BEHAVIOR AND DESIGN OF EARTHQUAKE-RESISTANT DUAL-PLATE COMPOSITE SHEAR WALL SYSTEMS

RESEARCH REPORT

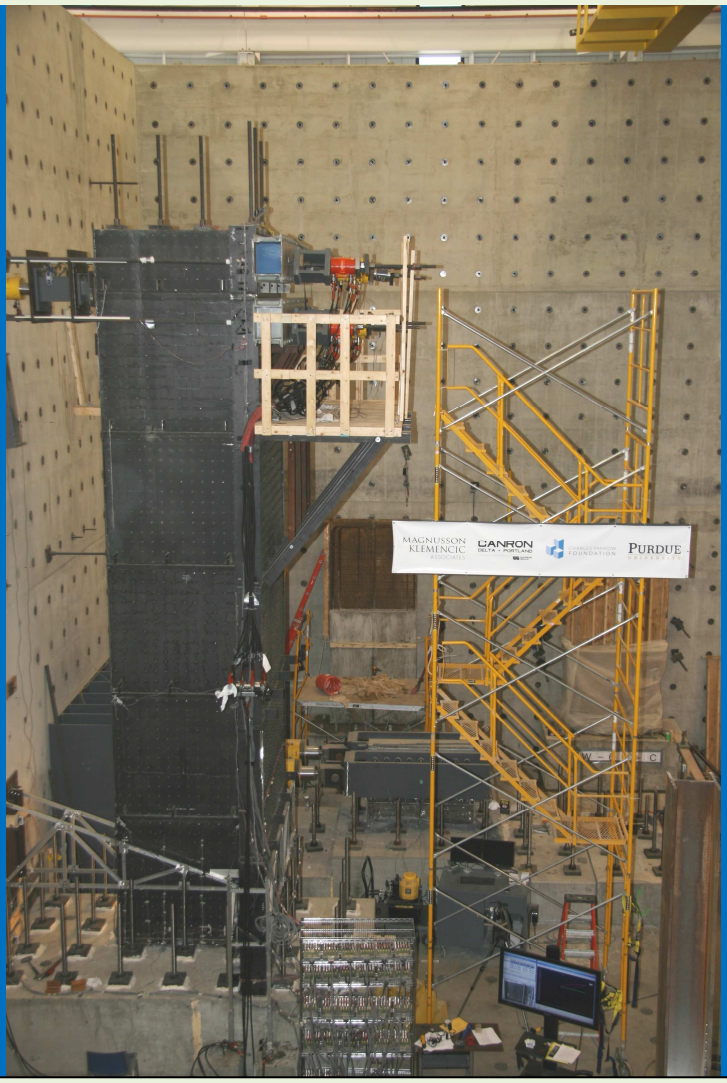

BY

SELVARAJAH RAMESH, MICHAEL E. KREGER, and MARK D. BOWMAN

SCHOOL OF CIVIL ENGINEERING
PURDUE UNIVERSITY

APRIL, 2013

This page intentionally left blank

BEHAVIOR AND DESIGN OF EARTHQUAKE-RESISTANT DUAL-PLATE COMPOSITE SHEAR WALL SYSTEMS

RESEARCH REPORT

SUBMITTED TO

CHARLES PANKOW FOUNDATION

BY

SELVARAJAH RAMESH
(Research Assistant, Purdue University)

MICHAEL E. KREGER
(Professor, Purdue University)

MARK D. BOWMAN
(Professor, Purdue University)

SCHOOL OF CIVIL ENGINEERING
PURDUE UNIVERSITY
WEST LAFAYETTE, INDIANA

APRIL, 2013

This page intentionally left blank

ACKNOWLEDGEMENTS

The authors gratefully acknowledge the financial support of the Charles Pankow Foundation, which sponsored this research program, and the administrative assistance provided by Mark J. Perniconi Executive Director, Dean Browning, Project Director, and Robert K. Tener, Executive Director (retired) of Charles Pankow Foundation. The authors wish to express their gratitude to Peter Timler, Corporate Business Development Officer and Vice President of Engineering, and the Supreme Group for the donation of steel plates used in test specimens, and for providing load frames that were used in the experimental program. The authors also are grateful for the valuable constructive conversations and feedback provided throughout the research program by Ron Klemencic, Chairman and CEO of Magnusson Klemencic Associates, and numerous MKA employees.

The authors wish to express their gratitude for the technical expertise provided by Dr. Jeesoo Kim during the initial analytical work. The authors wish to thank David Koppes, Ricardo Arrechea, Christopher Wilcox, Adythia Soendjojo, and Steve Giffin for their assistance during the study. Professor W. Jason Weiss and his students Robert Spragg and Dr. Mohammad Pour-Ghaz are recognized for providing guidance in the design and development of the concrete mix used in the large laboratory specimen tested during the research program. Finally, the authors gratefully acknowledge the technical and administrative assistance provided by Kevin Brower, Harry Tidrick, and Molly Stetler.

DISCLAIMER

The opinions, findings, conclusions and recommendations expressed in this report are those of the authors and do not necessarily reflect the views of the individuals or organizations acknowledged previously.

TABLE OF CONTENTS

Page

Page

Page

Page

Page

Page

Page

LIST OF TABLES

LIST OF FIGURES

Figure Page

Figure Page

Figure Page

Figure Page

Figure Page

Figure Page

Figure Page

Appendix Figure

Appendix Figure Page

Appendix Figure Page

Appendix Figure Page

Appendix Figure Page

Appendix Figure Page

Appendix Figure Page

ABSTRACT

This report discusses research related to behavior and design of earthquake-resistant dual-plate composite shear wall systems that was conducted at Purdue University with the financial sponsorship of the Charles Pankow Foundation. The analytical and experimental research conducted in this study and conclusions obtained from the results are detailed in this report.

The dual-plate composite shear wall concept was introduced to reduce the construction time of tall buildings. A dual-plate composite shear wall is a concrete-filled steel plate assembly. The steel plate assembly is composed of two steel plates connected with steel rods spaced uniformly in orthogonal directions. The objective of this research was to develop details to be used in dual-plate composite shear walls and to investigate the behavior and adequacy of those details.

A 3/8-scale dual-plate composite shear wall was constructed and tested as part of the experimental evaluation conducted during this research effort. First, foundation details and the connection between the specimen and foundation were designed and investigated. Next, details of the shear wall were selected using available standard design provisions. The behavior of dual-plate composite shear walls was investigated through four distinct experimental tests to study the following features: (a) stability of plate assemblies for resisting vertical construction loads, (b) strain compatibility between steel plates and concrete - to determine whether the steel plates and concrete act together for the selected details used in the plate assembly, (c) shear strength of horizontal splice connections between adjacent plate assemblies, and (d) behavior of dual-plate composite

shear walls under cyclic load - to determine whether composite shear walls have sufficient strength and ductility to resist earthquake and wind loads.

From the experimental and analytical investigation of the stability behavior of a 3/8-scale two-story dual-plate assembly, it was determined that the plate assembly was able to resist a maximum load of 18 times the maximum expected construction load. Behavior of the composite shear wall under cyclic lateral loading was investigated using a 3/8-scale 5-1/2 story 30-ft tall T-shaped shear wall specimen. It was determined from the test that if buckling of the plate could be prevented, then the design approach used for the test specimen can be used to design the structural components for dual-plate composite shear walls to resist cyclic lateral loads up to at least 2% drift.

CHAPTER 1: INTRODUCTION

1.1: Dual-plate composite shear wall

A shear wall is designed primarily to resist lateral loads, typically from wind and earthquakes, while also resisting the axial load from the gravity load system framing into the shear wall. The lateral load capacity and ductility of the shear wall are the primary features of the shear wall that need to be considered when designing for cyclic lateral loading. Concrete core walls have been traditionally used to resist lateral loads in tall buildings. Steel plate shear walls also have been used to a lesser degree in recent years.

A dual-plate composite shear wall is a concrete filled steel plate assembly intended to be incorporated in tall buildings to resist lateral loads. The steel plate assembly is composed of two steel plates connected with steel rods at a regular spacing in orthogonal directions (Fig. 1.1). The transverse steel rods can be bolted or welded to the steel plates.

The moment developed due to cyclic lateral load results in cyclic tension and compression stresses in the vertical fibers of the shear wall. In the dual-plate composite shear wall, the steel plates can resist tension until they fail in a tensile fracture mode and can resist compression until they fail by buckling. The steel plates also develop significant ductility under tension. The concrete in the dual-plate composite shear wall can resist compression force until it fails by crushing and can resist tension force until it cracks. Investigation of the combined, composite behavior of the steel plates connected by transverse bars and filled with concrete is an important step in understanding the behavior of dual-plate composite shear walls. Based on an understanding of the behavior,

design criteria can be formulated to facilitate efficient construction practices of the dual-plate composite shear walls.

When a concrete core wall is used in a steel-framed building, the construction schedule is influenced by the cycle time associated with the climbing forms. When a dual-plate composite shear wall is used, the steel plate assembly itself acts as a form and provides sufficient strength to resist the construction loads transmitted from the floor framing. Hence, the time required for the construction of tall buildings can be significantly shortened by using dual-plate composite shear walls instead of concrete core walls. Thickness of the shear wall may possibly be reduced when a dual-plate composite shear wall is used. In a reinforced concrete shear wall, cracking, splitting, and spalling during lateral load cycles can lead to a severe reduction in stiffness and strength (Zhao and Astaneh-asl, 2002). In a dual-plate composite shear wall, steel plates provide tensile resistance upon cracking of the concrete. The steel plates and transverse bars provide confinement to the concrete and prevent spalling and limit the reduction in stiffness and strength.

The primary disadvantage of the steel plate shear wall is buckling of the steel plate (Zhao and Astaneh-asl, 2002). In the dual-plate composite shear wall, the in-fill concrete and transverse bars will help to delay buckling of the steel plates.

The main factors that need to be considered in the design of dual-plate composite shear walls are the following:

1. The dual-plate assembly should be strong enough to resist construction loads that occur prior to casting of concrete. The dual-plate assembly also should resist the hydraulic forces due to the fresh concrete during casting, with minimal displacement and residual stresses.

2. The steel plates and concrete in the dual-plate composite shear wall should act together as a unit.

3. The horizontal joint between adjacent plate assemblies should be able to transfer the axial and shear forces between the top plate assembly and bottom plate assembly.

4. The dual-plate composite shear wall should be able to resist in-plane and out-of-plane cyclic loads. The composite shear wall should have sufficient strength and ductility to resist earthquake and wind loads in combination with axial loads due to the wall self weight and the loads delivered by the floor systems framing into the wall.

5. In order for the composite shear wall to achieve sufficient strength and ductility, the horizontal connection between the dual-plate assemblies and the foundation, the vertical connection between intersecting dual-plate assemblies, and the foundation details also should be able to resist the forces developed due to the lateral cyclic loads applied to the composite shear wall.

1.2: Historical background of the dual-plate composite shear wall

The concept of steel-concrete-steel composites was first proposed for a submerged tube highway tunnel in the United Kingdom in 1986 (Xie and Chapman, 2006). Shear studs were designed to make the steel-concrete-steel units act as a composite structure. Shear studs were welded only at one end of the shear stud. There are many research studies about steel-concrete-steel panels with shear studs. In the United States, a steel-concrete composite shear wall which had only two layers, steel plate on one side and concrete on the other, was developed and studied by Zhao and Astaneh-asl (2004). The steel plate and concrete (cast in place or precast) were connected by bolts.

Bi-Steel, which is very similar to the dual-plate composite shear wall, was developed by Corus UK Limited (currently TATA Steel). Bi-Steel is composed of two steel plates connected by steel rods friction stir-welded to the steel plates at both ends of the steel rods. Figure 1.2 shows a photograph of the Bi-Steel plate assembly. Even though the friction welding technique existed before the development of Bi-Steel, it was not used to make the steel panels with steel rods friction stir-welded to the steel plates at both ends of the steel rods prior to the development of Bi-Steel.

A fabrication unit of the Bi-Steel plate assembly is shown in Fig. 1.3 (Xie and Chapman, 2006). Steel rods are rotated while the steel plates at the locations of the end of each rod are compressed against the steel rod so that fusion can occur because of the heat developed by friction. The process is automatically controlled by machines. The dimensional limits of Bi-Steel are shown in Fig. 1.4.

The shop fabricated Bi-Steel plate assemblies can be brought to the field, assembled (welded and bolted) in place and can be filled with concrete to erect shear walls. Plate assemblies can be connected together in the shop as much as is practical and transported to the field as a unit to reduce the construction time needed in the field. Such a unit is shown in Fig. 1.5. Steel framing surrounding the shear wall can be attached to the steel plate assemblies in the field prior to the placement of concrete in the shear walls. This will speed the construction process.

Bowerman and Chapman (2002) reported the manufacturing process of Bi-Steel. Design guidelines of Bi-Steel have been reported by Bowerman et al. (1999). Clubley et al. (2003a, 2003b) studied the shear strength of Bi-Steel panels. The shear strength of the concrete core relative to the steel plates was also investigated in their study. Xie, Foundoukos, and Chapman (2004) studied the behavior of the friction welded bar to plate connections in Bi-steel under static and fatigue shear loading. All these research studies were conducted in the United Kingdom. In South Korea, a double-skin composite wall,

which is also very similar to Bi-Steel, has also been studied by Eom et al. (2009). Details of these research studies are reported in Chapter 2.

1.3: Motivation and research need

This research was motivated by the significant reduction in construction time of tall buildings when a concrete shear wall is replaced by a dual-plate composite shear wall. The design guideline of Bi-Steel by Bowerman et al. (1999) was developed mostly from existing theories and design procedures. Even though there are few research studies related to Bi-Steel as mentioned above, the behavior of Bi-Steel has not been widely investigated. Because Bi-Steel, used as a dual-plate composite shear wall, is not a traditional shear wall and there is no standard design code for the design of dual-plate composite shear walls, the performance of the dual-plate composite shear wall needs to be widely investigated for different configurations and dimensions of the shear wall to understand the behavior. The stability of the plate assembly for construction loads has not been experimentally investigated. This research study was conducted to investigate the stability of the plate assembly for construction loads and to check the adequacy of the connections and other structural elements of the dual-plate composite shear wall for cyclic lateral loading.

1.4: Research goals, objectives and scope

The goal of this research is to develop details to be used in dual-plate composite shear walls and to investigate the adequacy of the details. The knowledge obtained from this study was used to recommend design procedures for dual-plate composite shear walls. The primary objectives of this research study are the following:

1. To determine the contribution of the transverse rods connecting the steel plates to the performance of the dual-plate composite shear walls.

2. To examine the stability of the steel plate assembly of the shear wall for supporting construction loads before casting concrete inside the plate assembly.
3. To examine the strain compatibility between the steel plates and concrete within those steel plates.
4. To investigate the details for joining steel plates at the horizontal interface between adjacent dual-plate units.
5. To investigate the behavior of details (such as the horizontal connection between the dual-plate assemblies and the foundation, the vertical connection between intersecting dual-plate assemblies, and the foundation details) in the intersecting wall elements under cyclic lateral loading.
6. To observe and report any constructability issues encountered during the testing program.
7. To develop a design procedure for dual-plate composite shear walls.

The scope of this study is limited to the following.

1. This study is limited to prototype 40~60 story steel buildings.
2. The experimental investigation is performed for a specific plate thickness, spacing between the plates, transverse bar diameter, and transverse bar spacing.
3. The behavior of intersecting wall elements for cyclic lateral loading is limited to the *T- Shaped* intersecting wall element.
4. Behavior of the composite shear wall when subjected to impact loading, fire loading, and fatigue loading was not investigated in this research study.

1.5: Methodology

The research objective was met through the following five phases.

1. Investigation of the stability of the dual-plate assembly for construction loads.

2. Investigation of the strain compatibility between the steel plates and concrete within those steel plates.
3. Investigation of the behavior of horizontal splice plate details used to connect adjacent plate assemblies.
4. Investigation of the behavior of intersecting wall elements for cyclic lateral loading.
5. Development of a design procedure for dual-plate composite shear walls.

A more detailed description of these five phases is provided below.

Phase 1: The primary objective of the first phase of this research program was to investigate the stability of the dual-plate assembly prior to adding concrete between the plates. An analytical investigation was performed to select the shape and details of the dual-plate assembly to be tested in the laboratory. The analytical investigation involved different plate thicknesses, different bar diameters, and different spacing of transverse bars in the plate assembly. The resistance of the plate assemblies to the hydrostatic pressure from the wet concrete during concrete casting and the stability of the plate assembly under vertical construction loads were analytically investigated to select the plate thickness, transverse bar diameter, and spacing of the transverse bars.

Different shapes of the dual-plate assembly were analytically investigated to select the worst-case configuration for stability of the dual-plate assembly for construction loads. These different shapes included a *planar shape* (to represent the case when there are no intersecting wall elements for a significant length of a core wall), *T-shape* (to represent when two wall elements intersect in the central part of a core wall) and a *C-shape* (to represent the intersection of wall elements at the end of a core wall). The modes of failure were monitored and studied to decide the shape of the wall element to be tested in the laboratory. Small-scale lab tests were performed to substantiate and calibrate the analytical models (refer to Appendix A).

Once the shape and optimum dimensions of the details were selected, the experimental investigation was carried out. It involved the stability test of a dual-plate assembly with a scale of three-eighths of typical wall units. Two stories of the dual-plate assembly were investigated in the experimental program. Finite element analysis was expanded to three and four-story plate assemblies.

Phase 2: Once the stability of the dual-plate assembly with the selected details was found to be sufficient to resist the expected construction loads, strain compatibility between the steel plates and the concrete was investigated for the same details. Strain gauges mounted on the steel plates, concrete strain gauges embedded in the concrete, and strain gauges bonded to the reinforcing bar were monitored while lateral load was applied to the specimen in the out-of-plane direction. Strain compatibility between the steel plates and concrete would indicate that both elements act together, rather than independently.

Phase 3: The primary objective of this phase was to investigate the behavior of the horizontal splice plate details. The splice plates will act as alignment devices during erection of the plate assemblies and transfer axial and shear forces between the adjacent panels (Fig. 1.6). Behavior of the splice plate connection for in-plane lateral load was investigated.

Phase 4: The observations made during the earlier phases were crucial for designing similar, non-critical details for the intersecting shear wall elements which were tested in this phase. The primary objective of this phase was to investigate the behavior of the intersecting wall elements subjected to cyclic lateral loads. The test specimen was a large-scale cantilever wall element, like that tested in the previous phase, but was "T"-shaped in plan. Moment-curvature diagrams for the unit of intersecting wall elements were developed.

Phase 5: Results obtained from phases 1 to 4 were used to develop design procedures for the dual-plate composite shear wall.

1.6: Report outline

This report consists of seven chapters and three appendices. Chapter 2 details the literature review related to this research study. Chapters 3 through 6 present the four major tests conducted in the laboratory. Chapter 3 describes the analytical and experimental investigation of the stability of the dual-plate assembly for construction loads. The experimental program describes the stability test of a 3/8-scale two-story dual-plate assembly. Chapter 4 presents the experimental investigation to evaluate the strain compatibility between the steel plates and the concrete in a 3/8-scale one-story dual-plate composite shear wall. Chapter 5 discusses the experimental investigation of the behavior of the horizontal splice plate details for transferring in-plane lateral loads. Chapter 6 presents the investigation of the behavior of intersecting wall elements subjected to cyclic lateral loads. This investigation includes the cyclic loading test of a 3/8-scale, 5-1/2 story T-shaped dual-plate composite shear wall composed of intersecting wall elements. Chapter 7 provides a summary of the research findings, conclusions derived from the results, and recommendations for future work.

Appendix A presents the investigation of the contribution of the transverse connecting rods to the lateral stiffness of the plate assembly. This investigation includes a series of small tests conducted in support of the stability test described in Chapter 3. Appendix B discusses the investigation of the weld between the reinforcing bar hook and the foundation connection plate. This investigation was performed to design the weld between the reinforcing bar hook and the foundation connection plate of the specimens in the stability test and the cyclic loading test described in Chapter 3 and Chapter 6, respectively. Appendix C details the investigation of the weld between the shear wall plate and the foundation connection plate. This investigation was conducted to design the weld between the shear wall plates and the foundation connection plates of the specimen in the cyclic loading test described in Chapter 6.

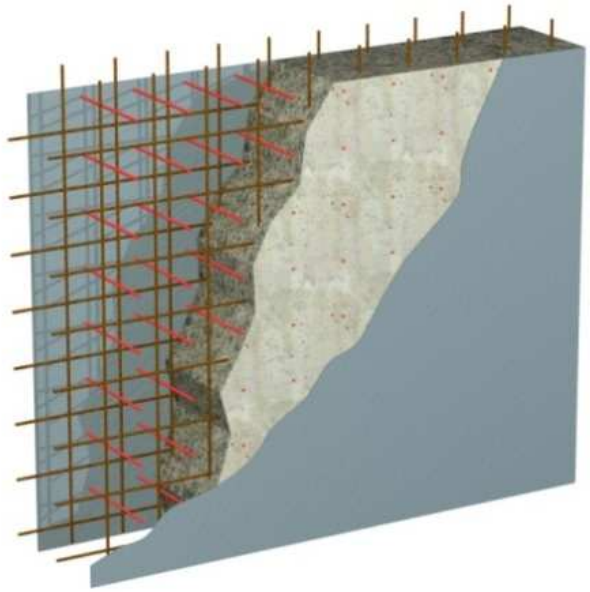

Figure 1.1 Schematic of Dual-Plate Composite Shear Wall Element (Wright et al., 2006)

Figure 1.2 Bi-Steel panel with friction welded rods (from brochures by Corus)

Figure 1.3 Fabrication of Bi-Steel panel assembly (Xie and Chapman, 2006)

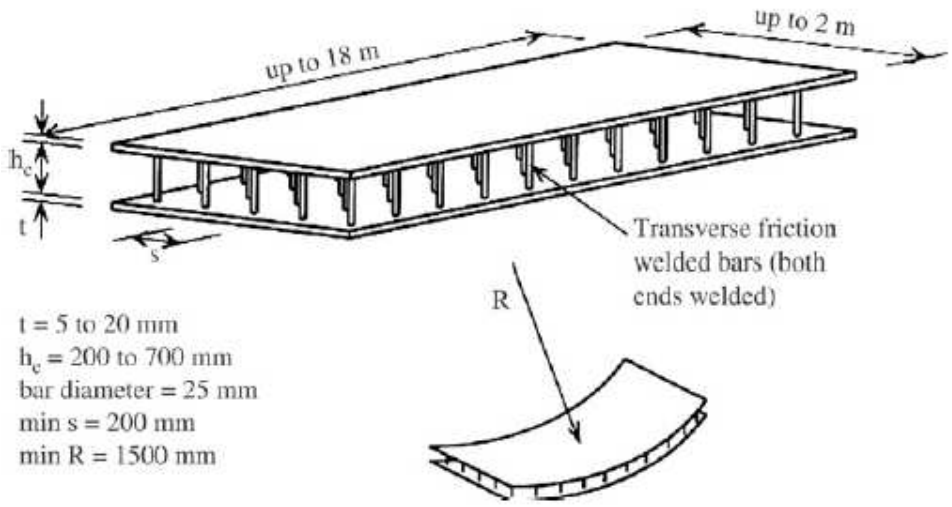

Figure 1.4 Dimensional limits of Bi-Steel (Xie and Chapman, 2006)

Figure 1.5 Lowering a Bi-Steel plate assembly unit in the field (from brochures by Corus)

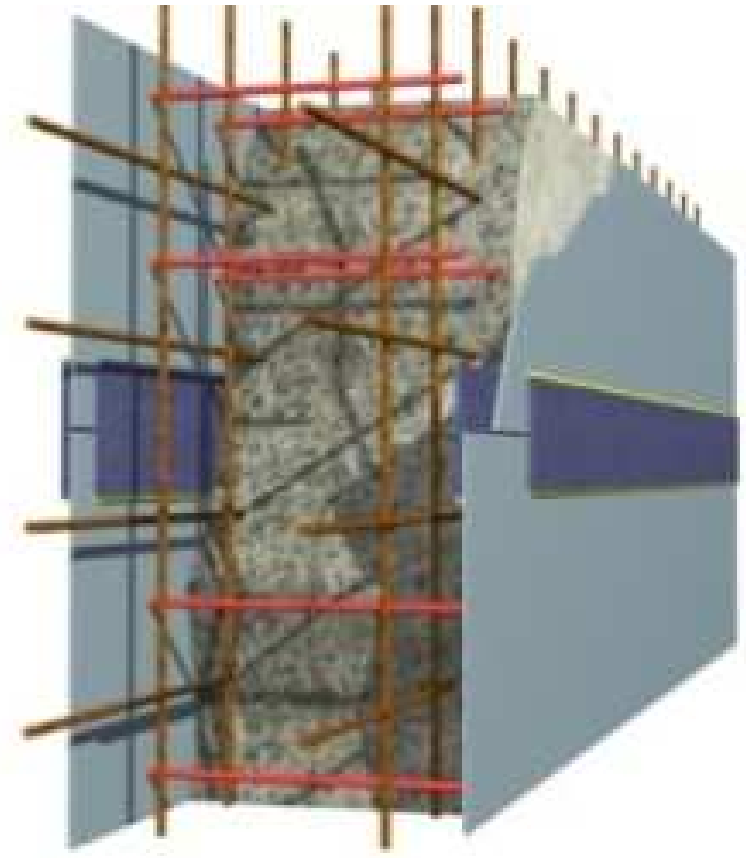

Figure 1.6 Schematic of Horizontal Connection between Dual-Plate Composite Wall Units (Wright et al., 2006)

CHAPTER 2: LITERATURE REVIEW

There is no standard design code for dual-plate composite shear walls for building structures. Some prior research studies, however, have been conducted on steel-concrete-steel composite shear walls which are similar to the dual-plate composite shear wall investigated in this study. Bi-Steel, which is very similar to the dual-plate composite shear wall, was developed by Corus UK Limited (currently TATA Steel) and few research studies have been conducted to investigate the behavior of the Bi-Steel panel, filled with concrete, under various loading conditions.

This research program includes four major but distinct investigations: (a) stability of the dual-plate assembly for construction loads, (b) strain compatibility between the steel plates and concrete under flexural loading, (c) behavior of the welded horizontal splice plate connection for in-plane shear loading, and (d) the behavior of dual-plate composite shear walls for cyclic loading. The background and prior studies related to this research are detailed in the following subsections divided according to the four major investigations.

2.1: Stability of the dual-plate assembly for construction loads

The stability of the dual-plate assembly can be influenced by plate thickness, distance between the plates (wall thickness), transverse bar diameter, and spacing of the transverse bars. The height and location of the bracing, which can influence stability of the dual-plate assembly, are governed mostly by the dimensions and location of structural elements in the building. Because the loads from beams that frame into the wall are always eccentric with respect to the center of the wall cross section, stability of the dual-

plate assembly for the vertical load and moment due to the eccentricity should be considered. The load transmitted from the cross beams is first transferred to one of the dual-plates, and the transverse rods welded or bolted to both plates transfer a portion of the load to the plate on the opposite side of the assembly. Hence, from a stability standpoint, the capacity of the dual-plate assembly lies between that for two individual plates and a plate assembly unit made of two steel plates rigidly connected together.

Even though an expression for the stability of a dual-plate assembly could not be found, there is considerable information in the literature on the stability of plates. Information is available that deals with the stability of plates under various loading conditions, various boundary conditions along the edges, and various stiffenening conditions.

As reported by Rees (2009), when a plate with length, width, and thickness of a, b, and t (as shown in Fig. 2.1) and with free side edges is uniformly compressed, the critical buckling stress (σ_{cr}) can be expressed by the following equation:

$$\sigma_{cr} = \frac{\pi^2 E}{12 L_e{}^2 (1/t)^2} \qquad \text{Eq. (2.1)}$$

where E = Young's modulus
L_e = equivalent length of the plate
t = thickness of steel plate

The equivalent length, L_e, depends on the boundary conditions along the loaded edges and can be expressed by the following equations.

$L_e = a(1 - v^2)^{1/2}$ for pinned ends Eq. (2.2a)

$L_e = (a/2)(1 - v^2)^{1/2}$ for fixed ends Eq. (2.2b)

$L_e = (a/\sqrt{2})(1 - v^2)^{1/2}$ for pinned-fixed ends Eq. (2.2c)

$L_e = 2a(1 - v^2)^{1/2}$ for fixed-free ends Eq. (2.2d)

where v = Poisson's ratio

a = length of the plate

Equation 2.1 is for a plate with free side edges. When all four edges are simply supported, the critical buckling stress (σ_{cr}) can be expressed by Equation 2.3 (Rees, 2009).

$$\sigma_{cr} = \frac{\pi^2 E}{3(1-v^2)(b/t)^2} \quad \text{Eq. (2.3)}$$

The elastic critical buckling stress, $(\sigma_{cr})_e$, for a uniformly compressed plate with various boundary conditions along its four edges and various a/b values is shown in Fig. 2.2. In the figure, σ_{cr} is the critical buckling stress for a plate with all four edges simply supported as given by Equation 2.3. Salmon and Johnson (2009) also reported similar equations for plate buckling.

2.2: Strain compatibility between steel plate and concrete

Strain compatibility between the steel plates and the infill concrete in a dual-plate composite shear wall ensures that the steel plates and concrete act together. When a lateral load is applied to the composite shear wall, the bond between steel and concrete and the interlock of the transverse rods and concrete minimize the slip between the steel

plates and concrete and help the composite shear wall to act as one unit. The primary factors which can affect strain compatibility are diameter of the transverse bars and spacing between the transverse bars.

Clubley et al. (2003) performed push-out tests to investigate the behavior of the concrete core in Bi-Steel composite panels for shear load applied to the concrete core relative to the steel plates. Different plate thicknesses, plate spacing, and transverse bar spacing were considered. Three plate spacings of 200 mm, 400 mm and 700 mm were considered for the laboratory test specimens. The test set-up for the 200 mm plate spacing is shown in Fig. 2.3 and the test set-up for the 400 mm and 700 mm plate spacings is shown in Fig. 2.4. Plate thicknesses of 6 mm, 8 mm, and 10 mm were considered for the specimens. Threaded studs of 16 mm diameter were provided perpendicular to the transverse bars in order to simulate the constraints in the panel. The failure load per number of welds between the transverse bars and plates was calculated and compared between the test results for specimens with different plate spacings.

It was observed that the shear strength of the concrete core was governed by the plate spacing, diameter of the transverse bars, and spacing between the transverse bars. The mode of failure was governed by the plate thicknesses and transverse bar spacing. When the composite panel was constructed with thick plates, failure was initiated by shearing of the transverse bars which experienced a brittle failure at the friction welds. When the composite panel was constructed with thin plates, failure was initiated by large deformation of the plate around the friction weld followed by tearing in the plate. Furthermore, Clubley et al. (2003) also reported that the transverse bars should have sufficient ductility to transfer load between the concrete and steel to ensure that all components fail as one unit.

It should be noted that shearing load was applied only to the concrete core in the study by Clubley et al. (2003). According to Xie and Chapman (2006), the behavior of

the composite panel for in-plane shear will be close to the behavior of the concrete core studied by Clubley et al. (2003) because the shear is resisted mostly by the concrete core.

A series of studies similar to the study by Clubley et al. (2003) were reported by Xie, Foundoukos and Chapman (2004) on the behavior of the friction welded bar-to-plate connections in Bi-steel under static shear loading. The specimens were made by casting concrete inside a Bi-steel unit which had only one transverse bar connecting both steel plates. A Bi-steel unit and a sample test specimen are shown in Fig. 2.5. Plate thicknesses of 6, 8, 10, 12, and 15 mm were used for the specimen. The test set-up is shown in Fig. 2.6. Load was applied to the concrete so that the concrete was sheared relative to the steel plate.

Three modes of failure were observed in the connections between the transverse bar and steel plate (see Fig. 2.7). Failure occurred by plate tearing around the bar, shear fracture of the bar, or fracture between the bar and plate. Increasing the plate thickness from 6 mm to 10 mm increased the shear strength by 25%, and there was no increase in shear strength when the plate thickness was increased to more than 10 mm.

2.3: Behavior of splice plate connection for in-plane shear loading

Adjacent plate assemblies can be connected by welding or bolting the splice plates to the adjacent plate assemblies. The splice plate connection should transfer vertical load and in-plane shear from one plate assembly to the other. When the splice plates are welded, the possible modes of failure for in-plane shear are shear yielding of the plate, shear rupture of the base metal, and failure of the weld metal along the weld line. The primary modes of failure for vertical load are bending in the out-of-plane direction (due to the moment developed by the eccentricity of the vertical load) and fracture of the base metal along the weld line. The steel construction manual (AISC, 2011) outlines the methods to calculate the shear strength of welded connections. However,

information regarding an investigation of the behavior of splice plate connections in a dual-plate assembly for in-plane shear loading could not be found.

2.4: Behavior of dual-plate composite shear wall for cyclic loading

The shear wall system should provide sufficient strength, stiffness, and ductility to withstand ground motions and wind loads. The strength of the shear wall limits the damage, stiffness limits the deformation, and ductility of the shear wall ensures the wall maintains sufficient lateral load capacity in the inelastic range of response (Massone and Wallace, 2004). In a steel-concrete-steel composite panel, bending is resisted primarily by the steel plates, and shear is resisted mostly by the concrete core (Xie and Chapman, 2006).

Ductility or deformation capacity of the steel-concrete-steel composite panel enables the composite shear wall to withstand lateral loads experienced by a building during a severe earthquake. The shear wall should be allowed to deform into the inelastic region to limit the load that is resisted by the shear wall. Hence, the other structural elements which receive load from the shear wall, such as the foundation, can be designed for the maximum load expected to be developed by the shear wall (Thomsen and Wallace, 2004). When the weld fracture at the base of the wall is avoided, plate buckling followed by concrete crushing and tie bar fracture is the primary mode of failure of the steel-concrete-steel double skin composite wall for in-plane cyclic loading (Eom et al., 2009). The research study performed by Eom et al. (2009) is detailed below.

2.4.1: Research study performed by Eom et al. (2009)

The behavior of double-skin composite walls for in-plane cyclic loading was investigated in the research study performed by Eom et al. (2009). Double-skin composite walls were made up of two thin steel plates connected by tie bars with

concrete cast between the steel plates. Even though five different specimen types were tested and reported in the research study, only two types, a rectangular cross-section wall and T-shaped cross-section wall, are detailed in this report. All five different specimen types are shown in Fig. 2.8. The rectangular cross-section wall alone is shown in Fig. 2.9 for better visualization of the dimensions.

The rectangular and T-shaped cross-section walls (DSCW1C and DSCW3, respectively in Fig. 2.8) were 1/3 scale models composed of 10-mm thick steel plates connected by 16-mm diameter tie bars spaced at 300 mm. The walls were 120 mm thick, 1000 mm deep and 3700 mm high. The flange width of the T-shaped wall was 600 mm.

The cyclic loading history is shown in Fig. 2.10. For the test of the rectangular cross-section wall, the wall plates were connected to the base plate using complete joint penetration groove welds. The base plate was attached to a support section which was then attached to the laboratory floor. For the applied in-plane cyclic loading, the weld joint failed in tensile fracture before the wall plate reached flexural yielding (at 1.5% drift ratio). Hence, two different strengthening methods were used: (a) welding triangular rib plates (10 mm thick) to the wall plate and base plate and (b) fillet welding cover plates (10 mm thick) to the wall plates and base plate. Use of the rib plates did not remedy the earlier observed failure. When the cover plates were used to strengthen the specimen at the wall base, stable cyclic behavior was observed up to +2.5% drift ratio without any failure in the weld at the wall base. Hence, the cover plates were used to strengthen the wall base for all remaining specimens.

The failure mode and load-displacement response for the rectangular cross-section wall are shown in Figs. 2.11 and 2.12, respectively. The rectangular cross section wall with cover plates failed at -2.5% drift ratio due to buckling of the wall plates near the wall base followed by fracture of the vertical weld joint, crushing of the concrete, and fracture of the tie bars.

The failure mode and load-displacement response for the T-shaped cross-section wall are shown in Figs. 2.13 and 2.14, respectively. The T-shaped cross section wall failed due to local buckling of the wall plate, tie bar fracture, and concrete crushing at -2% drift ratio. Positive monotonic loading was applied until the wall plate failed in tensile fracture near the wall base at +4.9% drift ratio.

The above observations show that tensile fracture of the weld joints at the wall base, local buckling of the steel plates, and concrete crushing and tie bar fracture following local buckling are the major failure modes for the double-skin composite walls for in-plane cyclic loading. Tensile fracture of the weld joint reduces the ductility of the specimen. This research study demonstrated that using cover plates worked well to improve the wall base strength, while the addition of rib plates did not demonstrate any improvement. In the rectangular cross-section wall and the T-shaped cross-section wall, the steel plate buckled at 0.021 to 0.028 mm/mm tensile strains. Due to the cyclic loading, compressive stresses can be developed as a result of residual tensile strain, even when the steel plate undergoes tensile strain. Because the concrete in tensile strain could not develop compressive strength, the steel plate had to resist all the compressive force and consequently buckled. Because, after buckling, the steel plate could not provide lateral confinement for the concrete, concrete crushing and tie bar fracture occurred following steel plate buckling. Reducing the ratio of tie bar spacing to plate thickness can reduce the susceptibility of the steel plate to buckling.

The ratios of the load-carrying capacity of the specimen, calculated using a plastic stress distribution, to the measured load-carrying capacity were between 0.98 and 1.18. This shows that the load-carrying capacity was achieved by the specimen as predicted. However, this research study shows that further work should be undertaken to improve the ductility of the specimen for in-plane cyclic loading.

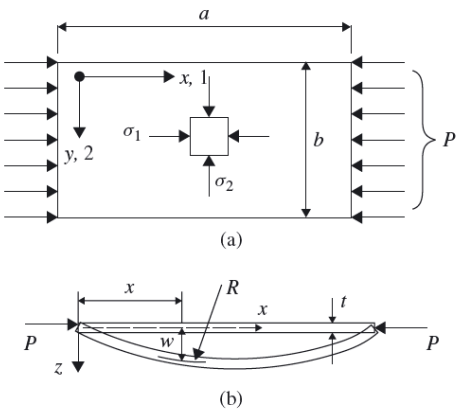

Figure 2.1 Buckling of a uniformly compressed plate (by Rees, 2009)

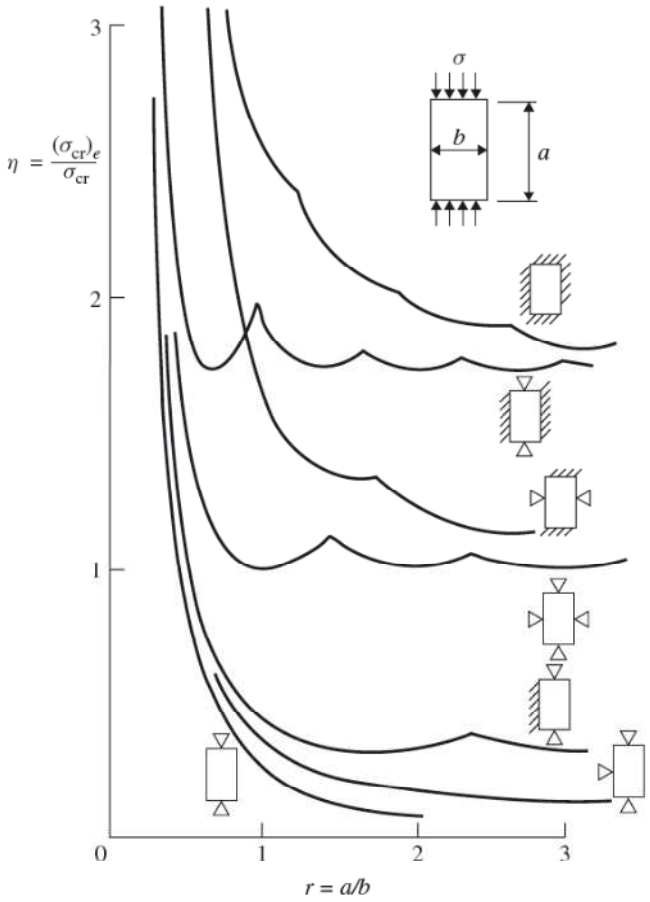

Figure 2.2 Critical buckling stresses of plate with various boundary conditions along the edges (by Rees, 2009)

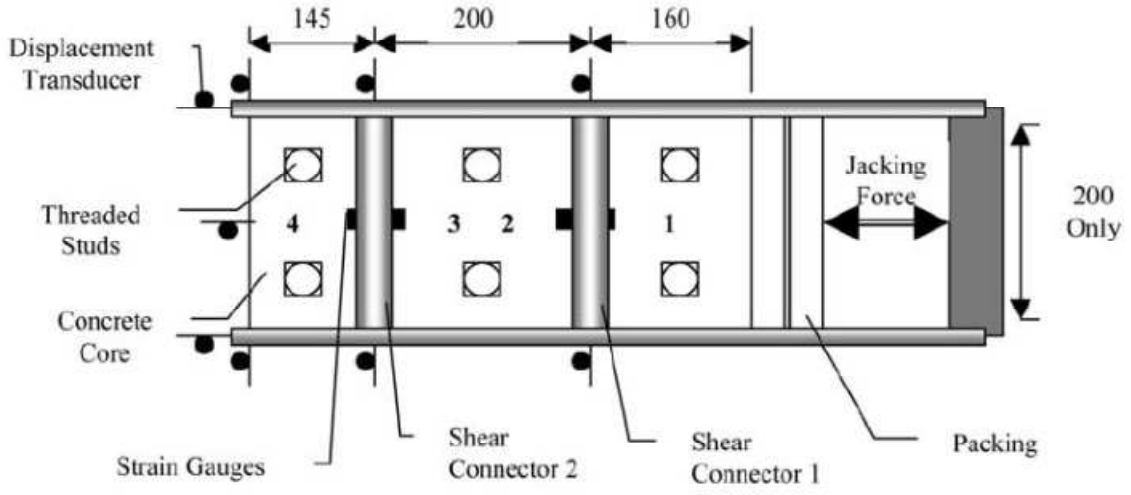

Figure 2.3 Push out test set-up for Bi-Steel panel with a plate spacing of 200 mm (by Clubley et al., 2003)

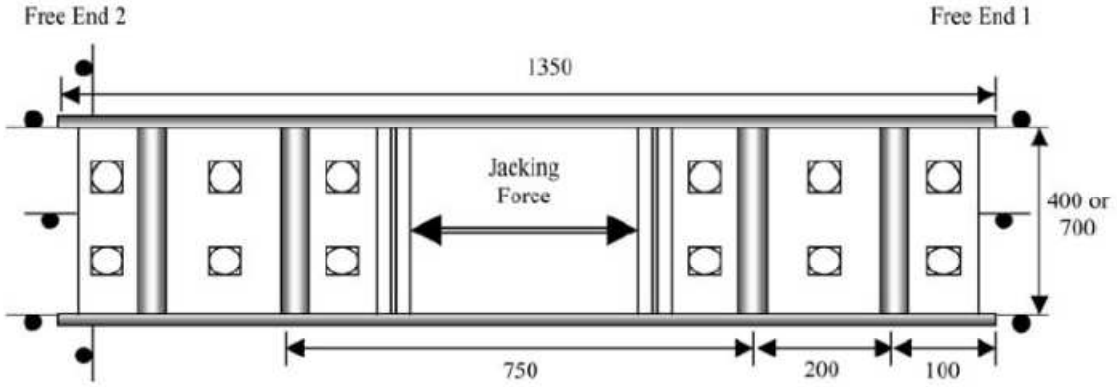

Figure 2.4 Push out test set-up for Bi-Steel panel with a plate spacing of 400 mm and 700 mm (by Clubley et al., 2003)

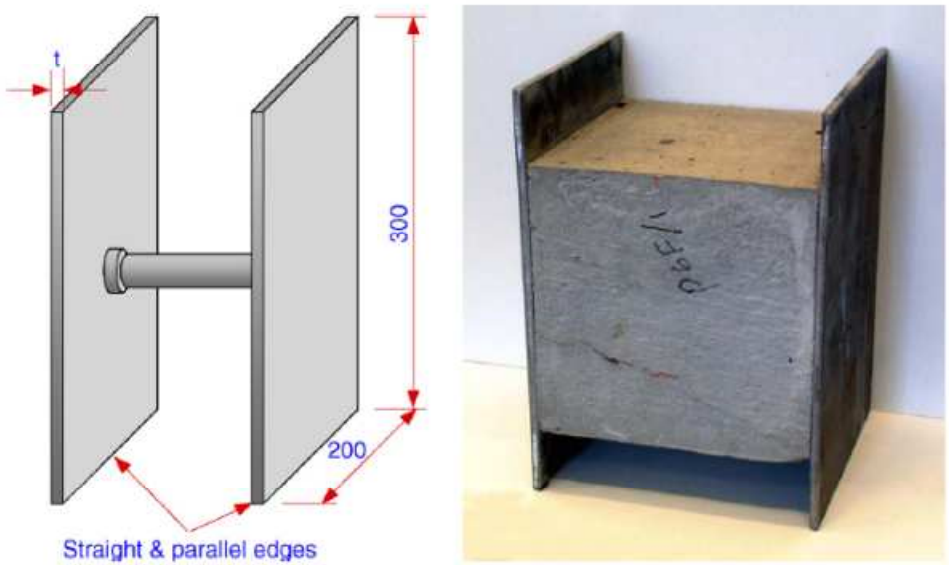

Figure 2.5 A Bi-steel unit and a test specimen for the study by Xie et al. (2004)

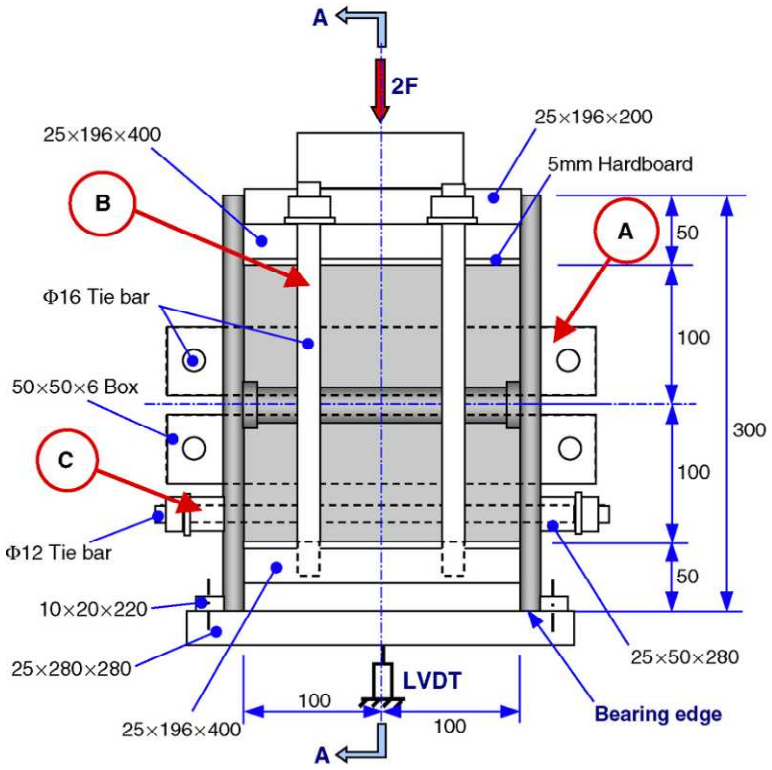

Figure 2.6 Test set-up for the study by Xie et al. (2004) – Elevation view

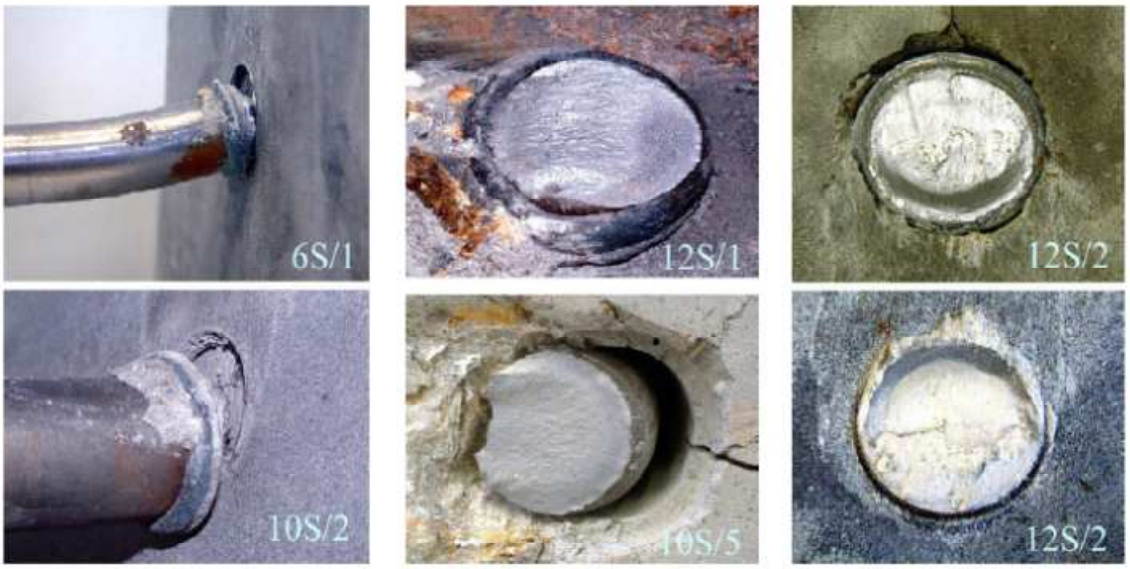

Figure 2.7 Modes of failure for the shear test by Xie et al. (2004)

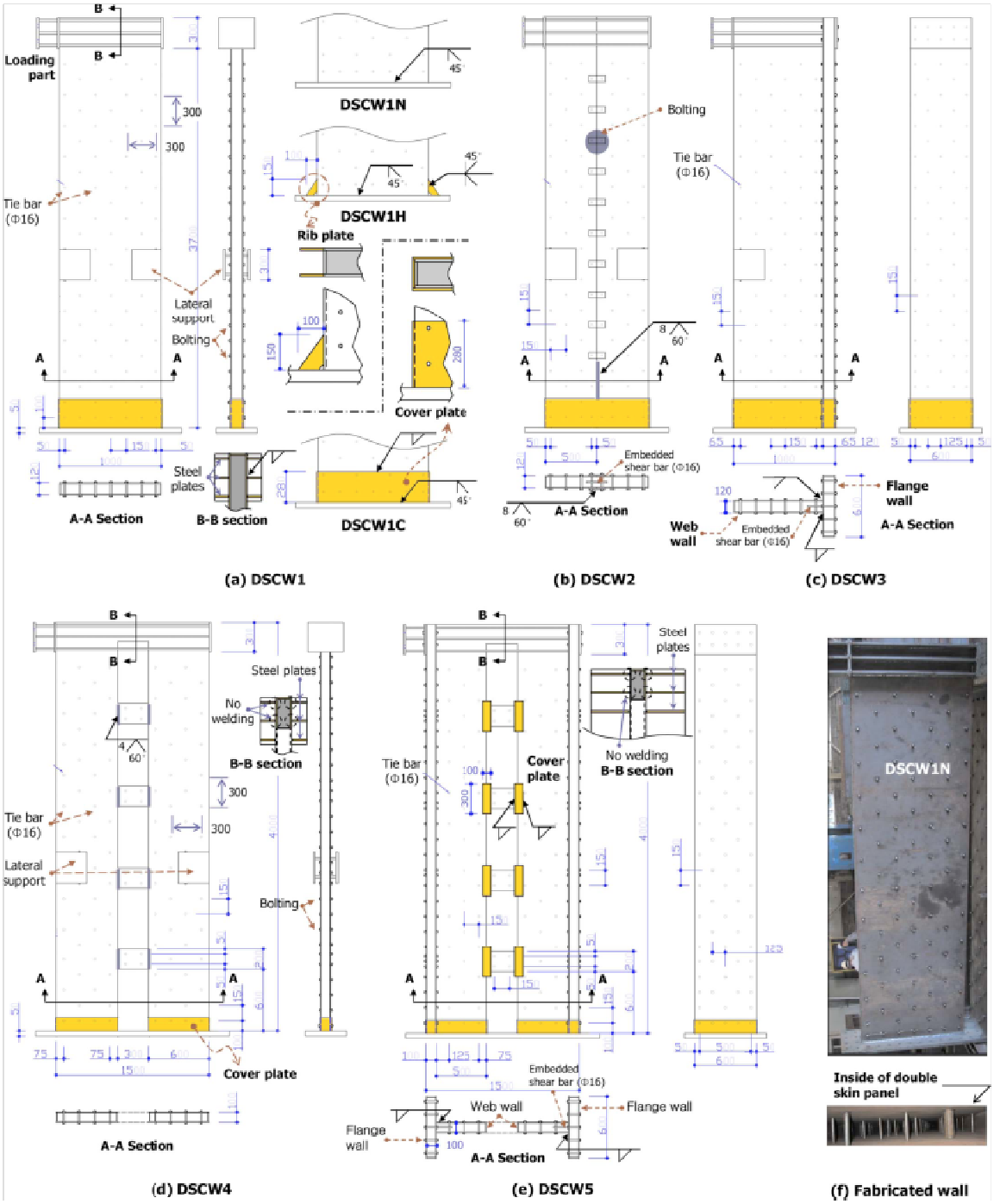

Figure 2.8 Double-skin composite wall specimens and test set-up for the study by Eom et al. (2009) – Dimensions are in mm.

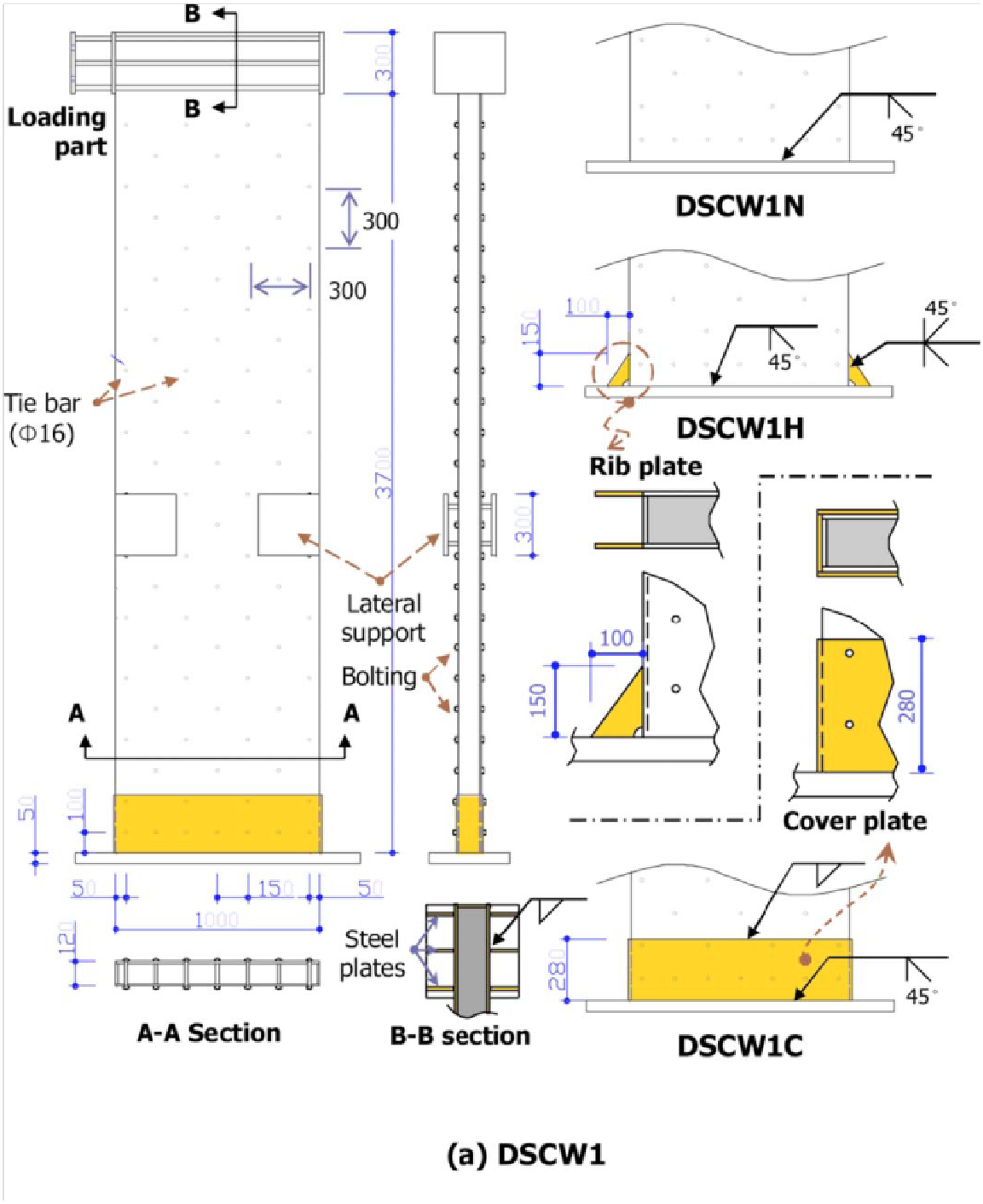

Figure 2.9 Rectangular shaped double-skin composite wall specimen and test set-up for the study by Eom et al. (2009) – Portion of the illustration in Figure 2.8 - Dimensions are in mm.

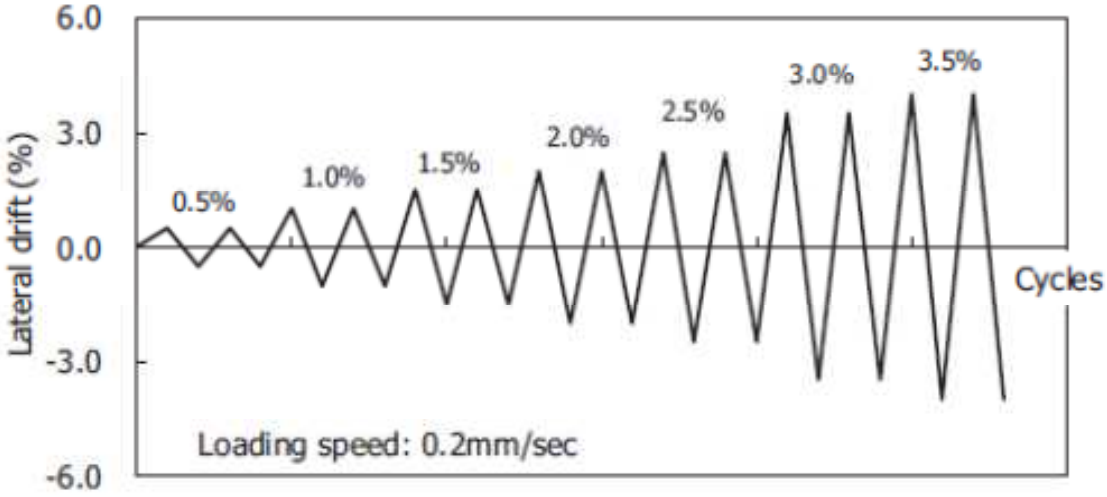

Figure 2.10 Cyclic loading history for the study by Eom et al. (2009)

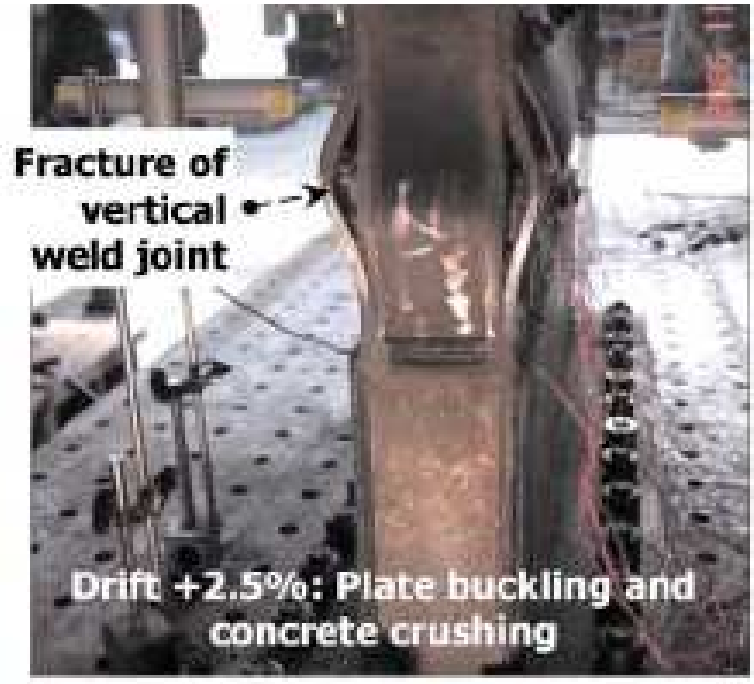

Figure 2.11 Failure of rectangular double skin composite wall – DSCW1C by Eom et al. (2009)

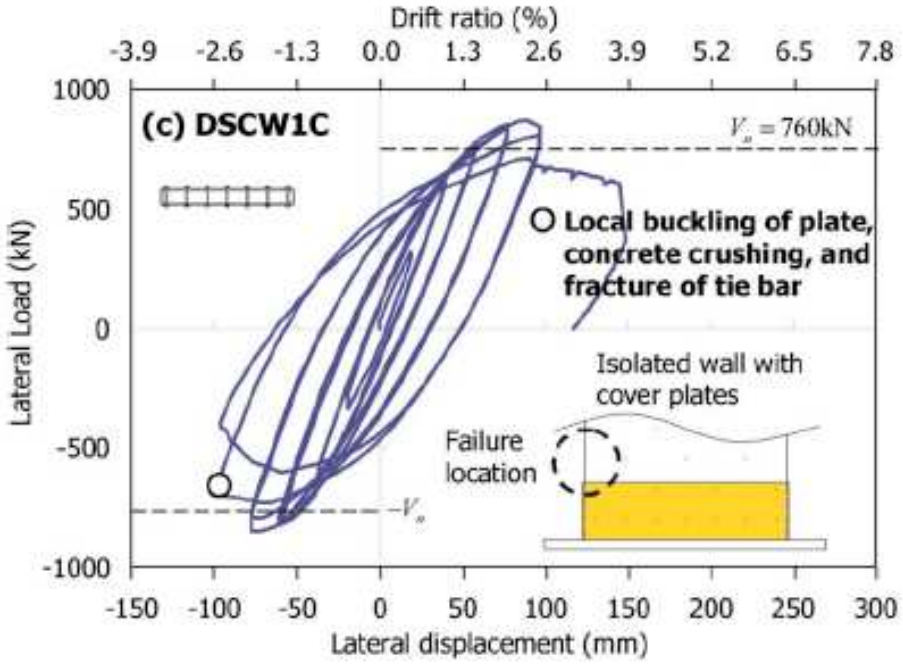

Figure 2.12 Lateral load versus displacement for rectangular double skin composite wall – DSCW1C by Eom et al. (2009)

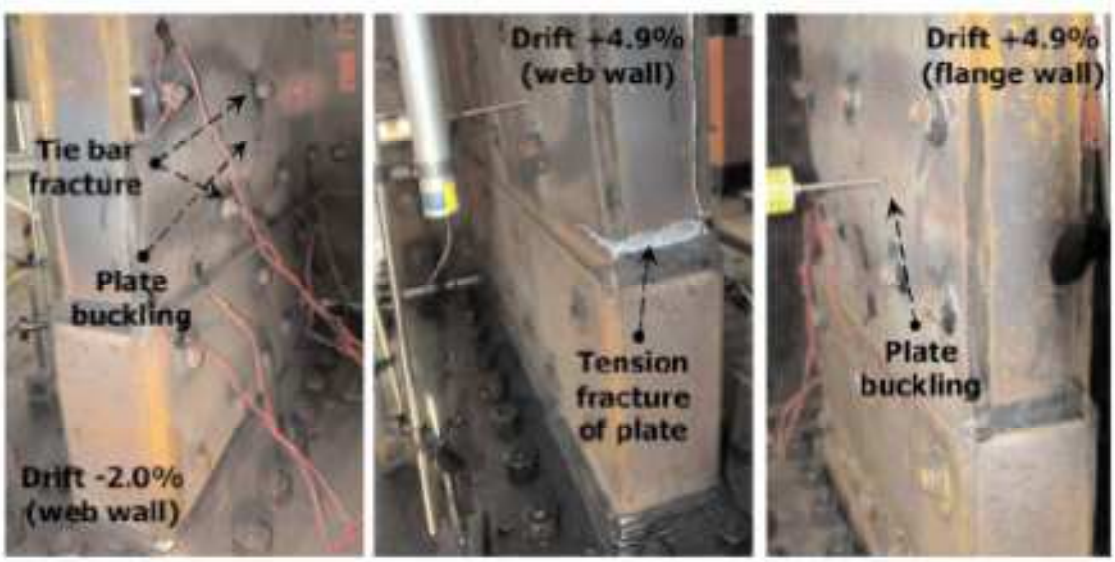

Figure 2.13 Failure of T-shaped double skin composite wall – DSCW3 by Eom et al. (2009)

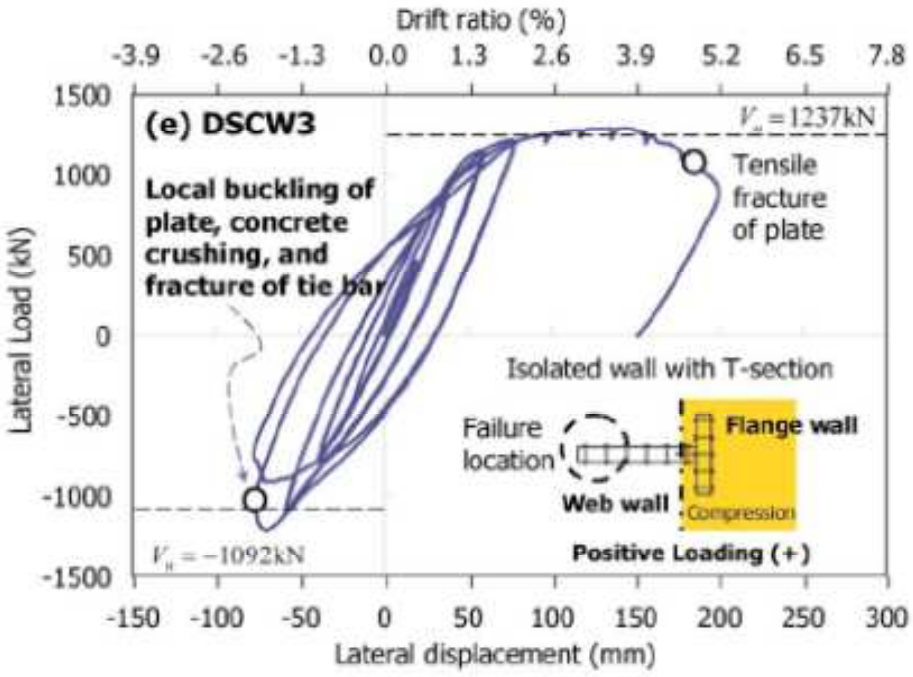

Figure 2.14 Lateral load versus displacement for T-shaped double skin composite wall – DSCW3 by Eom et al. (2009)

CHAPTER 3: BEHAVIOR OF DUAL-PLATE ASSEMBLY FOR CONSTRUCTION LOADS

3.1: Introduction

One of the advantages of the steel plate composite shear wall system is that during the construction operation steel framing can be attached to the steel plate assemblies prior to placement of concrete in the shear walls. This will allow construction to proceed a few floors ahead of the level of hardened concrete within the dual-plate composite shear wall. For this to occur successfully, however, the two steel plates interconnected with tie rods must be capable of safely supporting an appropriate portion of the steel framing dead load and typical construction live loads. To assess the behavior and buckling load resistance of the interconnected dual-plate system, finite element models were assembled and the response of the dual-plate assembly with various parameters for vertical loads was evaluated. An experimental investigation was performed for a planar dual-plate assembly with the parameters which are typically used in the industry and were selected from the finite element analysis. The analytical and experimental investigations are discussed in the following sections.

3.2: Analytical Investigation

Stability of the plate assembly for the vertical construction loads was investigated in this phase of the research study. This investigation was performed to assist in the selection of the plate thickness, transverse bar diameter, and spacing of the transverse bars in a dual-plate assembly. In a dual-plate assembly, the plates provide (1) the necessary rigidity to safely support their own weight plus the weight of structural steel

framing into the core wall before concrete is cast inside the plate assemblies, (2) the necessary rigidity and strength to resist the hydraulic forces that develop when concrete is cast between the plates, and (3) act as formwork to cast the concrete. The transverse bars provide (1) bracing for the stacked plate assemblies to develop the necessary rigidity for stability under vertical construction loads, (2) tensile strength to resist the hydraulic forces, and (3) the mechanical connection that facilitates composite action of the plates and reinforced concrete cast between the plates. The plate thickness and transverse bar diameter are the main parameters expected to influence the stability of the wall panels for resisting the vertical construction loads. Spacing of the transverse bars is the main parameter influencing the resistance of the plate assemblies to hydrostatic pressure.

Earlier analytical work performed by a postdoctoral fellow (Dr. Jeesoo Kim) for this research project is briefly summarized in Section 3.2.1. This earlier analytical work includes two main aspects: (1) the resistance of the plate assembly to the hydrostatic pressure due to concrete casting, and (2) the behavior of various dual-plate configurations such as *planar, T-shape,* and *C-shape* for vertical construction loads. From this earlier analytical work, the maximum spacing of the transverse bars was selected. Furthermore it was verified that the *planar* dual-plate configuration would be the worst-case scenario for the buckling resistance of the dual-plate assembly for vertical load.

Considering results from the earlier work, further analysis was performed in this phase of the research study. Finite element models were modified according to the typical field boundary conditions. This analysis includes the investigation of the stability of the planar dual-plate assembly for vertical construction loads.

3.2.1: Analytical work for dual-plate assembly

The resistance of the plate assembly for hydrostatic pressure due to concrete casting, and the behavior of various dual-plate configurations for vertical construction loads were investigated.

3.2.1.1: Behavior of dual-plate assembly for concrete hydrostatic pressure with change in transverse bar spacing

Selection of Parameters

It was anticipated that approximately 13-ft tall plate assemblies, 30-ft in length, will be shipped to the jobsite, lifted into place, and joined with other plate assemblies to form a complete core wall. It has been anticipated that concrete will be cast one or two stories at a time. For this analysis, a ½-in. rod diameter and a ½-in. plate thickness were considered. Bar spacing could be adjusted from one plate assembly to the next to optimize the number of bars and connections required, but it was anticipated that one constant spacing will be used.

Modeling

Finite element analysis (Abaqus) was used to investigate the behavior of dual-plate assemblies for hydrostatic pressure with varying rod spacing. The rod stress was evaluated for different spacing and plate heights. Analysis was performed for half-scale models in anticipation of the specimen size that would be used in the laboratory study. Plates were modeled as shell elements and rods were modeled as solid elements. Because height of the plate, that is, height of the concrete cast, affects the stress, five different plate heights were considered.

Findings

Stress in the rods at various elevations (various rows) was monitored and is shown in Figs. 3.1 and 3.2 for a rod spacing of 6 and 12 in., respectively. In the figures, “H” refers to the height of the plate or the height of concrete casting. As shown in those

figures, stress in the rods at the second row (from bottom of the plate) was higher than the other locations.

Next, stress in the rods at the second row was monitored for various plate heights and rod spacings. Figure 3.3 shows the stress in the rods at the second row versus rod spacing for various plate heights.

In parallel with the finite element analysis (FEA), stress in the rods at the second row also was calculated by considering the force developed by the hydrostatic pressure in the tributary area around the rod. The hydrostatic pressure was taken as the unit weight of the concrete multiplied by the height of concrete cast above the rods at the second row. The tributary area was taken as a square with both of its sides equal to the rod spacing. This method led to Eq. 3.1 to calculate stress in the rods at the second row.

$$\sigma_{rod} = \frac{\gamma(H-1.5S)*S^2}{\frac{\pi}{4}D^2} \qquad \text{Eq. (3.1)}$$

Where σ_{rod} = Rod stress (ksi)

γ = Unit weight of fresh concrete (kip/in^3)

H = Height of the plate (height of concrete casting) (in)

S = Spacing between rods (in)

D = Diameter of the rod (in)

Table 3.1 shows the stress in transverse rods at the second row calculated using both finite element analysis (FEA) and Eq. 3.1. The difference in the stress calculated using these two methods is also tabulated as a percentage of the stress values calculated using finite element analysis. The difference in the calculated stress ranged from 4.4 percent to a maximum 6.4 percent, with the stress from Eq. 3.1 consistently lower than the FEA predicted stress.

In the laboratory tests, a 3/8-scale model of a prototype with a rod diameter of 1 in. and a rod spacing of 12 in. was considered. Hence, the rod diameter and rod spacing were 3/8 in. and 4.5 in. in the laboratory specimen. Table 3.2 and Table 3.3 show the variation of the maximum stress in transverse rods with the height of concrete casting for a 3/8-scale laboratory specimen and the full-scale prototype, respectively. It can be noted from these tables that the rod stress was not the same for the laboratory specimen and prototype at a particular story level. However, the rod stress at a particular story level was proportional to the scale (equal to 3/8 in this research study). This is also evident from Eq. 3.1.

It can also be noted from Table 3.2 and Table 3.3 that the rod stresses were very small compared to the design yield strength of the rod of 50 ksi. Hence, the concrete hydrostatic pressure did not govern the selection of the transverse bar diameter and spacing. The reason for the selection is explained in Section A.4 of Appendix A of this report.

3.2.1.2: Behavior of various dual-plate configurations for vertical construction loads

Different shapes of the dual-plate assembly, *planar*, *T-shape*, and *C-shape* were analyzed to select the worst-case configuration for resisting vertical construction loads. These shapes of shear wall components are present in typical shear wall layouts. For the different shapes considered, it was found that the *planar shape* was the worst-case configuration for stability considerations.

3.2.2: Stability of planar shape two-story plate assembly for vertical loads

Following the earlier investigation of the behavior of the dual-plate assembly for hydraulic pressure with the change in transverse bar spacing and the stability of the

various dual-plate configurations for resisting vertical construction loads, finite element models to examine the stability behavior of the planar shape dual-plate assemblies were developed. The models were modified to model the field and laboratory boundary conditions. The finite element analysis of the stability test specimen tested in the laboratory is described in this section.

The contribution of the diameter of the transverse rods to the stiffness of the plate assembly was experimentally investigated in the laboratory at the same time finite element models of the test were developed. The test and the analysis are described in detail in Appendix A. It was concluded from the test program that the diameter of the transverse bars has a significant impact on the stiffness of the plate assembly. Furthermore, it was decided to use transverse bar diameters with 3/8-in. diameter and 4.5-in. spacing in the 3/8-scale models (which corresponds with 1-in. diameter and 12-in. spacing in the full scale).

3.2.2.1: Selection of parameters

Dimensions from drawings of prototype buildings

Four prototype buildings were analyzed to select typical dimensions of the shear walls. Figures 3.4 through 3.7 show plan drawings of the shear walls in the prototype buildings. It was evident from the drawings that the cross beams frame into the shear wall at a horizontal spacing of about 10 ft. Furthermore, the center to center distance between flanges of the shear walls ranges from 28’-9” to 46’-2”. The shear wall layout in the 55-story Washington Mutual building (Fig. 3.7) was taken as a typical layout. Hence, it was determined that the cross beams frame into the shear wall at 10 ft lateral spacing and the center to center distance between the flanges of the shear wall is 30 ft. The length of the shear wall to be analyzed was taken as 30 ft. It was reasonably assumed that the cross beams frame into the shear wall 5 ft below the top of each wall panel with a

corresponding story height of 13 ft and a wall thickness of 2 ft. Considering the scale (3/8) of the specimen to be tested in the laboratory, the lateral spacing of the cross beams, story height, wall thickness, and length of the wall were taken as 45 in., 58.5 in., 9 in., and 135 in., respectively.

Dimensions from Bi-Steel panels

Bi-Steel panels are the dual-plate assemblies produced by Tata Steel Europe (formerly known as the Corus Group). Refer to Section 1.2 for more details about the Bi-Steel panels. Typical details of the Bi-Steel panels are shown in Fig. 1.4. In the typical details, the plate thickness ranges from 5 to 20 mm (0.20 to 0.79 in.) and the clear spacing between the plates ranges from 200 to 700 mm (7.9 to 27.6 in.). The minimum transverse bar spacing is 200 mm (7.9 in.). The bar diameter used in the Bi-Steel panel is fixed at 25 mm (≈1 in.). Hence, a bar diameter of 1 in., bar spacing of 12 in., plate thickness of ½ in., and clear spacing of 23 in. were selected for a full-scale model. For the experimental program, these dimensions will be 3/8 in., 4.5 in., 3/16 in., and 8-5/8 in. for bar diameter, bar spacing, plate thickness, and clear spacing, respectively. The conclusion from Appendix A also suggests using a diameter of transverse bar of at least 3/4 in. in the full-scale wall when all the other parameters are selected as mentioned above.

Dimensions and boundary conditions from the laboratory test set-up

The finite element models were developed to simulate the test set-up for the 3-story laboratory stability test. The laboratory stability test set-up is shown in Fig. 3.8. The top two stories were not filled with concrete to study the axial capacity of the plate assemblies prior to concrete placement. The details of the load set-up are described in Section 3.3.1.3. Cross beam members (W12 x 50) were framed into the plate assembly using a shear tab connection with two bolts; the beams were framed into the laboratory strong wall using another shear tab connection with three bolts. The cross beam and the shear tab connections are shown in Fig. 3.9. The shear tabs were welded to the plate

assembly as well as to the plate on the strong wall. The shear tabs on the strong wall had oversized bolt holes with 1-in. diameter for 7/8-in. bolts to allow the cross beam to freely rotate at that end. The shear tabs on the plate assembly had standard bolt holes with 15/16-in. diameter for the 7/8-in. diameter A325 bolts.

Material Properties of the Steel Plate and Transverse Bar

Figure 3.10 shows a representative stress-strain curve of the plates obtained from tensile coupon tests. Because the direction of rolling of the plates used for the plate assembly was not known, totally eight coupons were made from the plates used for the plate assembly by cutting the coupons both in the vertical and horizontal directions relative to the orientation of the plate assembly. The average yield strength and tensile strength were 64.3 and 74.4 ksi, respectively, for the coupons taken in the horizontal direction of the plate assembly. The average yield strength and tensile strength were 66.6 and 74.1 ksi, respectively, for the coupons taken in the vertical direction of the plate assembly. For the finite element analysis, elastic perfectly plastic stress-strain behavior with a yield strength of 66.6 ksi was used. Figure 3.11 shows a stress-strain curve for the transverse rods obtained from tensile coupon tests. For the finite element analysis, an elastic perfectly plastic stress-strain behavior was used with a yield strength of 70 ksi.

Calculation of vertical loads to be resisted

The vertical construction loads to be carried by the plate assembly were calculated using the prototype building drawings shown in Figs. 3.4 through 3.7. The vertical construction load transferred by the cross beam at each shear tab connection was calculated considering the self weight of the cross beam, the deck weight (5 psf), and construction live load (20 psf). The factored vertical load (1.2DL + 1.6 LL) transferred to the shear tab connection varied from 6.0 kips to 10.5 kips at different load points and for different prototype buildings. The factored vertical construction load of 10.5 kips in the prototype building is equivalent to 1.48 kip (= 10.5 kip x $(3/8)^2$) per cross beam in the

3/8-scale model when the stress developed at the cross section of the plate assembly in the prototype building is equal to that of the 3/8-scale model.

3.2.2.2: Modeling

Finite element analysis (Abaqus-Riks analysis) was used to investigate the behavior of the dual-plate assembly for vertical construction loads. Analysis was performed for laboratory-scale models. Plates were modeled as shell elements and rods were modeled as beam elements. The cross beams which frame between the shear tabs on the laboratory strong wall and the shear tabs on the specimen were modeled as beam elements with appropriate cross section (W12 x 50). Refer to Fig. 3.9 for a drawing of the cross beams and shear tab connections. Because of the oversized bolt holes on the shear tabs, the end of the cross beams at the strong wall was assumed to freely rotate in the vertical plane perpendicular to the strong wall. A two-story laboratory-scale (3/8-scale) model is illustrated in Fig. 3.12 in a deformed state. Both pinned and fixed boundary conditions at the bottom were considered in the analysis. The connection between the transverse rods and the plate was assumed rigid. Imperfections in the specimen were not considered. Vertical load versus lateral deformation responses were plotted from the Riks analysis.

3.2.2.3: Findings

The deformed shape of the analytical model is shown in Fig. 3.12. For this model, the boundary condition at the bottom was assumed to be pinned. The vertical load versus lateral displacement response is shown in Fig. 3.13. The locations of the displacements shown match the locations of the displacements measured using wire potentiometers during the stability test (refer to Section 3.3.2.). The maximum load the 3/8-scale specimen resisted, according to the FE analysis, was 204 kips (see Fig. 3.13). The estimated vertical construction load on the specimen was 8.9 kips (= 1.48 kips/cross

beam x 6 cross beams, refer to Section 3.2.2.1). Hence, the maximum load capacity calculated from the FE analysis was well beyond (by nearly 23 times) the estimated vertical construction load level.

When the bottom was assumed to be fixed, the deformed shape was similar to that shown in Fig. 3.12 except at the very bottom. The maximum load the 3/8-scale specimen resisted when the bottom was assumed to be fixed was 267 kips.

3.2.3: Analytical investigation of stability behavior of planar shape plate assembly for multiple levels

Prior to the analytical investigation of stability behavior of a planar shape two-story plate assembly for vertical loads described in Section 3.2.2, finite element models were developed for multiple stories (one to four stories) of full-scale prototypes. However, a 1/2-in. diameter rod was used for modeling the full-scale prototypes. Later, in the research program, a 3/8-in. diameter rod was used for the 3/8-scale finite element models as well as for the 3/8-scale laboratory specimens, which is equivalent to a 1-in. diameter in the full-scale prototype. The other dimensions (a plate thickness of ½ in., wall thickness of 24 in., transverse bar spacing of 12-in., story height of 13 ft, and the location of applied load 5 ft from the top of each story) were the same as the prototype dimensions considered for the experimental program.

Figure 3.14 shows a finite element model of a one-story plate assembly. A fixed boundary condition at the bottom was considered in the analysis. An x-symmetry boundary condition was considered for the edges of the plate assembly to simulate the continuity of the plate in the x-direction (see Fig. 3.14 for the direction of the x-axis). Two boundary conditions were considered at the loading points: (1) the loading point was constrained for lateral movement perpendicular to the plate assembly, and (2) there was no constraint for the loading point. The buckling load per each load point, calculated from the finite element analysis, for each case is tabulated in Table 3.4. Table 3.4 also

shows the ratio of the buckling load for one to four-story plate assemblies to the buckling load for the two story plate assembly. These ratios are tabulated to provide a relative indication of the buckling load for the one to four-story plate assemblies. Because the stability behavior of a two-story plate assembly was analytically and experimentally investigated in detail in this research study, as described in Sections 3.2.2 and 3.3, respectively, one may extrapolate from the analytical results to estimate the buckling load of the taller plate assemblies.

3.3: Experimental Investigation

Following the analytical investigation, a stability test set-up was designed considering the results from the analytical investigation and the details anticipated to be used in a typical dual-plate composite shear wall. It was decided to test a two story *planar shaped* dual-plate assembly at 3/8-scale of a typical dual-plate composite shear wall. To investigate the behavior of the splice plate connection for the vertical load applied and to simulate the boundary condition at the bottom of the plate assembly (splice plate connection), which will be representative for most typical construction, it was decided that the two-story dual-plate assembly would be constructed above a concrete-filled dual-plate assembly. Using the concrete-filled dual-plate assembly for the strain compatibility test (which is detailed in Chapter 4) was another reason for making a three-story dual-plate assembly and filling the first story with concrete (see Figs. 3.8 and 3.15). Later, the same specimen was also used for investigating the horizontal splice plate connection test for in-plane shear loading (which is detailed in Chapter 5).

3.3.1: Test Set-up

Figures 3.8 and 3.15 show the AutoCAD drawing of the test set-up for the stability test and a photograph of the test set-up. Notable features include the foundation, specimen, and the loading apparatus. In addition to the three story specimen, an 18-in.

thick foundation block was constructed to transfer the forces from the specimen to the lab strong floor. Loading frames were also erected to apply the vertical load required during the test. Details of the foundation block, specimen, and load set-up are described in Sections 3.3.1.1, 3.3.1.2, and 3.3.1.3, respectively.

3.3.1.1: Foundation Details

The foundation block was designed to adequately transfer the vertical load applied during the stability test and the lateral load applied during the splice plate connection test to the laboratory strong floor. Figures 3.16 and 3.17 illustrate the foundation components. The foundation components include the concrete block, foundation connection plates which connect the specimen to the foundation block, and high-strength bars to post-tension (PT) the concrete block to the laboratory strong floor. Other features include: reinforcing bar hooks and shear studs welded to the foundation connection plate, reinforcement to prevent or intercept splitting of concrete from post-tensioning forces, and reinforcement to distribute shrinkage cracks. A capacity design approach was used to design the foundation components. That is, the foundation components were designed for yielding of the shear wall plates and for the expected maximum loads during testing.

Foundation connection plate

The foundation connection plate was welded to the shear wall plate and partially embedded in the foundation block to transfer the vertical and shear forces transmitted from the shear wall plate to the foundation. Figures 3.16 and 3.17 show the location and dimensions of the foundation connection plates. The total height of the foundation connection plate was 18 in., and the embedded height of the plate was 13 in.

Moment at the base of the wall was developed due to the horizontal eccentricity of the vertical load transferred to the shear wall through the shear tabs during the stability

test, and due to the vertical eccentricity of the applied lateral load during the splice plate connection test. This moment developed tension in the vertical fibers at the bottom of the 3/16-in. shear wall plate.

Shear was developed due to the lateral load applied during the splice plate connection test. The foundation connection plate was designed considering the yielding of the shear wall plate in combined tension and shear. The yield strength of the 3/16-in. shear wall plate was taken as 50 ksi (later it was found to be 66.6 ksi from coupon tests, see Section 3.3.1.2). Consequently, a thickness of ¾ in. was selected for the ASTM A36 foundation connection plate. A fillet weld of 5/16 in. between the 3/16-in. shear wall plate and the 3/4 -in. foundation connection plate was provided to transfer load from the 3/16-in. plate to the 3/4-in. connection plate.

Reinforcing bar hooks

Reinforcing bar hooks were welded to the foundation connection plate and embedded in the foundation block to transfer the tension forces from the foundation connection plate to the foundation block. The reinforcing bar hooks were designed for the tension forces developed when the shear wall plate yields in tension. It was determined that No.7 reinforcing bar hooks welded on both sides of the foundation connection plate at a 7-in. spacing would be sufficient (see Figs. 3.16 and 3.17).

The weld between the foundation connection plate and each reinforcing bar hook was made with two passes: (a) first with a 1/8-in. electrode with amperage of 110 and (b) then with a 3/16-in. electrode with amperage of 160. Voltage was kept constant at 30V for both passes. Figure 3.18 shows the reinforcing bar hooks welded to both sides of the foundation connection plate. A two inch length weld was provided on both sides of the reinforcing bar hook (see Figs. B.3 and B.4 in Appendix B). Appendix B describes further details of this weld and the procedures developed to determine those details.

Shear studs

Shear studs were designed to resist the lateral load capacity of the shear wall. See Figs. 3.16 and 3.17 for the locations of the shear studs. Headed shear studs of 3/4-in. diameter (S3L 3/4-in. diameter and 4 3/16-in. long MS shear studs) were welded to the 3/4-in. steel connection plate on both sides at a horizontal spacing of 7 in.

Reinforcement

Minimum reinforcement consisting of No.4 reinforcing bars and No.3 stirrups were provided to resist shrinkage and uplift forces on the foundation block (see Figs. 3.19 and 3.20). Figures 3.19 and 3.20 also show the reinforcing bar hooks provided to confine the splitting forces in the concrete due to the post-tension force applied by the PT bars which were used to attach the foundation element to the structural strong floor. Vertical reinforcing bars (No. 5's) at a 4.5-in. spacing were provided along the mid plane of the shear wall (see Fig. 3.20) to provide additional shear resistance. The vertical reinforcing bars were extended up through the first story.

Foundation block

The dimensions of the foundation block were selected so that the foundation block combined with the force in the post-tensioned bars could resist the moment developed during the stability test and the splice plate connection test. The foundation block was 141-in. long, 36-in. wide and 18-in. deep. The foundation block was anchored to the laboratory strong floor using eight 1-3/8-in. diameter PT bars that were post tensioned to 240 kips each. The strength of the concrete on the day of the stability test (after approximately 98 days) was 6690 psi.

3.3.1.2: Specimen Details

A 3/8-scale specimen with a plate thickness of 3/16 in., wall thickness of 9 in., transverse bar diameter of 3/8 in., and a transverse bar spacing of 4-1/2 in. was selected in this research study to experimentally investigate the stability behavior of the dual-plate assembly. The plate assembly for each story was 135-in. long and 58-½-in. high (see Figs. 3.8 and 3.15). As mentioned in Section 3.3, the top two stories of the three-story specimen were used for the stability test. Material properties of the steel plates and threaded rods are detailed in Section 3.2.2.1.

Fabrication of steel plate assembly

Figure 3.21 shows a photograph of a steel plate assembly. First, strain gauges which were located on the inside of the steel plate assembly were mounted and coated (see Section 3.3.2 for details of the strain gauges). Then, the bottom steel plate (3/16-in. thick) was laid down on the wooden support frame. Next, the threaded rods with two nuts and two washers (for inside the plate assembly) were inserted into the holes. The threaded rods were 10.5-in. long. The nut and washer beneath the steel plate were installed. After that, wooden spacers were laid down on top of the steel plate. The height of the wooden spacers was set at 8-5/8 in. so that the out-to-out dimension of the plate assembly would be 9 in. Care was exercised to ensure the edges of the two steel plates were aligned vertically. The threaded rods were lifted and inserted into the holes in the top plate assembly then a washer and nut were installed above the top steel plate for each threaded rod. Next, all the nuts inside the plate assembly were tightened by hand so that the spacing between the steel plates was fixed at the desired 8-5/8 in. Finally, the outside nuts were wrench tightened while holding the inside nuts in place. No additional mechanical advantage (ie. a cheater bar) or impact wrench were used.

Concrete strain gauges were mounted inside the steel plate assembly (see Fig. 3.22 for a photograph and see Section 3.3.2 for locations and other details of the concrete strain gauges). Small plate pieces of 3/16-in. thick were tack welded to the inner side of

the plate assembly and continuous splice plates of 3/16-in. thick were tack welded to the outer side of the plate assembly (see Figs. 3.23 and 3.24). The small plate pieces were tack welded and were intended to facilitate dual-plate construction. They made positioning the second story plate assembly on top of the first story plate assembly possible. Totally three plate assemblies were made for the specimen used for the stability test. Shear tabs were welded to the second and third story plate assemblies to attach the cross beams as detailed in Section 3.3.1.3.

Fabrication of specimen

The first story plate assembly was positioned in between the foundation connection plates then fillet welded (5/16-in. size) to the foundation connection plates. The spacing between the foundation connection plates was 9 in. so that the steel plate assembly fit tightly between the foundation connection plates. The 5/16-in. fillet weld was made in one pass using 3/16-in. electrodes (E7018). The voltage and amperage for welding were 30 and 160, respectively. After attaching the formwork, concrete was added between the plates to a level just below the lowest set of horizontal splice plates (see Fig. 3.15). The strength of the concrete on the 14^{th} day and on the day of the stability test (after approximately 98 days) was 6510 psi and 7644 psi, respectively.

After three days, the formwork was removed and the second-story plate assembly was positioned on top of the first story plate assembly (see Fig. 3.25). The 2-in. wide splice plates were welded to the top and bottom plate assemblies with 3/16-in. continuous fillet welds. The 3/16-in. fillet weld was made using a 1/8-in. (E7018) electrode. The voltage and amperage for welding were 30 and 110, respectively. The measured average effective throat thickness for the splice plate fillet weld was 0.149 in. instead of the 0.133 in. theoretical effective throat for a 3/16-in. leg size. Similar procedures were used to erect the third story plate assembly of the specimen.

3.3.1.3: Loading Set-up

After fabrication, the specimen was positioned in the test frame and prepared for testing. Figures 3.8 and 3.15 show the loading set-up for the stability test. Care was taken to make the loading set up resemble the loads a steel gravity frame system would apply on a typical core wall. According to the finite element analyses that had been performed, the shear wall specimen was expected to buckle at a total vertical load of 204 kips (34 kips at each of six loading points). The testing set-up had the capacity to apply a vertical load of up to 330 kips, which is 1.6 times the expected vertical load for buckling.

Cross beams and shear tab connections

Six cross beams framed into the dual-plate assembly using shear tab connections with two bolts. Figure 3.9 shows the cross beam and the shear tab connection in the second story. Cross beams framed into the dual-plate assembly 22-½ in. below the top of each panel assembly. The other end of each cross beam framed into the strong wall also using a shear tab connection with three bolts (see Fig. 3.26). Instead of a strong wall, there would be columns at the end of the cross beams in a typical building. Load was applied on the top of each cross beam near its mid point. A loading frame with two levels of beams with three double-acting hydraulic cylinders at each level was used to apply the load on the cross beams. Load was transferred to the dual-plate assembly by the cross beams.

Loading frame and hydraulic rams

The loading frame was composed of two W16 x 100 columns and two W18 x 71 beams. The loading frame had a steel box assembly at the bottom of each column and the steel box assembly was anchored to the strong floor using post-tensioned bars (see Fig. 3.27).

The loading ram for each beam was 45 in. from the shear tab (bolt line) on the strong wall and 41.75 in. from the shear tab (bolt line) on the plate assembly. The shear tab (bolt line) on the plate assembly was 1.75 in. and 6.25 in. from the outside of the plate assembly and the center of the plate assembly, respectively. Bolts on the shear tabs were wrench tightened only to the level needed for a bearing connection. Hence, the connections at both ends of the cross beams were considered as pin connections, allowing simple statics to be used to calculate the load transferred to the plate assembly. Six Power Team RH 605 double acting hydraulic cylinders (with an effective area of 12.31 in^2) were used to apply the vertical load with one double acting pump.

3.3.2: Instrumentation

A pressure transducer, wire potentiometers (wire pots), and strain gauges were used to measure the load, displacements, and strains, respectively. The pressure transducer (Omega PX302-10KGV with an accuracy of 0.25% BFSL) was used to infer the load applied from the loading cylinders by multiplying the measured pressure by the effective area of the loading cylinders. The pressure transducer was calibrated prior to the load test using an Instron tensile testing machine. The calibration factor for the pressure transducer was 125.83 psi/mv.

Load transferred to the shear tab was calculated from the load measured at the loading cylinders by applying the lever arm rule. Delta rosettes were attached to the webs of the cross beams to calculate the shear force in the cross beams so that the vertical load transferred to the shear tab could be verified by comparing with the load inferred from the pressure transducer readings. In total, five delta rosettes (CEA-06-125UY-350) were used. The locations of the delta rosettes are shown in Fig. 3.28.

The lateral displacements were monitored using wire potentiometers mounted on the strong wall with their wires attached to the specimen (top two stories) in order to develop vertical load - lateral displacement response curves and the deflected shape of

the specimen. A total of 12 wire potentiometers (UniMeasure PA-10-NJC-DS-L3M or UniMeasure PA-20-NJC-DS-L3M with a linearity of ± 0.15% of full scale) were used on the loading side of the specimen. The locations of the wire potentiometers are shown in Fig. 3.29. All the wire potentiometers were calibrated prior to attaching to the specimen.

Three dial gauges were placed on the strong floor against the foundation block of the specimen to monitor any sliding of the specimen during testing. All the dial gauges were located on the north side of the specimen (opposite the loading frame side). Two dial gauges were located near ends of the specimen and the third was located between them.

Strain gauges were mounted on steel plates of the dual-plate assembly to infer the stress levels in the plates. Figures 3.30 and 3.31 show the location of the strain gauges for the stability test. Strain gauges were attached on both sides (inside and outside) of the steel plates where the greatest bending was expected. Strain gauges were also attached around the shear tabs to monitor local yielding of the plates. Strain gauges installed in the first story of the specimen (which was filled with concrete) were intended for use in the strain compatibility test, and they are discussed in Section 4.3 of Chapter 4. The outside of the top two stories of the specimen was whitewashed to monitor any yielding during the stability test. All measurements were monitored and recorded using a high-speed data acquisition system (Vishay's Strain Smart System 5000).

3.3.3: Test Method

All the sensors were zeroed in the data acquisition system prior to starting the test. The stability specimen was loaded by initially applying 1000 lb, followed by 2000 lb load increments, at each of the six shear tabs on the stability specimen. Data readings were recorded at a speed of 10 readings per second during loading. At the end of each load increment, data recording was paused and the specimen was inspected for any damage, large deflection, yielding (from strain readings as well as from flaking of whitewash), or

any movement of the foundation (from dial gauges). Loading was applied until a maximum total load of 168 kips (28 kips at each shear tab) was reached when the specimen started buckling. Loading could have been continued till some portion of the wall plate assembly failed, but it was decided not to jeopardize tests that were planned to follow.

3.3.4: Test Results and Analysis

The specimen started buckling at a total load of 168 kips on the specimen. The distorted specimen at that load is shown in Figs. 3.32 and 3.33. As mentioned in Section 3.3.2, the load transferred to the specimen was calculated from the pressure transducer attached to the hydraulic pump and the rosettes (delta or rectangular) attached to the webs of the cross beams. Calculation of load, load-deflection response, and load-strain relationship of the specimen for the vertical load applied are discussed below.

Calculation of Load

The total load applied from the six hydraulic rams was calculated by multiplying the pressure measured from the pressure transducer by the total effective area of the six rams (6 times 12.31 in^2). The load transferred to the plate assembly via the shear tab was calculated using the lever arm rule and assuming the connections at the shear tabs were pin connections. Load transferred to the six shear tabs was assumed to be the same for this calculation.

To verify the above calculated load, measurements from the rosettes attached to the cross beams also were used to calculate the load. A total of four delta rosettes and one rectangular rosette were attached on the web of each cross beam close to the shear tabs on the plate assembly. The rosettes were attached near mid-depth of the cross section of the beam on the side of the web (see Fig. 3.28 for locations of rosettes). Derivation of the equation relating the shear force and the strain measurements from rosettes is detailed

below. For the closed cross section of the beam, the shear flow across the web of the beam can be written as in Eq. 3.2.

$$\tau = \frac{VQ}{It_w} \qquad \text{Eq. (3.2)}$$

where τ = Shear stress; V= Shear force; Q = First moment of area; I = Second moment of area, and t_w = web thickness.

In the W12 x 50 cross beam, the maximum shear stress occurs at the neutral axis, or mid-depth of the web. Considering the properties of the W12 x 50 shape, the relationship between shear force, V, and the shear stress at the center of the web, τ_{max}, can be derived as follows (Eq. 3.3).

$$V = 4.086\ \text{in}^2 * \tau_{max} \qquad \text{Eq. (3.3)}$$

The shear stress, τ_{max}, can be calculated from the delta gauge reading measured at mid-depth of the web using the following equation (Eq. 3.4).

$$\tau_{max} = G * \gamma_{xy} \qquad \text{Eq. (3.4)}$$

where, G = Shear modulus = ½*E/(1+ υ); E = Young's modulus = 29000 ksi, υ = Poisson ratio = 0.3; and γ_{xy} = Shear strain. For a delta rosette, $\gamma_{xy} = 2/\sqrt{3} * (\epsilon_1 - \epsilon_3)$ when strains ϵ_1 and ϵ_3 are oriented (+) 60° and (-) 60° with respect to the positive x – axis,

respectively, as attached on the cross beams in this test. For a rectangular rosette, $\gamma_{xy} = (\epsilon_1 - \epsilon_3)$ when strains ϵ_1 and ϵ_3 are oriented (+) 45° and (-) 45° with respect to the positive x – axis, respectively, as attached on one of the cross beams in this test. Hence, combining equations 3.2 and 3.3, shear force measured from delta rosettes and rectangular rosettes can be summarized in Eq. 3.5 and 3.6, respectively.

$$V_{Delta} = 52600 \text{ kip} * (\varepsilon_1 - \varepsilon_3) \qquad \text{Eq. (3.5)}$$

$$V_{Rectangular} = 45600 \text{ kip} * (\varepsilon_1 - \varepsilon_3) \qquad \text{Eq. (3.6)}$$

The variation of the shear force calculated from the rosettes and normalized with respect to the load per shear tab (inferred from the pressure transducer) is shown in Fig. 3.34. It can be seen from Fig. 3.34 that the load transferred to the plate assembly via each shear tab is not exactly the same. However, they were close (within ± 20% of the load inferred from the pressure transducer). For the load–deflection and load-strain relationship calculations, the load inferred from the pressure transducer (assuming same load at each shear tab) has been used.

Load – deflection response

Load-deflection responses measured at three different locations over the height of the steel plate assemblies are shown in Fig. 3.35 (please refer Fig. 3.29 for locations of the wire pots). The maximum reading from the dial gauges attached to measure the movement of the foundation was only 0.002 in. and was subsequently neglected in the plotting of the deflection response of the plate assembly. The response of the specimen at low load levels (beneath a total of 10 kips) indicated that the wall panels were completely stable with nearly no discernable distortion at load levels corresponding with the maximum expected construction loads (1.6 kips at each shear tab). The maximum load that was applied at each shear tab went well beyond the maximum expected construction

load level (by nearly 18 times) before loading was discontinued. Deflections were growing rapidly under these extreme loads, largely as the result of P-delta effects.

Load-deflection responses measured at three locations (wire pots 3, 9 and 12) at an elevation 18 in. above the joint between the bottom two plate assemblies are shown in Fig. 3.36. The figure shows that even though the deflections of these three locations in the plate assembly exhibited small deviations before the peak load, they exhibited large deviations around the peak load (168.3 kips). Load-deflection responses measured at all the wire pot locations are summarized in Fig. 3.37. The deflection of the plate assembly over the height of the specimen is shown in Fig. 3.38 (compare with the distorted shape shown in Figs. 3.32 and 3.33). Figures 3.38, 3.32, and 3.33 show that the largest deflection occurred between 18 in. and 22.5 in. from the bottom of the second story plate assembly.

The load-displacement graph (see Fig. 3.13) obtained from the FE analysis shows behavior similar to the experimental results (see Fig. 3.35). However, the maximum load the test specimen resisted was 168 kips compared to 204 kips computed by the finite element analysis. Imperfection of the plate assembly was not measured and consequently was not considered in the finite element analysis. If the imperfection had been considered, the maximum load obtained from the finite element analysis would have been smaller and would have been closer to the measured value. It can be noted that the connection between the transverse rods and plate was assumed to be a rigid connection and no imperfections were considered in the finite element analysis. The assumption of a pinned condition at the bottom of the plate assembly in the finite element model (see Fig. 3.12) can be judged by examining the specimen just above the top level of concrete during the stability test (Fig. 3.32). The pinned condition is reasonable considering there is minimal reverse curvature evident at the top of the concrete.

Load versus Strain

The yield strength of the steel plate used for the fabrication of the plate assembly was 66.6 kips in the vertical direction (see Section 3.2.2 for material properties of the steel plate). Hence, the yield strain would be 2,300 με when the young's modulus is assumed as 29,000 ksi. Strain gauge readings indicated there was no yielding in the plate assembly. Also, no flaking of the whitewash was observed, which reinforces the strain measurements. The maximum measured strain on the plate assembly was (-) 1058 με (compressive strain) at strain gauge C12 which was around the shear tab in the third story assembly (see Fig. 3.30 for the location of the strain gauge). This indicated that there was no local yielding around the shear tab. The maximum measured strain on the plate assembly other than around the shear tabs was (-) 711 με at strain gauge B12 which was 18 in. above the first-story level.

Large deflection and bending of the plate assembly occurred at 18 in. above the first-story level. The variation of strains measured from four strain gauges (B12, B4, B6, & B19) at this location with the load is plotted in Fig. 3.39. All four strain gauges were at a horizontal distance of 67.5 in. from either side of the specimen. There was good strain linearity with distance through the cross section of the plate assembly up to a total load of approximately 80 kips (see Fig. 3.39). For example, at a total load of 80 kips, the measured strains at B12, B4, B6, and B19 were (-) 132, (-) 77, (-) 25, and 39 με, respectively, which is nearly linear when plotted versus the distance through the cross section.

However, close to the peak load, B12 and B6 measured compressive strains while B4 and B19 measured tensile strains. At the peak load of 168.3 kips, the measured strains at B12, B4, B6, and B19 were (-) 686, 151, (-) 391, and 447 με, respectively. These strain values demonstrate that the strains were not linear with respect to the distance across the cross section (along strain gauges B12, B6, B4, and B19). This behavior indicates that the plate assembly acted like a frame, primarily as two individual

plates connected by the transverse rods, and not as a solid integral unit at this load level. This behavior may be the result of large bending of the plate assembly.

3.4: Conclusions

The stability behavior of the plate assembly was investigated both experimentally and analytically. The finite element results were in good agreement with the experimental results. However, the maximum load the test specimen resisted was 168 kips compared to 204 kips from the finite element analysis. Imperfection of the plate assembly was not measured and consequently was not considered in the finite element analysis.

Typical vertical construction loads calculated from prototype buildings varied from 6.0 kips to 10.5 kips (which is 1.48 kips at 3/8-scale) at different load points. The plate assembly resisted a maximum load of 28 kips at each load point. This was well beyond the maximum expected construction load level by nearly 18 times. When the ratios of the computed buckling loads for three and four-story plate assemblies to the buckling load for the two-story plate assembly tabulated in Table 3.4 (for case II in Table 3.4, which is closer to field conditions) are considered, the three and four-story plate assemblies could resist a vertical load of approximately 9 and 5 times the typical vertical construction loads, respectively.

The specimen was completely stable at low load levels (1.6 kips at each shear tab). The plates behaved elastically up to the maximum load applied. The plate assembly acted like an integral unit at low load levels (less than a total load of 100 kips) and like a frame at higher load levels. This behavior may be attributed to the larger bending moments developed due to the P-delta effects.

The experimental program was carried out for the two-story plate assembly. Hence, it could be concluded from this study that construction of gravity-load framework around a two story core-wall plate assembly before casting the concrete is safe.

Furthermore, from the finite element analysis, it was found out that construction of gravity-load framework around three and four story core-wall plate assemblies before casting the concrete is also safe. However, further experimental research need to be done to verify this result.

Table 3.1 Rod stress versus spacing for different plate heights (for ¼-in. rod diameter)

Spacing [in]	Rod stress [ksi]								
	H = 6 ft			H = 7 ft			H = 8 ft		
	FEA	Eq. 3.1	Difference (%)	FEA	Eq. 3.1	Difference (%)	FEA	Eq. 3.1	Difference (%)
6	4.2	4.0	4.6	5.0	4.8	4.6	5.8	5.5	4.6
8	7.1	6.8	4.4	8.6	8.1	5.3	10.1	9.5	6.0
12	14.5	13.7	5.2	17.7	16.8	5.1	20.9	19.9	5.0
16	23.2	21.7	6.4	28.8	27.2	5.7	34.4	32.6	5.3

Table 3.2 Rod stress versus height of concrete casting from Eq. 3.1 (for 3/8-scale laboratory specimen with 3/8-in. rod diameter and 4.5-in. rod spacing)

Story level	Height = H (ft)	Rod stress from Eq. 3.1 [ksi]	1.1 * Rod stress from Eq. 3.1[ksi]
1	4.875	0.8	0.9
2	9.75	1.7	1.9
3	14.625	2.7	2.9
4	19.5	3.6	4.0

Table 3.3 Rod stress versus height of concrete casting from Eq. 3.1 (for a full-scale prototype with 1-in. rod diameter and 12-in. rod spacing)

Story level	Height = H (ft)	Rod stress from Eq. 3.1 [ksi]	1.1 * Rod stress from Eq. 3.1[ksi]
1	13	2.2	2.4
2	26	4.7	5.1
3	39	7.1	7.8
4	52	9.6	10.6

Table 3.4 Buckling load per loading point for plate assemblies of multiple levels

Story	Height of Plate [ft]	Case I: No constraint at loading point		Case II: Lateral constraint at loading point	
		Pcr [kip]	Ratio of Pcr/(Pcr of two story plate assembly)	Pcr [kip]	Ratio of Pcr/(Pcr of two story plate assembly)
1	13	57.75	2.66	192.06	2.71
2	26	21.67	1.00	70.92	1.00
3	39	10.09	0.47	35.88	0.51
4	52	5.07	0.23	21.41	0.30

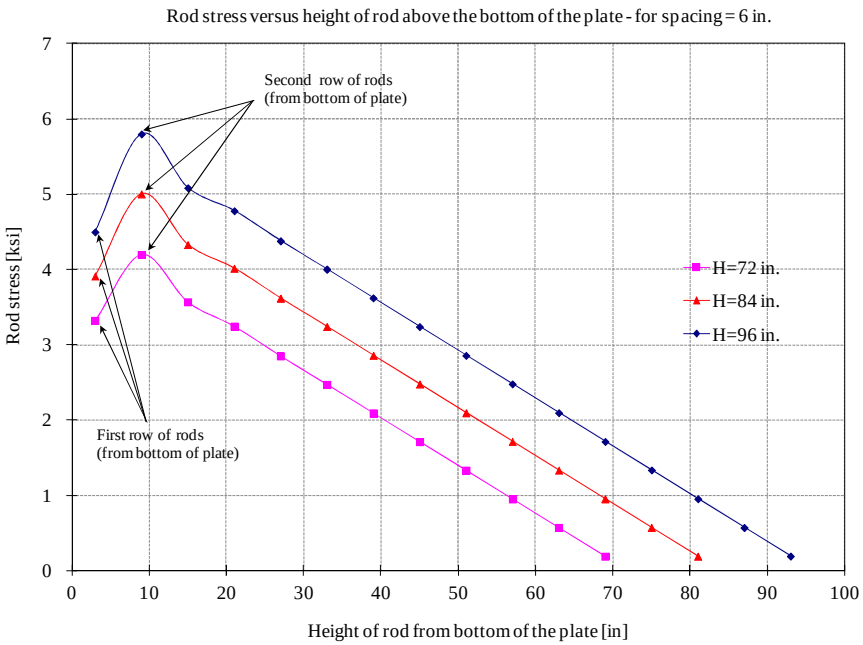

Figure 3.1 Rod stress versus height of rod above the bottom of the plate for various concrete heights – ½ scale model, spacing = 6 in. (Kim, J., 2007)

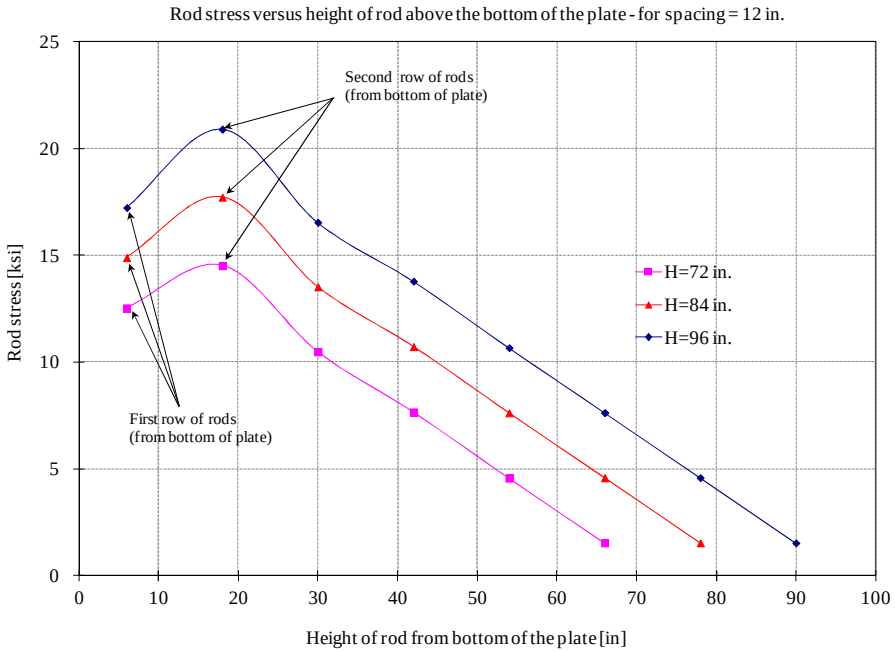

Figure 3.2 Rod stress versus height of rod above the bottom of the plate for various concrete heights - ½ scale model, spacing =12 in. (Kim, J., 2007)

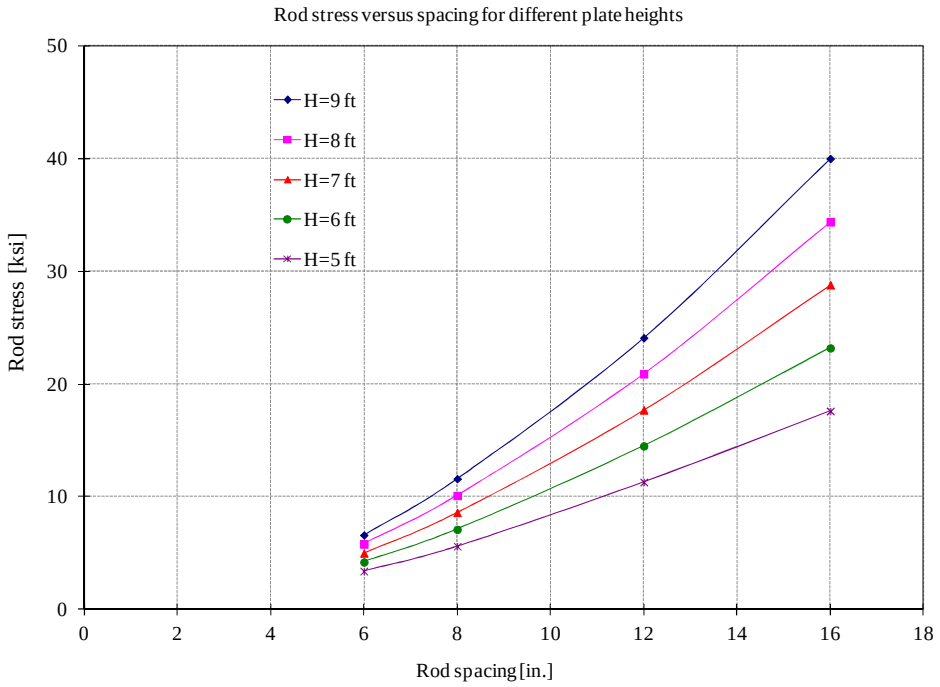

Figure 3.3 Stress in the rod (in the second row) versus transverse rod spacing for various concrete heights (in a ½ scale model) (Kim, J., 2007)

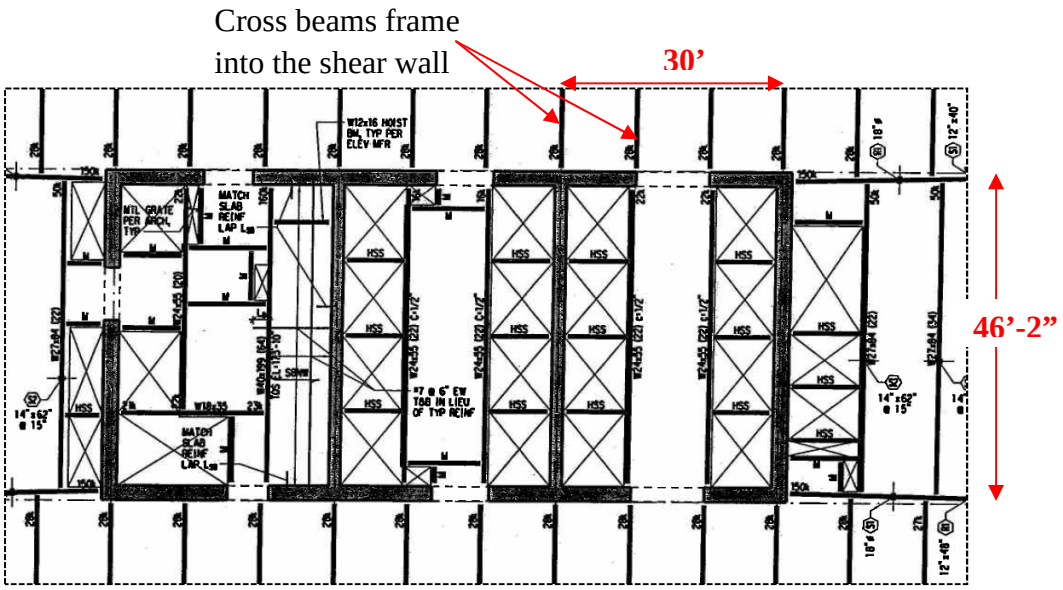

Figure 3.4 Shear wall layout (155 N.Wacker, Chicago, IL – 48 story, provided by Magnusson Klemencic Associates, 2006)

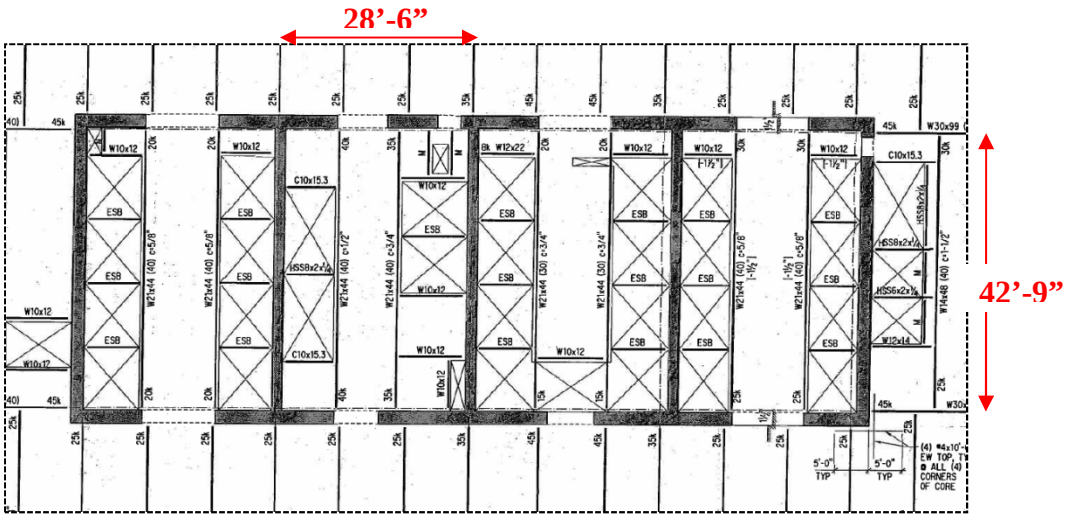

Figure 3.5 Shear wall layout (300 North LaSalle, Chicago, IL – 60 story, provided by Magnusson Klemencic Associates, 2006)

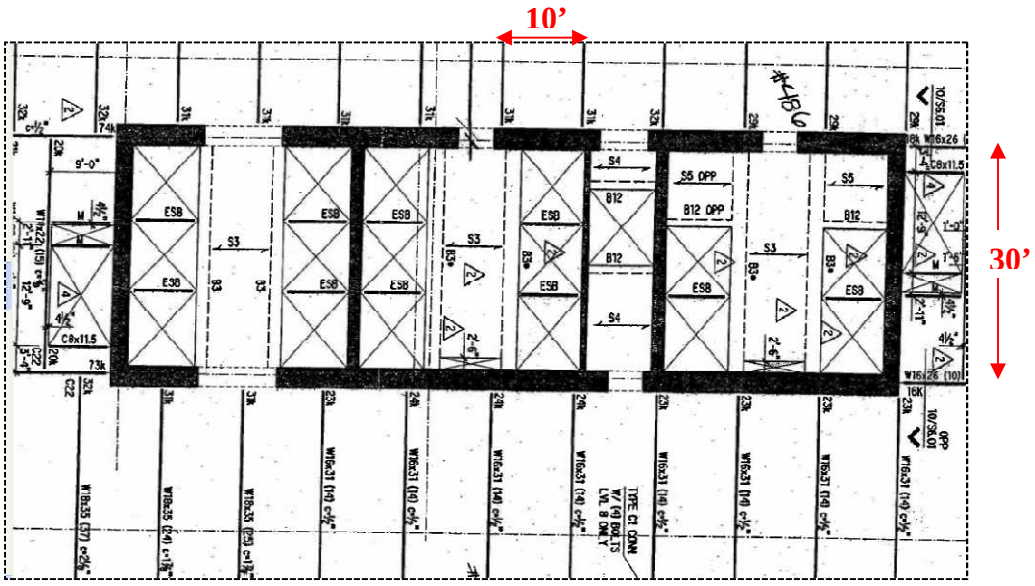

Figure 3.6 Shear wall layout (IDX Tower, Seattle, WA – 40 story, provided by Magnusson Klemencic Associates, 2006)

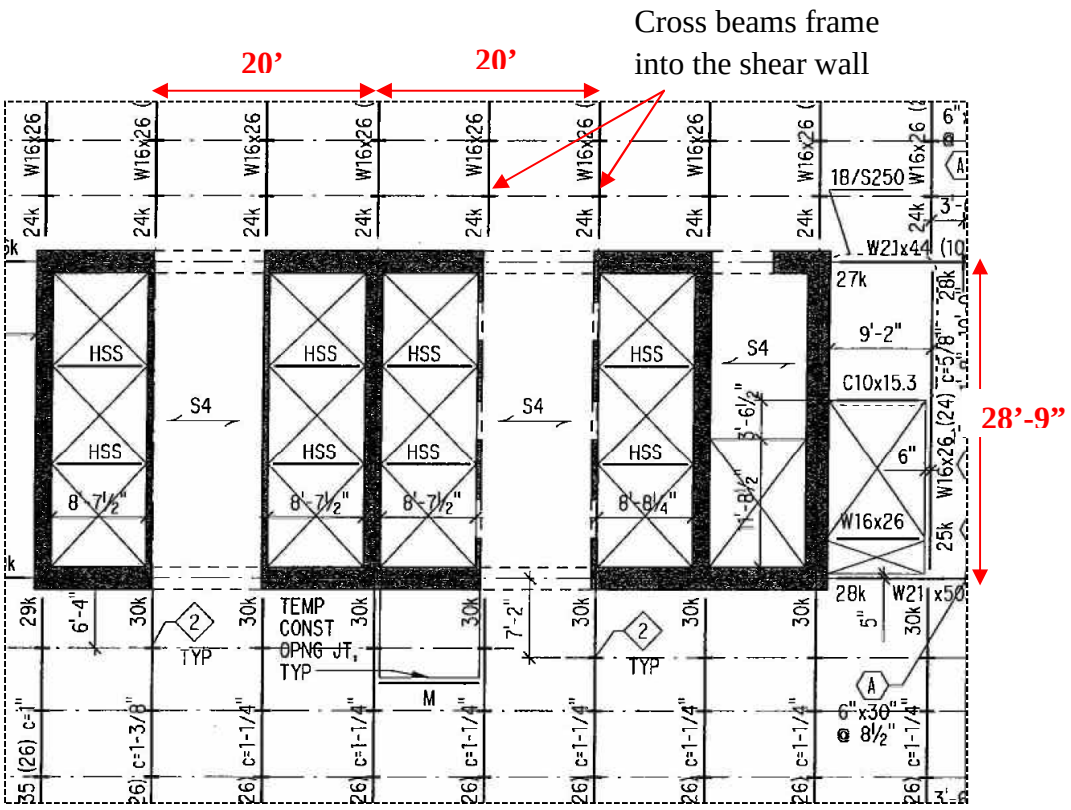

Figure 3.7 Shear wall layout (Washington Mutual / Seattle Art Museum, Seattle, WA – 55 story, provided by Magnusson Klemencic Associates, 2006)

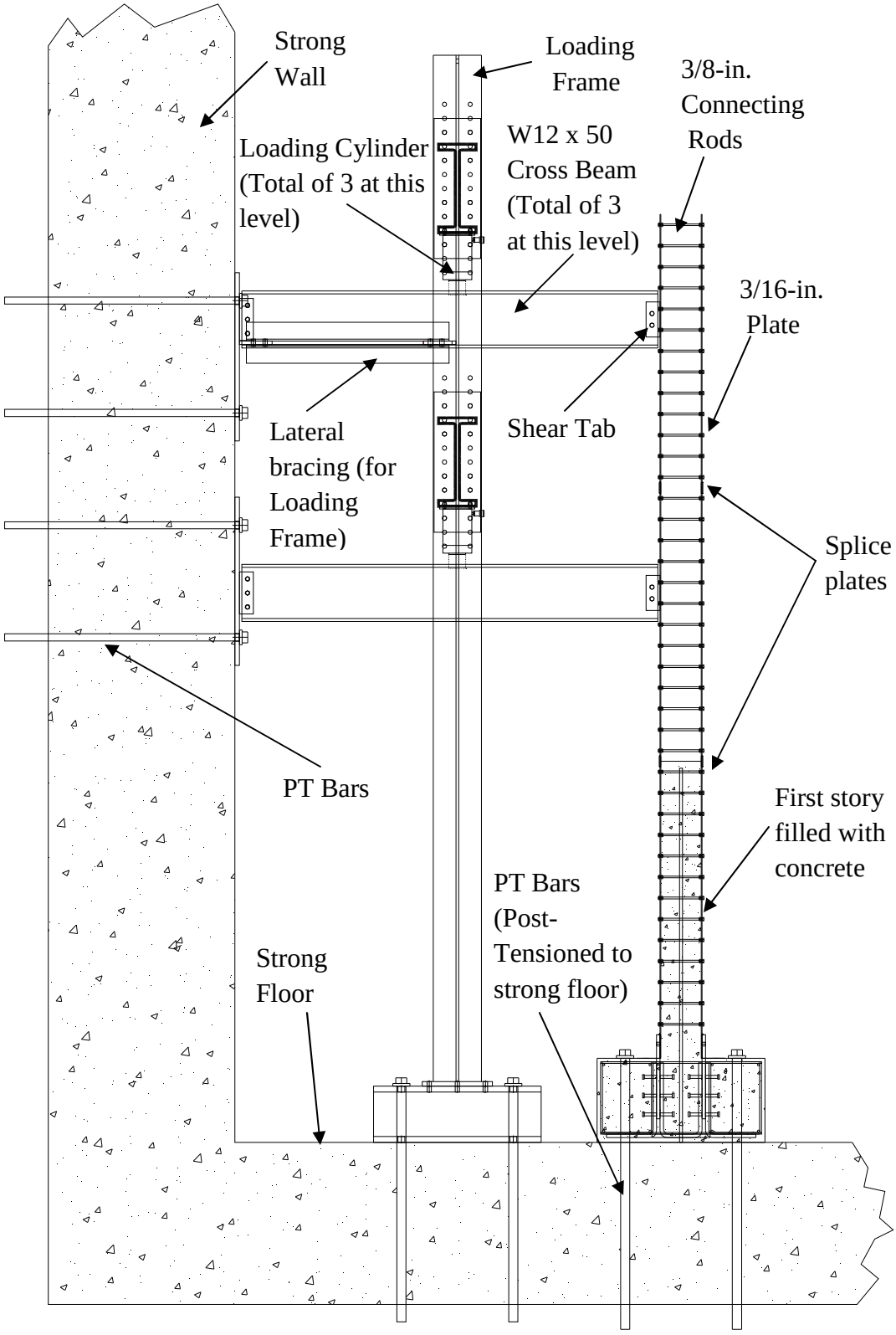

Figure 3.8 End view of the stability test set-up

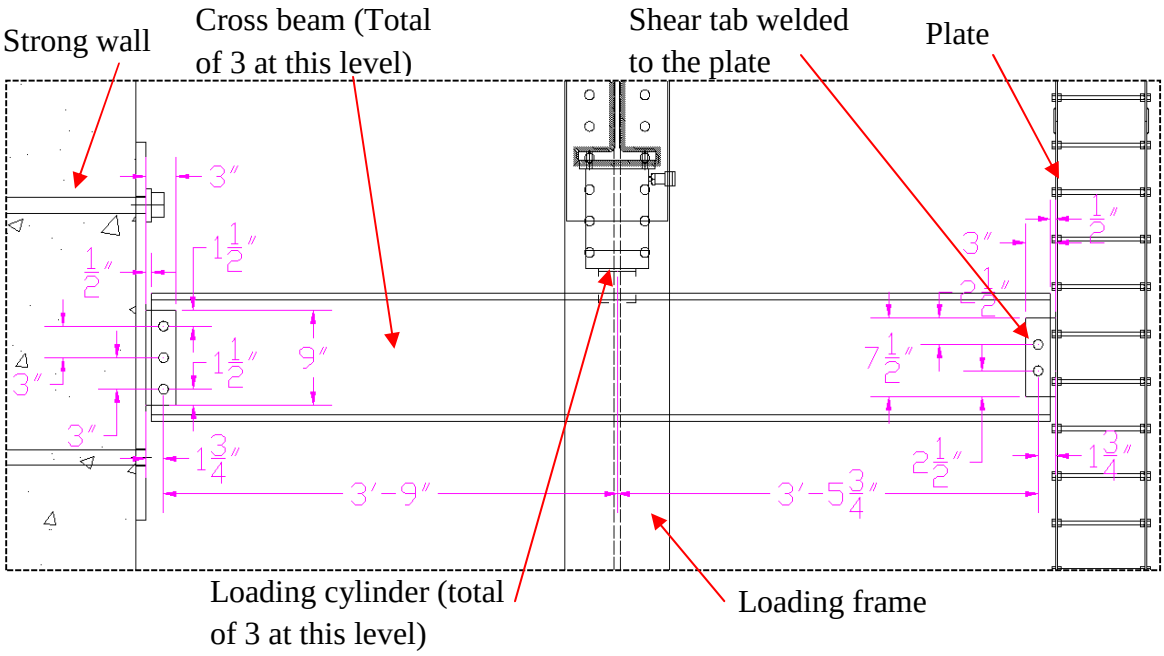

Figure 3.9 Cross beam and shear tab connections (at second story)

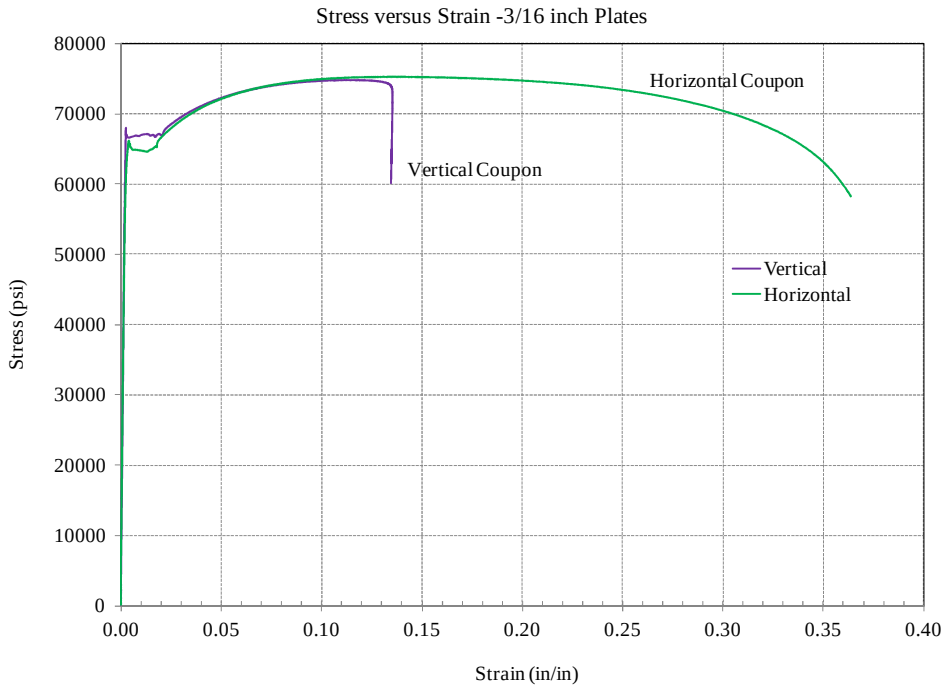

Figure 3.10 Stress – strain curves for plates from tensile coupon tests

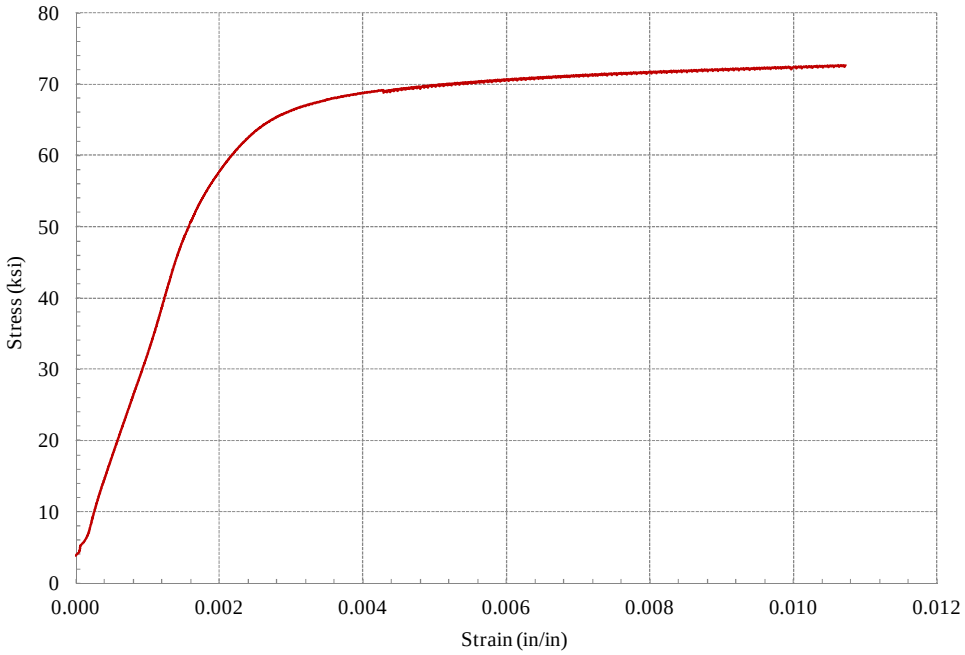

Figure 3.11 Stress – strain curves for transverse bar from tensile coupon tests

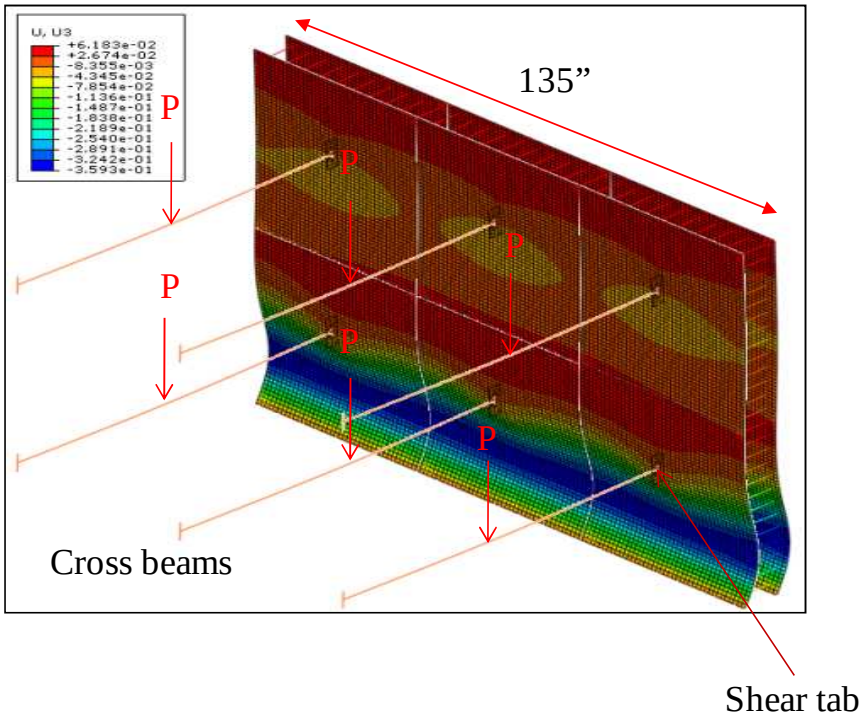

Figure 3.12 Deformed shape of the 3/8-scale specimen – FE Analysis

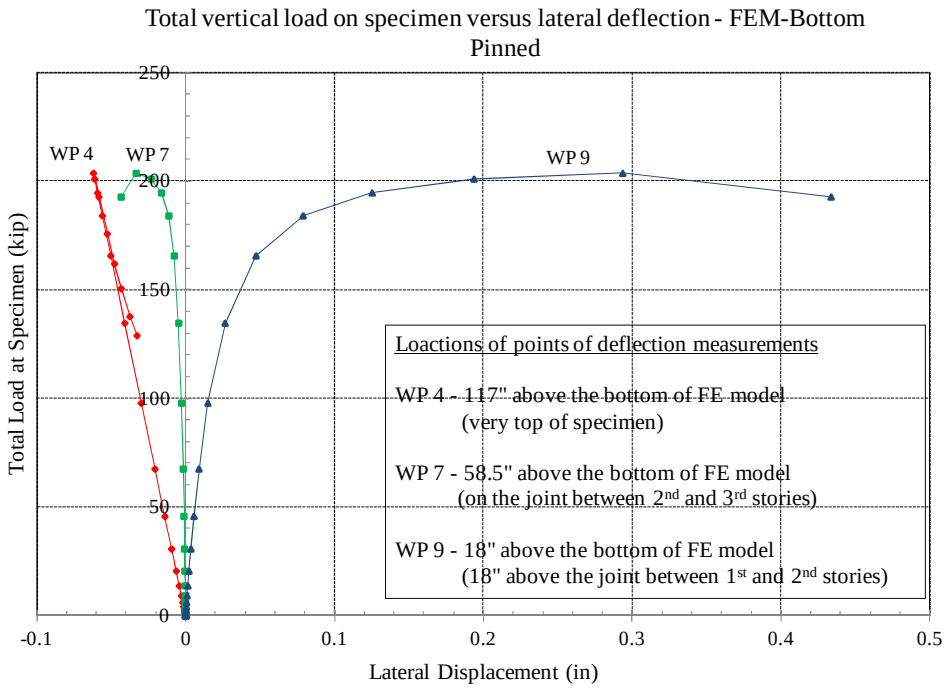

(Note: The locations of the points of deflection measurements are comparable with the Wire Pot locations shown in Figure 3.29)

Figure 3.13 Vertical load versus lateral displacement – From FE analysis - 3/8-scale stability test specimen

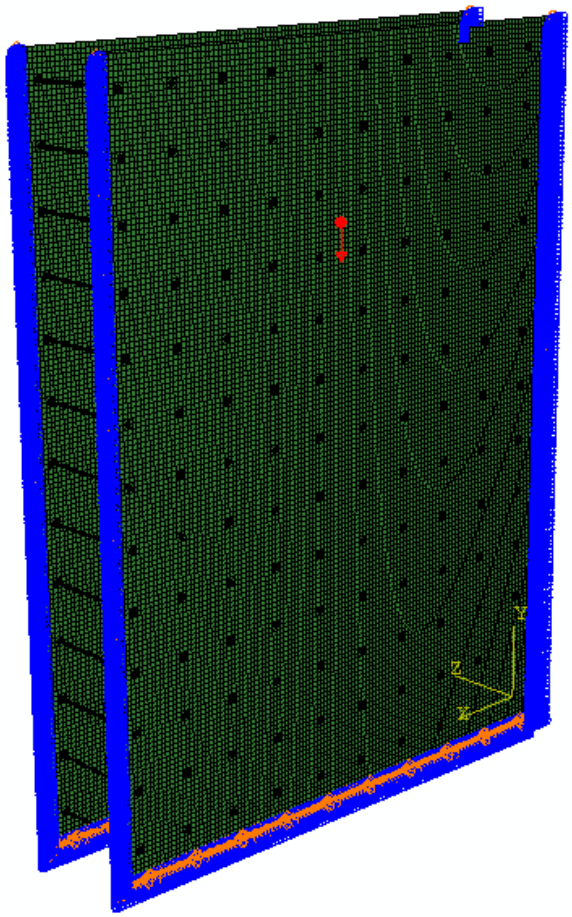

Figure 3.14 Finite element model of one story plate assembly with load and boundary conditions

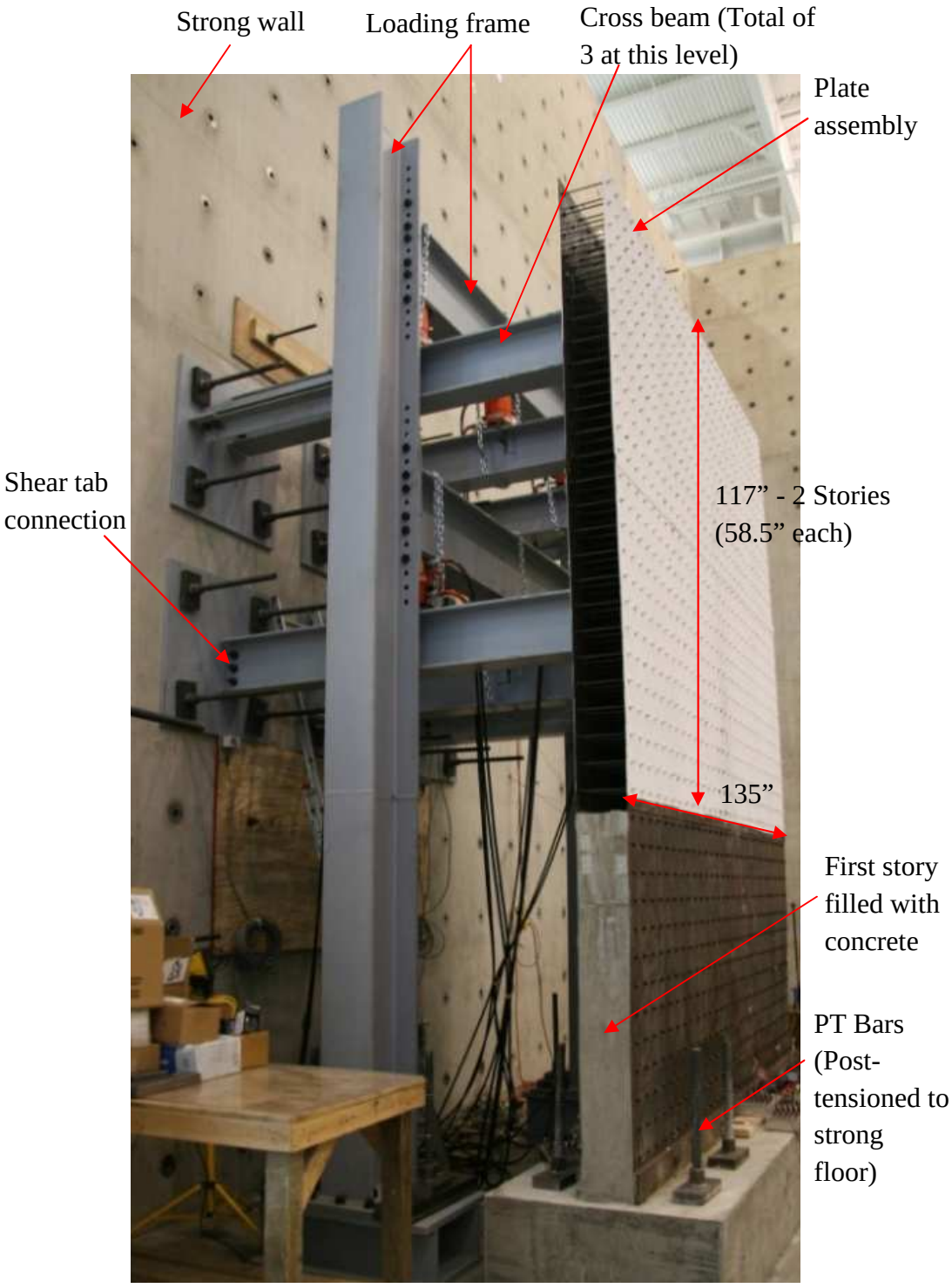

Figure 3.15 Stability Test set-up

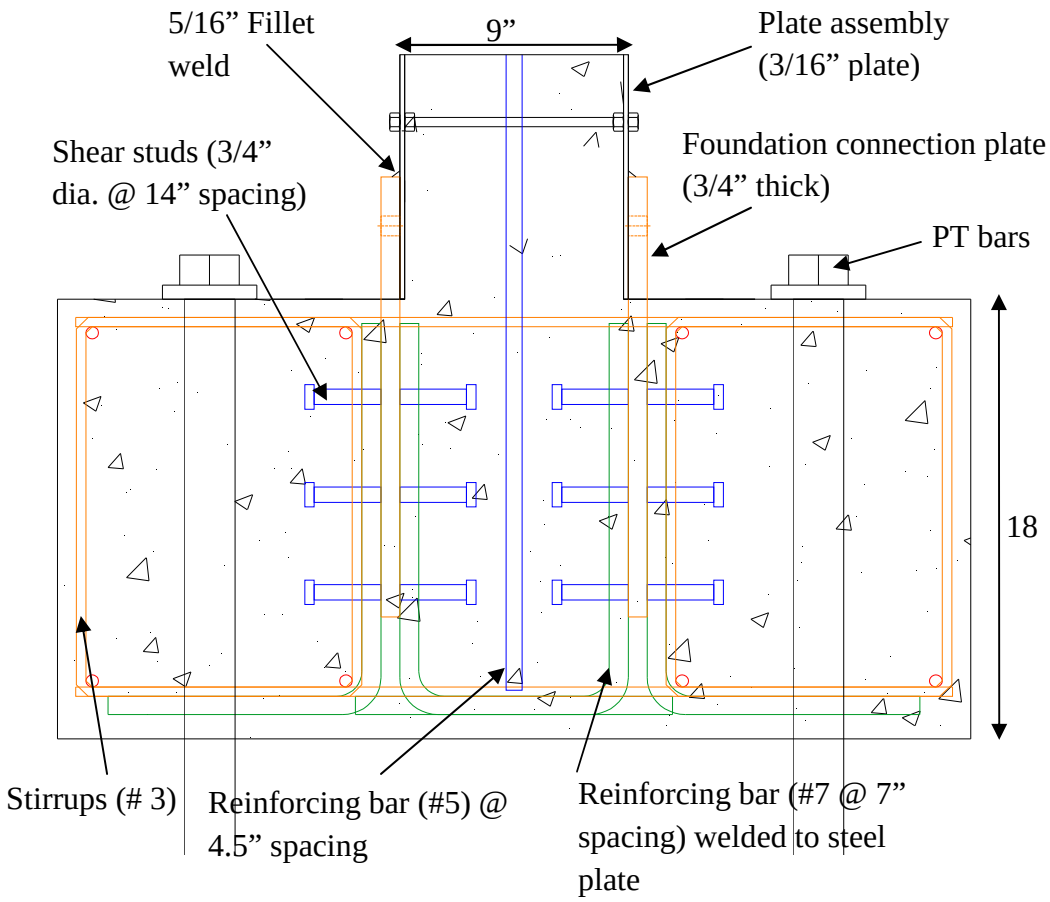

Figure 3.16 Foundation of shear wall assembly – Side View

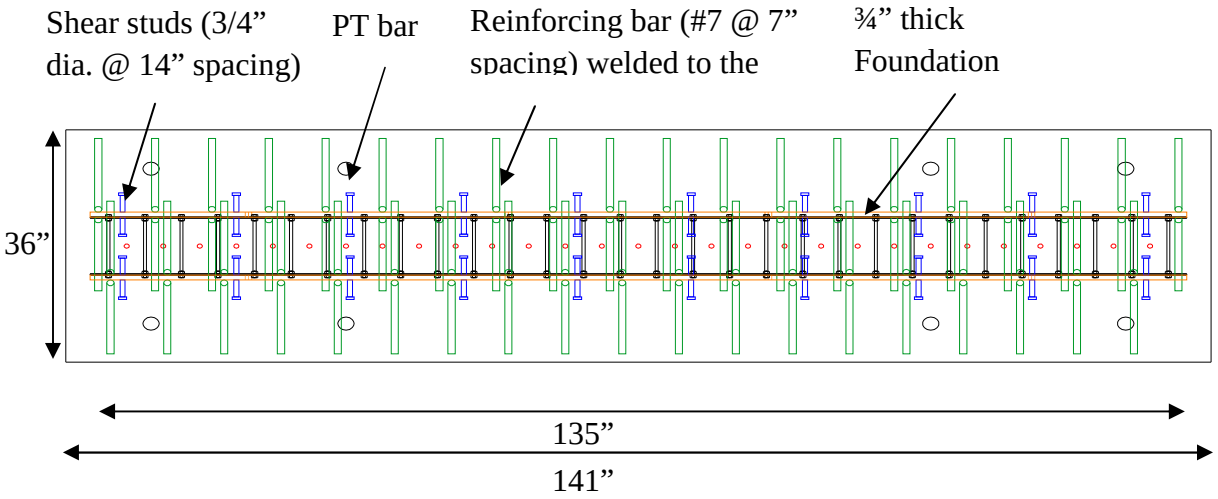

Figure 3.17 Foundation of shear wall assembly - Plan View

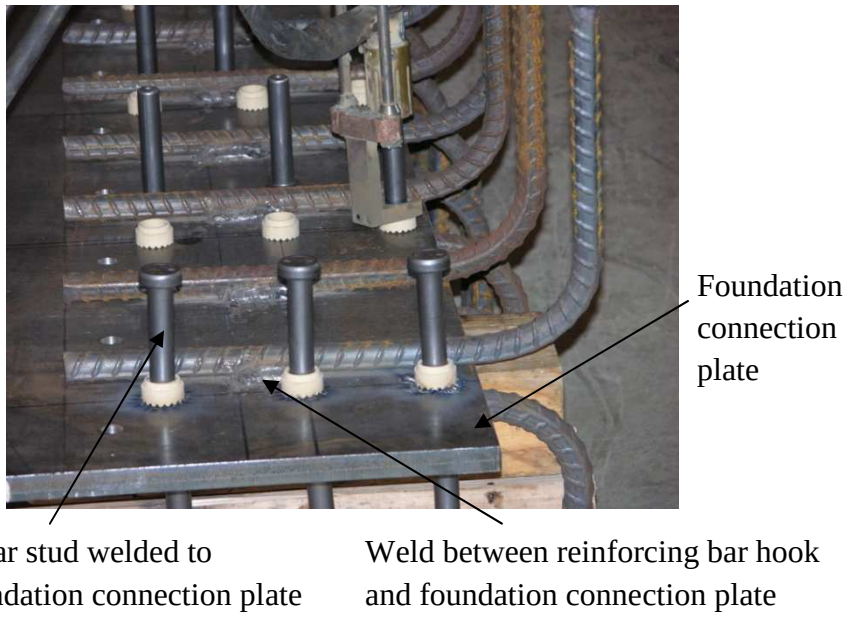

Figure 3.18 Reinforcing bar hooks and shear studs welded to foundation connection plate

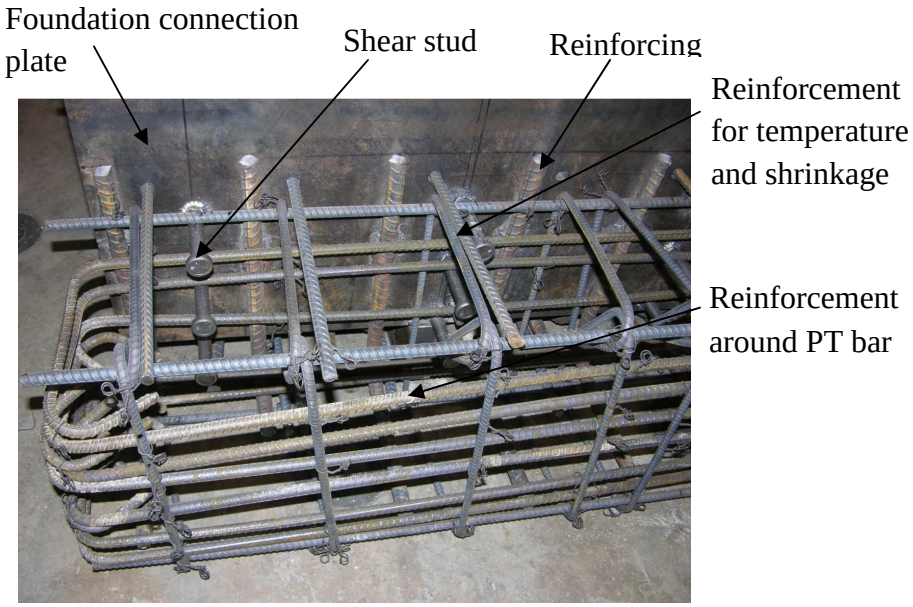

Figure 3.19 Foundation elements

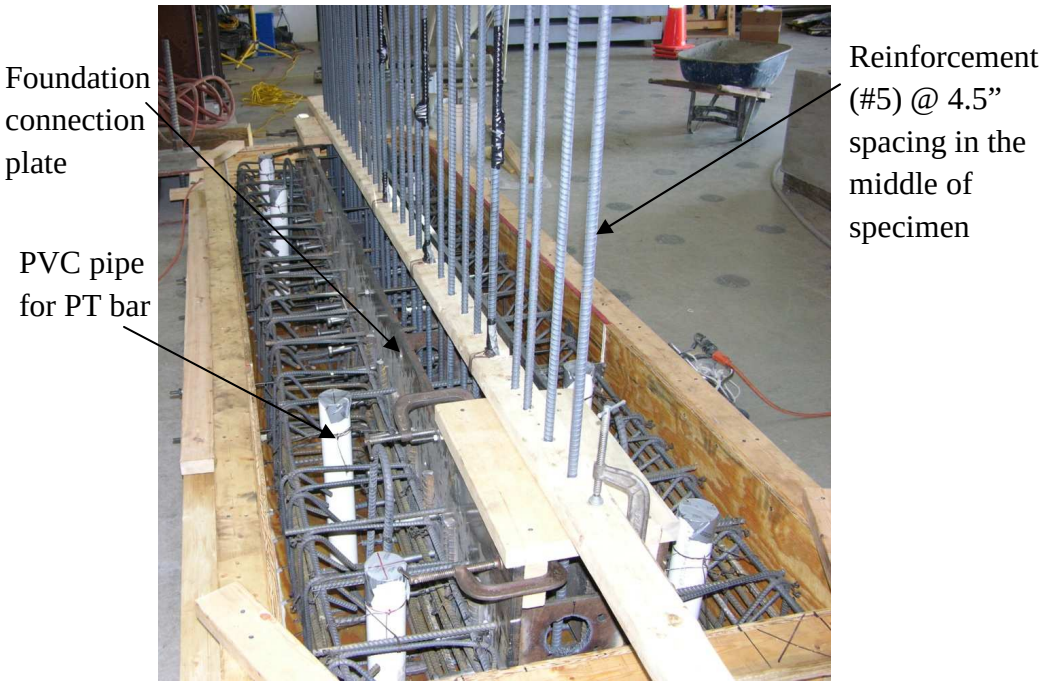

Figure 3.20 Foundation elements with specimen reinforcement

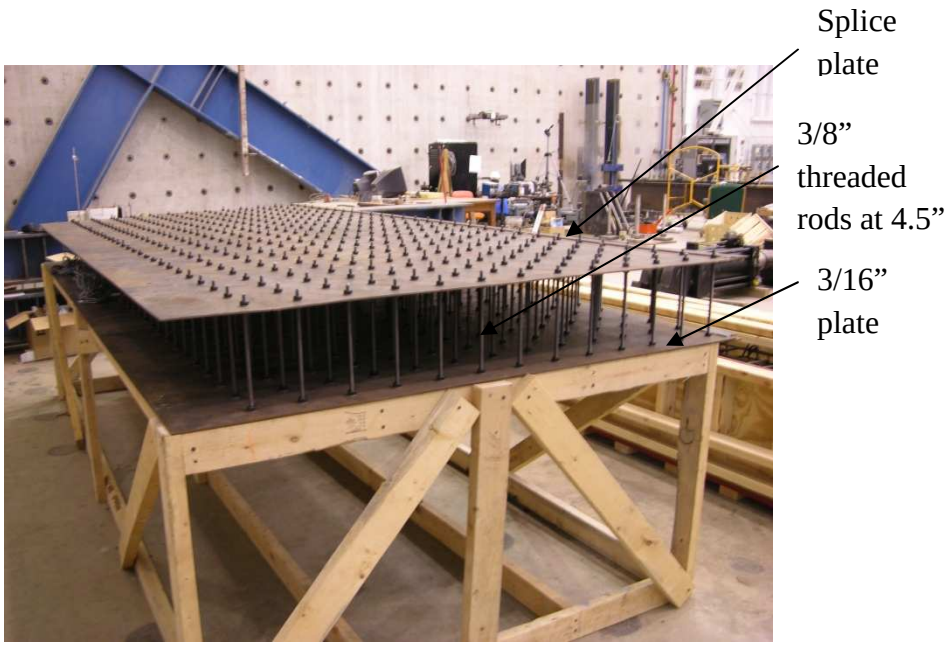

Figure 3.21 Plate assembly for stability test

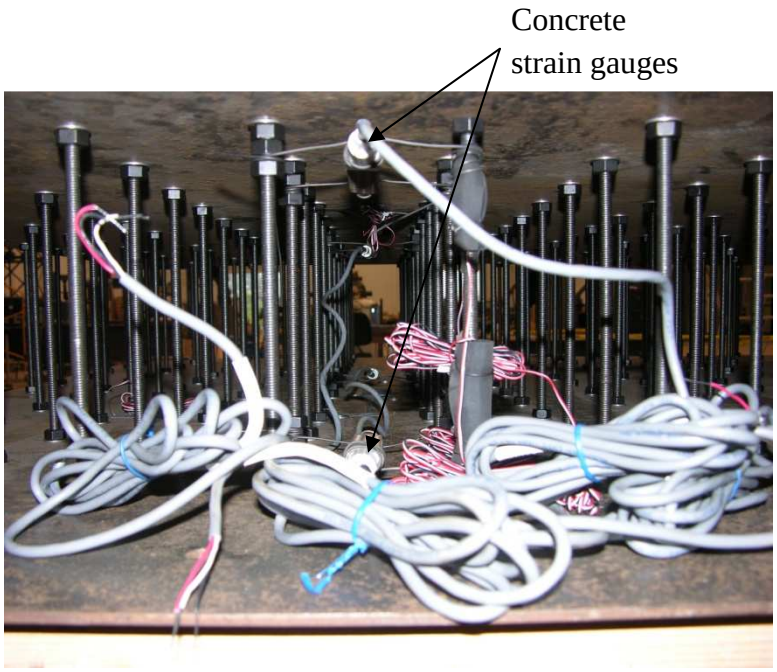

Figure 3.22 Plate assembly with strain gauges attached inside

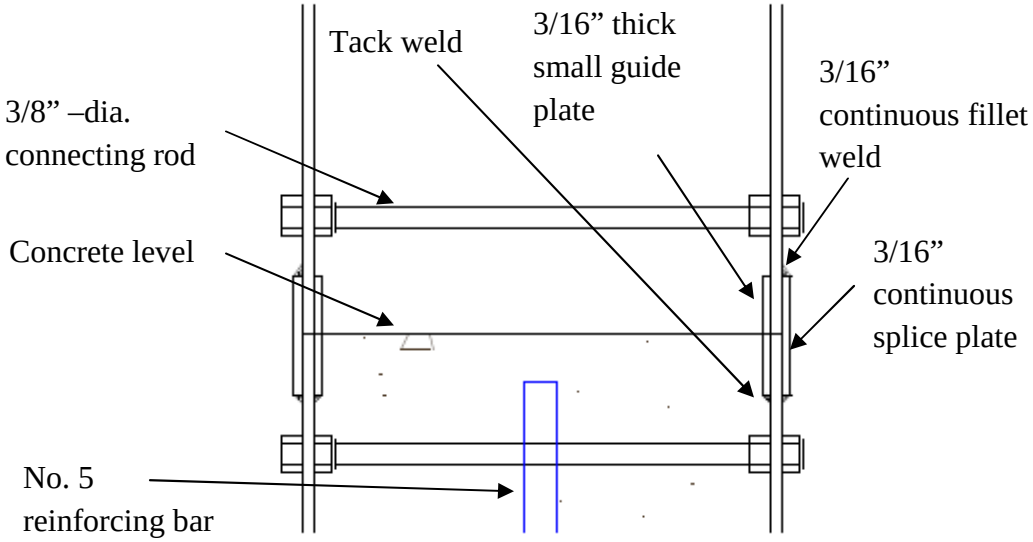

Figure 3.23 Connection of adjacent wall plate assemblies using horizontal splice plates

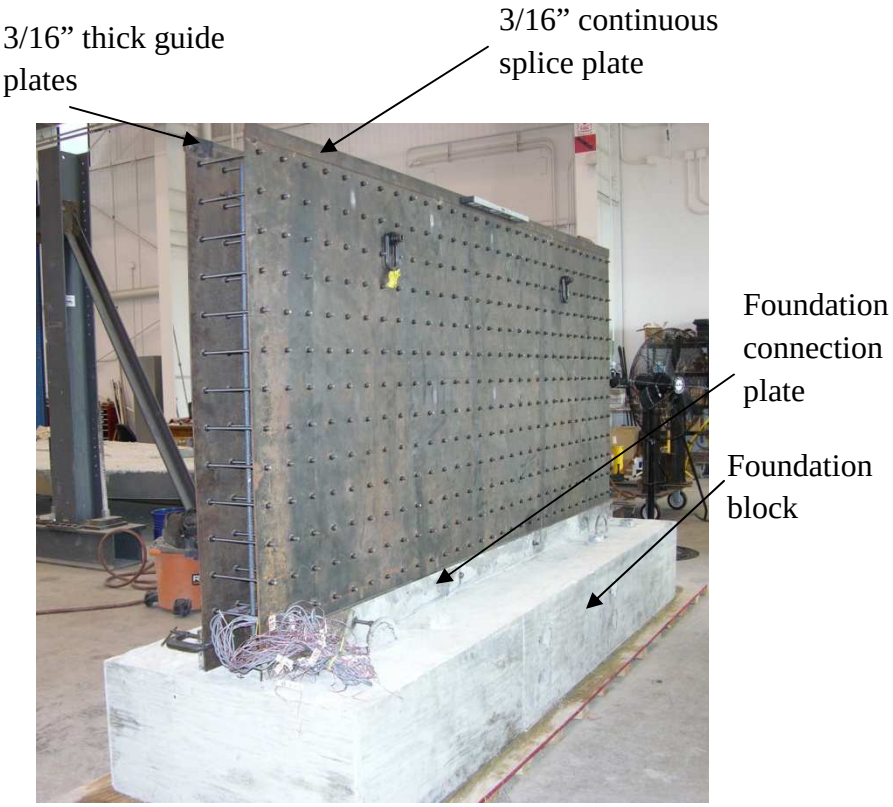

Figure 3.24 Plate assembly with splice plates

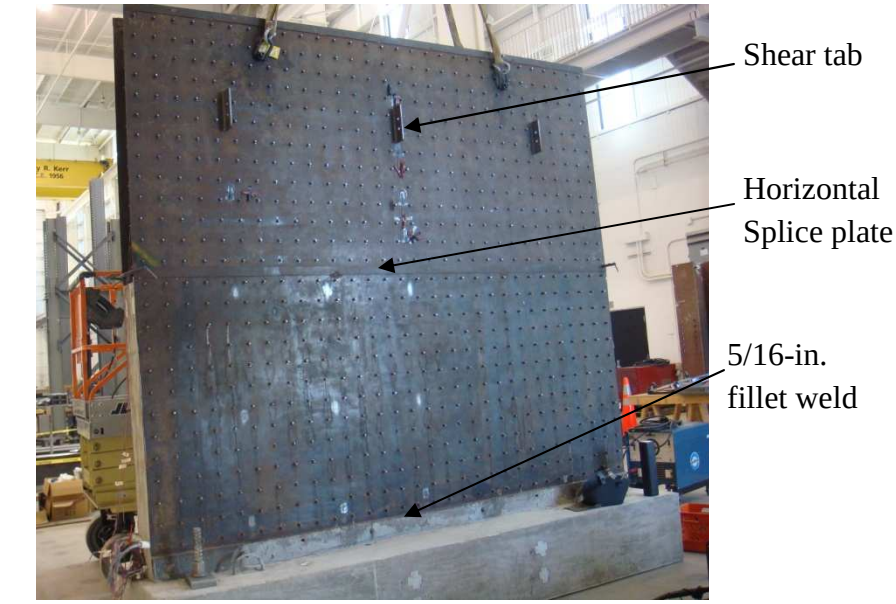

Figure 3.25 Erection of second story plate assembly

Figure 3.26 Test set - up (view from west side)

Figure 3.27 Anchoring the loading frame to the strong floor

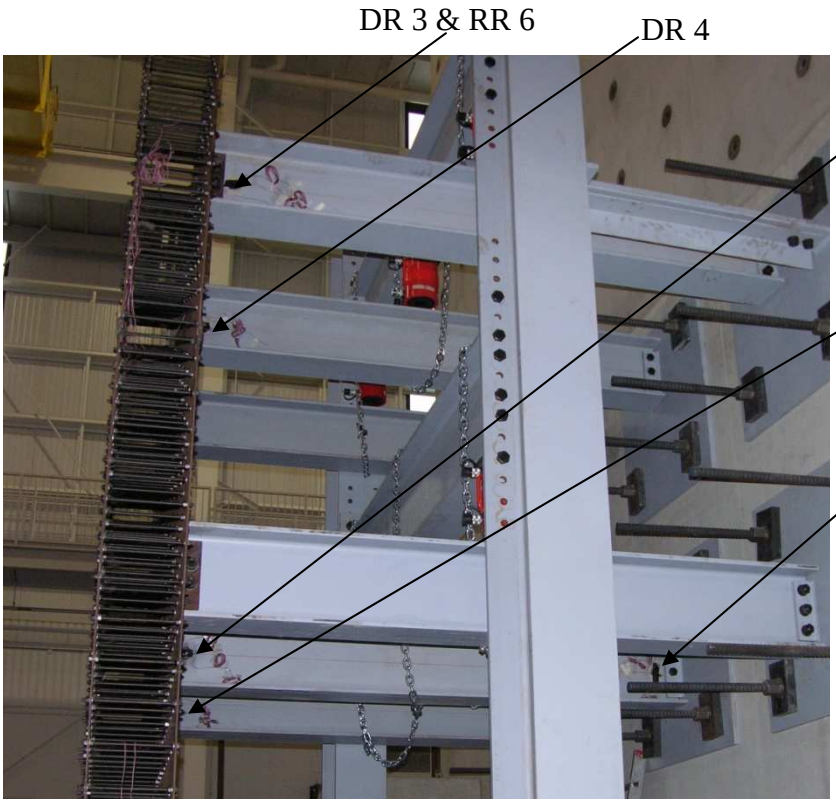

Note:

DR – Delta Rosette (1-5); RR – Rectangular Rosette (6)

DR 1 - Bottom level, middle cross beam, close to specimen

DR 2 - Top level, west side cross beam, close to strong wall

DR 3 - Top level, west side cross beam, close to specimen

DR 4 - Top level, middle cross beam, close to specimen

DR 5 - Bottom level, east side cross beam, close to specimen

RR 6 - Top level, west side cross beam, close to specimen

Figure 3.28 Locations of delta and rectangular rosettes (view from west to east)

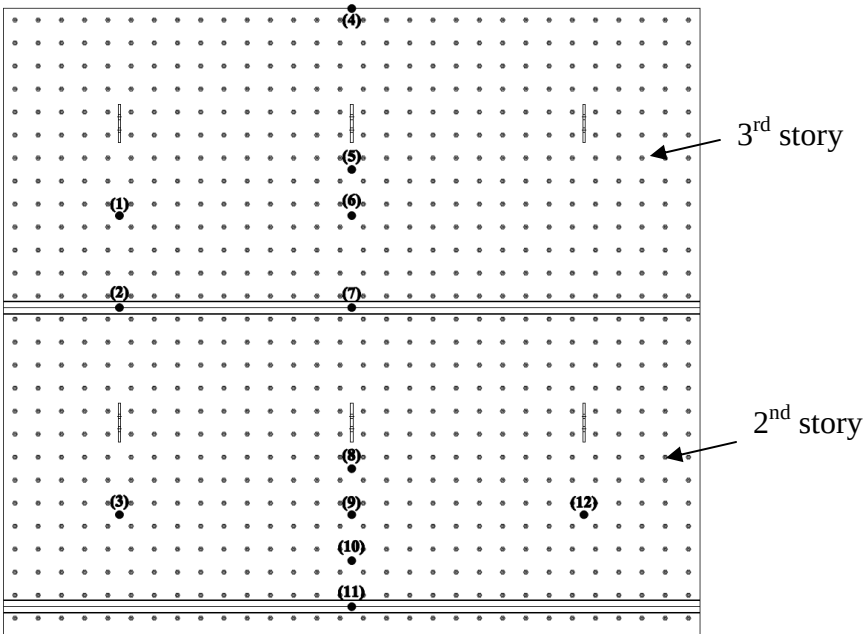

Figure 3.29 Locations of wire potentiometers (view from south to north - from strong wall to specimen)

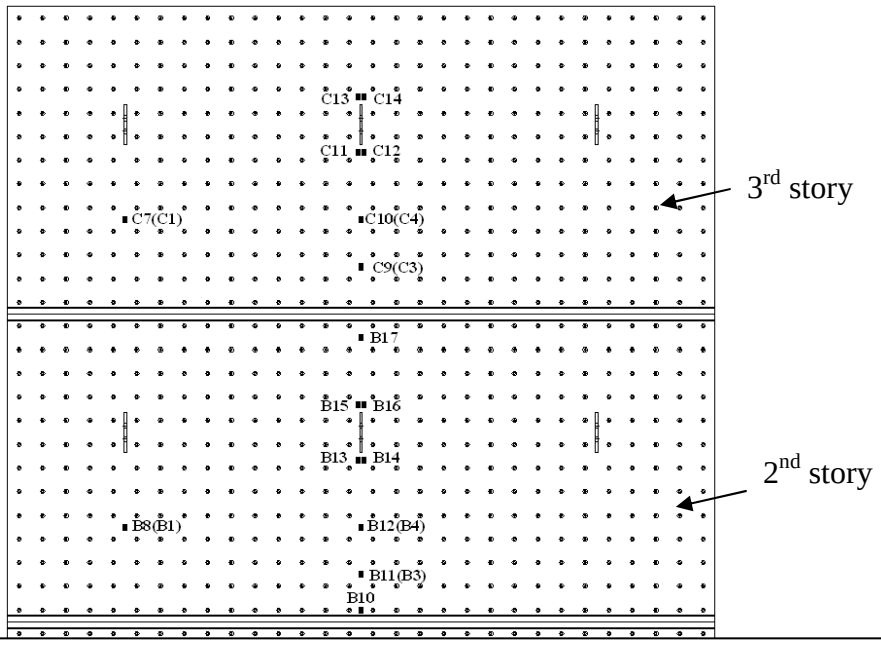

Note: Strain gauges marked within bracket (example: B1) are on inside of plate

Figure 3.30 Locations of strain gauges on south plate (view from south to north)

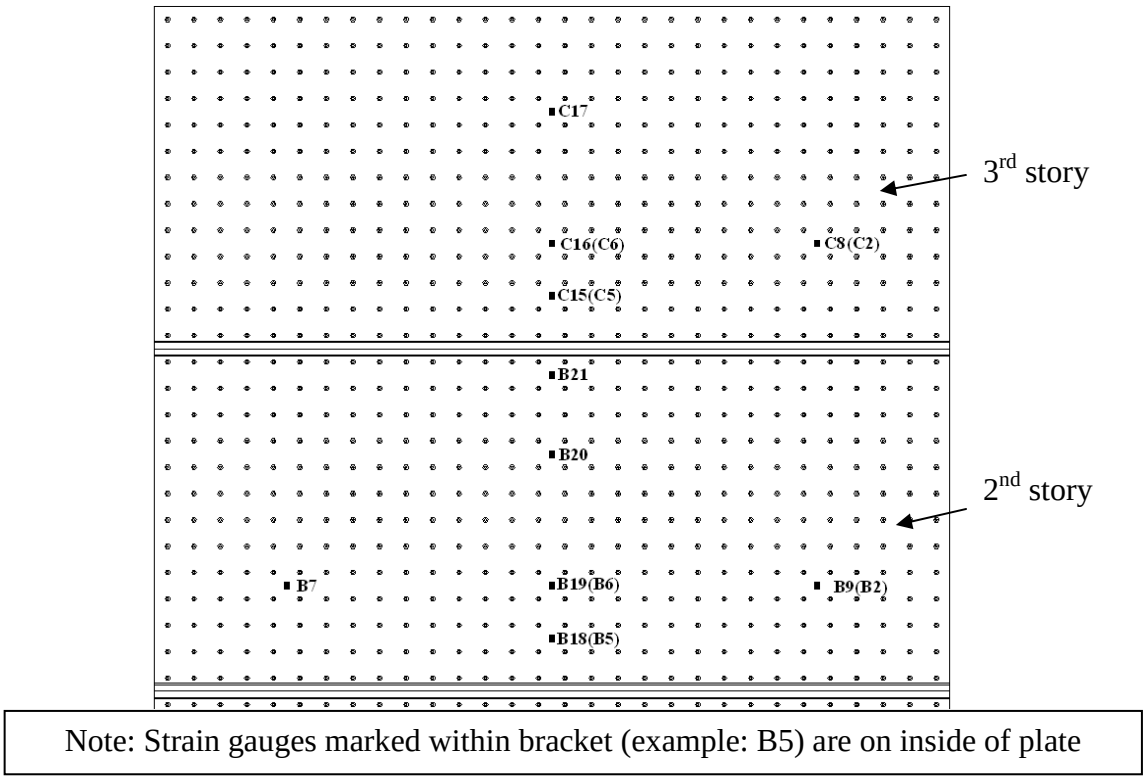

Figure 3.31 Locations of strain gauges on north plate (view from north to south - from specimen to strong wall)

Figure 3.32 Distorted stability specimen at maximum applied load (168 kips) – View 1

Figure 3.33 Distorted stability specimen at maximum applied load (168 kips) – View 2

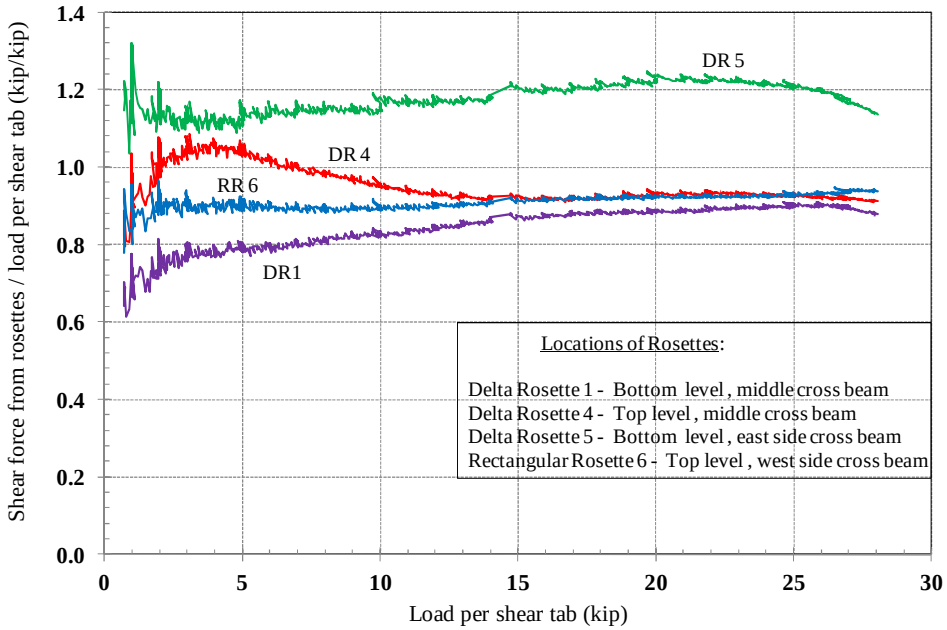

Figure 3.34 Ratio of load measured by rosettes to load per shear tab inferred from pressure transducer readings versus load per shear tab

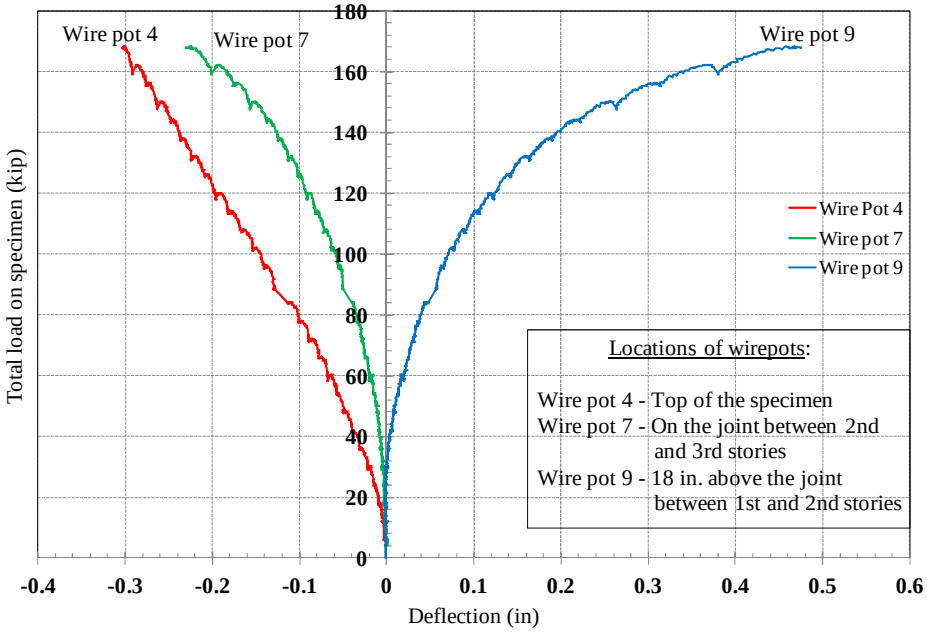

Note: Positive deflection indicates the specimen moved away from the strong wall.

Figure 3.35 Total load on specimen versus deflection at wire pots 4, 7, and 9

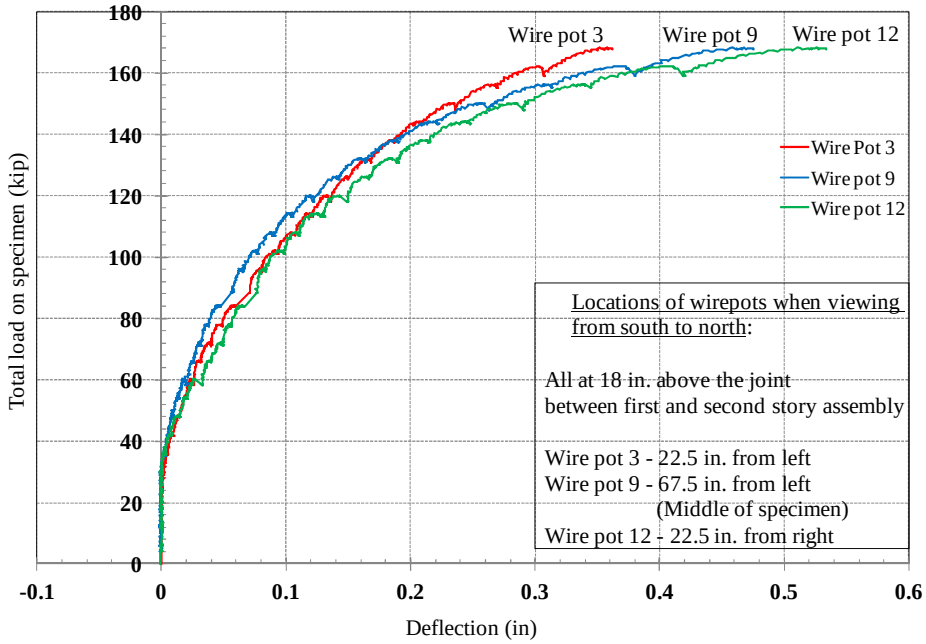

Figure 3.36 Total load on specimen versus deflection (Wire pots 3, 9 & 12)

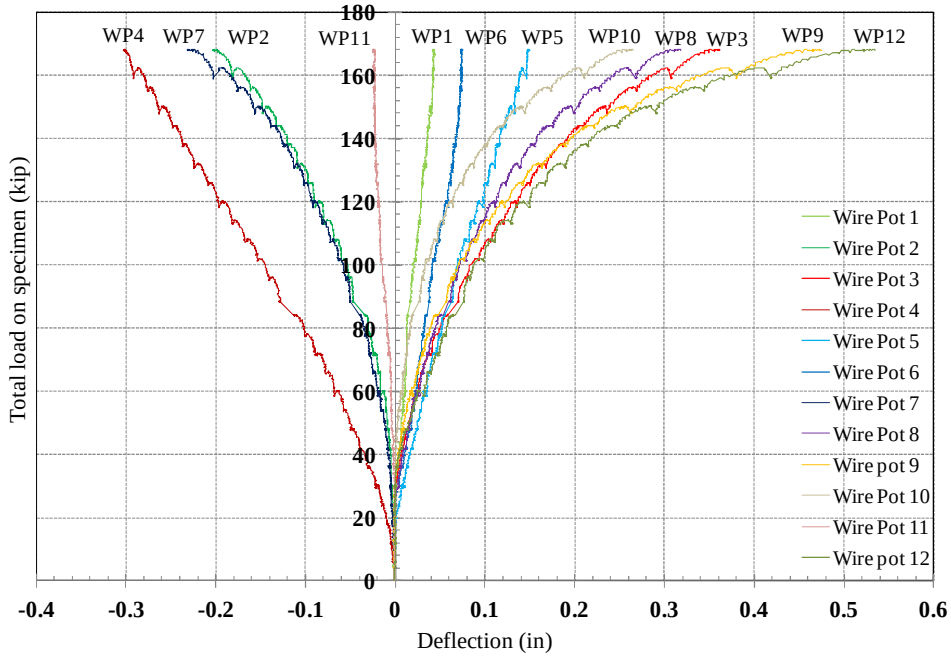

Figure 3.37 Total load on specimen versus deflection (Wire pots 1-12)

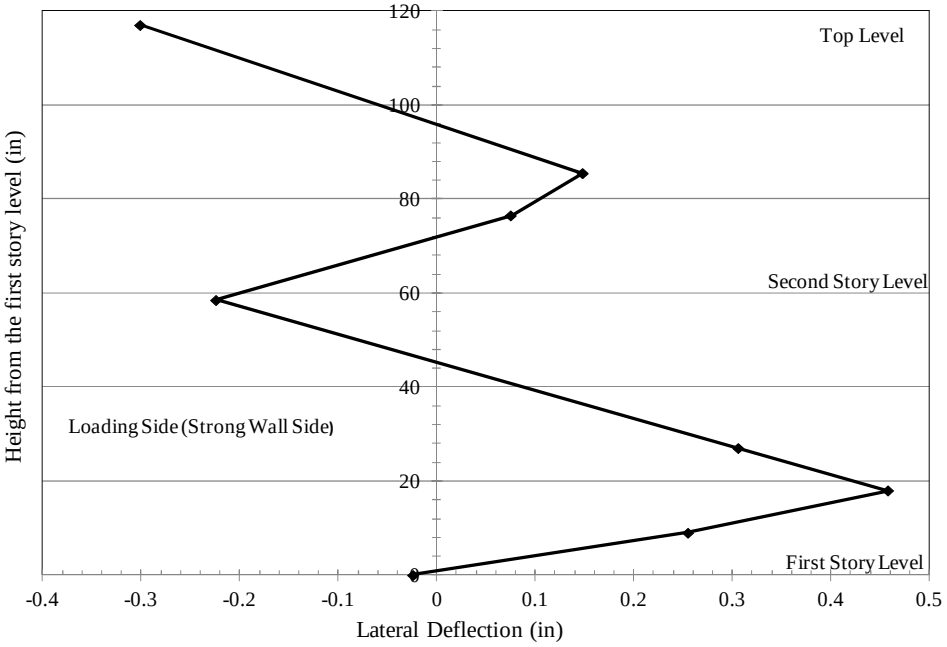

Figure 3.38 Lateral deflection at middle section of the shear wall versus height from the first story level at peak load (total load of 168.3 kips on plate assembly)

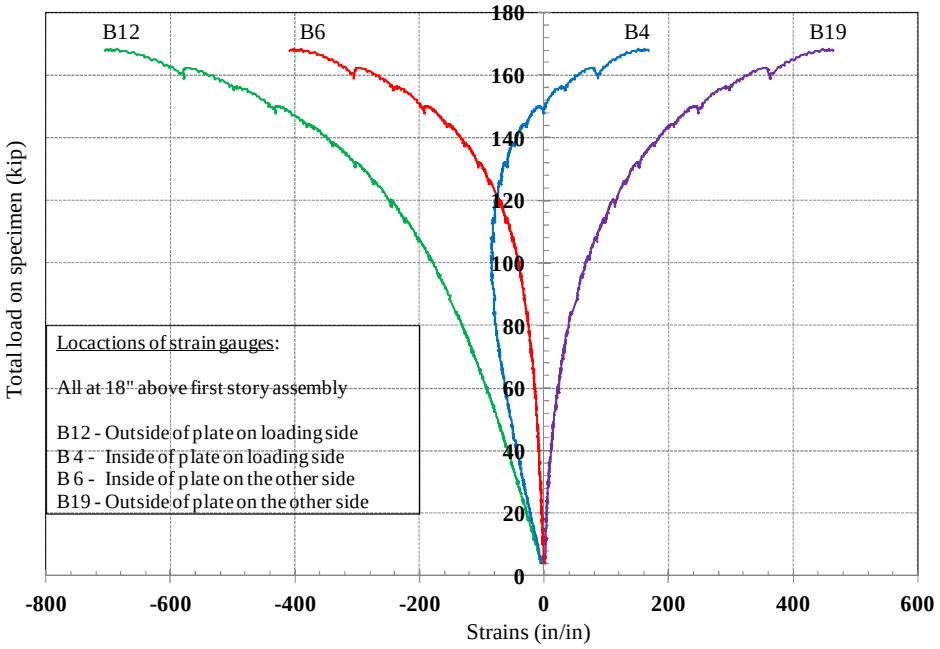

Figure 3.39 Total load on specimen versus strain at 18 in. above first story

CHAPTER 4: INVESTIGATION OF STRAIN COMPATIBILITY BETWEEN WALL PLATES SAND CONCRETE

4.1: Introduction

Investigation of strain compatibility between the steel plates and the concrete cast between the plates was the objective of the strain compatibility test. Strain compatibility between the steel plates and concrete would reveal that both materials deform together and that there is strain continuity through the cross section. Spacing of the transverse bars is one of the primary parameters that affect development of strain compatibility. Bar spacing was selected considering the hydrostatic forces resulting from freshly cast concrete (see Section 3.2.1.1). It was intended to determine whether the selected bar spacing develops sufficient strain compatibility between the steel plates and concrete through this experimental study. If there is insufficient strain compatibility, the bar spacing could be reduced to improve strain compatibility. For the strain compatibility investigation, out-of-plane lateral load was applied to the concrete-filled dual-plate assembly (first story of the specimen used for the stability test). Strains in the steel plates, concrete, and vertical reinforcement were measured and evaluated for strain compatibility at different lateral load levels.

4.2: Test set-up

Following completion of the stability test, the specimen was relocated along the laboratory strong wall to perform the strain compatibility test. The set-up used to load the lower third of the overall test specimen in its weak direction is shown in Figs. 4.1, 4.2, and 4.3. The foundation block was anchored to the strong floor by post tensioning eight

high-strength thread bars. The shear wall plate that was expected to resist tension was predicted to yield at a total lateral load of 320 kips applied at 49.5 in. from the bottom of the shear wall specimen. Three single-acting hydraulic cylinders (RCH 306 with a load capacity of 60 kips each) were used to apply a lateral load that would crack the concrete between the steel plates but not yield the plates so as to not jeopardize the shear test that was planned to follow this test. The load from the hydraulic cylinders was transferred to the strong wall via the W-shapes (see Fig. 4.2).

4.3: Instrumentation

Similar to the stability test, a pressure transducer, wire potentiometers (wire pots), and strain gauges were used to measure the load, displacements, and strains, respectively. The same pressure transducer, with the same calibration factor for pressure as was used in the stability test, was used to measure the load.

The lateral displacements from the wire potentiometers mounted on a wooden frame with their wires attached to the specimen (the bottom story) were monitored in order to develop lateral load - lateral displacement response curves and the variation of deflection along the height of the specimen. A total of five wire potentiometers were connected to the specimen opposite the side used for loading. The wooden frame and a few of the wire pots are visible in Figs. 4.2 and 4.3. The locations of all the wire potentiometers are shown in Fig. 4.4. Two dial gauges were placed on the strong floor against the foundation block of the specimen to monitor any sliding of the specimen during testing. The dial gauges were located on the north side of the specimen (opposite the loading frame side) near each end of the specimen.

A total of five strain gauges (on the compression-side steel plate, in the concrete near the compression-side steel plate, on the reinforcing bar in the middle of the wall, in the concrete near the tension-side steel plate, and on the tension-side steel plate) were installed in a line through the cross section in which strain compatibility was investigated.

These sets of five strain gauges were installed in five locations (lines through the cross section). These locations are listed in Fig. 4.5. The concrete strain gauges were located 1-1/8 in. from the outer side of the steel plates. The strain gauges on the No.5 reinforcing bars were located 4-3/16 in. from the outer side of the tension plate (i.e. the south plate or the plate on the loading side). All the measurements were monitored and recorded using a high-speed data acquisition system (Vishay's Strain Smart System 5000).

4.4: Test Method

A procedure similar to that used in the stability test was followed during testing. Load versus strain plots were monitored for the strain gauges along line 4. At approximately a total load of 60 kips the concrete strain gauge on the tension side registered a strain that indicated the concrete had cracked at that location (see Fig. 4.6). The reinforcing bar started resisting tension at that stage. Loading was continued after concrete cracking but was stopped well before the steel plates yielded so the same specimen could be used for the horizontal splice plate connection test detailed in Chapter 5. The strain gauge on the tension-side steel plate reached a maximum strain of about 600 με. Loading was applied until a maximum total load of 114 kips (38 kips at each loading cylinder) was applied.

4.5: Results and Analysis

A maximum load of 114 kips was applied to the specimen, and resulted in maximum measured strains of approximately 550 to 670 με in the steel plate (which corresponds with stresses of 16 to 19.4 ksi). The load versus strain response measured along the line that was 4.5 in. from the bottom of the specimen and midway along the length of the specimen (Line 4) is shown in Fig. 4.6. The measured responses on the compression side of the cross section (the two responses on the left side of Fig. 4.6) demonstrate reasonable agreement with the assumption of strain compatibility. Measured

responses on the tension side of the section also appear to be in reasonable agreement with strain compatibility until the concrete cracks at a total applied load of approximately 60 kips. The onset of concrete cracking is indicated in the plots when strains were measured in the no.5 reinforcing bar in the center of the wall section.

The load versus strain responses measured at the other locations (lines 1, 2, 3, and 5) are shown in Figs. 4.7 through 4.10. It is evident in Figs. 4.7 and 4.8 that the measured concrete strains at Lines 1 and 2 (which are 22.5 in. from the ends of the specimen) deviate from mostly-linear behavior at approximately 40 kips. Fig. 4.9 shows that the concrete cracked and the reinforcing bar started resisting tension at approximately 50 kips at Line 3 (which is 45 in. from the end of the specimen). Figures 4.6 and 4.10 show that the reinforcing bars started resisting tension at approximately 60 kips at Lines 4 and 5 (which are 67.5 in. from the specimen ends). The concrete in the middle (at 67.5 in. from the edge) is more confined than the concrete near the ends (at 22.5 in. from the ends). Also, larger shrinkage strains likely developed near the ends of the specimen than in the middle of the specimen, which might have been a possible reason for different load levels at which concrete cracked.

Strains measured through the cross section of the wall are plotted against the distance from the outer side of the tension side plate in Figs. 4.11 through 4.14 at different load levels (30, 60, 90, and 114 kips). Figure 4.11 shows strain readings before concrete cracked while Figs. 4.12 through 4.14 illustrate strain readings after concrete cracked on the tension side of the wall. Hence, the readings from tension-side concrete strain gauges have been removed from Figs. 4.12 through 4.14. Figure 4.11 (strains at a total load of 30 kips) shows close to a linear relationship of strains with distance. However, it is evident from Figs. 4.11 through 4.14 that the distribution of strains through the cross section is less linear with increased applied total load. The average R^2 values of the linear trend lines were 0.973, 0.957, 0.928, and 0.924 at a total load of 30, 60, 90, and 114 kips, respectively (from Figs. 4.11 through 4.14). Lines 1, 3, and 4 (which were 4.5

in. above the bottom) measured greater bending than Lines 2 and 5 (which were 27 in. above from bottom) as is evident from Figs. 4.11 through 4.14.

4.6: Conclusions

Strain compatibility through the cross section of the shear wall would reveal that the steel plate and concrete act together as one unit. To evaluate strain compatibility for the dual-plate system, a test was conducted on the composite shear wall. For the test, lateral load was applied to a concrete-filled steel plate assembly in the out-of-plane direction. During the test, the reinforcing bar in the middle of the shear wall did not resist any significant tension prior to concrete cracking (before a total load of 40 kips). However, after the concrete cracked, the reinforcement started resisting tension due to bending. Concrete cracked at different load levels depending on the distance from the ends of the specimen. The concrete in the middle of the specimen (far away from the ends) cracked around a total lateral load of approximately 60 kips while the concrete near the ends cracked at approximately 40 kips. This behavior was likely due to more shrinkage cracks occurring near the ends of the specimen than in the middle.

The strain compatibility test also demonstrated that strains through the cross section were reasonably linear before concrete cracked, and the linearity decreased when the lateral load was increased. Threaded rods in the plate assembly clearly facilitated the transfer of strains from the steel plate to concrete. Decreasing the spacing of the threaded rods may increase the strain linearity through the cross section of the wall.

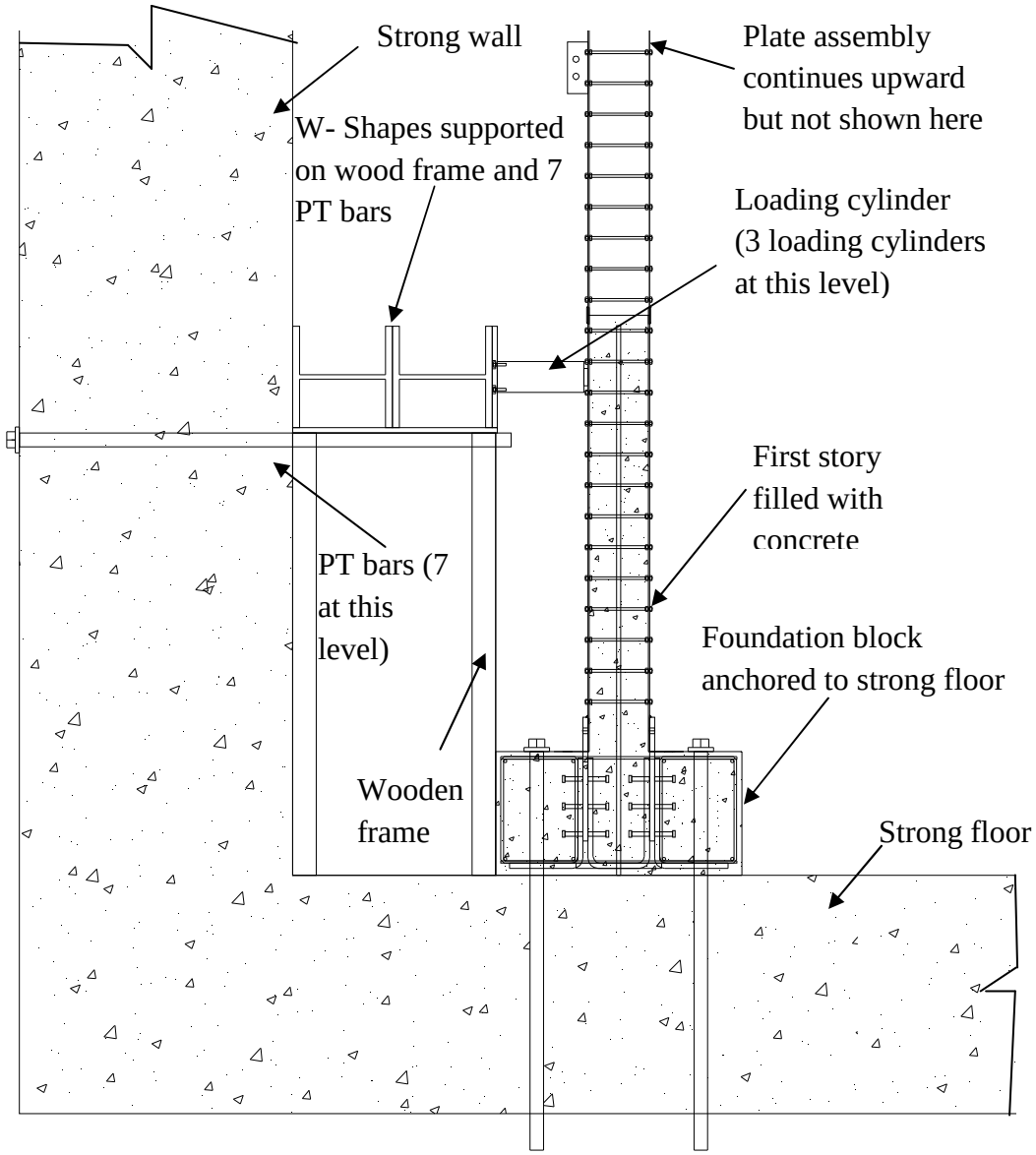

Figure 4.1 Test set-up for the strain compatibility test - End View

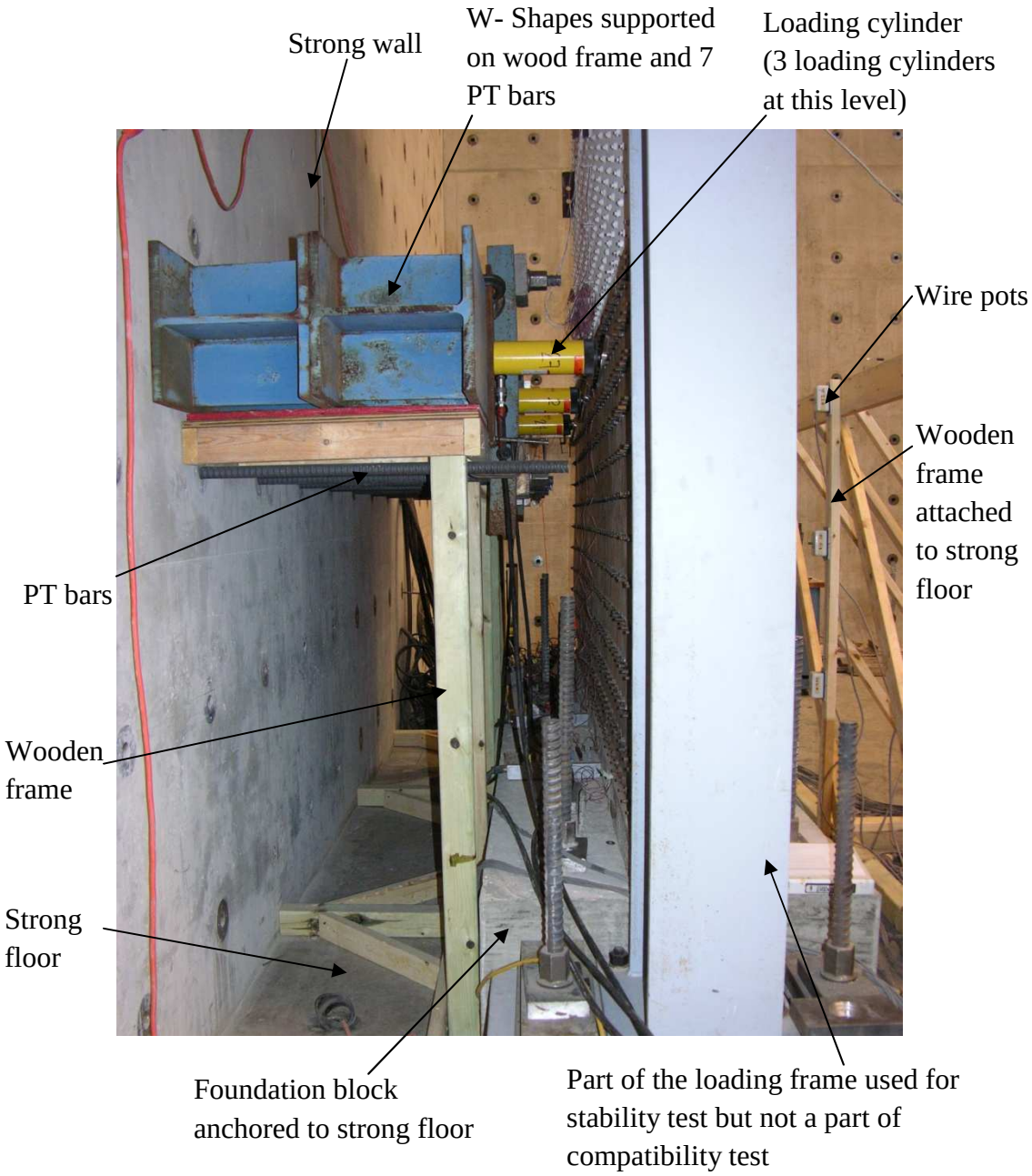

Figure 4.2 Test set-up for the strain compatibility test – View from east to west

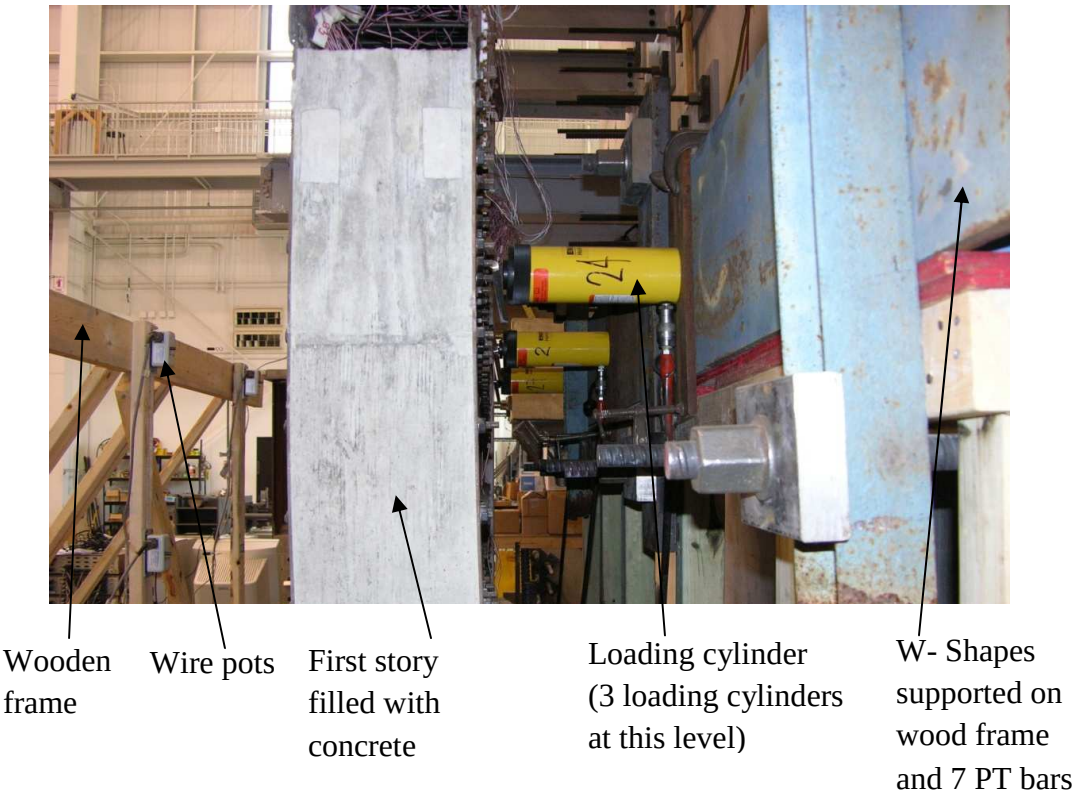

Figure 4.3 Test set-up for the strain compatibility test – View from west to east

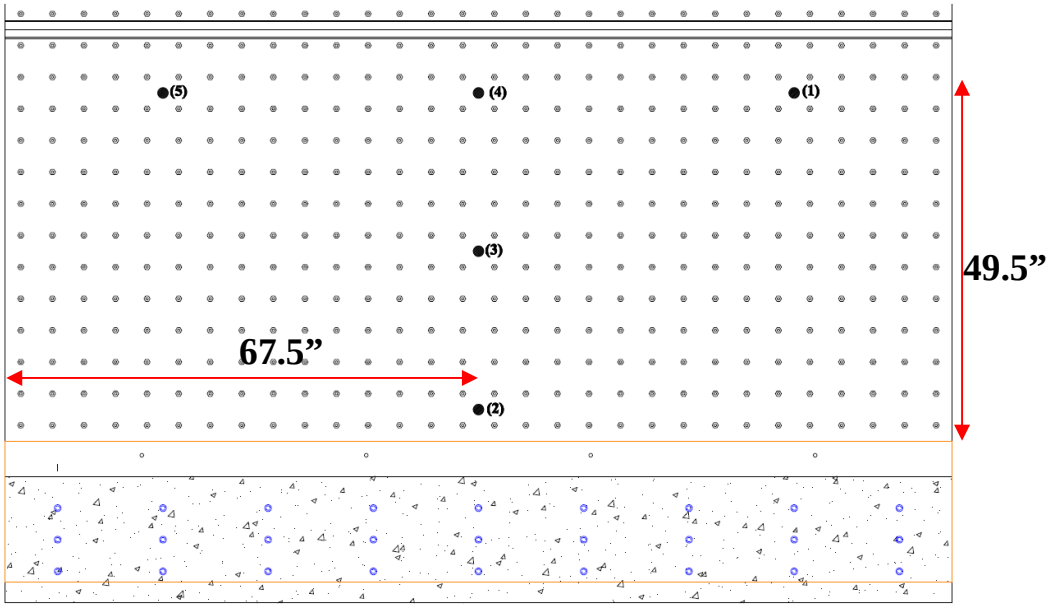

Figure 4.4 Wire pot locations (view from north to south – from specimen to strong wall)

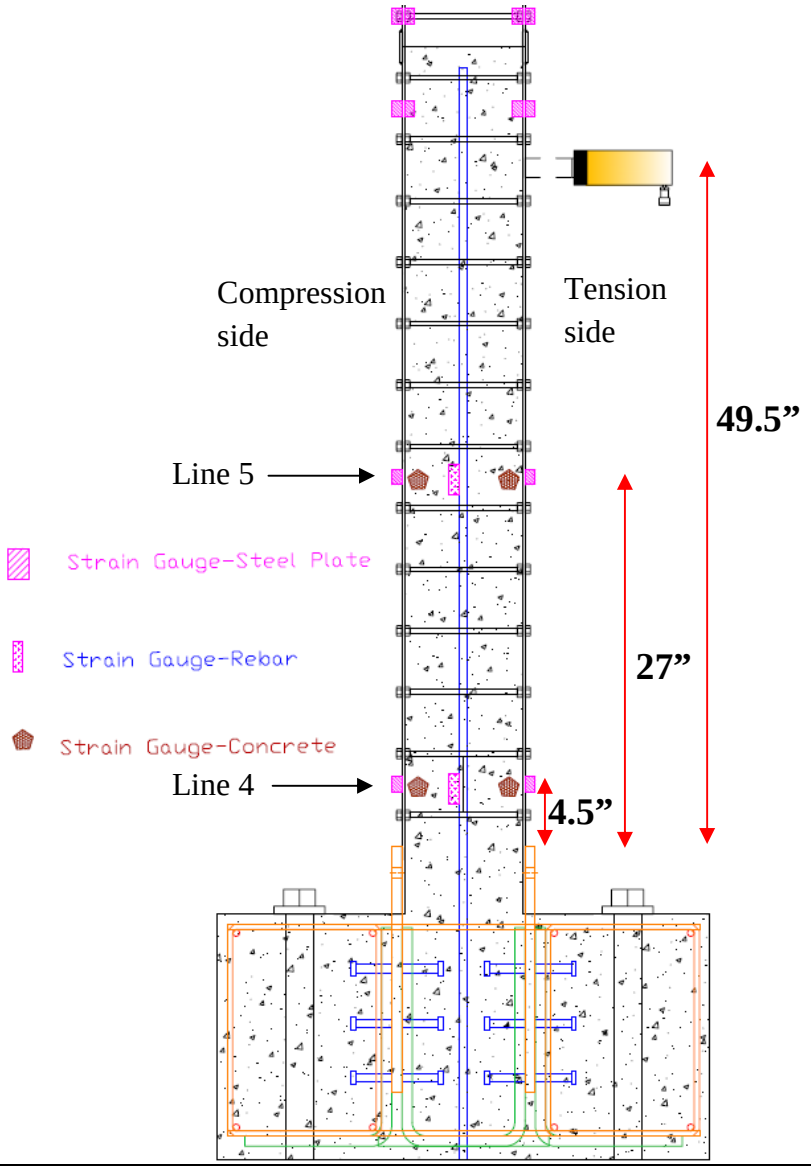

Note: Locations of 5 sets of strain gauges (lines)

Line 1: At a horizontal distance of 22.5 in. from west edge of the specimen and at a vertical distance of 4.5 in. from bottom

Line 2: Horizontal distance = 22.5 in.; Vertical distance = 27 in.

Line 3: Horizontal distance = 45 in.; Vertical distance = 4.5 in.

Line 4: Horizontal distance = 67.5 in.; Vertical distance = 4.5 in.

Line 5: Horizontal distance = 67.5 in.; Vertical distance = 27 in.

Figure 4.5 Strain gauge locations for strain compatibility test

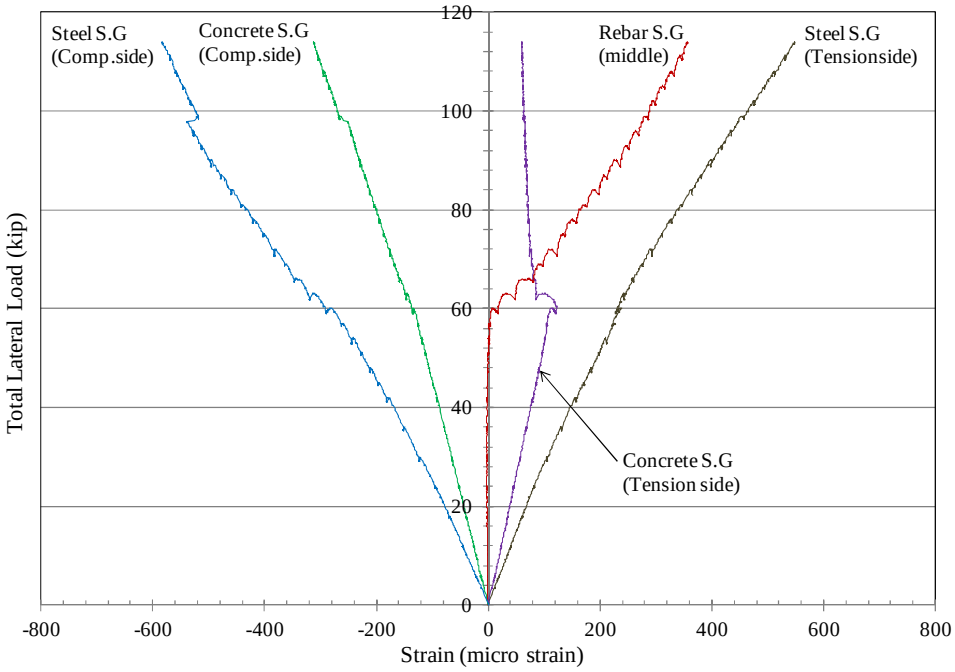

Figure 4.6 Load versus strain along Line 4

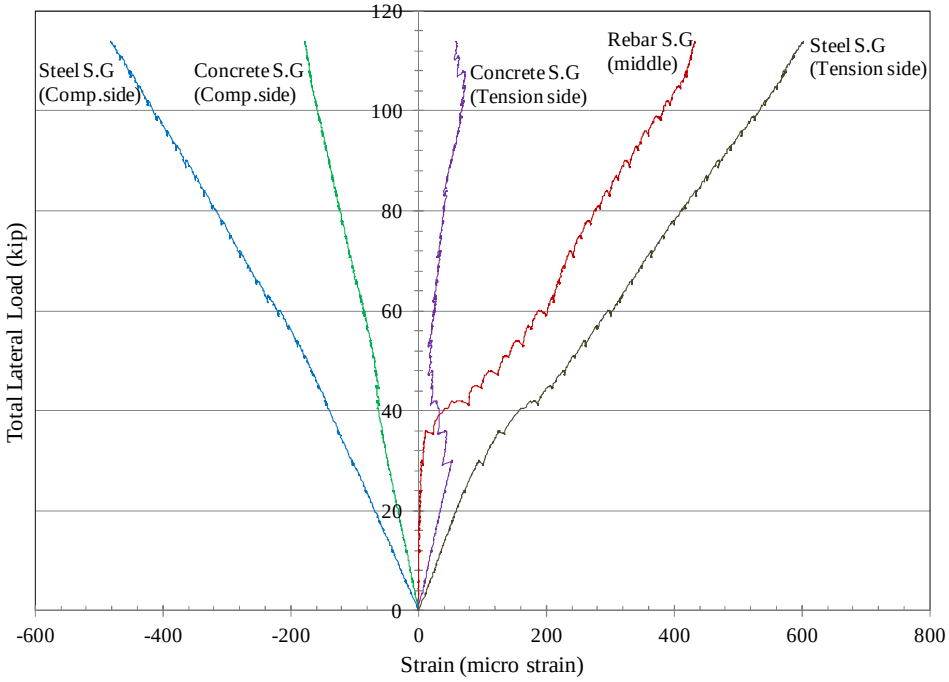

Figure 4.7 Load versus strain along Line 1

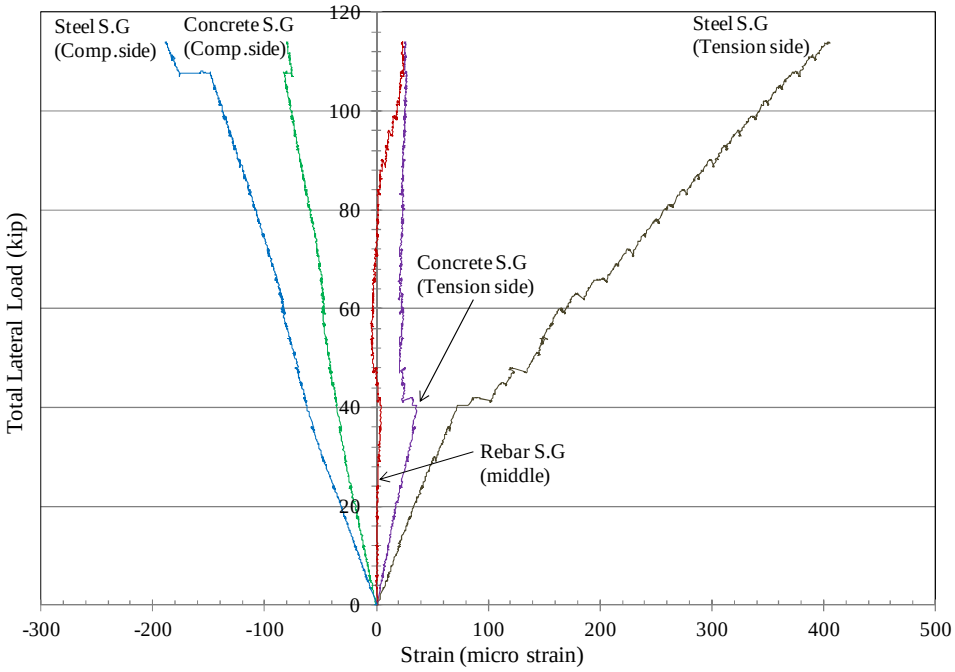

Figure 4.8 Load versus strain along Line 2

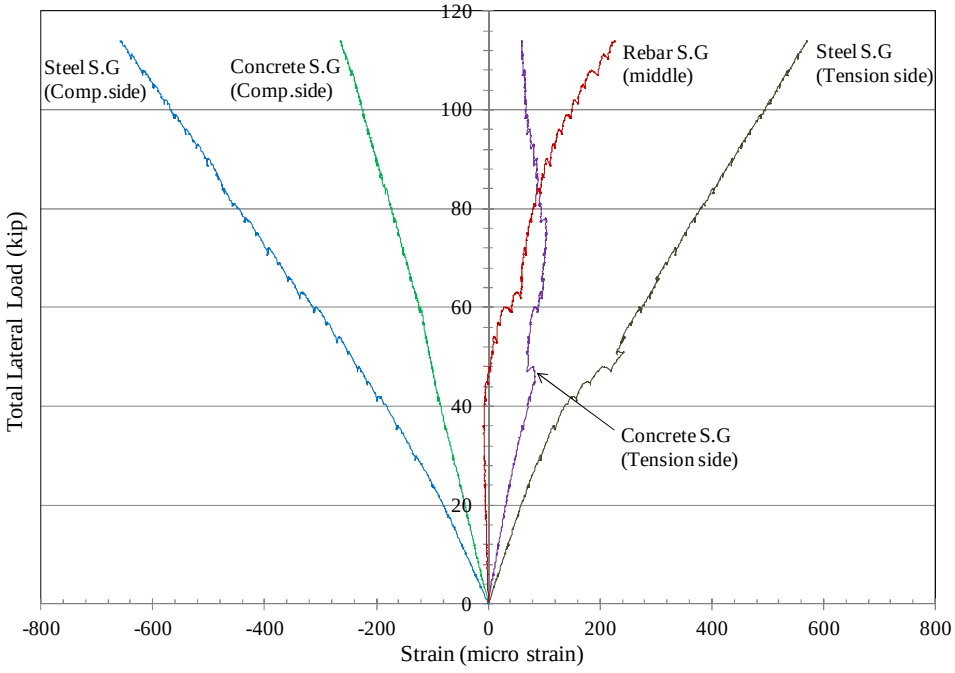

Figure 4.9 Load versus strain along Line 3

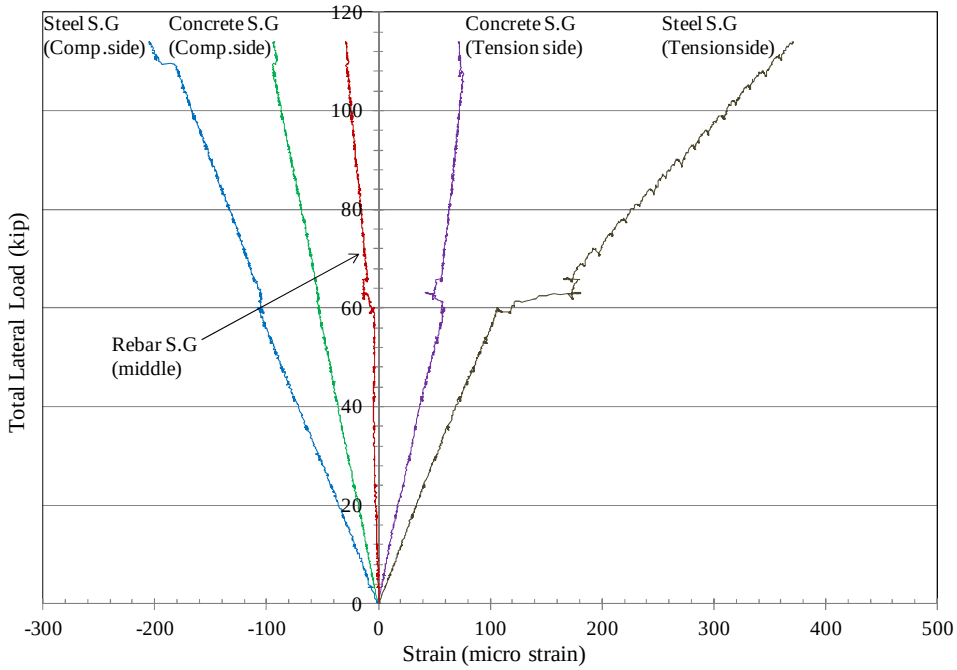

Figure 4.10 Load versus strain along Line 5

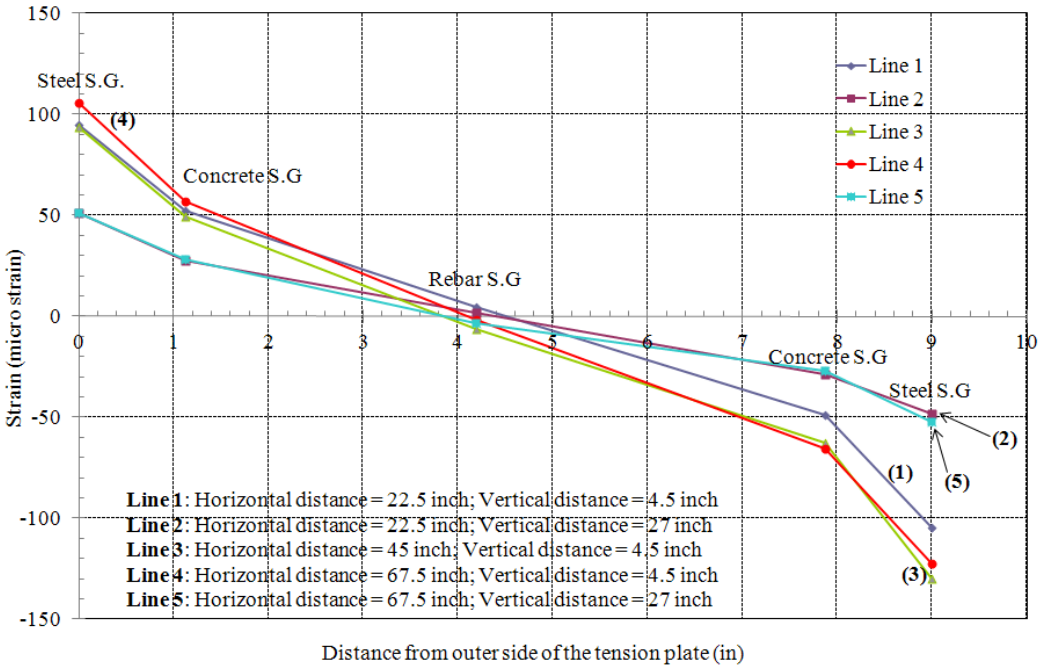

Figure 4.11 Strains versus Distance (at a total load of 30 kips)

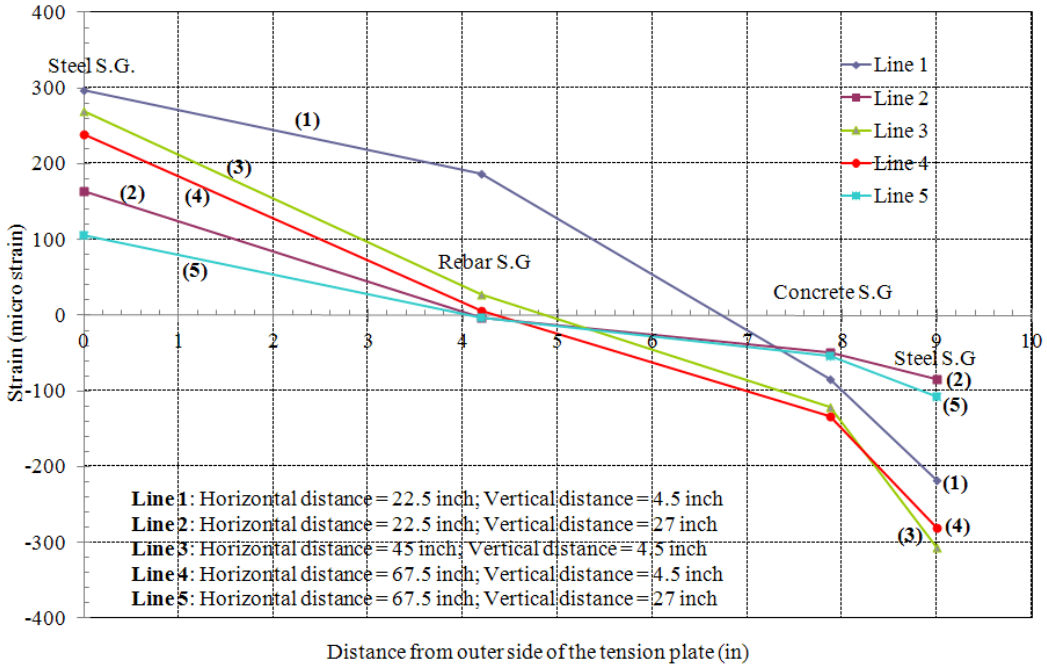

Figure 4.12 Strains versus Distance (at a total load of 60 kips)

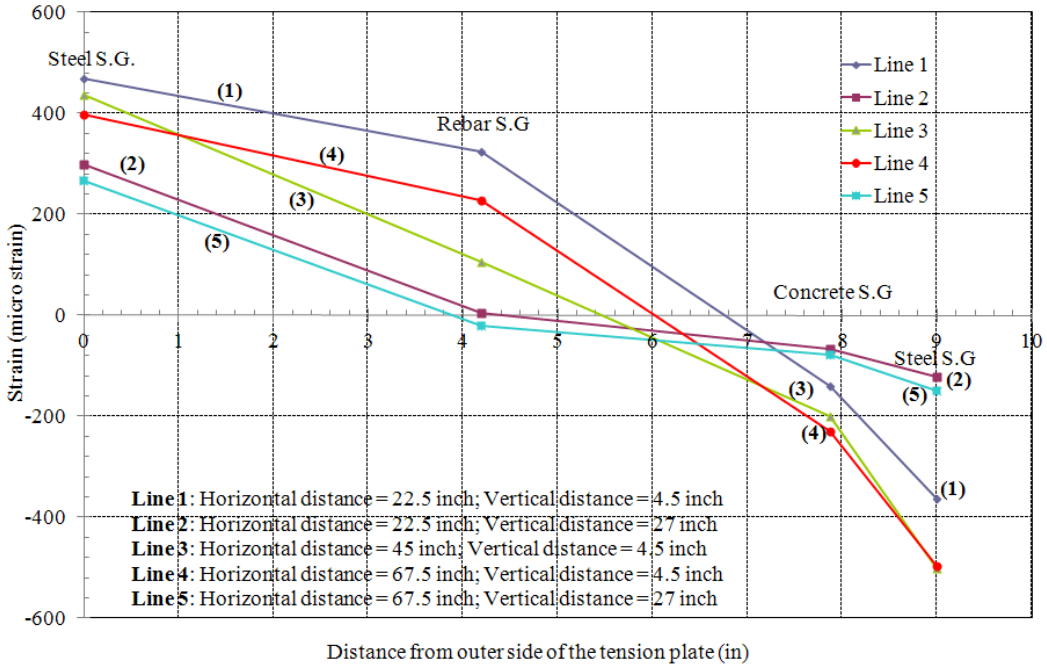

Figure 4.13 Strains versus Distance (at a total load of 90 kips)

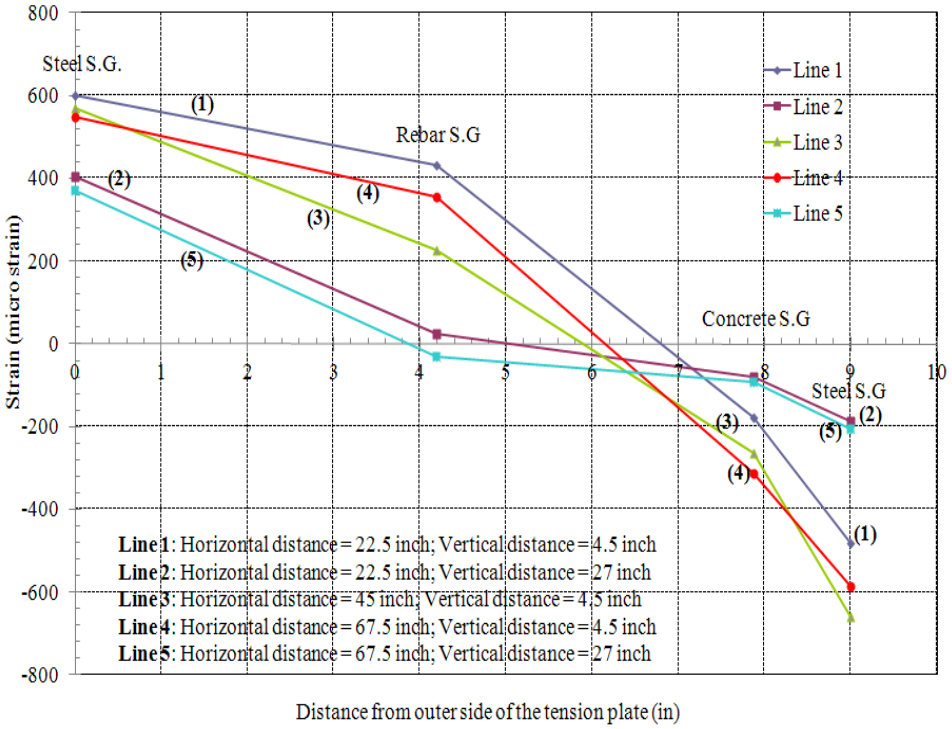

Figure 4.14 Strains versus Distance (at a total load of 114 kips -the maximum load applied)

CHAPTER 5: BEHAVIOR OF SPLICE PLATE CONNECTION FOR IN-PLANE SHEAR

5.1: Introduction

The horizontal splice plate connection between two plate assemblies transfers axial, shear and bending forces from a plate assembly to the adjacent plate assembly. Axial forces are due to self weight of the shear wall and from load transferred to the shear wall by the gravity load system. Shear forces are from the lateral load developed by wind or earthquake. Bending forces are due to a combination of the lateral load applied at vertical eccentricity and the vertical load applied at lateral eccentricity.

The adequacy of the splice plate connection for vertical and bending forces was indirectly verified by the stability test (Chapter 3) and the cyclic loading test (Chapter 6), respectively. Because there was no failure of the splice plate connection during the stability test, it could be concluded that the connection was sufficient to resist a vertical load of 168 kips (1.24 kips/in. length of plate assembly) applied on the plate assembly during the test. Similarly, because there was no failure of the splice plate connection during the cyclic loading test, it could be concluded that the connection was able to resist the axial load developed as a result of an axial stress of 0.1 A_g*f'_c (where A_g = cross section area of the wall and f'_c = compressive strength of concrete) on the cross section of the wall combined with bending effects resulting from a 2% drift at a height of 295 in.

In this experimental program, the behavior of the splice plate connection for the lateral load applied in the plane of the shear wall was investigated. Figure 3.23 shows an AutoCAD drawing of the splice plate connection while Fig. 3.24 provides a photograph of the splice plates welded to a bottom plate assembly before the assembly was lowered

onto the plate assembly below. Fabrication of this connection is described in Section 3.3.1.2.

5.2: Test Set-up

Specimen Details

Due to the limited capacity of the foundation, only 1/3 of the plate assembly width (depth of the wall specimen) was used to evaluate the strength of the horizontal splice connection. The central portion of the plate assembly above the cast concrete was removed using a plasma torch. This action resulted in two advantages: (1) the required load to be resisted by the foundation was reduced, and (2) two shear tests of the horizontal splice plates - one test at each end of the specimen - were possible. The plate was coped to provide a 30-in. test length beneath where the horizontal load was applied with the intent of precipitating a failure in the plate or weld rather than the bolted connection to the loading system. Figure 5.1 shows the AutoCAD drawing of the test set-up with only one test connection shown for ease of illustration. Figure 5.2 shows a photograph of the test set-up with test connections on both ends. After completing the first shear test (Test-1), the specimen was turned end-for-end to conduct the second shear test (Test-2) on the opposite end of the specimen.

A weld size of 3/16 in. was used to attach the 3/16 in. splice plate to the 3/16 in. shear wall plate. The weld sizes on the specimen were measured at several locations along the length, and the horizontal leg size was almost always 3/16 in. while the vertical leg size varied. The average vertical leg sizes were 0.250 in. and 0.245 in. in specimen 1 and specimen 2, respectively. The calculated average effective throat thickness for the splice plate fillet weld from the measured leg sizes was 0.149 in. and 0.148 in. for specimen 1 and specimen 2, respectively. For comparison, if the vertical leg size was 3/16 in., then the effective throat thickness would have been 0.133 in.

Load Set-up

Expected shear strength of the 30-in. long test specimen was calculated considering the failure modes of shear fracture of weld (from calculated effective throat thicknesses of 0.149 in. and 0.148 in. for specimen-1 and specimen-2, respectively), shear yielding of the plates (considering a yield strength value of 64.3 ksi for the plates), and shear rupture of the plates (considering a tensile strength value of 74.4 ksi for the plates) and selecting the minimum value from the three failure modes. The expected shear strength of the test specimen obtained from the above calculation was 376 kips for Test-1 and 373 kips for Test-2 by shear fracturing of weld for both specimens. Strength reduction factors were excluded from the above calculation. The load set-up was designed for a maximum load of 600 kips.

Figures 5.1 and 5.2 show the test set-up for the splice plate connection test. During the test, the loading axis was kept as close as possible to the expected failure region to minimize flexural effects. Shear applied to the connection by the hydraulic cylinder was distributed along the horizontal splice connection using two T-sections bolted on the outside of the 3/16 in. plates. The flanges of the T-sections were bolted to the vertical plates, and the webs pointed outward from the shear wall. Both T-sections were welded to a single 1 in. thick plate on which the hydraulic cylinder bore. The bottom of the loading cylinder was attached to the laboratory strong wall. The center of the loading cylinder was located 5-3/4 in. above the splice plate. A single-acting high tonnage hydraulic cylinder (CLSG-5006 with a load capacity of 1000 kips) was used to apply the lateral load to the steel plates.

Because the laboratory strong floor was relatively smooth (it provided a friction coefficient of 0.1 between the foundation block and the strong floor), it was questioned whether the frictional resistance between the foundation concrete and the strong floor (developed using post tensioning) would be sufficient to resist the lateral load. It was decided that a more positive lateral restraint was needed. Accordingly, a steel bearing

block and post-tensioned high-strength thread bars were added as shown in Figs. 5.1 and 5.2 to resist the lateral load. The four post-tensioned bars (1-1/4 in. dia.) could resist a total lateral load of 600 kips. The moment resulting from the applied lateral load was resisted by the post-tensioned bars anchored to the strong floor.

5.3: Instrumentation

Strain gauges were positioned above the splice plate on the dual-plate section and below the splice plate on the composite section. Strain gauge locations on the specimen are shown in Fig. 5.3. The top strain gauges were attached approximately ½ in. above the weld toe and 5 in. below the loading axis. The bottom strain gauges were located 4-1/2 in. below the center of the splice plate and 11-1/4 in. below the loading axis. Strain gauges J1-J7 were located on the right side plate (when facing in the loading direction), while strain gauges J8-J14 were located on the left side plate of the plate assembly. A pressure transducer was used to measure the load.

The shear wall plates and splice plate connection were whitewashed to monitor any yielding during Test-1. Two dial gauges were placed on the strong floor against the foundation block of the specimen to monitor any rotation of the specimen during testing. These dial gauges were positioned 7 in. from each end of the foundation block. A third dial gauge was placed to monitor any sliding of the specimen during testing.

5.4: Test Method

Load was applied slowly while watching for any indication of failure of the specimen including flaking of the whitewash. A display of the load versus strain response was monitored during the test. The test was discontinued when the specimen reached the maximum load it was able to resist. After Test-1 was completed, the specimen was turned

end-for-end and the same procedure was repeated for Test-2 on the opposite end of the specimen.

5.5: Test Results and Analysis

Both specimens failed in a similar manner. Figures 5.4 and 5.5 show photographs of the Test-1 specimen at maximum applied load. Figures 5.6 and 5.7 show photographs of the Test-2 specimen at maximum applied load. The maximum lateral load the 30 in. length specimen was able to resist was 360 kips and 350 kips for Test-1 and Test-2, respectively. The splice plate connection did not fail at that maximum applied load. Figures 5.8 and 5.9 show the load versus strain relationships along the connection (strain gauges above the splice plate) for Test-1 and Test-2, respectively (see Fig. 5.3 for the strain gauge layout). Following the maximum load, the hydraulic pump was continuously pumped, resulting in the deformation increasing and the load dropping off. It is evident from Figs. 5.8 and 5.9 that a dramatic increase in strains (very large non-linear load-strain behavior of the connection) was observed after a lateral load of 310 kips and 300 kips was attained in Test-1 and Test-2, respectively. The dual-plate section started displacing laterally in the out-of-plane direction after a lateral load of 310 kips and 300 kips was developed in Test-1 and Test-2, respectively. Due to this out-of-plane displacement, measured strains in gauges J13 and J14 changed from compressive to tensile (see Figs. 5.8 and 5.9).

No undesirable behavior was observed until a lateral load of 300 kips. At 300 kips, the 3/16-in. shear wall plate would have developed a shear stress of 26.7 ksi (300 kips/ [2 x 3/16 in. x 30 in.]). Hence, a shear stress of 26.7 ksi was deemed to be acceptable for a horizontal splice connection prior to failure. The 26.7 ksi stress is 0.9 times the nominal shear strength of the 3/16 in. plates used for the test, which is equal to 30 ksi ($0.6*F_y$). At a lateral load of 300 kips, the maximum strain measured at the dual-plate section from Test-1 was 560 $\mu\epsilon$ (approximately 0.25 ε_y). At a lateral load of 300 kips, the maximum strain measured at the dual-plate section from Test-2 was 830 $\mu\epsilon$ (approximately 0.37 ε_y)

at strain gauge J12. The strain gauge J12 in Test-2 behaved differently from Test-1 and the strains increased more rapidly than the other strain gauges in Test-2. At a lateral load of 300 kips, the maximum strain measured at the other strain gauges in Test-2 was 380 με (approximately 0.17 ε_y).

Figures 5.10 and 5.11 show the load versus strain relationships along the strain gauges below the splice plate for Test-1 and Test-2, respectively. The bottom strain gauges measured larger strains than the top strain gauges which were 6.25 in. directly above them. Furthermore, along the line from J1 to J4 or J8 to J11, the strains generally increased with an increase in applied shear.

The dial gauge readings indicated that the rotation of the foundation block was very minimal (0.01 in. over a length of 154 in.) in Test-1 while it was 0.18 in. over a length of 154 in. in Test-2.

5.6: Conclusion

The splice plate connection did not fail during the test (until an equivalent stress of 31.1 ksi on the shear wall plates when compared to the nominal shear strength of 30 ksi of the steel plates). The dual plate assembly displaced laterally in the out of plane direction at a shear stress of 26.7 ksi on the shear wall plates probably because of eccentricity in the alignment of specimen and loading set-up. Hence, an average stress of 26.7 ksi was observed to be acceptable for the horizontal splice plate connection prior to failure. This is slightly less (0.89 times) than the nominal shear strength of the 3/16 in. plates used for the test, which is equal to 30 ksi ($0.6*F_y$).

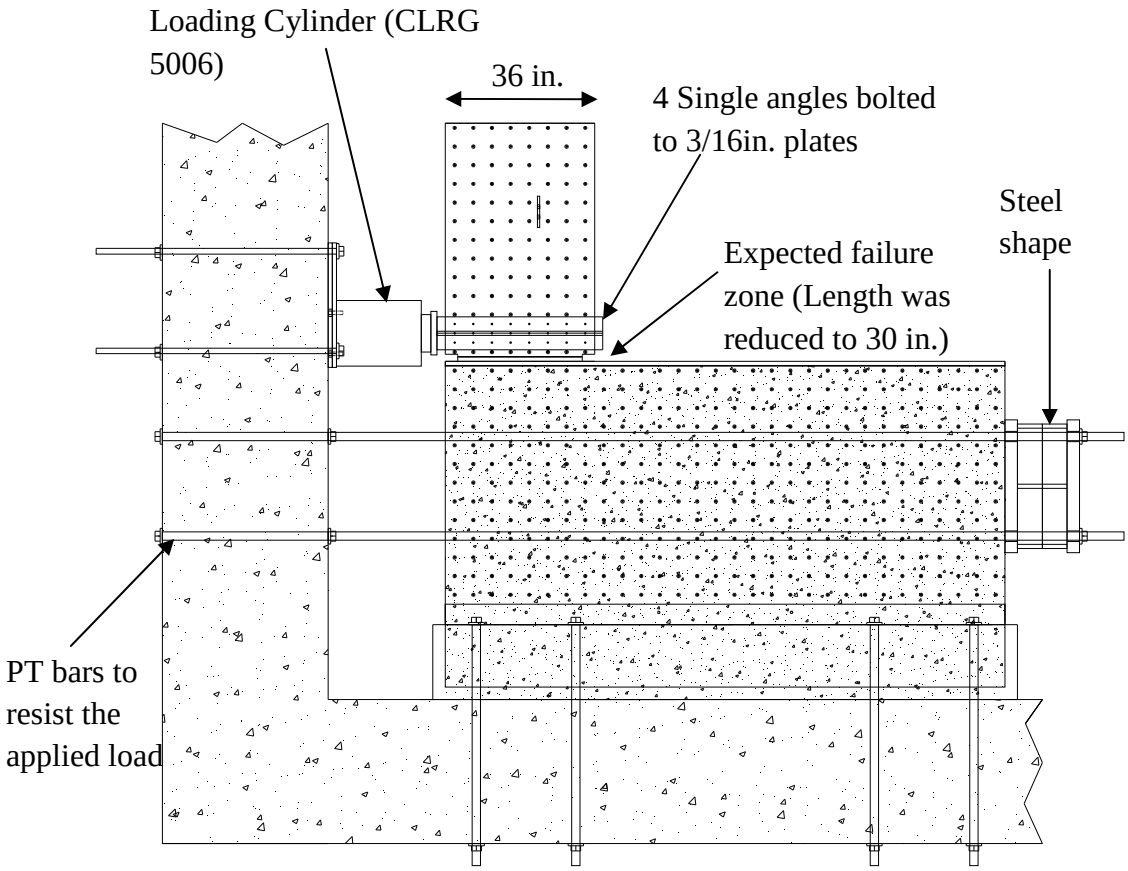

Figure 5.1 Test set-up for the Horizontal Connection Test - Side View

Steel shape	PT bars to resist the applied load	T-Sections bolted to plate assembly	Loading Cylinder (CLRG 5006)

Figure 5.2 Test set-up for the Horizontal connection test

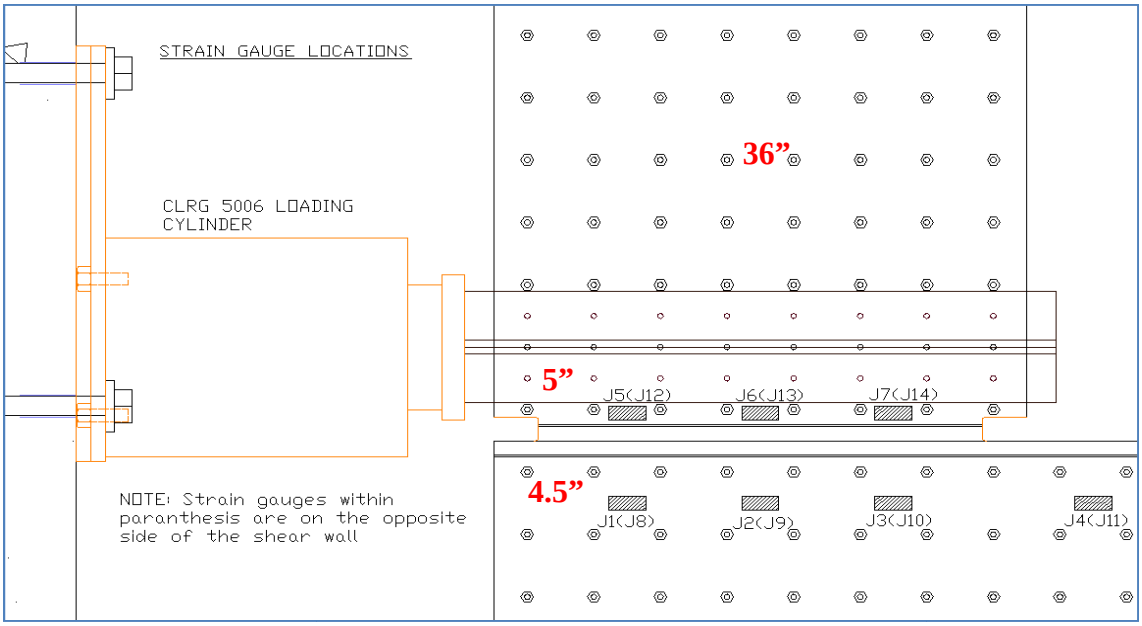

Figure 5.3 Strain gauge locations for Horizontal Connection Test - Side View

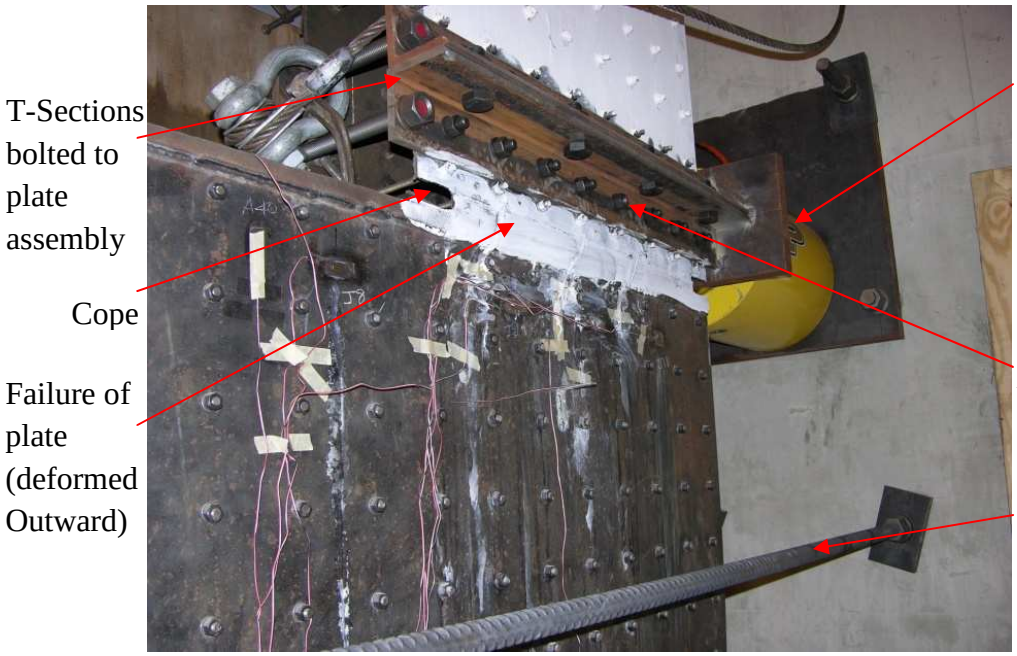

Figure 5.4 Failure of the Horizontal Connection - Test-1: View 1

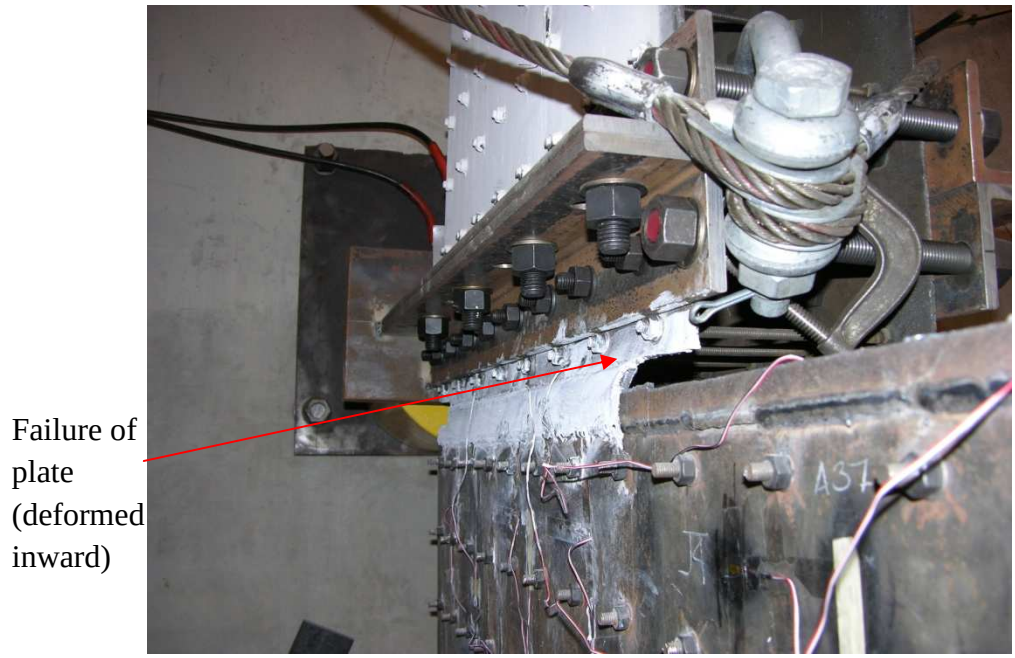

Figure 5.5 Failure of the Horizontal Connection - Test-1: View 2

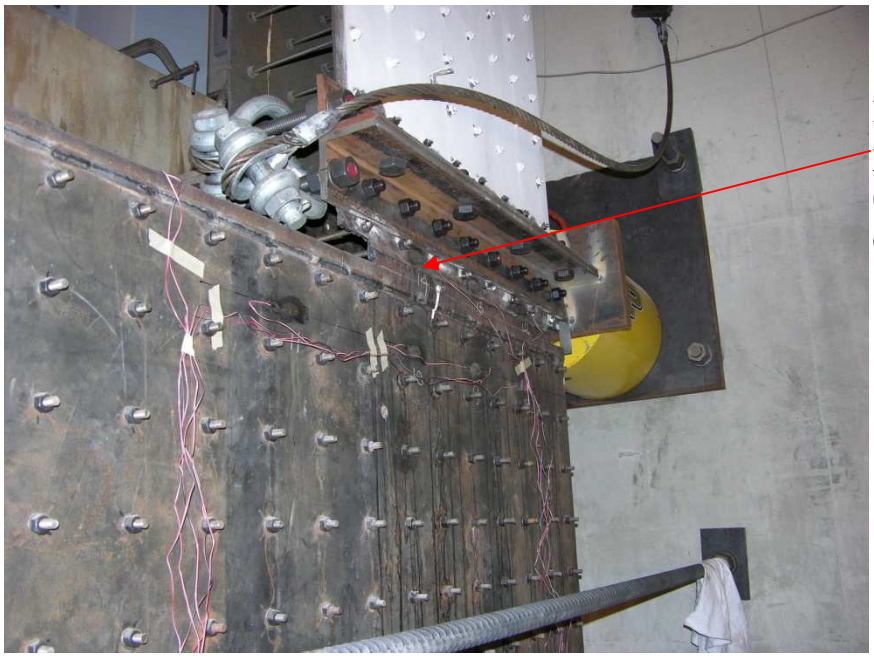

Figure 5.6 Failure of the Horizontal Connection - Test-2: View 1

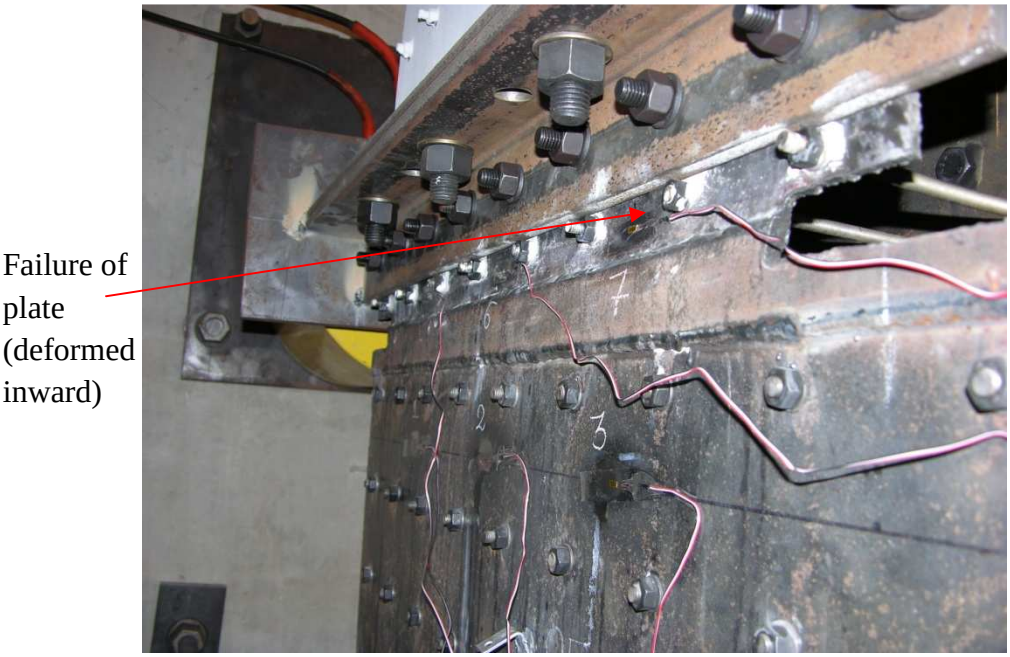

Figure 5.7 Failure of the Horizontal Connection - Test-2: View 2

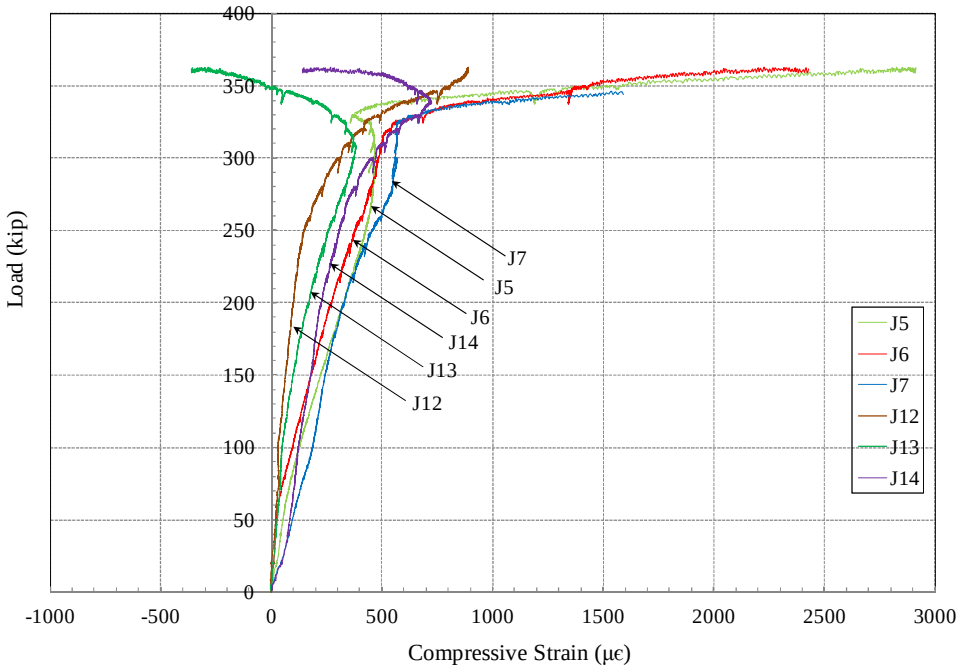

Figure 5.8 Load versus strain - along horizontal connection- Test 1

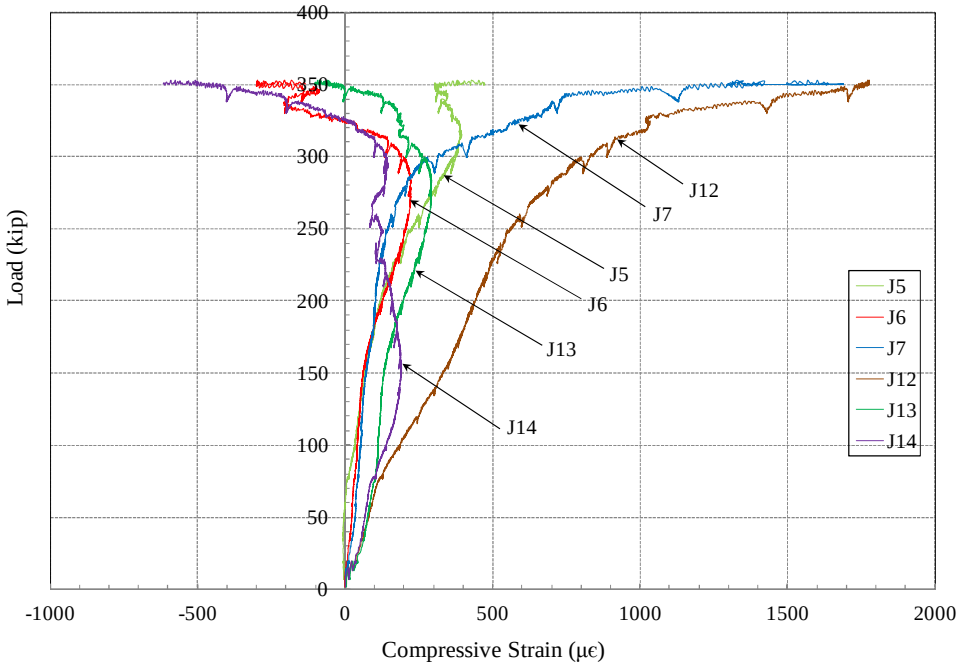

Figure 5.9 Load versus strain - along horizontal connection- Test 2

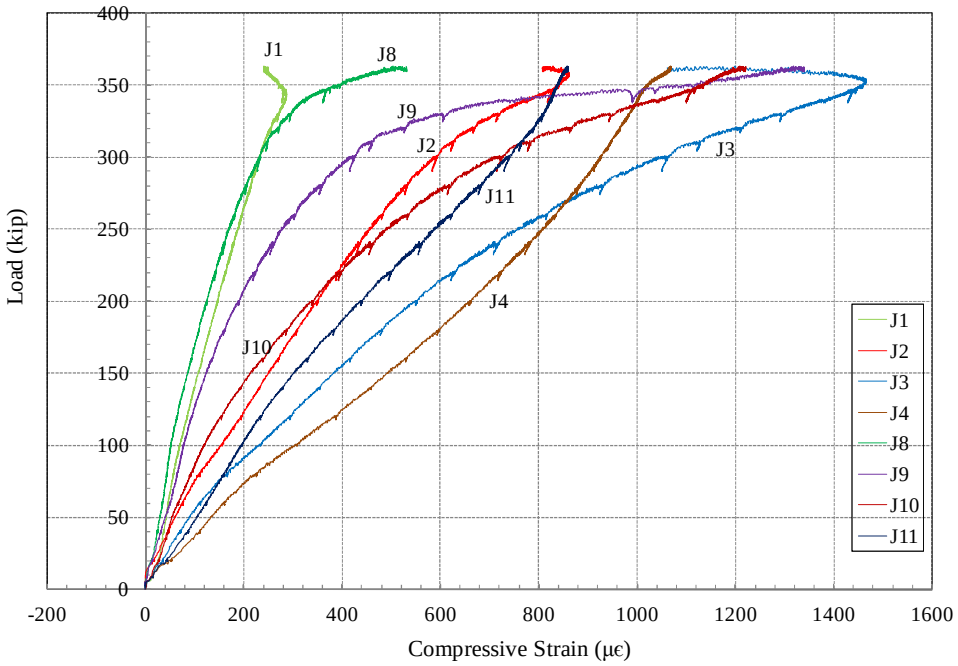

Figure 5.10 Load versus Strain - On the composite section- Test 1

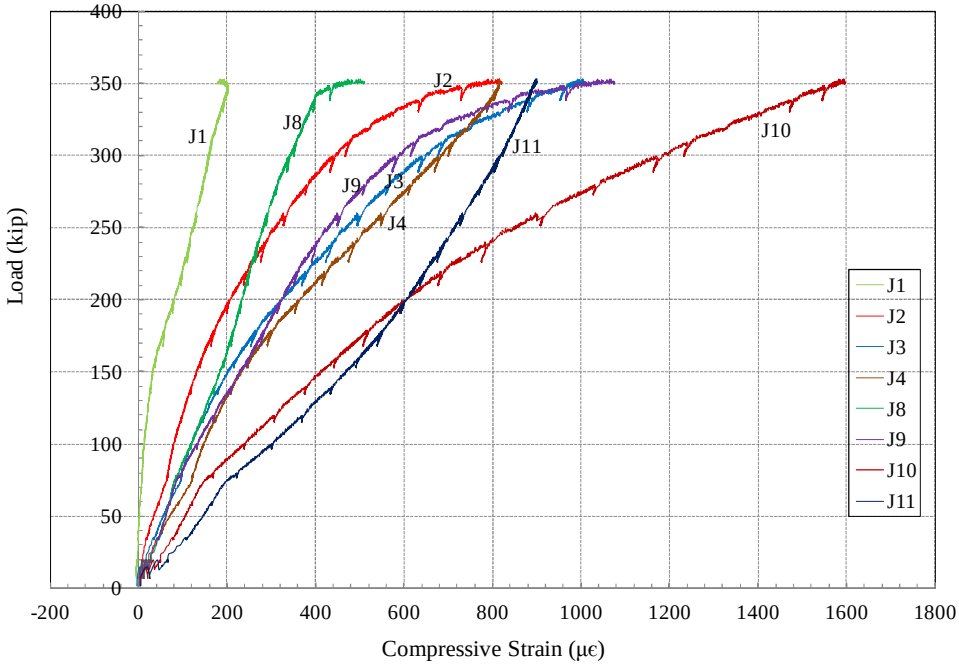

Figure 5.11 Load versus Strain - On the composite section- Test 2

CHAPTER 6: BEHAVIOR OF DUAL-PLATE COMPOSITE SHEAR WALL FOR CYCLIC LOADING

6.1: Introduction

Shear wall systems are designed primarily to resist the cyclic lateral load resulting from wind and earthquakes, while also resisting the axial load from the gravity-load system that frames into the shear wall. The lateral load capacity and ductility of the shear wall both need to be considered when designing for cyclic lateral load. The moment developed due to the cyclic lateral load generates cyclic tension and compression stresses in the vertical fibers of the shear wall. In the dual-plate composite shear wall, the steel plates can resist tension until they fail by tensile fracture, and they can resist compression until buckling occurs. The concrete infill can resist compression until it fails by crushing and can resist tension until it cracks. This chapter presents the results of an experimental investigation of the behavior of steel plates connected by transverse bars with concrete infill in the dual-plate composite shear wall construction.

An intersecting dual-plate composite shear wall element with a T-shaped configuration, rather than a planar configuration which was used in the stability test, was selected in order to include the investigation of the behavior of the connection at the intersection of the two wall elements. Furthermore, the specimen was selected so that the wall section was symmetric about the direction of lateral loading to minimize twisting. Geometries with an I-shape, T-shape (half portion of an I-shape) and C-shape (combination of two L-shapes to be symmetric) were initially considered. Moment-curvature diagrams were developed for each geometry to understand the behavior of each shape for static lateral load and the maximum load that would be needed to be applied during the laboratory test. Development of moment-curvature diagrams of these three

shapes is described in Section 6.2. The results indicated that the I-shape possessed a much larger moment for a particular curvature compared to the T-shape or C-shape. Therefore, the I-shape was eliminated early in the selection process because a loading set-up with a very large load capacity would be needed for the laboratory test. Of the T-shape and C-shape, the T-shape was selected for the testing program due to time and budgetary limitations – the C-shaped wall would have necessitated a more complex loading set-up to restrain or accommodate testing of the specimen.

The behavior of a T-shaped composite shear wall under cyclic lateral load was experimentally investigated. A 3/8-scale model of a 5-1/2 story composite shear wall element was fabricated in the laboratory. Specific items investigated during testing include (1) the vertical connection between the two intersecting wall elements, (2) the horizontal splice plate connection between adjacent plate assemblies, (3) the connection between the specimen and the foundation, and (4) the elements used to transfer load to the concrete foundation. Development of moment-curvature diagrams and a detailed description of the laboratory test are presented in the following sections of this chapter.

6.2: Preliminary Analysis (Moment-Curvature Diagrams)

Initially, moment-curvature diagrams of the I-shaped, T-shaped and C-shaped intersecting dual-plate composite shear walls were developed. Different shapes of the shear walls in a prototype building plan in Seattle, WA are illustrated in Fig. 6.1. Force equilibrium equations were used assuming strain linearity over the cross section of the shear wall to develop the moment-curvature diagrams. Because cyclic loading was applied during the laboratory test, moment-curvature relationships were developed in both loading directions (for the outer end of the web in compression and the outer end of the web in tension).

After the selection of the T-shaped wall for the laboratory test, as mentioned in Section 6.1, moment-curvature diagrams for the T-shape were developed for a range of possible material properties.

6.2.1: Moment-Curvature Diagrams for Different Shapes of Intersecting Wall Elements

Dimensions of the 3/8-scale model of the T-shaped intersecting wall element specimen are shown in Fig. 6.2. The T-shaped specimen is made up of a 90 in. wide flange and a 63 in. deep web. One end of the web intersects with the flange at the middle of the flange width. The 3/8-scale I-shaped wall is made up of a 126 in. deep web and 90 in. wide flanges at both ends of the web. Lastly, the C-shaped wall is made up of 99 in. wide flange and 63-in. deep webs at both ends of the flange (the outer sides of the webs align with the ends of the flange).

Two cases of loading were considered: (a) stem in compression – the strong direction and (b) stem in tension – the weak direction. An elastic-perfectly plastic bilinear stress-strain response with yield strength of 50 ksi (design yield strength) was assumed for the steel plates. The Hognestad model (MacGregor and Wight, 2005) was used to represent the stress-strain compressive strength of the concrete. The maximum compressive stress of the concrete was taken to be 6 ksi (f'_c = 6 ksi).

Moment curvature diagrams of for the I, C and T-shaped walls are shown in Fig. 6.3. For the stem in compression, I, C and T-shaped walls had a maximum flexural capacity of 36,300 kip-ft, 13,300 kip-ft and 8,900 kip-ft, respectively. As mentioned in Section 6.1, the I-shape developed much larger moment for a particular curvature compared to either the T-shape or C-shape. Therefore, the I-shape was not selected for the laboratory testing. Finally, only the T-shape was selected in this research study because of time and money limitations.

6.2.2: Moment-Curvature Diagrams for the T-shaped Wall

The moment-curvature diagram for the T-shaped wall was developed using appropriate material properties for the steel plate and concrete. The design yield strength of the steel plate was 50 ksi, and the design compressive strength of the concrete was 10 ksi. The plate used for the cyclic loading test was ASTM A572 grade 50 steel. Stress-strain curves from the coupon tests of the 3/16-in. plates are shown in Fig. 6.4. The average yield strength and average tensile strength of the plate were 60.0 ksi and 70.1 ksi, respectively.

The moment-curvature diagram for the T-shaped wall was developed for two different cases: (a) elastic-perfectly plastic bilinear stress-strain response with a yield strength of 55 ksi for the steel plates and a maximum compressive strength of 10 ksi for the concrete (to predict the behavior based on the material properties considered for design) and (b) a tri-linear curve with a yield strength of 60 ksi and an ultimate strength of 69 ksi (as shown in Fig. 6.5) for the steel plates and a maximum compressive strength of 11.5 ksi for the concrete. The 55 ksi yield strength was calculated by multiplying the design yield strength of 50 ksi by a factor of 1.1 to account for strain hardening of the steel plates.

The concrete model generalized by Thorenfeldt et al. (1987), as reported by MacGregor and Wight (2005), for high-strength concrete was used for the stress-strain response of the concrete. The stress-strain graph developed using this model is shown in Fig. 6.6.

The moment-curvature diagrams for the T-shaped specimen (see Fig. 6.2) for case (a) and case (b) are shown in Figs. 6.7 and 6.8. For case (a), the peak moment capacity was computed to be 9,820 kip-ft when the web is in compression and 4,990 kip-ft when the web is in tension. For case (b), the peak moment capacity was computed to be 10,790 kip-ft when the web is in compression and 6,040 kip-ft when the web is in tension.

6.3: Design of Specimen for the Laboratory Test

The behavior of intersecting wall elements for cyclic lateral load was experimentally investigated using a 3/8-scale cantilever T-shaped composite wall which was anchored to the laboratory strong floor via a 3-ft deep foundation block. A cross section of the T-shaped intersecting wall specimen (3/8-scale of prototype) is shown in Fig. 6.2. The specimen had a 90-in. long flange and a 63-in. long web with a uniform wall thickness of 9-inces. The side and plan views of the test set-up are shown in Figs. 6.9 and 6.10, respectively. The specimen height was 319.5 in. (26'-7 1/2") above the foundation connection plate. The foundation block was 3-ft high and the foundation connection plate extended 5 in. above the foundation block. Hence, the total height of the specimen measured from the strong floor was 360.5 in. (30'-½").

6.3.1: Selection of Plate Assembly Details

Details of individual plate assemblies, except for the wall geometry, were kept the same as those used in the stability test. A T-shaped wall specimen (as shown in Figs. 6.9 and 6.10) was used in this cyclic loading test while a planar plate assembly was used in the stability test (as shown in Fig. 3.15). Refer to Section 3.3.1.2 for the plate assembly details. A plate thickness of 3/16 in., a transverse bar diameter of 3/8 in., transverse bar spacing of 4-½ in., and a wall thickness of 9 in. were used for the cyclic loading test.

It was decided to build a specimen approximately 5-1/2 stories tall (where the story height is 58.5 in. in 3/8-scale). The height of the specimen was determined as follows:

1. The specimen should be sufficiently tall so that failure will be dominated by flexural behavior and not shear. A specimen with a height of at least three times the specimen depth was expected to develop significant flexural behavior under cyclic loading. The depth of the specimen was 6 ft.

2. The hydraulic rams used to apply lateral load should have sufficient capacity and stroke. A target 3% maximum drift for the specimen was considered. When the height of the specimen is increased, the required load is decreased but the required stroke of the rams is increased. In addition, when the specimen is pushed laterally in the strong direction the elongation of the PT bars in the loading system will use up a portion of the available stroke of the rams.

3. The horizontal PT bars used to pull the specimen towards the laboratory strong wall (Figs. 6.9 and 6.10) can have a maximum diameter of 1-¼ in. due to the size of the hole openings in the strong wall. Moreover, the tension force in the PT bars was limited to prevent repeated-load damage to the PT bars. Hence, it was determined that a maximum tension force of 112.5 kips ($0.6\ f_{pu}\ A_{ps}$) could be safely applied to each PT bar for the anticipated 20 cycles of load.

4. The maximum moments needed to be applied in the strong and weak directions were estimated to be 10,790 kip-ft and 6,040 kip-ft, respectively (see Section 6.2.2).

To satisfy these requirements, it was decided that a specimen height of 27 ft above the top of foundation should be used with the lateral loading applied at a height of 25 ft (see Fig. 6.9). For a 25-ft loading height, a lateral load of 432 kips and 242 kips were expected to be needed in the strong and weak load directions to achieve peak moments of 10,790 kip-ft and 6,040 kip-ft, respectively. A displacement equal to 9 in. at the top of the wall was needed to attain the target drift ratio of 3%.

6.3.2: Weld Joint between the Shear Wall Plate Assemblies and Foundation Connection Plate

The weld joint between each 3/16-in. shear wall plate and 3/4-in. foundation connection plate was used to transfer forces from the shear wall plate to the foundation connection plate. The fillet weld size (7/16 in.) was designed for the forces developed by tensile fracture of the shear wall plate. Innershield NR-232 flux-cored self-shielded (FCAW-S) wires (AWS E71T-8, 70 ksi F_{EXX}) from Lincoln Electric were used to make the weld joint. Only the static material properties, rather than the cyclic material properties of the steel plate and weld, were considered for weld design. Furthermore, an alternate welded connection was also proposed to be used for this connection if the fillet weld joint were to fail during the cyclic loading test of the wall. The detailed design of the two weld connections and the cyclic behavior of the two connections are described in Appendix C.

6.3.3: Splice Plate Connection Details

The splice plate connection used in the test specimen was slightly different from that used in the stability test. In the stability test, splice plates were 3/16-in. thick with 3/16-in. fillet welds on the top and bottom of the splice plates. For the stability test, the 3/16-in. shear wall plates were not expected to yield. However, for the cyclic loading test, the 3/16-in. shear wall plates up to an elevation between the third and fourth stories were expected to develop large strains well beyond the yield strain. Hence, the fillet weld size had to be increased so that there would be no failure in the splice plate connection. The fillet weld was designed for the tensile strength of the shear wall plate. A 3/8-in. thick splice plate with 5/16-in. fillet weld on the top and bottom of the splice plate were used for the bottom three stories. A 3/16-in. thick splice plate with 3/16-in. fillet weld on the top and bottom of the splice plate were used for the top two levels.

6.3.4: Connection between the Web and Flange Plate Assemblies

The joint between the flange and web of the specimen is shown in Fig. 6.11. A single angle (L2-1/2 x 2-1/2 x 1/4 of A36 steel) was welded to the flange and web. Considering the forces in the flange to be transferred to the web for suitable shear flow, an angle thickness of 1/4 in. and a fillet weld size of 3/16 in. were used. The total force from the flange was transferred to the web via these welds and angles. The angles were welded to each side of the web along the specimen height. At every horizontal intersection of two plate assemblies, 1-1/2 x 1-1/2 x 1/4-in. bent plates were used to join the L2-1/2 x 2-1/2 x 1/4 angles from the plate assemblies above and below the joint (see Figs. 6.11 and 6.12). Bent plates rather than single angles were used so that they fit into the curved portion of the L2-1/2 x 2-1/2 x 1/4 single angles. The 3/8-in. threaded rods which would interfere with the L2-1/2 x 2-1/2 x 1/4 angles were filler-welded as shown in Fig. 6.11. Those threaded rods were 3/32 in. short of reaching the outer sides of the plate assembly.

6.4: Test Set-up

Following the calculation of maximum load that would need to be applied in each direction during the cyclic loading test, and the design of specimen details, the test set-up was designed and constructed so that the calculated load could be applied to the specimen and transferred to and resisted by the lab strong floor and strong wall. AutoCAD drawings of a side view and a plan view of the test set-up for the cyclic loading test are shown in Figs. 6.9 and 6.10. The test set-up had three main components: (a) the foundation block, (b) the specimen and (c) the loading system. They are detailed in the following subsections.

6.4.1: Foundation Details

The purpose of the foundation block was to transfer forces from the specimen to the strong floor. The size of the foundation was determined by considering the moment demand from the lateral load applied for failure of the wall specimen. The foundation was anchored to the strong floor using post-tensioned (PT) bars to resist uplift of the foundation during the test and to prevent slip between the foundation and strong floor when the maximum lateral load was applied.

Dimensions of the foundation block and locations of the PT bars are shown in Figs. 6.9 and 6.10. Plan and elevation views of the foundation block are shown in Figs. 6.13 and 6.14, respectively. In addition, Figs. 6.13 and 6.14 also show the location of the foundation connection plates, reinforcing bar hooks, shear studs, PT bars inside the specimen to apply the vertical load, and PT bars used to anchor the foundation block to the strong floor. These components are described later in this section.

6.4.1.1: Foundation block and post-tensioned bars

Using strut and tie models to establish a force path and calculating contact stresses between the foundation block and strong floor for maximum lateral load for the wall, it was determined that a 14’-long, 8’-wide, and 3’-thick foundation with 28 post-tensioned bars (PT bars) of 1-¾-in. diameter would be sufficient to resist a 10,790 kip-ft moment at the base of the wall (peak moment for strong direction of loading). Each PT bar was post-tensioned to 240 kips so that the total post-tensioning force would be 6720 kips from the 28 PT bars.

When a friction coefficient of 0.1 was considered between the foundation block, underlain with tar paper, and the smooth laboratory strong floor, the foundation block was expected to resist a total lateral load of 672 kips (6720 kips x 0.1 = 672 kips). From the moment curvature diagrams, the maximum expected lateral load on the specimen was

430 kips and 240 kips in strong and weak directions, respectively. The foundation block, which was cast in place, is shown in Fig. 6.15. The foundation connection plates, PT bars enclosed in plastic ducts and intended for applying vertical load, and the vertical reinforcing bars provided along the mid plane of the specimen can also be seen in Fig. 6.15.

6.4.1.2: Foundation connection plate

A foundation connection plate was welded to each shear wall plate and partially embedded in the foundation block to transfer the vertical and shear forces from shear wall plates to the foundation. A 7/16-in. fillet weld was used between each shear wall plate and 3/4-in. foundation connection plate. Refer to Section 6.3.2 for details of this connection. The shape, location, and dimensions of the foundation connection plates are shown in Figs. 6.13, 6.14, and 6.15. The total height of the foundation connection plate was 18 in., with the bottom 13 in. embedded in concrete.

The bending moment caused by the lateral load applied at the top of the specimen results in tension and compression in the vertical fibers at the bottom of the 3/16-in. plates. During the test, the 3/16-in. plates developed large strains well beyond yield. These vertical forces were transferred into the ¾-in. thick foundation connection plates, in addition to the shear developed from the lateral load.

Hence, the foundation connection plates were designed to resist the combined effects of tensile fracture of the shear wall plate and shear transferred to the foundation connection plates during the cyclic loading test. Based upon tensile coupons, it was determined that the yield strength and tensile strength of the 3/16-in. plates was equal to 60.0 ksi and 70.1 ksi, respectively. The maximum expected lateral load was 430 kips. Based upon the forces developed from tensile fracture of the shear wall plates and the shear transferred to the foundation connection plates, it was determined that the required thickness of the foundation connection plates need be 3/4 in. for A36 steel plate.

6.4.1.3: Reinforcing bar hooks

Number 7 reinforcing bar hooks were welded to the ¾-in. foundation connection plates to transfer the vertical forces from the 3/16-in. wall plates to the foundation via the foundation connection plates. Section 3.3.1.1 describes the weld details between the reinforcing bar hooks and the ¾-in. foundation connection plate. For the stability test, the reinforcing bar hooks were designed for the tension forces developed by yielding of the shear wall plates. However, for the cyclic loading test, the reinforcing bar hooks were designed for the tension forces developed by tensile fracture of the shear wall plates. It was determined that No.7 reinforcing bar hooks (of ASTM A706) welded on both sides of each foundation connection plate at a 4.5-in. spacing, instead of the 7-in. spacing used in the stability test, was needed to transfer the maximum expected tensile forces. See Figs. 6.13 and 6.14 for the layout of the reinforcing bar hooks. Figure 6.16 shows a photograph with the foundation reinforcement layout before casting, and Figs. 6.17 and 6.18 show reinforcing bar hooks welded to a foundation connection plate.

6.4.1.4: Shear studs

Shear studs welded to the ¾-in. thick foundation connection plate were designed to resist the maximum lateral load of 430 kips during cyclic load tests. See Figs. 6.13 and 6.14 for the locations of the shear studs. Headed shear studs of 3/4-in. diameter (S3L 3/4-in. diameter and 4-3/16-in. long MS shear studs) were welded to each 3/4-in. steel connection plate on both sides, three shear studs in a vertical line at a horizontal spacing of 18 in. Fig. 6.17 shows a portion of the foundation reinforcement with shear studs welded to a foundation connection plate.

6.4.1.5: Reinforcement

The minimum reinforcement consisted of No.4 bars and No.3 stirrups to resist shrinkage and uplift forces on the foundation block (see Figs. 6.14 and 6.16).

Temperature and shrinkage reinforcement equal to $0.0018A_g$ (A_g is the cross-sectional area of the concrete block), as required by ACI 318-08 (Section 7.12 of ACI 318-08), in both horizontal directions was provided. Reinforcement in the vertical faces of the foundation block was provided to distribute cracking of the concrete in the vertical faces and to provide confinement to the foundation concrete (see Fig. 6.16).

Figures 6.13 and 6.14 show AutoCAD drawings with spiral reinforcement provided to prevent concrete splitting due to post-tensioning of the foundation PT bars. Figure 6.17 shows a photograph of the foundation reinforcement with spirals around PVC pipes. The amount of spiral reinforcement was calculated using the strut-and-tie method (Edward G. Nawy, 2006). Number 4 reinforcing bar spirals of standard grade 60 steel with outside diameter of 10 in., pitch spacing of 3 in. and height of 24 in. were used for the spiral reinforcement around each PT bar.

Vertical reinforcing bars (No. 6 reinforcing bars), at 9-in. spacing, were provided at mid-thickness of the shear wall to provide additional shear resistance. However, this vertical reinforcement in the test program was not considered in the design for shear resistance at the base of the wall. Figure 6.13 shows the AutoCAD drawing with locations of the vertical reinforcing bars and Fig. 6.15 shows a photograph of the cast foundation block with the reinforcing bars extending out from the foundation block. The vertical reinforcing bars were extended to 3 ft above the top of the foundation.

6.4.1.6: Vertical load applied by post-tensioned bars

Vertical load was applied to the specimen by eight 1-3/8-in. diameter PT bars. Calculation of vertical load and the selection of the PT bars are described in Section 6.4.3.3. The 1-3/8-in. diameter PT bars enclosed in corrugated plastic ducts were installed in the center of the specimen. The plastic ducts had an outside diameter of 2-7/8 in. and an inside diameter of 2-9/32 in. The PT bars were threaded into washer plates with exit

pipes and nuts at the bottom of the PT bars. Figures 6.9, 6.10, and 6.14 show locations of the PT bars in the foundation block.

Because it would have been difficult to support each of the 33-ft long PT bars (which extend to the top of the specimen) while casting the foundation, 8-ft long PT bars were placed while casting the foundation (see Fig. 6.16). The bottom of the PT bars and the inside surface of the nuts were greased so that the 8-ft long PT bars could be replaced with 10-ft long PT bars after casting the foundation block so that the PT bars would extend above the first story after casting. Figure 6.18 shows a photograph of the washer plate attached to the bottom of the PT bar encased in plastic duct.

6.4.1.7: Casting of foundation concrete block

The foundation block was cast in place. A target concrete cylinder strength of 6,000 psi was needed for the foundation block. The 28-day cylinder strength of the foundation concrete reached 7,700 psi.

Several measures were taken to keep the foundation plate assemblies in place while casting the concrete. Plates of 1/2-in. thick and 9-in. width were welded between the two foundation connection plates to keep them at the specified spacing (see Fig. 6.19). The foundation plate for the web of the wall was tack welded to the foundation plate for the flange of the wall. The plastic ducts around the PT bars (intended for applying vertical load) were secured in position using two steel bars around the ducts as shown in Fig. 6.20. The foundation plate assembly was supported by reinforcing bar chairs which were placed between the No.7 hooked bars and the strong floor. Wood shims glued under those reinforcing bar chairs were used to position the top of the foundation connection plate at the required level. Figure 6.21 shows the formwork before casting the foundation block. The PT bars enclosed in plastic ducts were secured in place using a wood frame attached to the PT bars and the foundation formwork.

6.4.2: Fabrication of steel plate assemblies and specimen

Following fabrication of the foundation block, the specimen was fabricated on top of the foundation block. The first four stories were cast story by story and the remaining 1-1/2 story was cast in one operation. The selection of specimen details and the design of the specimen have been described in Section 6.3. The following sub-sections describe fabrication of the plate assembly and the specimen.

6.4.2.1: Fabrication of steel plate assemblies

The same general fabrication method used to make the steel plate assemblies (panel assemblies) for the stability test (see Section 3.3.1.2) was also used for the cyclic load test. Filler welds were used to connect the transverse steel rods to the steel plates at the intersections of the web and flange plate assemblies as described in Section 6.3.4 and Fig. 6.11. Figure 6.11 shows the locations of filler welds at the intersection of web and flange panel assemblies. Threaded rods were positioned half-way through the 3/16-in. plates (3/32 in. shy of the outer surface of the 3/16-in. plates). The space between the end of the threaded rod and the outer surface of the 3/16-in. plate was filled with weld metal, and the excess weld material on the steel plate surface was ground off so that the steel angles (L2-1/2x2-1/2x1/4 in.) could be mounted on a smooth, flat surface. Figures 6.22 and 6.23 provide photographs of a web panel assembly and a flange panel assembly. The filler welds to connect the transverse steel rods to the steel plates can also be seen in Figs. 6.22 and 6.23.

Small, 3/16-in. thick guide plates were tack welded to the inner side of the plate assembly to facilitate erection of the plate assemblies (see Section 3.3.1.2). Concrete strain gauges were installed. The type and locations of concrete strain gauges are described in Section 6.5.5. A total of 12 steel plate assemblies, six web assemblies and six flange assemblies, were fabricated. Five web assemblies and five flange assemblies were 58.5-in. tall, and one web assembly and one flange assembly were 27-in. tall.

6.4.2.2: Fabrication of specimen

Figure 6.15 shows a photograph of the foundation block with foundation connection plates. PT bars were enclosed in ducts, and vertical dowel bars extended from the foundation block. The 8-ft long PT bars were replaced with 10-ft long PT bars after casting the foundation block (see Section 6.4.1.6 for details). The specimen was erected on top of the foundation block. Figure 6.24 depicts the first story panel assembly erected on top of the foundation block. The plate assembly was placed between the foundation connection plates so that the bottom 4 in. of the plate assembly was inserted into the foundation connection plates. The spacing between the foundation connection plates was 9 in. The steel plate assembly fit tightly between the foundation connection plates, and helped to ensure that the plate assembly remained in position as it was leveled vertically and horizontally.

6.4.2.2.1: Joint between the foundation connection plate and the shear wall plate

A 7/16-in. fillet weld was used to connect each ¾-in. thick foundation connection plate to a 3/16-in. shear wall plate (see Section 6.3.2 for the design criteria for this weld). Innershield NR-232 flux-cored self shielded (FCAW-S) wires (E71T- 8, 0.068 in. dia.) from Lincoln Electric were used to deposit the 7/16-in. fillet weld. The Lincoln Electric Company product catalog (2010 C1.10) claims that this electrode meets AWS D1.8 seismic lot waiver requirements and can be used for all welding positions in mild steels.

The 7/16-in. fillet weld for the shear wall specimen was achieved with three passes. After each weld pass, the weld locations with any discontinuities were back gouged (by grinding). The voltage, amperage, and the speed of each weld pass were recorded and are summarized in Table 6.1. After welding, the actual size of the weld was measured every 6 in. along the length of the weld. The average sizes of the fillet weld for different parts of the connection are shown in Table 6.2. The fillet welds were made in

short increments (stitch welding) at various locations along the plate to minimize local heating and warping of the plates.

6.4.2.2.2: Joint between the flange and web of the specimen

Design of the joint between the flange and web of the specimen has been described in Section 6.3.4. Refer to Fig. 6.11 for an AutoCAD drawing of the joint and Fig. 6.24 for a photograph of the first story panel assembly with the joint at the corner. A single angle (L2-1/2x2-1/2x1/4 of A36 steel) was welded to the 3/16-in. plates of the flange and web.

The 3/16-in. vertical weld along the joint between the L2-1/2x2-1/2x1/4 in. steel angles and the 3/16-in. shear wall plate (refer to Fig. 6.11) was made with Innershield NR-232 flux-cored self-shielded wires and E7018 electrodes. Initially, Innershield NR-232 flux-cored self-shielded wires were intended to be used for the entire length (57.5 in.) of this vertical weld. For the upper part of this vertical weld (40-3/8 in. the west side and 47 in. the east side), the Innershield NR-232 flux-cored wire resulted in a uniform weld. However, for the lower part of the weld (17-1/8 in. the west side and 10-1/2 in. the east side), the Innershield NR-232 flux-cored wire could not produce a uniform weld. Difficulty in maintaining the desired angle of the electrode with the weld line (for the upper and lower parts) might have been a possible reason for this behavior. Therefore, E7018 sticks were used for the lower part of the vertical weld.

When the Innershield NR-232 flux-cored wire was used for the upper part, the 3/16-in. weld was made with one weld pass. The voltage and amperage of the weld pass were 19.9V and 144~175 AMP, respectively. When the E7018 stick was used for the lower part, the 3/16-in. weld was made with one weld pass. The voltage, amperage, and the speed of the weld pass were 15~28.5V 103~105 AMP, and 3.5 in./min, respectively. The average sizes of the fillet weld for different parts of the joint are tabulated in Table

6.3. The average effective throat of the fillet weld was 0.140 in. while the designed effective throat of the fillet was 0.133 in.

6.4.2.2.3: Closure plates and concrete casting

The 3/16-in. closure plates as shown in Figs. 6.2 and 6.24 were welded to all three ends of the specimen to simulate the field conditions. The weld to attach the 3/16-in. closure plates to the 3/16-in. shear wall plates was made using NR-232 flux-cored wires. The closure plate acted as formwork that could resist the hydraulic forces of wet concrete during casting. Tack welds of 1/8-in. leg size and ½-in. long at 6-in. spacing were placed to attach the closure plates to the panel assembly.

The plastic ducts around PT bars were positioned in the center of the plate assembly by placing reinforcing bars at the sides of the ducts and tying those reinforcing bars to the ducts and the threaded rods (see Fig. 6.25). The PT bars were also positioned in place using a wooden frame as shown in Fig. 6.21. After caulking along the joint between the closure plates and the shear wall plates, concrete was placed in the plate assembly. The design strength of the concrete was 10,000 psi. The 28 day strength of the concrete was 9,360 psi and the strength of the concrete on the day of testing (246 days ≈ 8 months) was 11,480 psi.

6.4.2.2.4: Horizontal splice plates and bent plates at the horizontal joint

Three days after casting the first story, continuous, 3/8-in. thick horizontal splice plates were tack welded to the outer side of the plate assembly. Then the pair of second-story steel plate assemblies was mounted on top of the pair of first-story plate assemblies. The 3/8-in. thick splice plates were welded to join the first and second-story steel plate assemblies. As described in Section 6.3.3, a 5/16-in. thick fillet weld was provided

between the splice plate and the 3/16-in. thick shear wall plate. Innershield NR-232 flux-cored wire was used for this weld.

Closure plates for the first and second story were joined together by tack welding 3/16-in. thick splice plates. At the horizontal intersection of the two plate assemblies, L1-1/2 x 1-1/2 x 1/4-in. bent plates were used to join the L2-1/2 x 2-1/2 x 1/4 angles from the plate assemblies above and below the joint (refer to section 6.3.4 for the details of this joint).

6.4.2.2.5: Fabrication of second to sixth story of the specimen

The erection procedures used in the remaining stories were similar to those used in the first story. As mentioned above, the first four stories were cast story by story and the final 1-1/2 story was cast together. However, Dual Shield II 70 Ultra flux-cored wire (from ESAB) instead of Innershield NR-232 flux-cored wire was used for all welding beyond the joint between the first and second story panel assemblies. Dual Shield II 70 Ultra flux-cored wires were selected because it produces a good weld with greater ease, and because of the availability of the wire in smaller diameters (0.045-in. dia.).

Plate tabs (3/8-in. thick and 4.5-in. deep and 5-in. wide) were fillet welded to the plate assembly on the outside surface to facilitate the installation of the platform for the work crew to stand and work. Totally, 10 plate tabs around the specimen were welded at each story level. Figures 6.26 and 6.27 show a photograph of the specimen prior to casting the second and third stories, respectively. The steel angles were bolted to the plate tabs and the platform was bolted to the steel angles.

A total of eight 1-3/8-in. diameter PT bars were used to apply the vertical load (see Section 6.4.1.6 for the details of these PT bars). After casting the first story, two 10-ft long PT bars (see Fig. 6.15) located at the far end of the flange panel assembly were

replaced with 20.5-ft long PT bars. The remaining six 10-ft long PT bars were replaced with 18.5-ft long PT bars.

If the two vertical PT bars at the far end of the flange panel assembly were continuous, they would intersect with the horizontal PT bars used to apply lateral load (see Section 6.4.3.3 for details). Hence, these two vertical PT bars were post tensioned at the third story level and discontinued above the third story level. After the concrete cast in the third story had achieved sufficient strength, these two PT bars were post tensioned and sealed so that the PT bar would not be exposed to the concrete.

Due to dimensional limitations associated with use of the overhead crane, it was not possible to place the panel assemblies over the vertical PT bars that extended 30.5 ft above the foundation block. Hence, each of these six vertical PT bars (3 in the web and 3 in the flange) were cut into two pieces and coupled at the third story level. Figure 6.28 shows the five PT bars in the flange section. It shows two discontinued PT bars at the end of the flange and three continuous PT bars located between those two discontinued PT bars.

The hardware used for the two discontinued vertical PT bars is shown in Fig. 6.29. After the concrete in the third story had cured, the duct was cut to the level of the top of the concrete, hydrostone was applied on top of the concrete, and the PT bar washer plate was positioned on top of the hydrostone and leveled. After the hydrostone hardened, the PT bar was post-tensioned, and the box made of sheet metal was attached (welded and caulked) to the washer plate covering the PT bar nut. The PT bar duct was inserted into the box via the top of the box, and the joint between the duct and the box was sealed. Steel plate, box, and part of the plastic duct were then covered with duct tape to protect the caulk from the mechanical force resulting from concrete casting in the next story. The PT bar and the duct were extended to 30 in. and 33 in. above the third story level, respectively. The duct was sealed at the top to prevent concrete leakage into the duct. A photograph of this hardware is shown in Figs. 6.30 and 6.31.

An AutoCAD drawing of the coupler joint used for the six spliced PT bars is shown in Fig. 6.32. After concrete had been cast to the third story level, the upper end of each continuing PT bar was coupled using a coupler from DSI (Dywidag-Systems International). The bottom PT bars extended 5-7/8 in. above the third story level while the top PT bars extended up to 30.5 ft above the 3-ft tall foundation (which is 3 ft above the top of the 5-1/2 story specimen). The joint between the PVC pipe and the PT bar duct was tightly sealed using glue, caulk, and duct tape. The six coupled vertical PT bars (to apply vertical load) were later post-tensioned at the top of the shear wall (at a height of 30'- 0.5" above the strong floor). A photograph of this coupler which was in the process of completion is shown in Fig. 6.30 and the completed hardware is shown in Fig. 6.31.

Above the third story level, the splice plate connection at the horizontal intersection between two plate assemblies (fourth story-to-fifth story joint, and fifth story-to-sixth story joint) was made using a 3/16-in. thick splice plate and 3/16-in. fillet welds as detailed in Section 6.3.3. Four 4-1/2-in.-diameter holes in the fifth and sixth story flange plate assembly were made for the purpose of accommodating a horizontal loading apparatus for loading towards the strong wall. This is detailed in Section 6.4.3.1. A photograph of the completed specimen is shown in Fig. 6.33. For the purpose of sense of scale, the distance between the holes on the strong wall is 2 feet.

6.4.3: Load Set-up

The calculated flexural capacity of the T-shaped specimen was 10,790 kip-ft and 6,040 kip-ft in the strong direction (towards strong wall/ towards south) and weak direction (away from strong wall/ towards north), respectively. For a 25-ft loading height, 430 kips and 240 kips of lateral load were needed to be applied in the strong and weak directions to achieve the anticipated peak moment capacities. A displacement of 9 in. was needed at this height to attain the target drift ratio of 3%. Furthermore, an axial compression load of approximately $0.1A_g f_c'$, equal to 1380 kips, was applied with the PT bars to simulate gravity load on the wall specimen.

6.4.3.1: Loading in the strong direction (towards strong wall)

The load set-up for the cyclic loading test is illustrated in Figs. 6.34 through 6.36. Eight PT bars with a loading ram at each end of the PT bar were used to push the specimen towards the strong wall. The load applied by the hydraulic rams was transferred to the strong wall via the horizontal PT bars. Four hydraulic rams at a 24-ft height and the other four at a 26-ft height from the top of foundation, with a total capacity of 1280-kip, were used to push the specimen in the strong direction. The middle four rams were Enerpac- RRH 1006 double-acting hollow plunger cylinders (effective area = 20.63 in^2) with a load capacity of 200 kips and a stroke of 6 in. The other four rams were Power Team- RH 605 double-acting hollow plunger cylinders (effective area = 12.31 in^2) with a load capacity of 120 kips and a stroke of 5 in. All eight of these rams were extended using one double-acting pump so that the pressure in each ram would be the same. Hence, the ratio of load at applied by Enerpac- RRH 1006 cylinders to the load applied by Power Team- RH 605 cylinders was 20.63 to 12.31.

Communication with Dywidag-Systems International indicated that the PT bars should not be loaded to more than 60% of their ultimate strength if they were to be loaded repeatedly for approximately 20 cycles. For a lateral load of 430 kips, the middle four PT bars would reach a maximum stress level of approximately 29% of ultimate strength. Hence, the upper stress limit for the repetitive loading was not obtained.

The loading channels (C-channels joined by plates welded to their legs) between the hydraulic rams and the specimen helped to distribute the applied load across the flange of the specimen and to minimize bending of the flange of the specimen about the web.

To achieve the 3% target drift ratio, steel chairs (shown in Figs. 6.34, 6.35, and 6.36) were used to lock in the displacement when the hydraulic rams reached their stroke limit. The rams were then retracted so the nut in front of each piston was moved forward,

thereby allowing the rams to apply additional displacement. Elongation of the PT bars due to the load applied was also considered in designing this load set-up.

6.4.3.2: Loading in the weak direction (away from strong wall)

A hydraulic ram with 400-kip capacity and 12-in. stroke (Enerpac-CLRG20012 cylinder with an effective area of 41.22 in^2) was used to push the specimen in the weak direction (see Figs. 6.34 and 6.36).

A link, 16-in. long, (W-shape welded to plates at both ends) was used to fill the space between the CLRG 20012 loading ram and the cylindrical bearing (see Fig. 6.34). A larger link (21-in. long) was designed and fabricated for the purpose of loading beyond 2% drift (6 in. lateral displacement). A link to "hold the specimen" (see Figs. 6.34 and 6.36) was attached to the load set-up so that the specimen could be restrained while replacing the smaller link with the larger link. However, the larger link and the link to "hold the specimen" were not used during the test because the specimen was finally pushed only to 2% drift away from the strong wall. The reason for this drift limit is explained in Section 6.6.

6.4.3.3: Vertical load to simulate the service load

The service load was calculated for a prototype tall building (from plan drawings of WAMU/SAM, 42 floors plus roof above grade and 6 levels below grade). A dead load of 70 psf and a live load of 24 psf were considered for the floors. The corresponding calculated axial service load was 10.6% of $A_g f_c'$ (where A_g is the gross cross-sectional area of the shear wall). Hence, it was proposed to apply an axial load of approximately $0.1A_g f_c'$ which was equal to 1380 kips for the cross section of the specimen for the cyclic loading test.

Axial load was applied by post-tensioning eight high-strength PT bars: two bars extended from the foundation block to the third floor level and six bars extended from the bottom of the foundation block to the top of the specimen (see Figs. 6.34, 6.35, and 6.36). The 1-3/8-in. diameter PT bars were enclosed in 2-3/8-in. internal diameter plastic ducts (see Section 6.4.1.6 for installation details). To apply a total load of 1380 kips ($0.1A_gf_c'$) with the eight PT bars, each PT bar would need to be post-tensioned to 172.5 kips, which is equal to 73 % of their ultimate strength. However, a post-tension force of 166 kips, which is equal to 70% of the ultimate strength ($0.096\ A_gf_c'$), was instead applied to the PT bars for safety purposes. The total axial load on the wall specimen was 1320 kips as measured by the pressure gauge attached to the loading pump.

Figure 6.35 shows the vertical PT bars in the flange section and the horizontal PT bars which were intended to apply lateral load. The two vertical PT bars which are at the far ends (9 in. from each end) of the flange would intersect with the horizontal PT bars if those two vertical PT bars were continuous over the height. Hence, those two vertical PT bars were post-tensioned above the third story and were discontinued beyond that level. The method used to achieve this has been explained in Section 6.4.2.2.5.

6.5: Instrumentation

The test specimen was instrumented in order to measure lateral load, vertical load, strains in the plates, concrete strains, curvature of the specimen, and lateral deflection of the specimen. All measurements were monitored and recorded using a high-speed data acquisition system (Vishay's Strain Smart System 5000). The measuring device or gauge used, the method of attaching them, and the method for calculating the desired measurements from the observed readings are described in the following subsections.

6.5.1: Instrumentation to measure applied loads

A pressure transducer (Omega PX302-10KGV) was attached to the loading pump to measure the output pressure delivered to the loading ram for loading in the north direction (away from the wall). This pressure was used to infer the load applied to the specimen in order to push the specimen away from the strong wall (in the north direction). The pressure transducer was calibrated prior to attaching it to the loading pump.

To measure the load applied for loading towards the strong wall (in the south direction), four load cells were used to measure the load in addition to the pressure transducer. Two load cells of 100-kip capacity (Honeywell 3632-100K) were attached to two of the four 120-kip cylinders, while two 150-kip capacity load cells (Lebow 3156-150K) were attached to two of the four 200-kip cylinders. Load cells were calibrated in a Forney test machine prior to attaching them to the loading set-up.

Strain gauges were attached to the vertical PT bars (which were used to apply vertical load) to monitor the change in vertical load during post-tensioning and cyclic loading. Strain gauges were attached only to the six vertical PT bars which extended up to the top of the specimen. No strain gauges were attached to the two discontinued PT bars. The locations of the strain gauges on the PT bars are shown in Fig. 6.37.

6.5.2: Instrumentation in the foundation block

Strain gauges were attached to the No.7 reinforcing bar hooks to monitor the stress levels reached during cyclic loading. Even though the reinforcing bar hooks were designed for yielding, it was intended to determine the actual stress the reinforcing bars experienced during cyclic loading and to, possibly, modify the design approach used to design the hooks. A total of eight strain gauges were attached on four reinforcing bar hooks.

Figure 6.38 shows the locations of those four reinforcing bar hooks. At each of the four reinforcing bar hooks, two strain gauges, one located 1 in. below and the other located 9 in. below the bottom of the ¾-in. foundation connection plate were attached to monitor the strain variation along the length of the reinforcing bar hook.

6.5.3: Horizontal wire potentiometers

Wire potentiometers were mounted on the strong wall and their wires were attached to the specimen to measure the lateral displacements of the specimen. Figure 6.39 shows the locations of the wire potentiometers on the specimen. Lateral displacement was used to calculate the lateral drift and deflected shape of the specimen.

A total of 10 wire potentiometers (UniMeasure PA-10-NJC-DS-L3M, UniMeasure PA-20-NJC-DS-L3M, and UniMeasure PA-25-NJC-DS-L3M with a linearity of ± 0.15% of full scale) were used on the south side of the specimen. All the wire potentiometers were calibrated using a height gauge prior to attaching to the specimen.

6.5.4: Strain gauges attached on steel plate to measure vertical strains

Strain gauges were mounted on the 3/16-in. steel plates to measure vertical strains developed by the bending of the specimen due to the applied lateral load. Figures 6.40 and 6.41 show the locations of the strain gauges attached on the second story web plate assembly and the first story web plate assembly, respectively. Figures 6.42 and 6.43 show the locations of the strain gauges attached on the second story flange plate assembly and the first story flange plate assembly, respectively.

In the bottom part of the specimen, two strain gauges 7 in. apart vertically on a vertical line were attached to measure the strain on the plates and to calculate the

curvature (see Figs. 6.41 and 6.43). The two strain gauges were 1 in. and 8 in. above the foundation connection plate. In the second story, strain gauges were attached to measure strain to compare with strains measured in the first story of the specimen and to evaluate the variation of strain over the height of the specimen. Type C2A-06-250LW-350 strain gauges from Vishay Micro-Mesaurements were used to measure vertical surface strains in the steel plates.

6.5.5: Concrete strain gauges

Concrete strain gauges were embedded in the first and second stories of the specimen to measure strains in the concrete. EGP-5-350 embedment gauges from Vishay Micro-Mesaurements were used for this purpose. The locations of the concrete strain gauges are shown in Figs. 6.40 through 6.43. Concrete strain gauges were mounted in the mid thickness of the wall (center of the wall).

6.5.6: Strain gauges attached on reinforcing bars

Strain gauges were mounted on the No. 6 reinforcing bars (refer to Section 6.4.1.5 for the details of the reinforcing bar) to measure the strains in the reinforcing bars and to see the variation of strains over the depth of the cross section of the specimen. The locations of the reinforcing bars which had strain gauges mounted on them are shown in Fig. 6.38. The locations of the strain gauges attached to the reinforcing bars are also shown in Figs. 6.41 and 6.43. The strain gauges on the reinforcing bars were 1-1/8 in. above the top of the foundation connection plate.

6.5.7: Shear strain gauges attached on shear wall plate and foundation connection plate

Shear strain gauges (Measurement Group Type CEA-06-187UV-350 shear pattern strain gauges) were attached on a foundation connection plate and shear wall plates to measure the shear strain and to see the variation of strains with depth along the cross section of the specimen and between the shear wall plate and foundation connection plate. Three shear strain gauges were attached on a shear wall plate in the web of the specimen, two on the east side of the wall at 4.5 in. and 54 in. from the far end of the web and the other on the west side of the wall at 54 in. from the far end of the web. All three gauges were located 4.5 in. above the foundation connection plate. The fourth strain gauge was attached on the foundation connection plate 54 in. from the far end of the web and 2 in. below the top of the foundation connection plate on the east side of the wall. The locations of the shear strain gauges are shown in Fig. 6.41.

6.5.8: Position transducers for strains at the bottom of the specimen

After the steel plates yield, strain gauges attached on the steel plates generally pop off and cannot be utilized further for strain measurements. Hence, position transducers (Novotechnik – Siedle Group, Model TR 50 with a mechanical stroke of 55 mm and a repeatability of ±0.002 mm) were attached on the bottom of the specimen to measure strains in the plates. Position transducers were attached the north side of the flange and the west side of the web (strong wall to specimen direction was south to north). Along a vertical line, two position transducers were attached, one at the top of the foundation connection plate and the other at 8 in. vertically above that so that the average strain can be calculated over a length of 8 in. The location of the position transducers are shown in Figs. 6.41 and 6.43. An aluminum frame was constructed around the specimen to attach the position transducers so that the readings from the position transducers were not affected by the deflection or movement of the specimen or the foundation block. Figure 6.44 depicts the aluminum frame which was mounted on the strong wall and was supported by four concrete blocks (1.5 ft x1.5 ft x1.5 ft) sitting on the strong floor.

6.5.9: Position transducers and LVDTs to measure shear and flexural deformations along web of specimen

In the first and second story webs of the specimen, the diagonal elongations and vertical elongations at both ends of the diagonals were measured to calculate shear and flexural deformations along the web of the specimen at the first and second stories of the specimen. The instrumentation method and calculation method are described by Massone and Wallace (2004).

A schematic diagram of the gauges used to measure the shear and flexural deformations is shown in Fig. 6.45. Four position transducers were used to measure the diagonal elongations. Four LVDTs were used to measure the vertical elongations. The vertical displacement of the foundation connection plate was obtained from the position transducers attached to the top of the foundation connection plate (attached for the purpose of measuring vertical strains as described in Section 6.5.8 and shown in Fig. 6.41). The vertical displacement measurements from these position transducers were deduced from the vertical displacement measurements from the LVDTs attached in the first story level to calculate the vertical elongation of the first story plate.

Figure 6.46 shows a photograph with position transducers and LVDTs attached in the first and second stories of the specimen. The LVDTs were attached to the same aluminum frame described in Section 6.5.8. Plots of shear and flexural deformations calculated from this data are provided in Appendix D.10.

6.5.10: DEMEC mechanical strain gauges to measure strains on shear wall plates

DEMEC mechanical strain gauges (with a resolution of 0.001 mm from Mayes Instruments Limited) were used to measure the strains on shear wall plates to provide additional strain data from a different source. Expectation of losing some strain gauges because of plate yielding was another reason to use the mechanical strain gauges so that there would be at least some strain measurements as back up. In order to measure the

strain between two points on the plate over a 100 mm distance, two DEMEC points were glued (using a two parts epoxy, BondAway 2011A/2011B, from Fielco Adhesives) to the plate at those points, and variation in the distance between those two DEMEC points was measured using the DEMEC invar beam with a digital dial gauge attached to that. The digital dial gauge reading was multiplied by a factor of 0.8 to get the variation in distance between those two DEMEC points. Figure 6.47 shows a photo of two DEMEC points attached to the plate and Fig. 6.48 shows a photo of the DEMEC invar beam.

Fifteen pairs of DEMEC points were attached to 3/16-in. shear wall plates in the first story of the specimen. Five pairs of points were located on the east side of the web; four pairs of points were mounted on the south east side of the flange, and the remaining five pairs of points were located on the north side of the flange. Refer to Figs. 6.41 and 6.43 for the locations of the DEMEC points on the web and flange of the specimen, respectively. Plots of strain measurements calculated from data collected using the mechanical strain gauges are provided in Appendix D.7.

6.5.11: Optotrak used to measure strains on shear wall plates

Optotrak Certus Motion Capture System (from Northern Digital Inc.) was also used to measure the movements of target points attached to the specimen (see Fig. 6.47). The Optotrak system measures the coordinates of target points. Strain was calculated by dividing the difference in distance between two points by the original distance. Plots of strain measurements calculated from data collected with the Optotrak system are provided in Appendix D.8.

6.5.12: Dial gauges attached to monitor the movement of foundation block

Dial gauges were installed on the strong floor against the foundation block of the specimen to monitor any sliding of the specimen during testing. Five dial gauges were

installed. Two dial gauges were installed to monitor any rotation of the foundation block, and two dial gauges were installed to monitor any movement of the foundation block in the loading direction. The fifth gauge was installed against the top of the foundation block (on the north side) to monitor any uplift of the foundation block.

6.6: Test Method

Cyclic lateral load was applied to the specimen by displacing it to a program of specified drift. In each load cycle, first, the specimen was pushed to a specified drift in the strong direction. Then, it was pushed to the same drift in the weak direction after the hydraulic rams used in the strong direction of loading were retracted. The same drift was repeated for one more load cycle most of the time. However, this pattern was not carried out for the first loading cycle, or for the last loading cycle. The drift level was then increased for the next set of load cycles. This pattern of cycles was continued up to 2% drift in the weak direction and 1% drift in the strong direction (towards the south or towards the strong wall). To achieve 2% drift, a stroke of 6 in. was needed at the loading height of 25 feet. For the first cycle, the specimen was displaced to a lateral displacement of 0.375-in. (0.125% drift) to carry out an elastic load cycle before the plates start yielding. The load cycle and corresponding lateral drift for each cycle are tabulated in Table 6.4.

At 0.75% drift in the strong direction, the steel plates at the far south end of the stem started buckling. The specimen was not pushed beyond 1% drift in the strong direction for the reminder of the test. In the last cycle (7^{th} cycle), the specimen was pushed to 2% drift in the weak direction, and then the test was stopped after the specimen was returned to approximately zero displacement.

During the test, the fillet welds between the 3/16-in. shear wall plates and the 3/4-in. foundation connection plates were monitored for cracking using a magnifying glass.

Splice plate fillet welds and welds in the corner connection were also checked for cracking during testing. No cracking of these welds was observed.

6.7: Results and Analysis

A total of seven load cycles were applied to the specimen. Refer to Table 6.4 for the lateral drifts applied during each cycle. A maximum lateral load of 252 kips and 442 kips were applied in the weak direction (away from strong wall/towards north) and in the strong direction (towards strong wall/towards south), respectively. Noise observed during testing was assumed to be due to slipping of concrete against the steel plate, presumably by breaking the bond between the steel plate and concrete or exceeding static friction along the steel-concrete interface. It was noticeable from early stages of loading. When the specimen was cycled through larger drifts, the noise increased and the originating location moved from the bottom of the specimen toward the top.

At approximately 0.75% drift in the 6th cycle, when the specimen was pushed towards the strong wall (towards south), the 3/16-in. closure plate at the far end of the web at the bottom of the specimen started distorting outward and the web plates started buckling. See Fig. 6.49 for a photo of the specimen when the plates started buckling. The buckling occurred between the first and second horizontal bolt lines from the bottom (about 4.5 in. from the bottom). The concrete in that area had already cracked and crushed from earlier load cycles.

When the specimen was pushed away from the strong wall (towards north), the buckled shear wall plates straightened somewhat. A threaded rod along the fifth bolt line (20.25 in.) from the bottom fractured and the nut popped off as shown in Figs. 6.50. Figure 6.51 shows a photograph of the specimen pushed back towards the strong wall (towards south) again. During this 7th cycle, buckling occurred along the second horizontal bolt line from the bottom (about 6.75 in. from bottom). More threaded rods fractured and the nuts popped off. Then, when the specimen was pushed away from the

strong wall (towards north), the shear wall plates straightened again. More threaded rods fractured and the nuts popped off. The specimen was pushed to a maximum of 2% drift (6-in. displacement) towards the north. The analysis of the important results is discussed in the following sub sections. Plots of all the measurements are provided in Appendix D.

6.7.1: Lateral deflection of the specimen

Lateral deflections at various locations on the specimen were measured using the wire potentiometers mounted between the strong wall and the specimen. Refer to Fig. 6.39 for the locations of the wire potentiometers on the specimen. The readings from the top two wire potentiometers (WP1 and WP2) were used to calculate the lateral drift ratio of the specimen along the loading axis. The height of the loading axis from the bottom of the specimen (from the top of the foundation connection plate) was 295 in. Hence, the lateral drift ratio was calculated by dividing the average of the deflection measurements from the top two wire potentiometers by the height, 295 in.

Figure 6.52 shows the height versus lateral deflection plots at various loading stages. It can be seen from the plots that the deflected shape of the specimen for a particular drift was very similar for different load cycles. Furthermore, it could be also noted that the slope of the height versus lateral deflection plots decreased along the height of the specimen. During the 7^{th} cycle, when the specimen was pushed to 2% drift towards the north, a large portion of the bending (curvature) was concentrated in the first story of the specimen.

6.7.2: Variation in vertical load during the test

Vertical (or axial) load was applied by post-tensioning eight 1-3/8-in. diameter PT bars, most of which extended from the bottom of the foundation block to the top of the specimen. During the cyclic loading of the specimen, the vertical load was expected to

vary as the specimen moved laterally. Strain gauges were attached to six PT bars to measure the strain and then calculate the load in the PT bars (see Section 6.5.1 for details). All three PT bars in the web and the three of the five PT bars in the flange were gauged (see Fig. 6.37). Loads measured in the three PT bars in the flange were very close (refer to Appendix D.1 for the vertical load versus lateral drift plot for each PT bar). Hence, the load in the other two PT bars in the flange was assumed to be same as the average load in the three gauged PT bars.

Initial total load in the PT bars measured using the strain gauges was 1170 kips while the total load measured using the pressure dial gauge on the loading pump used to apply post-tensioning was 1320 kips. Past experience shows that load inferred from strain gauge measurements is more reliable than the load computed using the pressure dial gauge on the loading pump. The total load in the PT bars versus lateral drift plot is shown in Fig. 6.53. It can be seen from the figure that the total load on the PT bars increased to a maximum of 1290 kips and decreased to a minimum of 1150 kips when the specimen was pushed away from the strong wall. It increased to a maximum of 1260 kips and decreased to a minimum of 1150 kips when the specimen was pushed towards the strong wall.

When the specimen moved laterally, the post-tensioned bars also moved along with the specimen. Hence, the vertical load was taken as the vertical component of the total load on the PT bars (referred as “vertical load” throughout this report). Similarly, the horizontal component of the total load on the PT bars was subtracted from the lateral load (refer to Section 6.7.3). The inclination of the specimen and the post-tensioned bars was calculated using lateral deflections of the specimen along the loading axis (at the fifth-story level) and at the fourth-story level. See Fig. 6.54 for the adjusted vertical load versus lateral drift plot. The adjusted vertical load differed by a maximum of less than 1 kip from the total load on the PT bars. This is because of very small inclination of the specimen.

6.7.3: Lateral load versus lateral drift

A lateral load of 442 kips was applied to push the specimen in the strong direction to a lateral drift of 1%. Similarly, a lateral load of 252 kips was applied to push the specimen in the weak direction to a lateral drift of 2%. Lateral load was applied using eight hydraulic rams to push the specimen in the strong direction and using a single hydraulic ram to push the specimen in the weak direction.

Lateral load was inferred using pressure measurements made with a pressure transducer attached to the loading pump. In addition to that, four load cells mounted on four of the eight horizontal PT bars used to apply load to push the specimen towards the strong wall were also used to measure load. Loads inferred or measured during the first half of the 6^{th} cycle (when the specimen was pushed towards the strong wall) using the pressure transducer and load cells are shown in Figs. 6.55 and 6.56. Those two approaches to determining loads produced very similar results as shown in Figs. 6.55 and 6.56. Hence, the pressure transducer readings were considered sufficient for inferring applied lateral load.

As mentioned in Section 6.7.2, the horizontal component of load in the vertical PT bars was subtracted from the load applied using hydraulic rams to get the actual lateral load (denoted as “lateral load” throughout this report). This “lateral load” was used for all the remaining plots and results analysis. See Fig. 6.57 for the variation of horizontal component of load on the PT bars with lateral drift. The maximum value of the horizontal component was 30 kips.

Figure 6.58 shows the lateral load versus drift ratio response for each of seven cycles, while Fig. 6.59 shows the lateral load versus drift response for the first three cycles (for the purpose of ease in viewing). The lateral loads have been adjusted for the horizontal component of the axial load. In the plots, the load and drift measured away from the strong wall (towards north or in the weak direction) was considered positive.

Slope of the lateral load versus drift ratio response gradually decreased over the load cycles, indicating that the stiffness of the shear wall decreased after each load cycle.

6.7.4: Strains in reinforcing bar hooks

The No.7 reinforcing bar hooks were designed to yield for the vertical forces generated from the 3/16-in. shear wall plates when tensile fracture of the shear wall plates occurs (as a capacity design approach). A tensile strength of 70 ksi for the shear wall plates and yield strength of 60 ksi for the reinforcing bar hooks were used for designing the reinforcing bar hooks (see Section 6.4.1.3 for details of design). A total of seven strain gauges were attached to the No.7 reinforcing bar hooks to monitor the stress levels they reached during cyclic loading.

Figure 6.38 shows the locations of the strain gauges. Figures 6.60 and 6.61 show the strain measurements from strain gauges R4 and R7, respectively. Strain gauge R4 which was located beneath the web of the specimen (29.25 in. from the south end) reached maximum compressive and tensile strains of -300 με and +1250 με. For 60 ksi yield strength for the reinforcing bar hook, the yield strain would be approximately 2070 με. Hence, the reinforcing bar hook at that location reached a stress level of only 0.63 times yield strength.

Strain gauge R7, which was located beneath the flange of the specimen, reached maximum compressive and tensile strains of -120 με and +300 με. Hence, the reinforcing bar hook at that location reached a stress level of only 0.14 times yield strength. It can be noted from Figs. 6.60 and 6.61 that when buckling occurred (after a lateral load of approximately 420 kips), strains increased dramatically in compression at R4 and in tension at R7.

Strain gauge R2 (which was 3.75 in. from the south end) did not work properly during the test. It must have been damaged before or during the test. If the strains from

R4 and R7 are extrapolated assuming that the strains over the depth of the section vary linearly, then the maximum strain in the reinforcing bar hook to which R2 was attached would be 2040 με. It would indicate that the reinforcing bar hook was close to yielding at that location.

6.7.5: Strains in concrete

A total of six concrete strain gauges, three near the bottom of the specimen and three in the second story, were used to measure strains in the concrete during the test. The locations of the concrete strain gauges are shown in Figs. 6.40 through 6.43.

Near the bottom of the wall specimen, the closest concrete strain gauge to the south end (concrete strain gauge C1) in the web was 18 in. away from the south end. From the strain measurements from that strain gauge (see Fig. 6.62), the maximum measured compressive strain was approximately 2850 με. From the stress-strain model of the high strength concrete used in Section 6.2.2, the concrete compressive stress at 2850 με would be 5.7 ksi (which occurs after reaching the peak stress of 11.5 ksi). When buckling occurred (between -0.75% and -1.0 % drift during cycle 6), after a lateral load of approximately 420 kips, strains increased dramatically as can be seen in Fig. 6.62. When buckling occurred and the plates could not resist significant load, the concrete had to resist most of the load transferred to that region. Figure 6.63 shows the strain measurements from a strain gauge (C3) in the flange near the bottom of the wall specimen. Maximum compressive strain was 330 με. Strain measurements from the remaining strain gauges are presented in Appendix D.4.

At or shortly after buckling of the plate occurred, concrete must have crushed at the south end. Crushed concrete could be seen in the photograph taken immediately after buckling and is shown in Fig. 6.49. However, it was not possible to determine whether crushing of the concrete occurred before or after buckling occurred.

A concrete with design compressive strength of 10 ksi was used for the specimen. The 28-day strength of the concrete was 9,360 psi (9.4 ksi) while the compressive strength of the concrete on the day of testing was 11,480 psi (11.5 ksi) based on 6 x 12 in. cylinder tests. Considering the very high strength of the concrete used to cast the specimen, crushing of concrete, and dramatic increase in concrete strains at the south end of the web when buckling of the steel plates occurred, prevention of plate buckling would be a very effective way to minimize the increase in concrete strains. The steel plates likely provided some confinement effect for the concrete that was effectively lost when the steel plates buckled.

6.7.6: Strains in the shear wall plates

Shear and bending moment over the height of the wall are developed due to the applied lateral load. The wall plates experienced vertical tension and compression cycles due to moment developed by the applied cyclic loads. Strain gauges were attached to the 3/16-in. shear wall plates to measure strains developed due to these tension and compression cycles. The locations of the strain gauges are shown in Figs. 6.40 through 6.43. The yield strength and tensile strength of the plate were 60.0 ksi and 70.1 ksi, respectively. The yield strain calculated from the yield strength (assuming a Young's modulus of 29,000 ksi) was 2070 με.

The strain gauges were attached to the plates after the vertical load was applied by the post-tensioning of the vertical PT bars. Hence, strains measured with the strain gauges did not include the strains resulting from the vertical load. The total vertical load was 1170 kips. It is very plausible to assume that the strains from the vertical load were distributed uniformly over the cross section of the shear wall. Considering the modulus of elasticity for the steel and concrete as 29,000 ksi and 6,100 ksi, respectively, then the vertical compressive strain on the steel plate was calculated to be 120 με.

The analysis of the important results is discussed in the following sub sections. Plots of all strain measurements from strain gauges on the shear wall plates are provided in Appendix D.5.

6.7.6.1: Strains in the shear wall plate at 1 in. above the foundation connection plate

Figure 6.64 shows the strains measured 1 in. above the foundation connection plate at the south end of the specimen (SG 45 on a web plate). During cycle 6, the strain gauge was damaged and the strain values for the latter part of cycle 6 and cycle 7 were not included in the plot. The plate yielded at that location in tension during cycle 2 (cycle 2N-when the specimen was pushed away from the strong wall) when the lateral deflection, lateral drift ratio, lateral load, and moment at that location were 0.49 in., 0.17%, 77.4 kips, and 1940 kip-ft, respectively.

The plate yielded at that location in compression during cycle 4 (cycle 4S-when the specimen was pushed towards the strong wall) when the lateral deflection, lateral drift ratio, lateral load, and moment at that location were 0.96 in., 0.32%, 231.7 kips and 5770 kip-ft, respectively.

During cycle 4, cycle 5 and cycle 6, when the specimen was unloaded after it was pushed towards the strong wall (towards south), significant plastic compressive strains (between 2100 to 2900 $\mu\epsilon$) were evident from Fig. 6.64.

Figure 6.65 shows the strains measured at 1 in. above the foundation connection plate at the north end of the specimen (SG 52 on flange plate). The plate yielded at that location in tension during cycle 6 (cycle 6S - when the specimen was pushed towards the strong wall) when the lateral deflection, lateral drift ratio, lateral load, and moment at that location were 1.67 in., 0.57%, 338.7 kips and 8470 kip-ft, respectively.

The plate yielded at that location in compression during cycle 7 (cycle 7N-when the specimen was pushed away from the strong wall) when the lateral deflection, lateral drift ratio, lateral load, and moment at that location were 3.00 in., 1.02%, 221.4 kips and 5740 kip-ft, respectively.

6.7.6.2: Average strains over the bottom 8 in. of shear wall plate

Position transducers were used to measure the average strains over the bottom 8 in. of the shear wall plates. Refer to Section 6.5.8, Fig. 6.41 and Fig. 6.43 for the instrumentation method and locations of the position transducers. Over a vertical distance of 8 in., the bottom position transducer was attached to the top of the foundation connection plate and the top position transducer was attached to the shear wall plate. Hence, the strain calculated from the readings from the position transducers includes strain over 8 inches of shear wall plate and the weld between the shear wall plate and foundation connection plate.

Figure 6.66 shows the strains calculated at 1.5 in. from the south end (between position transducers 17 and 18). The strain exceeded the yield strain of the plate (2070 με) during the second and fourth cycles in tension and compression. During cycle 6, when the specimen was pushed towards the strong wall, the specimen started buckling at approximately a lateral load of 410 kips (- 410 kips in the plot). Buckling occurred between the top and bottom position transducers. In Fig. 6.66, a sudden increase in strain at that load can be noted. Because strain was calculated from the distance between the position transducers, the calculated strain values after buckling cannot be taken as actual strain over that distance. Buckling extended up to about half the web length from the south end. Hence, this will also be the case for strains calculated between position transducers 15 and 16.

Figure 6.67 shows the strains inferred from measurements at the outer fibers of the flange of the specimen (between position transducers 7 & 8). Strains exceeded the

yield strain of the plate (2070 με) during the sixth and seventh cycles in compression and tension. The plots of strains calculated using the position transducers at other locations are provided in Appendix D.

6.7.6.3: Strains on the shear wall plate at 22.25 in. and 49.25 in. above the foundation connection plate

Strains at 22.25 in. and 49.25 in. above the foundation connection plate were measured using the DEMEC mechanical strain gauges (refer to Section 6.5.10 and Figs. 6.41 and 6.43 for the measurement method and locations of DEMEC points). The readings (distances between the points) were manually recorded at certain intervals until completion of the 5th load cycle.

DEMEC gauges DG2 and DG12 were located 22.25 in. above the foundation connection plate. DG2 was on a web plate at 18 in. from the south end and DG12 was on the outer flange plate. Figures 6.68 and 6.69 show the strains calculated at DEMEC gauges DG2 and DG12. During the 5th load cycle, the plate at location DG2 reached maximum tensile and compressive strains of 1576 με and 824 με, respectively. The plate at location DG12 reached maximum tensile and compressive strains of 872 με and 528 με, respectively.

DEMEC gauges DG1 and DG11 were 49.25 in. above the foundation connection plate. DG1 was on a web plate 18 in. from the south end and DG11 was on the outer flange plate. Figures 6.70 and 6.71 show the strains calculated at DEMEC gauges DG1 and DG11. During the 5th load cycle, the plate at location DG1 reached maximum tensile and compressive strains of 1,512 με and 720 με, respectively. The plate at location DG11 reached maximum tensile and compressive strains of 896 με and 392 με, respectively.

6.7.6.4: Strains on the shear wall plate at 85.5 in. above the foundation connection plate

Figure 6.72 shows the strains measured at 85.5 in. above the foundation connection plate at the south end of the specimen (SG 15 on web). The plate yielded at that location in tension during cycle 6 (cycle 6N-when the specimen was pushed away from the strong wall) when the lateral deflection, lateral drift ratio, lateral load, and moment at that location were 2.77 in., 0.94%, 216.4 kips and 4,010 kip-ft, respectively. At that location, the plate underwent a maximum strain of 1,145 $\mu\epsilon$ (0.50 ϵ_y) in compression during the test.

Figure 6.73 shows the strains measured at 85.5 in. above the foundation connection plate at the north end of the specimen (SG 21 on flange). The plate experienced a maximum strain of 1090 $\mu\epsilon$ (0.47 ϵ_y) in tension and a maximum strain of 621 $\mu\epsilon$ (0.27 ϵ_y) in compression during the test.

6.7.6.5: Variation of strains along the depth of the shear wall

Plots of variation of strain along the depth of the wall at different heights are shown in Figs. 6.74 through 6.79. Strain measurements from strain gauges were used to generate the plots. Figures 6.74 and 6.75 show the variation in strain along the depth of the wall for various load stages at an 85.5-in. height from the bottom of the wall (85.5 in. above the foundation connection plate) on the east and west sides of the wall, respectively. From the plots, it can be seen that the strain versus distance relationship was almost linear at that height during the entire test. Furthermore, strains on the east and west sides of the wall are numerically very similar.

These figures show that the web plate up to about 31.5 in. from the south end yielded in tension at this height while the other parts of the plates remained elastic. It could be noted that the tensile strains developed at the south end when the specimen was pushed towards the north for a certain drift were always larger than the compressive

strains developed at the south end when the specimen was pushed towards the south for the same drift. This trend could be noted at both the 8-in. height and 1-in. height discussed below.

Figures 6.76 and 6.77 show the variation in strain along the depth of the wall at 8 in. above the foundation connection plate on the east and west sides of the wall, respectively. From the plots, it could be seen that the strain versus distance relationship was close to linear till the end of cycle 6. Strains steadily increased from south to north when the specimen was pushed towards the north, and strains steadily decreased from south to north when the specimen was pushed towards the south. However, this behavior was not consistent for cycle 7. Possible reasons might be that the strain gauges which reached very high strains in the earlier cycles had been damaged and the steel plates sustained large residual strains.

Figures 6.76 and 6.77 show that the web plate up to about 54 in. from the south end yielded in tension, while the web plate up to a distance between 18 and 36 in. from the south end yielded in compression.

Figures 6.78 and 6.79 show the variation in strain along the depth of the wall at 1 in. above the foundation connection plate on east and west sides of the wall, respectively. From the plots, it can be seen that the strain versus distance relationship was close to linear till the end of cycle 5. However, this behavior was not consistent for cycle 6 and cycle 7.

Figures 6.78 and 6.79 show that almost the entire web and both flange plates yielded in tension, while the web plate up to a distance between 18 and 36 in. from the south end and the outer flange plate yielded in compression.

6.7.7: Moment versus curvature along the depth of the wall

For applied lateral load, moment decreases with height of the horizontal section considered. Moment versus curvature plots were developed at 1-in., 8-in. and 85.5-in. heights above the foundation connection plate.

Moment at a particular section was calculated by considering three components: (a) load applied by the hydraulic rams multiplied by the height difference between the loading axis and the horizontal section considered, (b) horizontal component of the total load on the vertical PT bars multiplied by the height difference between the top of the specimen and the horizontal section considered and (c) vertical component of the total load on the vertical PT bars multiplied by the difference in lateral deflections at top of the specimen and the horizontal section considered.

Curvature at a particular section was calculated from the strain measurements from the strain gauges along the depth of the wall. Curvature was calculated as the gradient of the strain versus distance relation. It was averaged from the values obtained for the east and west side of the wall at a horizontal section. Strain measurements from the same strain gauges used to plot the variation of strains along the depth of the shear wall (as detailed in Section 6.7.6.5) were also used to calculate curvature for the moment versus curvature plots.

Moment versus curvature plots at 1-in., 8-in., and 85.5-in. heights are shown, respectively, in Figs. 6.80, 6.81 and 6.82. Curvature for a particular moment was the largest at the 1-in. height and smallest at the 85.5-in. height. For example, at the peak of cycle 5N when the wall was pushed away from the strong wall, the moment and curvature values are listed in Table 6.5. The ratios of curvature/moment at 1-in., 8-in., and 85.5-in. heights were 0.35, 0.14 and 0.10, respectively. At the 1-in. height, strains in steel and concrete fell into the non-linear stress-strain region earlier than the other two sections. This might be a possible reason for higher curvature/moment at a 1-in. height than at 8-in. and 85.5-in. heights. At the 1-in. height, there was no available strain data

for part of the 6th cycle and all of the 7th cycle. Hence, the curvature could not be calculated for these portions of the cycles and the moment versus curvature response is not shown in Fig. 6.80 for these portions of the cycles.

The moment-curvature diagram developed considering the measured properties of the steel and concrete is shown in Fig. 6.8. The moment capacity was 10,790 kip-ft and 6,040 kip-ft for the web in compression case and web in tension case, respectively. The maximum moment the specimen resisted during the test was 11,180 kip-ft for the web in compression case, and 6,830 kip-ft for the web in tension case, respectively. The concrete in the specimen was confined to some degree by the steel plate assembly while confinement was not considered in the preliminary analysis. In the moment-curvature diagram developed in the preliminary analysis, the moment started decreasing after a curvature of 0.000975 ft^{-1}. This was because of the reduction in concrete strength after it reached the peak as shown in Fig. 6.6. However, the moment was increasing at that curvature in Fig. 6.80, possibly because of the confinement of concrete.

Vertical load was not included in the moment-curvature diagrams developed in the preliminary analysis. The curvature in Figs. 6.80, 6.81 and 6.82 (for the moment-curvature diagram from the test) calculated from the measured strains also did not include strains from the vertical load. When calculating the moment for the moment-curvature diagram from the test, the effect of the horizontal component of the PT bar load and the moment calculated by multiplying the vertical load by the lateral deflection of the specimen were considered. Strains in the steel plate from the total vertical load of 1170 kips were calculated to be 120 με.

6.8: Summary and Conclusions

The behavior of the intersecting wall elements for cyclic lateral load was experimentally investigated using a 3/8-scale cantilever T-shaped composite wall. The specimen was 319.5 in. (26’-7 1/2”) above the foundation connection plate which

extended 5 in. above the 3-ft tall foundation block. The foundation block was anchored to the strong floor using post-tensioned bars.

A plate thickness of 3/16 in., a transverse bar diameter of 3/8 in., bar spacing of 4-½ in. and a wall thickness of 9 in. were used for the plate assembly. The plates were A572 grade 50 steel. From coupon tests, yield strength and tensile strength of the plate were 60.0 ksi and 70.1 ksi, respectively. Design strength of the concrete was 10 ksi. The 28-day strength of the concrete was 9,360 psi (9.4 ksi) while the compressive strength of the concrete on the day of testing was 11,480 psi (11.5 ksi) from cylinder tests.

6.8.1: Load and Moment capacities

A total vertical load of approximately $0.1A_g f_c'$ (where A_g is the gross cross-sectional area of the shear wall) was applied by post-tensioning eight high-strength PT bars, most of which extended from the bottom of the foundation block to the top of the specimen. This vertical load was used to simulate the self weight of the shear wall and service load transferred to the shear wall by the gravity-load framing. During the test, the load on the PT bars varied as the specimen was subjected to cyclic lateral loads. Initial total load on the PT bars was 1,170 kips. It varied between 1,290 and 1,150 kips during the test. Hence, the vertical load varied by a maximum of 10 percent during the test. Inclination of the specimen due to the lateral load was considered in calculating the vertical load on the specimen and the horizontal component which was subtracted from the lateral load applied using by the hydraulic rams.

From the test, the maximum moment the specimen was able to resist was 11,180 kip-ft in the strong direction (compared to 10,790 kip-ft calculated in the preliminary analysis). The plate at the far end of the web buckled at this applied moment. In the weak direction, the maximum moment the specimen resisted during the test was 6,830 kip-ft (compared to 6,040 kip-ft calculated in the preliminary analysis). This occurred when the specimen was pushed to approximately a 2% drift ratio in the weak direction. The higher

moment capacity of the shear wall from the test compared with the moment capacity from the preliminary analysis may be due to the confinement of concrete by the steel plate assembly. During the preliminary analysis, the moment-curvature diagram was developed using force equilibrium equations assuming strain linearity over the cross section of the shear wall. Buckling of the plate was not considered when developing the moment-curvature diagram.

6.8.2: Design and behavior of specimen components

During the test, no cracking (or fracture) was observed in the splice plates, the fillet welds between the splice plates and the shear wall plates, the angles in the corner connection, the fillet weld between the angles and the splice plates, and, perhaps most importantly, the fillet weld between the 3/16-in. shear wall plates and the 3/4-in. foundation connection plates. It indicates that these welds were successfully designed using the method used to design the specimen in this study (as detailed in Section 6.3).

The splice plates and fillet welds between the two adjacent plate assemblies were designed to transfer forces from the top plate assembly to the bottom plate assembly. The 3/16-in. shear wall plates up to an elevation between the third and fourth stories were expected to strain beyond yield. Hence, the fillet weld was designed for the tensile strength of the shear wall plate for the bottom three levels. A 3/8-in. thick splice plate with 5/16-in. fillet weld on top and bottom of the splice plate was used for the splice plate connections for the bottom three levels. A 3/16-in. thick splice plate with 3/16-in. fillet weld on top and bottom of the splice plate was used for the splice plate connections for the top two levels.

The vertical joint between the flange and web of the specimen was made by welding single angles (L2-1/2x2-1/2x1/4 of A36 steel) to the 3/16-in. plates of the flange and web. Considering the forces in the flange to be transferred to the web, the angle thickness and weld size were calculated to be 1/4-in. and 3/16-in., respectively. It was considered that the total force from the flange was transferred to the web via the two welds which extended the specimen height on each side of the web.

The weld joint between 3/16-in. shear wall plates and 3/4-in. foundation connection plates was provided to transfer forces from the shear wall plates to the foundation connection plates. The fillet weld size (7/16 in.) was designed based upon the forces developed assuming tensile fracture of the shear wall plate. Sample weld joint specimens were made and tested under cyclic tension loading to evaluate their performance. Tensile testing of sample specimens proved that the fillet weld joint would resist the forces developed upon tensile fracture of the shear wall plate.

The foundation connection plate was designed considering the combined effect of fracturing of the shear wall plate in tension and the shear transferred to the foundation connection plate during the cyclic loading. The thickness of the foundation connection plate was calculated to be 3/4 in. for a plate of grade A36 steel. Even though there were no strain gauges attached on the plate to measure vertical strains, there was no visible yielding (flaking of mill scale) or fracture of the plate.

The No.7 reinforcing bar hooks were designed considering yielding of the reinforcing bar hooks for the vertical forces from the 3/16-in. shear wall plates upon tensile fracture of the shear wall plates. Yield strain of the reinforcing bar hook was 2070 με. At 29.25 in. from the south end, maximum compressive and tensile strains in No.7 reinforcing bar hook were 1,300 με and 1,250 με, respectively. Maximum compressive and tensile strains in a reinforcing bar hook beneath the flange were 120 με and 300 με, respectively. If extrapolated assuming that the strains over the depth of the section are linear, then the maximum strain at the reinforcing bar hook near the south end would be 2,040 με compared to the yield strain of 2,070 με. Hence the reinforcing bar near the south end was expected to have been close to yielding during the test.

However, this higher strain was concentrated only at that location and the reinforcing bars at the other locations had smaller strains. For example, the maximum strain beneath the flange was 300 με which is only 15% of the yield strain. Hence,

reinforcing bar hooks can be designed considering the actual forces expected from the foundation connection plate at each location instead of designing the reinforcing bars considering tensile fracture of the shear wall plates at all locations. However, further research needs to be conducted to validate this method.

Shear studs welded to the ¾-in. thick foundation connection plate were designed to resist the maximum lateral load applied to the specimen during cyclic load tests. Even though there were no sensors used to monitor fracture of the shear studs, there were no obvious indications of shear stud failures.

Almost the entire length of the 3/16-in. shear wall plates at the foundation yielded during the test (however not at the same time) as expected. At the 85.5-in. height, the web plate up to about 31.5 in. from the south end yielded in tension while the other parts of the plate remained elastic. At the 8-in. height, the web plate up to about 54 in. from the south end yielded in tension, while the web plate up to a distance between 18 and 36 in. from the south end yielded in compression. At the 1-in. height, almost the entire web and both flange plates yielded in tension, while the web plate up to a distance between 18 in. and 36 in. from the south end and the extreme flange plate yielded in compression.

6.8.3: Expectation and results from the test

The main purpose of the cyclic load test was to verify whether the designed components of the specimen fulfilled the purpose for which they were designed. Splice plates, fillet welds between the splice plates and shear wall plates, the angles in the corner connection, fillet weld between the angles and splice plates, fillet weld between the shear wall plate and foundation connection plate, the foundation connection plate, reinforcing bar hooks welded to the foundation connection plate, and shear studs welded to the foundation connection plate all resisted the forces transferred to them when the specimen was pushed to 2% drift in the north direction.

Tensile strains developed at the south end when the specimen was pushed towards the north for a given drift were always larger than the compressive strains developed at the south end when the specimen was pushed towards the south for the same drift. This trend was noticed for different load cycles and at various heights of the specimen. Hence, pushing the specimen in the north direction would develop larger tensile strains in the splice plates, fillet welds between the splice plates and the shear wall plates, fillet weld between the shear wall plates and foundation connection plates, the foundation connection plate and reinforcing bar hooks at the south end. The plate at the south end buckled at approximately 0.75% drift when the specimen was pushed towards the south. If buckling of the plate could have been prevented, then the splice plates, fillet welds between the splice plates and the shear wall plates, fillet welds between the shear wall plates and the foundation connection plates, the foundation connection plates, and the reinforcing bar hooks might have been able to resist the forces when the specimen was pushed to 2% drift in the south direction too.

Buckling of the plate could be delayed by the following methods.

1. Decreasing the vertical spacing between the transverse bars in the web (especially at the extreme end of the web) so that the height of the plate for buckling would be reduced.

2. Decreasing both vertical and horizontal spacing between the transverse bars in the web (especially at the extreme end of the web) so that the concrete could be confined more.

3. Providing more reinforcement in the web (especially at the extreme end of web) so that the concrete could be confined more.

4. Increasing the thickness of the shear wall plates in the web while keeping the thickness of the shear wall plate in the flange unchanged. By doing this,

the moment capacity of the section would be increased. Then all the other shear wall components (welds and connections) would need to be redesigned.

5. Welding the end plate at the end of the web solidly to the shear wall plates so that the concrete could be confined more. Shear studs can be welded to the end plate to prevent buckling of the end plate and subsequently buckling of the shear wall plates.

6. Building a smaller flange at the south end similar to that used on the north side of the wall. Then the neutral axis would be moved towards the south end. The new flange would take a larger portion of the load taken by the web earlier. The moment capacity of the section would be notably increased. All the other shear wall components (welds and connections) would need to be redesigned.

If buckling of the plate could be prevented by implementing some of the methods described above, then the design approach used in this test could be used to design the structural components for dual-plate composite shear walls to resist cyclic lateral loading up to 2% drift ratio, and perhaps even greater drift ratios.

Table 6.1 Voltage, amperage, and speed of each three passes of the 7/16-in. fillet weld

Weld Pass	Voltage	Amperage (average)	Speed (average) (inch/min)
1st	23.5	238~280	9.1
2nd	23.5	234~280	9.9
3rd	21.5	205~255	10.2

Table 6.2 Average measured weld size of the 7/16-in. fillet weld between foundation connection plates and shear wall plates

Location in the joint	Leg Size Horizontal (in)	Leg Size Vertical (in)	Final Effective Throat size (in)	Designed Effective Throat size (in)
Web (East side)	0.538	0.428	0.335	0.309
Web (West side)	0.530	0.459	0.347	0.309
Flange (North side)	0.512	0.469	0.346	0.309
Flange (South side)	0.517	0.453	0.341	0.309

Note: North side – strong wall to specimen direction (or web to flange direction)

Table 6.3 Average measured weld size of the fillet weld between the angle and shear wall plate at web-to-flange intersection – First story

Location in the joint	Leg Size Perpendicular to 3/16" plate (in)	Leg Size Along 3/16" plate (in)	Final Effective Throat size (in)	Designed Effective Throat size (in)
East joint - Flange plate	0.192	0.205	0.140	0.133
East joint - web plate	0.203	0.189	0.138	0.133
West joint - web plate	0.175	0.215	0.136	0.133
West joint - Flange plate	0.187	0.225	0.144	0.133

Table 6.4 Displacement and drift ratio achieved during each cycle

Cycle	Deflection (in)	Drift (%)
1-S	0.375	0.125
1-N	0.375	0.125
2-S	0.75	0.25
2-N	0.75	0.25
3-S	0.75	0.25
3-N	0.75	0.25
4-S	1.5	0.5
4-N	1.5	0.5
5-S	1.5	0.5
5-N	1.5	0.5
6-S	3	1.0
6-N	3	1.0
7-S	3	1.0
7-N	6	2.0

Table 6.5 Moment and curvature at the peak of cycle 5N

Height (in)	Moment (kip-ft)	Curvature ($1/ft*10^{-6}$)	Ratio of Curvature/Moment ($Kip^{-1}*ft^{-2}*10^{-6}$)
1	4028	1395	0.35
8	3890	555	0.14
85.5	2840	284	0.10

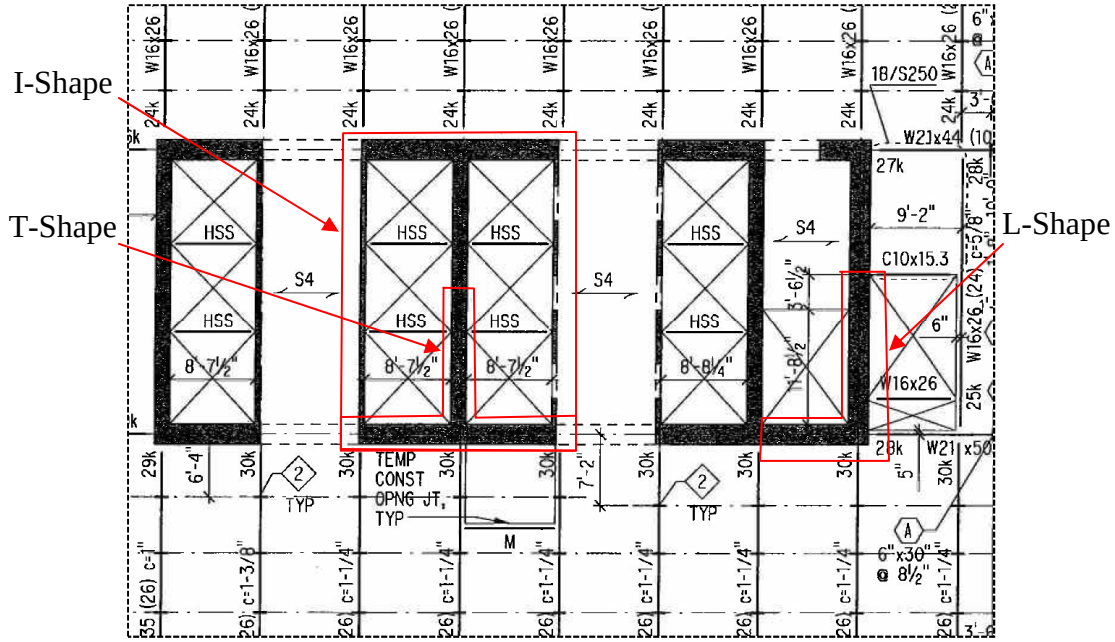

Figure 6.1 Different shapes of shear wall components in a typical shear wall layout (Washington Mutual / Seattle Art Museum, Seattle, WA – 55 story)

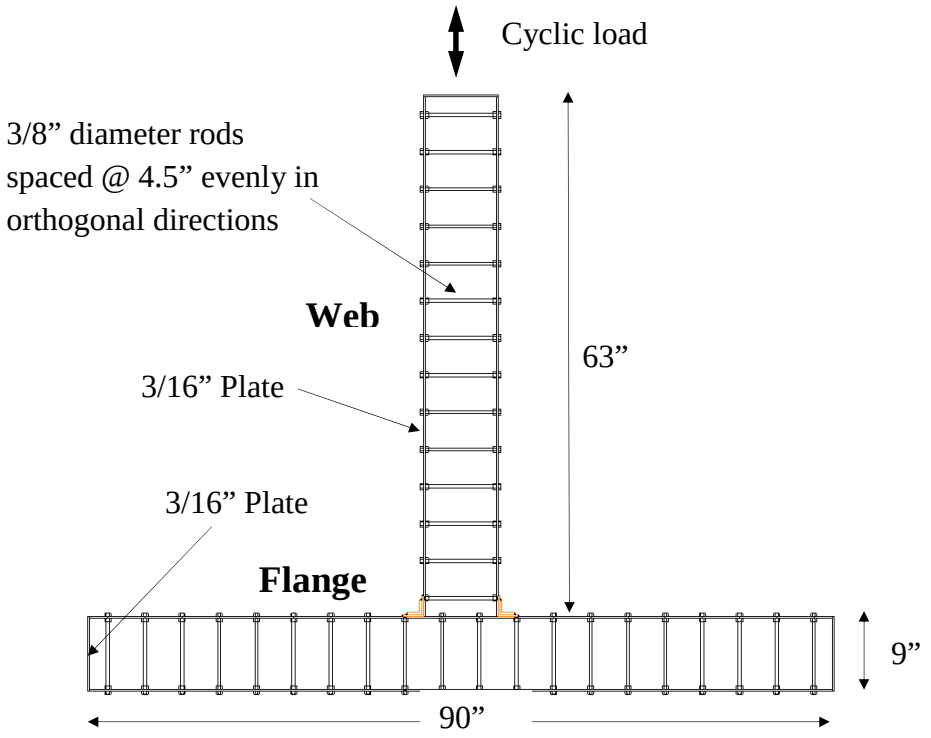

Figure 6.2 T-shaped intersecting wall specimen (3/8-scale of prototype)

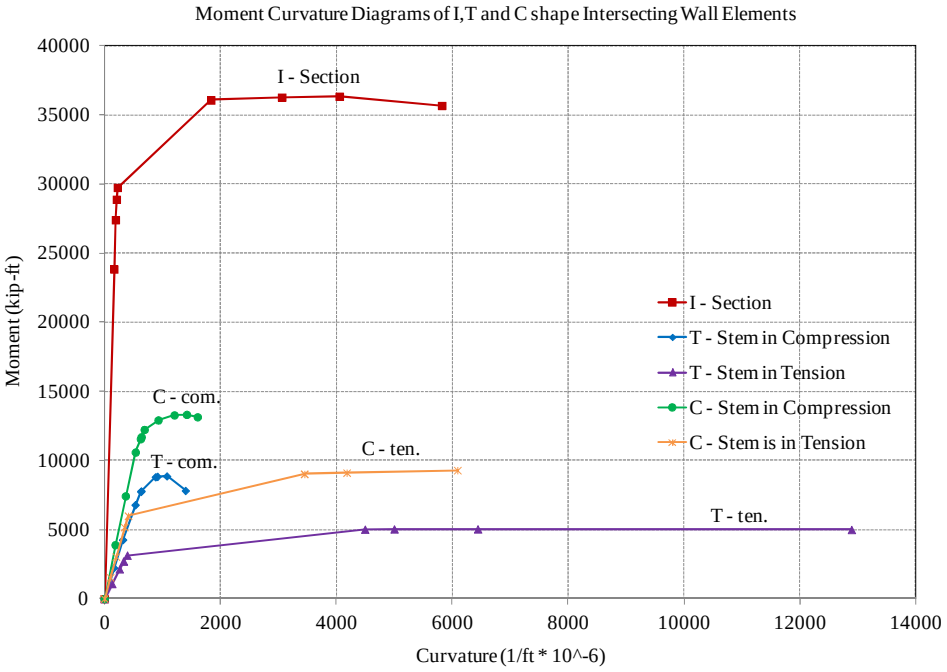

Figure 6.3 Moment curvature diagrams for I, T and C-shaped walls

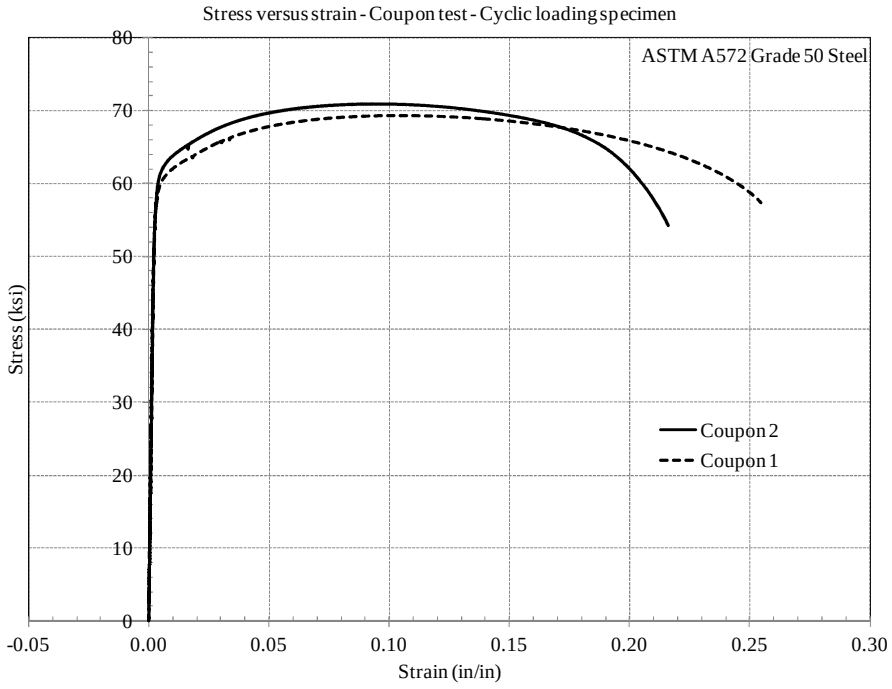

Figure 6.4 Stress versus strain response from coupon test – 3/16-in. plates

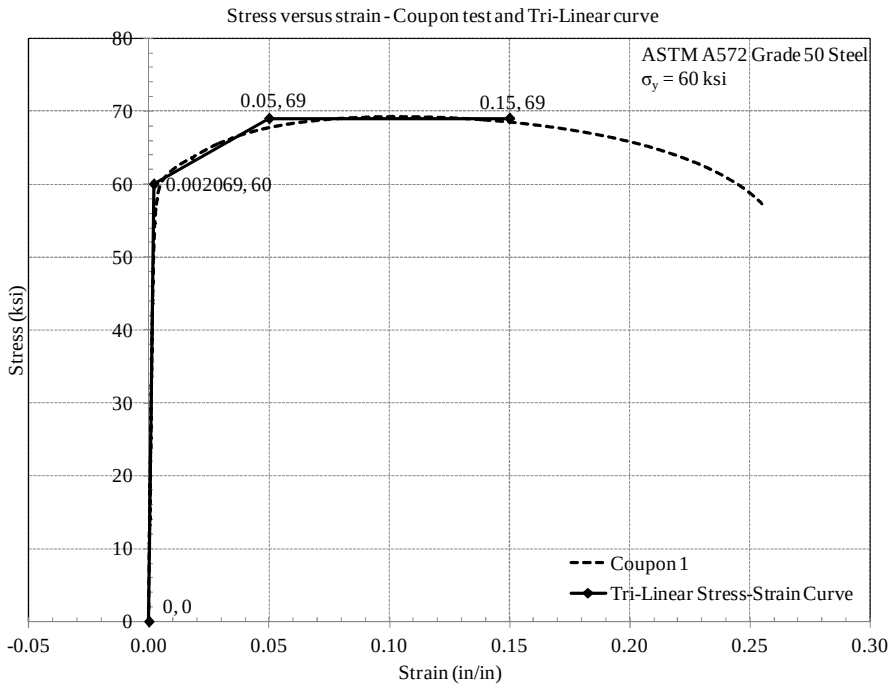

Figure 6.5 Tri-linear model of stress versus strain curve from coupon test

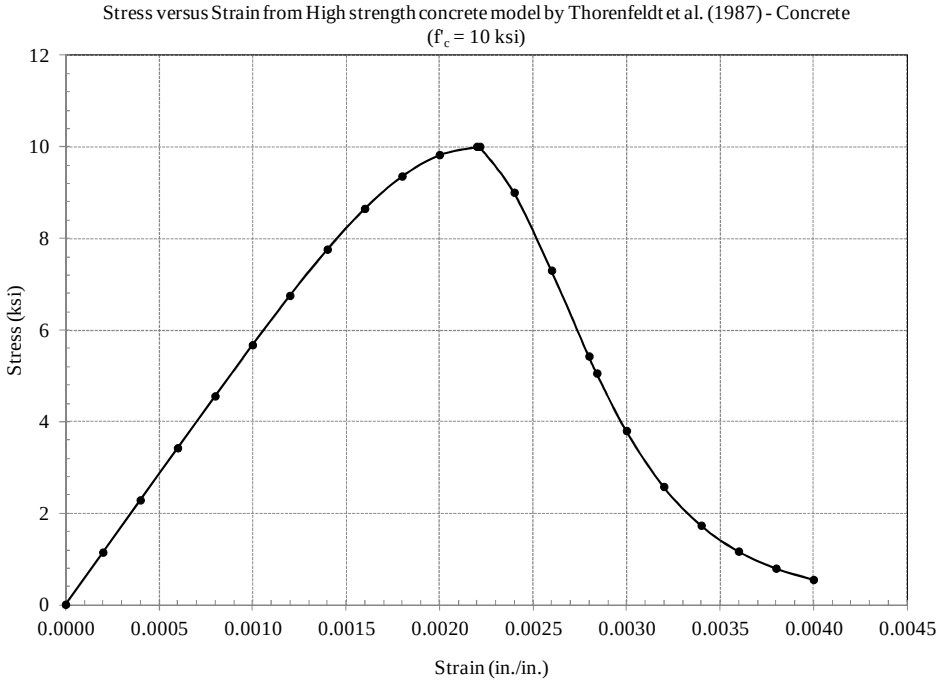

Figure 6.6 Stress-strain model for concrete (10 ksi)

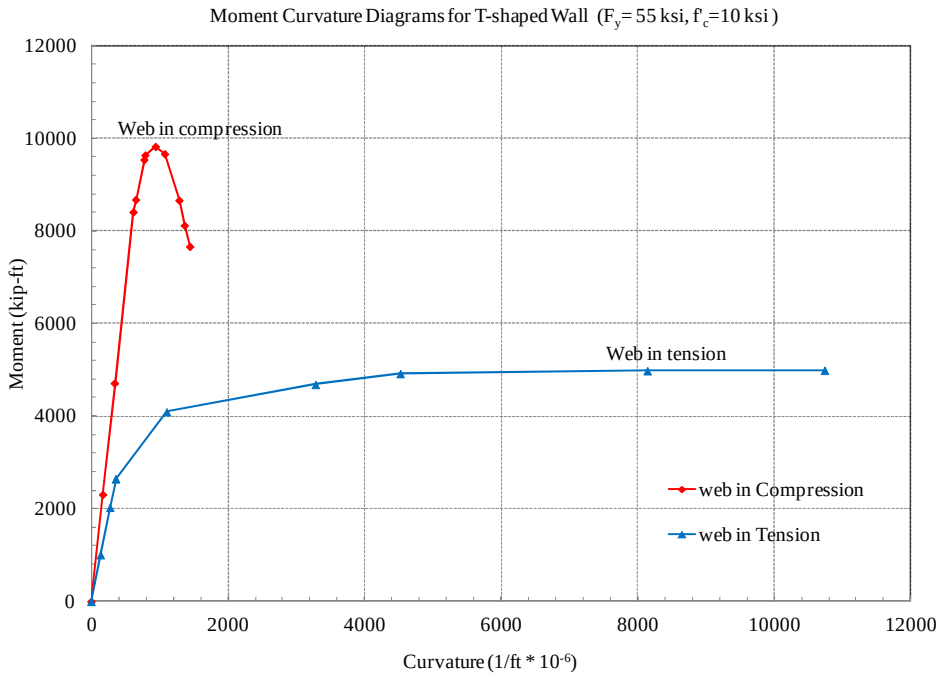

Figure 6.7 Moment curvature diagrams for the T-shaped wall for F_y = 55 ksi and f'_c = 10 ksi

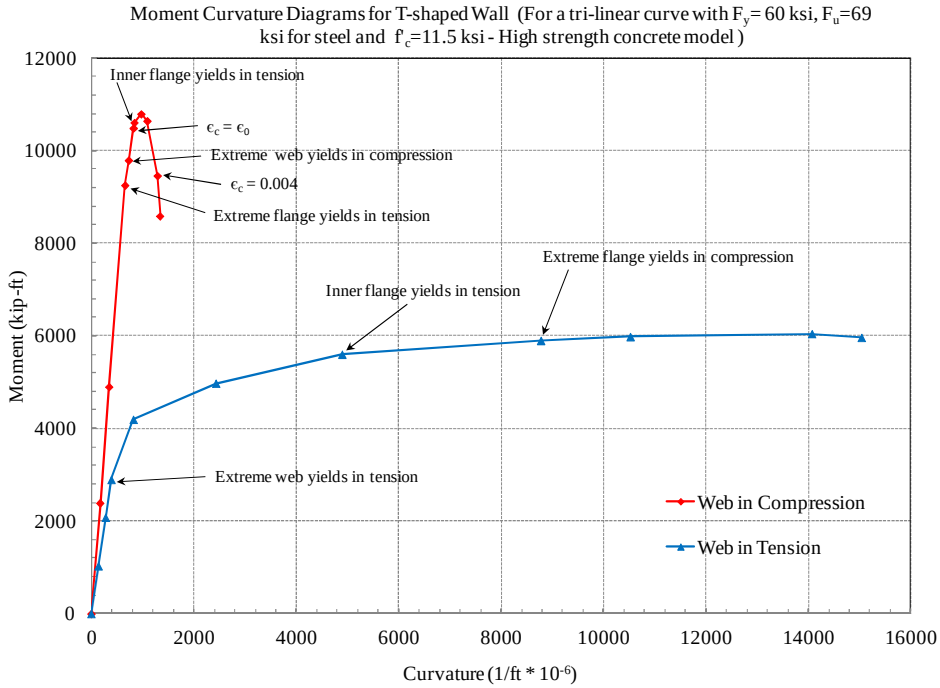

Figure 6.8 Moment curvature diagrams for the T-shaped wall for F_y = 60 ksi, F_u = 69 ksi and f'_c = 11.5 ksi

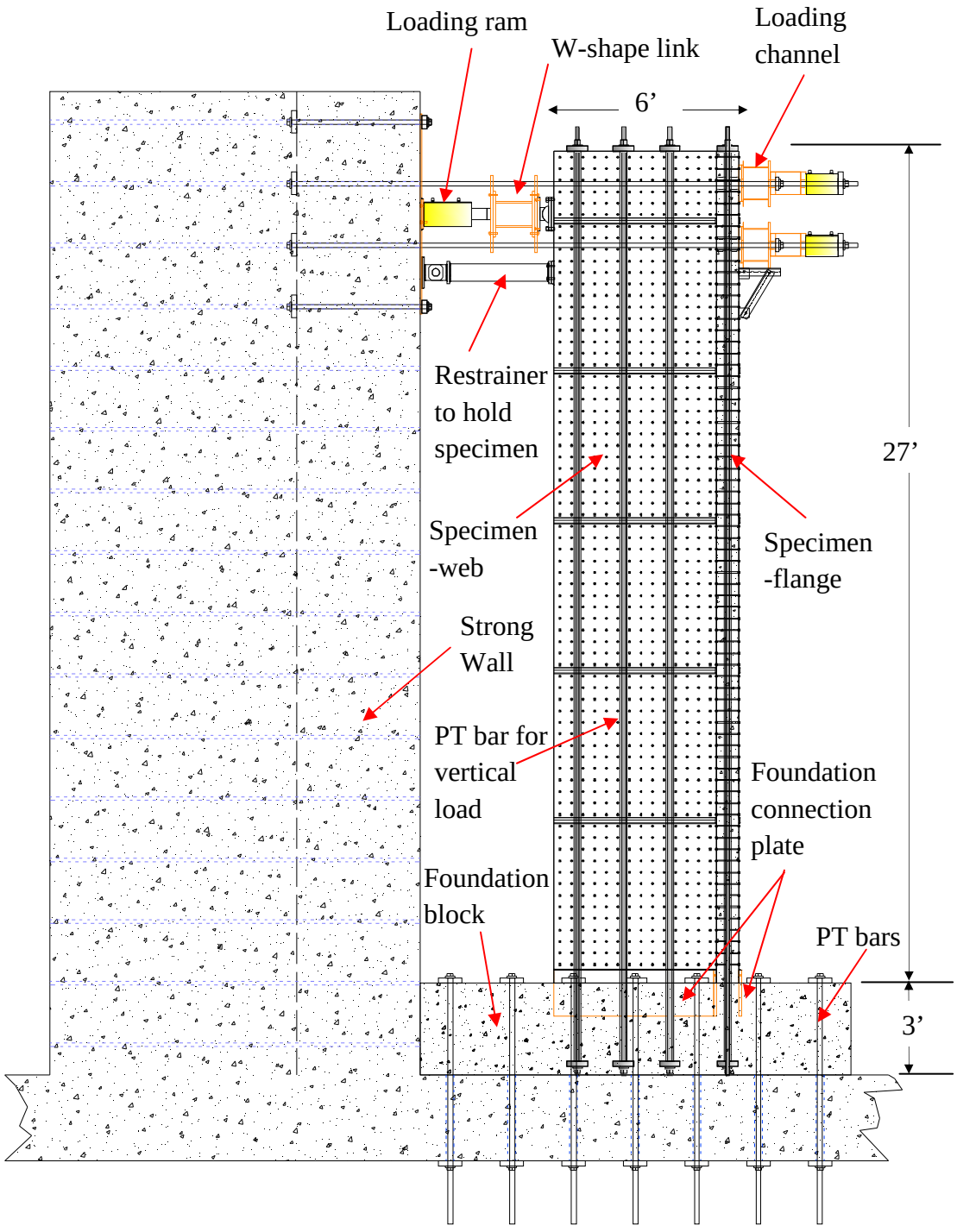

Figure 6.9 Side view of cyclic loading test set-up (view from East to West)

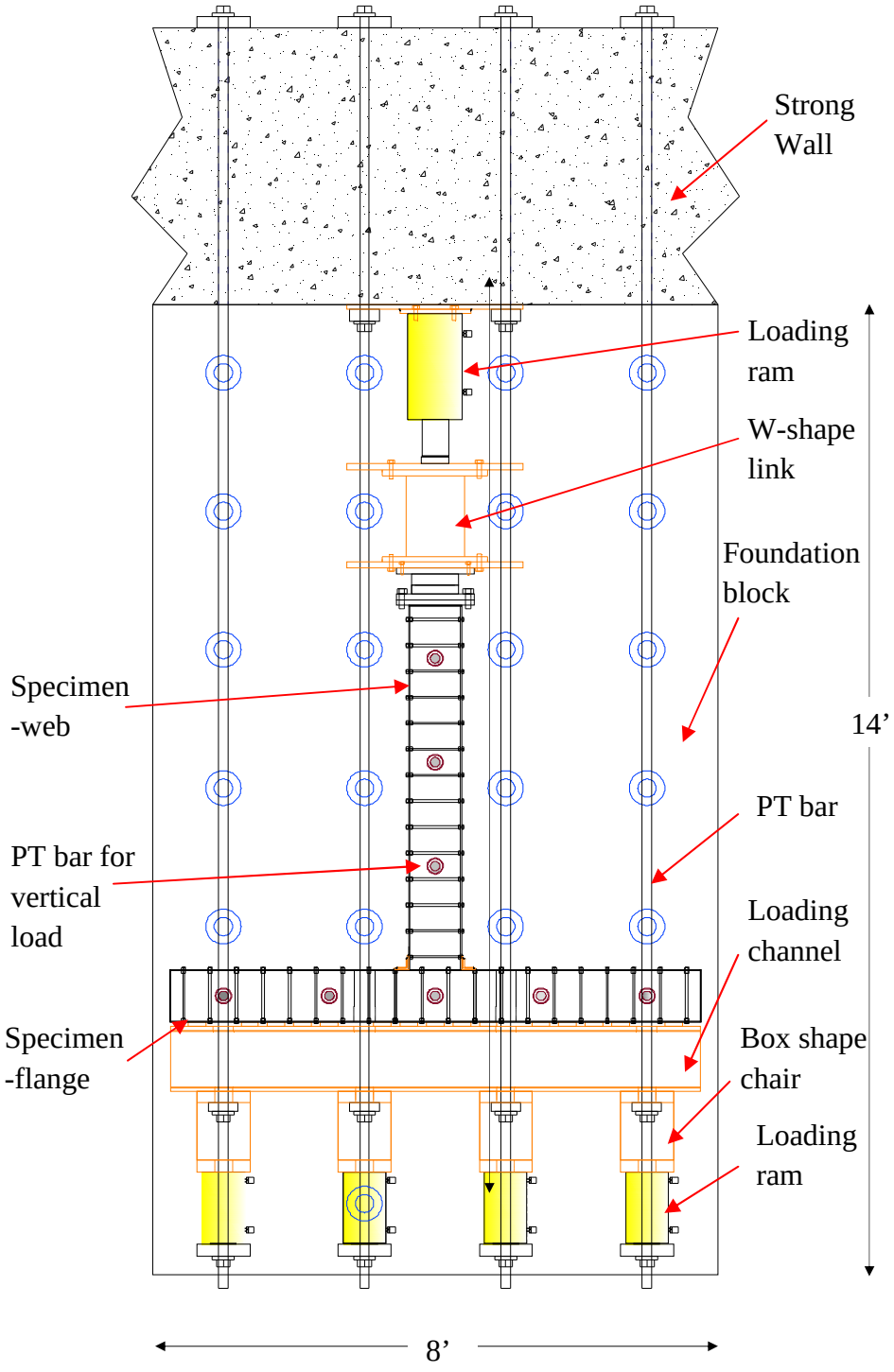

Figure 6.10 Plan view of cyclic loading test set-up

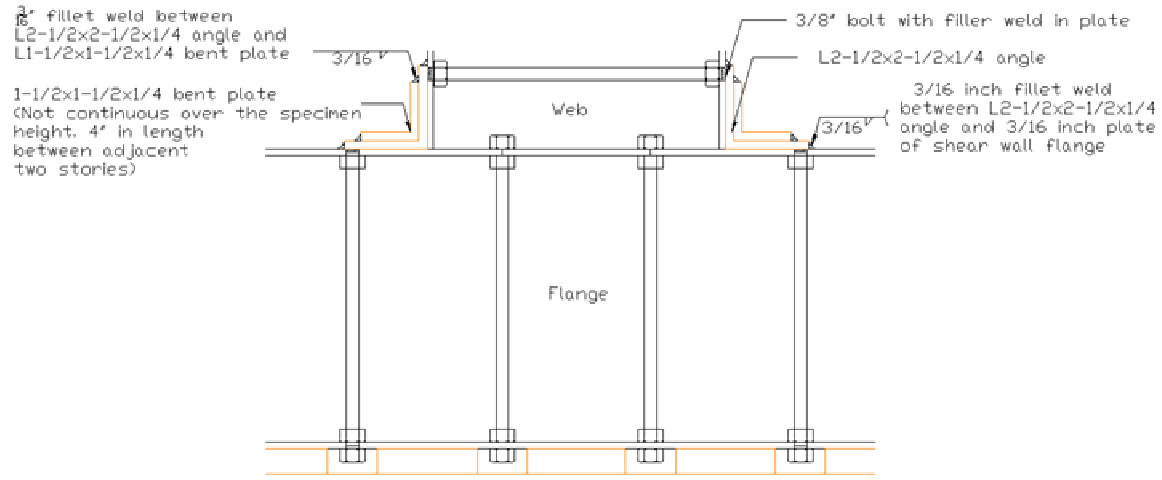

Figure 6.11 Connection details at the intersection of the web and flange plate assemblies – Plan view

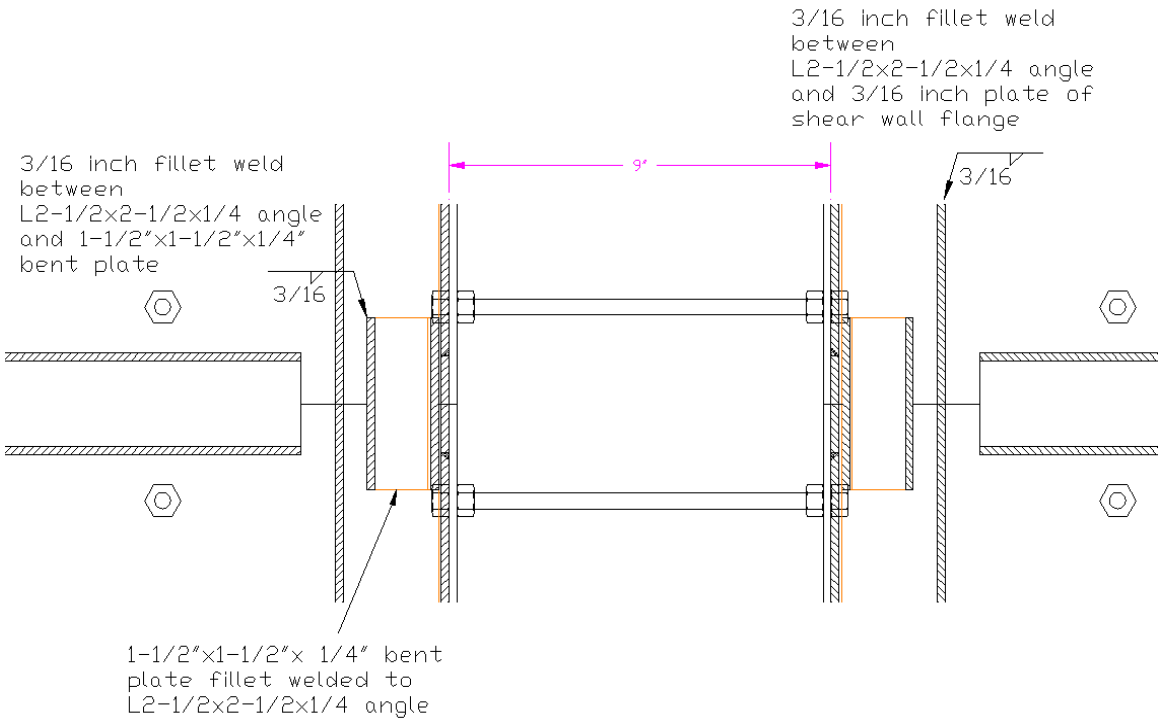

Figure 6.12 Joint details at intersection between 2nd and 3rd Story – Front view

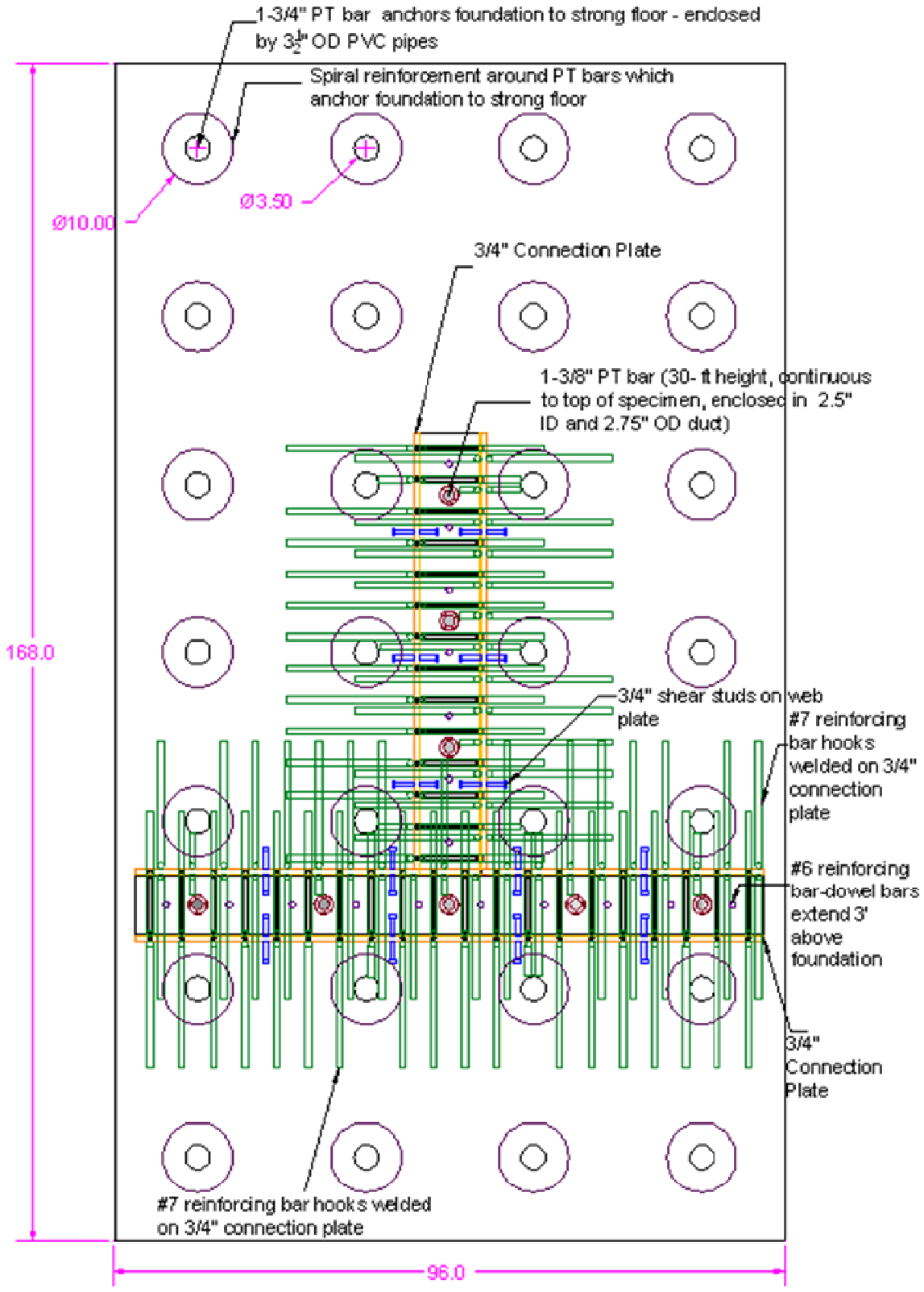

Figure 6.13 Plan view of the foundation block

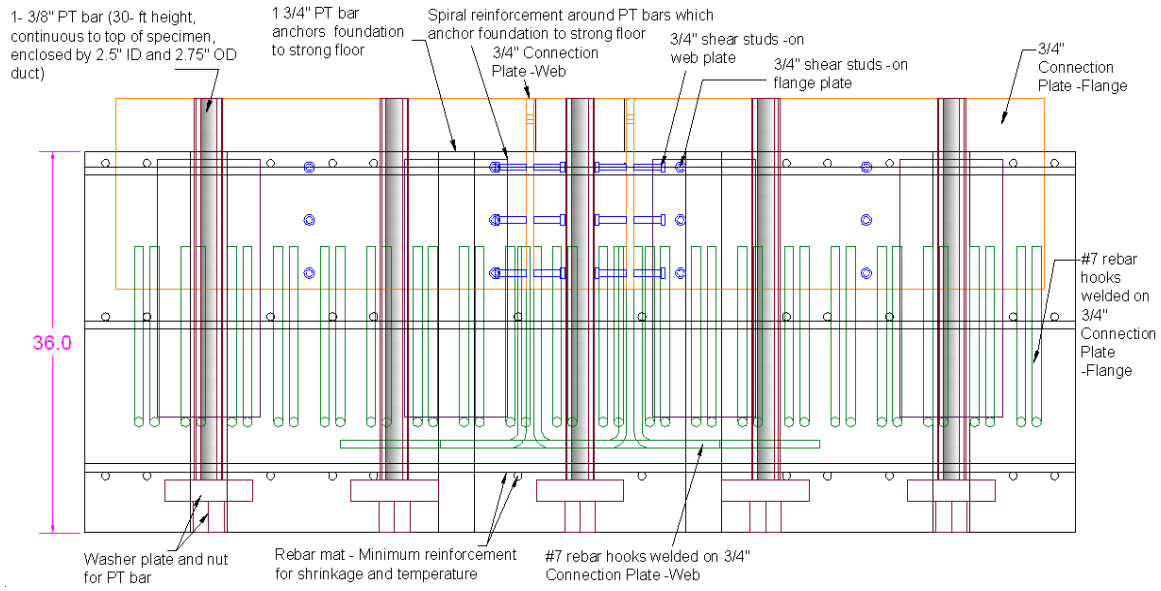

Figure 6.14 Elevation view of the foundation block

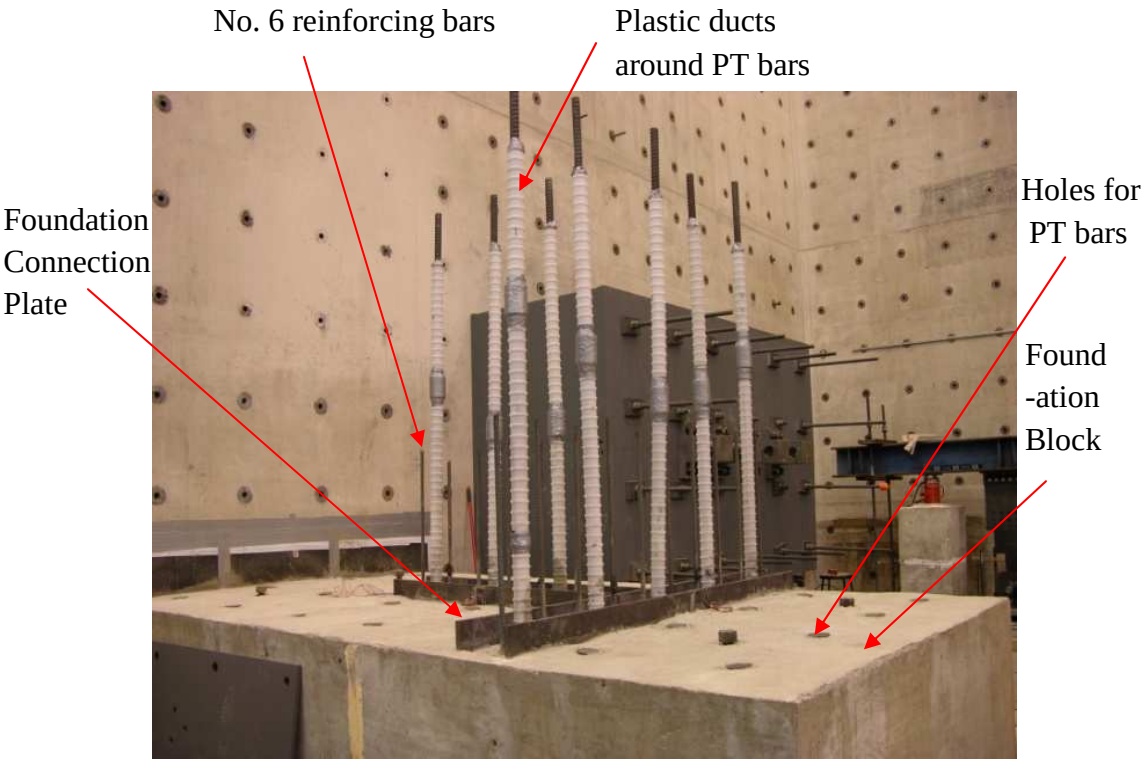

Figure 6.15 Foundation block for the cyclic loading test (view from NE to SW)

Figure 6.16 Foundation reinforcing bar cage before enclosed by forms

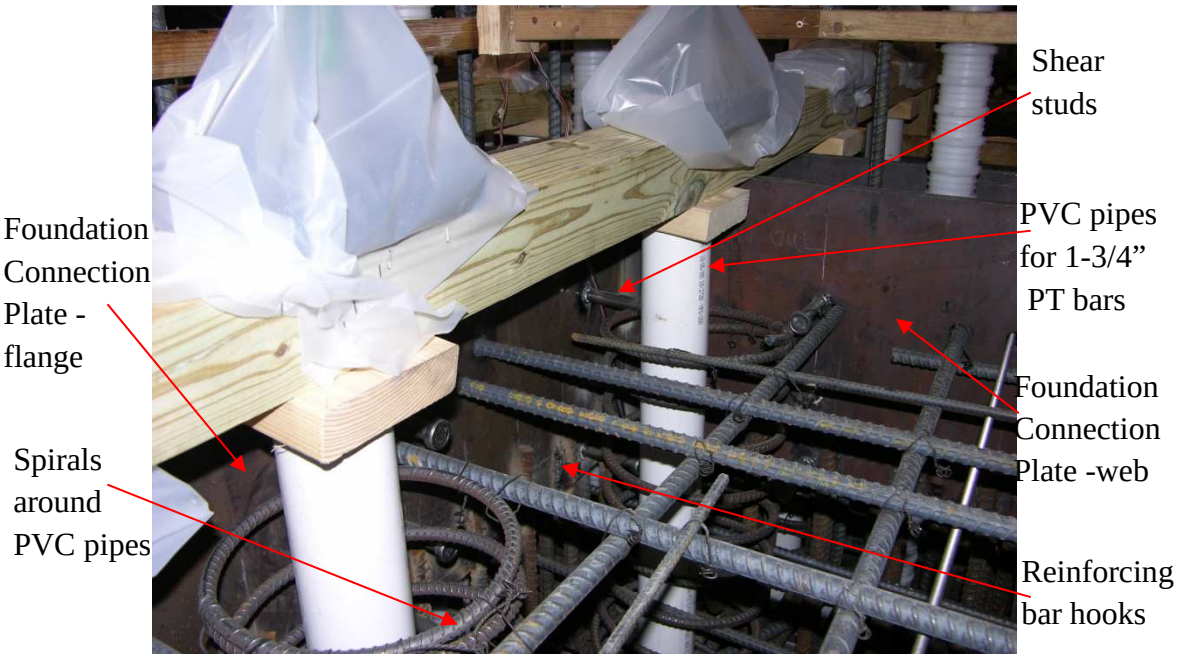

Figure 6.17 Spirals, shear studs and reinforcing bar hooks – view from SW to NE

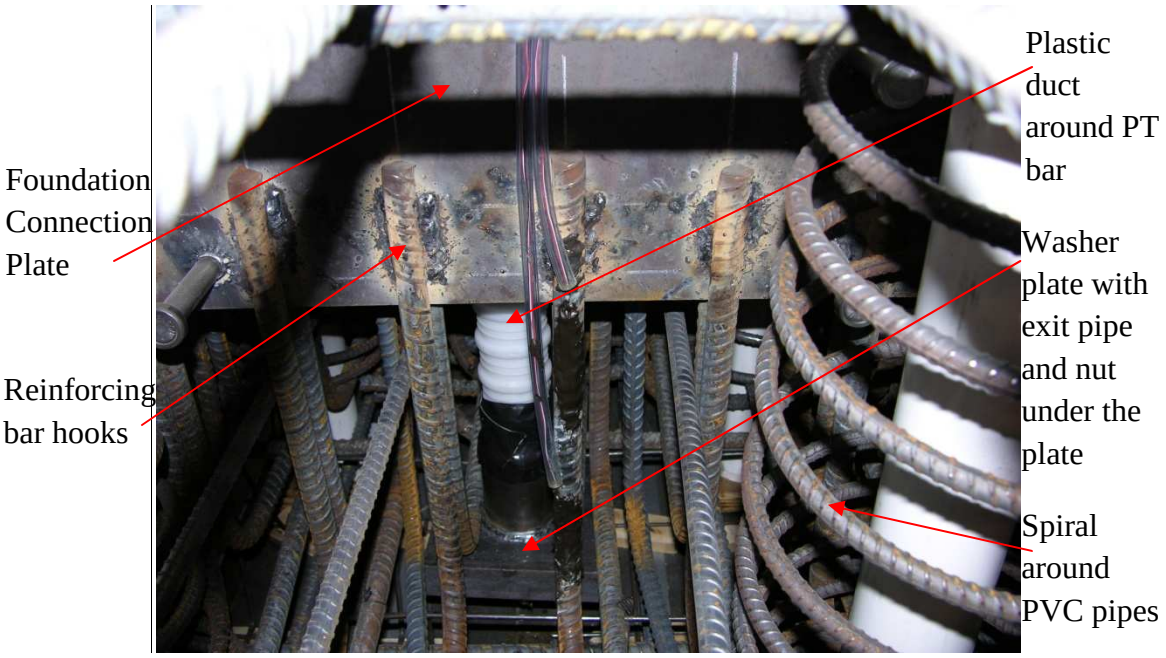

Figure 6.18 Washer plate with exit pipe at bottom of the PT bar

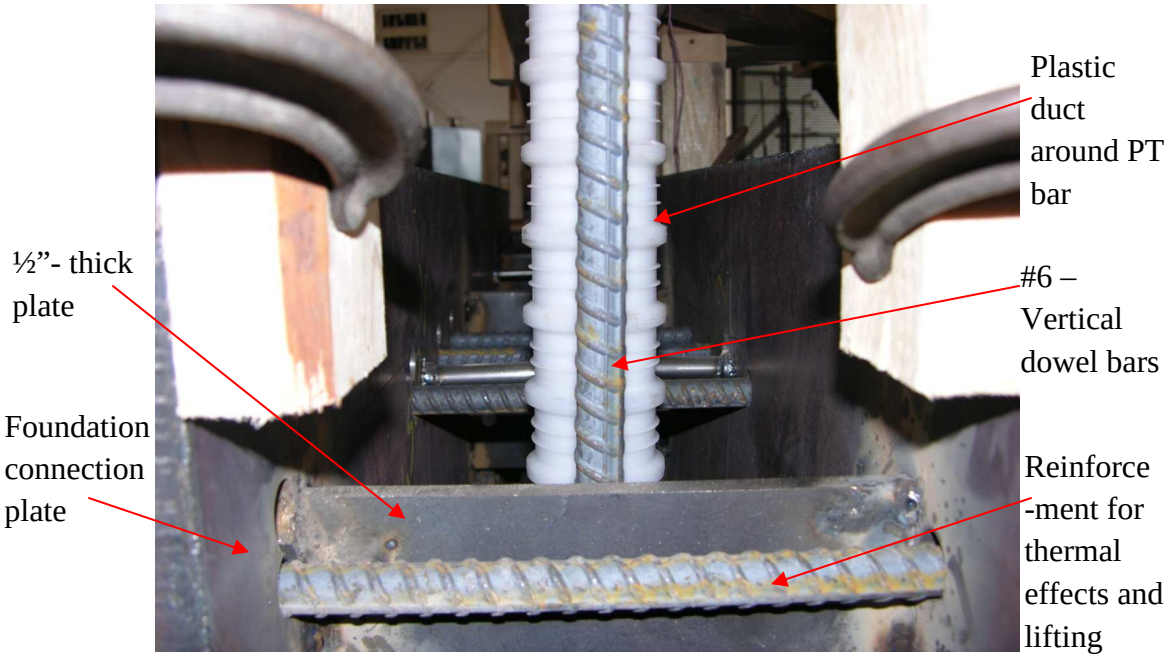

Figure 6.19 Securing foundation connection plates

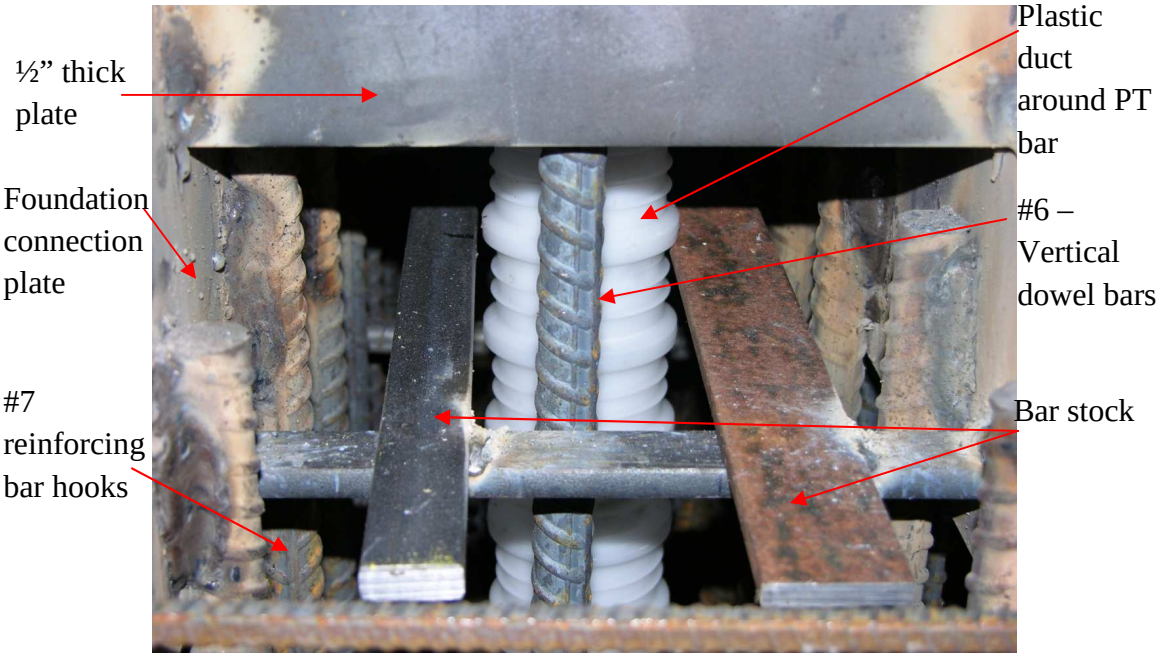

Figure 6.20 Securing ducts around PT bars intended for vertical load

Figure 6.21 Foundation formwork before casting concrete

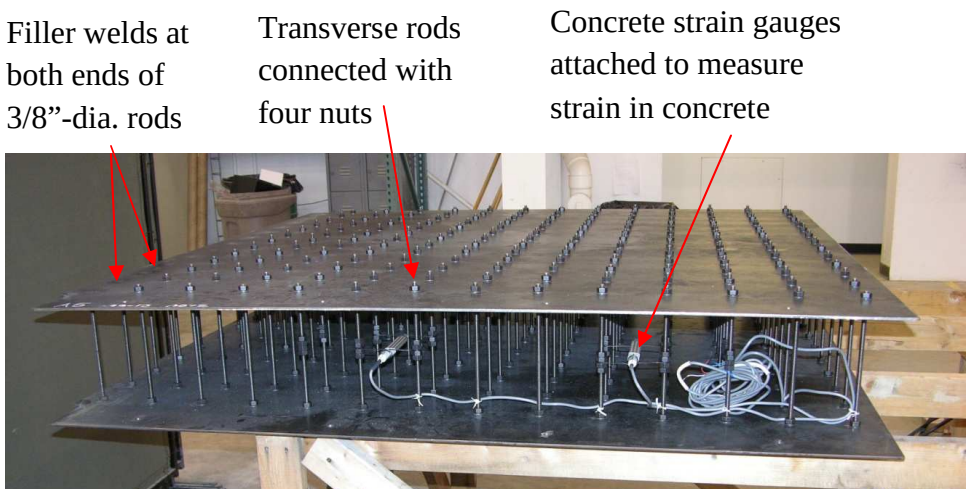

Figure 6.22 A web panel assembly (first story)

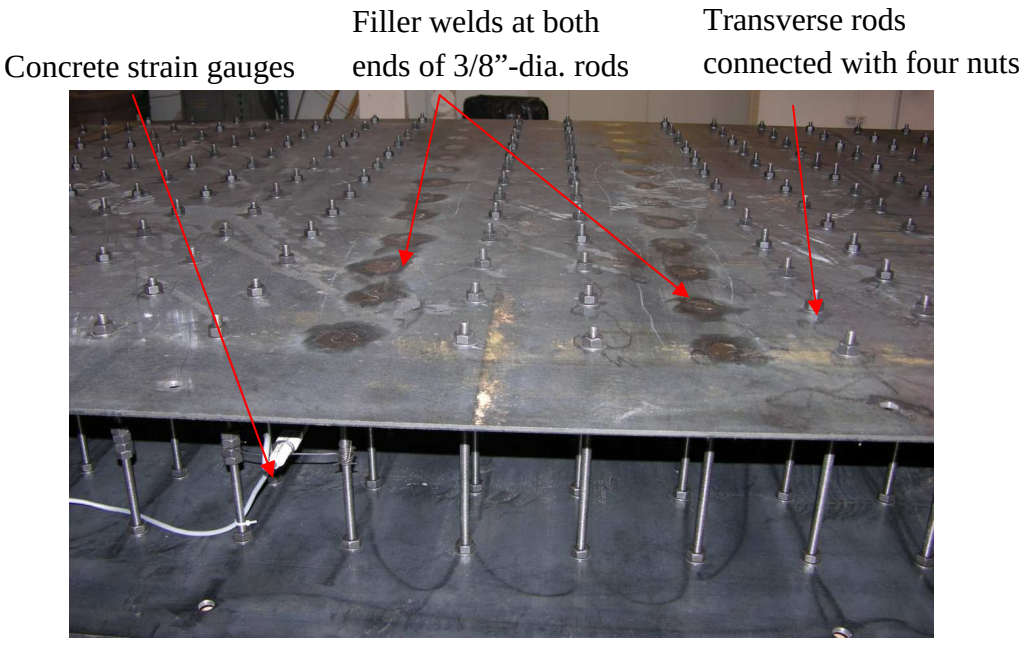

Figure 6.23 A flange panel assembly (first story)

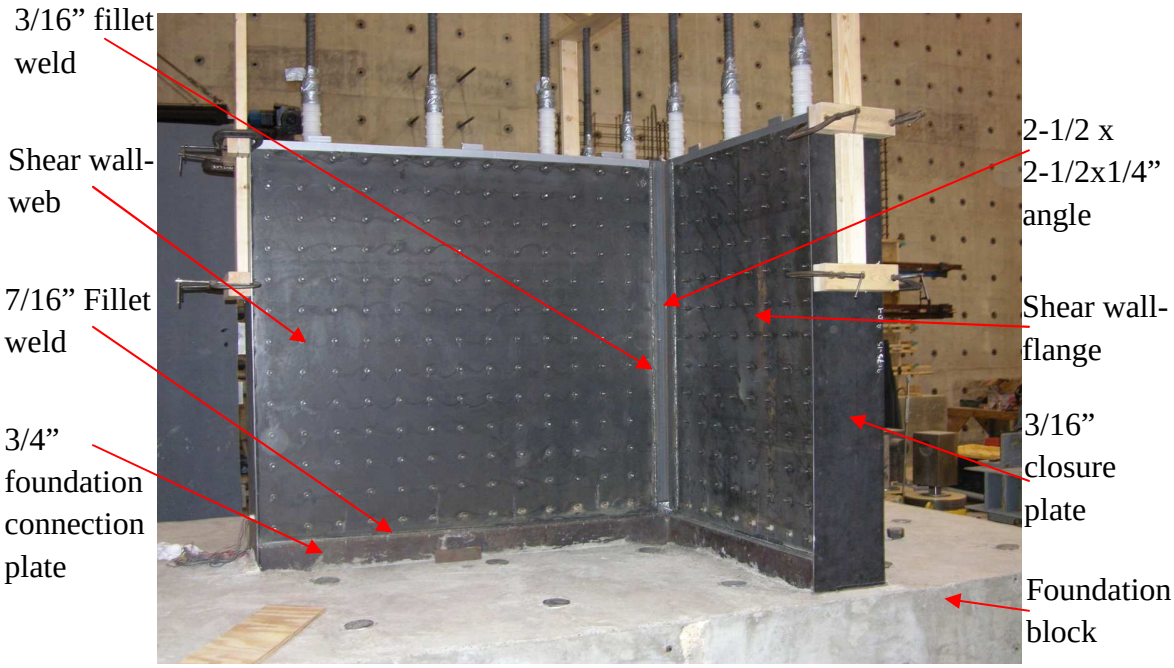

Figure 6.24 First story panel assembly erected

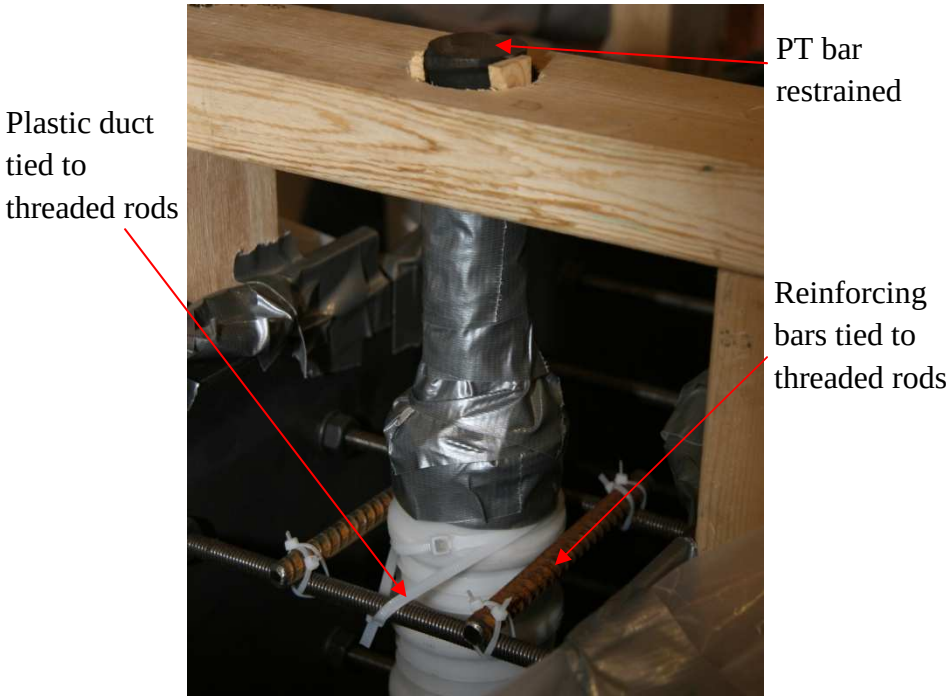

Figure 6.25 Securing vertical PT bar and the plastic duct around the PT bar

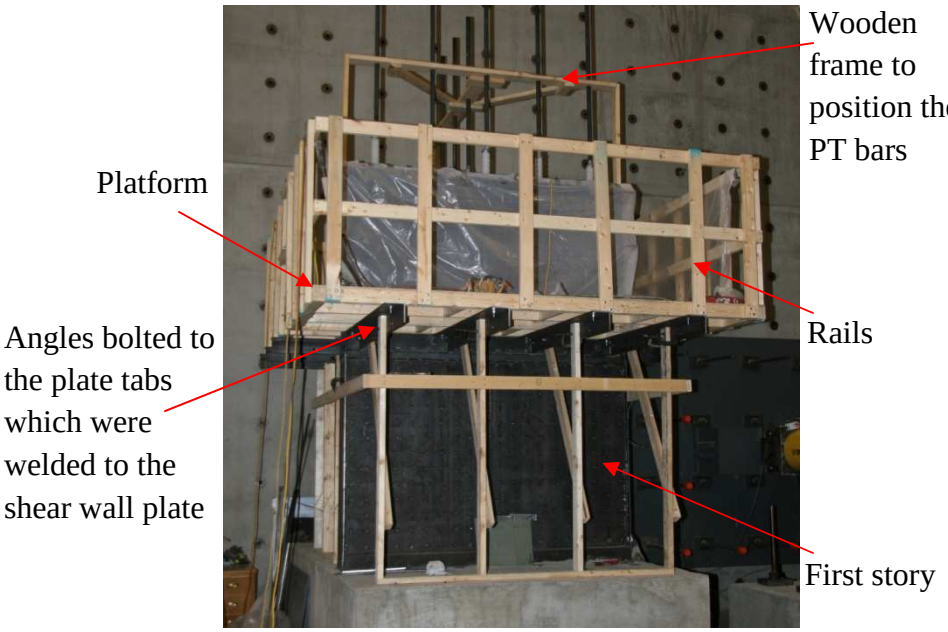

Figure 6.26 Second story ready for casting- with platform attached

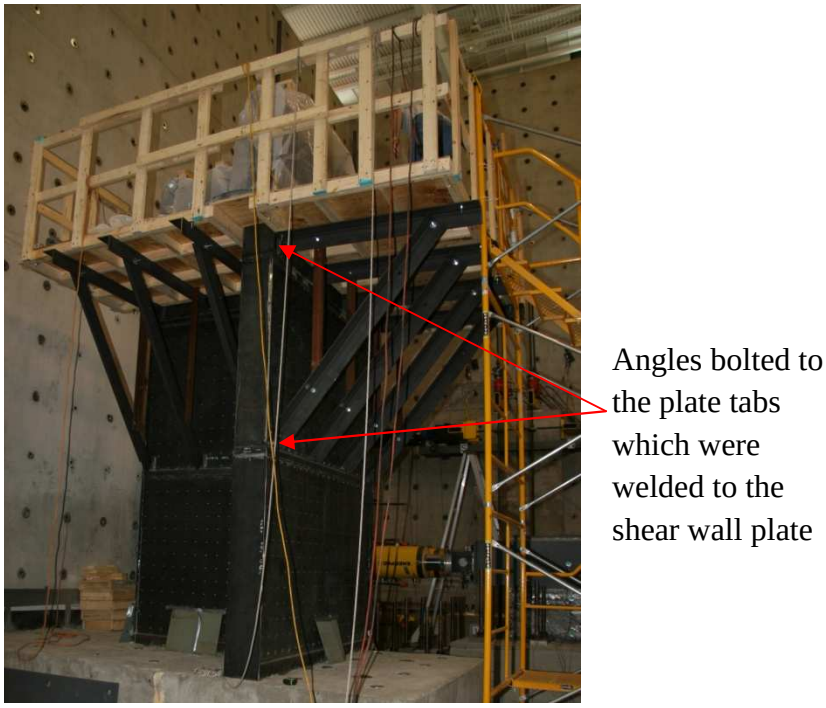

Figure 6.27 Third story ready for casting- with platform attached

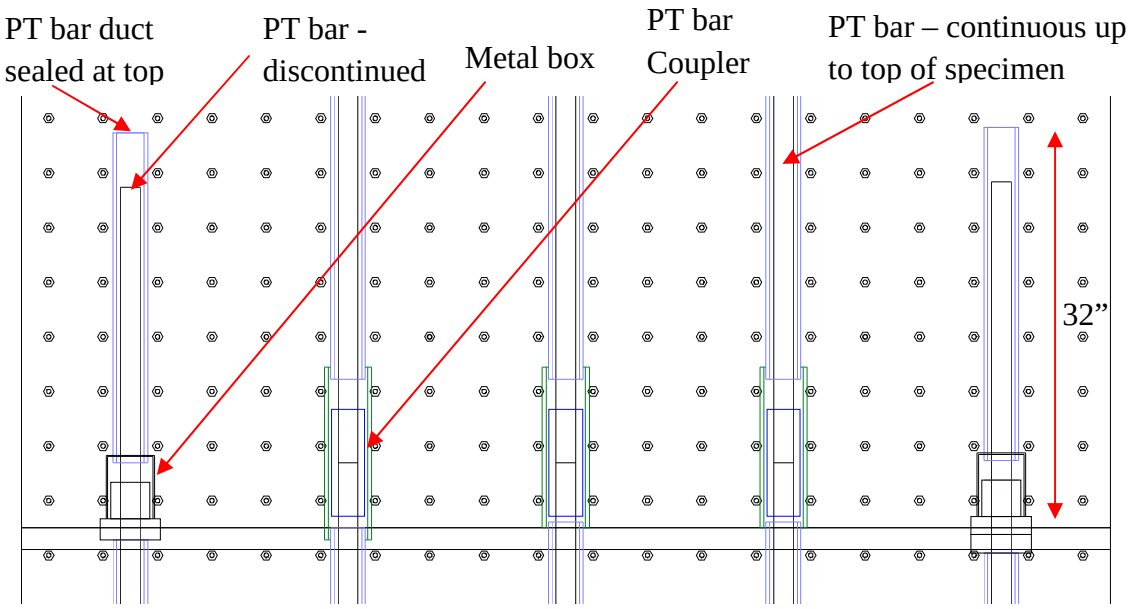

Figure 6.28 PT bars in the flange at third story level

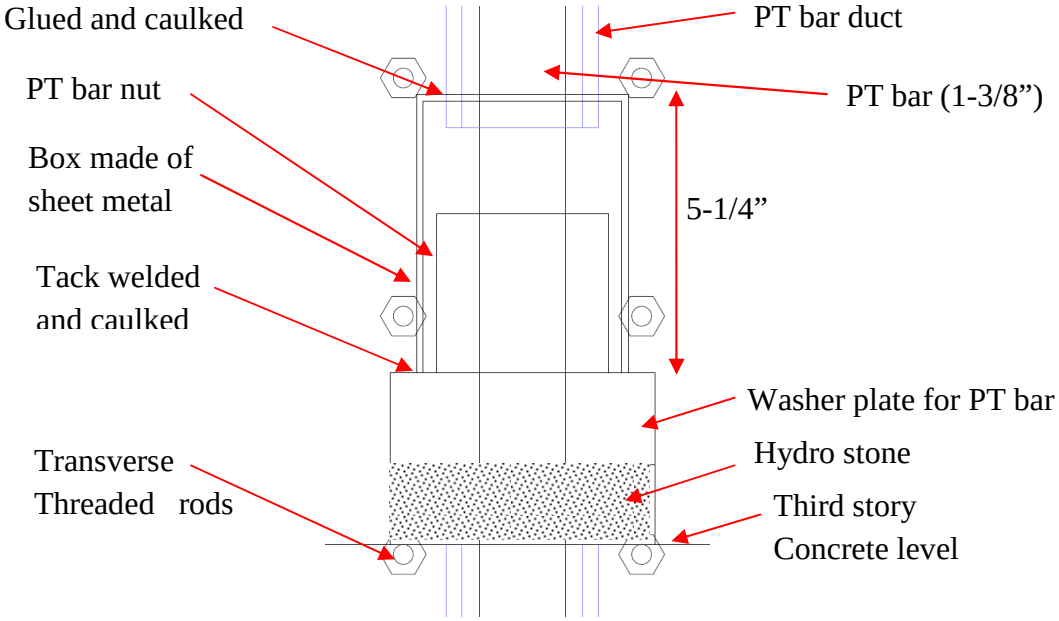

Figure 6.29 Hardware for the discontinued PT bars at the third story level

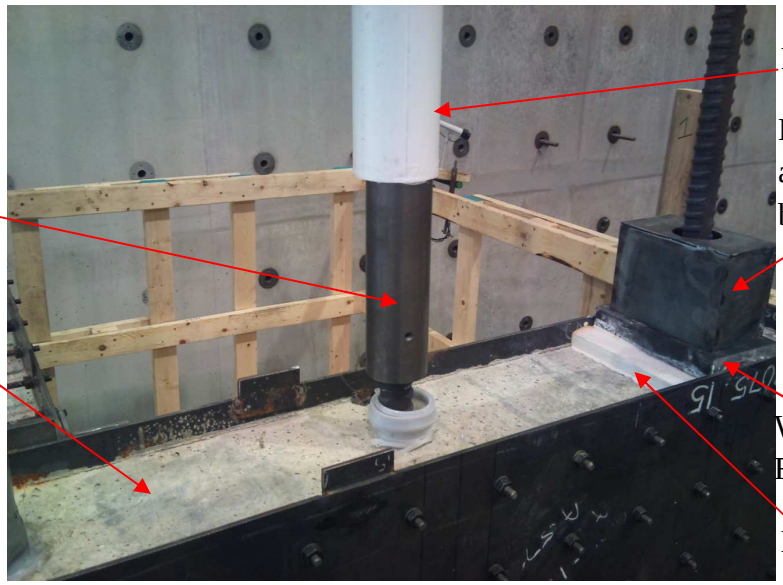

Figure 6.30 Coupler joint for a continued PT bar and hardware for discontinued PT bar –in process- at third story level

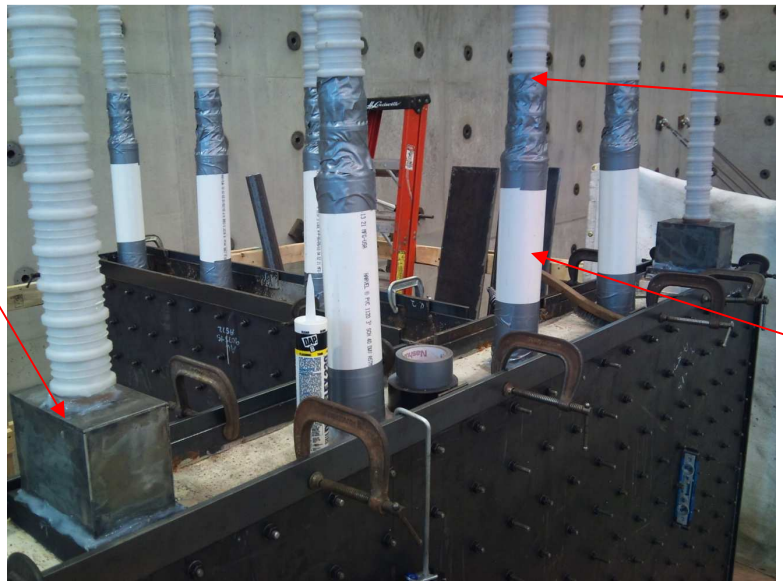

Figure 6.31 PT bars at the third story level

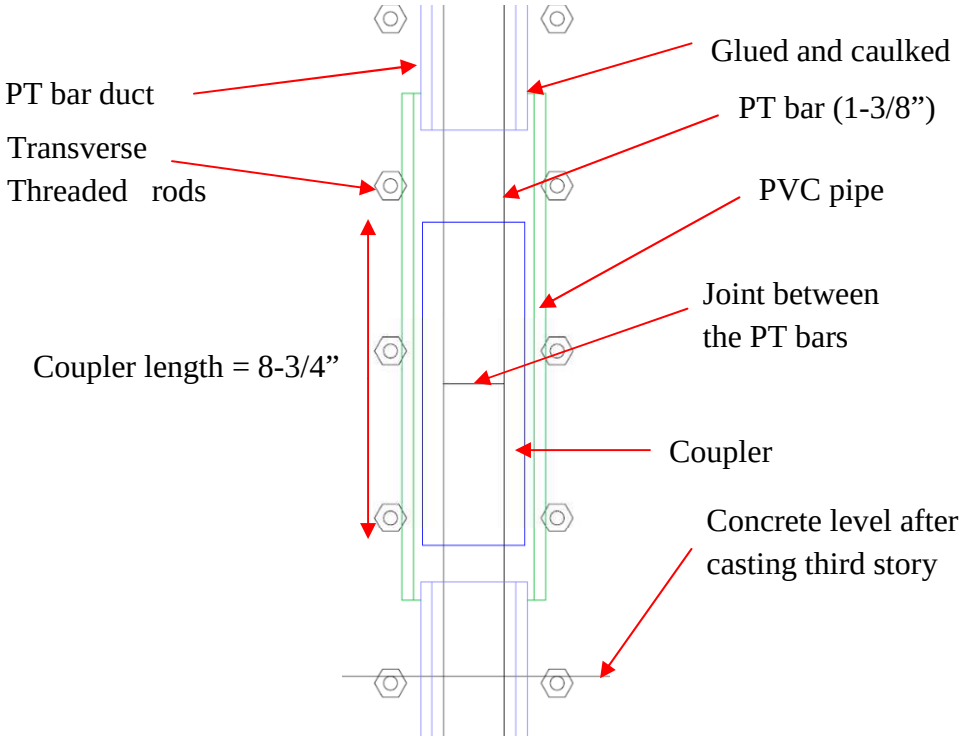

Figure 6.32 Coupler joint for vertical PT bar at the third story level

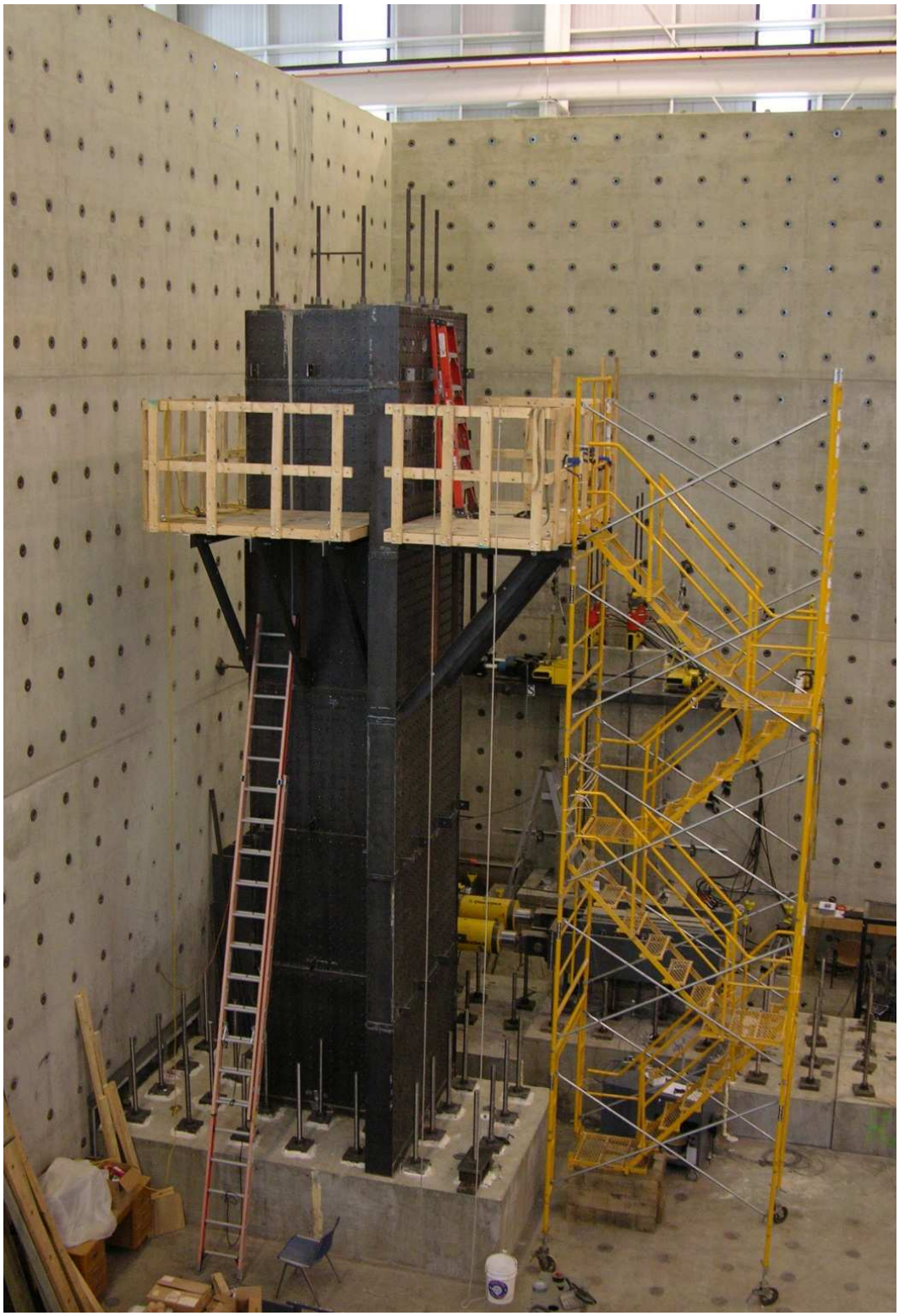

Figure 6.33 Specimen - completed

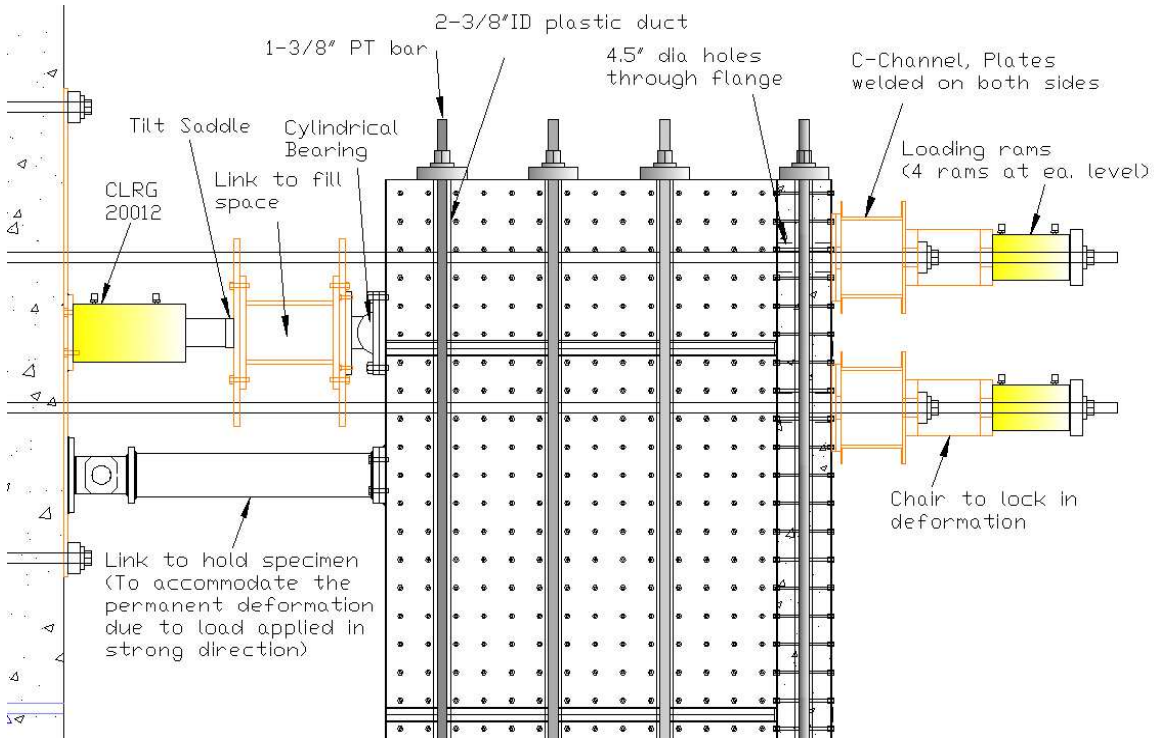

Figure 6.34 Loading Set up - Side view of the cyclic loading test set-up

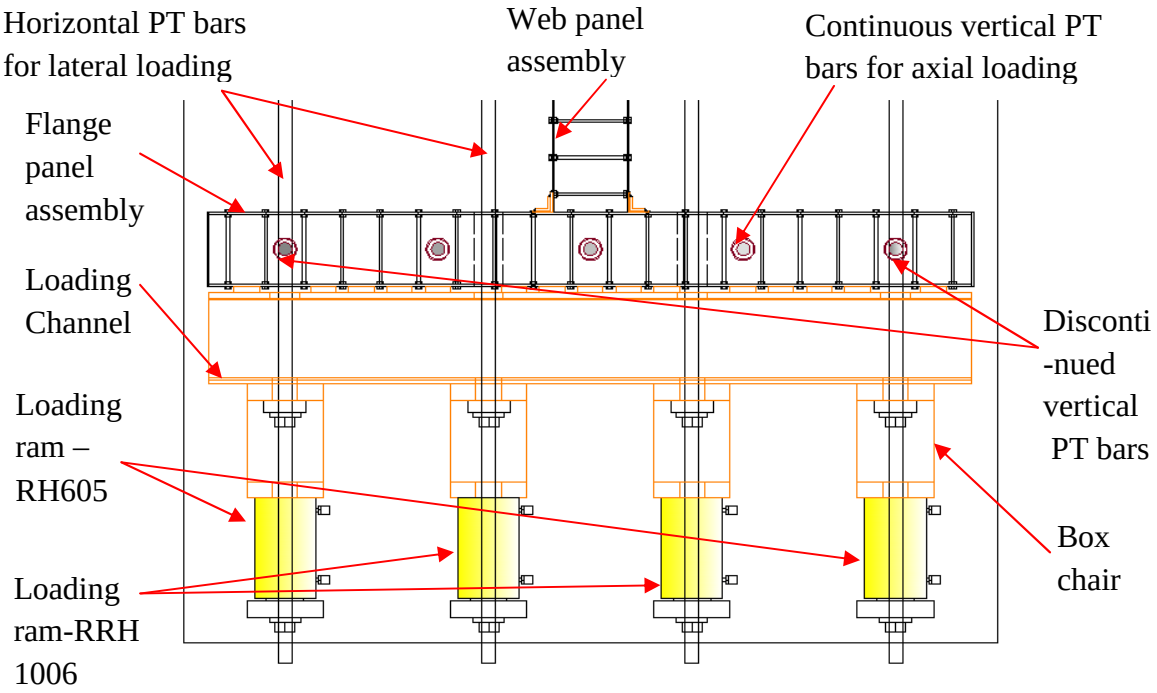

Figure 6.35 Plan view of a portion of the loading system

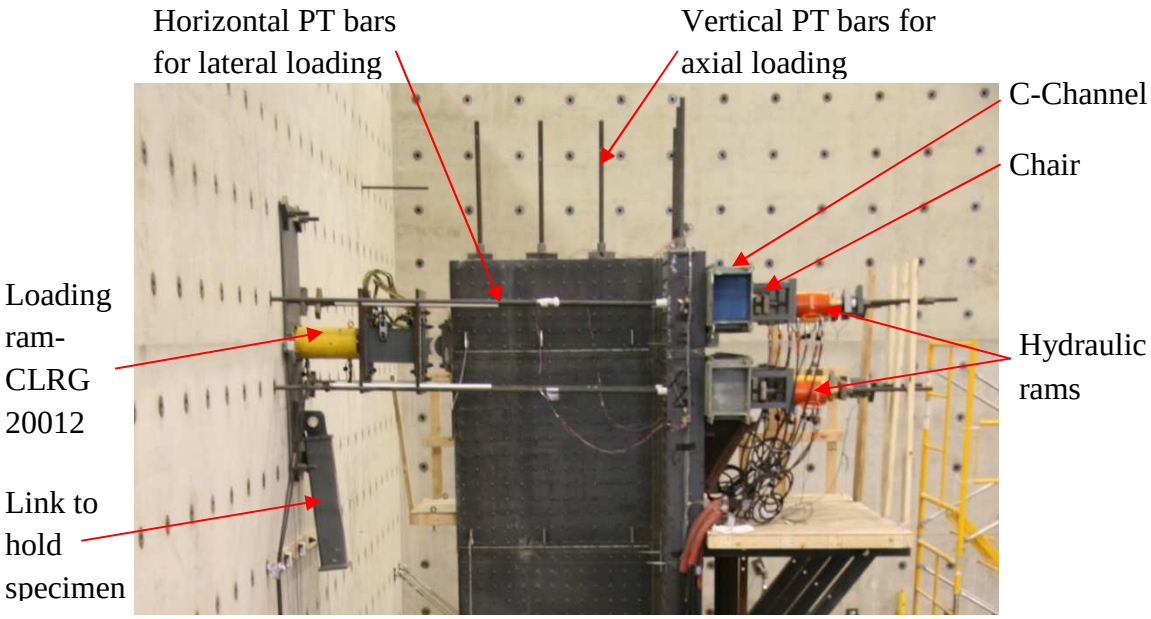

Figure 6.36 Side view of the cyclic loading test set-up

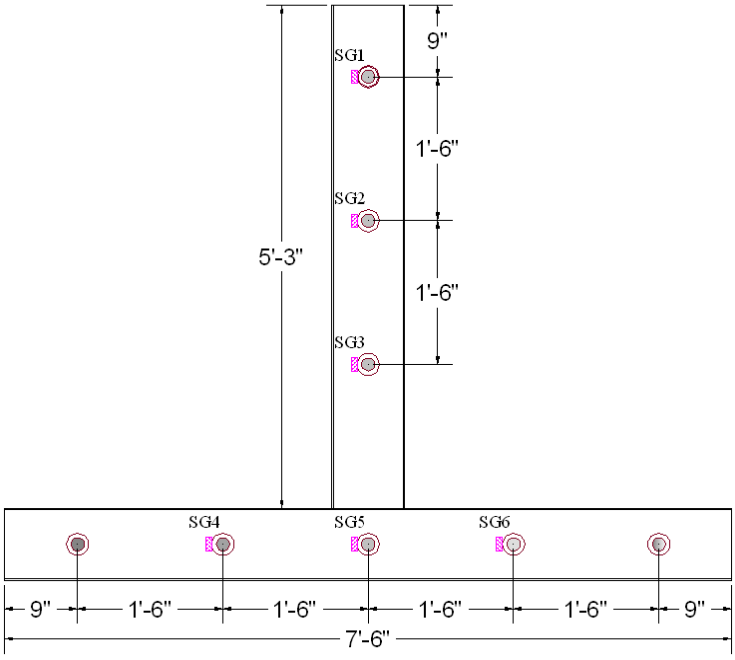

Figure 6.37 Strain gauges attached on vertical PT bars to infer axial load

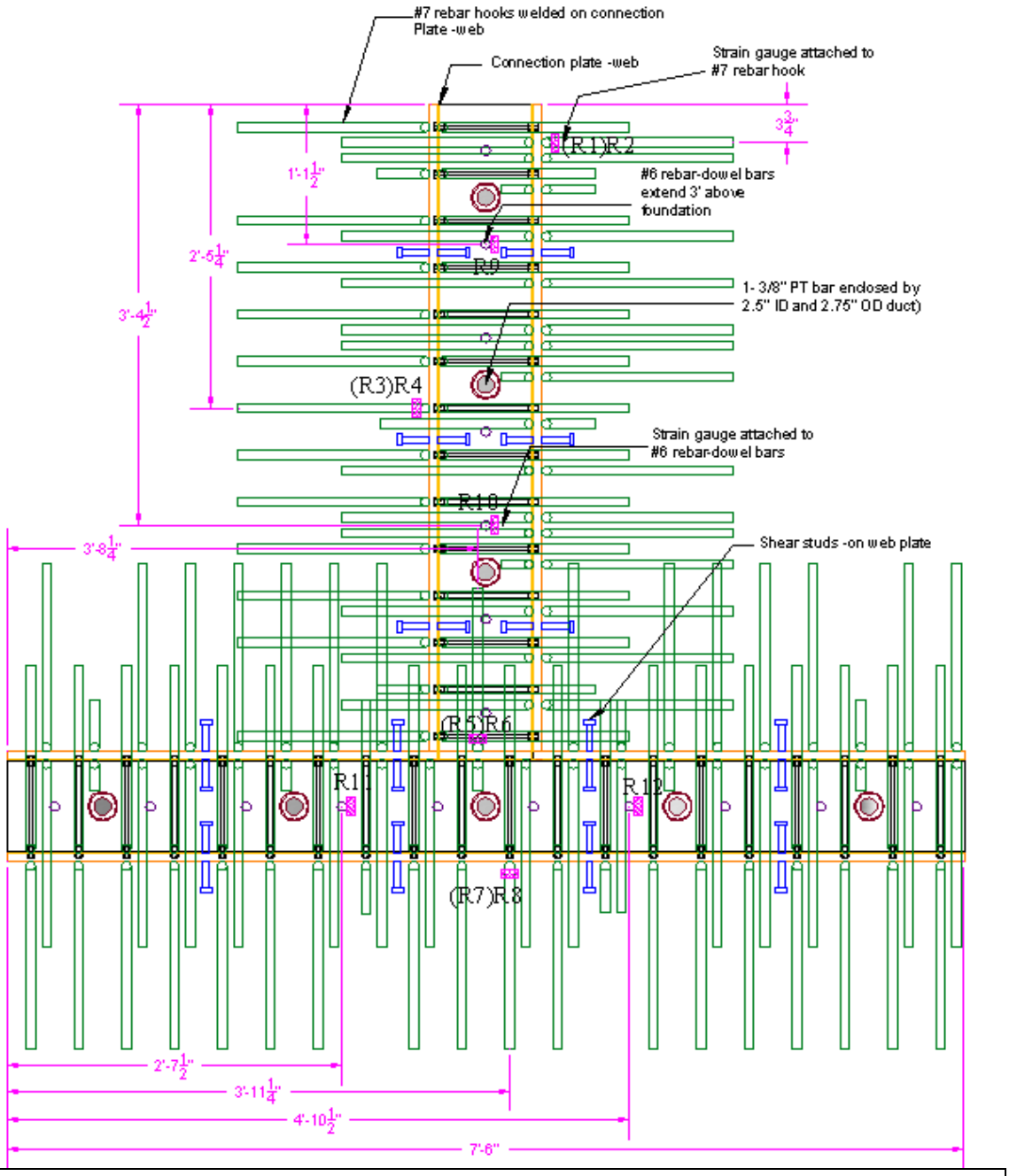

Note: Gauges on the reinforcing bar hooks marked within bracket are 9 in. below the bottom of the foundation connection plate, and the other gauges (not within bracket) on the reinforcing bar hooks are 1 in. below the bottom of the foundation connection plate.

Gauges on the No.6 reinforcing bar dowels are 2.25 in. above the foundation

Figure 6.38 Strain gauges attached on reinforcing bar hooks and dowel bars

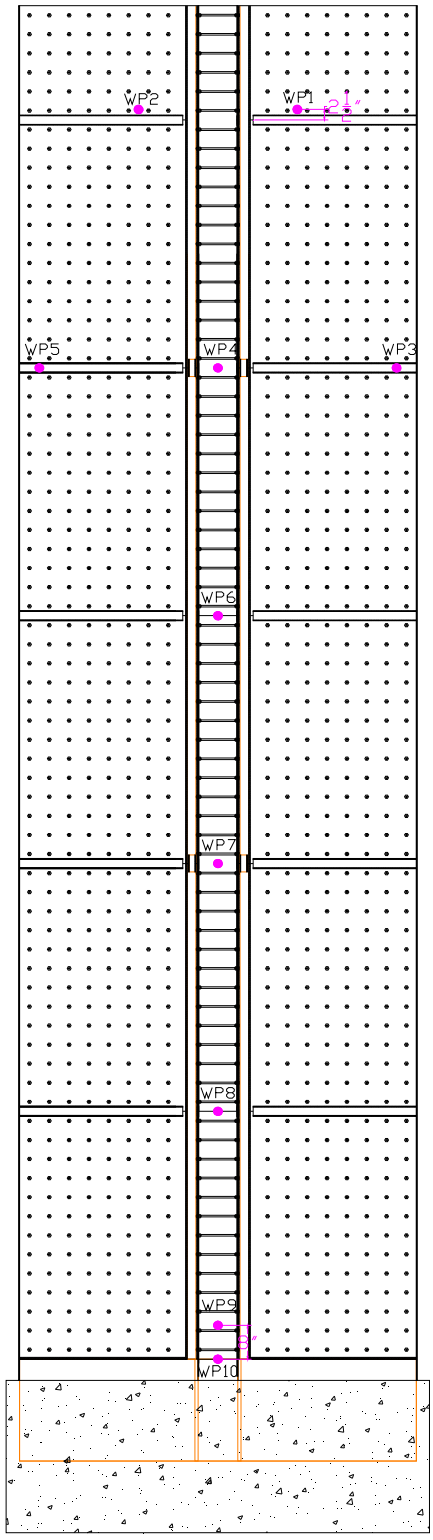

Figure 6.39 Locations of wire potentiometers for the cyclic loading test (view from south to north)

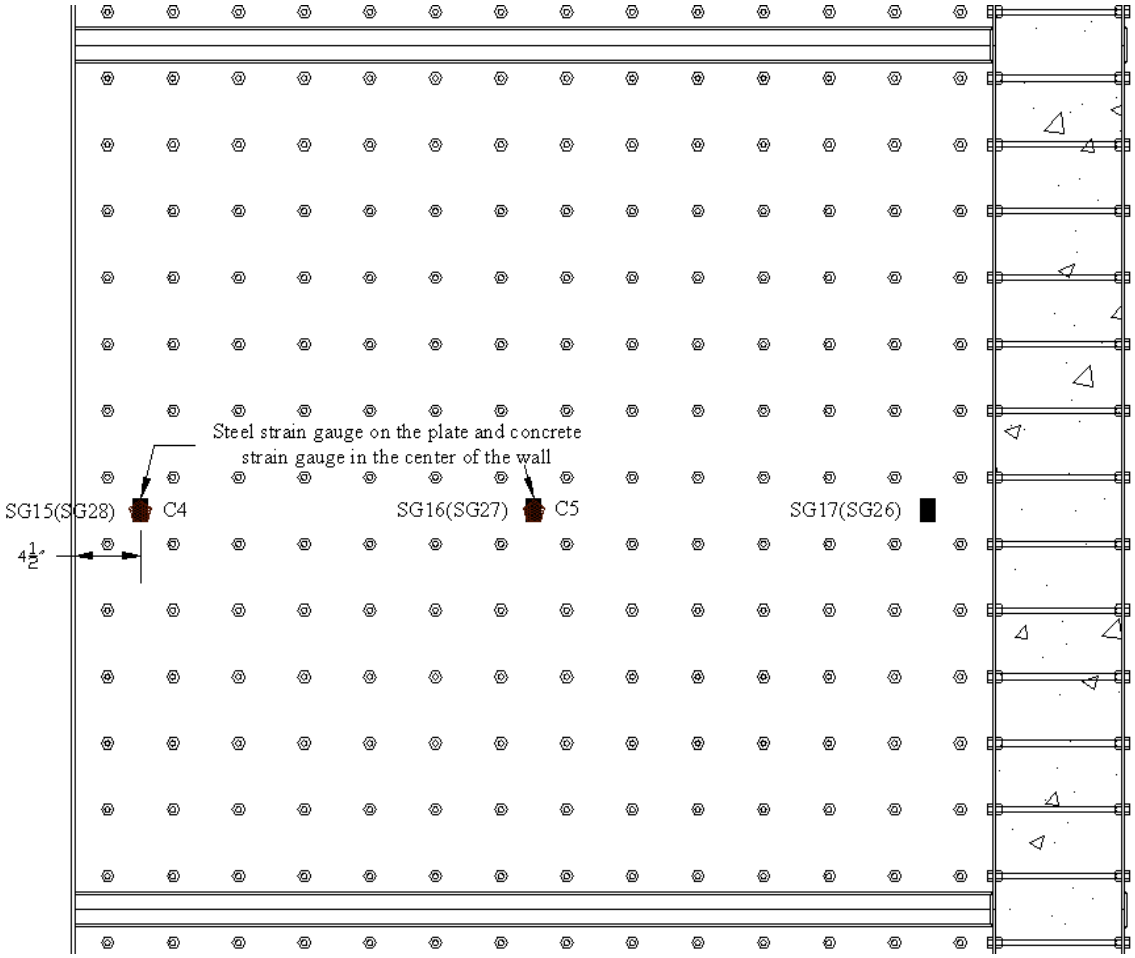

Figure 6.40 Sensors for the second story web (view from east to west)

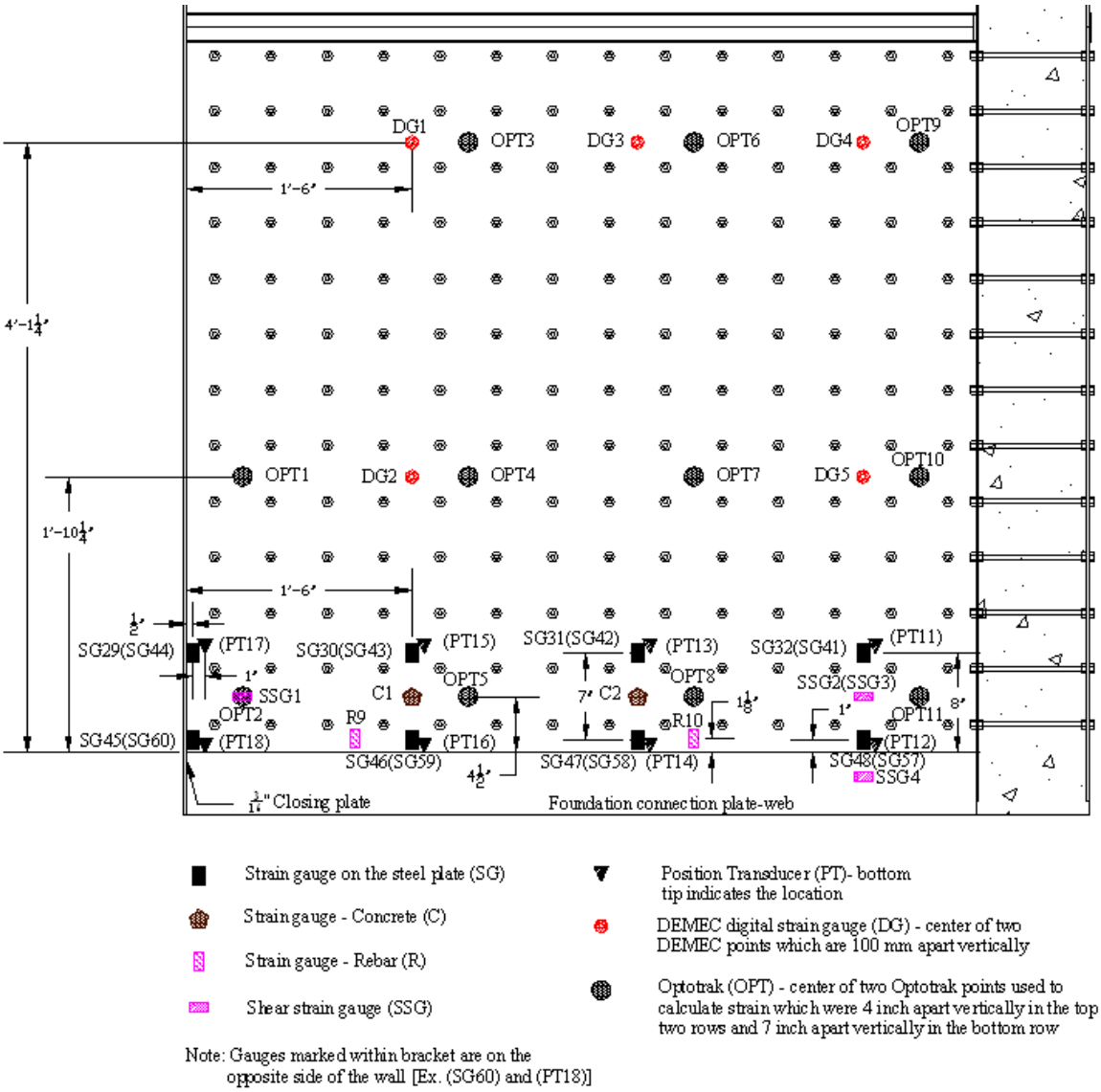

Figure 6.41 Sensors for the first story of specimen web (view from east to west)

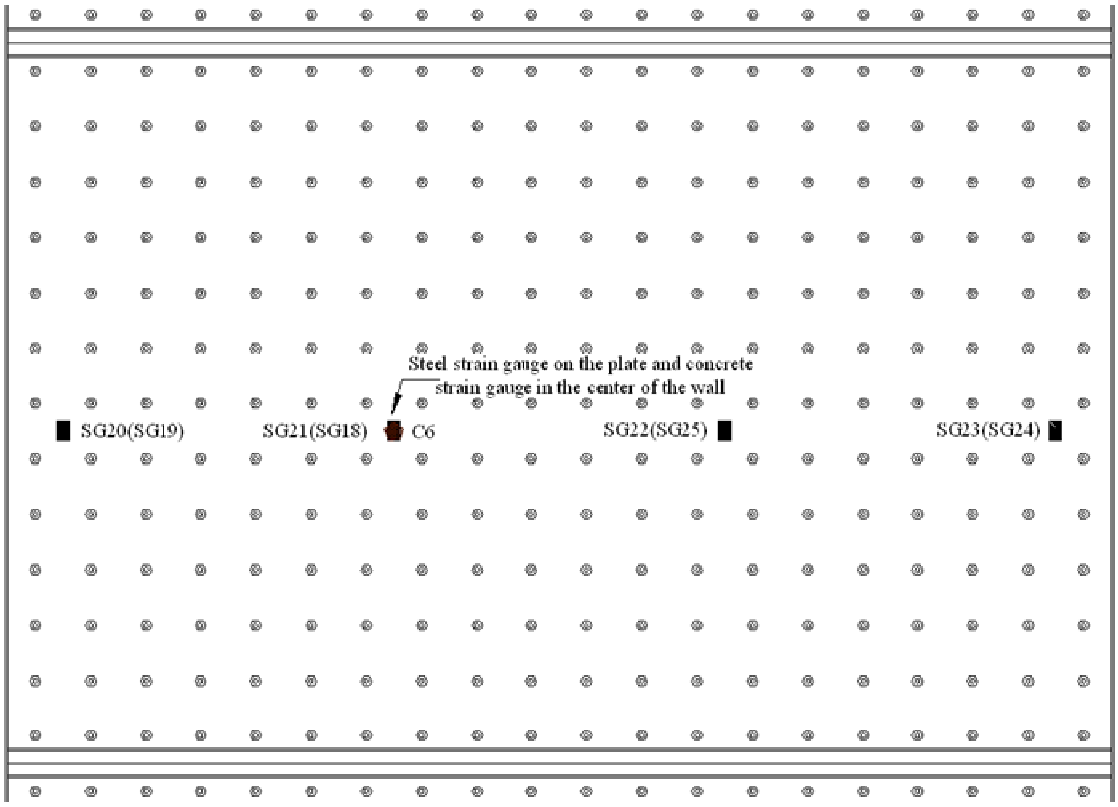

Figure 6.42 Sensors for the second story flange (view from north to south)

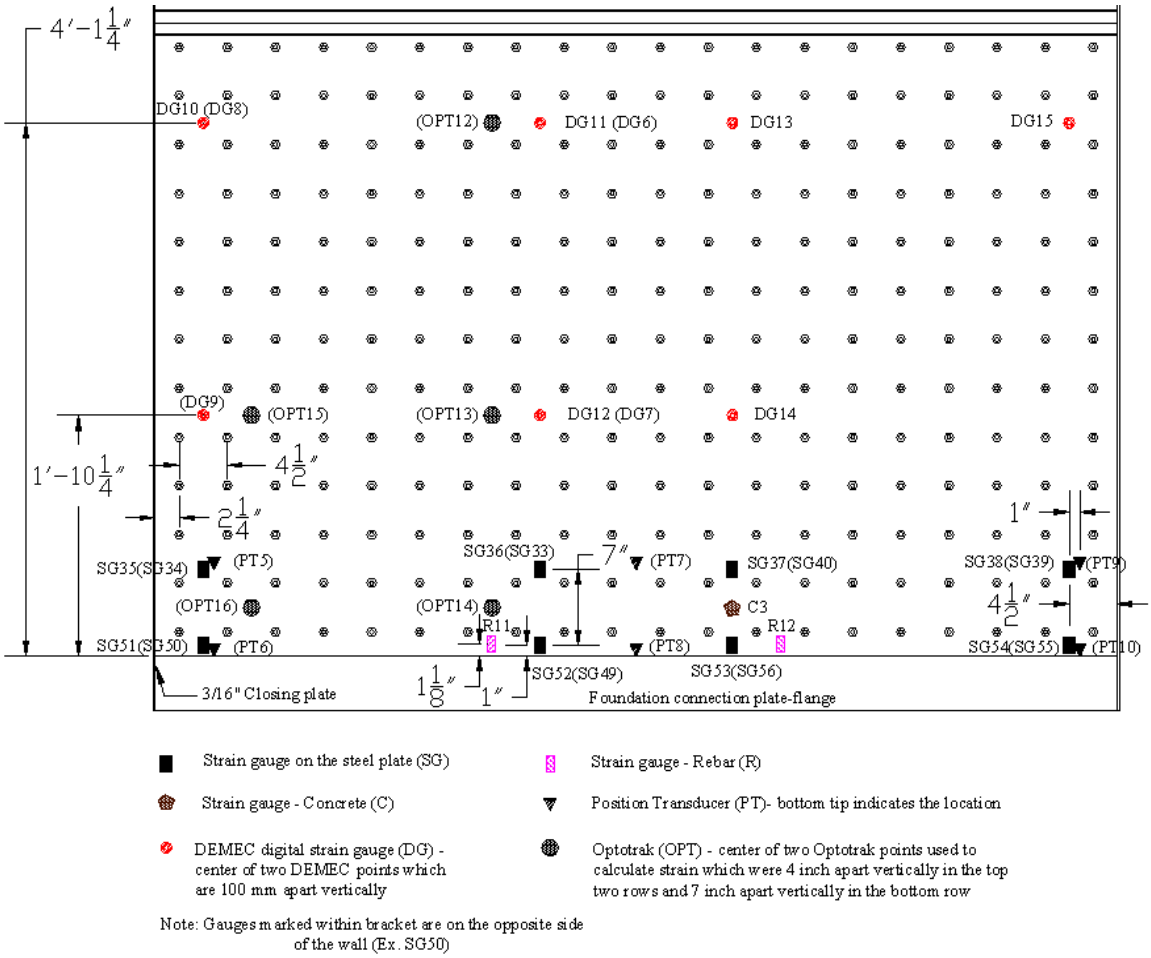

Figure 6.43 Sensors for the first story of specimen flange (view from north to south)

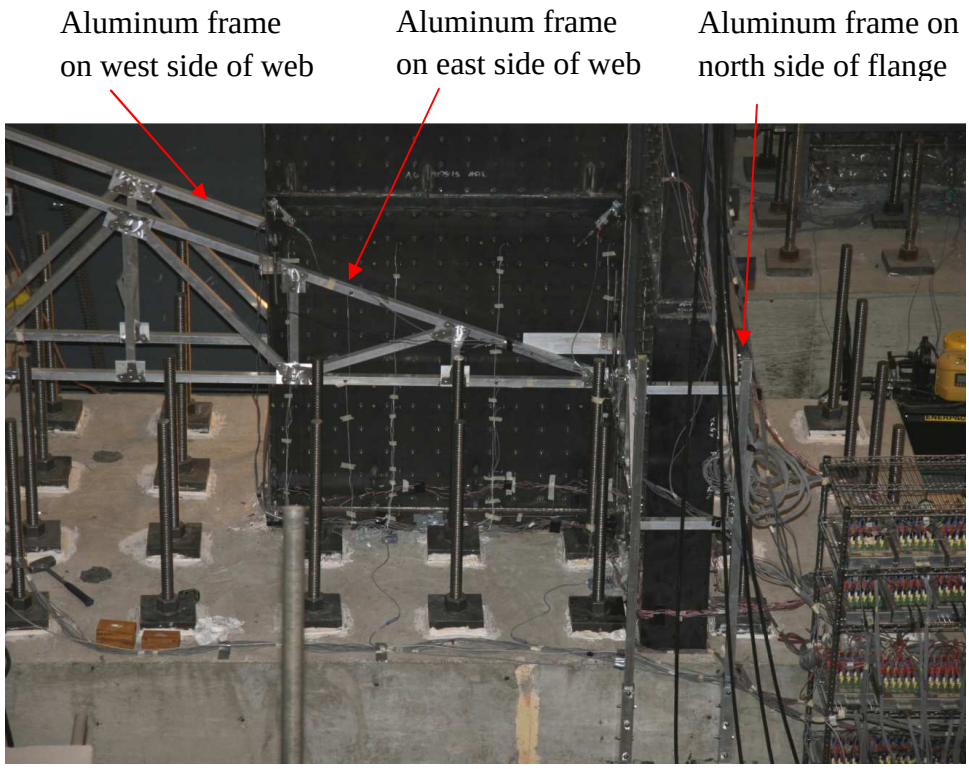

Figure 6.44 Aluminum frame in which position transducers and LVDTs were attached (view from east to west)

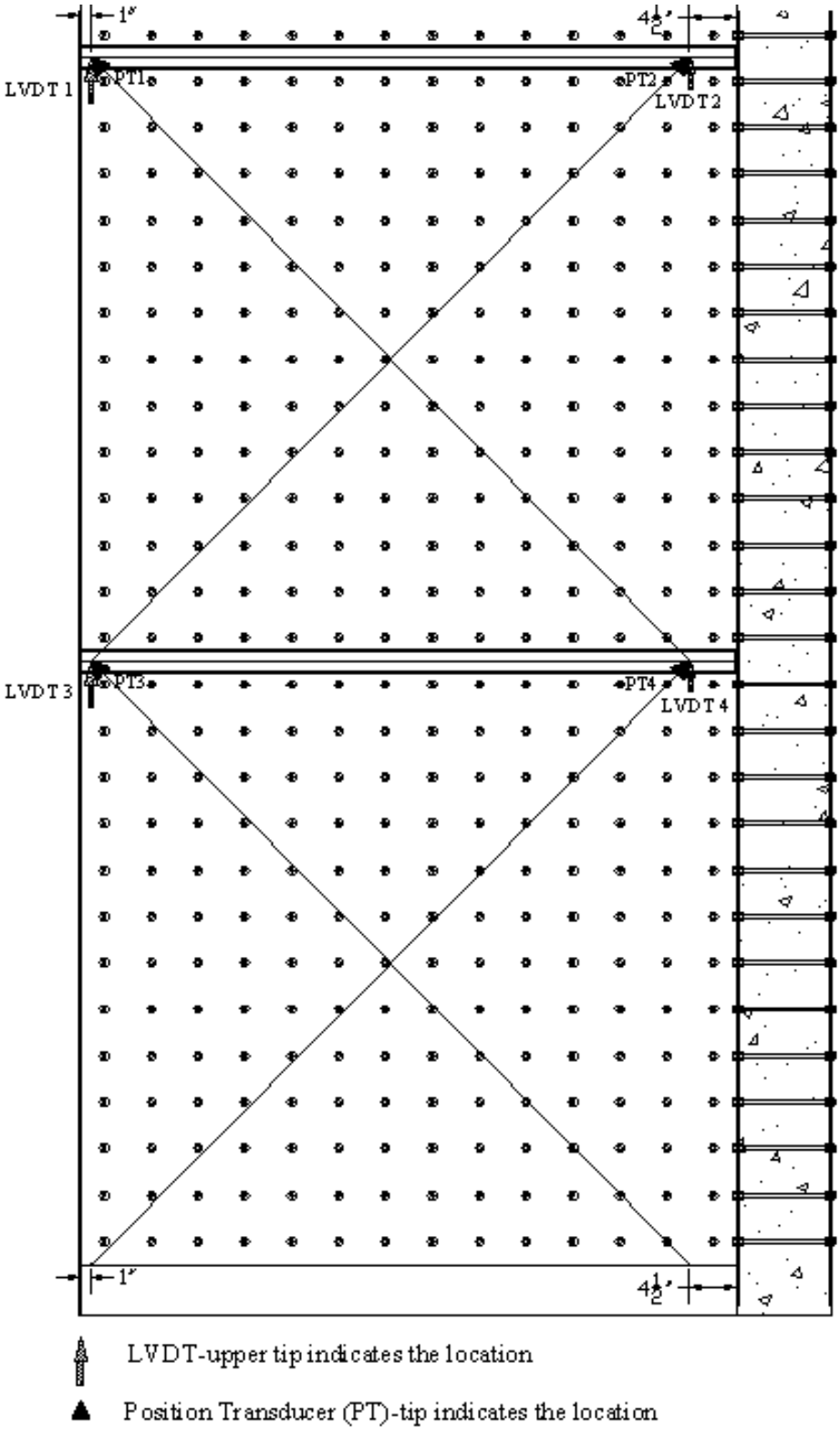

Figure 6.45 Instrumentation to measure shear strain along the web

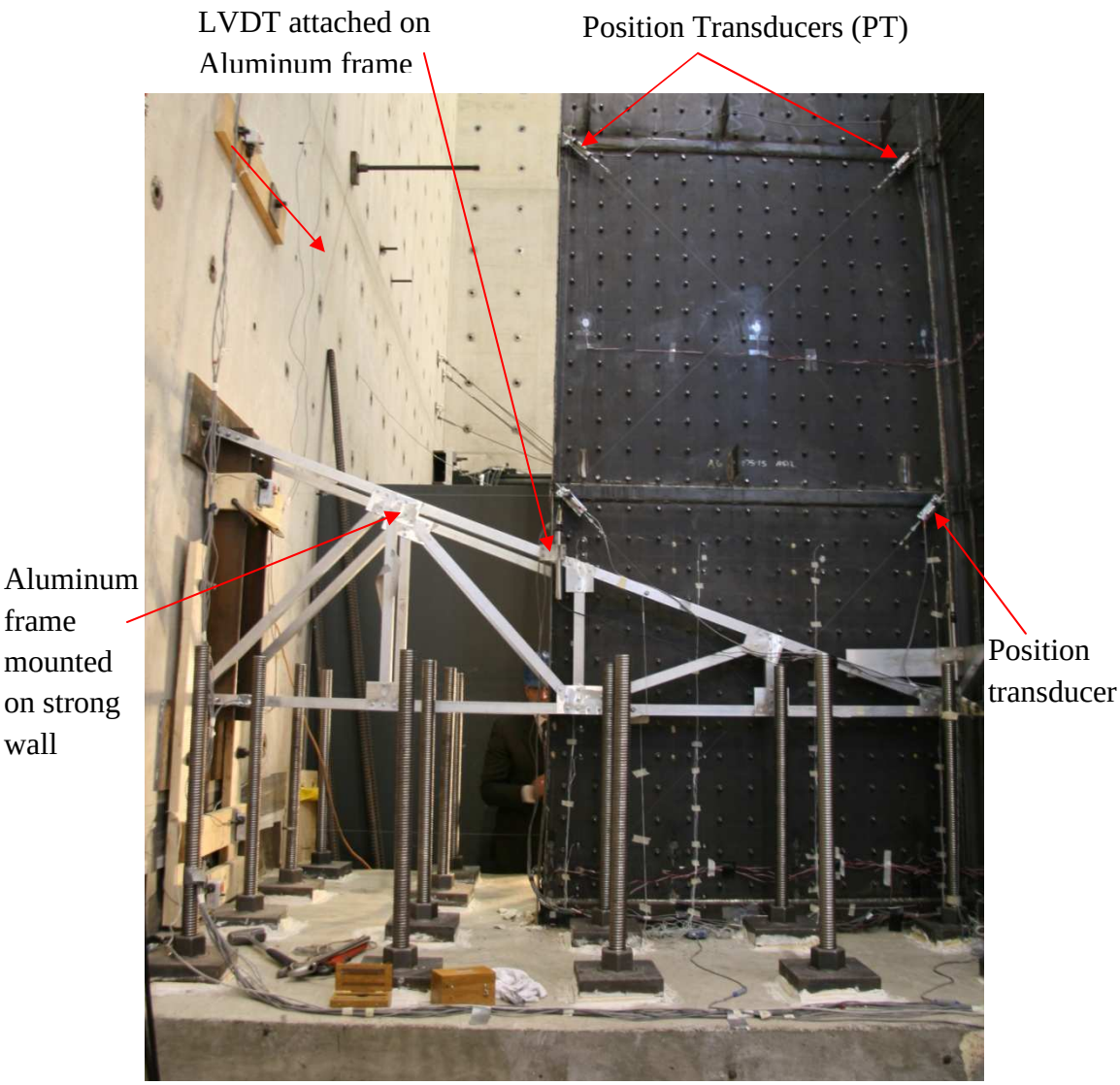

Figure 6.46 Aluminum frame and position transducers and LVDTs to measure shear strain along web (view from east to west)

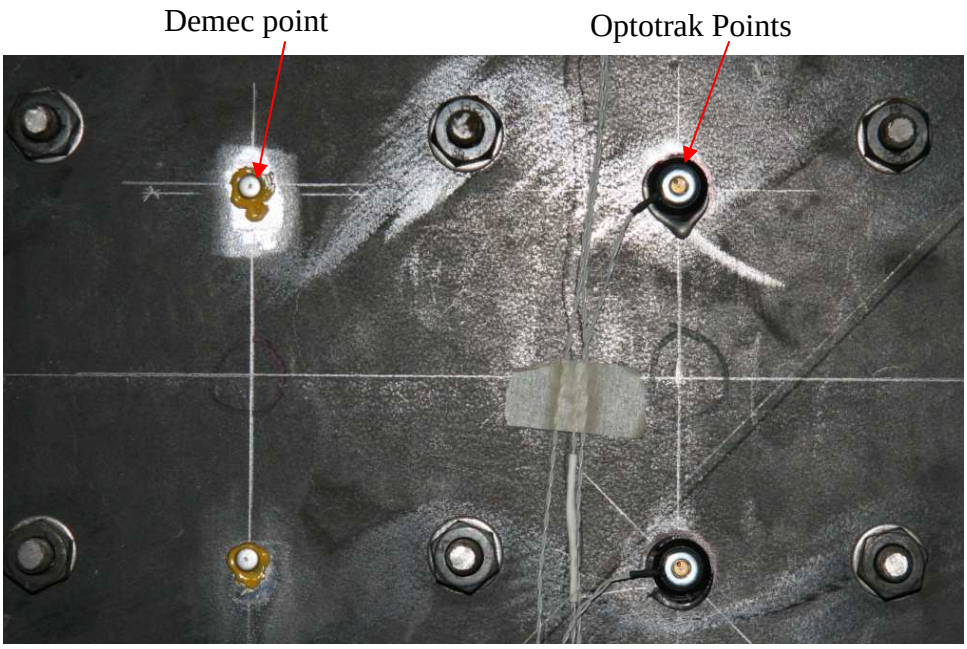

Figure 6.47 DEMEC points and Optotrak points attached to the plate

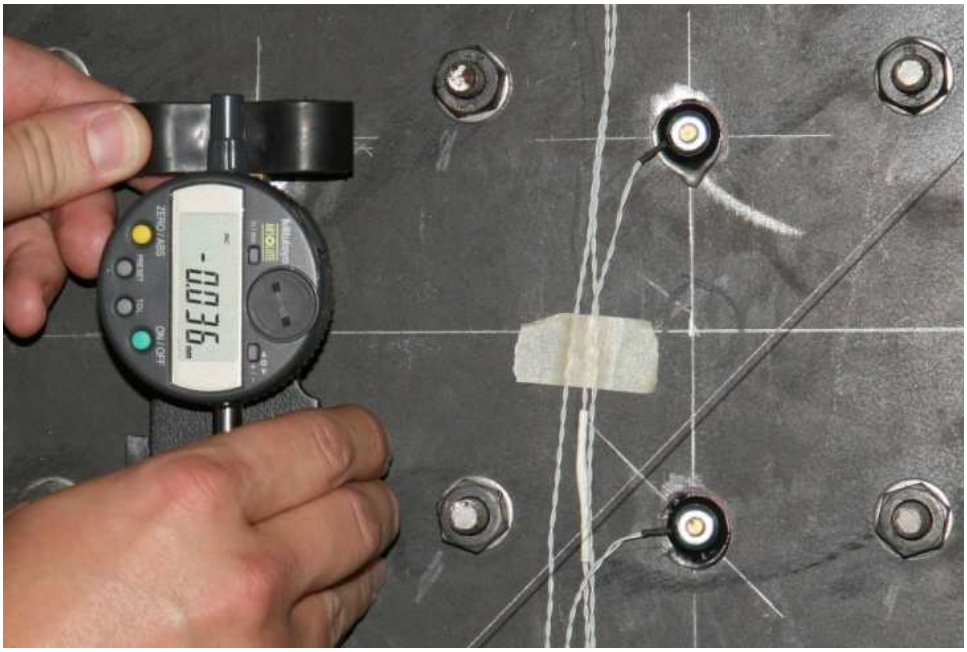

Figure 6.48 Invar beam with digital gauge over a pair of DEMEC points

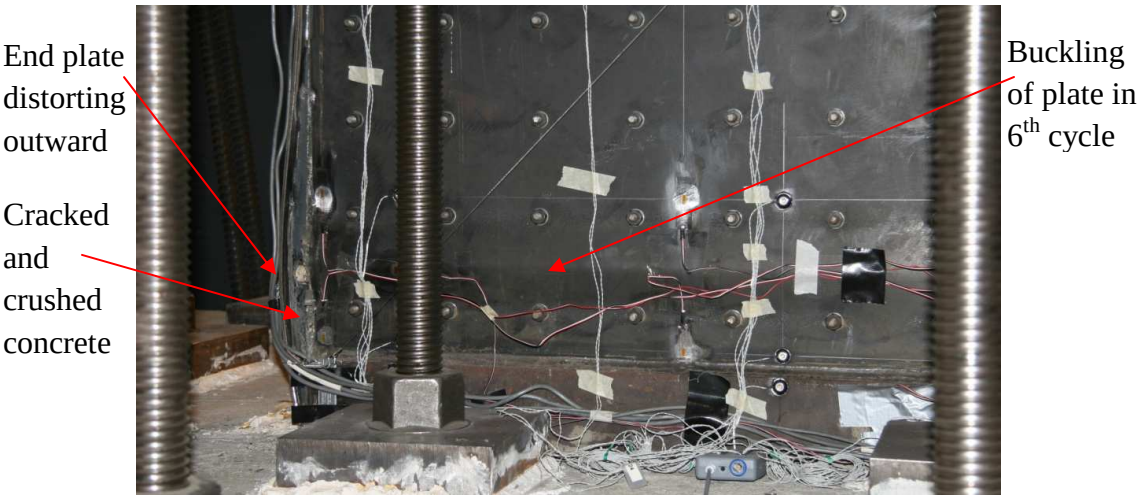

Figure 6.49 Buckling of plate at 1% drift in the 6th cycle towards the strong wall – towards south (Cycle 6S)

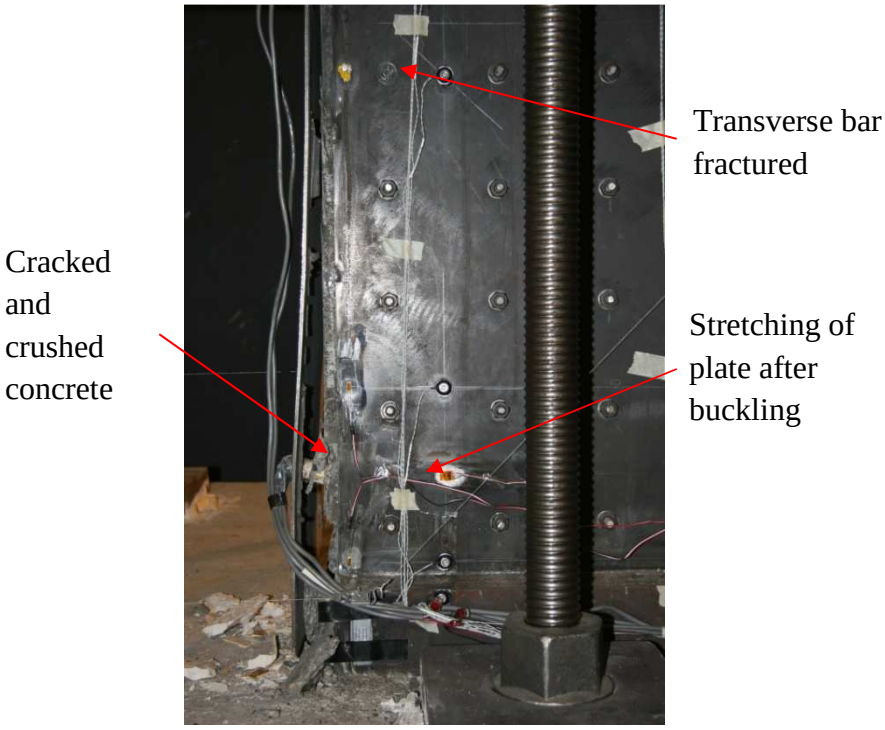

Figure 6.50 Specimen during 6th cycle – loaded away from the strong wall (6N)

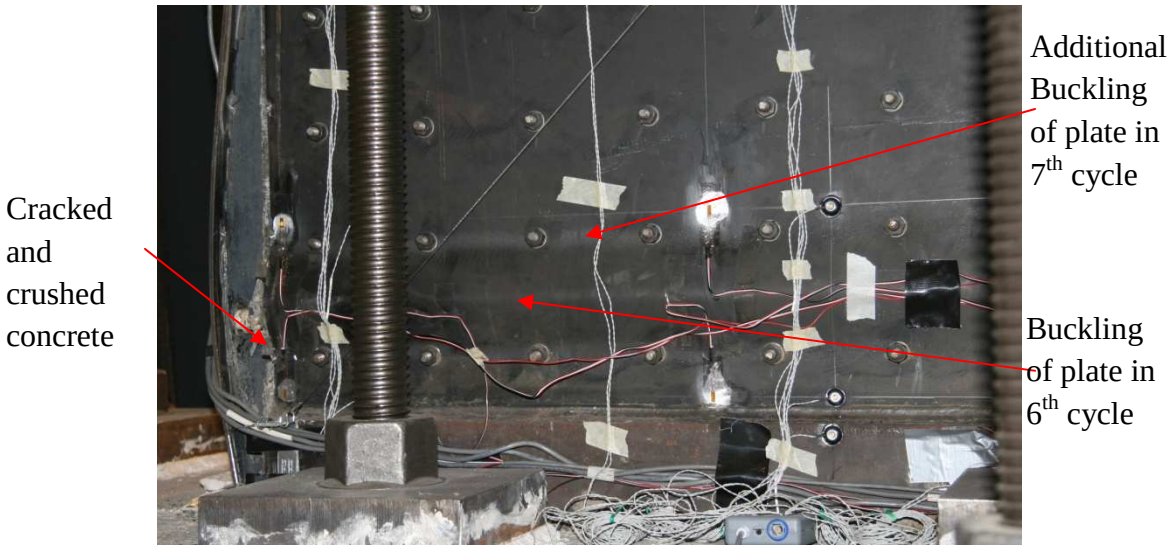

Figure 6.51 Bottom of the specimen at 1% drift in the 7th cycle towards the strong wall - towards south (Cycle 7S)

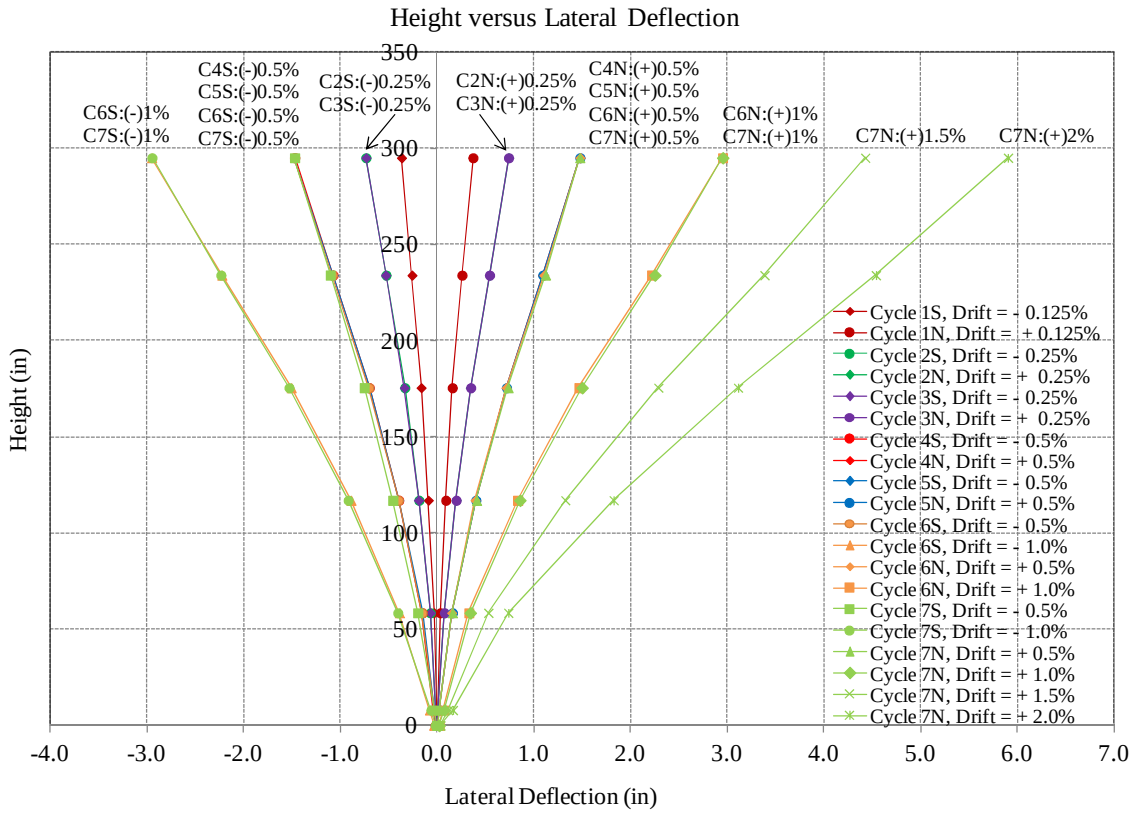

Figure 6.52 Height versus lateral deflection

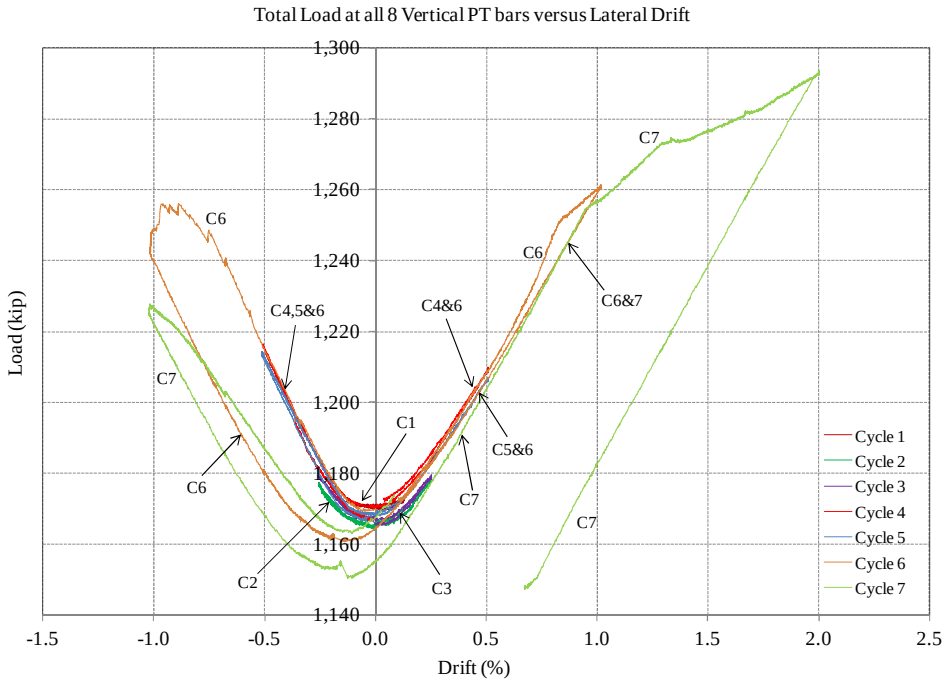

Figure 6.53 Total load in PT bars versus lateral drift

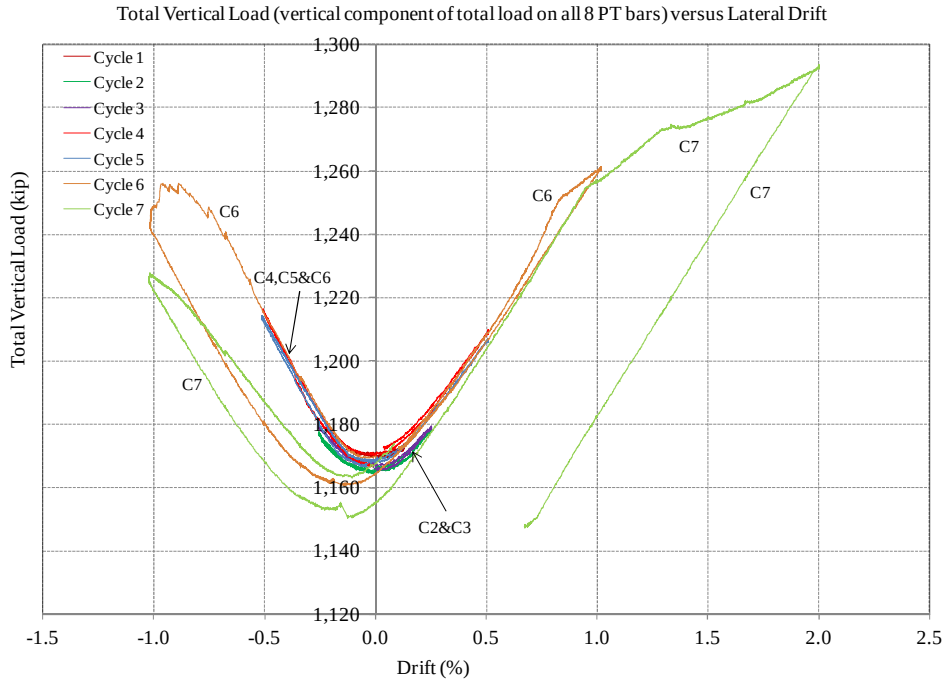

Figure 6.54 Adjusted total vertical load versus lateral drift

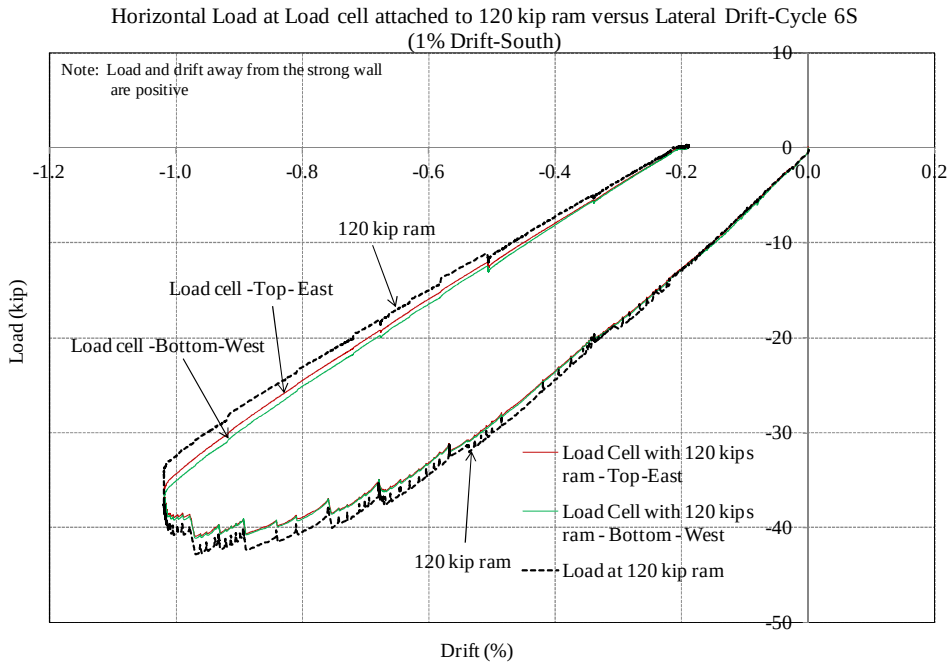

Figure 6.55 Horizontal load measured by load cell compared to load inferred from pressure transducer readings during cycle 6 - 120 kip ram

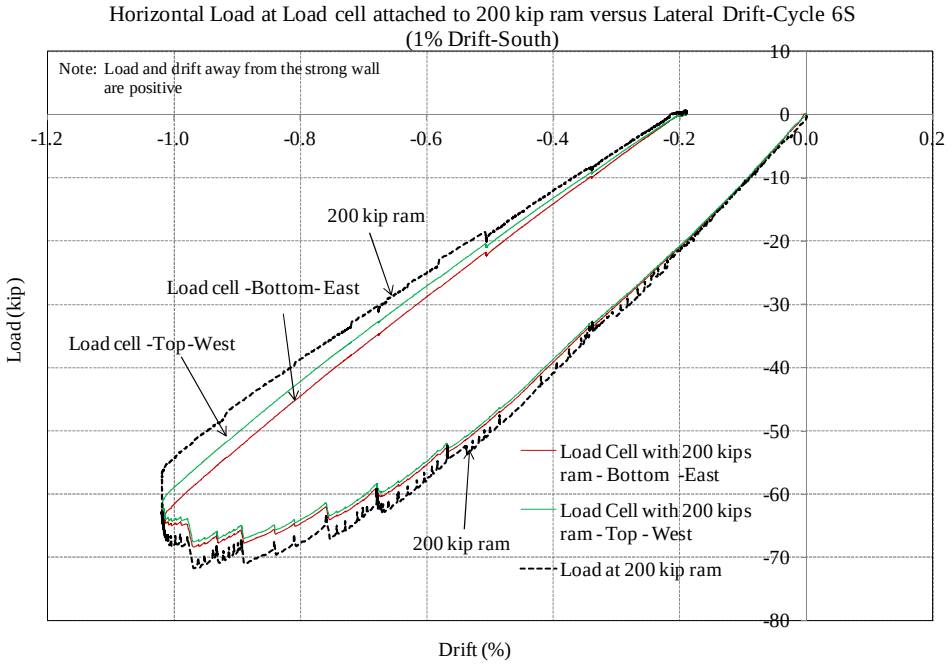

Figure 6.56 Horizontal load measured by load cell compared to load inferred from pressure transducer readings during cycle 6 - 200 kip ram

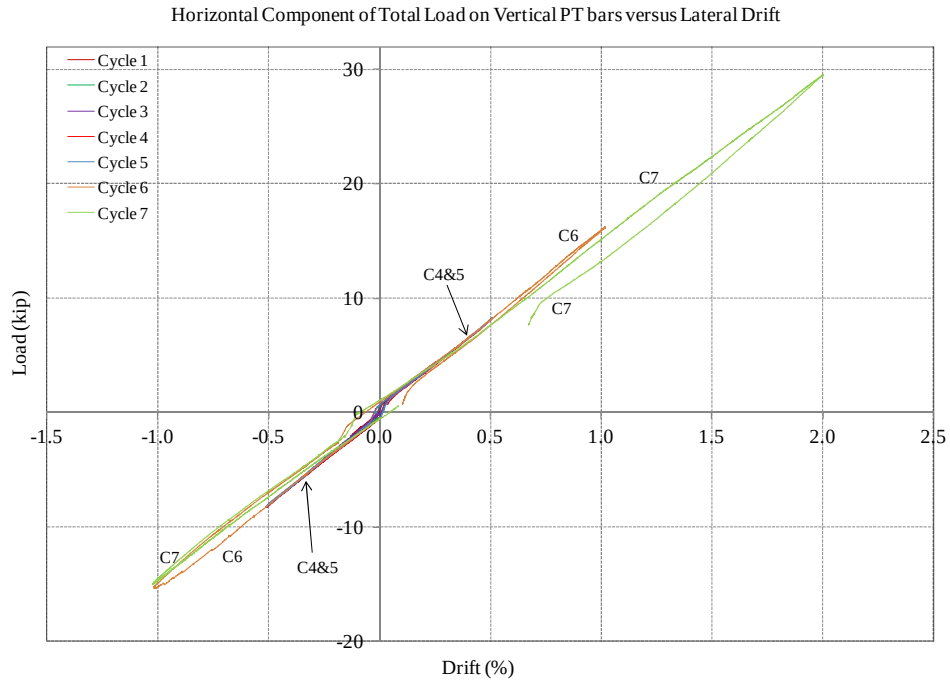

Figure 6.57 Horizontal component of total load on vertical PT bars versus drift ratio

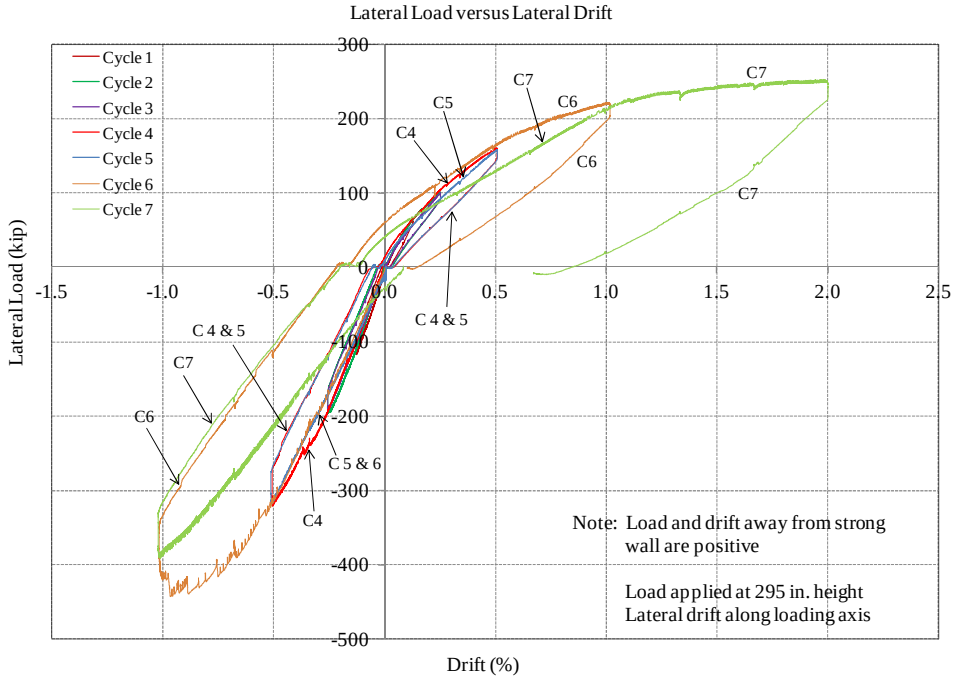

Figure 6.58 Lateral load versus lateral drift ratio

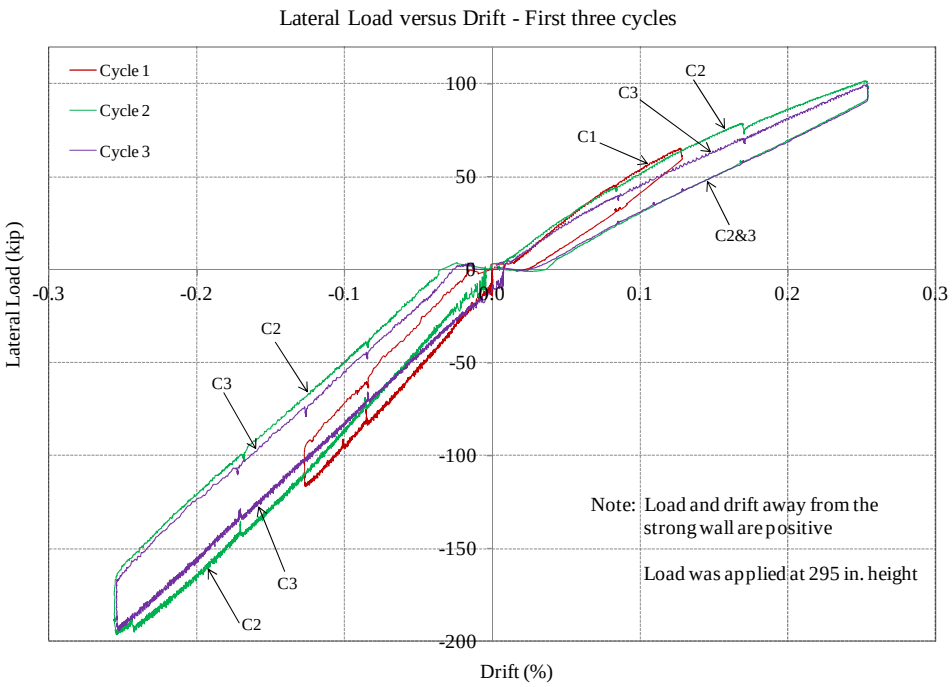

Figure 6.59 Lateral load versus drift ratio– First three cycles

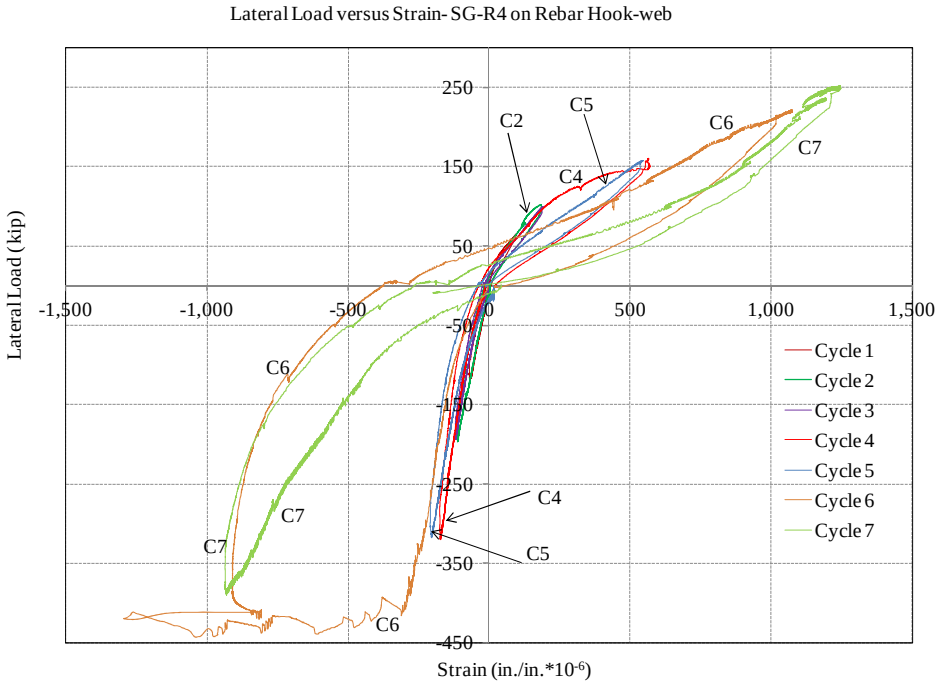

Figure 6.60 Lateral load versus strain – strain gauge on reinforcing bar hook – R4 on web

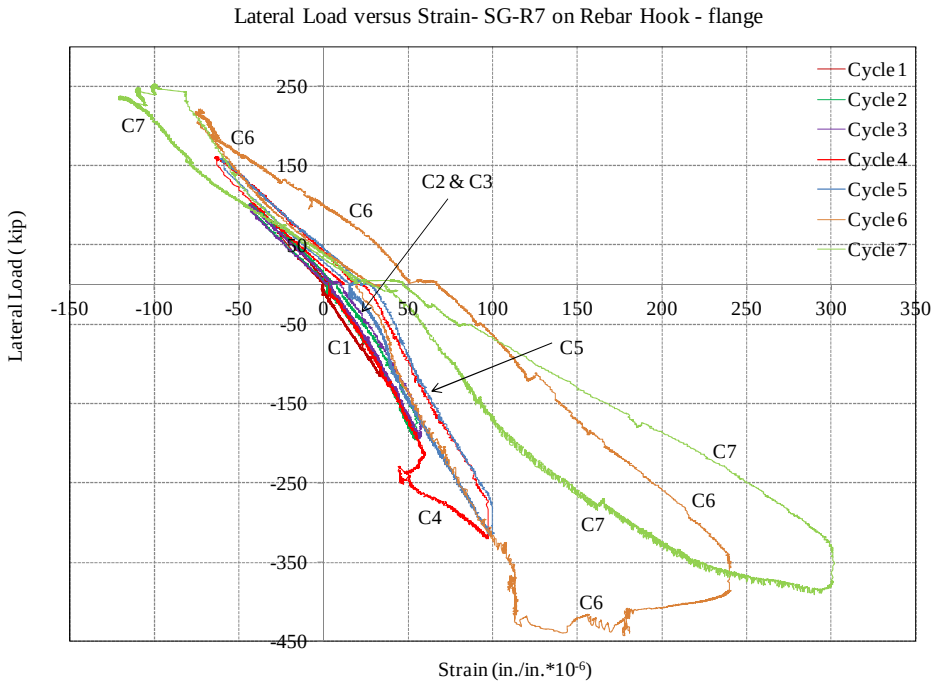

Figure 6.61 Lateral load versus strain – strain gauge on reinforcing bar hook – R7 on flange

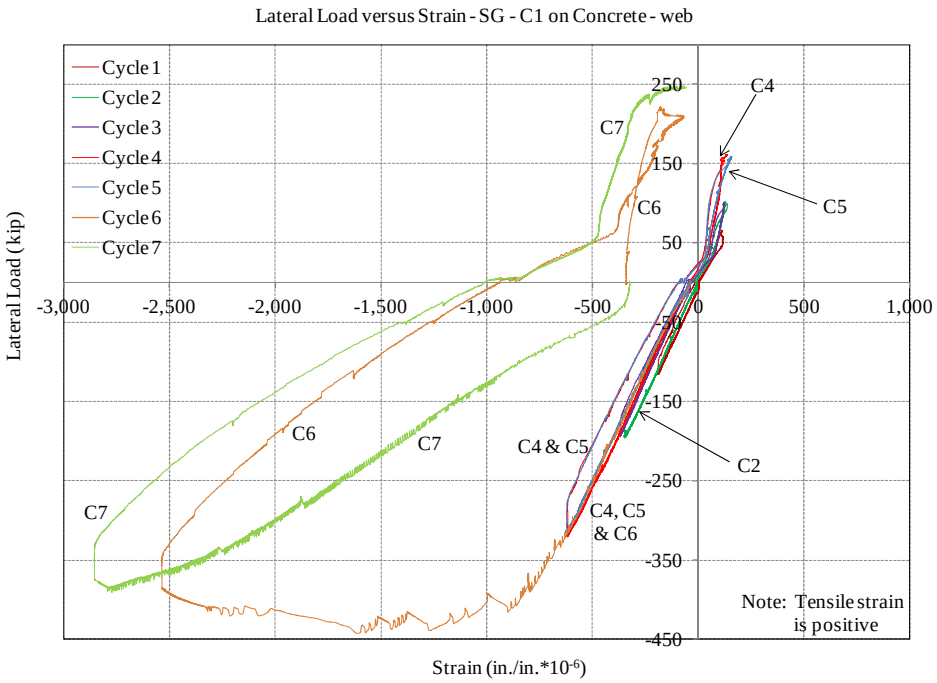

Figure 6.62 Lateral load versus strain – concrete strain gauge C1 in web

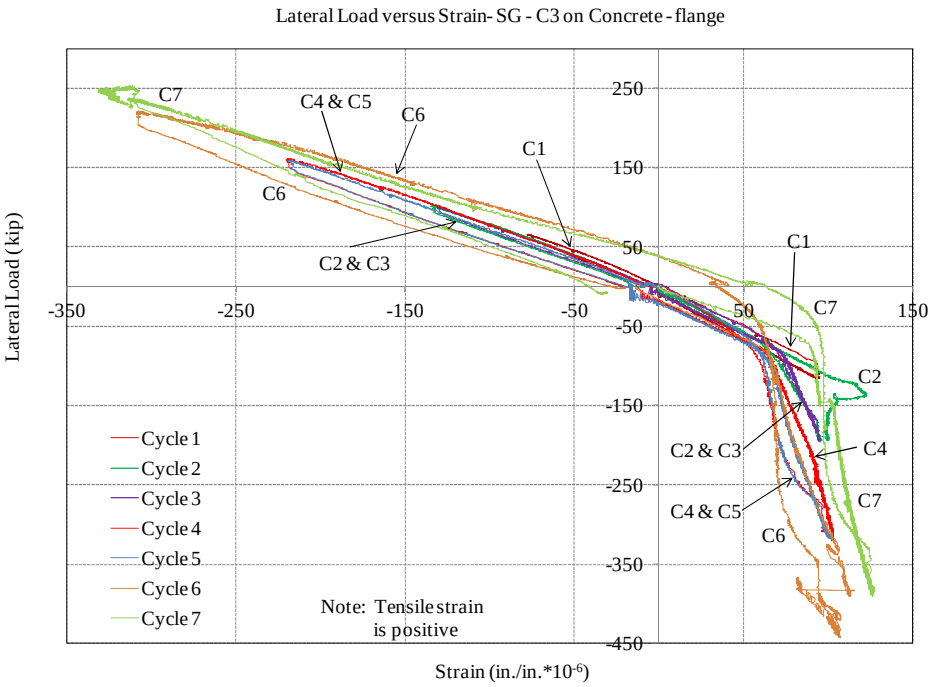

Figure 6.63 Lateral load versus strain – concrete strain gauge C3 in flange

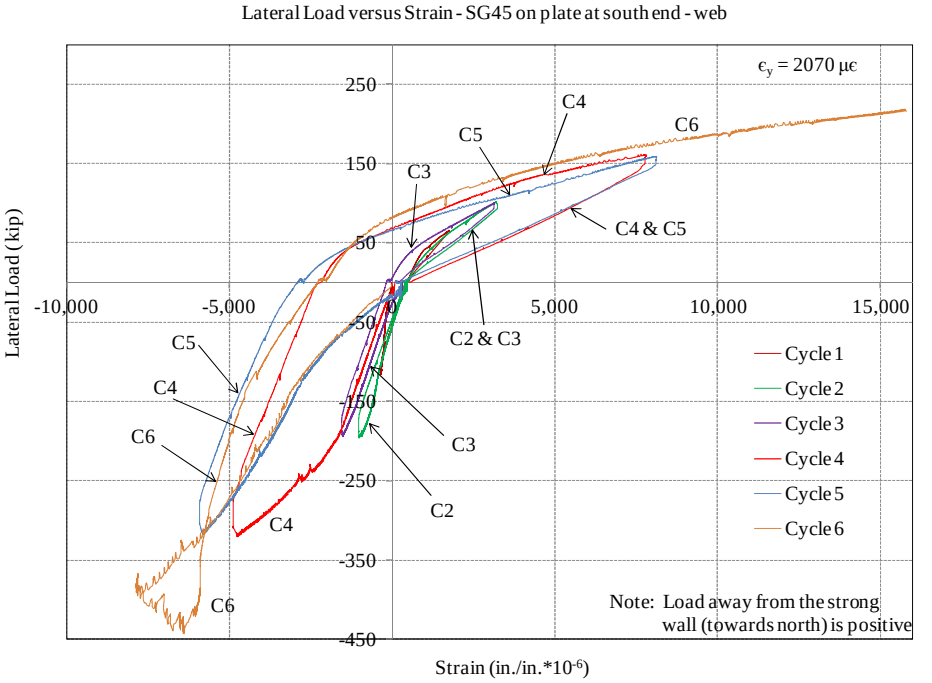

Figure 6.64 Lateral load versus strain – strain gauge on web plate - SG 45

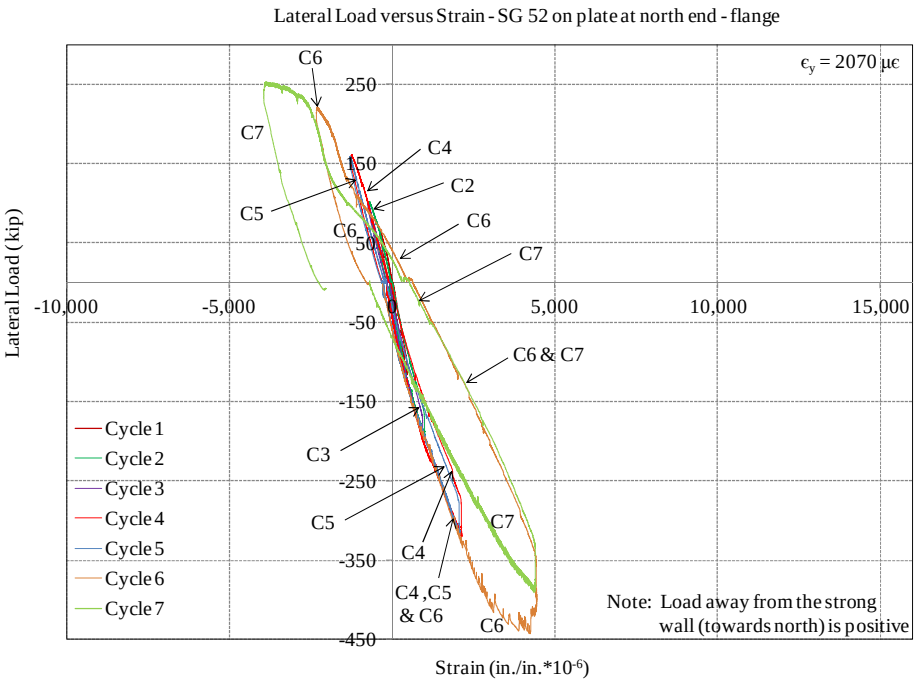

Figure 6.65 Lateral load versus strain – strain gauge on flange plate - SG 52

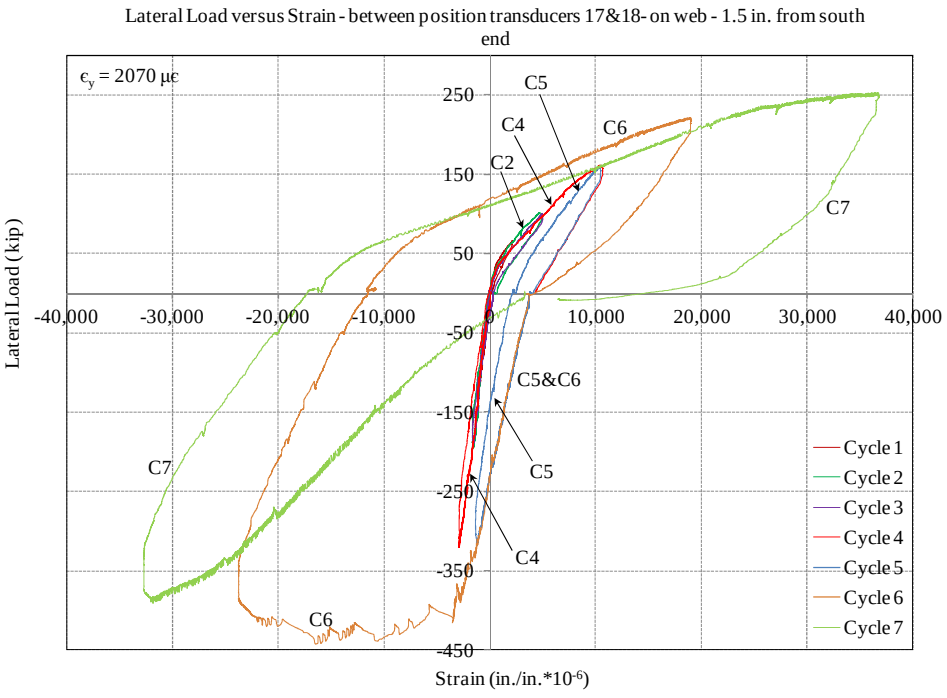

Figure 6.66 Lateral load versus strain – between position transducers 17 & 18 -web

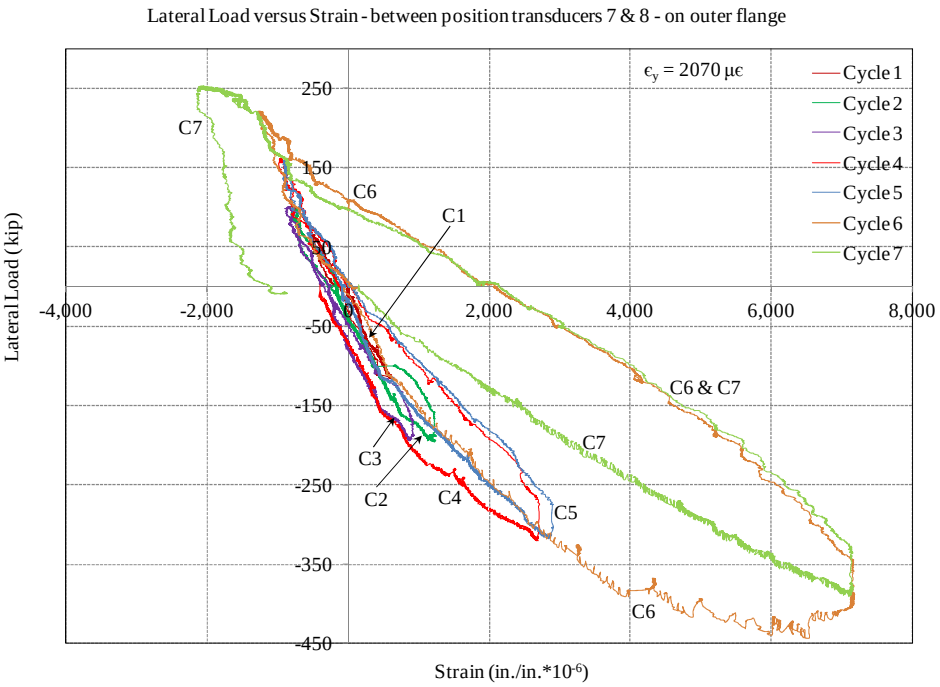

Figure 6.67 Lateral load versus strain – between position transducers 7 & 8 – flange

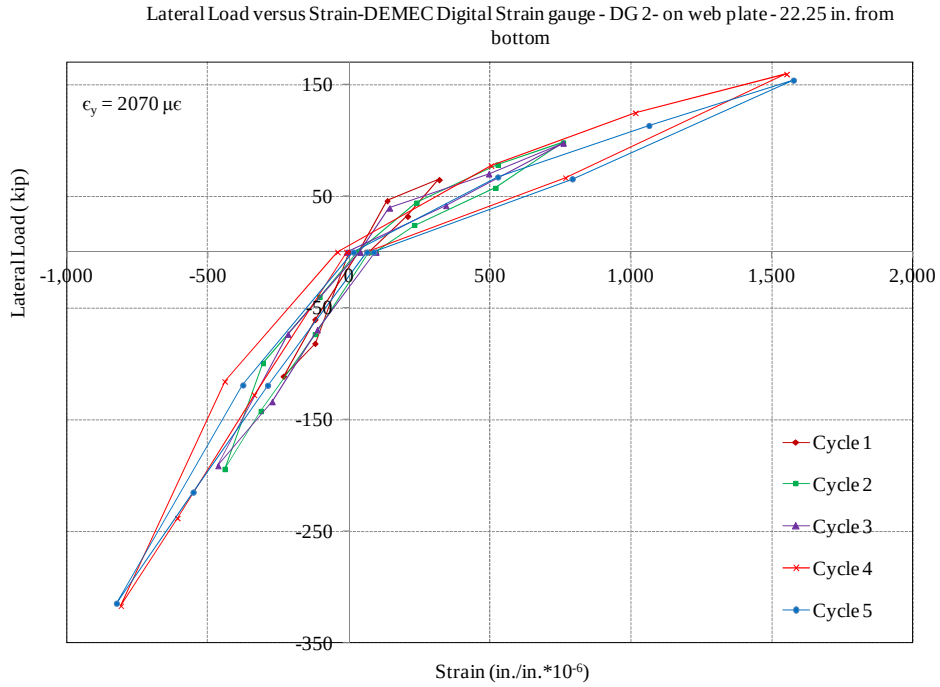

Figure 6.68 Lateral load versus strain – from DEMEC points – DG2 on web plate at 22.25 in. from bottom

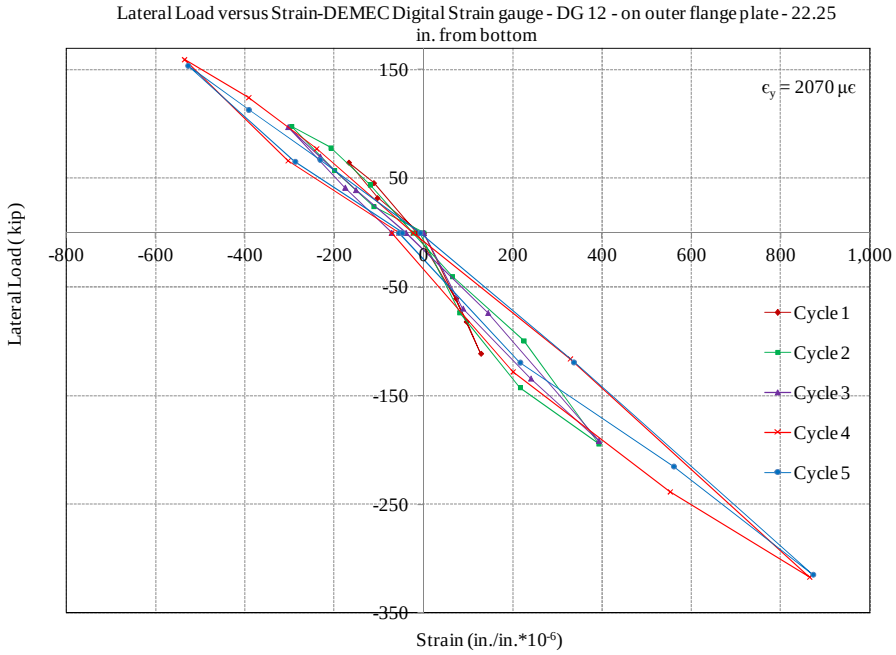

Figure 6.69 Lateral load versus strain – from DEMEC points – DG12 on outer flange plate at 22.25 in. from bottom

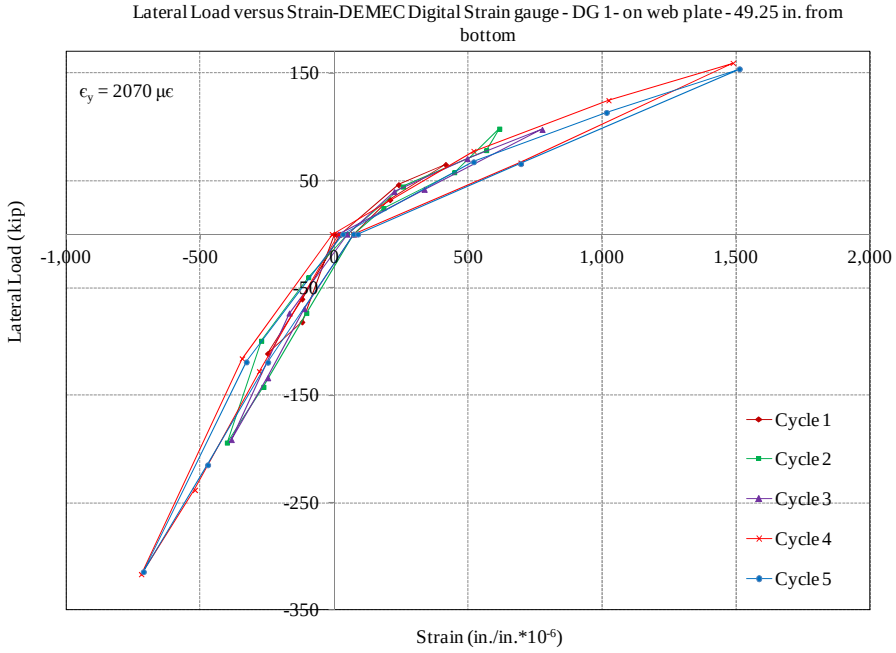

Figure 6.70 Lateral load versus strain – from DEMEC points – DG1 on web plate at 49.25 in. from bottom

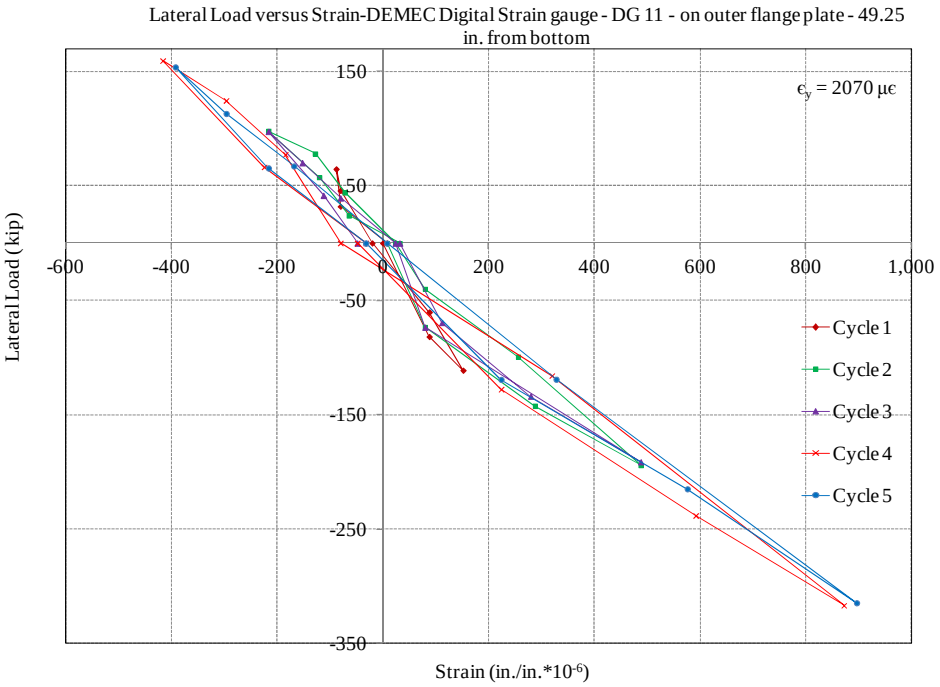

Figure 6.71 Lateral load versus strain – from DEMEC points – DG11 on outer flange plate at 49.25 in. from bottom

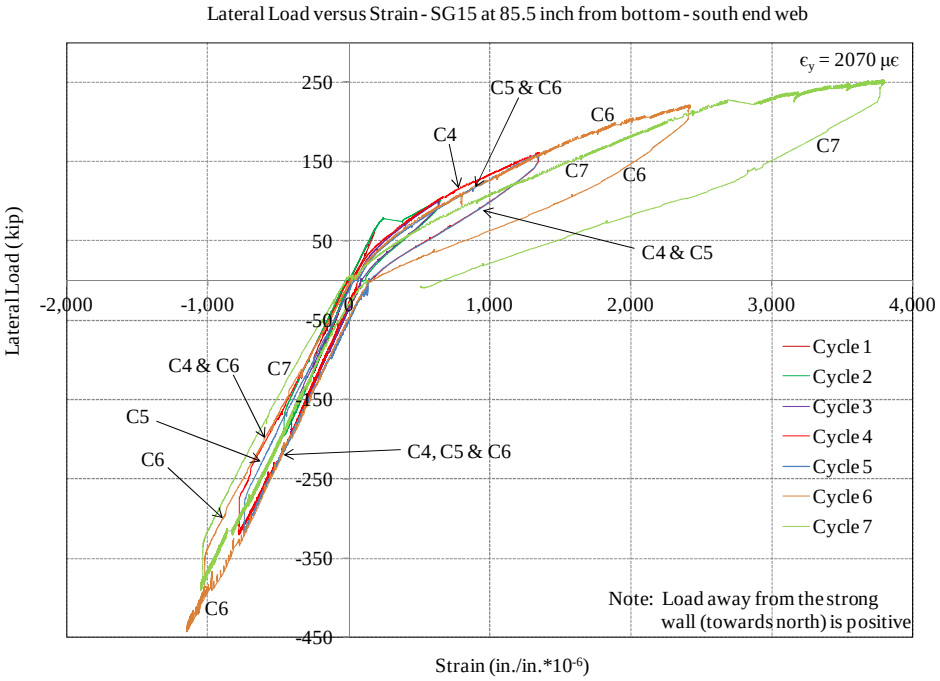

Figure 6.72 Lateral load versus strain – strain gauge on web plate - SG 15

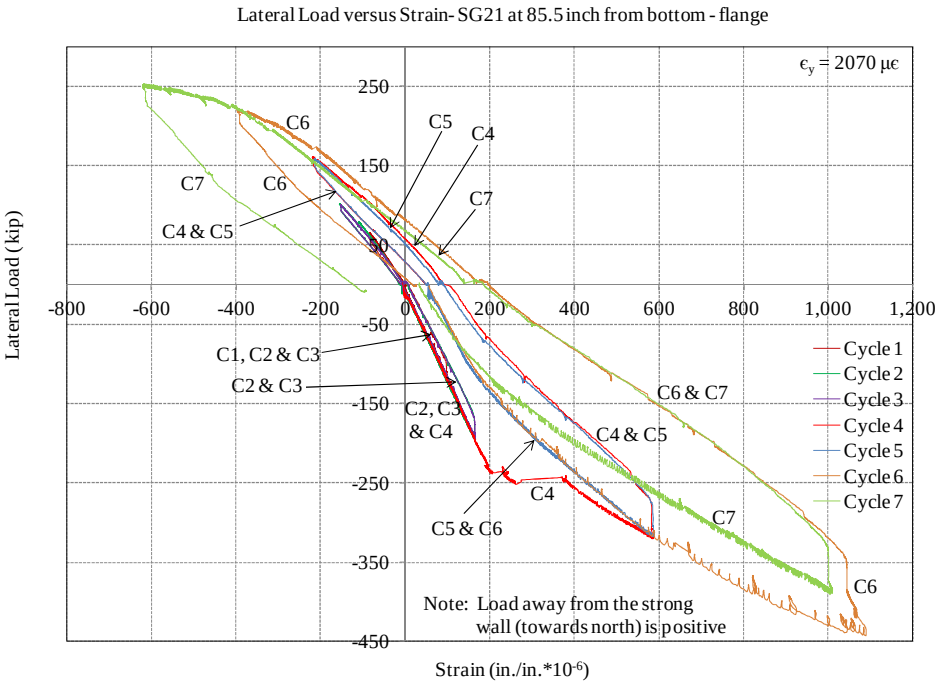

Figure 6.73 Lateral load versus strain – strain gauge on flange plate - SG 21

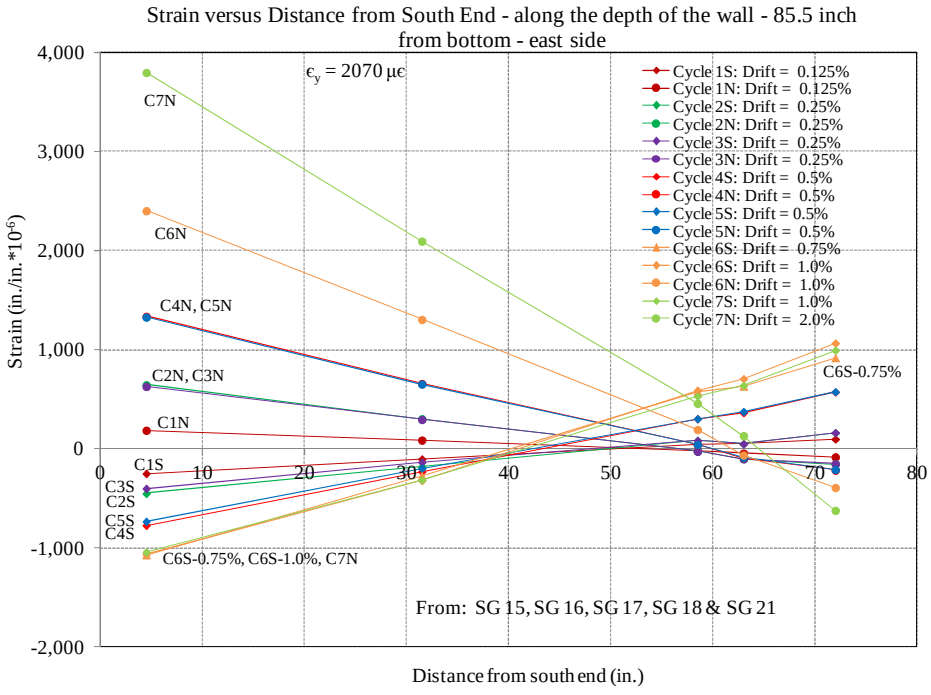

Figure 6.74 Strains along the depth of the wall at 85.5 in. from bottom - east side

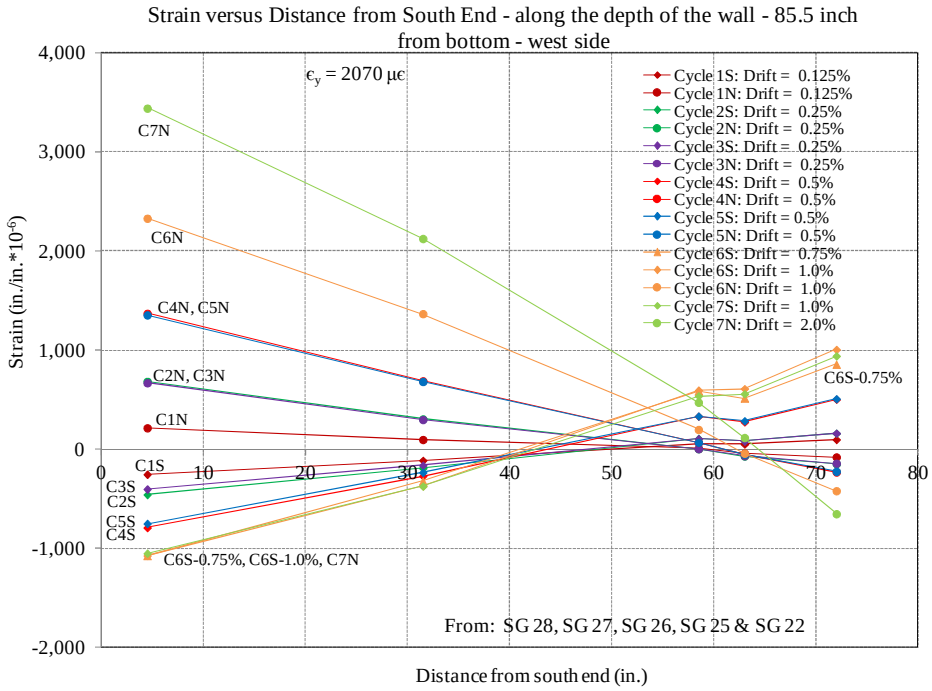

Figure 6.75 Strains along the depth of the wall at 85.5 in. from bottom - west side

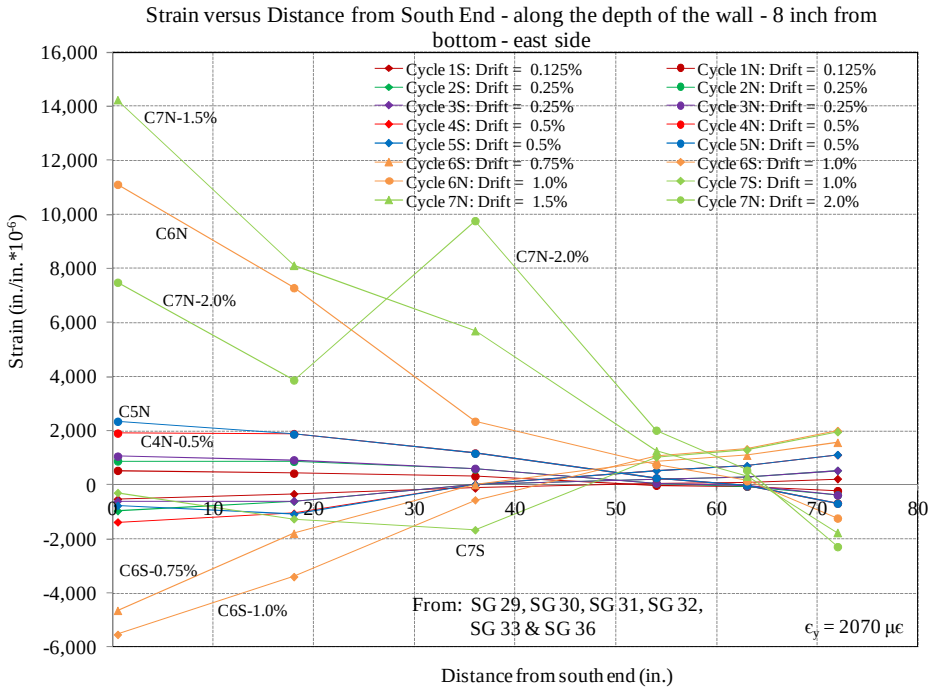

Figure 6.76 Strains along the depth of the wall at 8 in. from bottom - east side

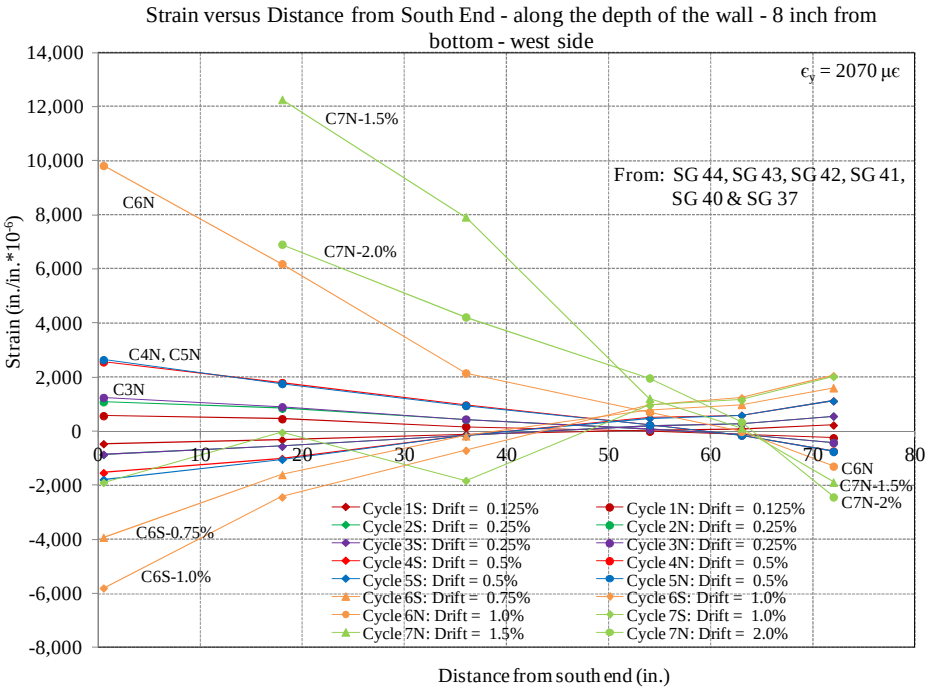

Figure 6.77 Strains along the depth of the wall at 8 in. from bottom - west side

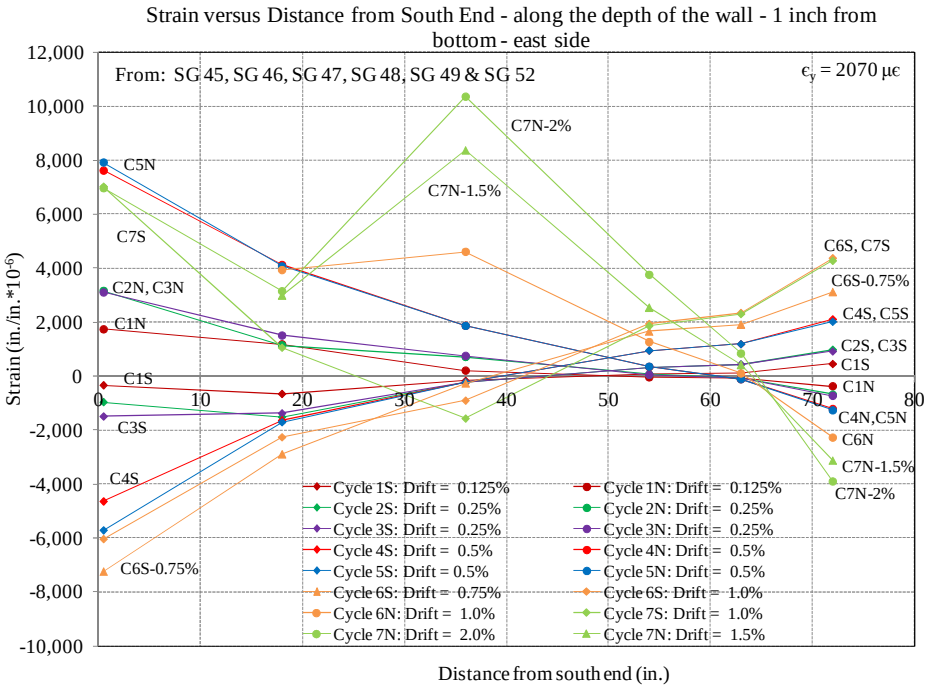

Figure 6.78 Strains along the depth of the wall at 1 in. from bottom - east side

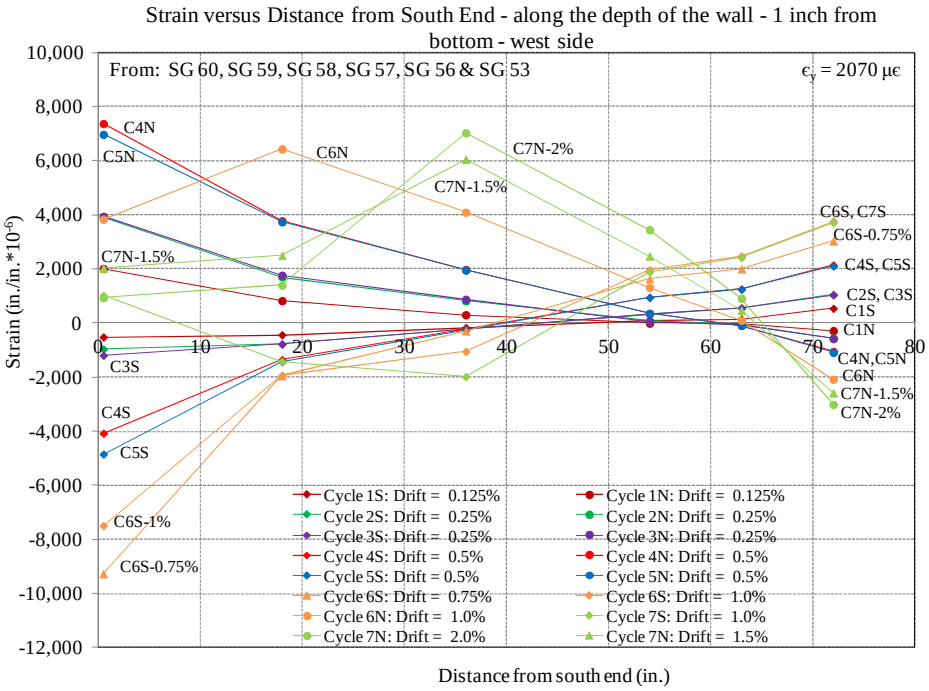

Figure 6.79 Strains along the depth of the wall at 1 in. from bottom - west side

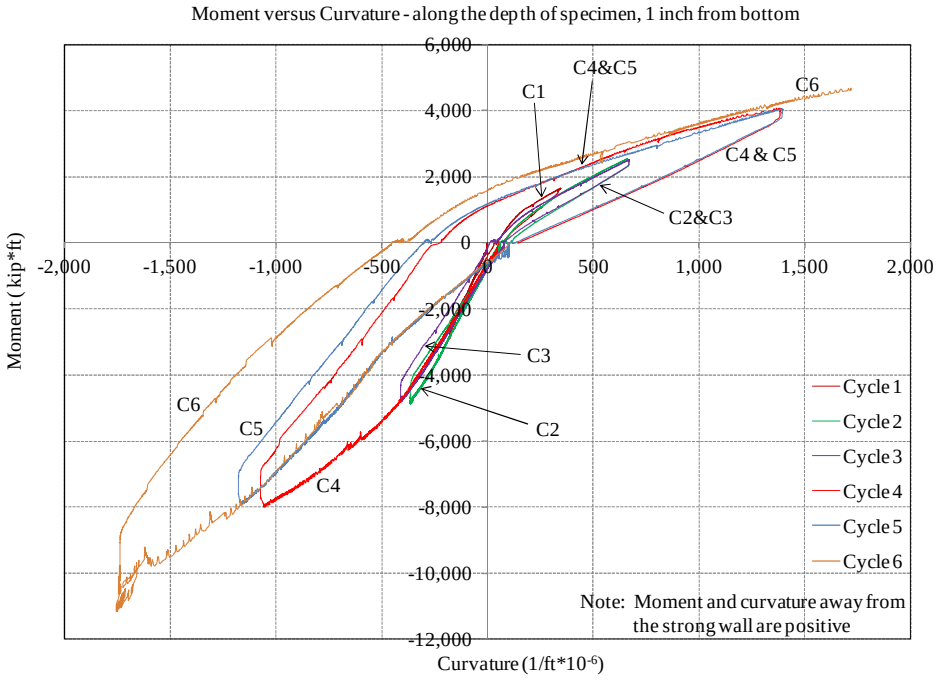

Figure 6.80 Moment versus curvature at 1 in. from bottom

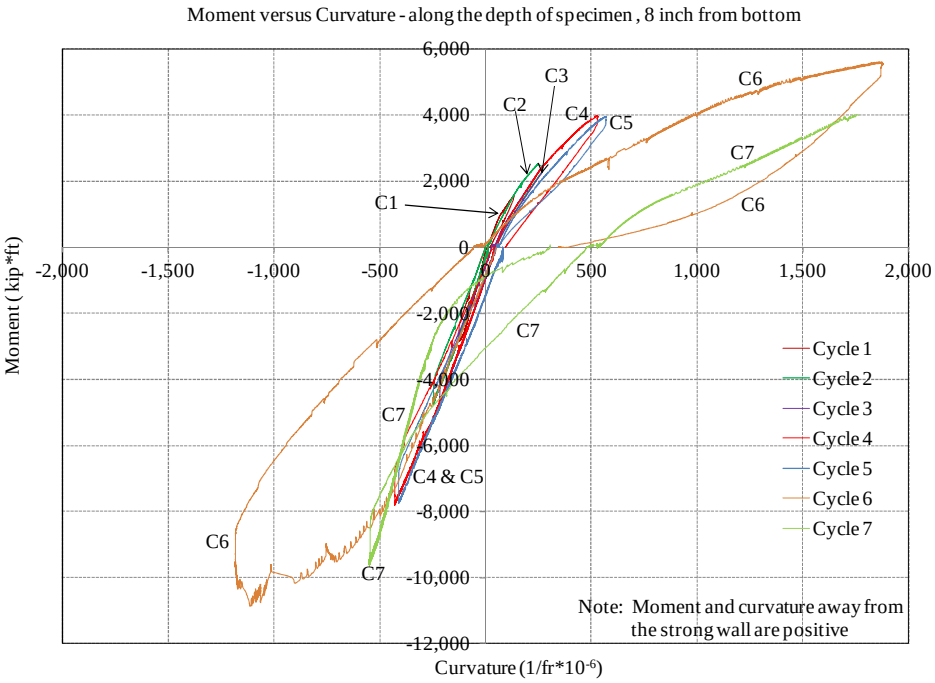

Figure 6.81 Moment versus curvature at 8 in. from bottom

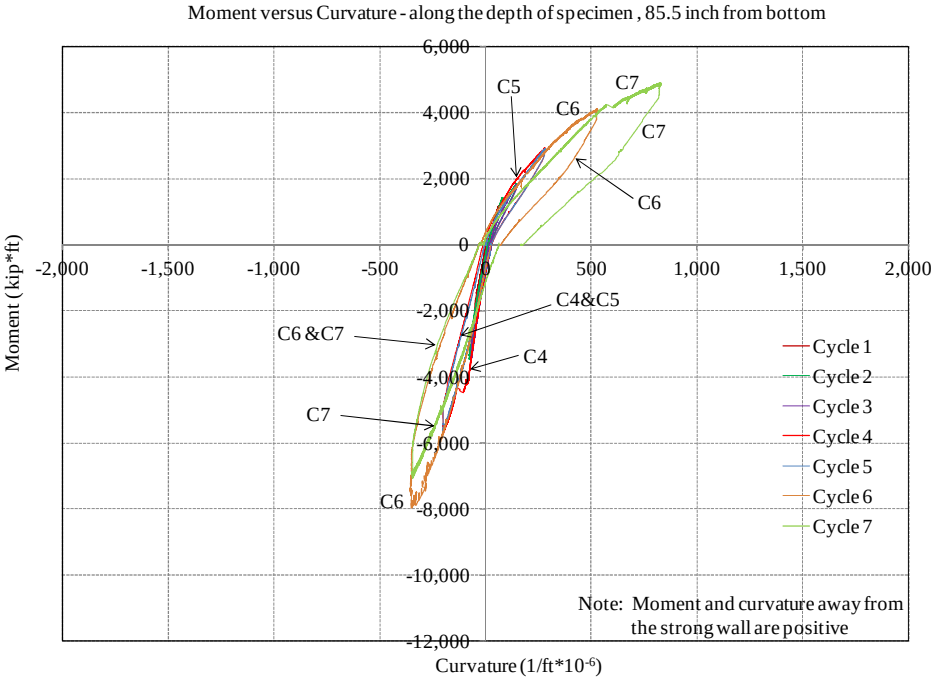

Figure 6.82 Moment versus curvature at 85.5 in. from bottom

CHAPTER 7: SUMMARY AND CONCLUSIONS

The objective of this research was to examine the behavior of a dual-plate composite shear wall subjected to cyclic lateral load and to develop suitable methods for the design of the corresponding structural components. Finite element analyses, together with characterizations of the structural strength and experimental investigations were used to accomplish this objective. This research program included four major investigations: (a) stability of the dual-plate assembly for construction loads, (b) strain compatibility between the steel plates and infill concrete, (c) behavior of the splice plate connection for in-plane shear loading, and (d) behavior of the dual-plate composite shear wall for cyclic loading.

7.1: Stability of dual-plate assembly for construction loads

Stability behavior of a dual-plate assembly to resist construction loads was analytically and experimentally investigated. The dual-plate assembly must be able to safely support an appropriate portion of the steel framing dead load and typical construction live loads to allow construction of steel framing to proceed before concrete is cast within the dual-plate assembly.

To assess the behavior and buckling load resistance of the dual-plate assembly, finite element models were assembled and the response of the dual-plate assembly with various parameters for vertical loads was evaluated.

An experimental investigation was performed using a two-story planar dual-plate assembly. A 3/8-scale specimen of a dual-plate composite shear wall with the parameters

that are typically used in the industry was constructed. A 3/8-scale specimen resulted in a specimen with a plate thickness of 3/16 in., wall thickness of 9 in., transverse bar diameter of 3/8 in., and a bar spacing of 4-1/2 in. The two-story unfilled dual-plate assembly was constructed on top of a one-story (58.5-in. tall) concrete-filled dual-plate assembly. Vertical load was applied to cross beams which framed into the dual-plate assembly. Load was transferred to the dual-plate assembly via shear tab connections. The bottom one-story concrete-filled dual-plate assembly was used for the strain compatibility test which followed. Later, the same specimen was also used for investigating the horizontal splice plate connection test for in-plane shear loading. Load was applied to the stability specimen until significant deflection was observed.

The finite element results were in good agreement with the experimental results. However, finite element analysis predicted a maximum load 20 percent higher than the maximum load measured during the test. Two reasons for a load less than predicted by the finite element analysis include: (a) loading was stopped before the specimen failed (buckled) and (b) imperfections in the plate assembly were not measured and, consequently were not considered, in the finite element analysis.

The plate assembly resisted a maximum load of 18 times the maximum expected construction load. The specimen was completely stable with almost zero deflection at low load levels (about 1.1 times the maximum expected construction load). The plates were still acting elastically when the maximum load was applied.

Prior to the analytical investigation of the stability behavior of a 3/8-scale two-story planar shape plate assembly for vertical loads, finite element models were developed for multiple stories (one to four stories) of full-scale prototypes. However, a 1/2-in. diameter rod, instead a 1-in. diameter rod, was used for modeling the full-scale prototypes. The ratios of the buckling loads for the three and four-story plate assemblies to the two-story plate assembly were 0.51 and 0.30, respectively. Hence, three and four-

story plate assemblies would resist a vertical load of approximately 9 and 5 times the typical vertical construction loads, respectively.

The experimental program was conducted for a two-story plate assembly. Hence, it can be concluded from this study that construction of gravity-load framework around a two-story core-wall plate assembly before casting the concrete is safe. Furthermore, from the finite element analyses, it was determined that construction of gravity-load framework around three and four-story core-wall plate assemblies before casting the concrete is also safe. However, further experimental research should be conducted to verify the results from the finite element analyses.

7.2: Strain compatibility between steel plates and concrete

Strain compatibility between the steel plates and concrete cast between the plates was investigated by applying out-of-plane lateral load to the concrete-filled dual-plate assembly (the first story of the three story specimen used for the stability test). Strains in steel plates, concrete, and reinforcement in the middle of the wall were measured to determine the strain distribution through the wall thickness and thereby evaluate the strain compatibility at different lateral load levels. Strain compatibility between the steel plates and concrete would reveal that both elements act together and there is strain linearity through the cross section.

The test demonstrated that the strain distribution was reasonably linear before the concrete cracked, and that the linearity decreased gradually when the lateral load was increased. Threaded rods in the plate assembly helped to transfer strains from the steel plates to the concrete. Decreasing the spacing of the threaded rods may increase the strain linearity through the cross section of the wall.

7.3: Behavior of splice plate connection for in-plane shear loading

The behavior of splice plate connections for in-plane shear loading was experimentally investigated using the second story dual-plate assembly of the specimen that was used for the stability test. The central portion of the plate assembly above the cast concrete was removed and two shear tests of 30-in. long horizontal splice plates, one test at each end of the specimen, were performed. A 3/16-in. fillet weld was provided to attach the 3/16-in. splice plate to the 3/16-in. shear wall plates. In-plane lateral load was applied to the dual-plate assembly to determine the maximum load the specimen was able to resist.

The splice plate connection did not fail during the test (until an equivalent stress of 31.1 ksi on the shear wall plates when compared to the nominal shear strength of 30 ksi of the steel plates). The dual plate assembly displaced laterally in the out of plane direction at a shear stress of 26.7 ksi on the shear wall plates probably because of eccentricity in the alignment of specimen and loading set-up. Hence, an average stress of 26.7 ksi was observed to be acceptable for the horizontal splice plate connection prior to failure. This is slightly less (0.89 times) than the nominal shear strength of the 3/16 in. plates used for the test, which is equal to 30 ksi ($0.6*F_y$).

7.4: Behavior of dual-plate composite shear wall for cyclic loading

The lateral load resistance and drift capacities of the shear wall need to be considered when designing for cyclic lateral load. To investigate the behavior of the composite shear wall for cyclic lateral load, a 30-ft tall T-shaped shear wall was tested under cyclic lateral load. The objective of this test was to check whether the selected dimensions of the structural elements and details used in the shear wall satisfy a drift capacity of 2 percent.

A 3/8-scale, 5-1/2 story T-shaped shear wall specimen with a 63-in. long web and a 90-in. wide flange was selected for the cyclic loading test. Plate thickness, wall thickness, transverse bar diameter and bar spacing were the same as used in the stability test.

The vertical and shear forces from the shear wall plate were transferred to the foundation via a foundation connection plate which was partially embedded in the concrete. Hence, each foundation connection plate was designed for the combined effects of the tensile fracture of the shear wall plate and the shear transferred to the foundation connection plate. The fillet weld joint between each shear wall plate and the foundation connection plate was designed for the forces developed by assuming tensile fracturing of the shear wall plate.

Tension forces from the foundation connection plate were transferred to the foundation via reinforcing bar hooks welded to the foundation connection plate. The reinforcing bar hooks were designed to resist the tension forces associated with tensile fracture of a shear wall plate. Shear studs welded to the foundation connection plate were designed to resist the maximum lateral load applied during the cyclic load tests.

The joint between the flange and web of the wall specimen was made by welding a single angle to the flange and web on each side of the web. The weld along the total length of the joint was designed to transfer the total vertical force transmitted from the flange to the web.

Horizontal connection between two plate assemblies was made by welding splice plates to the top and bottom plate assemblies. The shear wall plates up to an elevation between the third and fourth stories were expected to strain well beyond yield. Hence, each splice plate connection in the bottom three stories was designed for the tensile strength of the shear wall plate. The splice plate connections at the top two levels were designed for the yield strength of the shear wall plate.

Moment-curvature diagrams were developed to provide an understanding about the behavior of the shear wall expected for static lateral load and the maximum load needed for application during the laboratory test.

Vertical load was applied to replicate the self weight of the shear wall and the service load transferred to the shear wall by gravity-load framing. A total vertical load of approximately $0.1A_g f_c'$ (where A_g is the gross cross-sectional area of the shear wall and f_c' is the 28-day design strength of the concrete) was applied by post-tensioning eight high-strength PT bars extending from the bottom of the foundation block to different levels over the height of the specimen.

Lateral load was applied to the specimen in a drift-control mode up to a maximum drift ratio of 1 percent in the strong direction and 2 percent in the weak direction. The shear wall plates at the extreme end of the web started buckling at about 0.75 percent drift ratio when the specimen was pushed in the strong direction.

During a full load cycle, larger strains were observed at the extreme end of the web at the bottom level of the specimen. This occurred when the specimen was pushed in the weak direction (so that the steel plate at that location experienced tensile strains). Splice plates, fillet welds between the splice plates and the shear wall plates, the angles in the corner connection, fillet welds between the angles and splice plates, fillet welds between the shear wall plates and foundation connection plates, the foundation connection plates, reinforcing bar hooks welded to the foundation connection plates, and the shear studs welded to the foundation connection plates did not exceed the stress level they were designed for when the specimen was pushed up to 2% drift in the weaker direction. Hence, it appears that these structural components can be designed as outlined herein.

Almost the entire plate at the bottom level of the specimen yielded during the test (however not at the same time) as expected. Strains at the extreme end of the web near

the bottom of the specimen exceeded five times the yield strain of the plates. Yielding of the plates was observed up to at least the middle of the second story. There were no strain gauges on the shear wall plates above that level to monitor strains in the shear wall plates.

The plates at the south end buckled at approximately 0.75% drift when the specimen was pushed in the strong direction (so that the steel plate at that location developed compressive strains). If buckling of the plate could be prevented, then it is believed that the splice plates, fillet welds between the splice plates and the shear wall plates, fillet weld between the shear wall plates and foundation connection plates, the foundation connection plates and the reinforcing bar hooks would adequately resist the forces developed when the specimen is pushed to 2% drift ratio in the strong direction also.

If buckling of the plate could be prevented by the methods described above, then the design approach used in this test can be used to design the structural components for dual-plate composite shear walls to resist cyclic lateral loading up to 2% drift ratio.

7.5: Recommendations for future work

In this research study, the structural components of the dual-plate composite shear wall were designed and tested in the laboratory to verify whether or not those structural components performed satisfactorily. Additional research on dual-plate composite shear wall behavior would be useful to address a number of issues observed as part of the present research effort. The primary recommendations for future work include the following.

1. The experimental investigation was conducted only for the selected dimensions of the structural components of the dual-plate composite shear wall even though a range of values are possible for those dimensions. Research can be expanded for various dimensions of the structural

components (for example wall thickness, plate thickness, transverse bar diameter and spacing).

2. The stability test was conducted only for a two story dual-plate assembly. Finite element analysis was conducted for two to four-story plate assemblies. The experimental research may need to be expanded up to the number of stories currently erected in the construction industry and as limited by concrete placement.

3. The cyclic loading test was performed only for a T-shaped shear wall configuration. However, testing should be expanded to include I-shaped and C-shaped configurations which are also very common in a typical shear wall layout. In this research study, the load was applied along the plane of the web as it was symmetric. Different loading directions should also be considered. Detailed finite element analysis can be performed considering the cyclic material properties of the steel plates and the concrete.

4. During the cyclic loading test, noise that developed by apparent breaking of the bond between the concrete and steel plates was noticeable from the early stages of loading. Simple composite shear wall models should be fabricated using bond breakers between the concrete and steel plates and tested to verify the success in reducing the noise.

5. A more detailed study to examine the behavior of the foundation elements and their design is needed. The elements in the current study were designed so as to not fail prematurely, and their dimensioning and efficiency may be improved through further study.

6. Typical building plans for tall buildings indicate that shear wall elements like the T-shaped specimen studied in this investigation will need to be coupled together at floor levels to make the elements perform together as a core wall unit. Details for these coupling elements need to be developed and their intended behavior verified in the laboratory.

LIST OF REFERENCES

LIST OF REFERENCES

ABAQUS (2010). ABAQUS/Standard Version 6.10 User's Manuals. Hibbitt, Karlsson, and Sorenson, Inc., Pawtucket, RI.

ACI-318-08 (2008). Building Code Requirements for Structural Concrete (ACI 318-08) and Commentary (318R-081). American Concrete Institute, Farmington Hills, Mich.

AISC (2011). Manual of Steel Construction, Load and Resistance Factor Design. 14th Edition, American Institute of Steel Construction.

AWS D1.4/D1.4M (1998, 2011). Structural welding code — reinforcing steel. American Welding Society.

ANSI/AISC 341-10 (2010). Seismic provisions for structural steel buildings. American Institute of Steel Construction.

ASCE-7 (2010). Minimum Design Loads for Buildings and Other Structures. American Society of Civil Engineers, Reston, VA.

ASME B1.1(2003). Unified Inch Screw Threads. American Society of Mechanical Engineers, New York, NY.

Bowerman, H. G., Gough, M. S., and King, C.M. (1999). Bi-Steel design and construction guide. British Steel Ltd.

Bowerman HG, Chapman JC. (2002). "Steel concrete steel sandwich construction." US Engineering Foundation ASCE. Composite construction in steel and concrete IV, ASCE.

Clubley, S. K., Moy, S. S. J., and Xiao, R. Y. (2003a). "Shear strength of steel–concrete–steel composite panels, Part I—testing and numerical modeling." *J. Construct. Steel Res.*, 59, 781-794.

Clubley, S. K., Moy, S. S. J., and Xiao, R. Y. (2003b). "Shear strength of steel–concrete–steel composite panels, Part I—testing and numerical modeling." *J. Construct. Steel Res.*, 59, 795-808.

Eom, T., Park, H., Lee, C., and Chang, I. (2009). "Behavior of double skin composite wall subjected to in-plane cyclic loading ." *J. Struct. Eng.*, *135*(10), 1239-1249.

Kim, J. (2007). "Design procedure for dual-plate composite shear wall." Report I, Bowen Laboratory, Purdue University.

Macgregor, J. E., Wight, J. K., (2005). Reinforced Concrete: Mechanics and Design. 4th Edition, Pearson Prentice Hall, Upper Saddle River, NJ.

Massone, L., M., and Wallace, J. W. (2004). "Load-deformation response of slender reinforced concrete walls." *ACI Struct. J.*, 101 (1), 103-113.

Rees, D. W. A. (2009). Mechanics of optimal structural design: Minimum weight structures. John Wiley & Sons, Ltd, West Sussex, United Kingdom.

Salmon, C. G., Johnson, J. S., and Malhas, F. A. (2009). "Steel structures: design and behavior: emphasizing load and resistance factor design." 5th edition, Pearson, Prentice Hall, Upper Saddle River, New Jersey.

Thomsen, J. H., IV, and Wallace, J. W., (2004). "Displacement-based design of slender RC structural walls—experimental verification." *ASCE J. Struct. Eng.*, *130* (4), 618-630.

Kreger, M. E. and Bowman M. D. (2006). "Design procedure for dual-plate composite shear wall." Research Proposal.

Xie, M., Foundoukos, J.C., and Chapman, J. C. (2004). "Experimental and numerical investigation on the shear behaviour of friction-welded bar–plate connections embedded in concrete ." *J. Construct. Steel Res.*, 61, 625-649.

Xie, M., and Chapman, J. C. (2006). "Developments in sandwich construction." *J. Construct. Steel Res., 62* (11), 1123–1133.

Zhao, Q., and Astaneh-Asl, A. (2004). ''Cyclic behavior of traditional and innovative composite shear wall." *J. Struct. Eng.*, *130* (2), 271-284.

APPENDICES

Appendix A: Contribution of Transverse Rods to the Lateral Stiffness of the Plate Assembly

A.1: Introduction

The effective inertia and hence the computed lateral stiffness of the interconnected dual-plates varies significantly when the rod diameter is varied. Because the moment of inertia of a given tie rod varies according to the fourth power of the diameter, the effective inertia of tie rods can vary greatly as the diameter is varied. A 1-in. diameter rod has been used successfully to interconnect dual-plates for other patented construction applications that utilize friction stir-welding to join the rods with the plates (Bowerman and Chapman, 2002). Because a three-eighths scale model was used in the experimental program of this research project, it was decided that a 0.25-in. to 0.75-in. diameter rod would be needed to effectively connect the two plates of the reduced-scale model if full fixity of the rod-to-plate connection is achieved.

A series of reduced-scale (3/8-scale) tests to investigate the contribution of the transverse connecting rods to the lateral stiffness of the plate assembly was performed. The plate assembly was 9-in. thick, 13.5-in. wide, and 22.5-in. high. The spacing between the transverse bars was 4.5 in. in both orthogonal directions. Transverse connecting rods (fully threaded rods) of ¼-in., ½-in., and ¾-in. diameters were considered while keeping all the other parts of the test set-up the same. Finite element analyses were performed for the three cases, as well as for a 3/8-in. diameter case. The analysis results were compared with the test results. Based upon the information gathered regarding the performance of the tie rods used in the reduced-scale tests, the tie rod diameter to be used in the three-eighths scale specimens was selected.

A.2: Experimental Investigation

Lateral load was applied to three plate assemblies with the 0.25, 0.5, and 0.75-in. diameter transverse rods in the direction perpendicular to the plate assembly. Lateral displacement and strains in the plates and rods were measured to calculate the lateral stiffness of each plate assembly and to study how load was transferred in the plate assemblies.

A.2.1: Test Set-up

A drawing and a photograph of the test set-up are shown in Figs. A.1 and A.2, respectively. Transverse rods were spaced at 4.5 in. (which is a scaled spacing comparable to the 12 in. spacing in the prototype). Hinges were used to attach the loading plate (13.5 in. x 15.5 in. x 1 in.) to the 3/16-in. plates. The 3/16-in. plates were made of grade A36 steel. Hinges helped to transfer the horizontal load to the plate assembly specimen without also transferring significant moments. The transverse rods were attached to the 3/16-in. plates using four nuts per each bar-two inside the plate assembly and two outside. These nuts were tightened using a typical wrench; neither a cheater bar nor an impact wrench was used for tightening the nuts. Listed minimum tensile strength of the transverse bar was 53 ksi. However, coupon tests of similar rods tested later showed the tensile strength to be 70 ksi. The 3/16-in. plates were bolted at the bottom to 5 in. x 5 in. x 3/4 in. single angles by turn-of-the-nut method (1/3 rotation). These 5 in. x 5 in. x 3/4 in. angles were tightly bolted (by turn of the nut method) to a base plate which was anchored to the strong floor using high-strength PT bars that were post-tensioned (see Figs. A.1 and A.2). The load was applied by rotating a turnbuckle attached to the loading plate on the top of the plate assembly.

A.2.2. Instrumentation

Lateral loads, lateral deflections, and strains in the plates and transverse connecting rods were measured. The outer side of the 3/16-in. plates was whitewashed to detect any evidence of yielding in the plates. A 5-kip load cell, attached between the turnbuckle and loading plate (see Fig. A.2), was used to measure applied lateral load. A linear potentiometer was installed to measure lateral deflections (see Fig. A.2). Lateral load and lateral deflection measurements were then used to calculate the lateral stiffness of the plate assembly to assess the behavior and effectiveness of the tie rods to make the plates function together as an integral unit. Strain gauges were attached to the 3/16-in. plates to infer the second moment of area of the cross section of the plate assembly (from the pure bending formula, $\sigma = M*y/I$). Strain gauges were also attached on top and bottom of the transverse rods to determine how much bending or axial force is transferred by the rods from one plate to the other. Strain gauges were attached to transverse bars only for the ½-in. diameter case. Strain gauge layouts for the test set-ups with 3/4-in., 1/2-in., and 1/4-in. diameter bars are shown in Figs. A.3, A.4, and A.5, respectively. Strain gauges which were installed, but did not function properly, are not shown in the figures.

A.2.3: Test Method

The reduced-scale specimen, which resembled a cantilever beam, was subjected to a lateral load at the top to induce bending of the interconnected 3/16-in. thick plates. Lateral load was applied by slowly rotating the turnbuckle being careful not to apply any impact load. The load cell, potentiometer, and strain gauges were monitored and recorded using a Vishay Micro Measurements data acquisition system (system 7000). Lateral load was applied to a certain load level (2163 lbs for ¾-in. diameter rod case, 1679 lbs for ½-in. diameter rod case, and 343 lbs for ¼-in. diameter rod case) so that at least a significant part of the linear curve was obtained. For the ½–in. and ¼–in. diameter cases, load, deflection, and strain measurements were recorded also for the unloading response. Load,

deflection, and strain measurements were zeroed before starting each test. During each test, whitewash on the steel plates was monitored for flaking to detect yielding of the steel plates.

A.2.4: Test Results

Lateral Load versus Lateral Deflection from Laboratory Tests

Lateral load versus lateral deflection curves are shown in Fig. A.6 for each of the three tests (3/4-in. dia. rod, ½-in. dia. rod, and ¼-in. dia. rod). Calculation of lateral stiffness from the initial linear portion of the curves using a linear trend line is shown in Fig. A.7. The lateral stiffnesses are tabulated in Table A.1. Upon unloading, permanent deformations of 0.92 in. and 0.44 in. were observed for the ½–in. and ¼–in. diameter cases, respectively (refer Fig. A.6).

Strain Measurements in Plates and Transverse Rods from Laboratory Test

There was no observation of flaking of the whitewash during the tests. Strains developed in the plates versus lateral load plots for the test set-ups with 3/4-in., 1/2-in., and 1/4-in. diameter bars are shown in Figs. A.8, A.9, and A.10, respectively. Strain readings were consistently compressive on the loading side of the plate and tensile on the opposite side, and decreased with distance from the base of each plate assembly suggesting cantilever behavior of the assemblies. Strains in transverse rods versus lateral load plots for the test set-up with 1/2-in. diameter bars are shown in Fig. A.11. The strain gauges on the transverse rods are shown in Fig. A.4. From Fig. A.11, it could be noted that strain gauges B2 and B3 measured compressive strains while strain gauge B1 measured tensile strains in the top level transverse rod. Similarly, strain gauges B5 and B6 measured compressive strains while strain gauges B4 and B7 measured tensile strains in the bottom level transverse rod. Hence, it could be concluded that the transverse rods

transferred significant bending from the plate on the loading side to the plate on the opposite side of the plate assembly.

A.3: Finite Element Analysis

Finite element analysis was performed to compare predicted response with the experimental results and to further expand the investigation to 3/8-in. diameter rods. Abaqus (Abaqus/CAE 6.10-1) was used to perform the finite element analysis for each of the four cases (1/4-in., 3/8-in., 1/2-in., and 3/4-in. diameter rods).

A.3.1: Finite Element Modeling

A finite element model of the specimen is shown in Fig. A.12. The 3/16-in. plates were modeled as shell elements (S4, a 4-node doubly curved general-purpose shell, finite membrane strains). The portion of the 3/16-in. plates which was clamped by the bolts and nuts to the ¾-in. angles at the base was assumed to be rigid and was therefore omitted.

Transverse bars were modeled as beam elements (B33, a 2-node cubic beam in space). The effective pitch diameter of the threaded transverse bars can be calculated using Equation A.1 (ASME B1.1, 2003). The calculated effective pitch diameters of the 1/4-in., 3/8-in., 1/2-in., and 3/4-in. diameter rods were used in the finite element modeling. The pitch and effective pitch diameters of the transverse bars are tabulated in Table A.2.

$$D_p = D_{maj} - 0.64952 * p \qquad \text{Eq. (A.1)}$$

Where, D_p = Effective pitch diameter (in.)

D_{maj} = Major diameter (in.)

p = pitch (in.) = 1/ (number of threads/in.)

Material behavior for the steel plate was assumed to be elastic-perfectly plastic with E = 29,000 ksi, σ_y = 36 ksi, υ = 0.3, and Mass density = 0.00073386 lbf * s^{-2}*in^4. Material behavior for the transverse bars also was assumed to be elastic-perfectly plastic with E = 29,000 ksi, σ_y = 70 ksi, υ = 0.3, and Mass density = 0.00073386 lbf * s^{-2}*in^4.

The 1-in. thick loading plate was modeled as a solid element (C3D8R, an 8-node linear brick, reduced integration, hourglass control). Mesh parts were created and assembled. Connection between each transverse bar and 3/16-in. plates was modeled as a "tie" constraint with rotational degree of freedom restricted. The joint between the 3/16-in. plate and the loading plate was modeled as a "tie" constraint without rotational degree of freedom restricted.

A fixed boundary condition was considered at the bottom of the modeled specimen (at the top of the nuts). When the specimen is pulled (towards the left) by applying tension in the turnbuckle, the ¾-in. angle restricts the lateral movement of the 3/16-in. plate on the left side while the 3/16-in. plate on the right side is free to move laterally. Hence, the lateral movement was restricted (U3=0) along the joint between the left side 3/16-in. plate and the 3/16-in. angle. Figure A.12 shows both boundary conditions.

Analysis was performed in two steps: (1) Static General and (2) Static Riks. In the first step, gravity loading (self weight) was considered. In the second step, lateral load was applied as a concentrated force at the location shown in Fig. A.12. Because all the sensors were zeroed at the start of the test (after gravity loading), the deflections and strains from the gravity loading of the finite element model were deducted from the final results of the finite element analysis that are reported in this report.

A.3.2: Finite Element Analysis (FEA) Results

Lateral Load versus Lateral Deflection from Finite Element Analysis

Lateral load versus lateral deflection curves from the finite element analyses are shown in Fig. A.13 for each of the four rod diameter cases (1/4-in., 3/8-in., 1/2-in., and 3/4-in. diameter rods). Calculation of lateral stiffness from the initial linear portion of the curves using a linear trend line is shown in Fig. A.14. The lateral stiffnesses are tabulated in Table A.3. Figure A.14 shows that the lateral stiffness of the plate assembly significantly increases with rod diameter.

A.4: Results Analysis and Comparison

The load-deformation curves for the specimens with 1/4-in., 1/2-in., and 3/4-in. diameter rods from the FE analyses and the tests are shown in Fig. A.15. The test results were in good agreement with the FEA results (except a small deviation for the ¾-in. diameter rod case, see Fig. A.15). Lateral stiffness versus effective pitch diameter of the transverse rods is plotted in Fig. A.16. It can be noted from Fig. A.16 that the lateral stiffness of the specimen increased significantly with the diameter of the rods.

It can be noted from Table A.1 and Table A.2 that the lateral stiffness of the dual-plate assembly with ¼-in. (2/3 in. in prototype) rods at 4.5-in. spacing (12 in. in prototype) is very small (193.2 lb/in from laboratory test and 256.3 lb/in from FEA) compared to the other specimens. Hence, the earlier consideration of using a ½-in. diameter rod in the prototype (which would have been 3/16 in. in the 3/8-scale lab models) was decided to be inadequate due to low lateral stiffness. Instead, a prototype with 1-in. diameter rods at 12-in. spacing (which provides 3/8-in. diameter bars at 4.5-in. spacing in the 3/8-scale lab models) was selected for the stability investigation to check whether the wall panels are

able to resist construction loads. Furthermore, in the patented production of the dual-plate assembly (Corus/TATA Bi-Steel), 1-in. diameter bars were used.

Table A.1 Variation of lateral stiffness (from the initial linear portion of the curve) with transverse rod diameter- Laboratory test

Rod Diameter (in.)	Lateral Stiffness – From Test (lb/in.)
0.25	193.2
0.50	1547.0
0.75	4450.1

Table A.2 Effective pitch diameters of the transverse bars calculated for finite element analysis (using Equation A.1)

Transverse bar Diameter, D_{maj} (in.)	Threads/in. (1/in.)	p = Pitch (in.)	Effective pitch diameter (in.)
0.25	20	0.050	0.218
0.375	16	0.062	0.334
0.50	13	0.077	0.450
0.75	10	0.100	0.685

Table A.3 Variation of lateral stiffness (from the initial linear portion of the curve) with transverse rod diameter- Finite element analysis

Rod Diameter (in.)	Lateral Stiffness – From FEM (lb/in.)
0.25	256
0.375	807
0.50	1780
0.75	3530

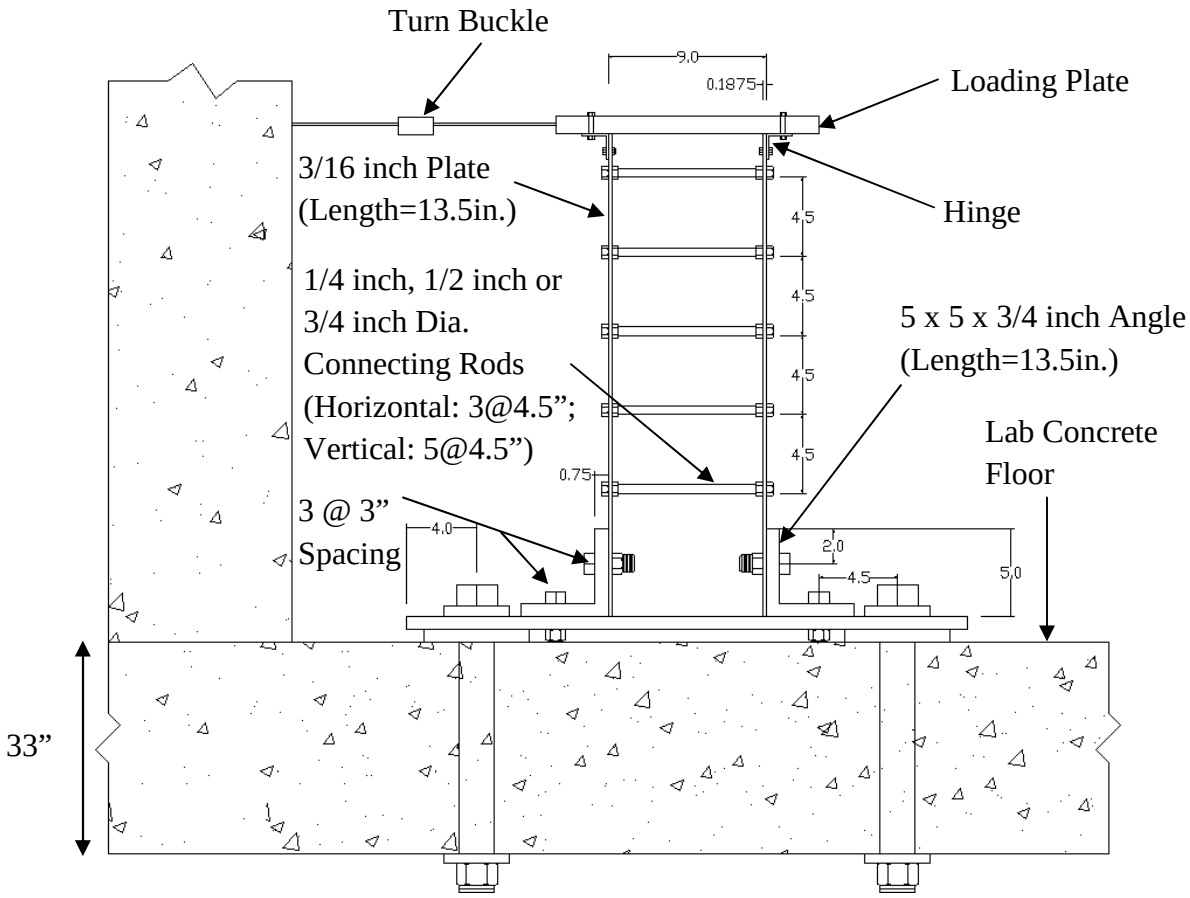

Figure A.1 Test set up for the investigation of transverse connecting rods (Front View)

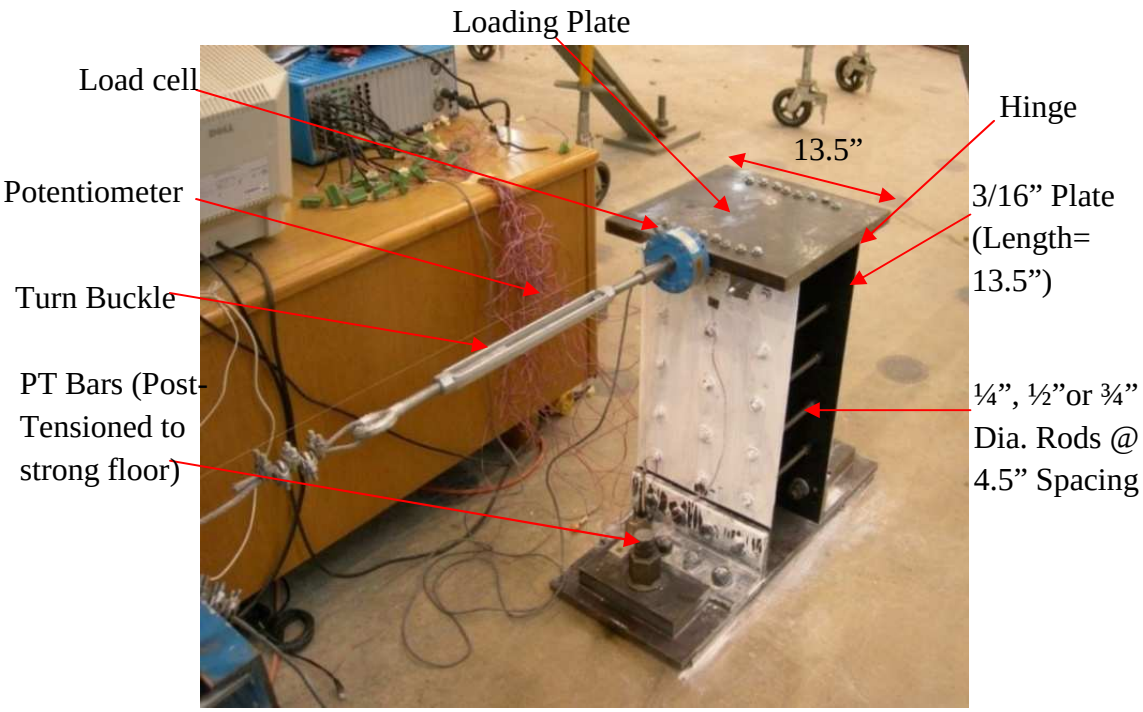

Figure A.2 Test set-up for the investigation of transverse connecting rods

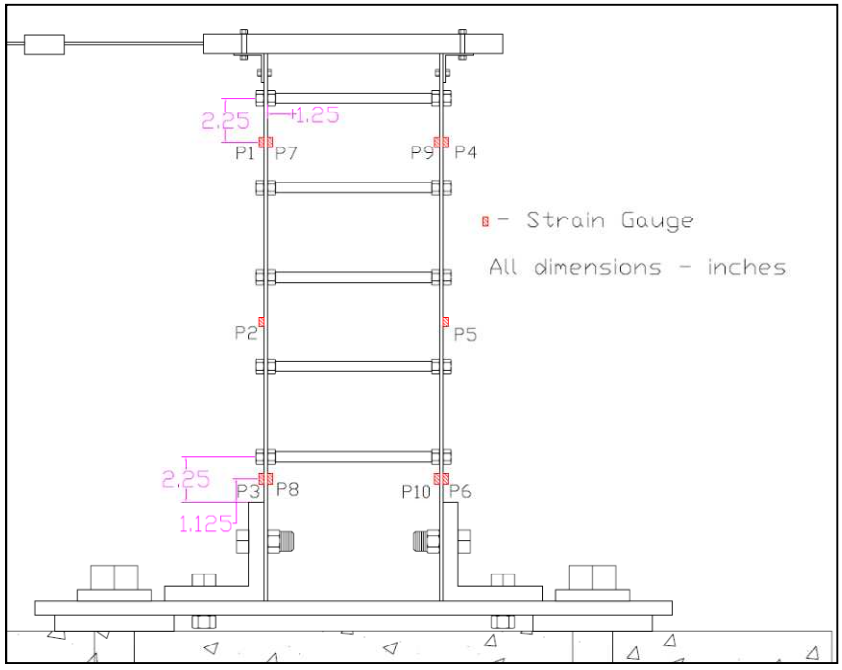

Figure A.3 Strain gauge layout for 3/4-in. bar diameter case (Test-1)

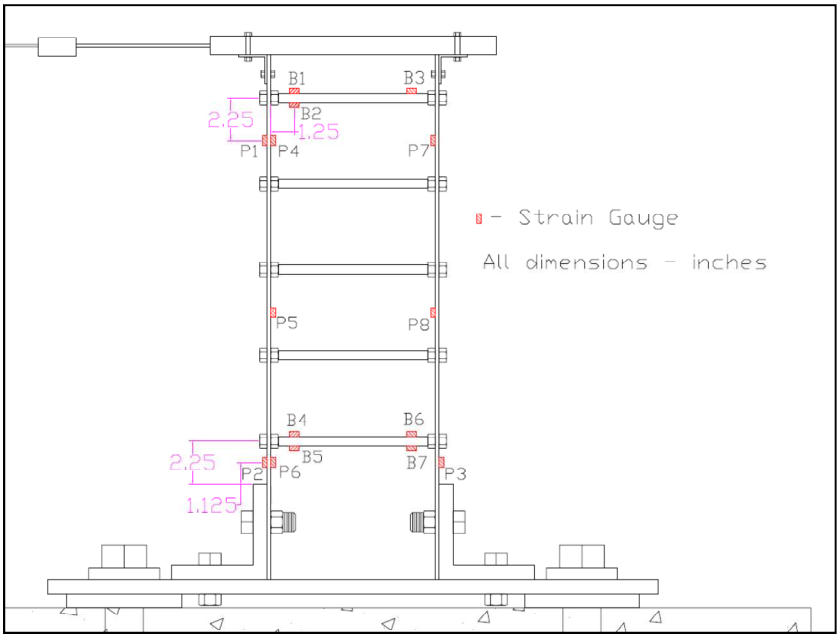

Figure A.4 Strain gauge layout for 1/2-in. bar diameter case (Test-2)

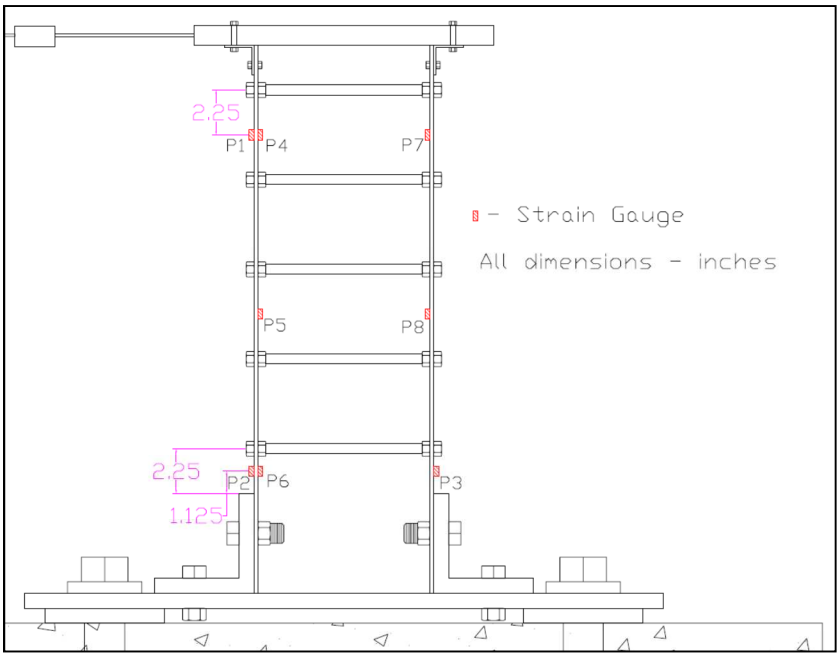

Figure A.5 Strain gauge layout for 1/4-in. bar diameter case (Test-3)

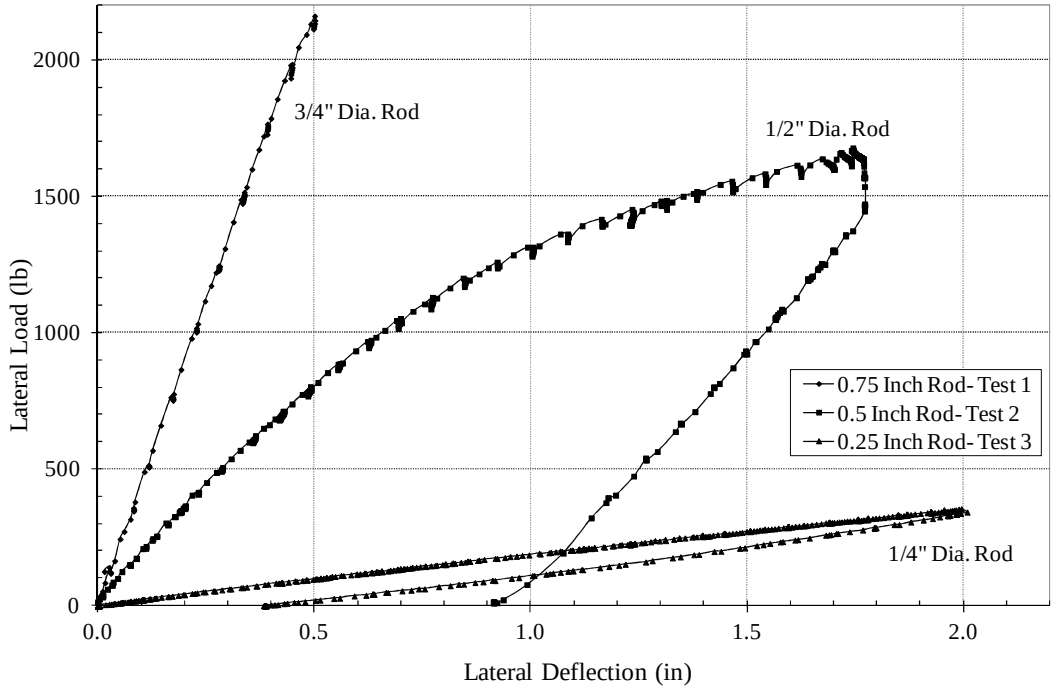

Figure A.6 Lateral load versus lateral deflection curves for 1/4, 1/2, & 3/4-in. rod diameters

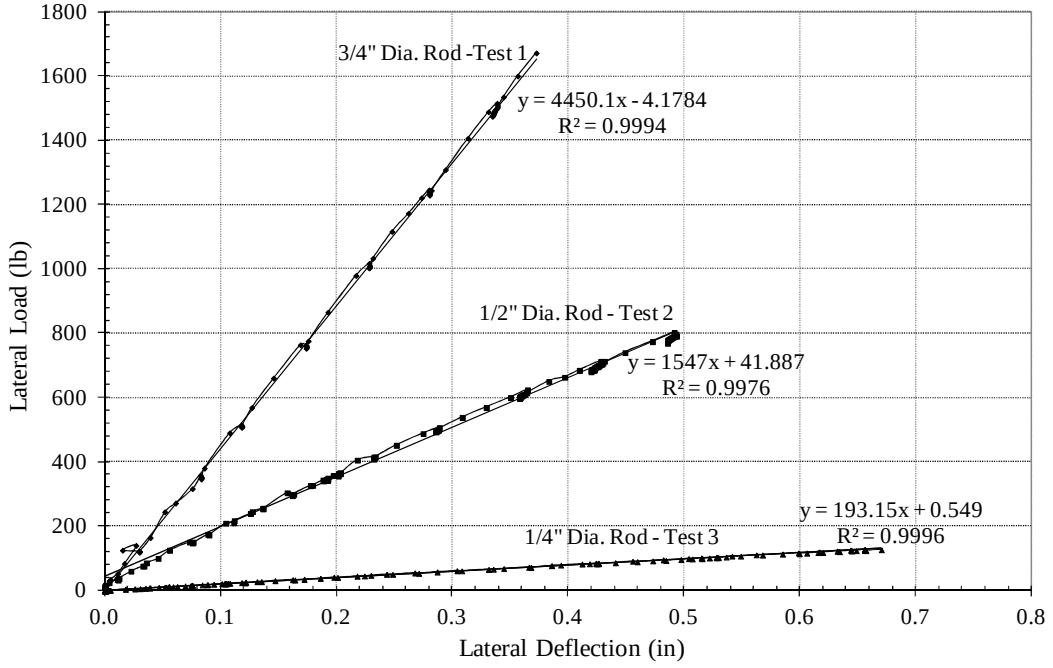

Figure A.7 Lateral load versus lateral deflection for 3/4, 1/2, & 1/4-in. dia. Rod tests - lateral stiffness calculation

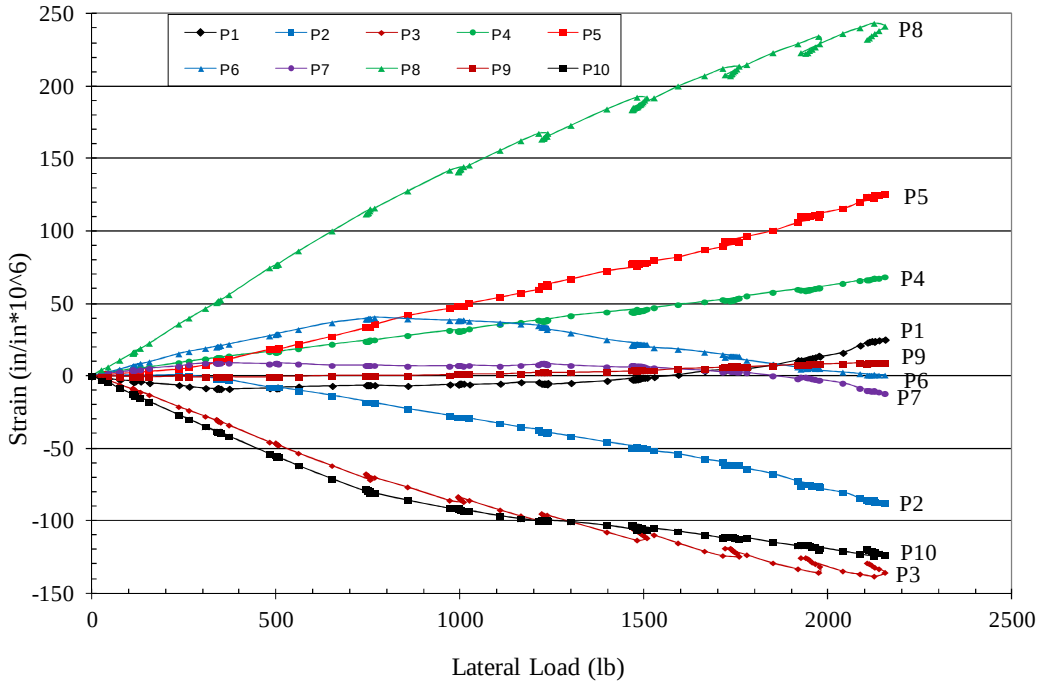

Figure A.8 Strain on plates versus lateral load-for specimen with 3/4-in. rod

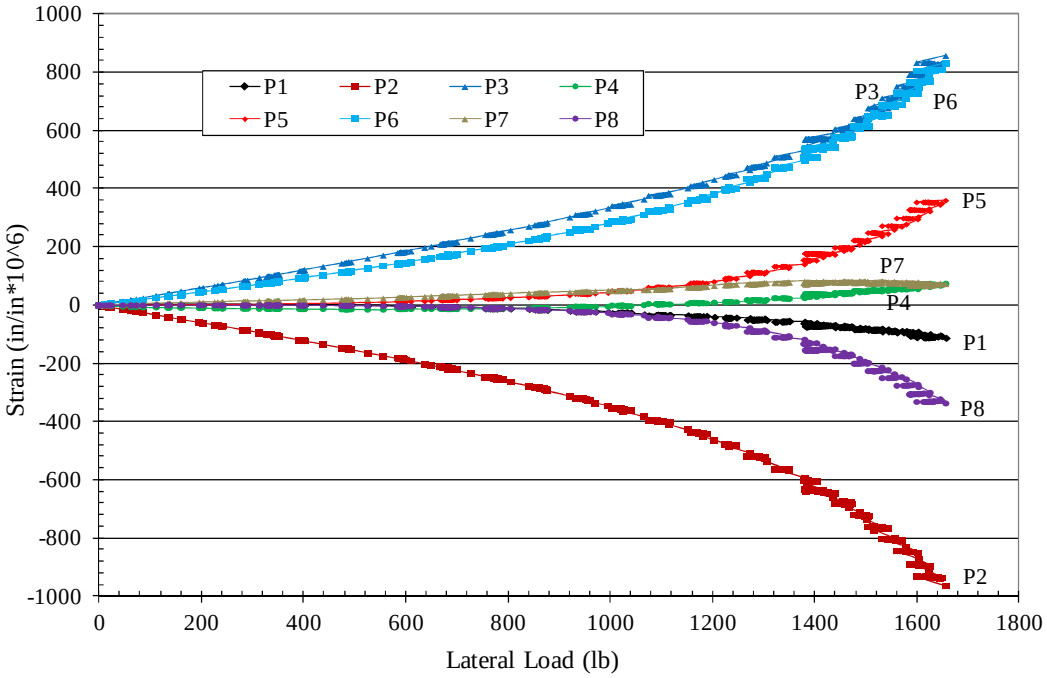

Figure A.9 Strain on plates versus lateral load-for specimen with 1/2-in. rod

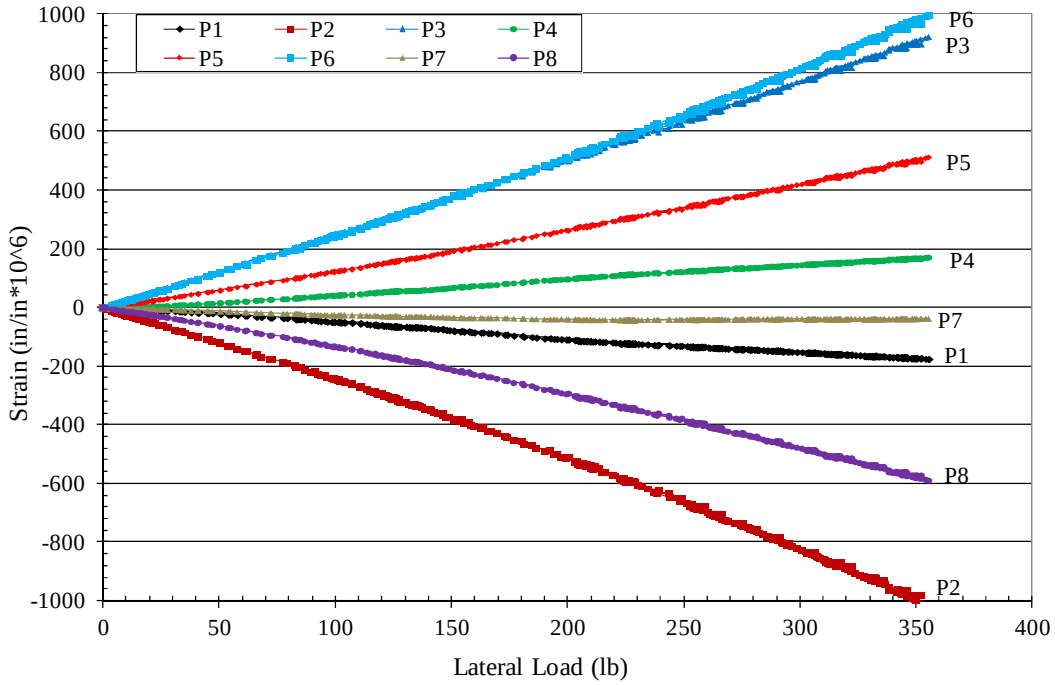

Figure A.10 Strain on plates versus lateral load-for specimen with 1/4-in. rod

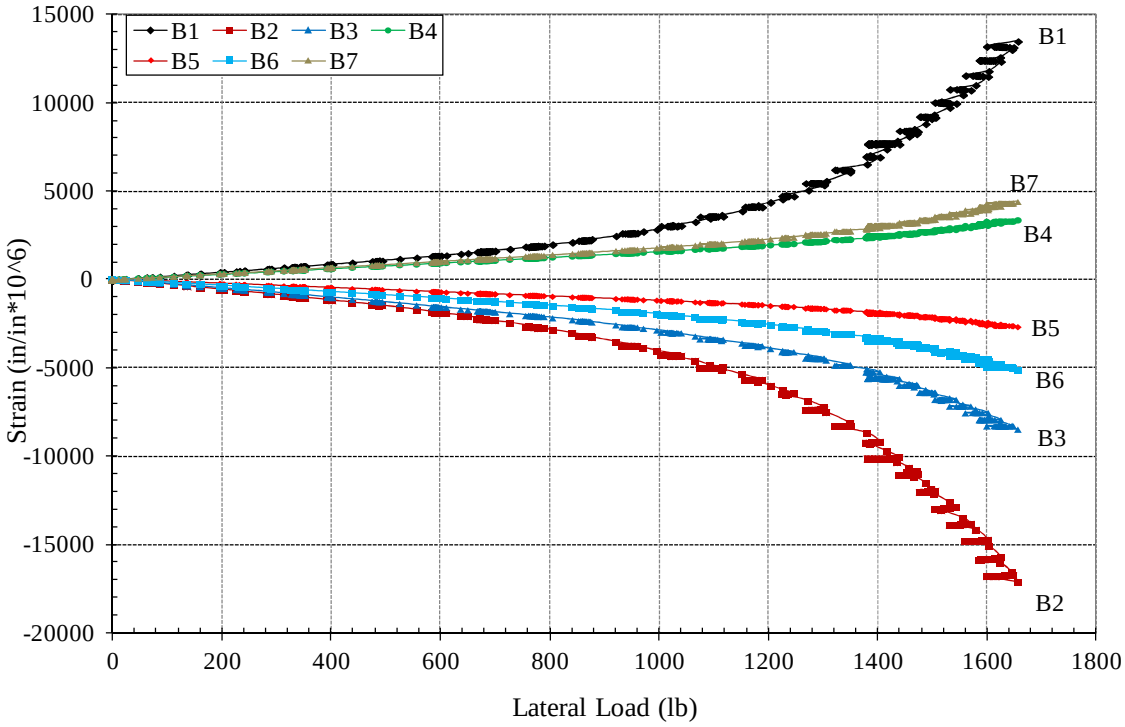

Figure A.11 Strain on rods versus lateral load-for specimen with 1/2-in. rod

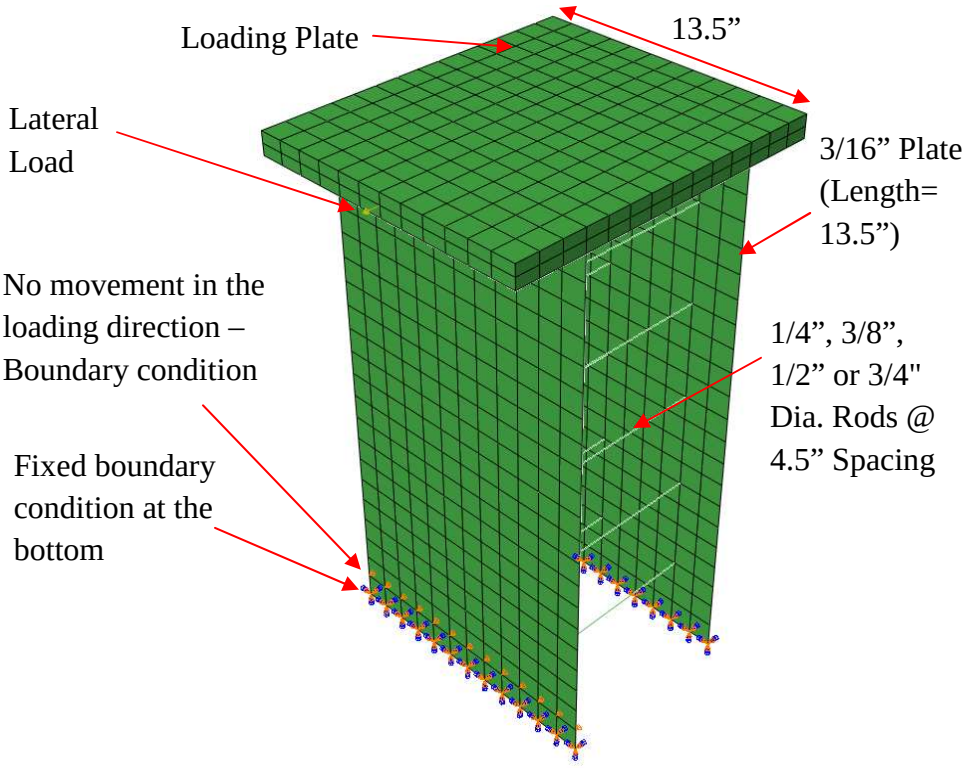

Figure A.12 Finite element model

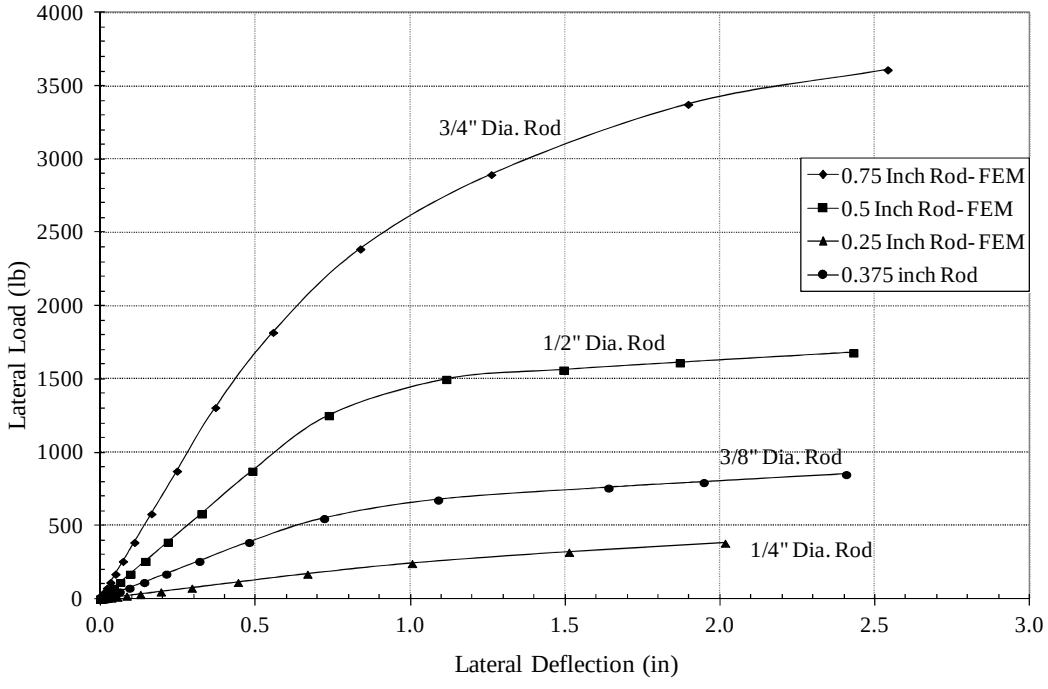

Figure A.13 Lateral load versus lateral deflection-3/4, 1/2, 3/8 & 1/4-in. rod-FEM

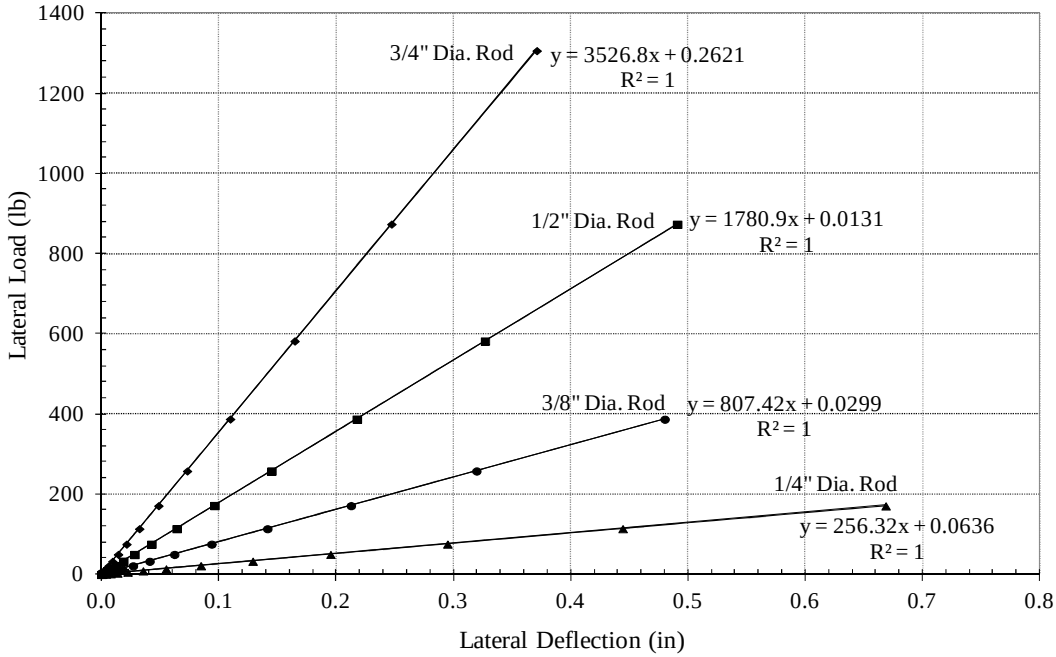

Figure A.14 Lateral Load versus Lateral Deflection-3/4, 1/2, 3/8 & 1/4-in. Rod-FEA-Lateral Stiffness Calculation

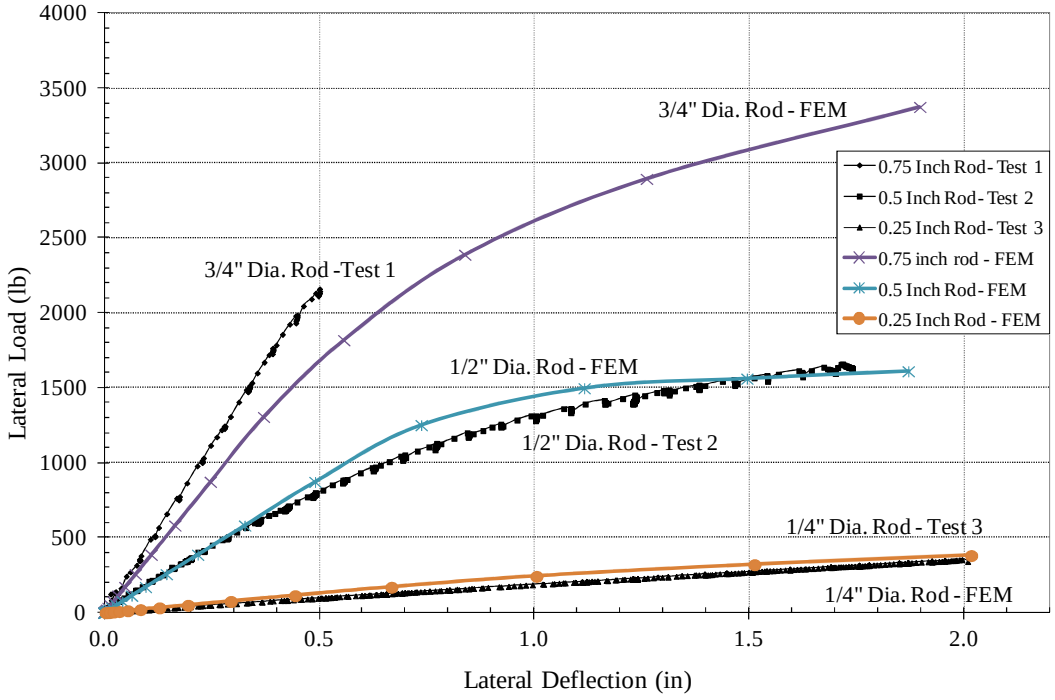

Figure A.15 Lateral Load versus Lateral Deflection-3/4, 1/2, & 1/4-in. Rod

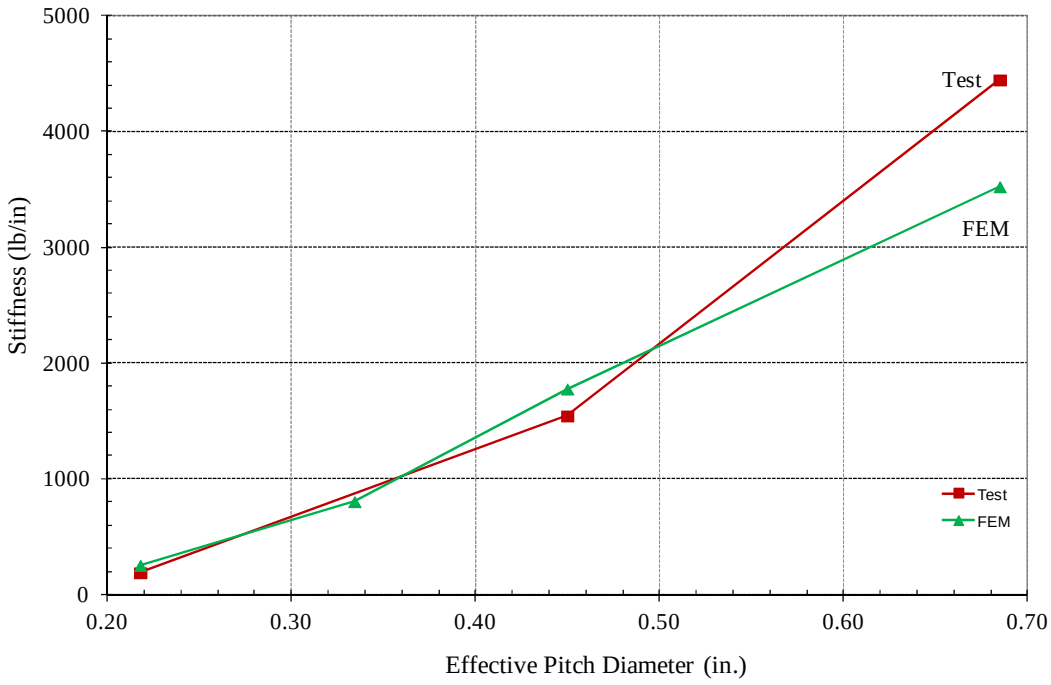

Figure A.16 Lateral stiffness of the plate assembly versus effective pitch diameter of the transverse rod- from laboratory test and finite element analysis

Appendix B: Investigation of Weld between the Reinforcing bar and the Foundation Connection Plate

B.1: Introduction

Tension force (developed from flexure) in each 3/16-in. shear wall plate has to be transferred to the foundation block first via the ¾-in. foundation connection plate and then via the no.7 reinforcing bars (see Fig. 3.16). The weld size and length of weld between the no.7 reinforcing bars and ¾-in. thick connection plate were determined to permit development of the yield strength of the no.7 bar. For stability test and cyclic loading test, the size and spacing of the no.7 bar were designed for yielding of the 3/16-in. shear wall plate and for tensile fracturing of the 3/16-in. shear wall plate, respectively.

AWS Specification D1.4 (AWS, 1998 and 2011) specifies the effective weld size to be 0.2*Bar diameters (refer to Fig. B.1) and the effective weld area to be the effective weld size multiplied by the weld length. Furthermore, AWS D1.4 (1998 and 2011) specifies an allowable weld stress of "0.3 times the nominal tensile strength of filler metal, except shear stress on the base metal shall not exceed 0.4 times the yield strength of the base metal for shear on the effective area". For the purpose of LRFD design, this design approach may be modified to consider a weld stress of 0.6 times the nominal tensile strength of filler metal with applicable strength reduction factor, 0.75, and applicable load factors. Hence, the shear strength of the weld (on either side of the reinforcing bar) can be calculated by using Equation B.1.

$$\emptyset R_n = 0.6 * F_{EXX} t_e L_{weld} \qquad \text{Eq. (B. 1)}$$

where $\emptyset$ = strength reduction factor (0.75 for shear)

R_n = shear strength

F_{EXX}= electrode strength (ksi)

t_e= effective weld size (0.2*Bar diameter)

L_{weld} = weld length

AWS D1.4 (1998 and 2011) specifies the type of electrodes (E8015, E8016, and E8018 for the SMAW process) to be used to weld ASTM A706 reinforcing bars to plates. However, the welding procedure is not specified. As a result, a number of weld pass combinations were attempted and each cross section was examined to identify the proper combination that would provide the necessary weld throat. Then the shear strength of the weld made by that combination was determined via tension tests and compared with the shear strength calculated using Equation B.1.

B.2: Test Set-up and Test Method

Two weld passes were considered for the weld between the ¾-in. foundation connection plate and the no.7 reinforcing bar. A 1/8-in. E8018 electrode was used for the first pass, while a 5/32-in. or a 3/16-in. E8018 electrode was used for the second pass. The DC voltage (on the Miller welding machine) was set to 30V. A number of samples were made with different Amperages to investigate the optimal welding procedure. After welding, the samples were cut and etched with a 2% Nital Solution. An example of the etched sample is shown in Fig. B.2. Figure B.2 (a) shows a sample weld made with a 1/8-in. electrode root pass and a 5/32-in. electrode used for the second pass. A good weld (with minimum included discontinuities and minimal burning of the reinforcing bar and the plate) was obtained with 110 amps for the 1/8-in. electrode and 140 amps for the 5/32-in. electrode. Figure B.2(b) shows a weld specimen made with a 1/8-in. electrode root pass and a 3/16-in. electrode for the second pass. A good weld (with minimum defects) was obtained with 110 amps for the 1/8-in. electrode and 160 amps for the 3/16-in. electrode. From the observations and measurements of the weld sizes of the specimens shown in Figs. B.2(a) and B.2(b), it was determined that a first weld pass on each side of the bar using a 1/8-in. electrode followed by a second pass using a 3/16-in. electrode produced the necessary weld throat. Although the procedure was not a formal welding procedure specification (WPS), it was adequate to demonstrate that the welds were suitable.

To demonstrate the structural performance, two specimens like those shown in Figs. B.3 and B.4 with different weld lengths (L_w in Fig. B.3) produced with E8018 electrodes were tested in a universal test machine to determine the weld length needed to develop the yield strength of the no.7 reinforcing bars. The first specimen had an average weld length of 1.81 in. and the second specimen had an average weld length of 1.00 in.

B.3 Results and Conclusions

In the first specimen, the yielding of the reinforcing bar initiated at 73.2 kips (61 ksi), and in the second specimen failure of the weld initiated along the weld line at 56.2 kips. Hence, it was determined that a 1.31-in. weld length (= 1.00 in. * 73.2 kips/ 56.2 kips) was needed to yield no. 7 bars used in the tension tests. The weld length calculated from Equation B.1, considering an 80 ksi electrode, excluding the strength reduction factor, and considering welds on both sides of the reinforcing bar, was 2.15 in. The shear strength to be resisted (R_n) was calculated by multiplying the yield strength of 60 ksi by the area of the no. 7 reinforcing bar. The lower weld length determined from the tension tests compared with that calculated from Equation B.1 may be primarily attributed to the weld size larger than 0.2*Bar diameter (as shown in Fig. B.1). Differences in deposited weld sizes between the two specimens also can be a reason for the lower weld length calculated from the tension tests.

For the experimental program a 2-in. weld length (a value between 1.31 in. and 2.15 in. determined from the tension tests and calculated using Equation B.1, respectively) was used to attach the hooked reinforcing bars to the connection plate for fabrication of the anchorage hardware in the base block. It is recommended to make the weld with two passes. For the first pass, a 1/8-in. electrode with Amperage of 110 and a deposition speed of 4.5 in./min. can be used. For the second pass, a 3/16-in. electrode with Amperage of 160 and a deposition speed of 5.6 in./min. can be used.

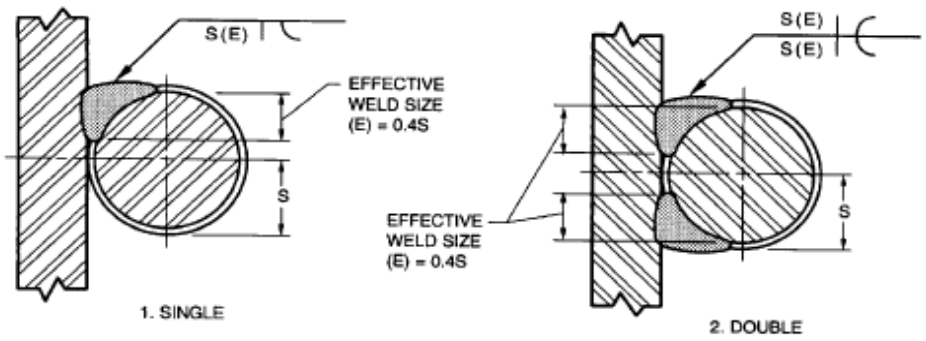

Figure B.1 Flare bevel groove weld (from AWS D1.4/D1.4M, 1998 and 2011)

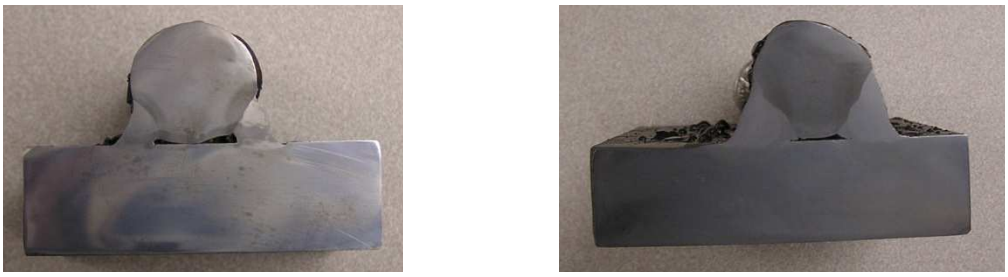

(a) (b)

Figure B.2 Etched weld samples: (a) Two weld passes with 1/8-in. electrode followed by 5/32-in. electrode and (b) Two weld passes with 1/8-in. electrode followed by 3/16-in. electrode

T

Weld (E8018 Electrodes)

3/4” thick Plate

No.7 Reinfor bar (A706)

L_W (Weld length)

T

Figure B.3 Tensile test set-up to evaluate reinforcing bar - plate weld strength – Front view

Weld

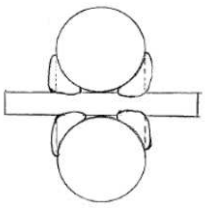

No.7 reinforcing ba (A706)

3/4” thick

Figure B.4 Tensile test set-up to evaluate reinforcing bar - plate weld strength – Cross Section

Appendix C: Investigation of Weld between Shear Wall Plate and Foundation Connection Plate

C.1: Introduction

The forces from the 3/16-in. shear wall plate have to be transferred to the ¾-in. foundation connection plate via the weld between the shear wall plate and the foundation connection plate (see Fig. 3.16). Even though the size of the weld was designed considering the static forces and static material properties for the in-plane cyclic loading test (which is detailed in Chapter 6), the behavior of the weld for cyclic loading had to be investigated. The purpose of this test was to verify that the failure will occur in the steel plates rather than in the weld.

In the study of "the behavior of double-skin composite walls for in-plane cyclic loading" by Eom et al. (2009), the shear wall plates were connected to the base plate using complete joint penetration groove welds. For the applied in-plane cyclic loading, the welded joint failed in tensile fracture before the wall plate reached flexural yielding (at 1.5% drift ratio). Motivated by this study, two types of welded connection were considered for the joint between 3/16-in. thick specimen plates and the ¾-in. thick foundation connection plates. Both were tested under tensile cyclic loading to select the necessary and sufficient weld connection.

C.2: Test Set-up and Test Method

For the two welded connections proposed for cyclic testing, the first welded connection option involved one load path, while the second involved two load paths. Details of the two options are outlined below.

(1) A 7/16-in. fillet weld was used between the 3/16-in. plate and ¾-in. plate as shown in Fig. C.1. The entire vertical tensile load from the 3/16-in. thick shear wall plate was intended to be transferred to the ¾-in. thick foundation connection plate via only a 7/16-in. fillet weld. The design philosophy was to size the weld so that it could develop the tensile capacity of the 3/16-in. plate.

(2) A 3/8-in. fillet weld and a bevel groove weld were used in addition to the 7/16-in. fillet weld as shown in Fig. C.2. The vertical tensile load from the 3/16-in. thick shear wall plate was intended to be transferred to the ¾-in. thick foundation connection plate via two load paths: (a) part of the load would be transferred from the 3/16-in. plate through the 7/16-in. fillet weld to the bevel groove weld, and (b) the remaining load would be transferred through the 3/8-in. fillet weld. Weld joint 2 was more time consuming and much more expensive to fabricate than weld joint 1 but it was expected to be stronger.

It was decided to test these two weld joints subjected to cyclic tensile loads. Cyclic compression was not introduced to avoid buckling of the specimen. Schematic diagrams of the two weld tests are shown in Fig. C.3. Specimens were made symmetric by combining with a mirror image of the actual weld joint so there would be no out-of-plane bending in the specimen during axial cyclic loading.

Preparation of weld test specimens

Innershield NR-232 flux-cored self shielded (FCAW-S) wires (0.068 in size) from Lincoln Electric were used to make the weld joint specimens. Prior to specimen fabrication, welding samples were prepared to check the penetration of the weld passes. Voltage and amperage were adjusted for each pass to obtain adequate weld penetration. Voltage, amperage, and deposit speed of each weld pass were recorded.

Progress made in the production of weld joint 2 is shown in the photos in Fig. C.4. Weld sample 1 had one pass for the 3/8-in. fillet weld and six passes for the bevel groove weld. The voltage ranged between 21.2 and 22.8 V, and the amperage ranged between 230 and 267 amps. It can be seen from Fig. C.4 (a) that the weld sample didn't have sufficient penetration in the first 3/8-in. fillet weld and the first three passes of the bevel groove weld didn't have adequate weld fusion. For sample 2 (Fig. C.4 (b)), the voltage and amperage were increased to 25.2 V and 300 amps (average), respectively, for the first 3/8-in. fillet weld and the first three passes of the bevel groove weld. Still, there was a large weld discontinuity in the first 3/8-in. fillet weld. Lastly, sample 3 (Fig. C.4 (c)) was made to check the penetration of the first 3/8-in. fillet weld and the first pass of the bevel groove weld. The voltage and amperage were increased to 25.7 V and 345 amps (average), respectively. The weld sample (made with only two passes) was satisfactory from observation. Furthermore, it was decided to back gouge (by grinding) the weld metal between the passes upon detecting any defect.

For the weld joint 1 specimen (Fig. C.3 (a)), the 7/16-in. weld was made with three passes. For the first pass, the voltage and amperage were 25.7V and 360 amps (average), respectively. For the other two passes, the voltage and amperage were 21.5V and 235 amps (average), respectively. After the first pass the weld metal was back gouged. The average measured weld size of the 7/16-in. fillet weld was 0.456 in. For the weld joint 2 specimen (Fig. C.3 (b)), the 7/16-in. weld was made with three passes. For the first pass, the voltage and amperage were 25.7V and 345 amps (average), respectively. For the other two passes, the voltage and amperage were 21.5V and 235 amps (average), respectively. After the first pass the weld metal was back gouged. The average measured weld size of the 7/16-in. fillet weld was 0.464 in.

The first 3/8-in. fillet weld in the weld joint 2 specimen was made with one pass. The voltage and amperage were 25.7V and 340 amps, respectively. The bevel groove weld was made with seven passes on one side and nine passes on the other side. The number of passes was dependent on the amount of back gouging. The voltage and

amperage for the first three passes of the bevel groove weld were 25.7V and 340 amps (average), respectively. The voltage and amperage for the fourth pass were 25.2V and 275 amps, respectively. The voltage and amperage for the remaining passes were 21.5V and 250 amps (average), respectively.

Testing Weld Joint Specimens

The yield strain (ε_y) of the 3/8-in. plate material was calculated from the two coupons tested in tension. The stress-strain curve for a coupon specimen is shown in Fig. C.5. The average yield strain was 0.002070 (2070 με). The weld joint specimen was first loaded until the strain reached $2\varepsilon_y$ then was unloaded until the load was zero. The specimen was then loaded until the strain reached $3\varepsilon_y$ and was subsequently unloaded till the load was zero. Similarly, the specimen was subjected to repetitions of loading to develop strain multiples of ε_y ($4\varepsilon_y$, $5\varepsilon_y$ …) until failure occurred.

Weld joint 1 specimen was subjected to 67 loading cycles before failure: One cycle of $2\varepsilon_y$ increment, another 19 cycles of ε_y increment (for each cycle), another 10 cycles of $2\varepsilon_y$ increment, another 10 cycles of $3\varepsilon_y$ increment, another 10 cycles of $4\varepsilon_y$ increment, and the remaining 16 cycles of $5\varepsilon_y$ increment. The weld joint 2 test specimen was subjected to 50 loading cycles before failure: One cycle of $2\varepsilon_y$ increment, another 9 cycles of ε_y increment, another 10 cycles of $3\varepsilon_y$ increment, and the remaining 30 cycles of $5\varepsilon_y$ increment.

The test specimens were configured with the test weld at one end and a bolted anchor connection at the opposite end. The bolted connection involved four high-strength bolts with a shear capacity in excess of the capacity of the welded connection at the test end of the specimen.

The test set-up for the weld joint specimens is shown in Fig. C.6. The tests were performed in a four pole MTS servo-hydraulic testing machine. The strain was measured

using a clip gage that was attached to the specimen, as can be seen at the top of Fig. C.6. The controller was programmed to apply cycles of loading automatically.

C.3: Results and Conclusions

The stress-strain response curves for weld joint specimens 1 and 2 are shown in Figs. C.7 and C.8, respectively. Figure C.9 shows the failure of a weld joint specimen. Failure occurred by fracturing the 3/8-in. thick plate above the 7/16-in. fillet weld in both specimens. The 3/8-in. thick plates stretched up to 0.394 and 0.395 in/in strains in specimens 1 and 2, respectively (see Fig. C.7 and C.8). No indication of failure was observed in the welds in either of the specimens. Both welds sustained load until the plate element failed. However, during the weld joint tests, the specimens were not subjected to compression loading. The compression part of the loading cycle was avoided so that the specimen would not fail due to buckling of the 3/8-in. thick plate. But in the intersecting wall element test, portions of the plate will be subjected to tension and compression as the specimen is pushed and pulled in the two loading directions.

Because both weld joints did not fail during the cyclic loading tests and because weld joint 1 is considerably less expensive than weld joint 2, weld joint 1 was selected for the joint between the 3/16-in. shear wall plates and the ¾-in. foundation connection plates in the specimen for the cyclic loading test.

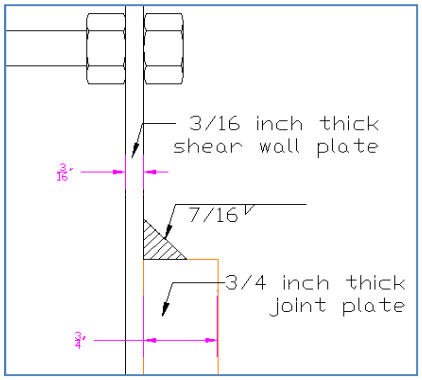

Figure C.1 Weld Joint 1 - A 7/16-in. Fillet weld between wall specimen plates and the foundation connection plates

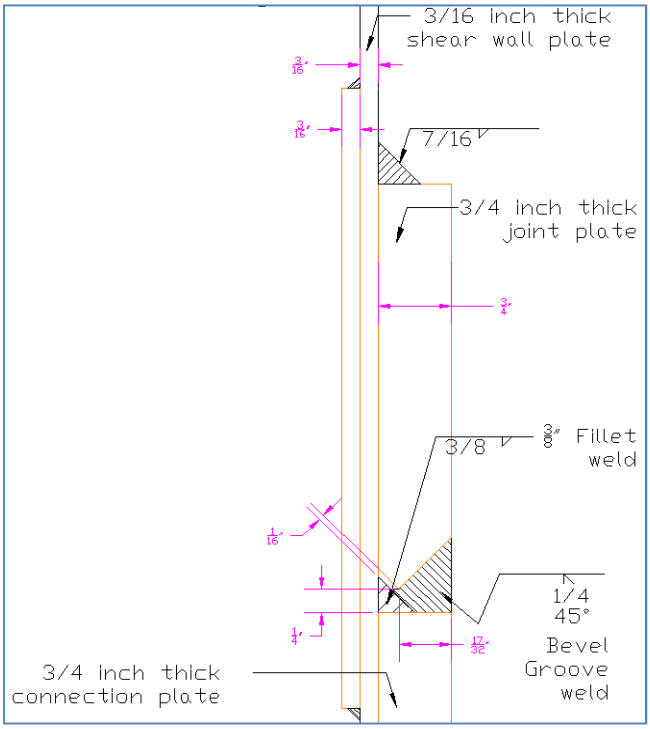

Figure C.2 Weld Joint 2 - A 3/8-in. fillet weld and bevel groove weld in addition to the 7/16-in. fillet weld

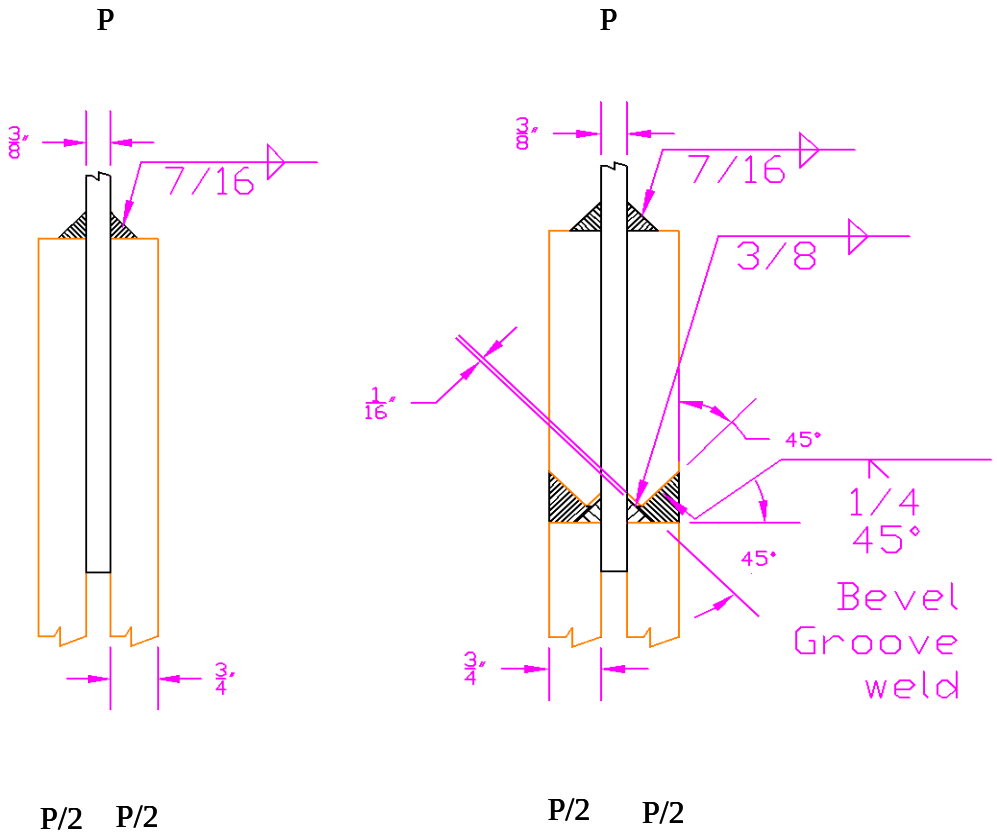

Figure C.3 Weld Joints (a) Weld Joint 1 specimen (b) Weld Joint 2 specimen

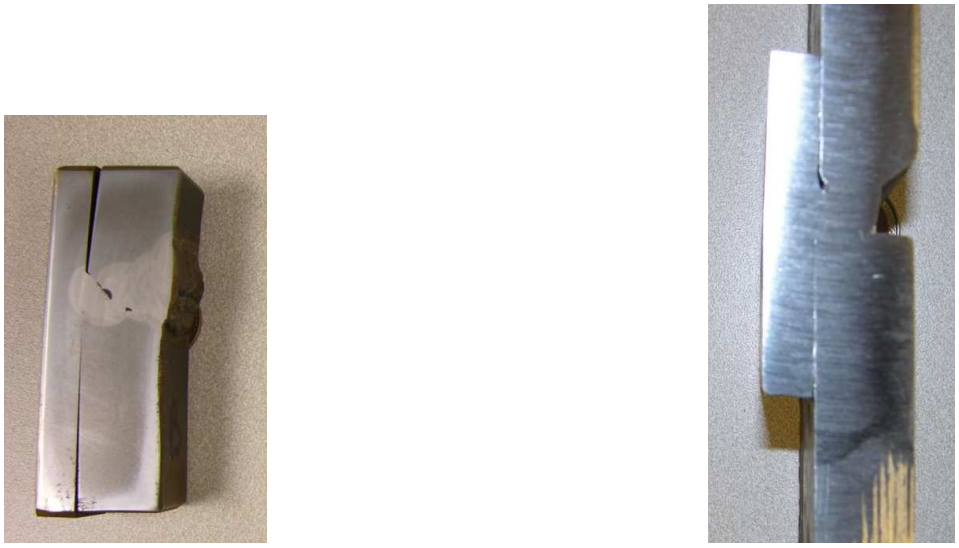

Figure C.4 Weld samples (a) Weld sample 1 (b) Weld sample 2 (c) Weld sample 3

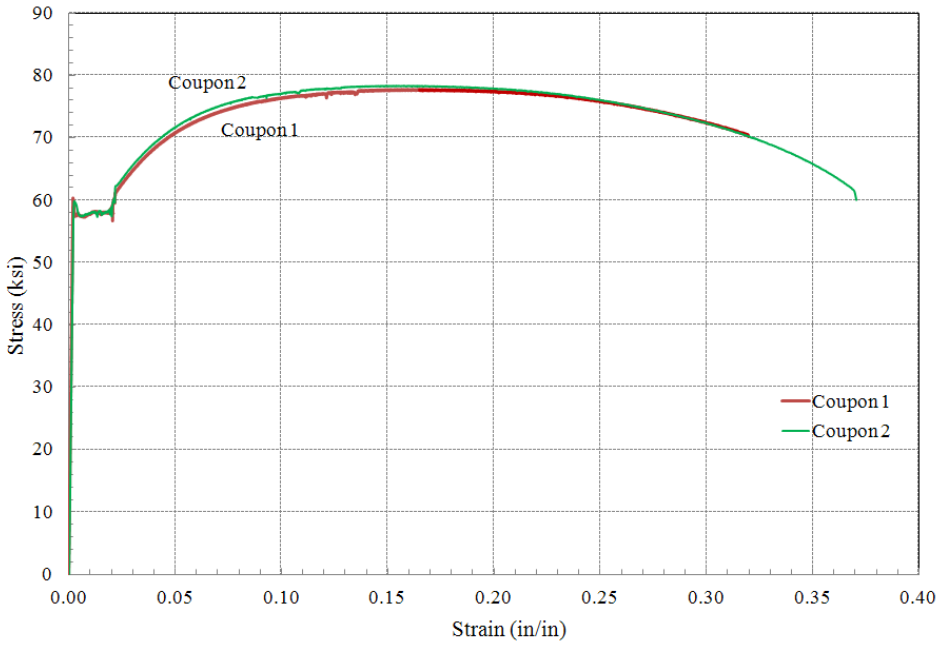

Figure C.5 Stress versus Strain Curve –Static Loading– Coupon Specimen1 and 2

Figure C.6 Weld Joint Specimen Tests - Cyclic Loading in Four Pole MTS Testing Machine (Specimen 1)

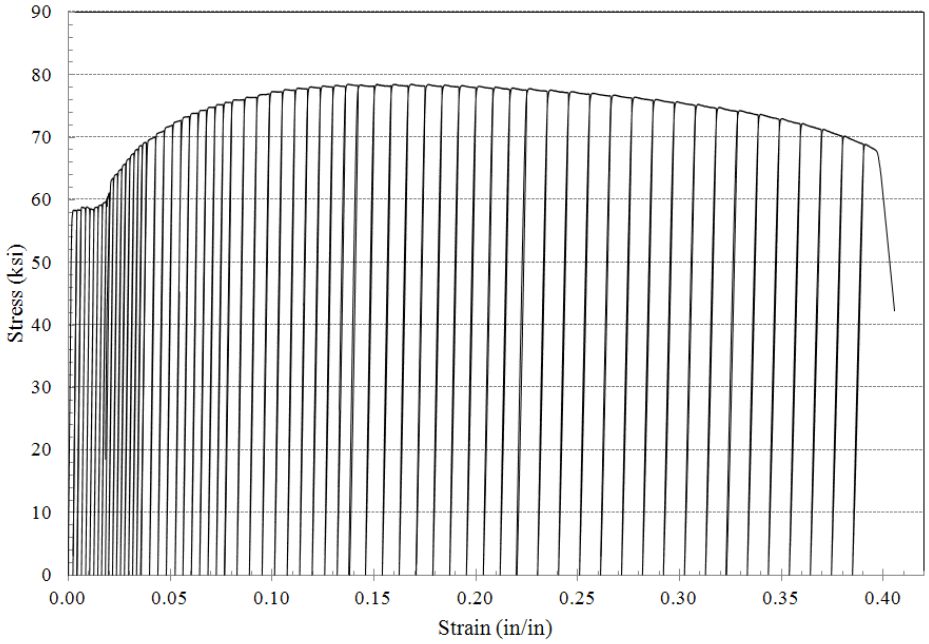

Figure C.7 Stress versus Strain Curve –Cyclic Loading– Weld Joint 1 Specimen

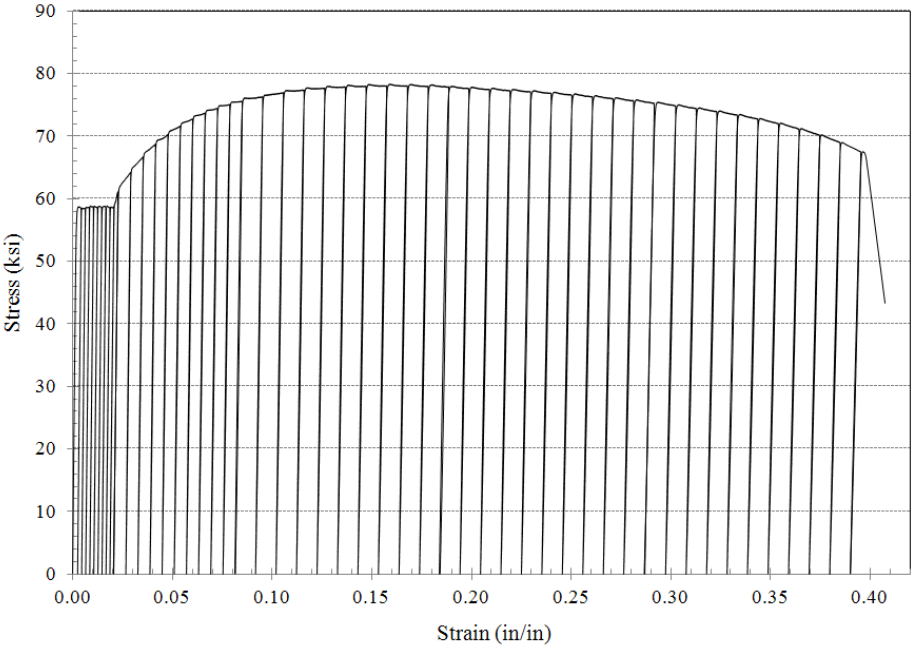

Figure C.8 Stress versus Strain Curve –Cyclic Loading– Weld Joint 2 Specimen

Figure C.9 Failure of the Weld Joint Specimen (Specimen 2)

Appendix D: Plots of Measurements from Gauges During Cyclic Loading Test of the Dual-Plate Composite Shear Wall

The primary findings from the cyclic loading test of the dual-plate composite shear wall were discussed in Chapter 6. Plots of measurements from the gauges which might be of interest to the reader and have not been discussed in Chapter 6 are presented in this Appendix. Instrumentation method and locations of the gauges are detailed in Section 6.5. Analysis of primary results and conclusions from the results are presented in Sections 6.7 and 6.8, respectively.

D.1: Variation in force in vertical PT bars during the test

Plots of lateral force in vertical PT bar versus lateral drift of the specimen are presented in Figs. D.1 through D.6. Refer to Section 6.5.1 for details on instrumentation (strain gauges) attached on vertical PT bars to measure variation in force in vertical PT bars during the test. Refer to Fig. 6.37 for strain gauge locations. Refer to Section 6.7.2 for a discussion of results on variation in force in vertical PT bars during the test.

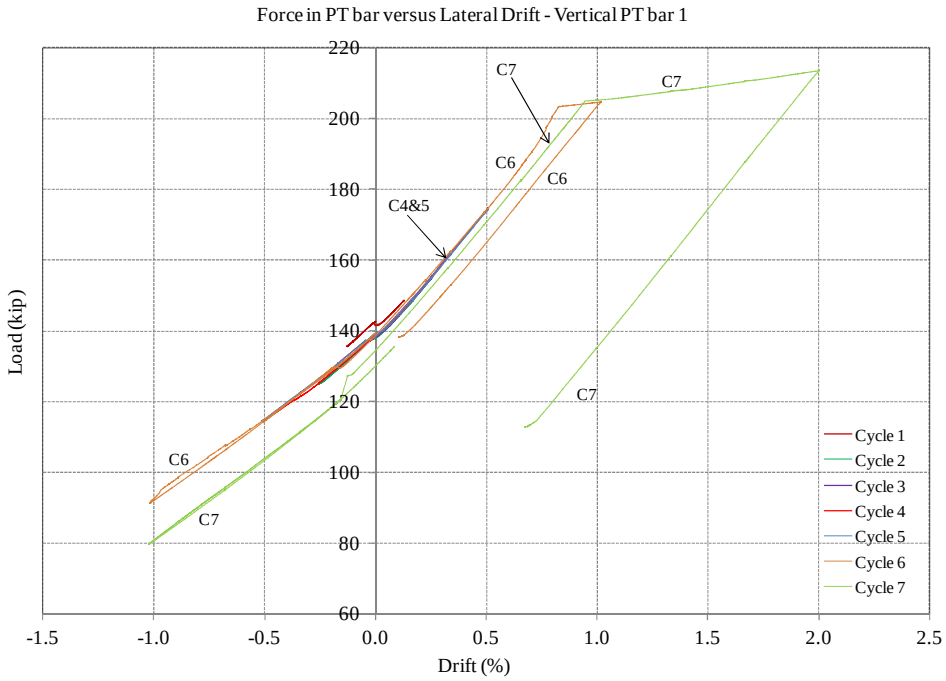

Figure D.1 Force in PT bar versus lateral drift – Vertical PT bar 1

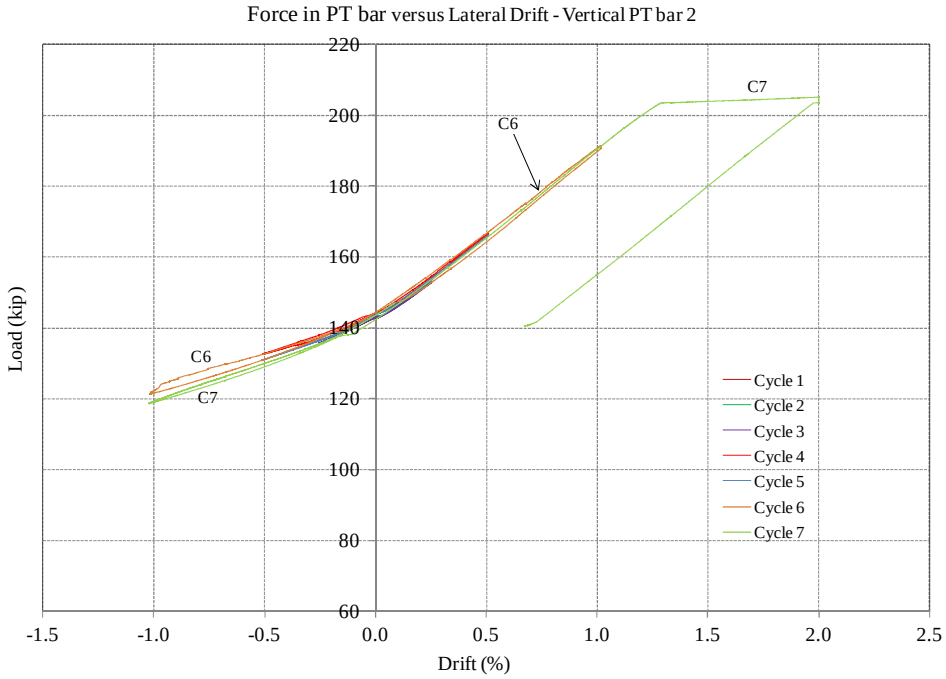

Figure D.2 Force in PT bar versus lateral drift – Vertical PT bar 2

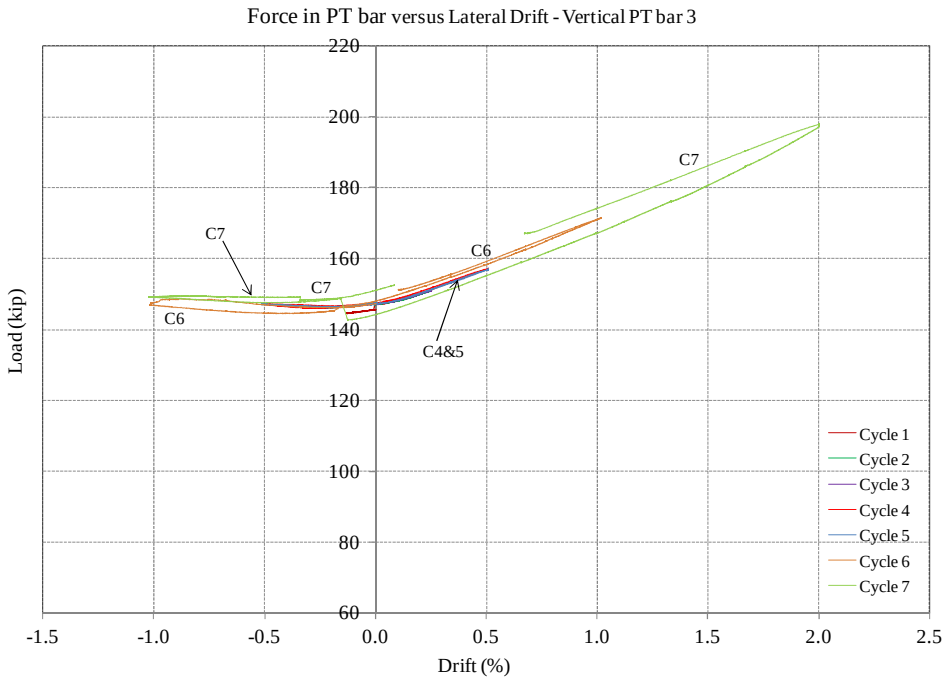

Figure D.3 Force in PT bar versus lateral drift – Vertical PT bar 3

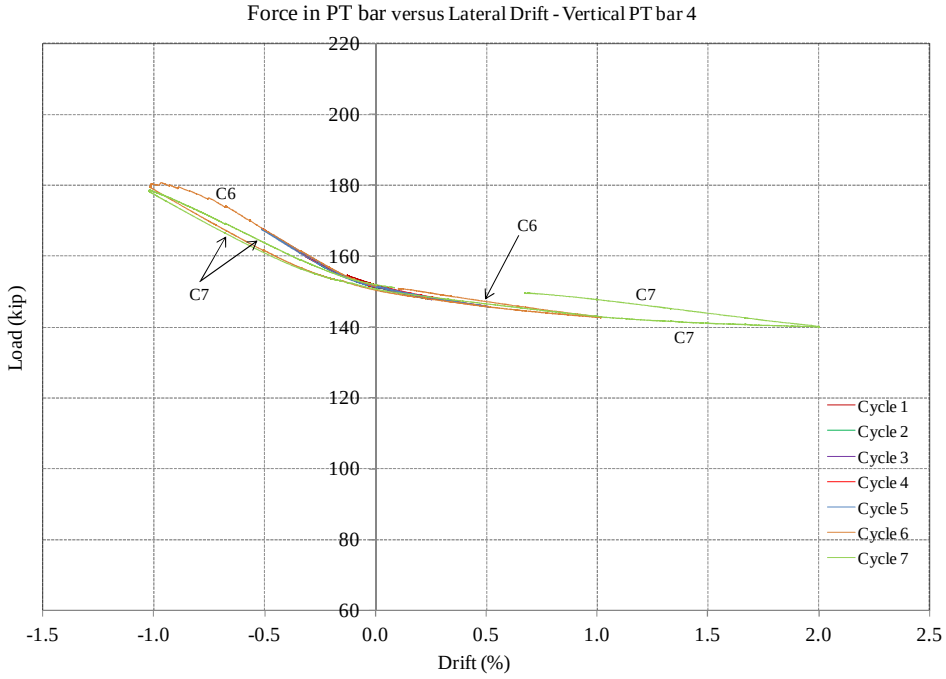

Figure D.4 Force in PT bar versus lateral drift – Vertical PT bar 4

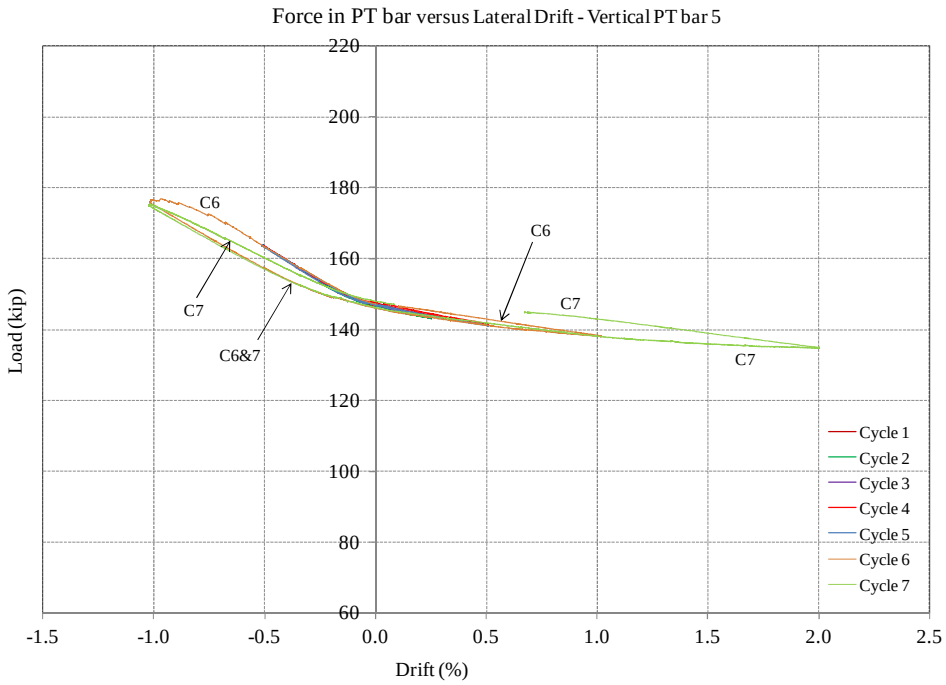

Figure D.5 Force in PT bar versus lateral drift – Vertical PT bar 5

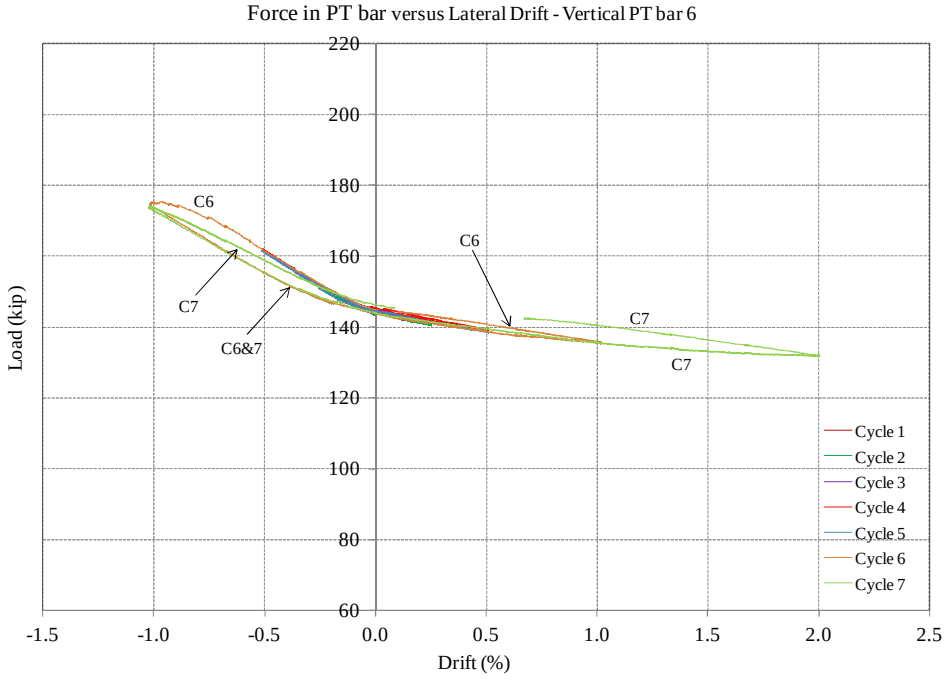

Figure D.6 Force in PT bar versus lateral drift – Vertical PT bar 6

D.2: Strain measurements on No.7 reinforcing bar hooks

Plots of lateral load versus strain measurements on No.7 reinforcing bar hooks are presented in Figs. D.7 through D.13. See Section 6.5.2 for details on instrumentation (strain gauges) attached on No. 7 reinforcing bar hooks to measure strains in reinforcing bar hooks. Refer to Fig. 6.38 for strain gauge locations. See Section 6.7.4 for a discussion of results on strains developed in reinforcing bar hooks during the test.

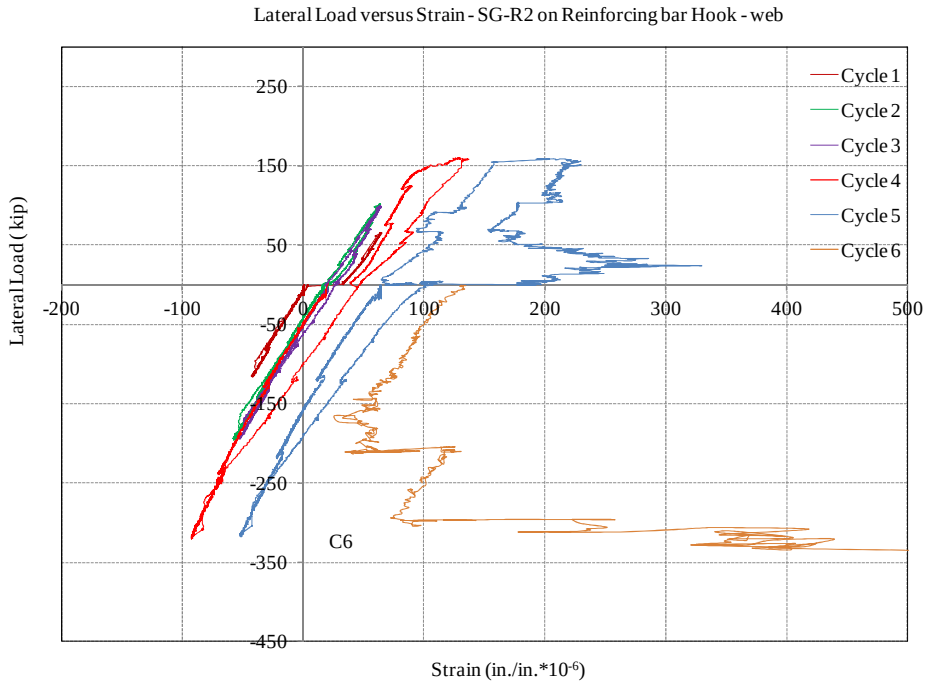

Figure D.7 Lateral load versus strain on No.7 reinforcing bar hook – R2

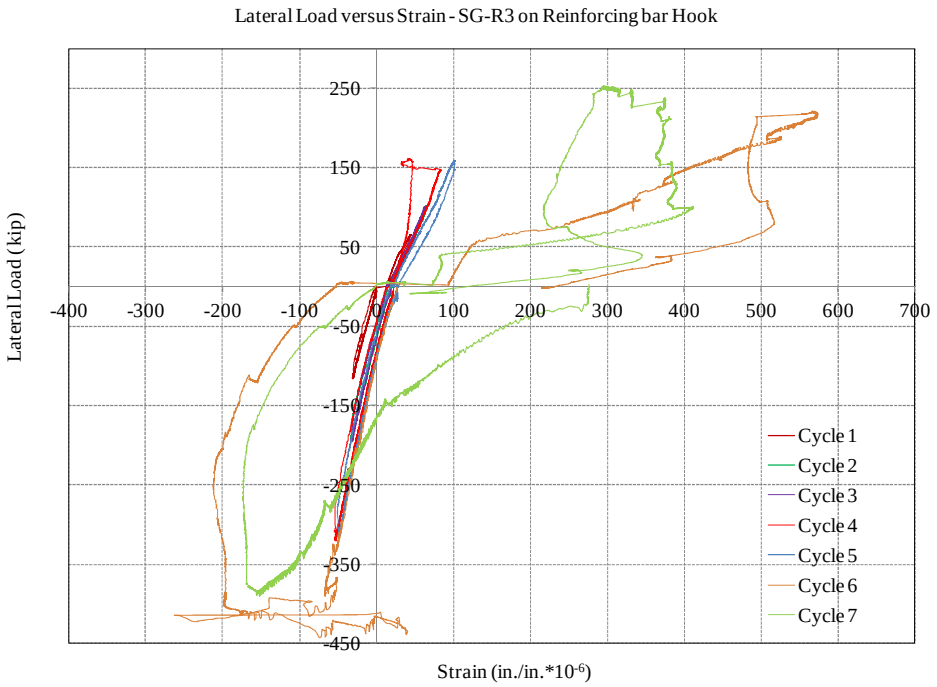

Figure D.8 Lateral load versus strain on No.7 reinforcing bar hook – R3

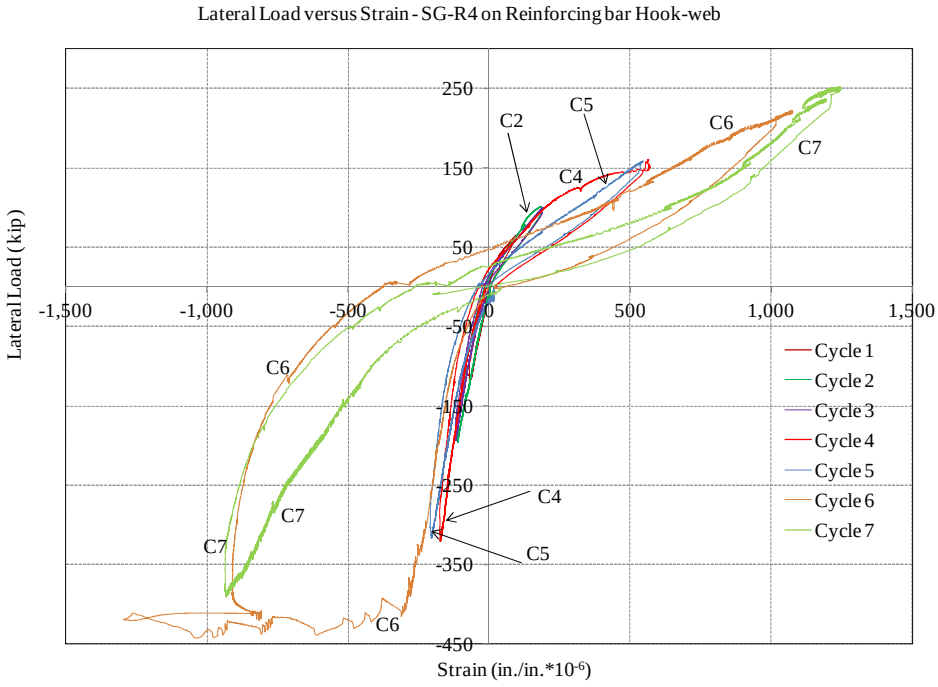

Figure D.9 Lateral load versus strain on No.7 reinforcing bar hook – R4

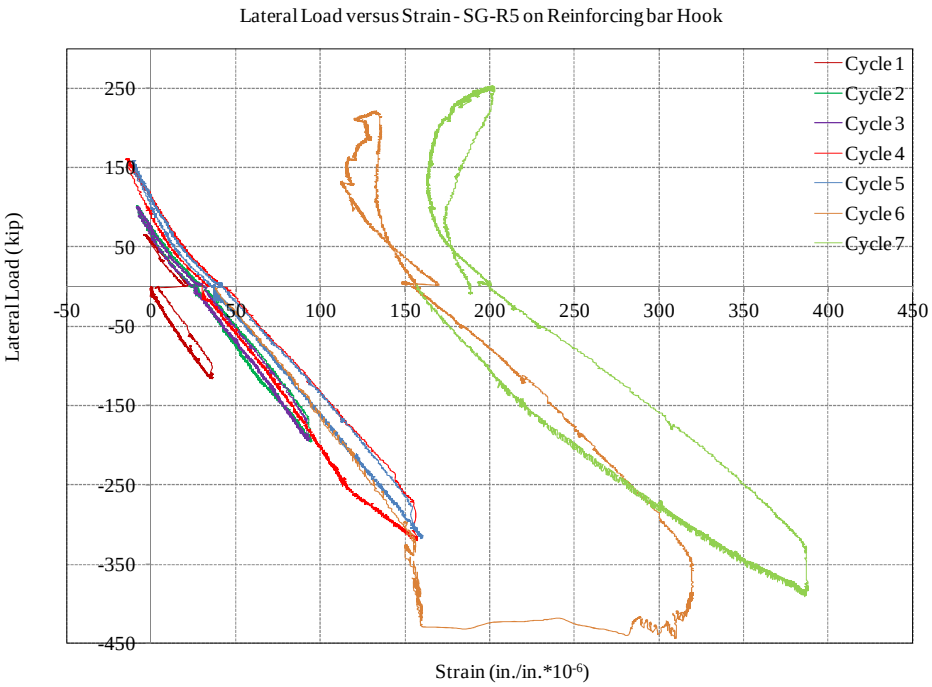

Figure D.10 Lateral load versus strain on No.7 reinforcing bar hook – R5

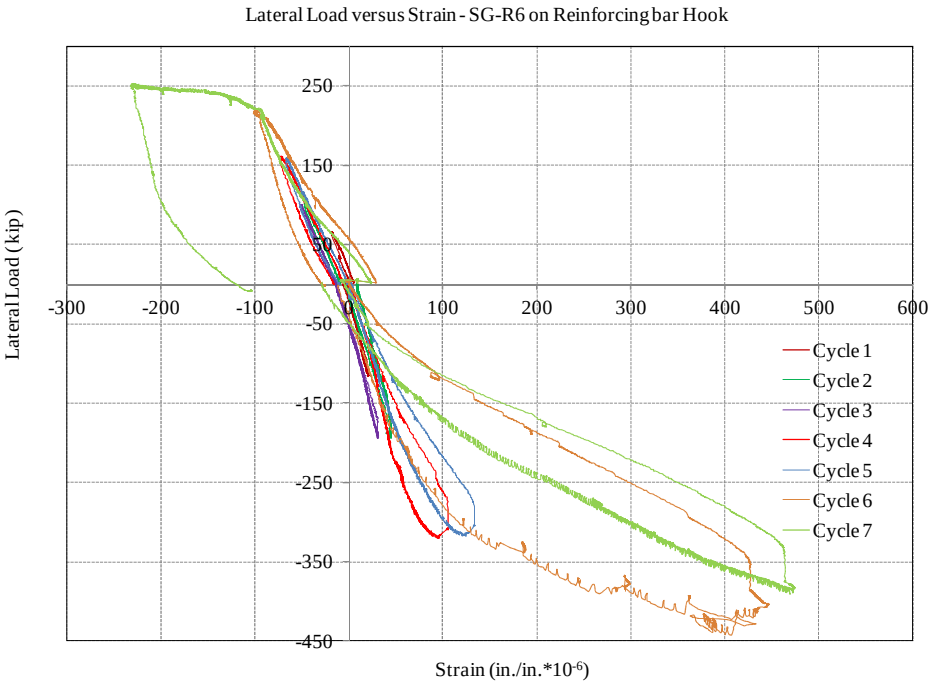

Figure D.11 Lateral load versus strain on No.7 reinforcing bar hook – R6

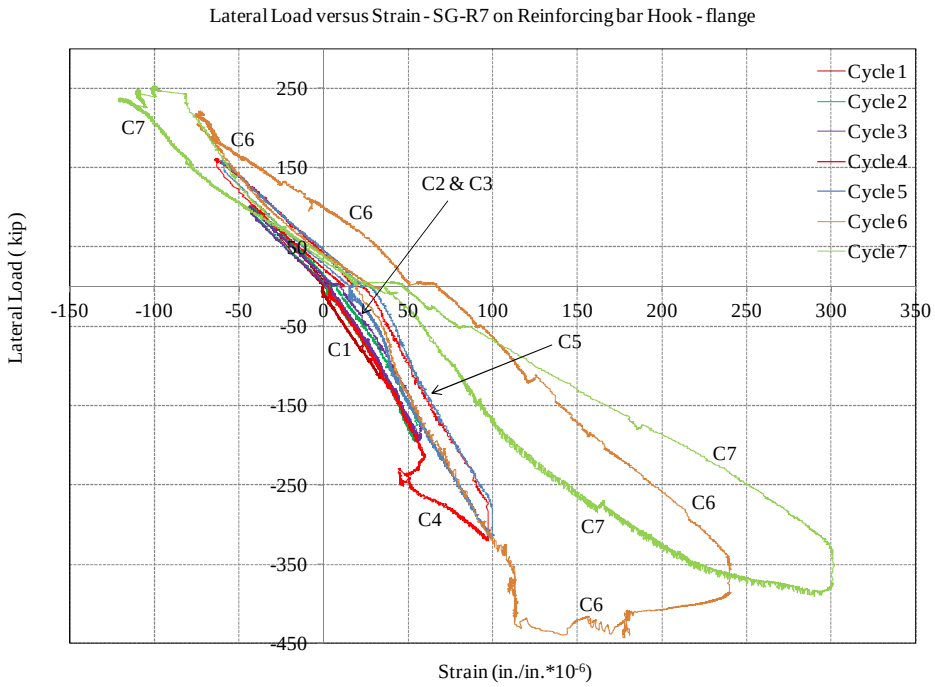

Figure D.12 Lateral load versus strain on No.7 reinforcing bar hook – R7

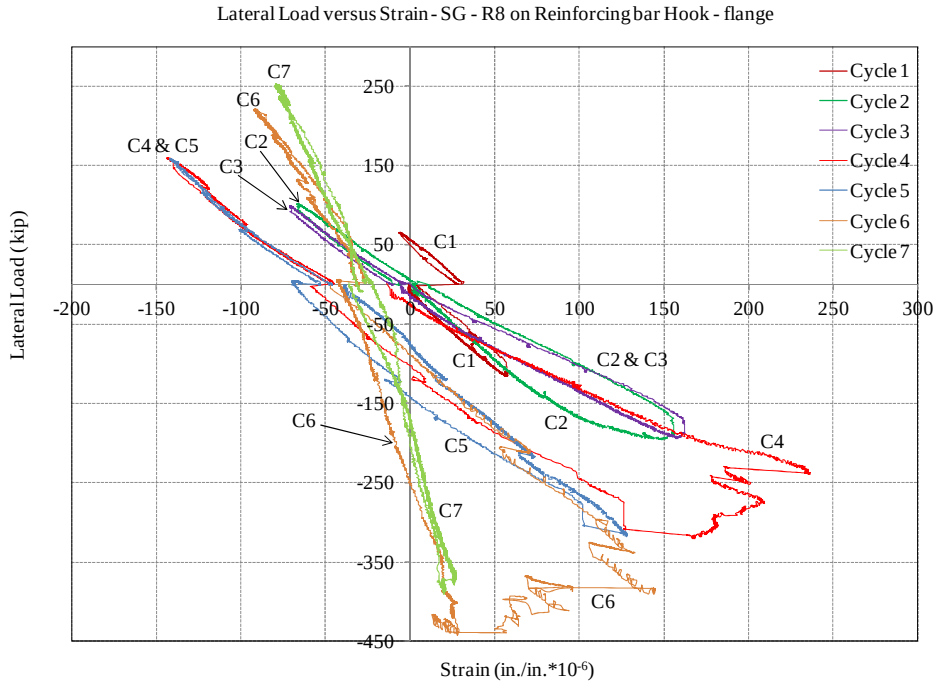

Figure D.13 Lateral load versus strain on No.7 reinforcing bar hook – R8

D.3: Strain measurements on No.6 reinforcing bar

Lateral load versus strain plots for No.6 reinforcing bars are presented in Figs. D.14 through D.17. See Section 6.5.6 for details on instrumentation attached on No. 6 reinforcing bars to measure strains in the reinforcing bars. Refer to Figs. 6.38, 6.41, and 6.43 for strain gauge locations.

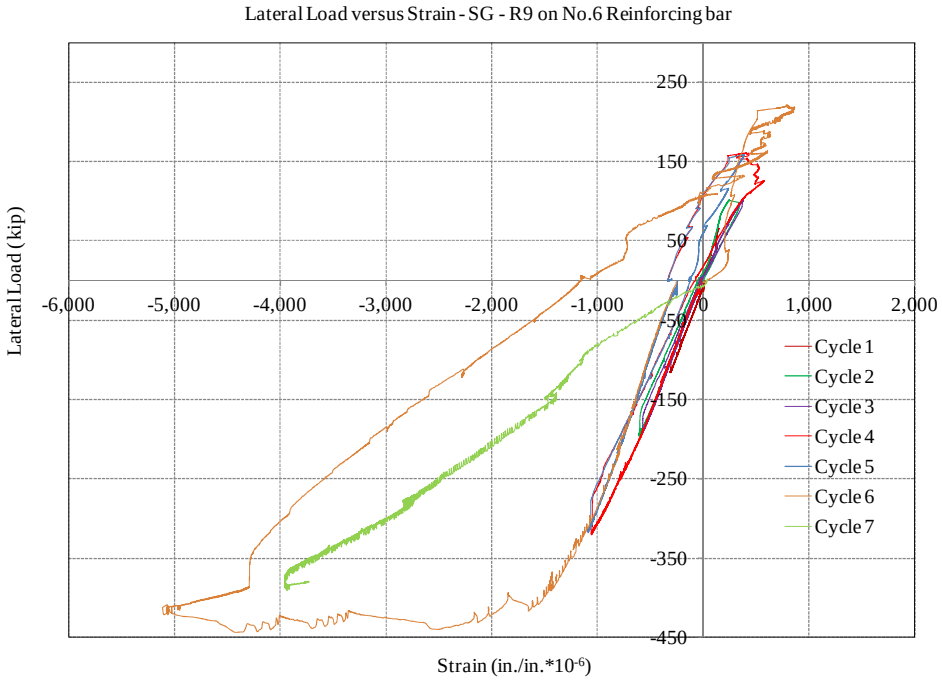

Figure D.14 Lateral load versus strain on No.6 vertical reinforcing bar – R9

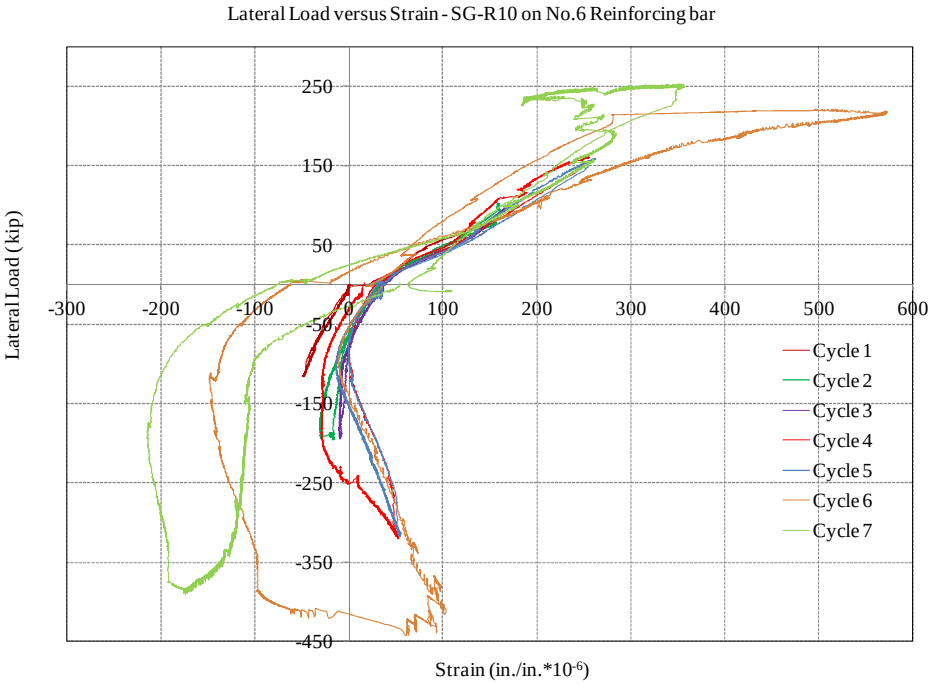

Figure D.15 Lateral load versus strain on No.6 vertical reinforcing bar – R10

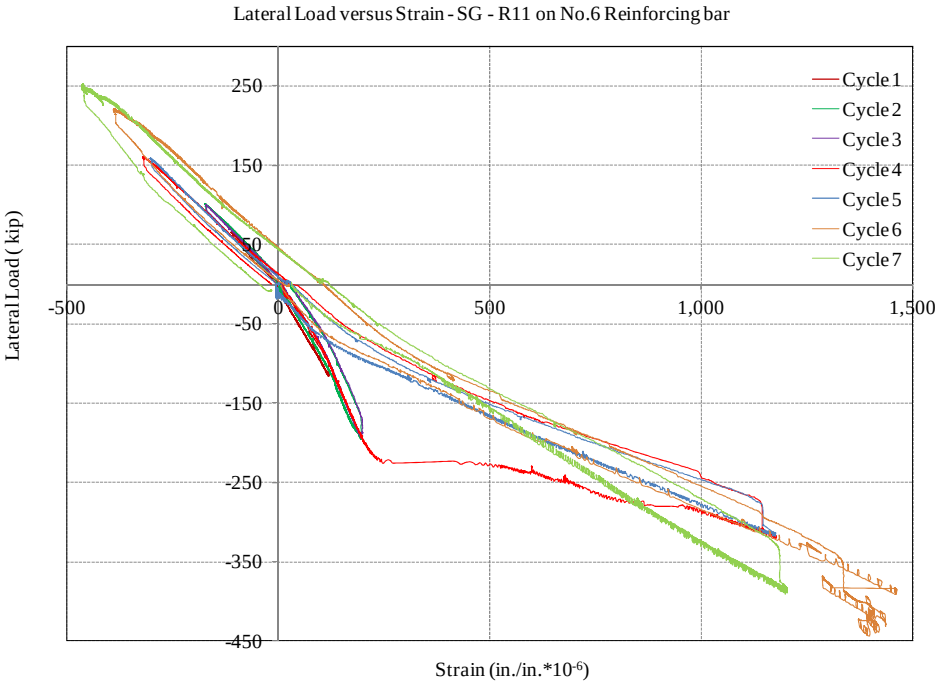

Figure D.16 Lateral load versus strain on No.6 vertical reinforcing bar – R11

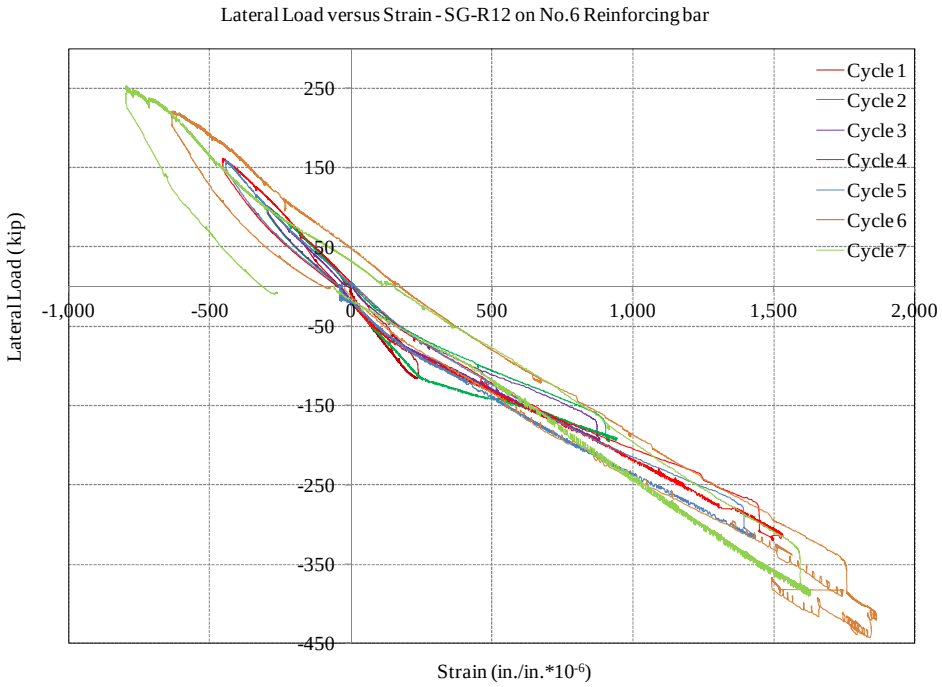

Figure D.17 Lateral load versus strain on No.6 vertical reinforcing bar – R12

D.4: Strain measurements from concrete strain gauges

Lateral load versus strain plots for concrete strain gauges are presented in Figs. D.18 through D.23. See Section 6.5.5 for details on instrumentation to measure strains in concrete. Refer to Figs. 6.40 through 6.43 for strain gauge locations. Refer to Section 6.7.5 for a discussion of results on strains developed in concrete during the test.

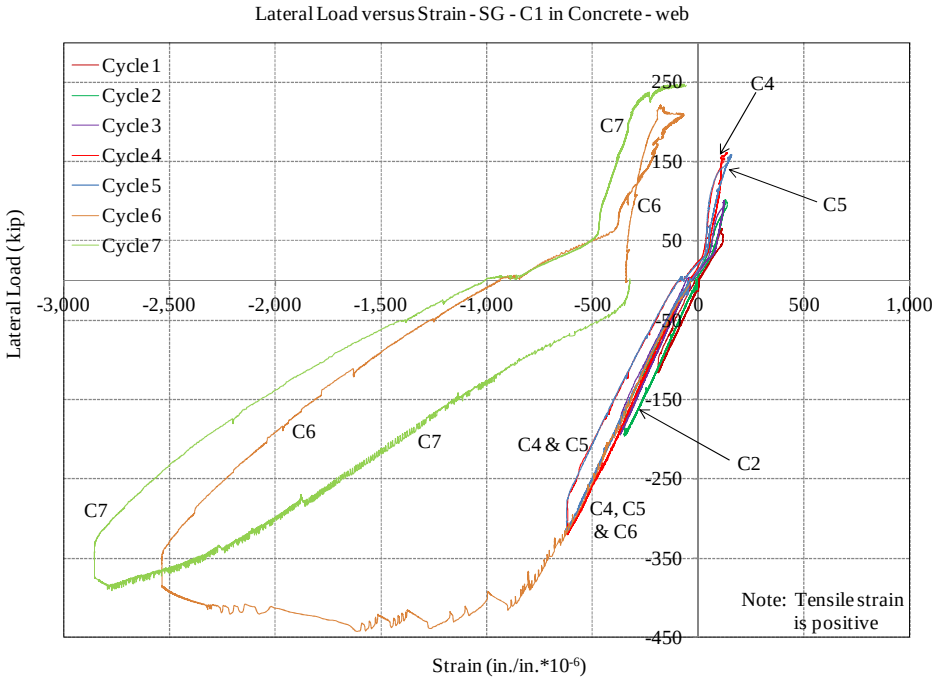

Figure D.18 Lateral load versus strain in concrete – C1

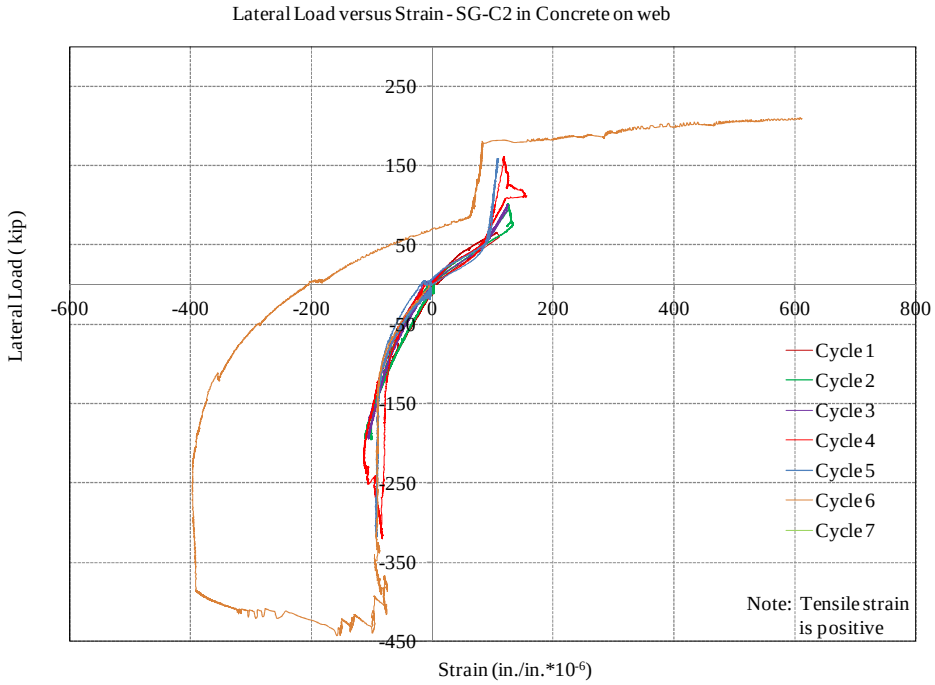

Figure D.19 Lateral load versus strain in concrete – C2

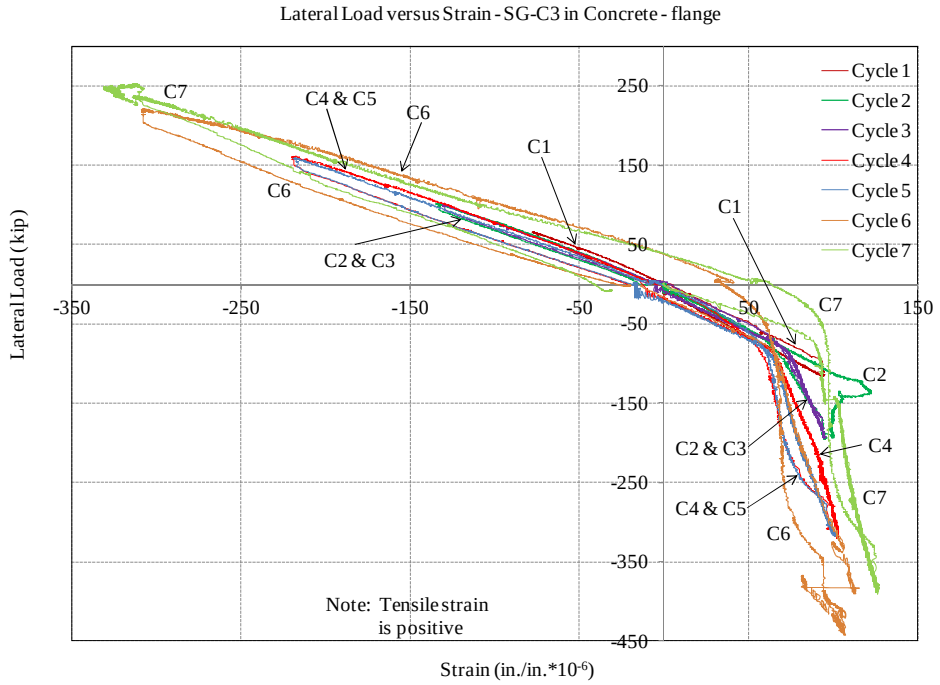

Figure D.20 Lateral load versus strain in concrete – C3

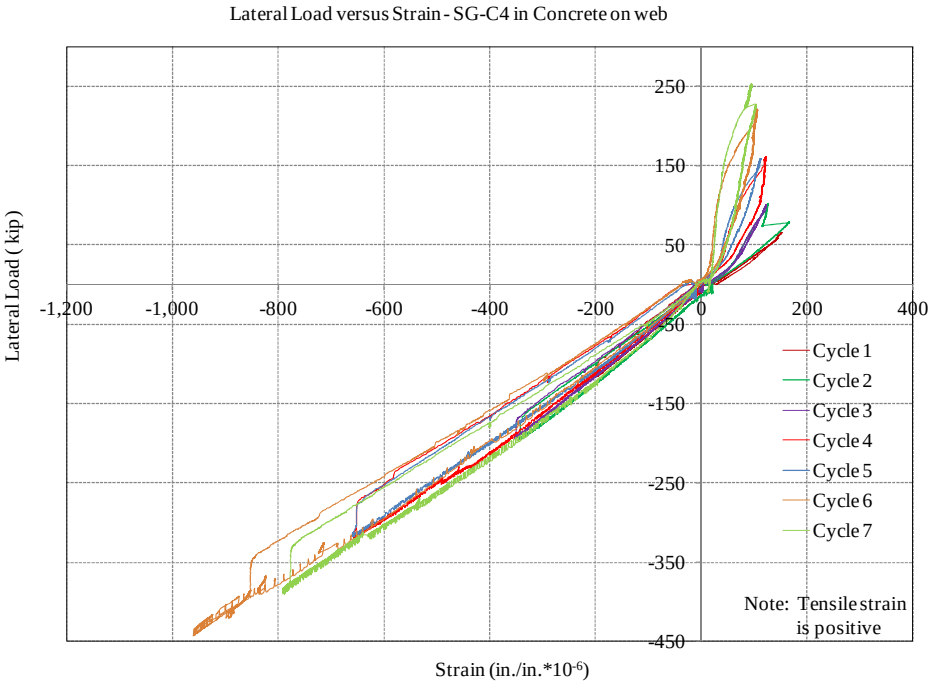

Figure D.21 Lateral load versus strain in concrete – C4

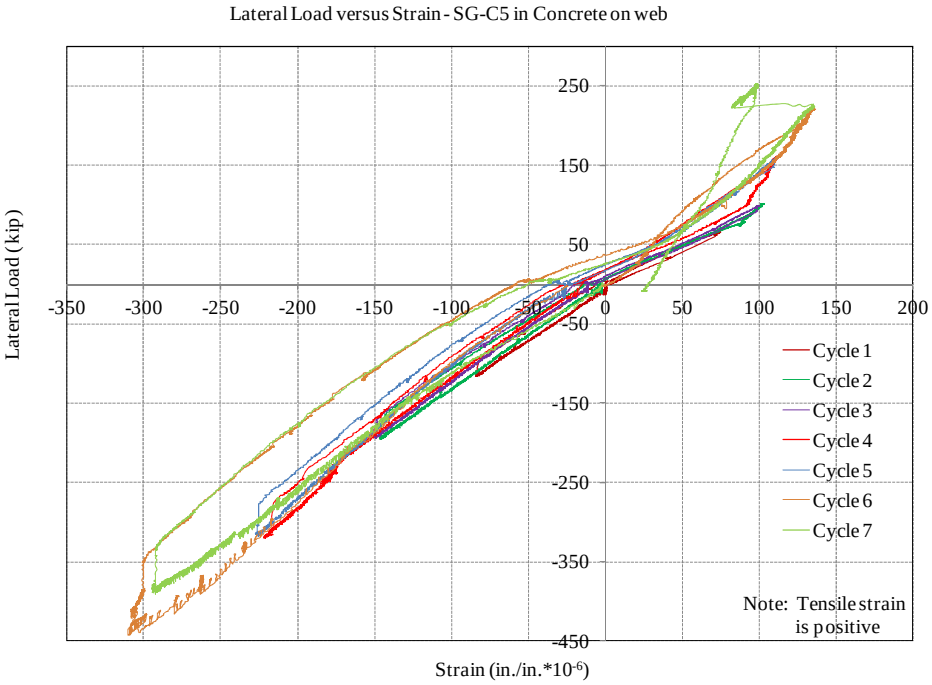

Figure D.22 Lateral load versus strain in concrete – C5

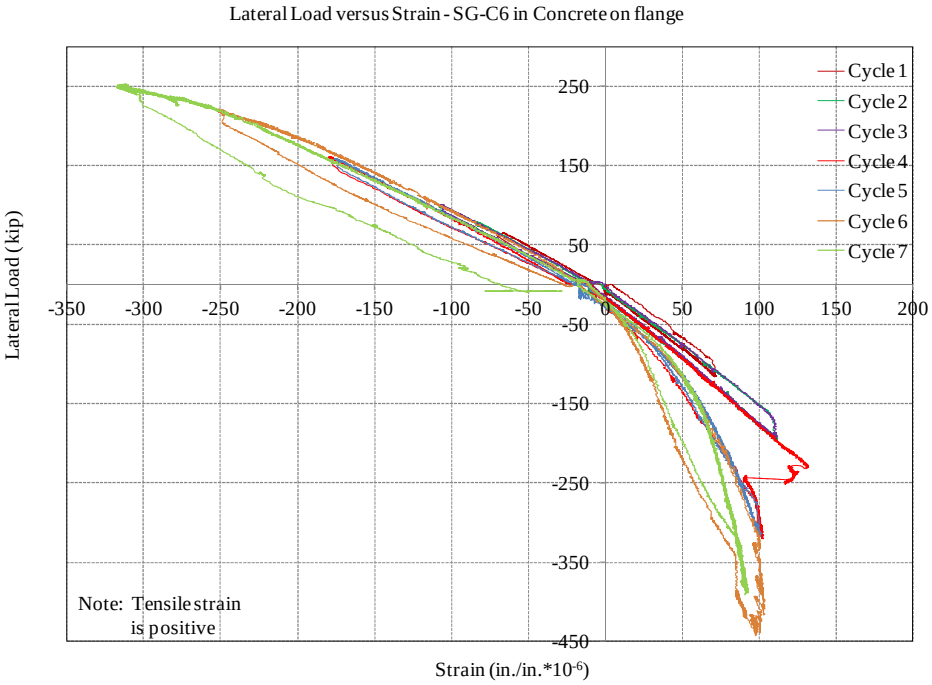

Figure D.23 Lateral load versus strain in concrete – C6

D.5: Strain measurements from strain gauges on shear wall plates

Lateral load versus strain plots for shear wall plates are presented in Figs. D.24 through D.68. Refer to Section 6.5.4 for details on instrumentation attached on shear wall plates to measure strains in shear wall plates. Refer to Figs. 6.40 through 6.43 for strain gauge locations. Refer to Section 6.7.6 for a discussion of results on strains developed in shear wall plates during the test.

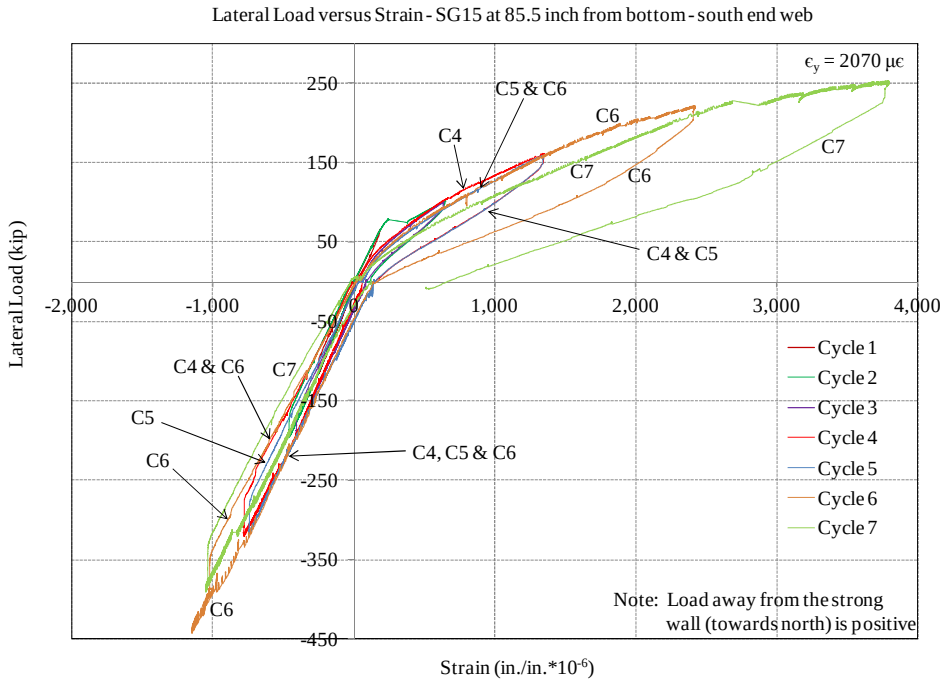

Figure D.24 Lateral load versus strain on shear wall plate – SG15

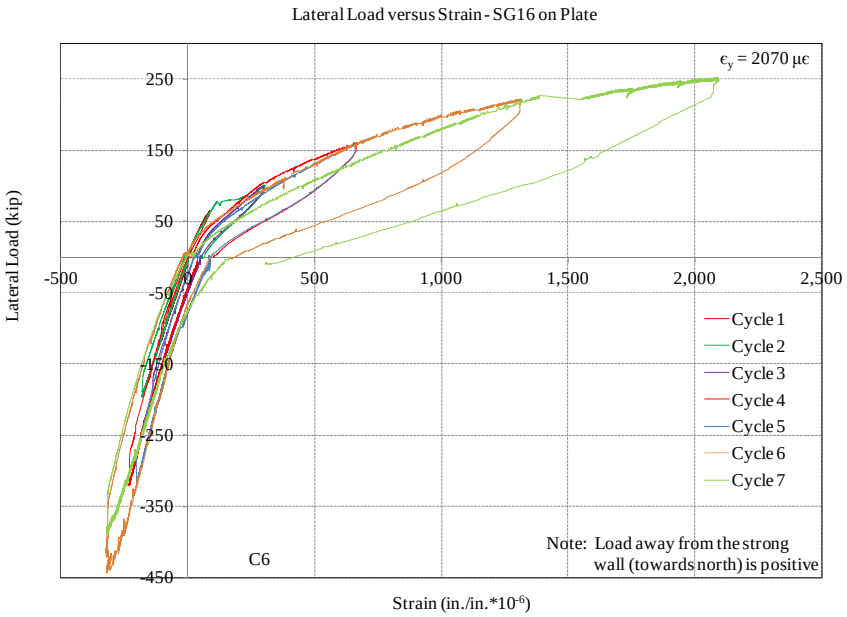

Figure D.25 Lateral load versus strain on shear wall plate – SG16

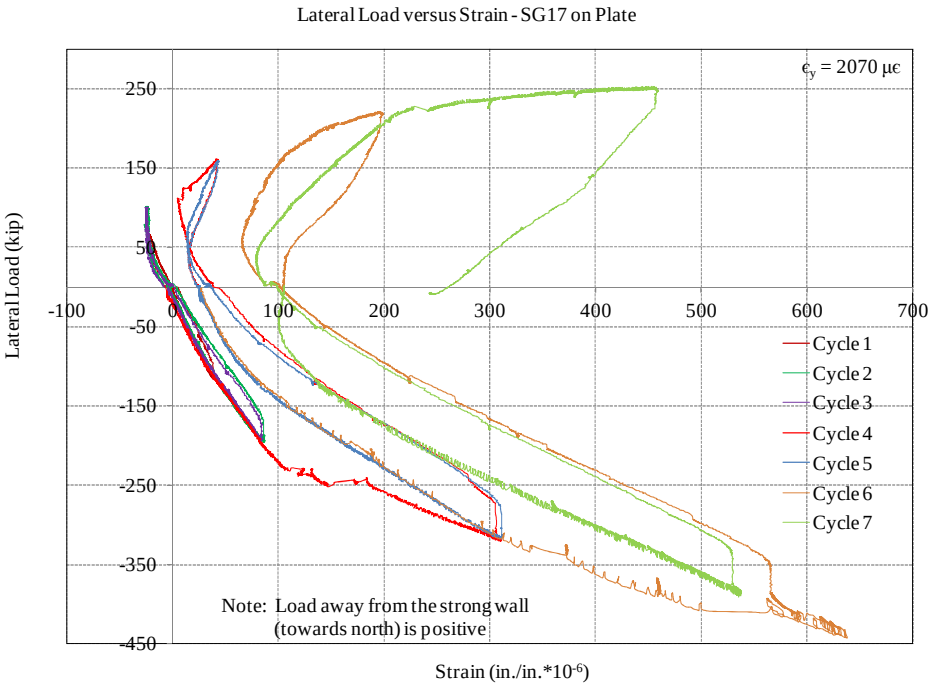

Figure D.26 Lateral load versus strain on shear wall plate – SG17

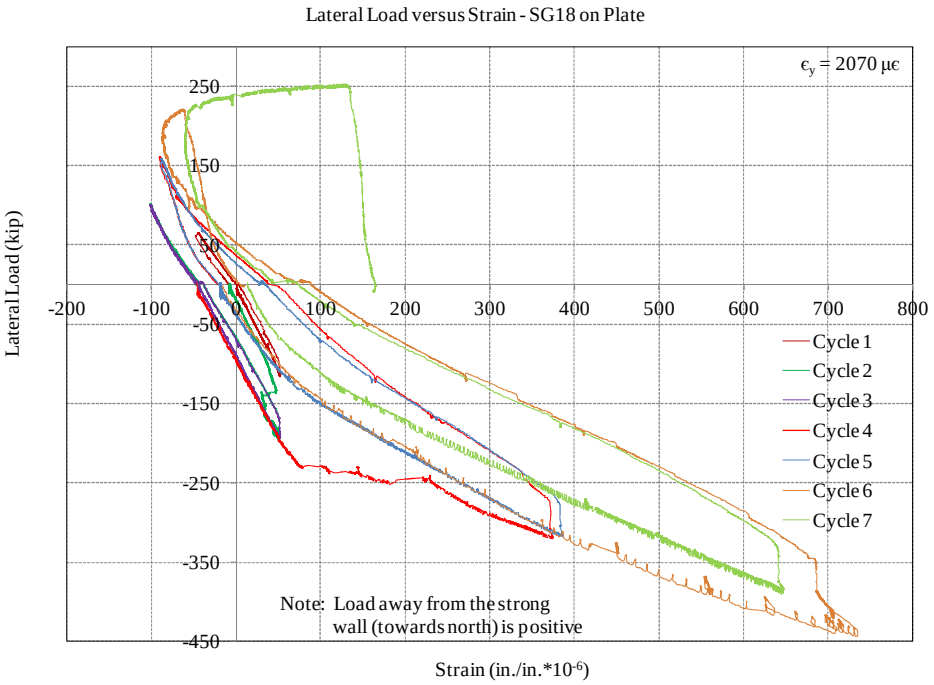

Figure D.27 Lateral load versus strain on shear wall plate – SG18

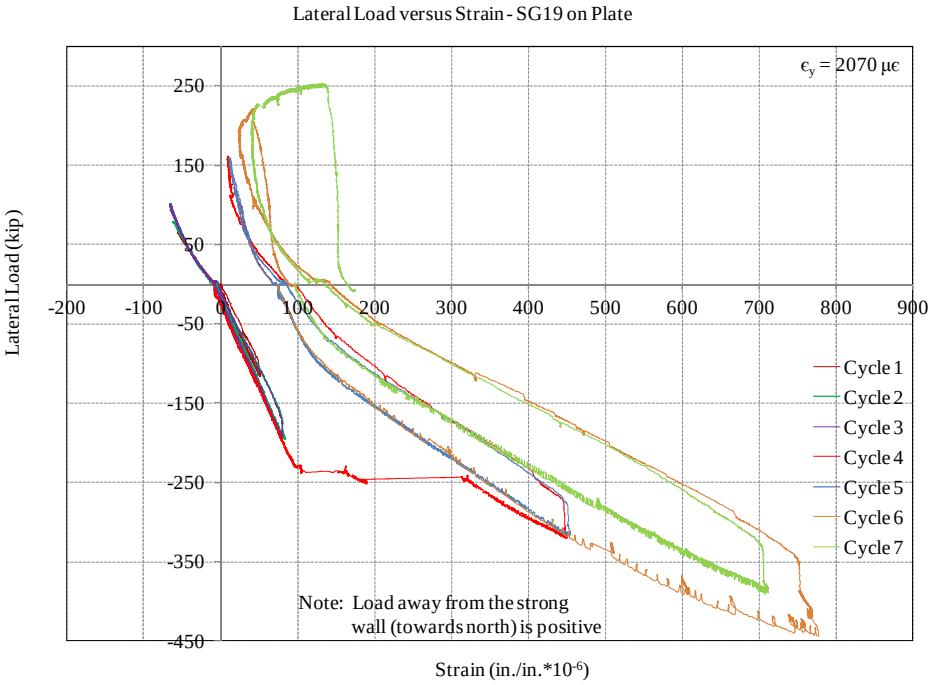

Figure D.28 Lateral load versus strain on shear wall plate – SG19

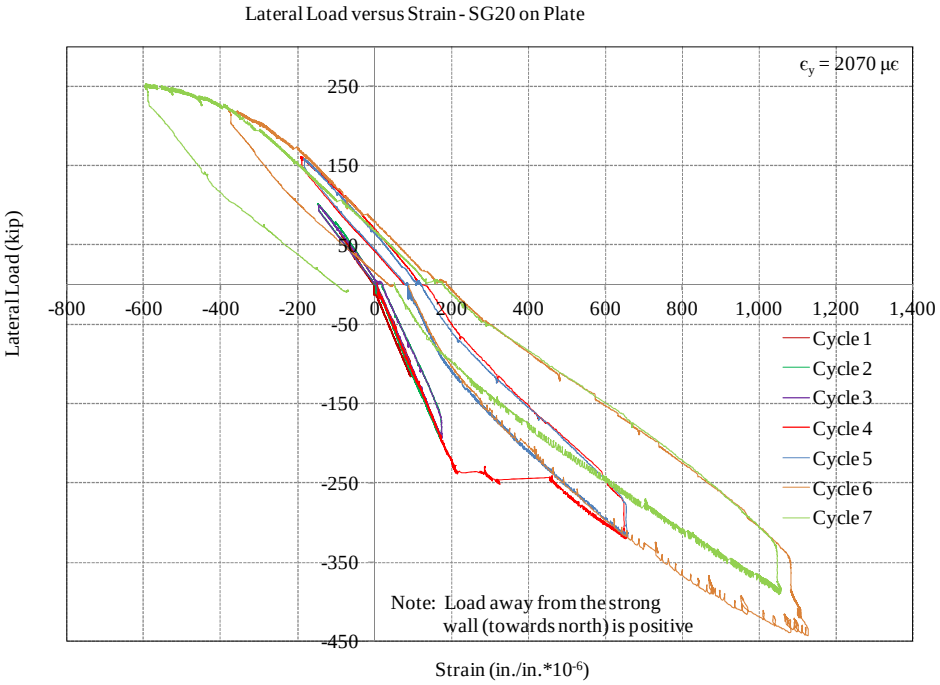

Figure D.29 Lateral load versus strain on shear wall plate – SG20

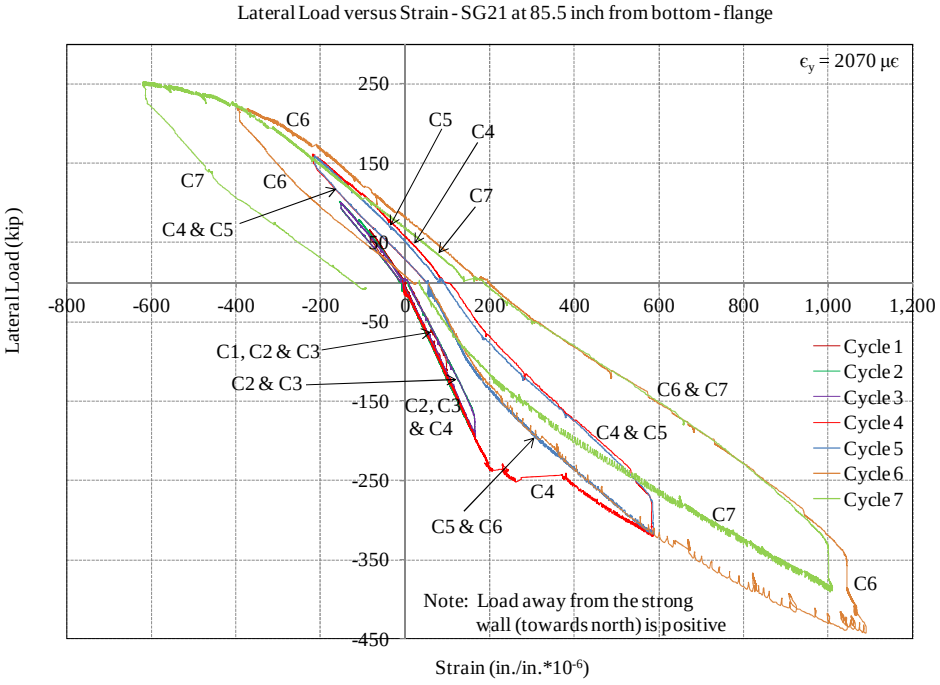

Figure D.30 Lateral load versus strain on shear wall plate – SG21

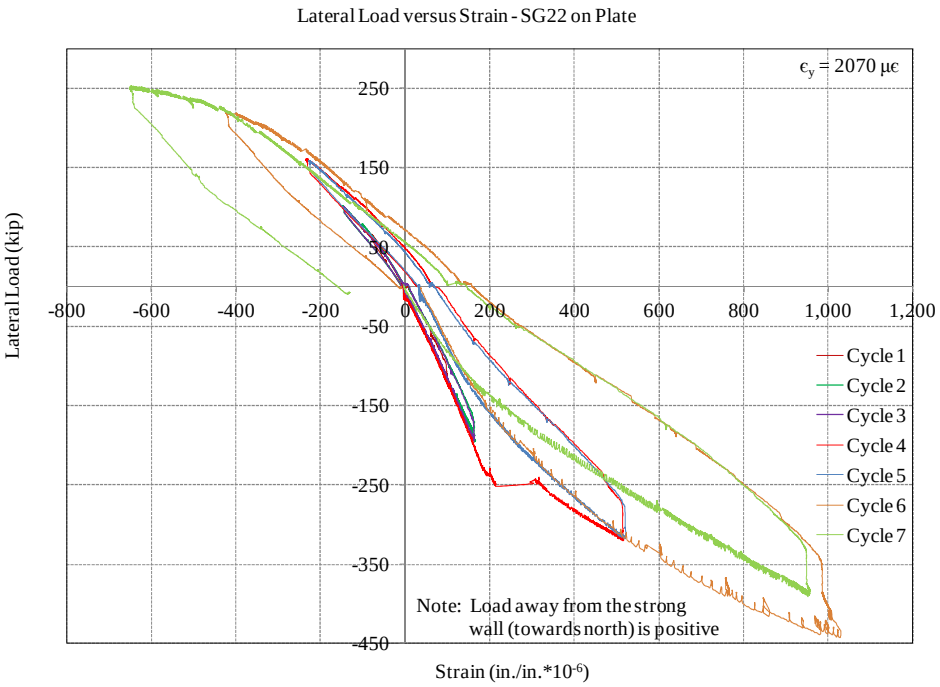

Figure D.31 Lateral load versus strain on shear wall plate – SG22

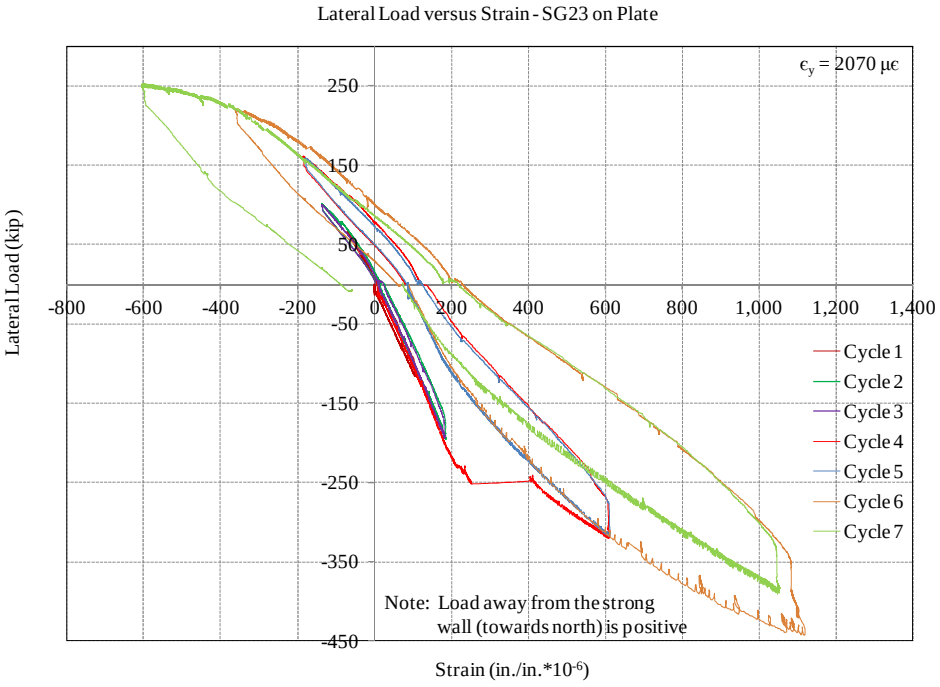

Figure D.32 Lateral load versus strain on shear wall plate – SG23

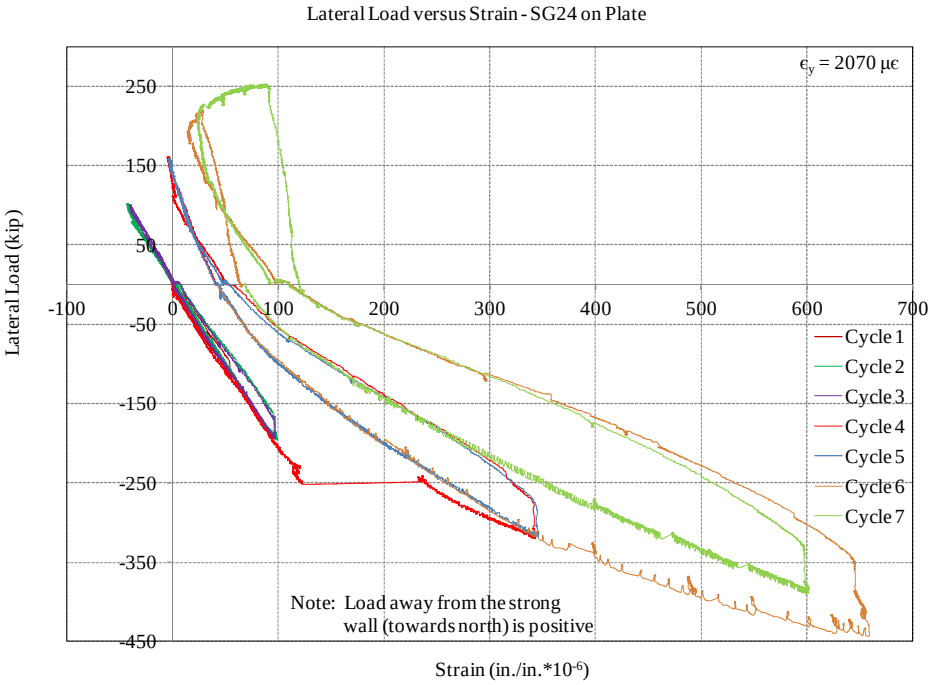

Figure D.33 Lateral load versus strain on shear wall plate – SG24

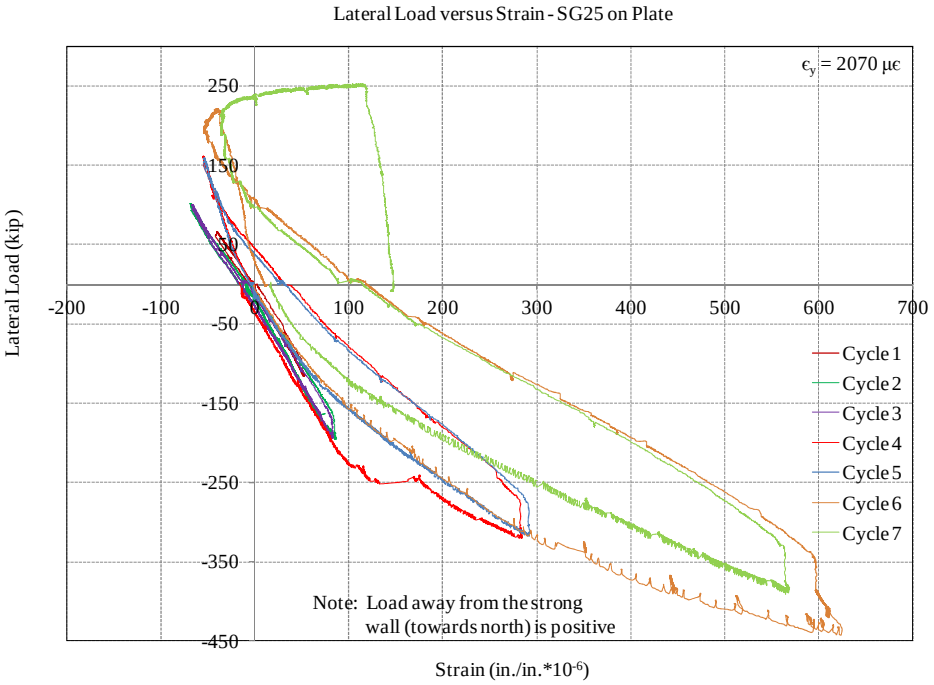

Figure D.34 Lateral load versus strain on shear wall plate – SG25

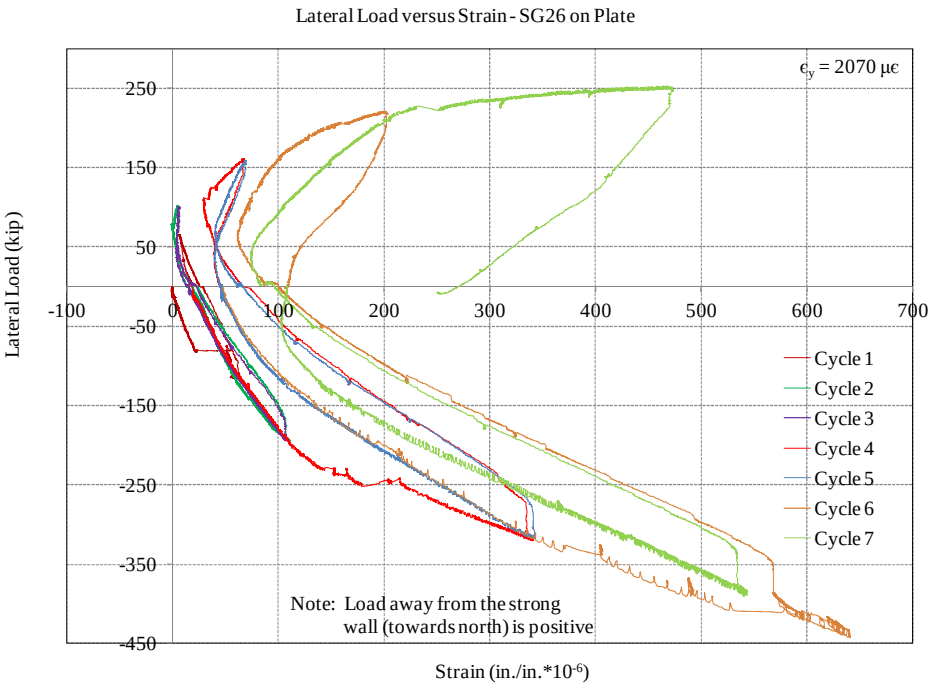

Figure D.35 Lateral load versus strain on shear wall plate – SG26

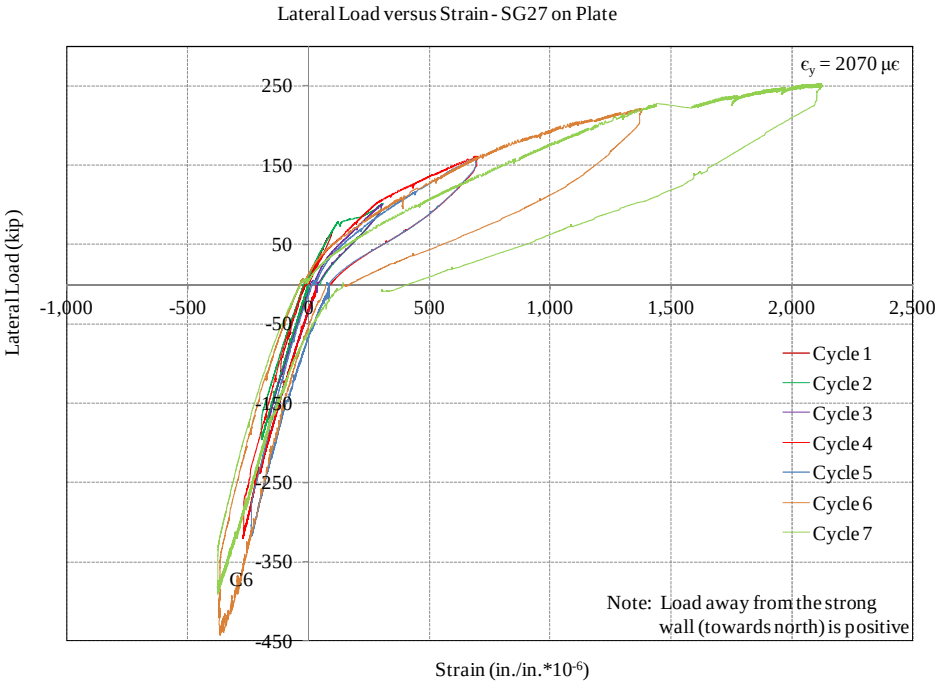

Figure D.36 Lateral load versus strain on shear wall plate – SG27

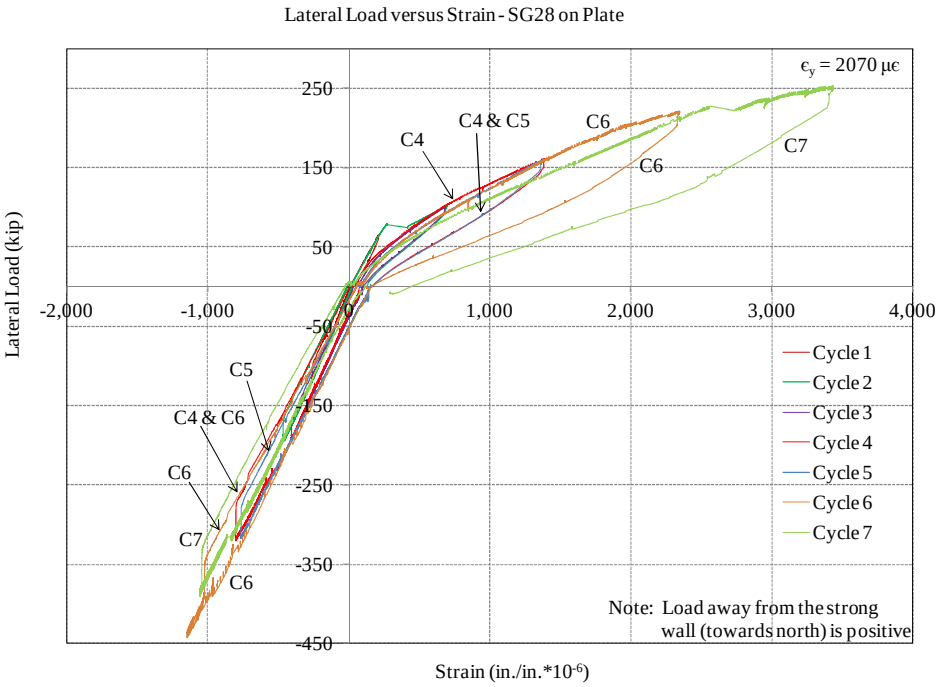

Figure D.37 Lateral load versus strain on shear wall plate – SG28

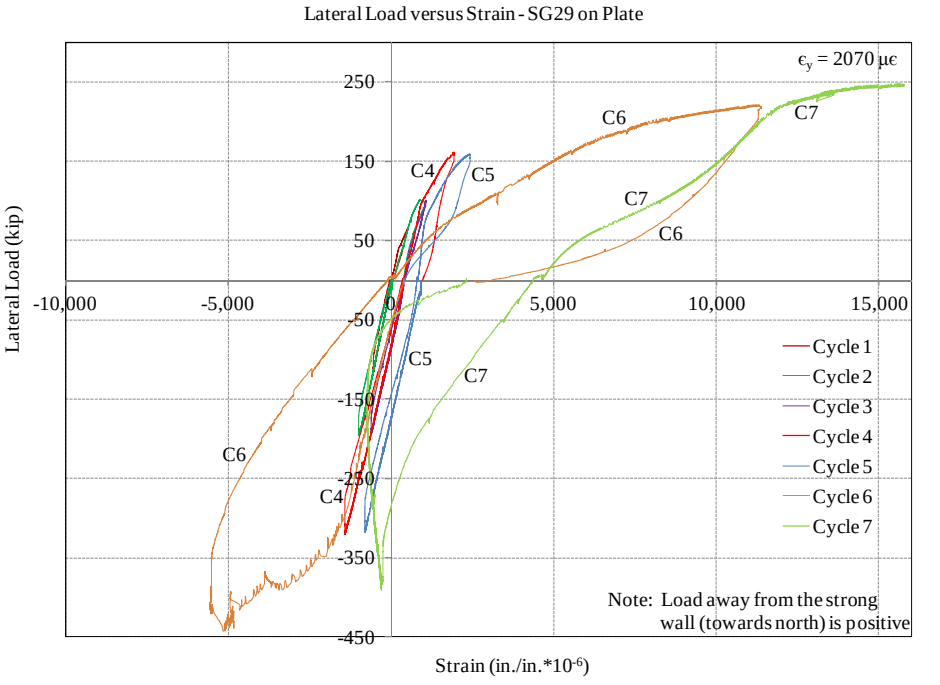

Figure D.38 Lateral load versus strain on shear wall plate – SG29

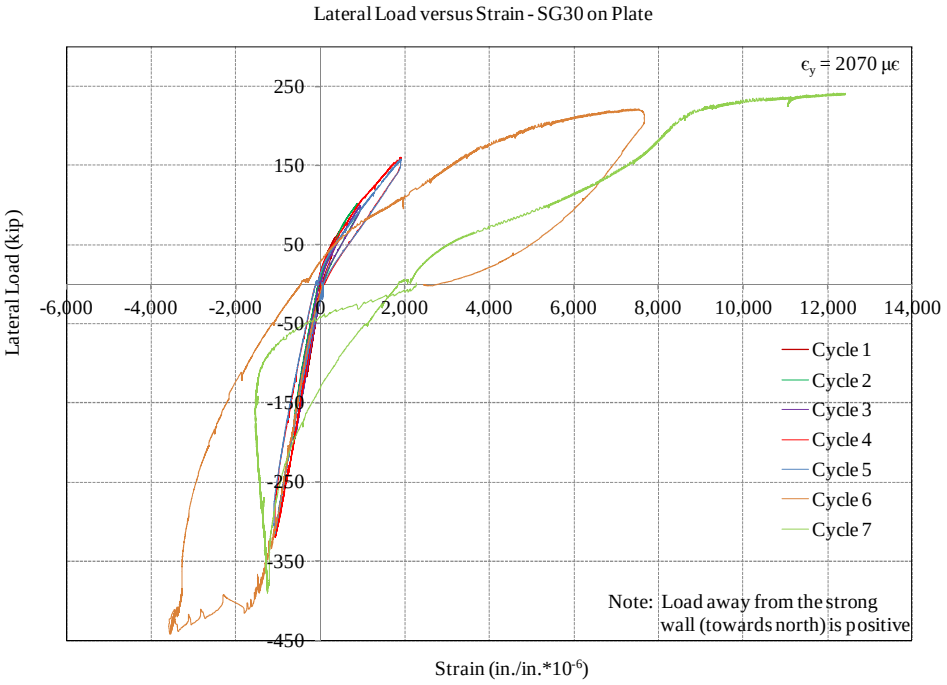

Figure D.39 Lateral load versus strain on shear wall plate – SG30

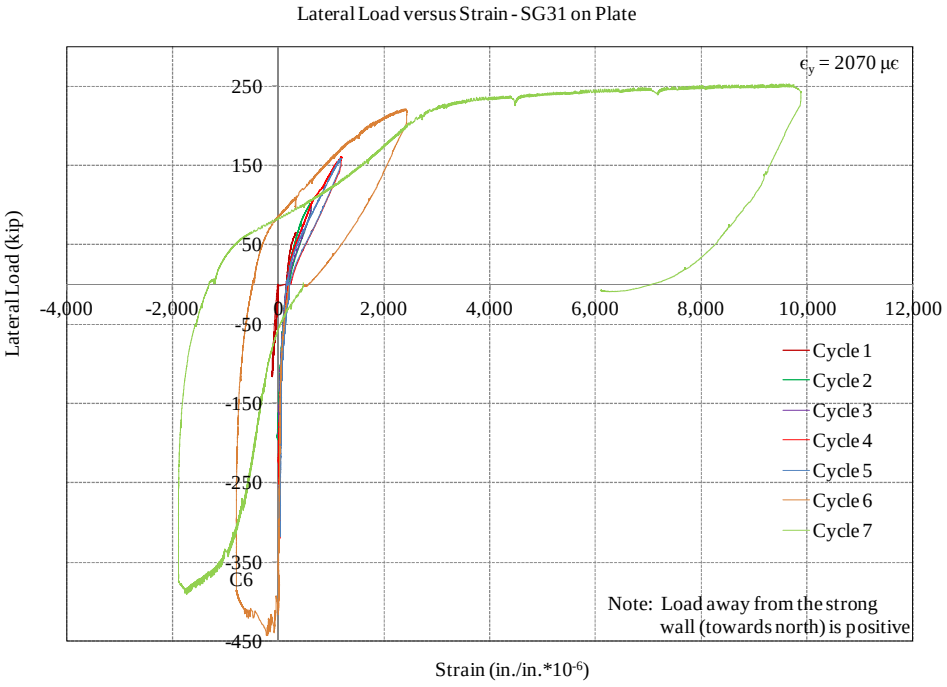

Figure D.40 Lateral load versus strain on shear wall plate – SG31

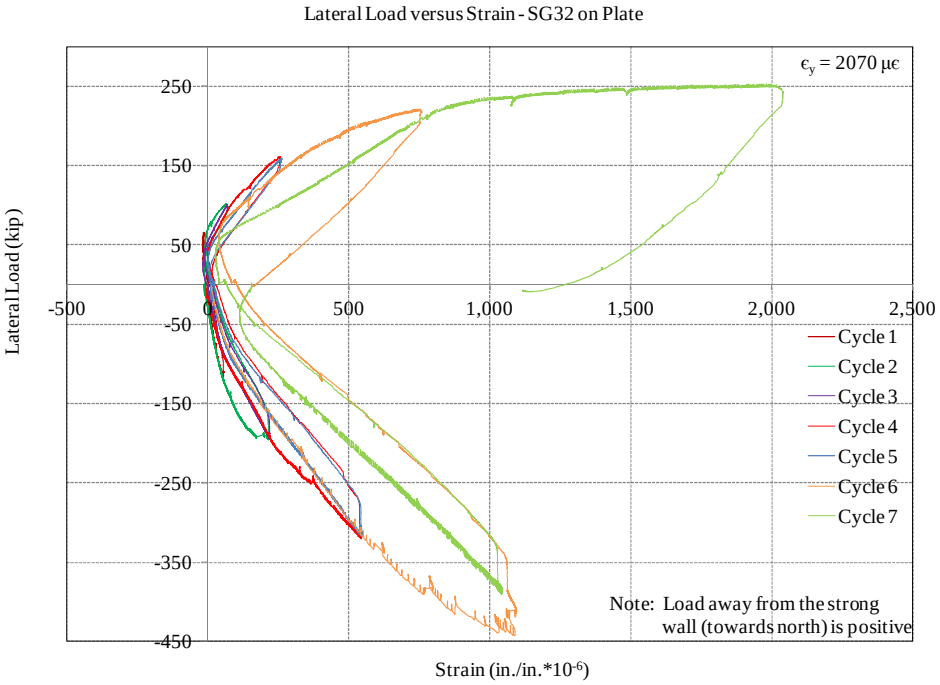

Figure D.41 Lateral load versus strain on shear wall plate – SG32

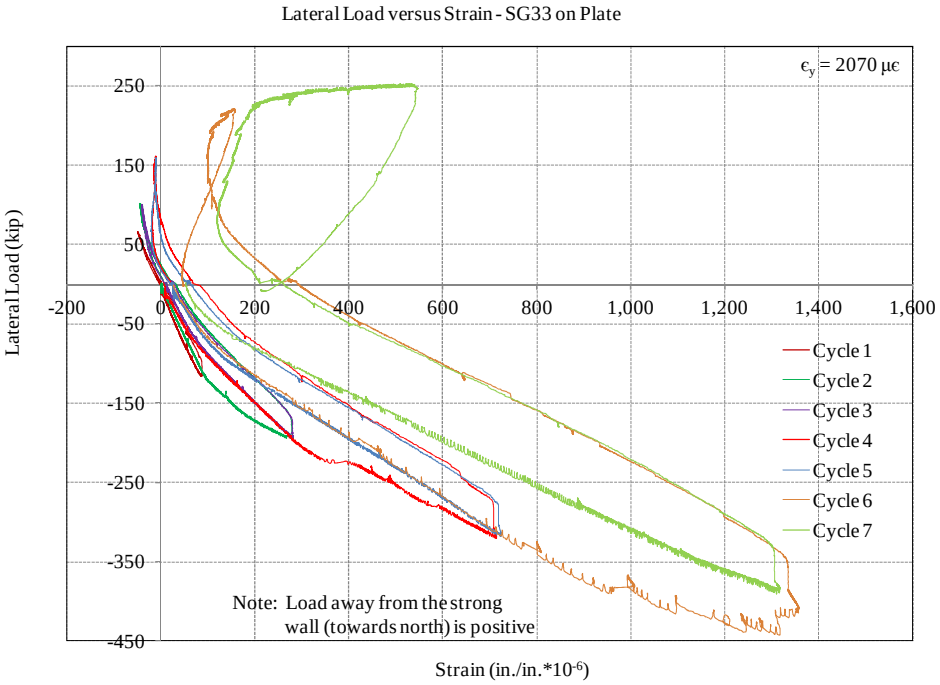

Figure D.42 Lateral load versus strain on shear wall plate – SG33

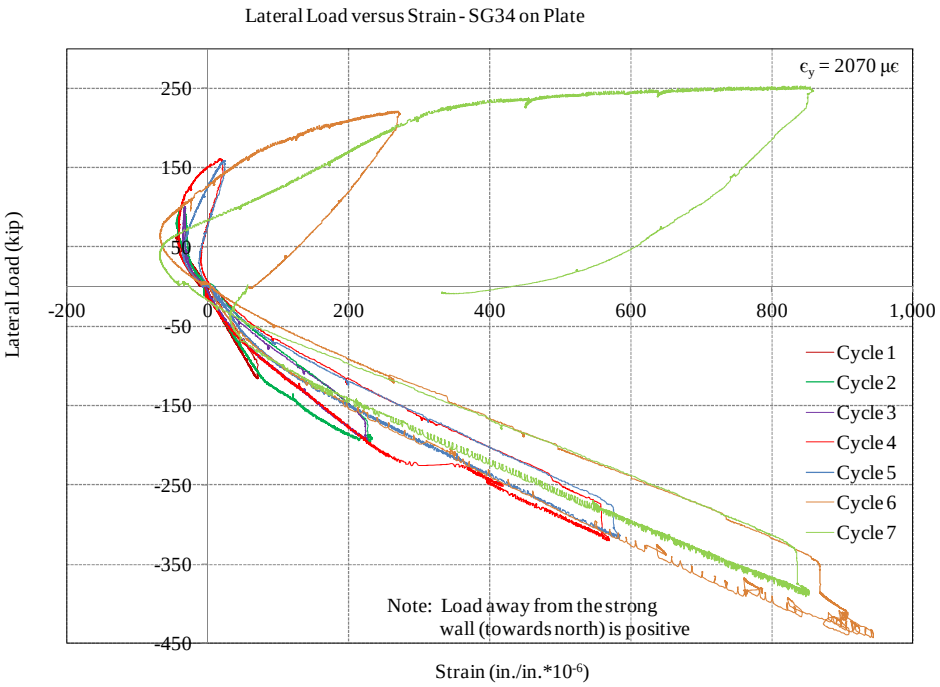

Figure D.43 Lateral load versus strain on shear wall plate – SG34

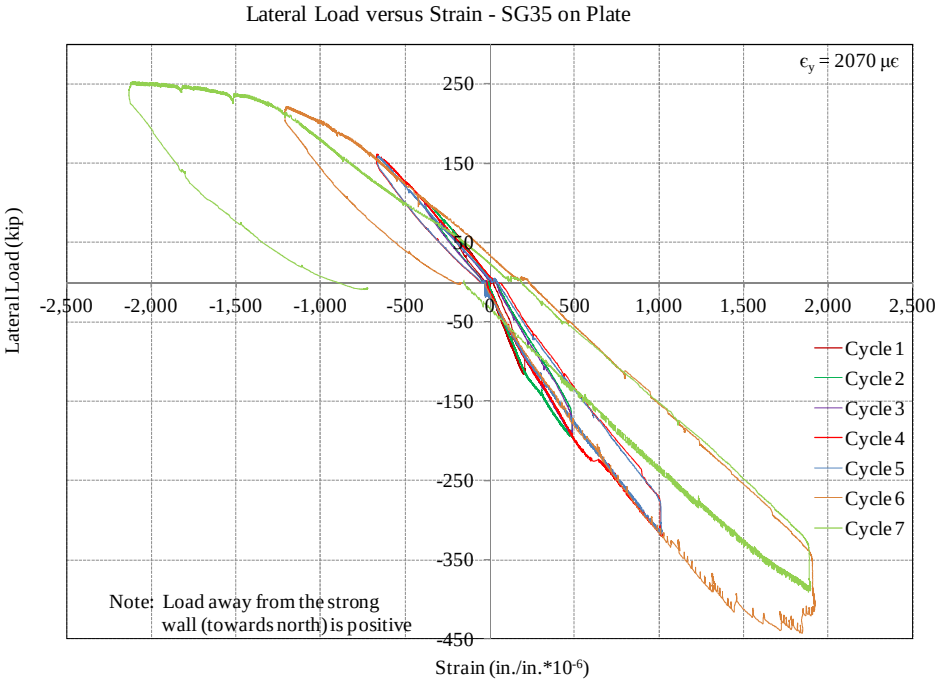

Figure D.44 Lateral load versus strain on shear wall plate – SG35

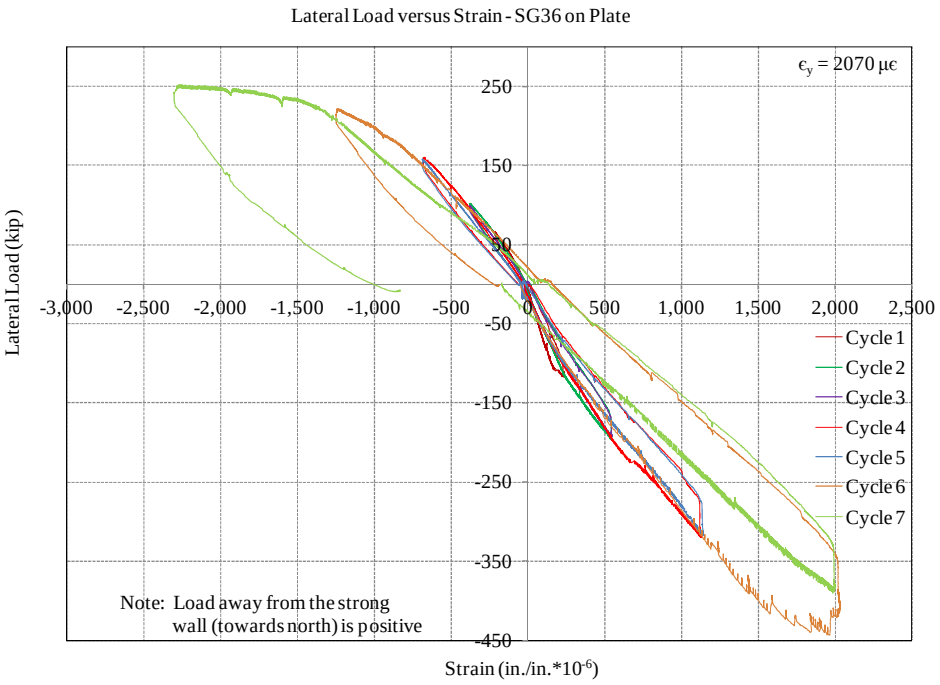

Figure D.45 Lateral load versus strain on shear wall plate – SG36

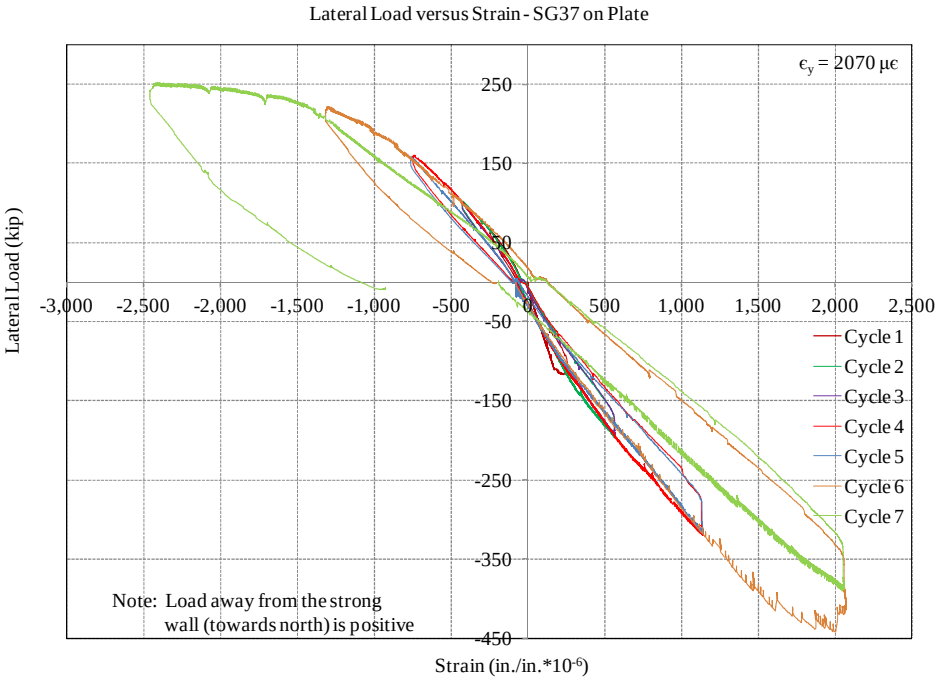

Figure D.46 Lateral load versus strain on shear wall plate – SG37

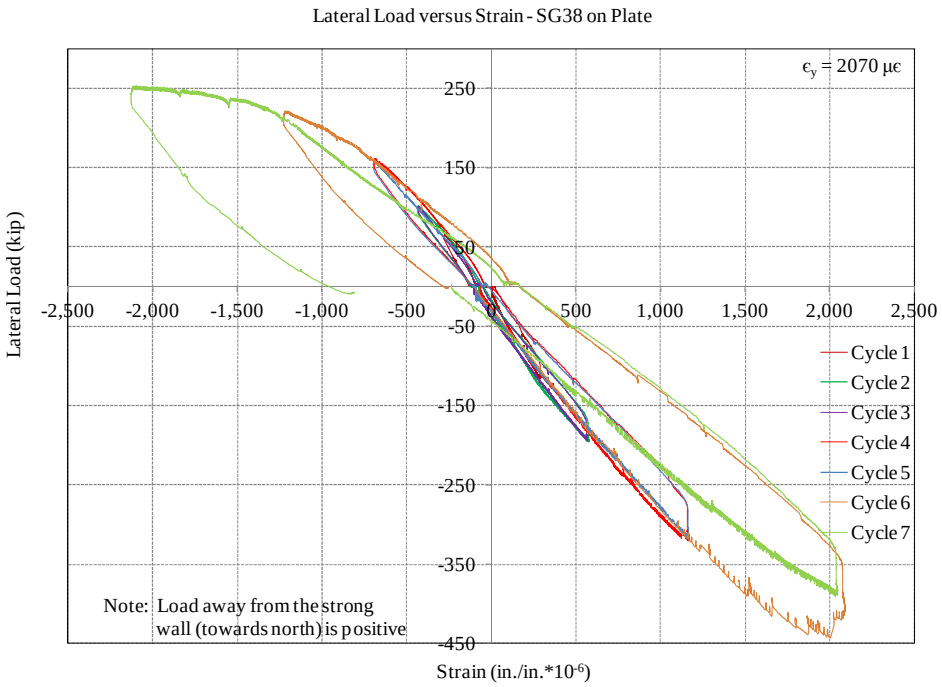

Figure D.47 Lateral load versus strain on shear wall plate – SG38

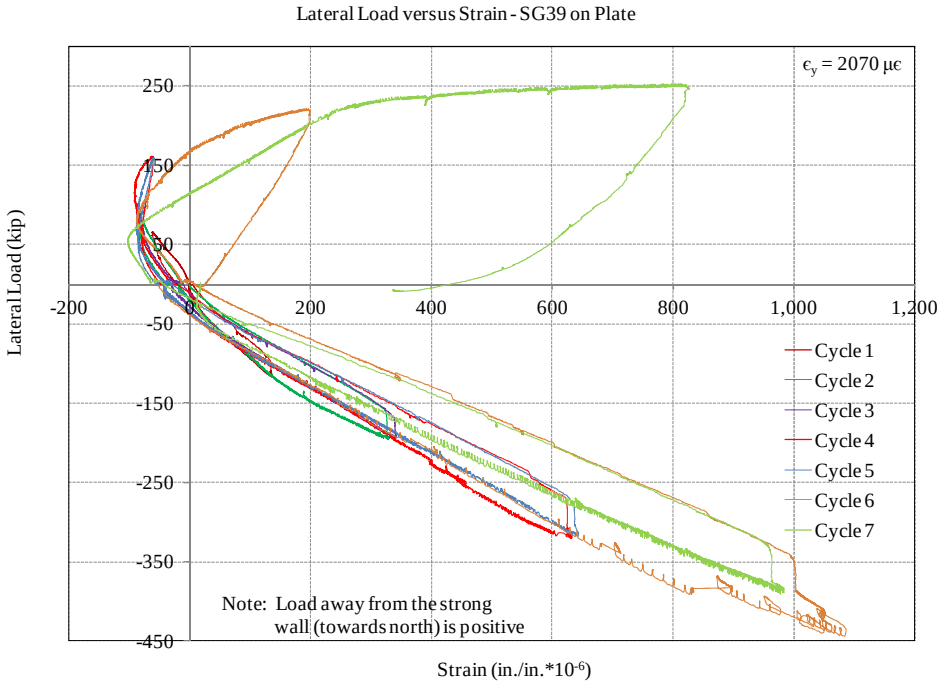

Figure D.48 Lateral load versus strain on shear wall plate – SG39

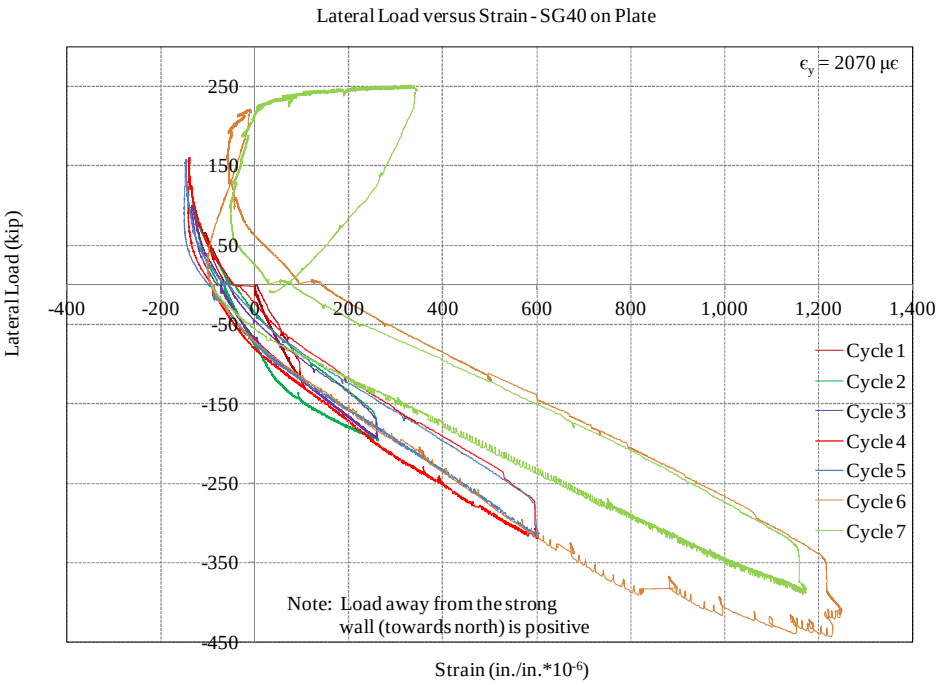

Figure D.49 Lateral load versus strain on shear wall plate – SG40

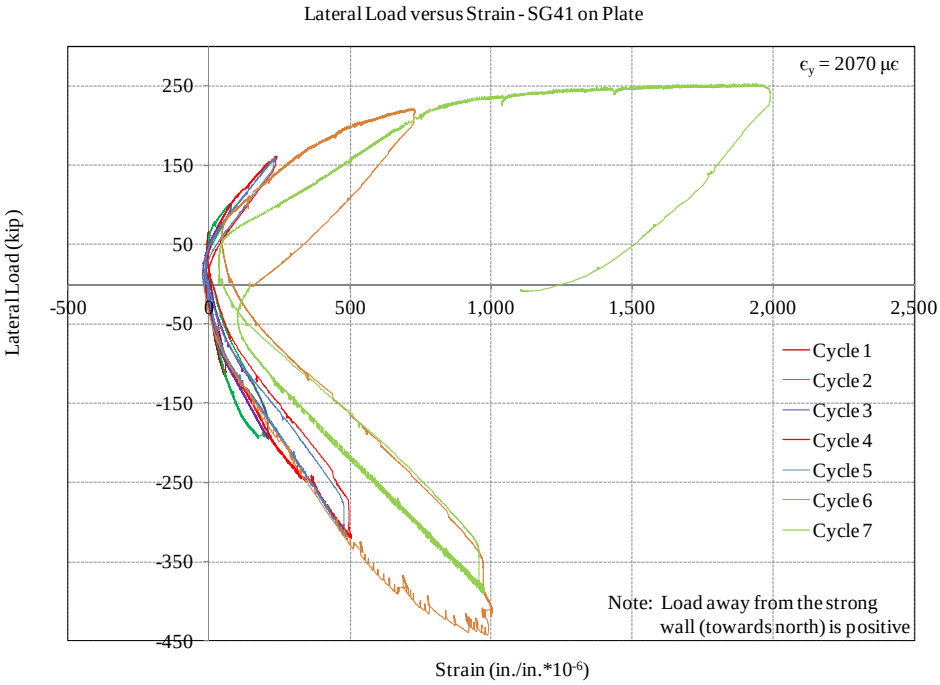

Figure D.50 Lateral load versus strain on shear wall plate – SG41

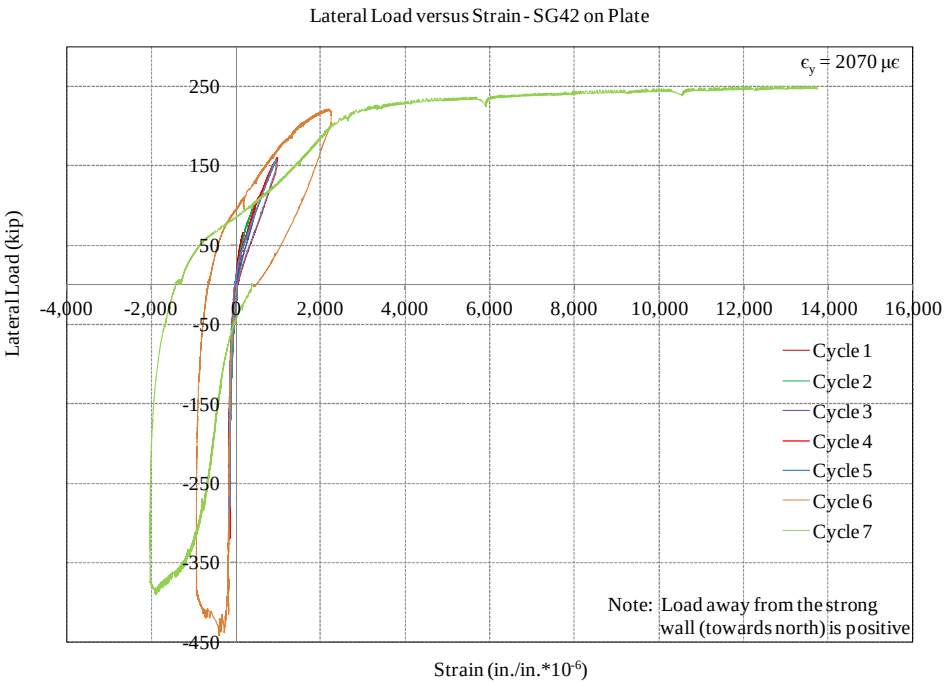

Figure D.51 Lateral load versus strain on shear wall plate – SG42

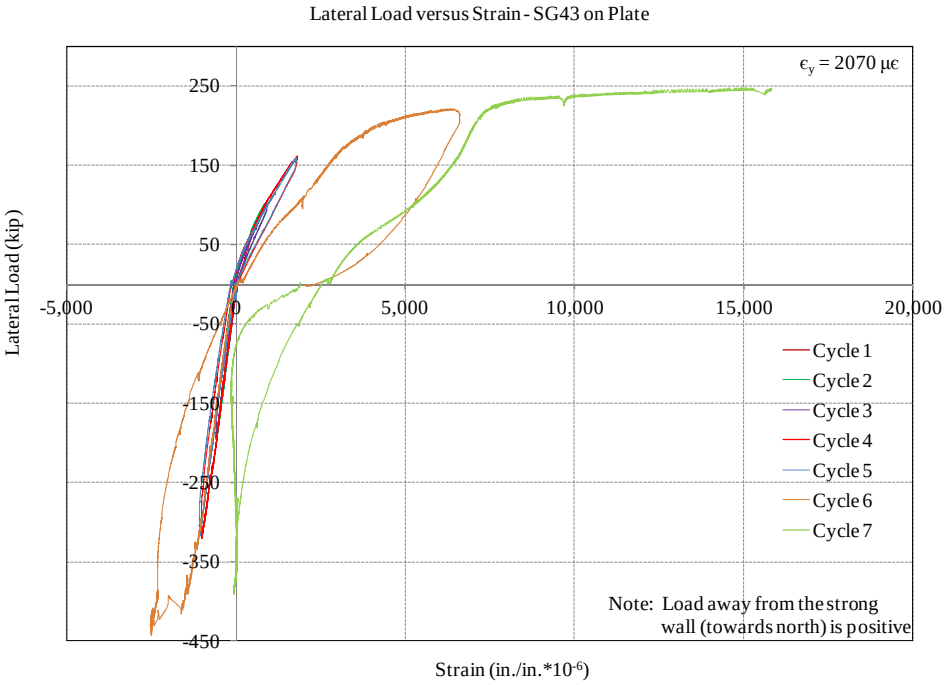

Figure D.52 Lateral load versus strain on shear wall plate – SG43

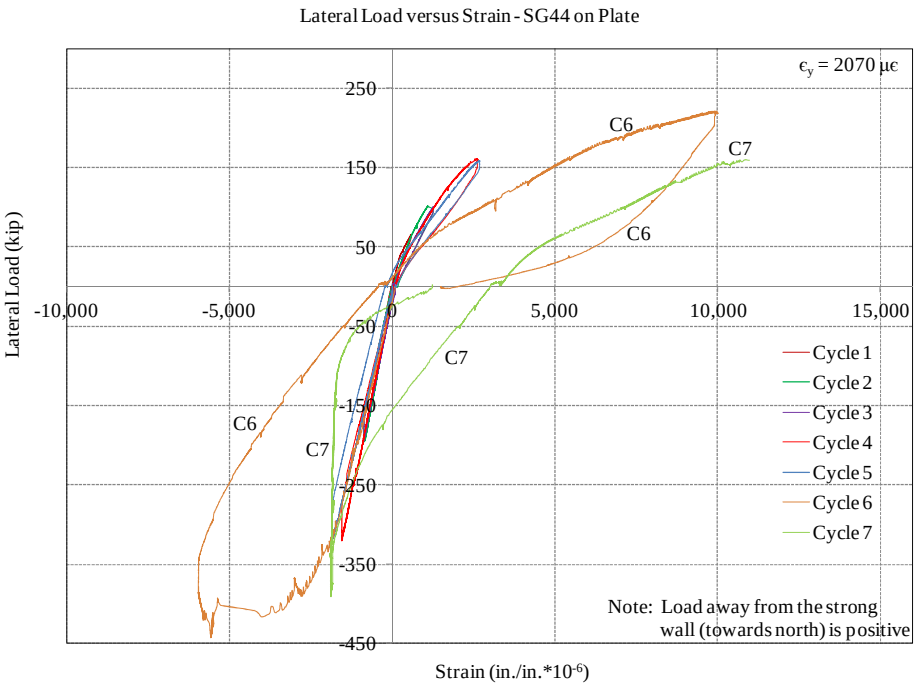

Figure D.53 Lateral load versus strain on shear wall plate – SG44

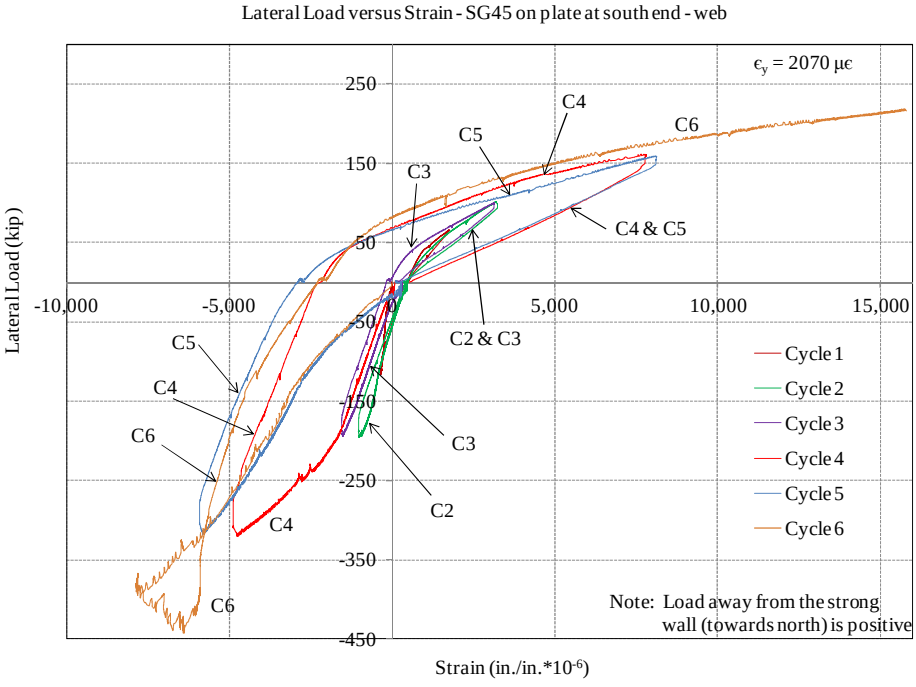

Figure D.54 Lateral load versus strain on shear wall plate – SG45

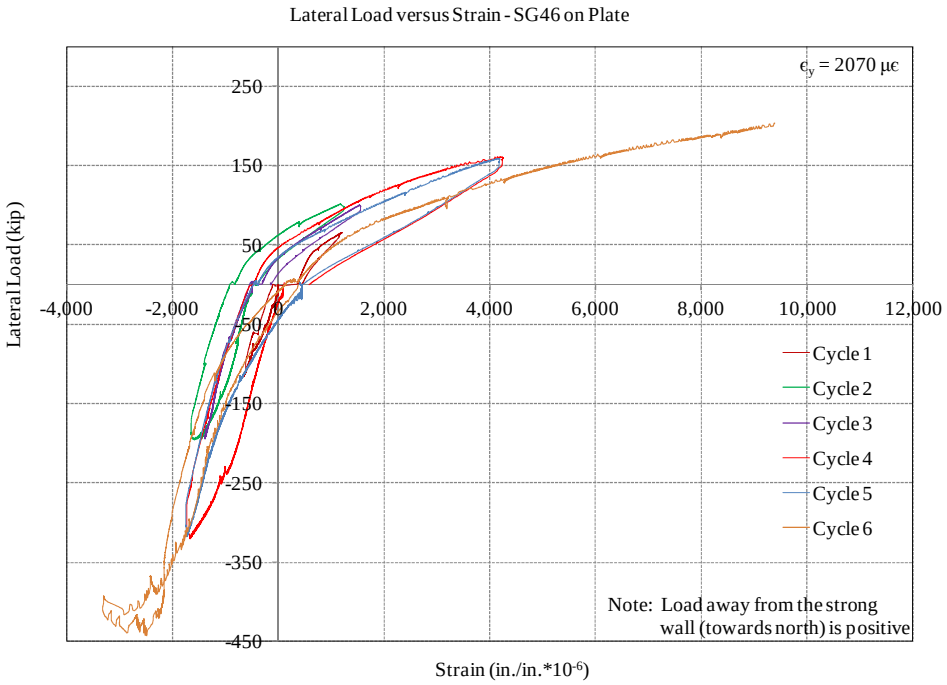

Figure D.55 Lateral load versus strain on shear wall plate – SG46

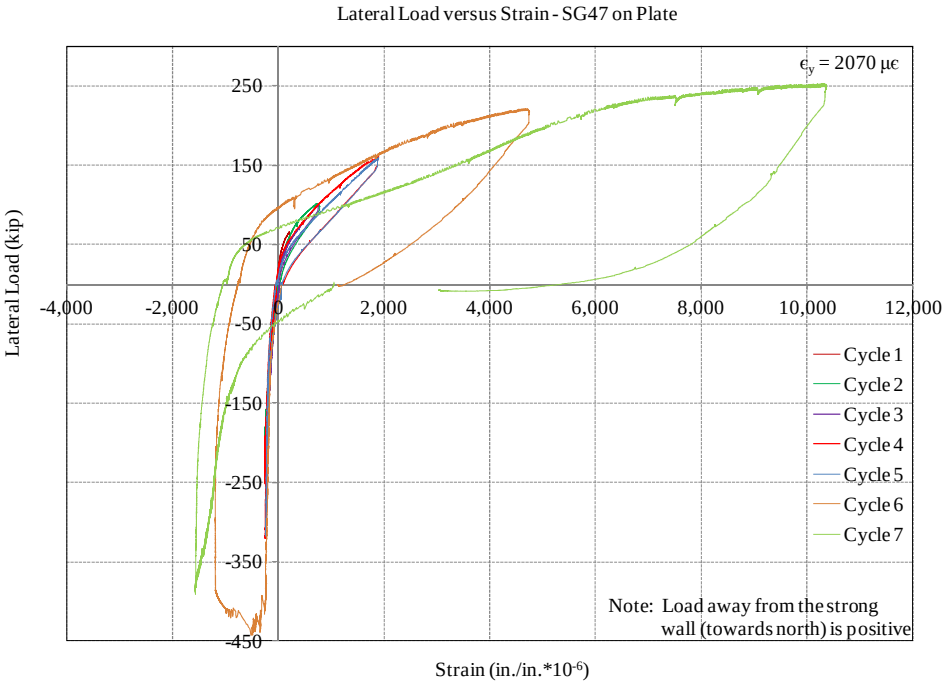

Figure D.56 Lateral load versus strain on shear wall plate – SG47

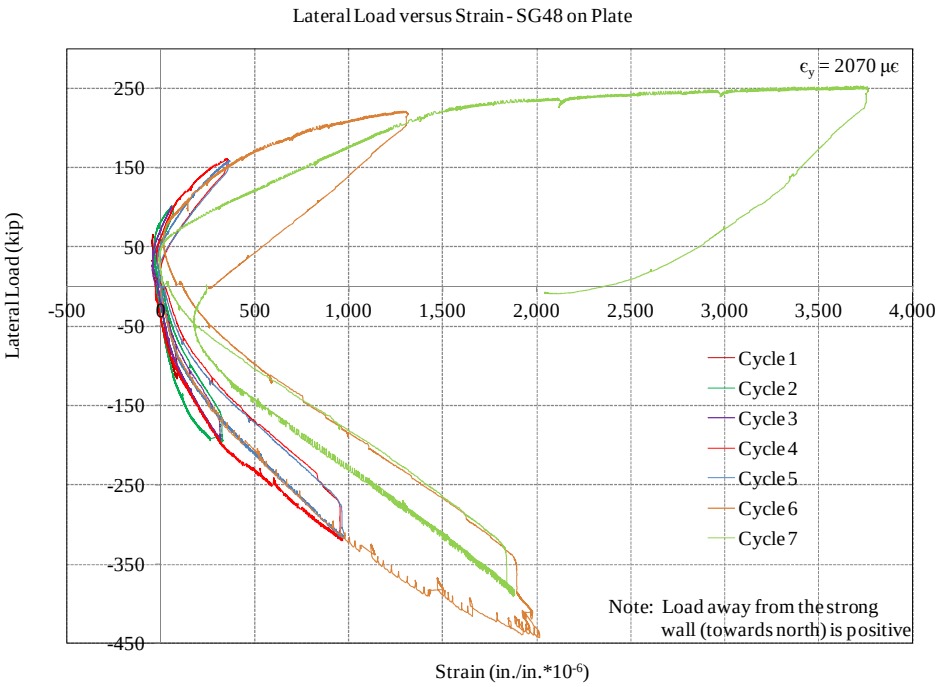

Figure D.57 Lateral load versus strain on shear wall plate – SG48

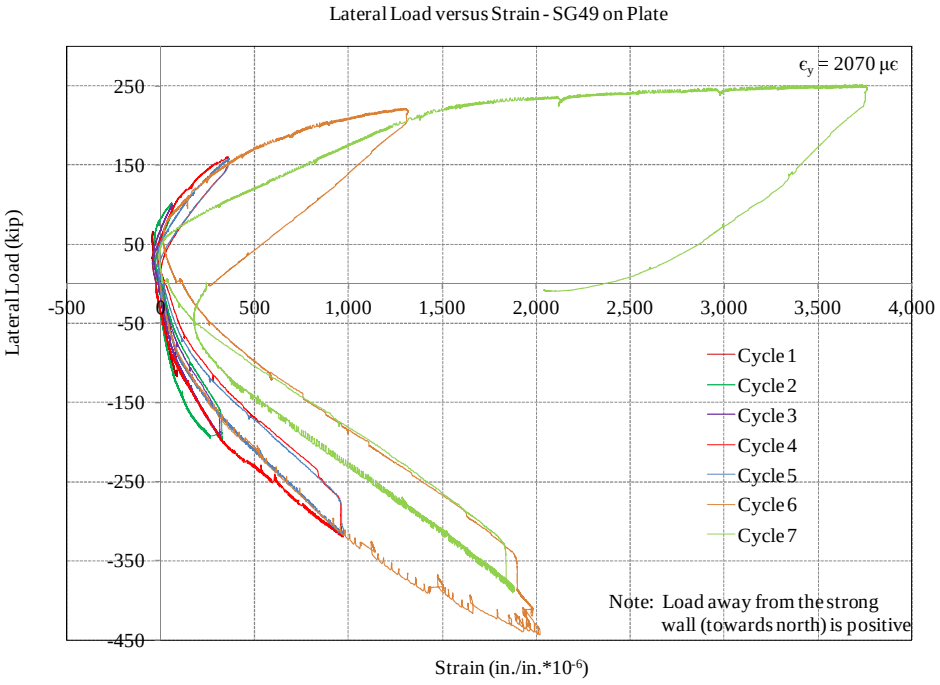

Figure D.58 Lateral load versus strain on shear wall plate – SG49

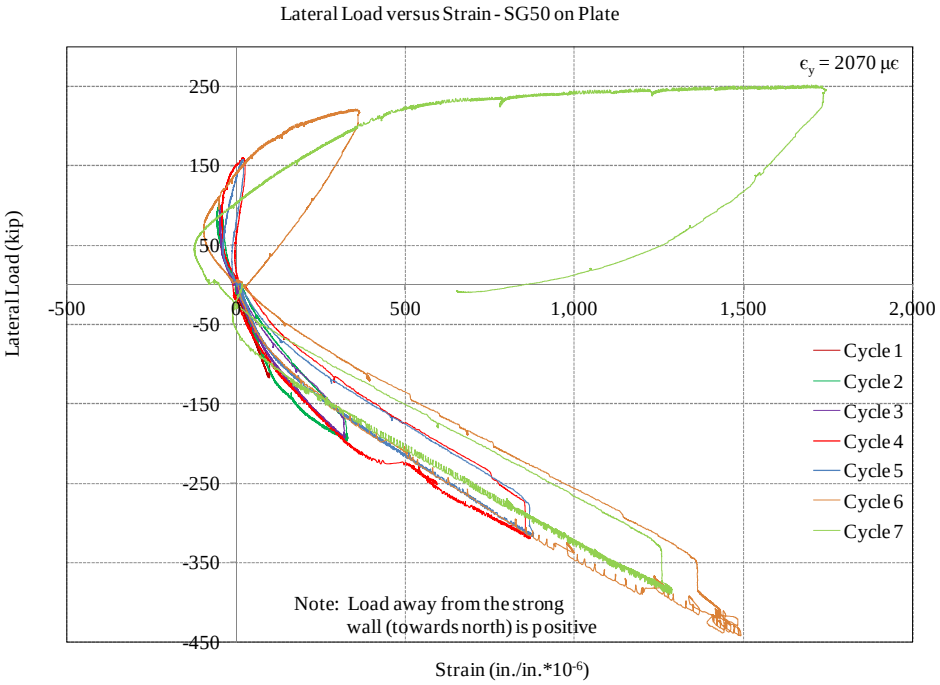

Figure D.59 Lateral load versus strain on shear wall plate – SG50

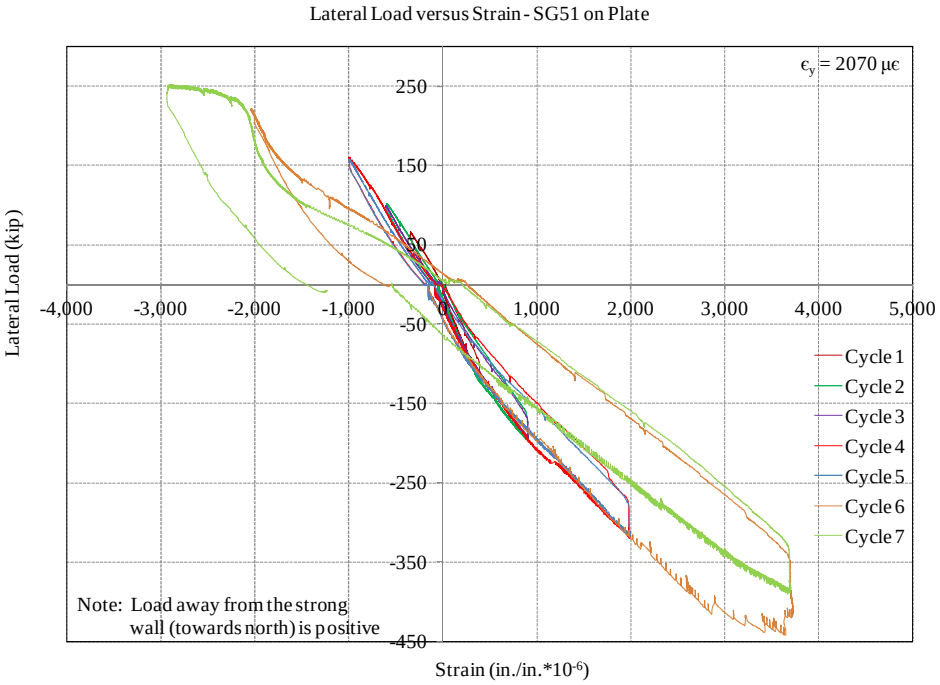

Figure D.60 Lateral load versus strain on shear wall plate – SG51

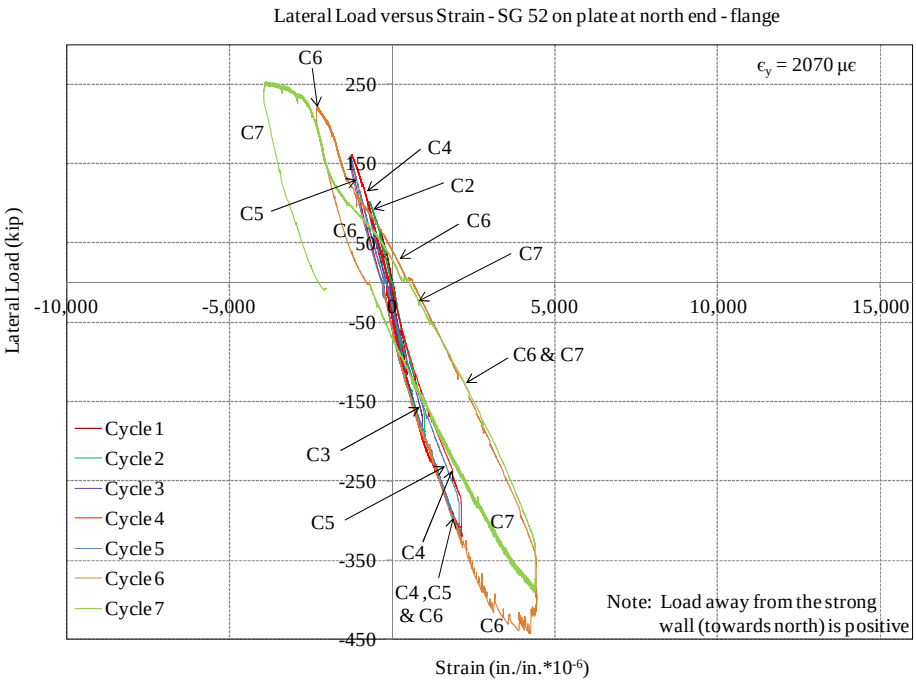

Figure D.61 Lateral load versus strain on shear wall plate – SG52

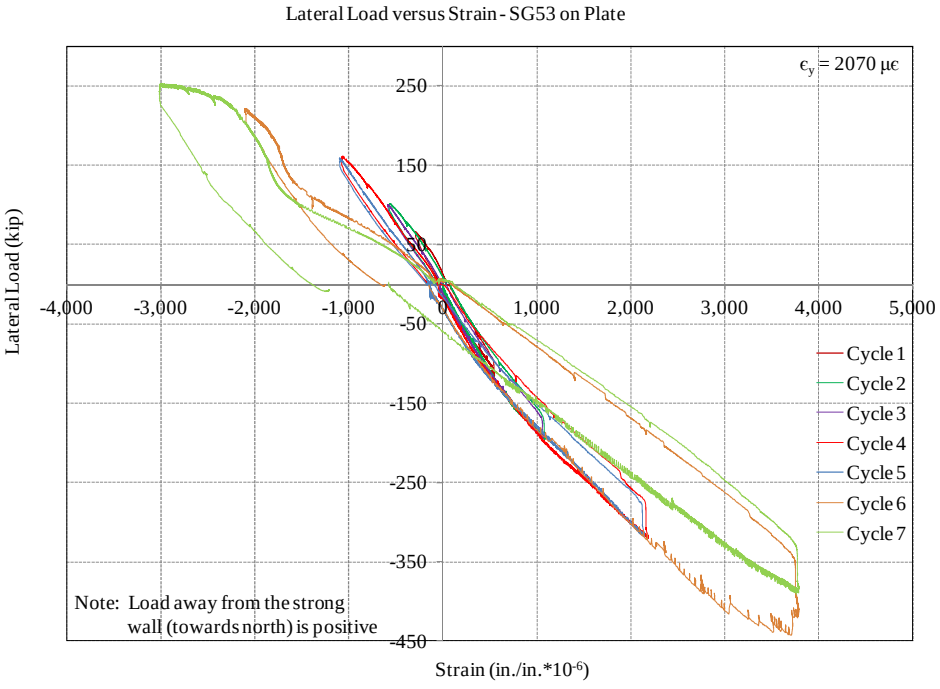

Figure D.62 Lateral load versus strain on shear wall plate – SG53

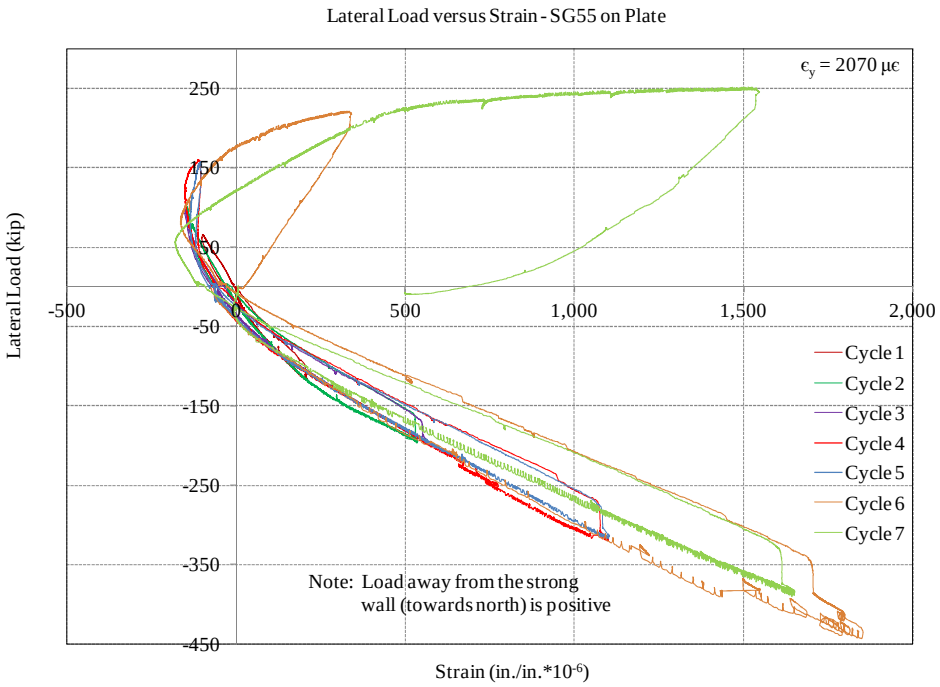

Figure D.63 Lateral load versus strain on shear wall plate – SG55

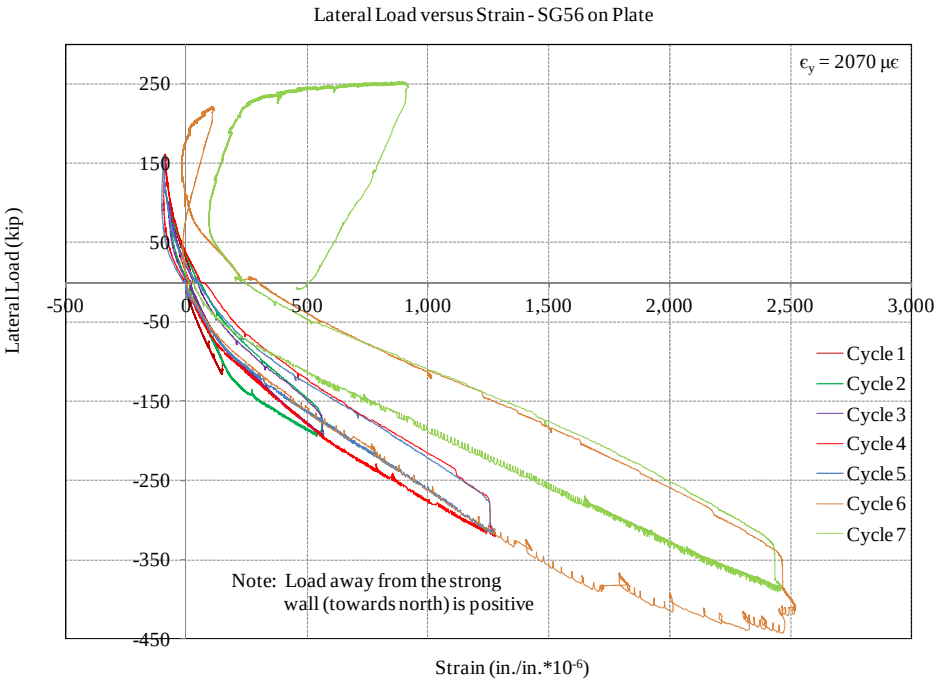

Figure D.64 Lateral load versus strain on shear wall plate – SG56

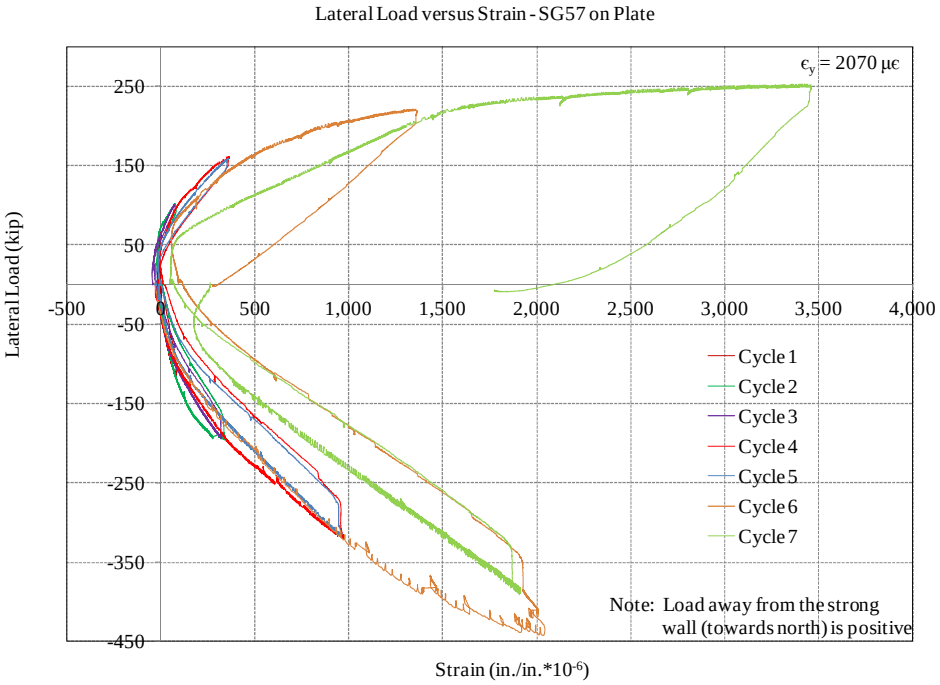

Figure D.65 Lateral load versus strain on shear wall plate – SG57

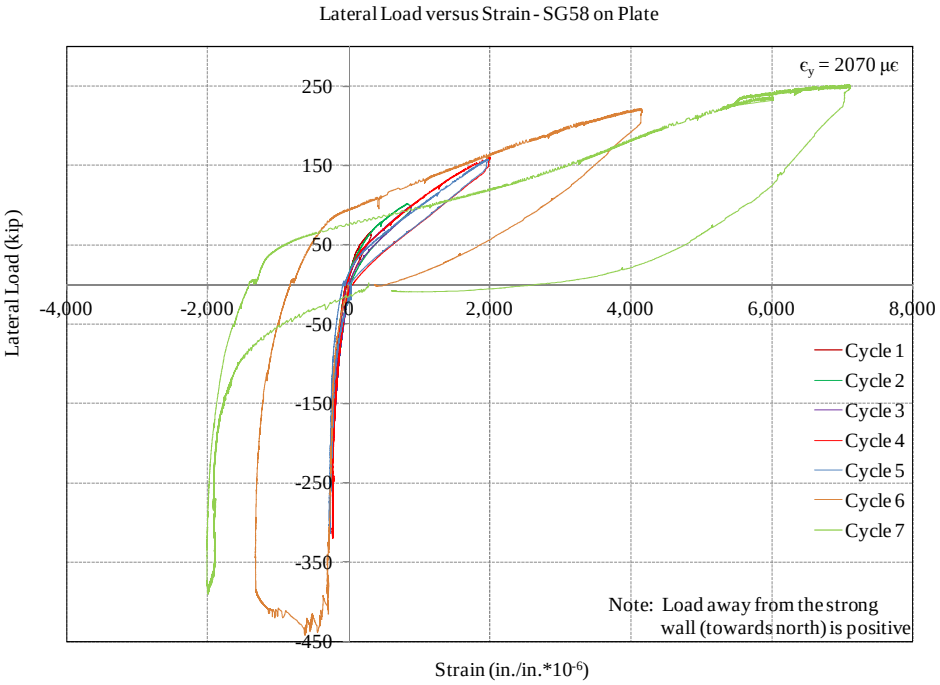

Figure D.66 Lateral load versus strain on shear wall plate – SG58

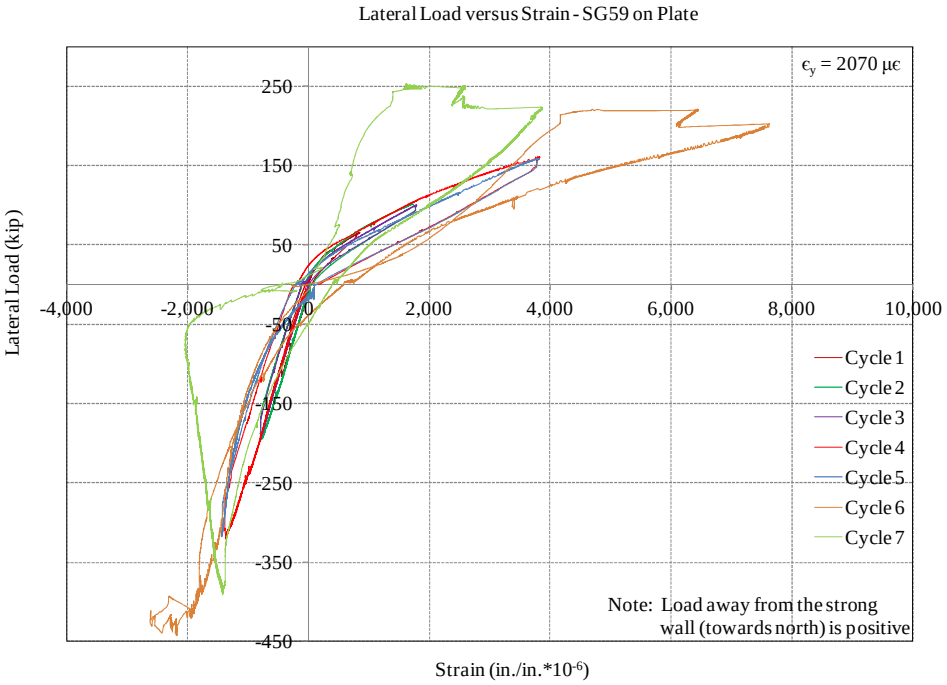

Figure D.67 Lateral load versus strain on shear wall plate – SG59

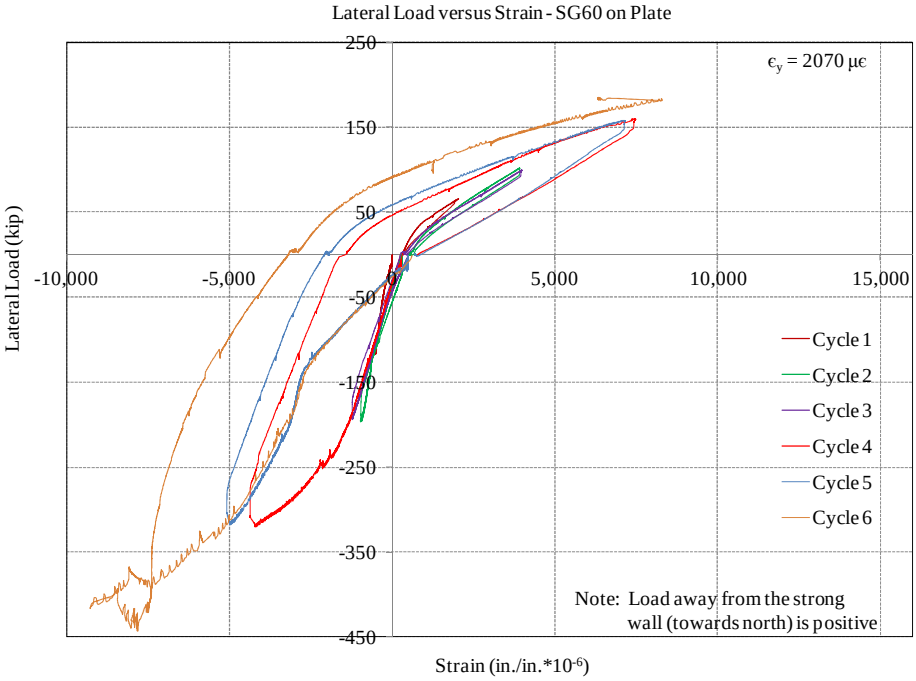

Figure D.68 Lateral load versus strain on shear wall plate – SG60

D.6: Average strains over the bottom 8-inch of shear wall plate measured by position transducers

Lateral load versus average strain measurements at the bottom of the wall are presented in Figs. D.69 through D.74. See Section 6.5.8 for details on instrumentation (position transducers) attached to measure average strains over the bottom 8 inches of shear wall plate. Refer to Figs. 6.41 and 6.43 for locations of position transducers. Refer to Section 6.7.6.2 for a discussion of results on average strains over the bottom 8 inches of shear wall plate.

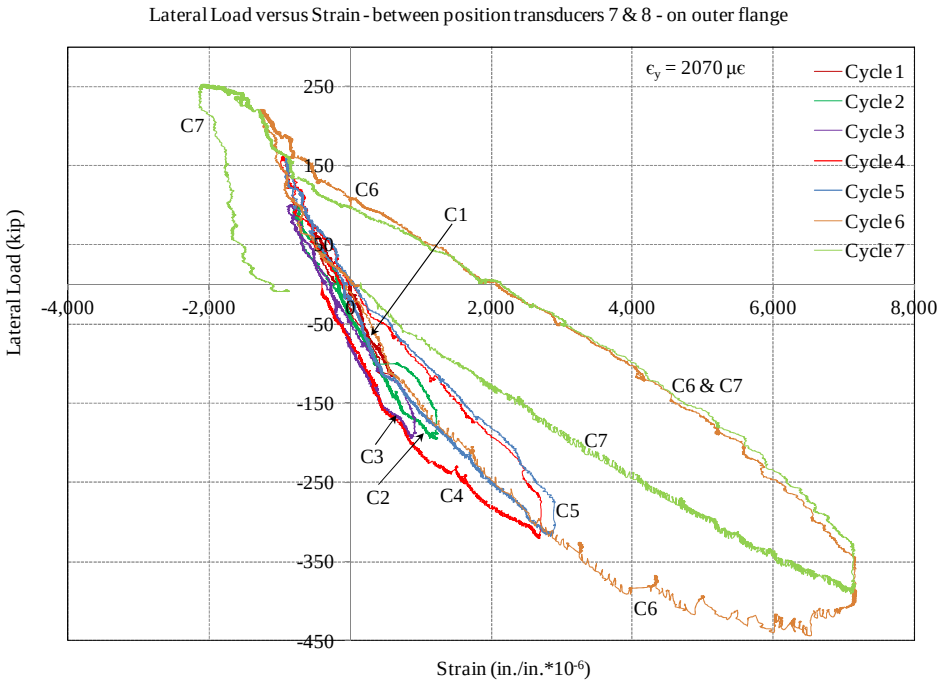

Figure D.69 Lateral load versus strain on shear wall plate – between PT7 & PT8

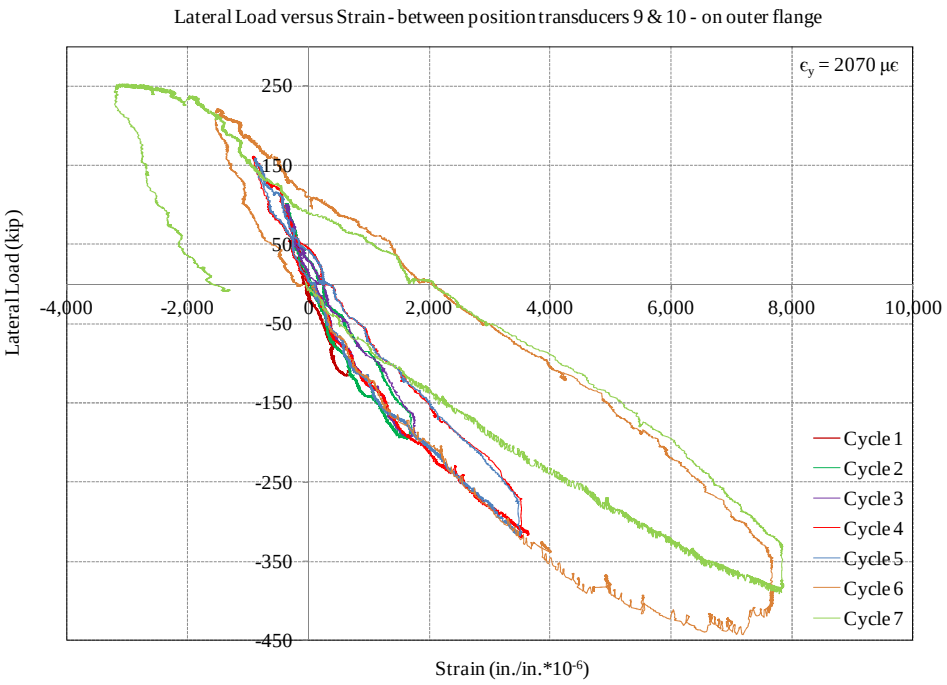

Figure D.70 Lateral load versus strain on shear wall plate – between PT9 & PT10

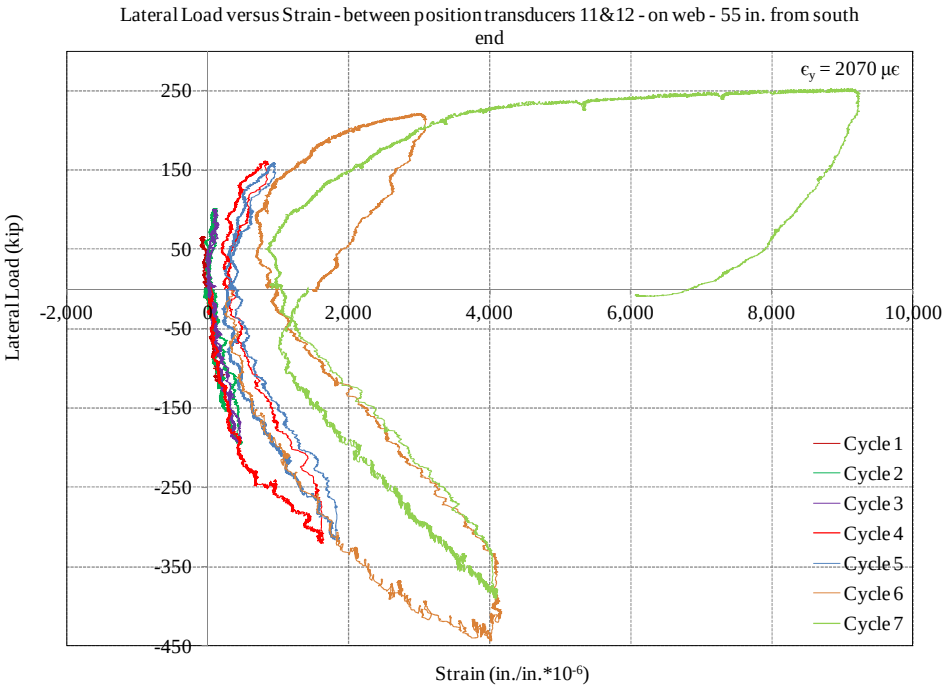

Figure D.71 Lateral load versus strain on shear wall plate – between PT11 & PT12

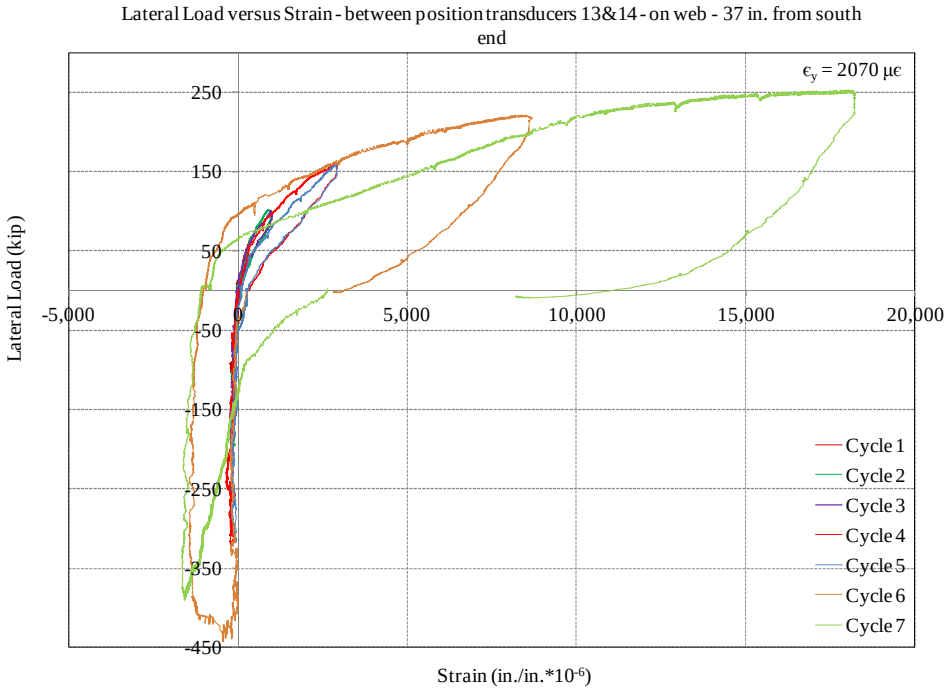

Figure D.72 Lateral load versus strain on shear wall plate – between PT713& PT14

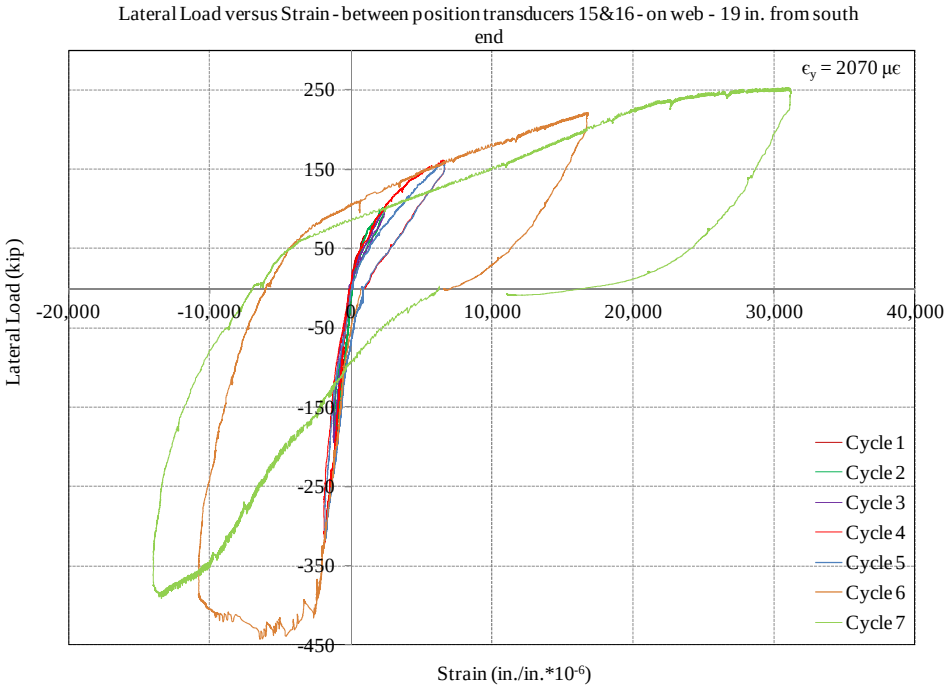

Figure D.73 Lateral load versus strain on shear wall plate – between PT15 & PT16

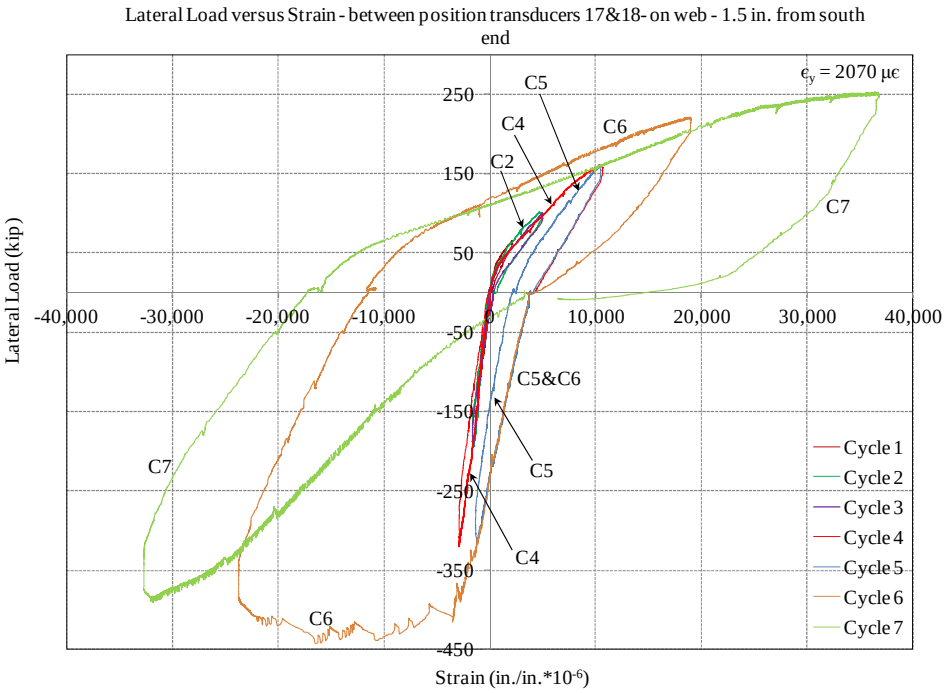

Figure D.74 Lateral load versus strain on shear wall plate – between PT17 & PT18

D.7: Strains on shear wall plate measured by DEMEC mechanical strain gauge

Lateral load versus strain plots for the shear wall plates are presented in Figs. D.75 through D.89. See Section 6.5.10 for details on instrumentation (DEMEC mechanical strain gauges) attached to measure average strains on shear wall plates. Refer to Figs. 6.41 and 6.43 for locations of DEMEC points.

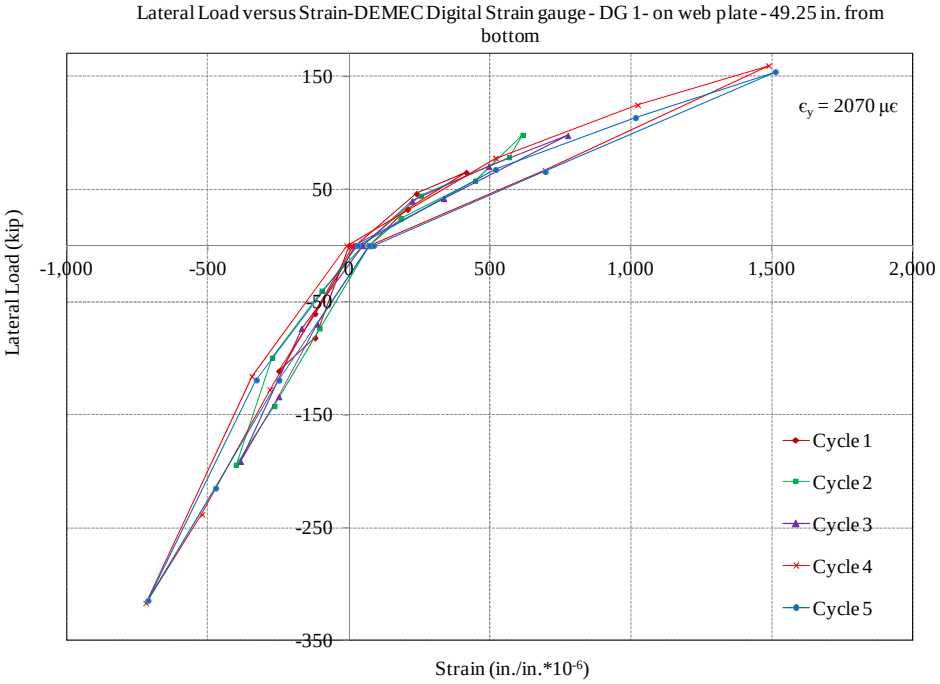

Figure D.75 Lateral load versus strain on shear wall plate – DG1

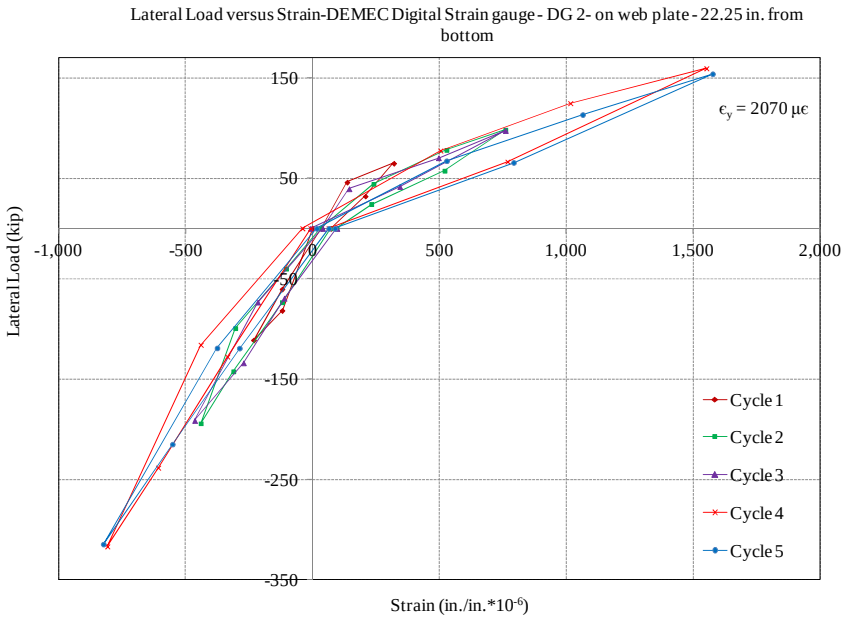

Figure D.76 Lateral load versus strain on shear wall plate – DG2

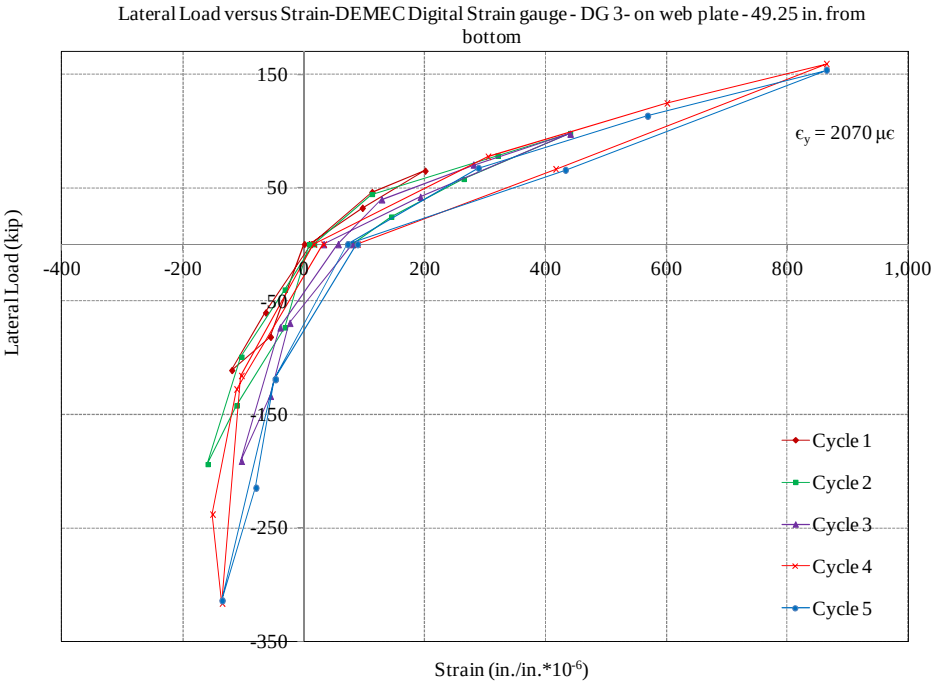

Figure D.77 Lateral load versus strain on shear wall plate – DG3

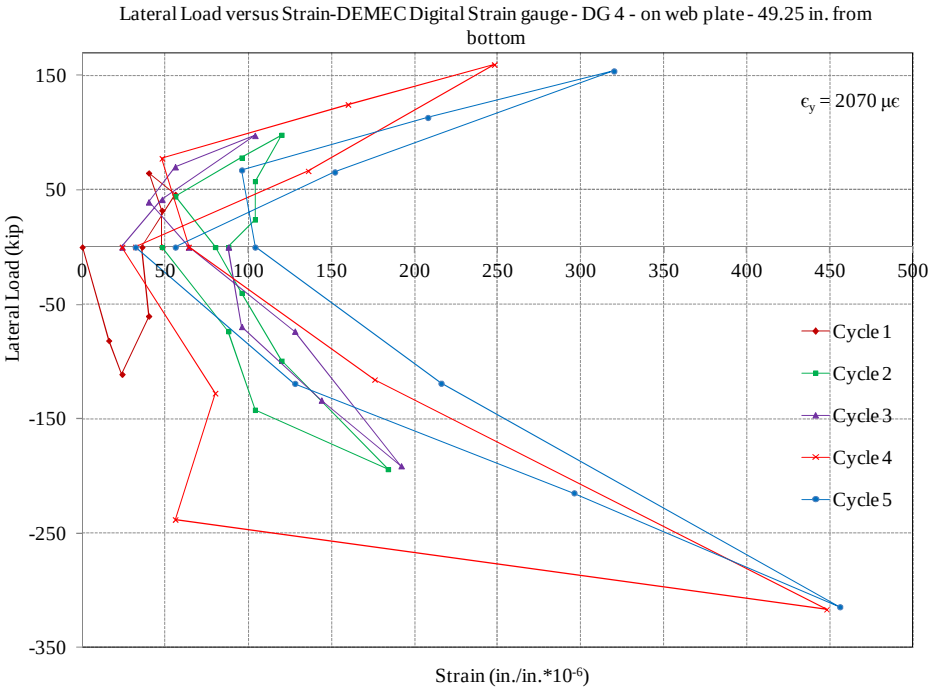

Figure D.78 Lateral load versus strain on shear wall plate – DG4

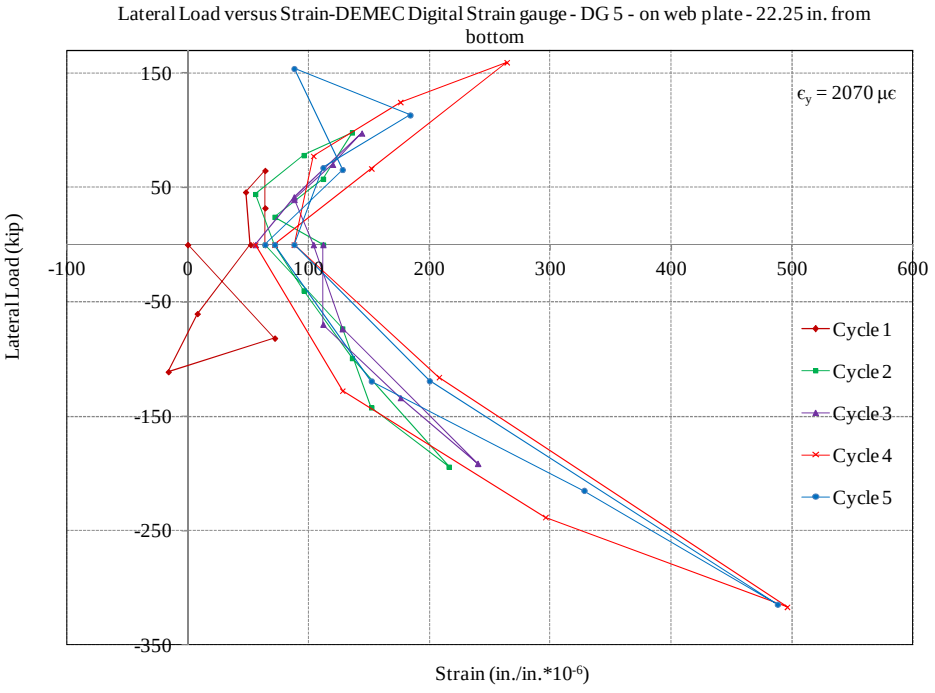

Figure D.79 Lateral load versus strain on shear wall plate – DG5

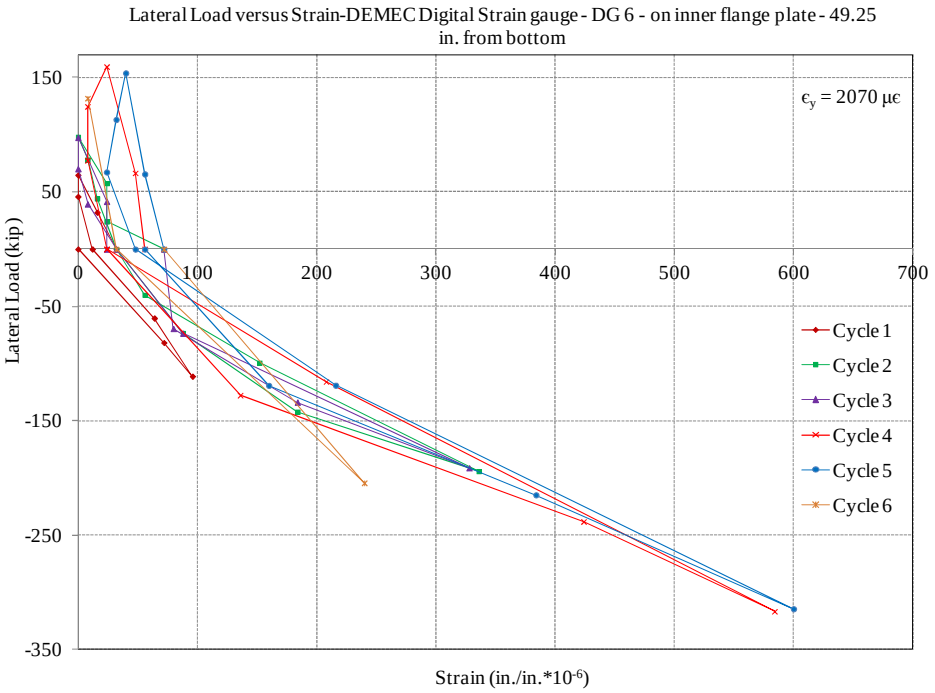

Figure D.80 Lateral load versus strain on shear wall plate – DG6

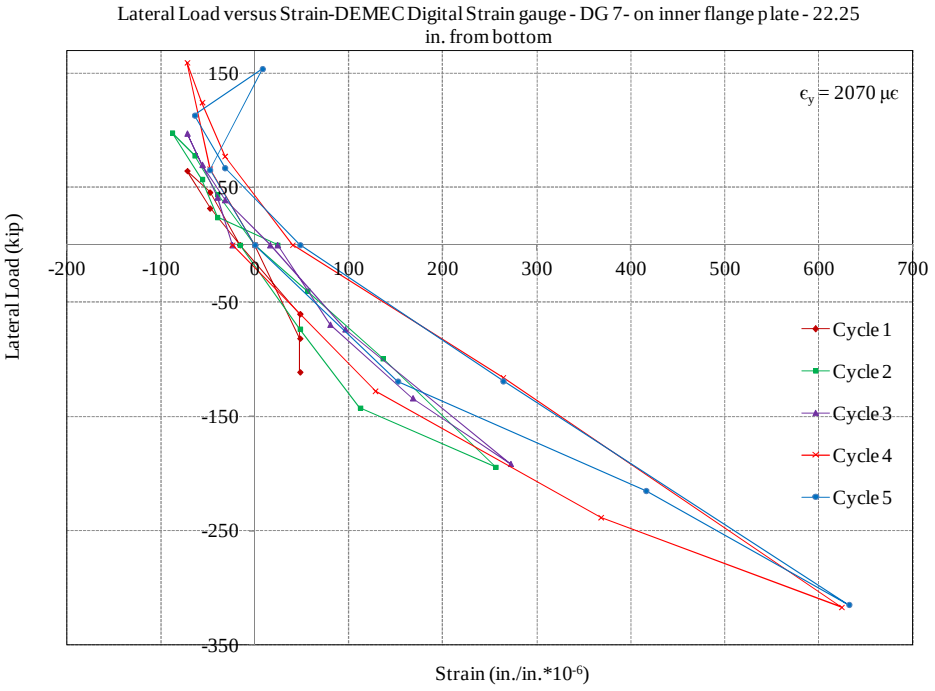

Figure D.81 Lateral load versus strain on shear wall plate – DG7

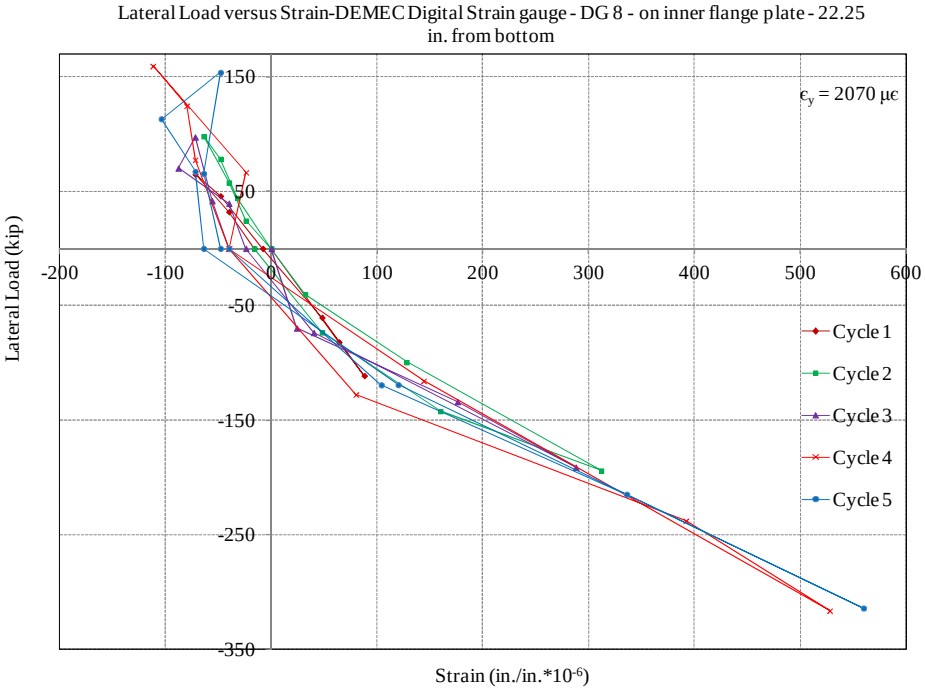

Figure D.82 Lateral load versus strain on shear wall plate – DG8

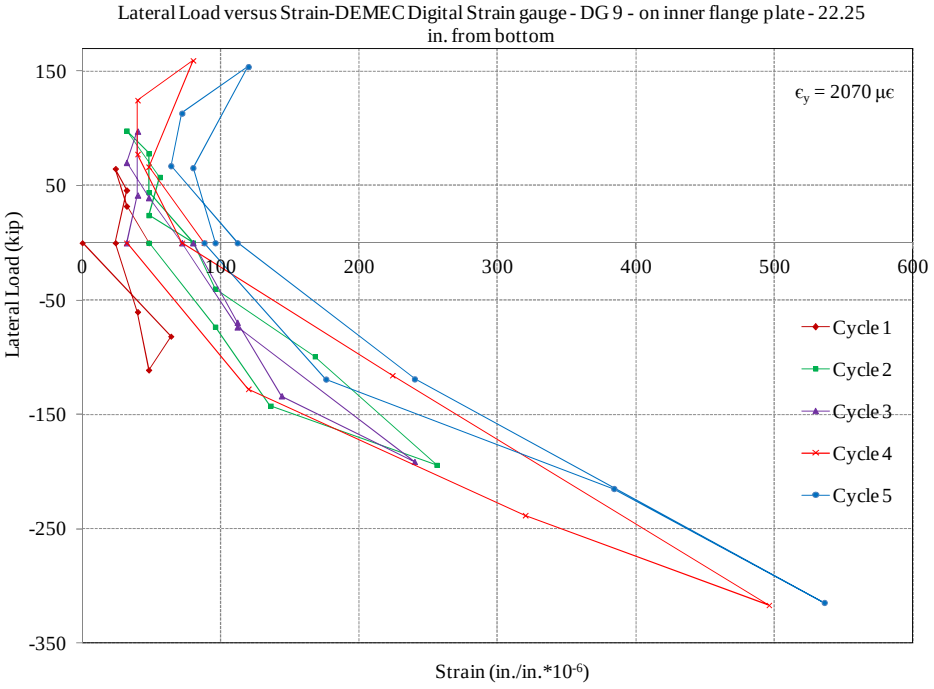

Figure D.83 Lateral load versus strain on shear wall plate – DG9

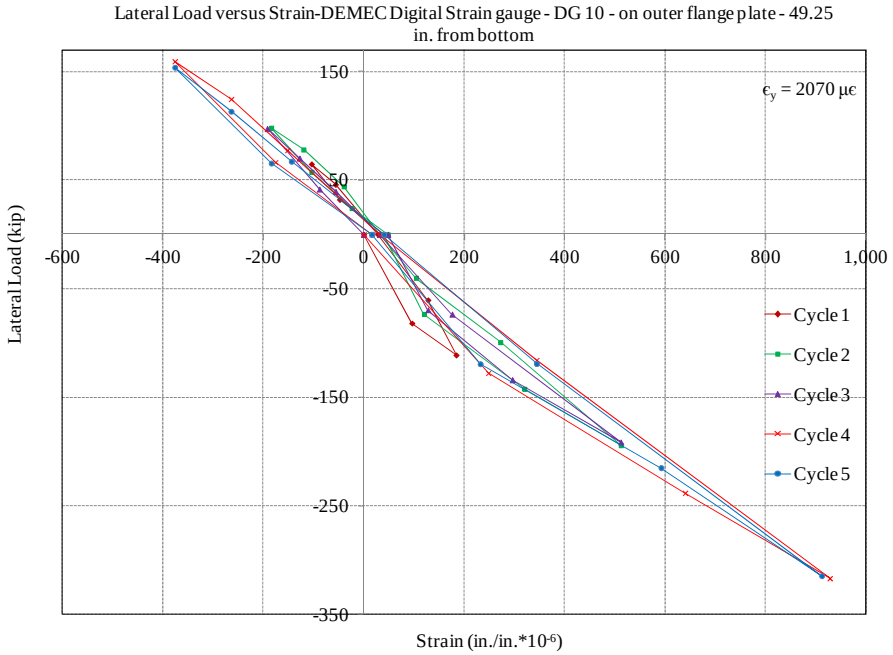

Figure D.84 Lateral load versus strain on shear wall plate – DG10

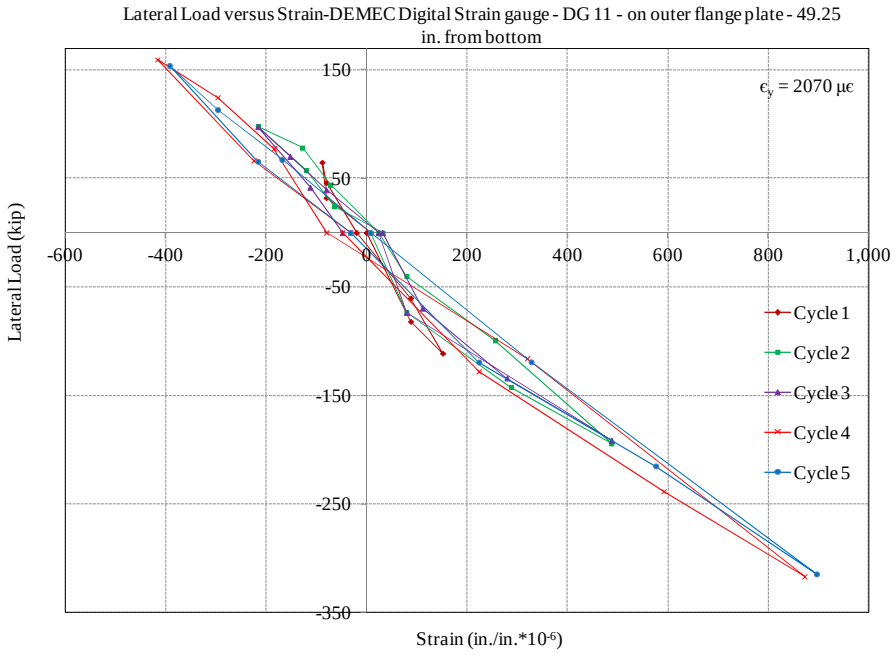

Figure D.85 Lateral load versus strain on shear wall plate – DG11

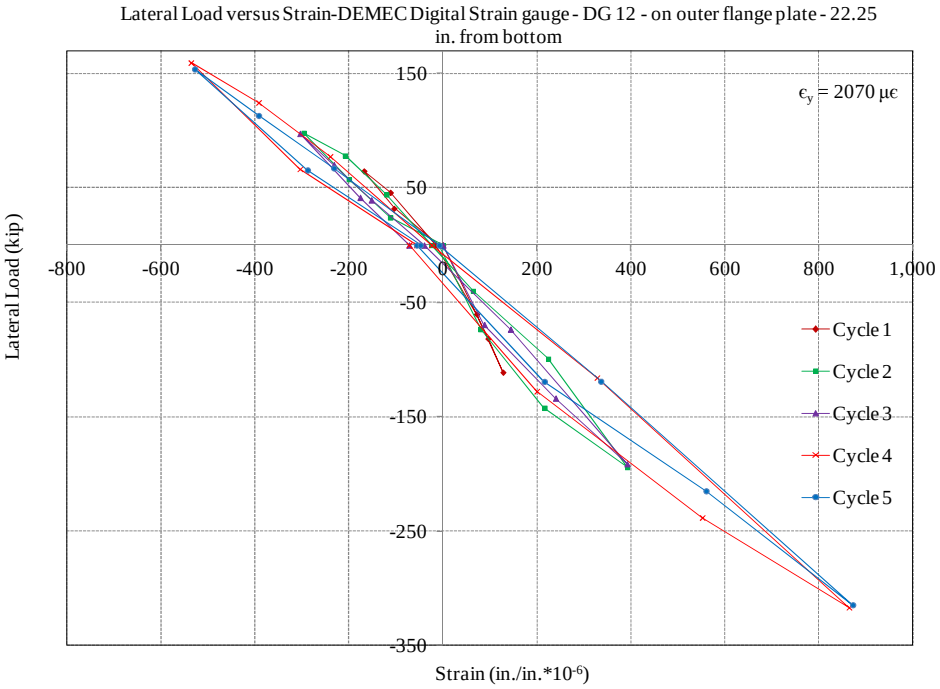

Figure D.86 Lateral load versus strain on shear wall plate – DG12

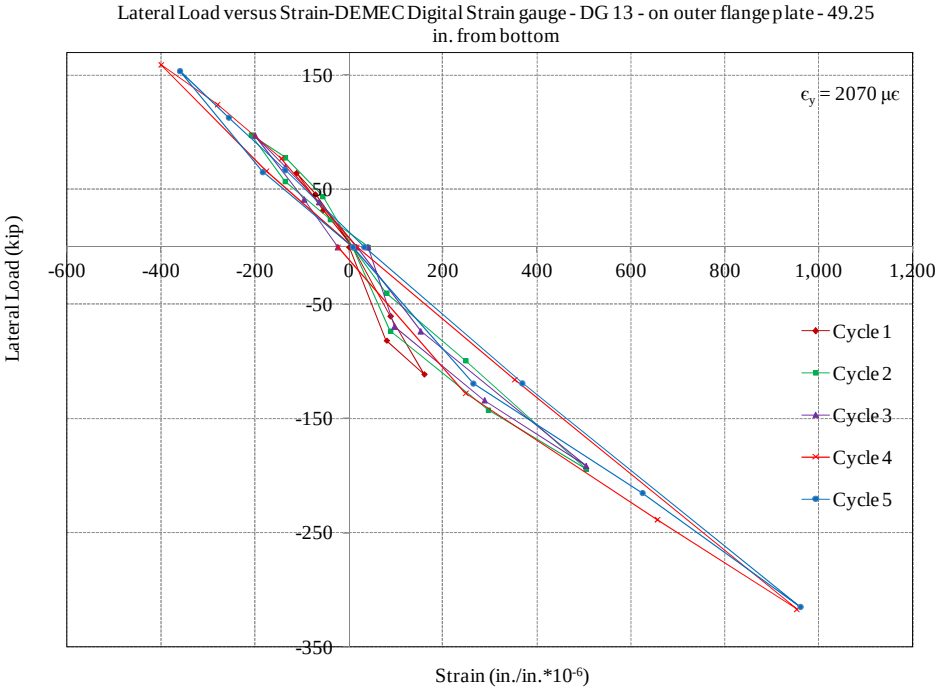

Figure D.87 Lateral load versus strain on shear wall plate – DG13

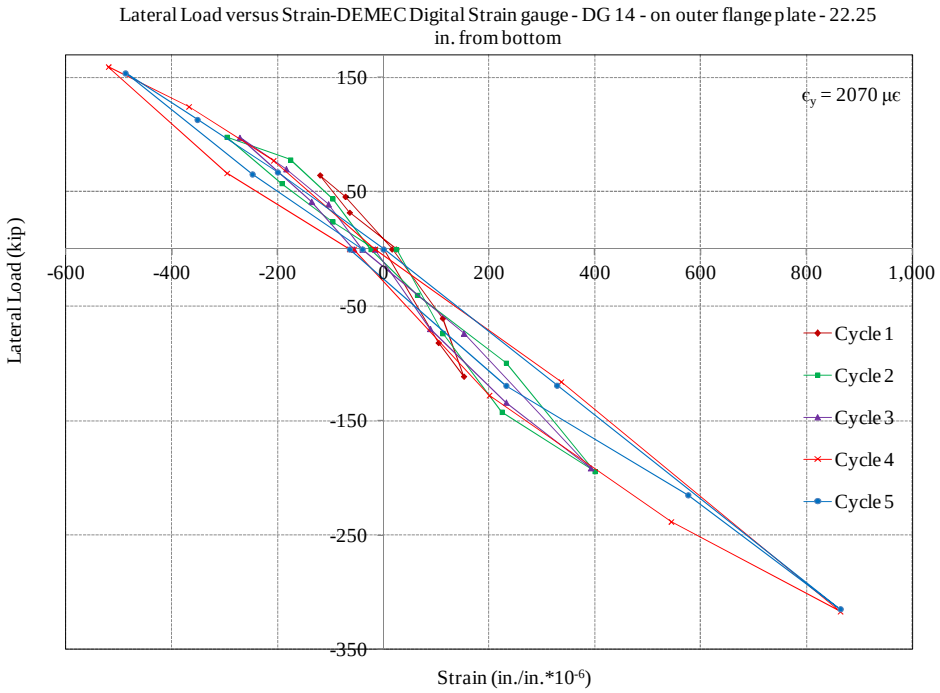

Figure D.88 Lateral load versus strain on shear wall plate – DG14

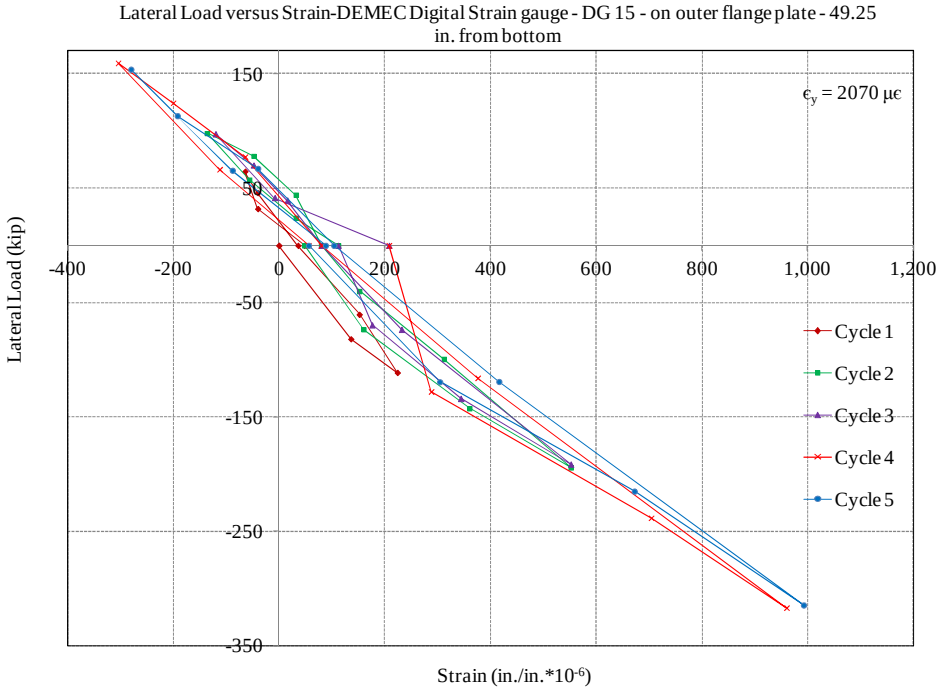

Figure D.89 Lateral load versus strain on shear wall plate – DG15

D.8: Strains on shear wall plate measured by Optotrak

Lateral load versus strain plots for the shear wall plates are presented in Figs. D.90 through D.105. The Optotrak system measures the spatial coordinates of target points on the specimen. Strain was calculated by dividing the difference in distance between two points by the original distance. See Section 6.5.11 for details on instrumentation (Optotrak system) used to measure average strains on shear wall plates. Refer to Figs. 6.41 and 6.43 for locations of Optotrak points. The location of the mid-distance between two Optotrak points is shown in Figs. 6.41 and 6.43.

During cycle 6, when the specimen was pushed towards the strong wall, plates at the base of the specimen started buckling at approximately a lateral load of 410 kips. Buckling occurred approximately 4.5 inches above the foundation connection plate (between the first and second rows of nuts). This occurred between the two points used to measure strain at OPT2 and OPT5 (see Fig. 6.41 for the locations). In Figs. D.91 and D.94, sudden increase in strain at approximately the load corresponding with the plate buckling can be noted. Because the strain was calculated from the distance between two Optotrak points, the calculated strain values after buckling could not be taken as the actual strain over that distance. Buckling extended up to about half the depth of the web from the south end.

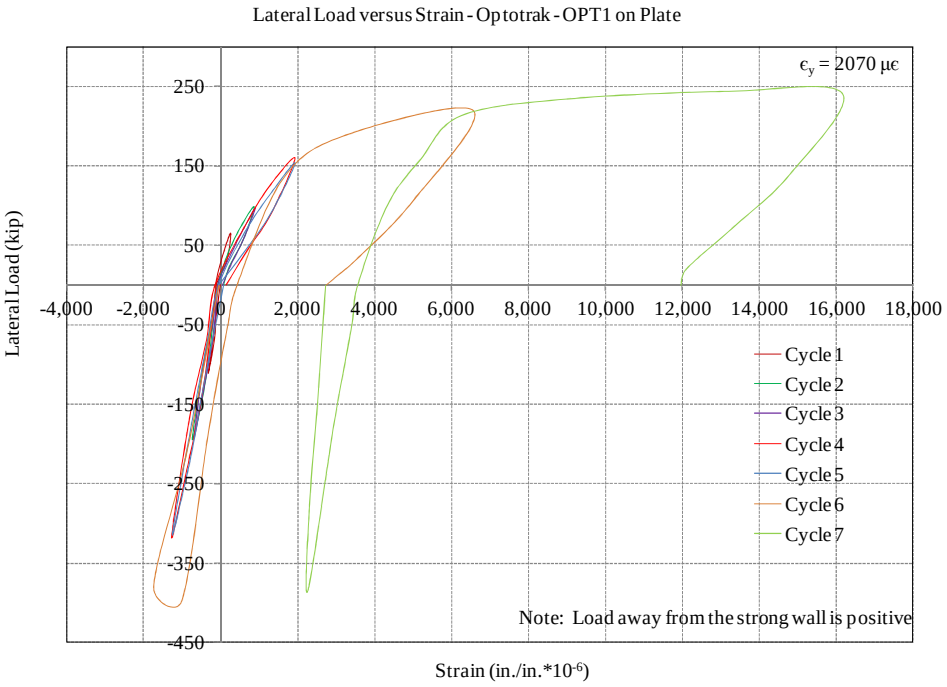

Figure D.90 Lateral load versus strain on shear wall plate – Optotrak – OPT1

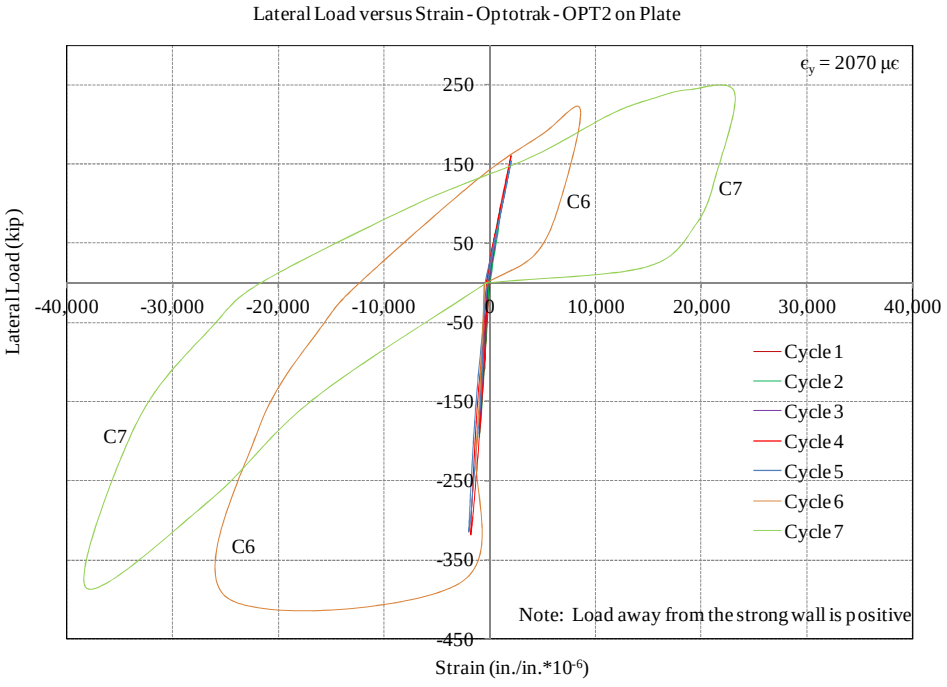

Figure D.91 Lateral load versus strain on shear wall plate – Optotrak – OPT2

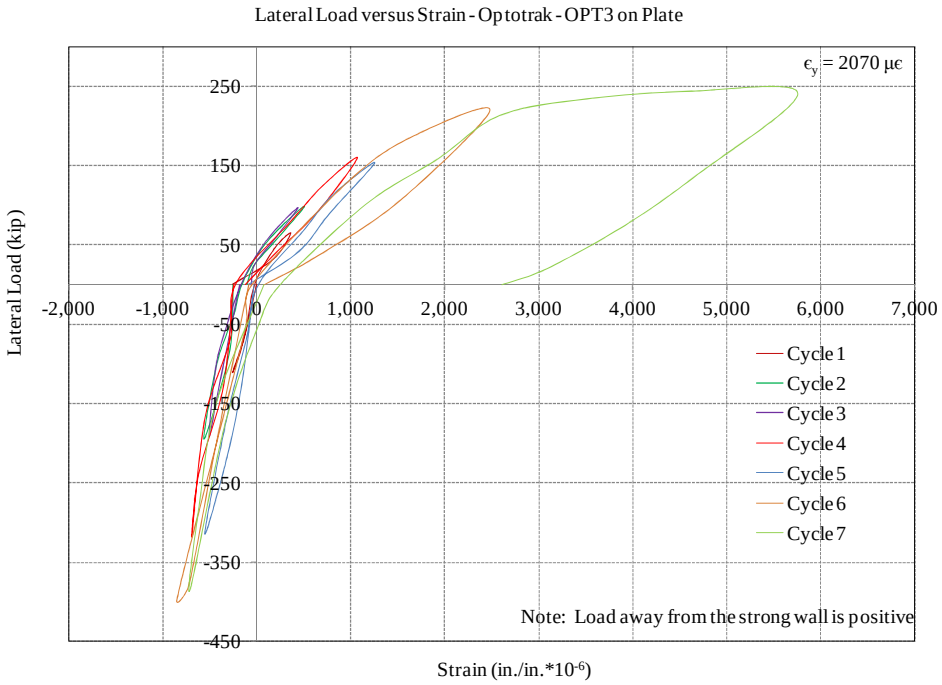

Figure D.92 Lateral load versus strain on shear wall plate – Optotrak – OPT3

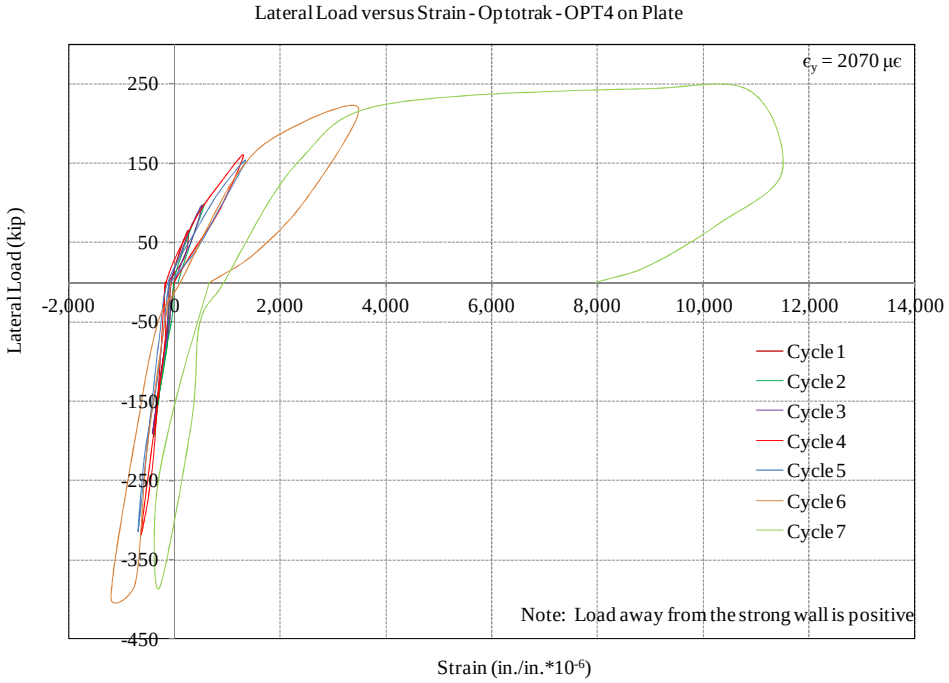

Figure D.93 Lateral load versus strain on shear wall plate – Optotrak – OPT4

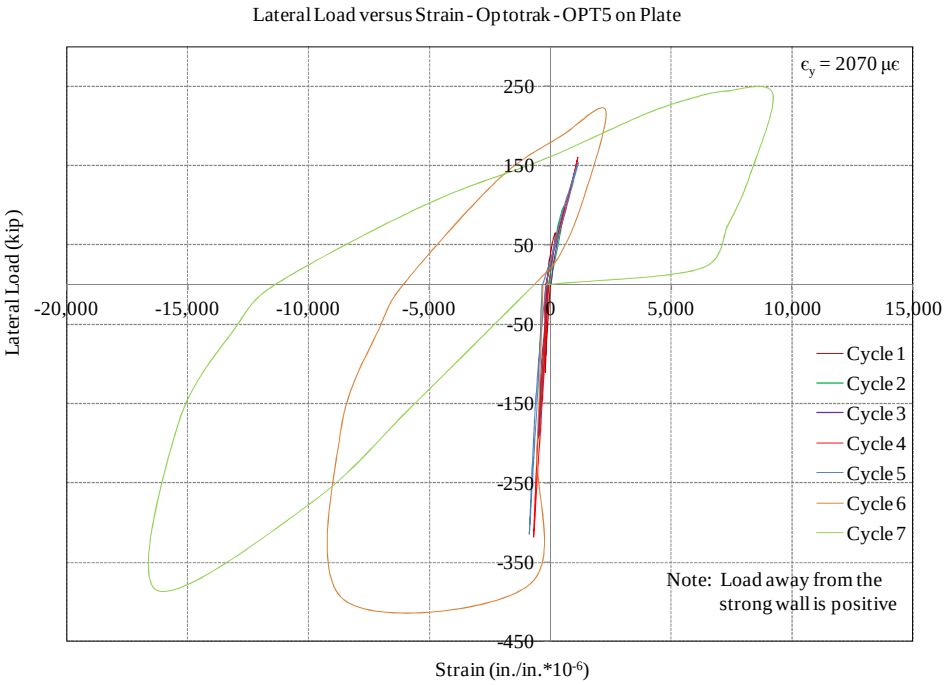

Figure D.94 Lateral load versus strain on shear wall plate – Optotrak – OPT5

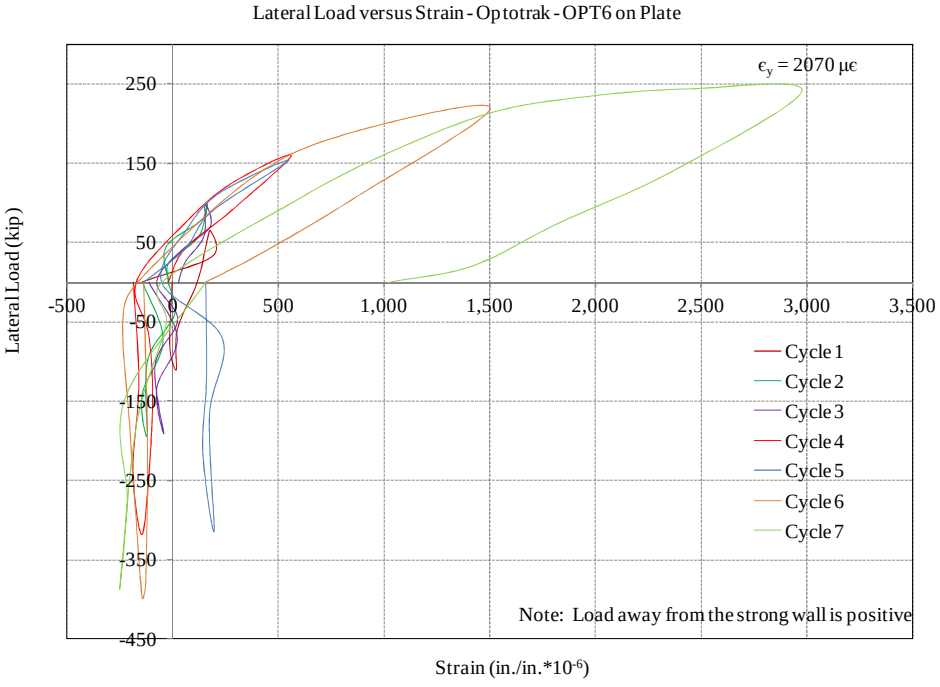

Figure D.95 Lateral load versus strain on shear wall plate – Optotrak – OPT6

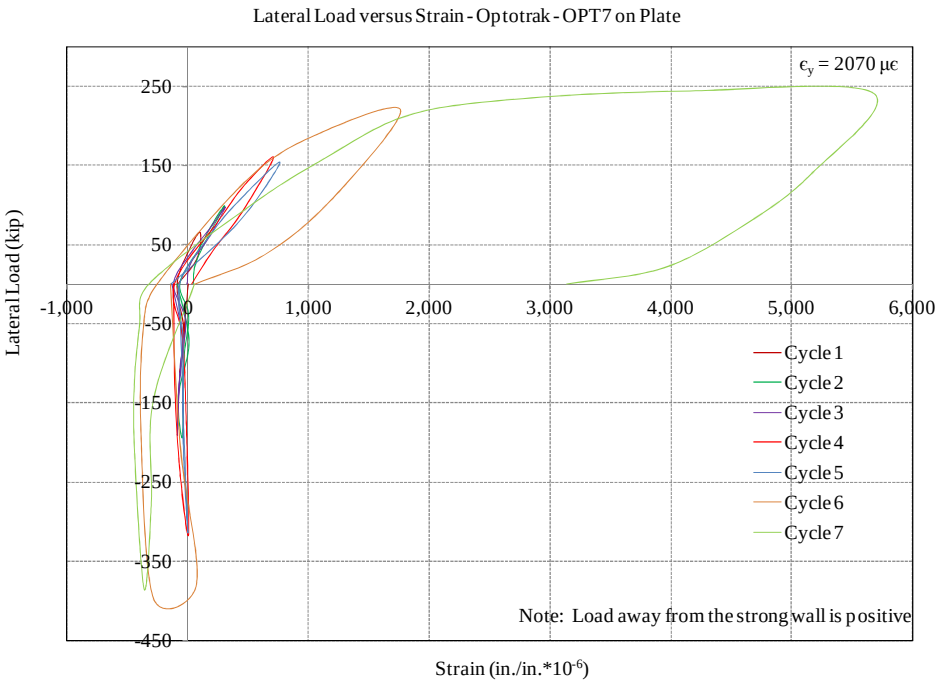

Figure D.96 Lateral load versus strain on shear wall plate – Optotrak – OPT7

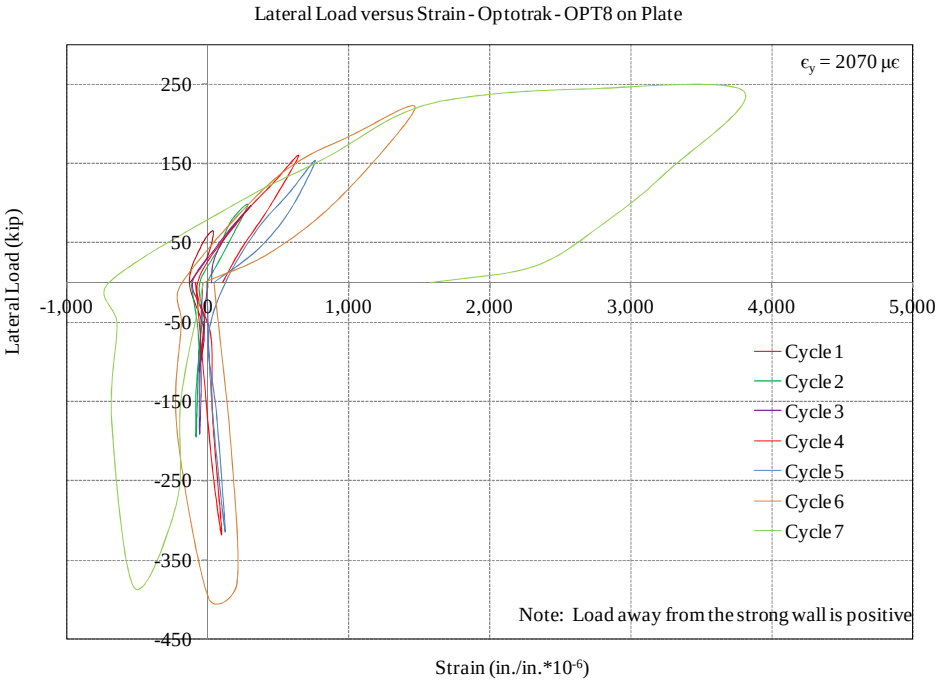

Figure D.97 Lateral load versus strain on shear wall plate – Optotrak – OPT8

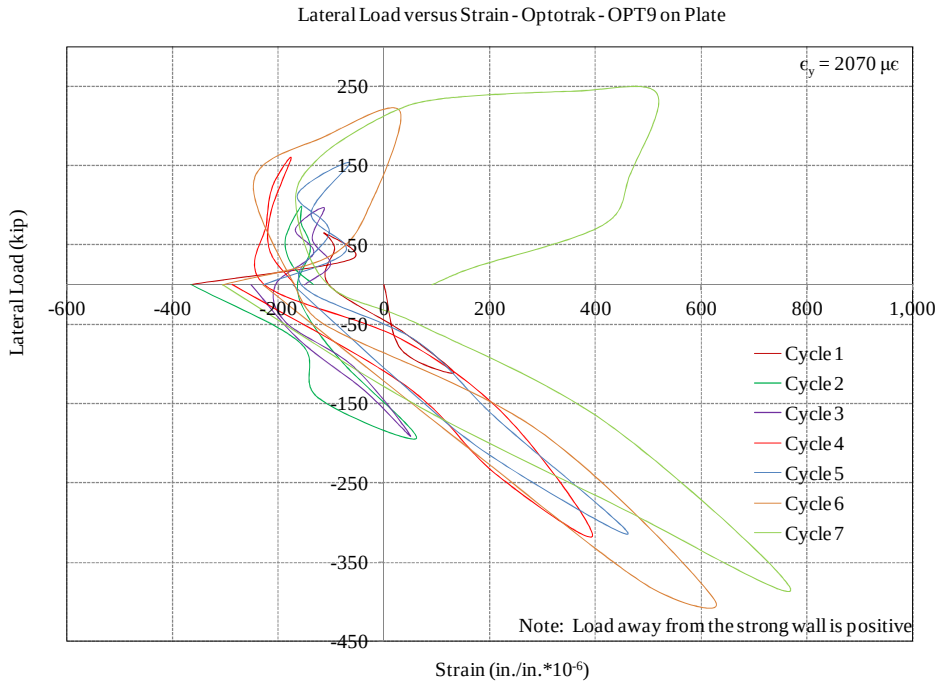

Figure D.98 Lateral load versus strain on shear wall plate – Optotrak – OPT9

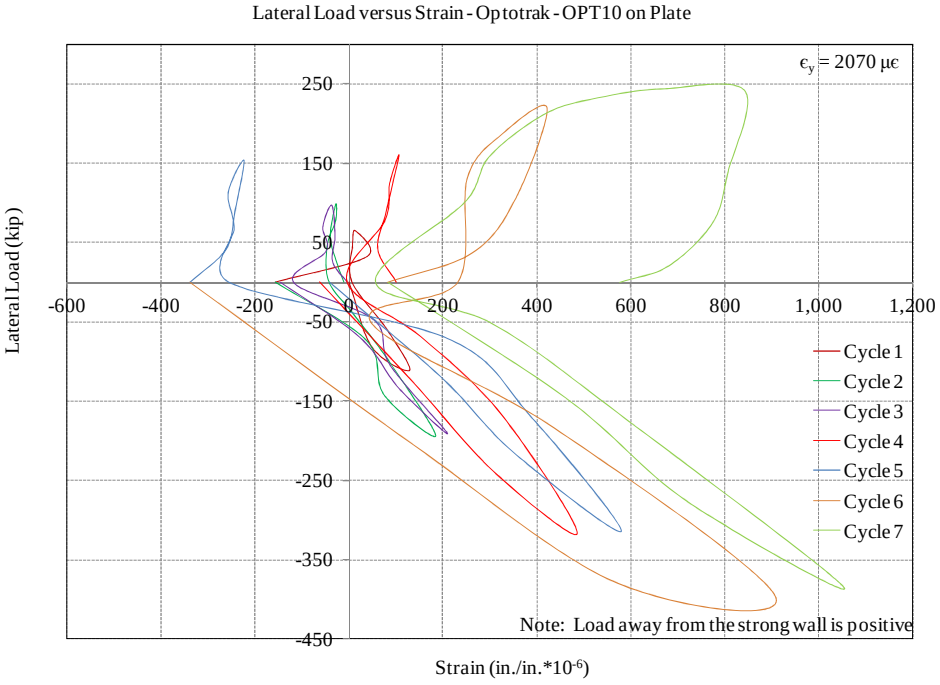

Figure D.99 Lateral load versus strain on shear wall plate – Optotrak – OPT10

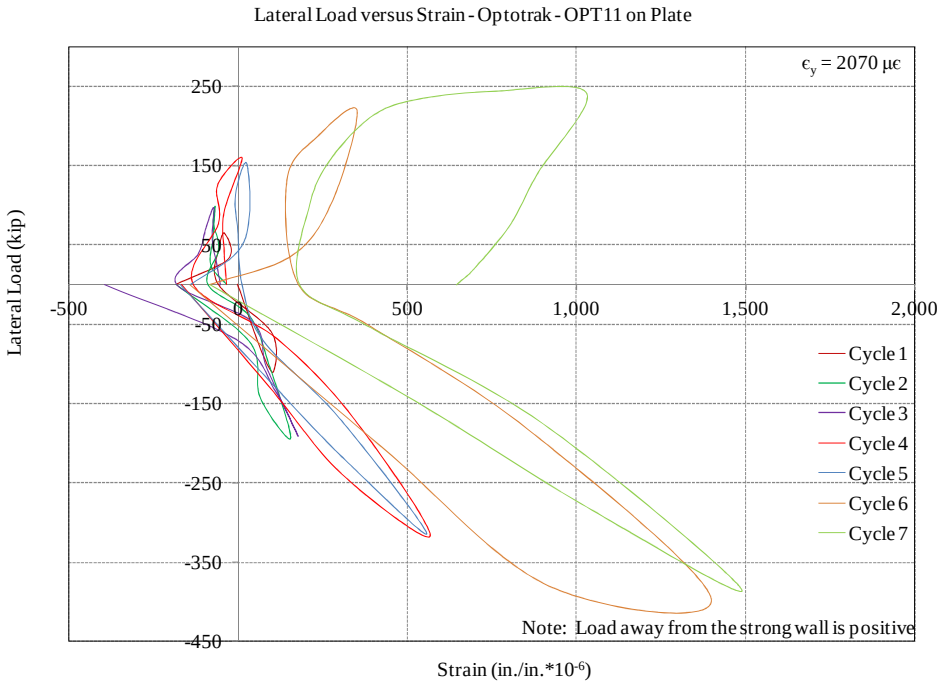

Figure D.100 Lateral load versus strain on shear wall plate – Optotrak – OPT11

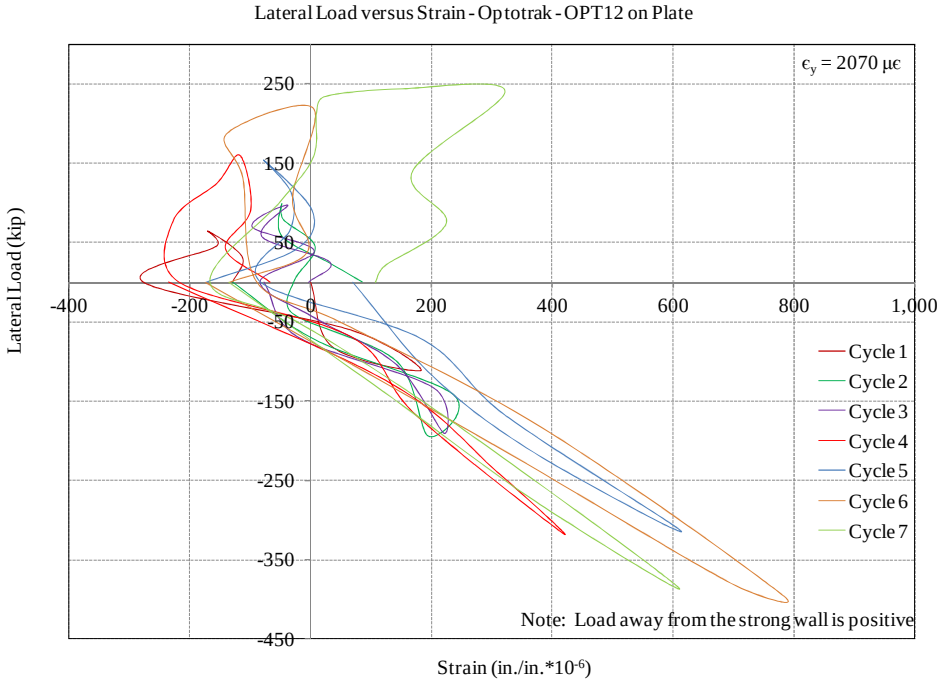

Figure D.101 Lateral load versus strain on shear wall plate – Optotrak – OPT12

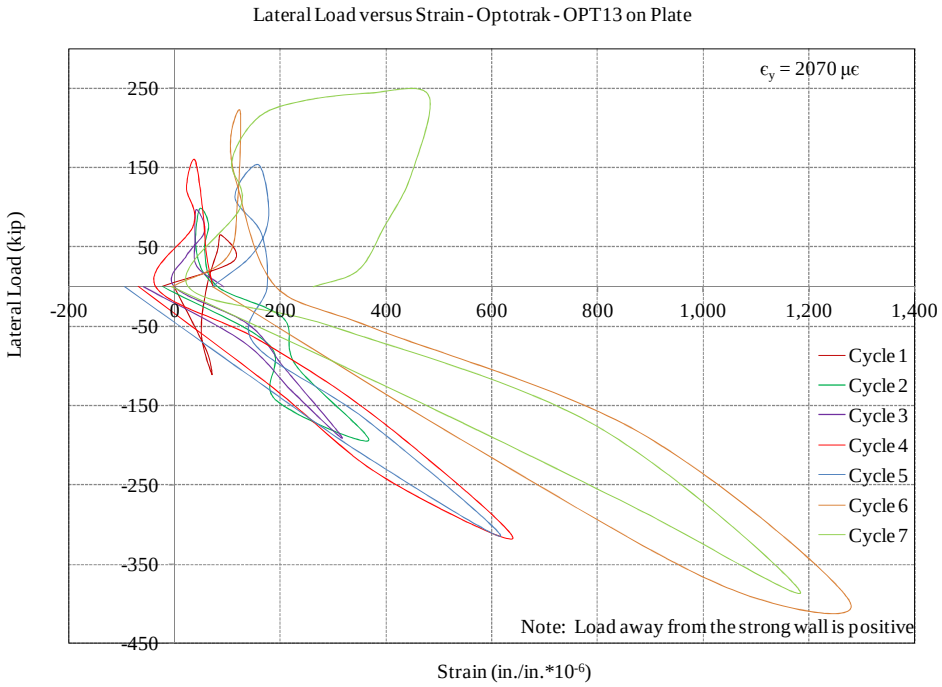

Figure D.102 Lateral load versus strain on shear wall plate – Optotrak – OPT13

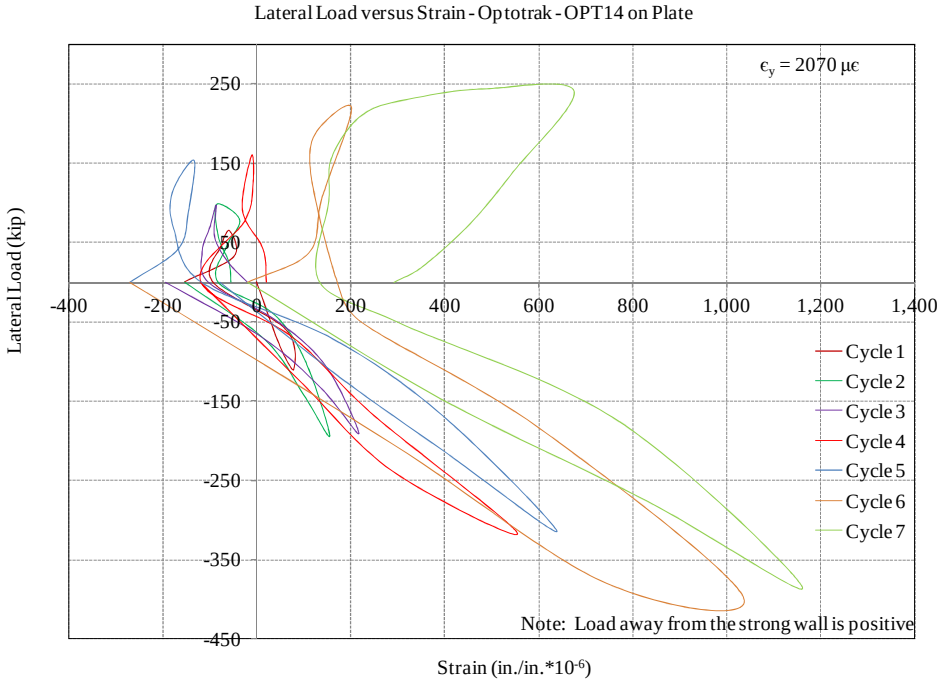

Figure D.103 Lateral load versus strain on shear wall plate – Optotrak – OPT14

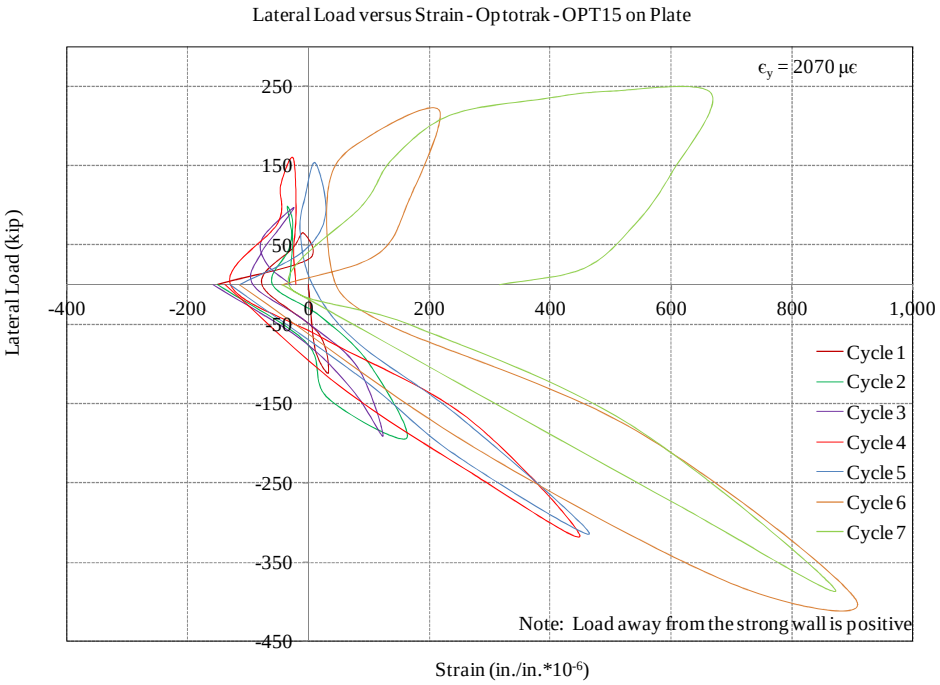

Figure D.104 Lateral load versus strain on shear wall plate – Optotrak – OPT15

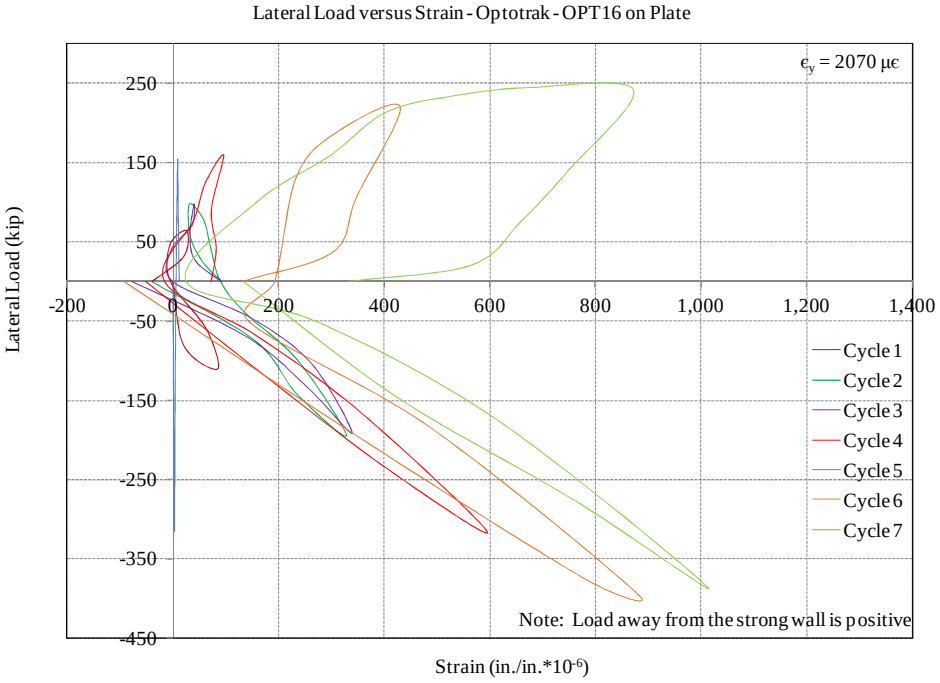

Figure D.105 Lateral load versus strain on shear wall plate – Optotrak – OPT16

D.9: Shear strains on shear wall plate and foundation connection plate

Lateral load versus shear strains measured on shear wall and foundation connection plates are presented in Figs. D.106 through D.109. See Section 6.5.7 for details on instrumentation (shear strain gauges) attached to measure shear strains on shear wall plates and foundation connection plates. Refer to Fig. 6.41 for locations of shear strain gauges.

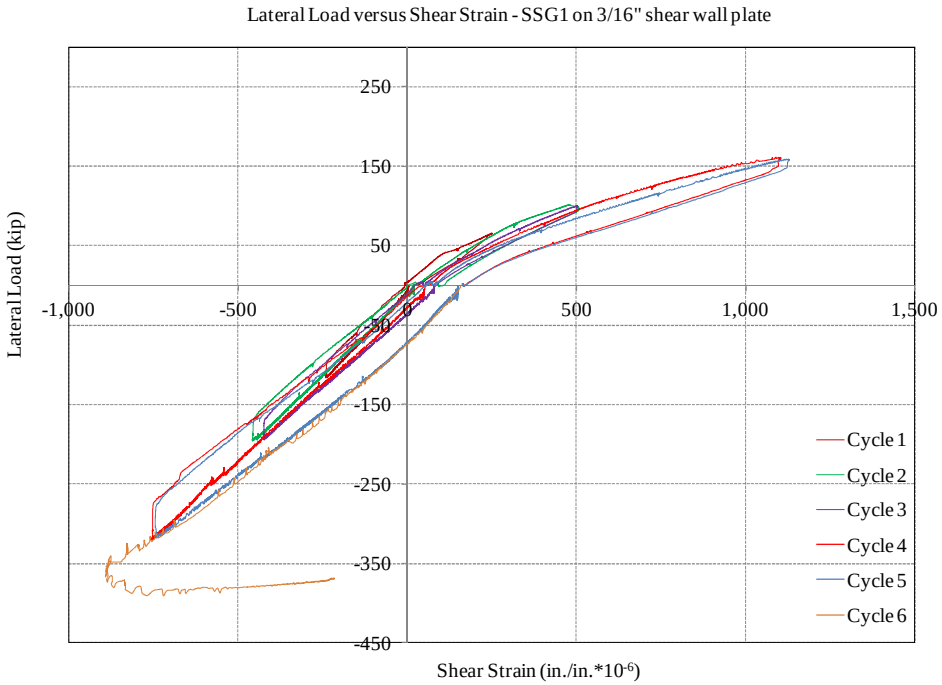

Figure D.106 Lateral load versus shear strain on shear wall plate – SSG1

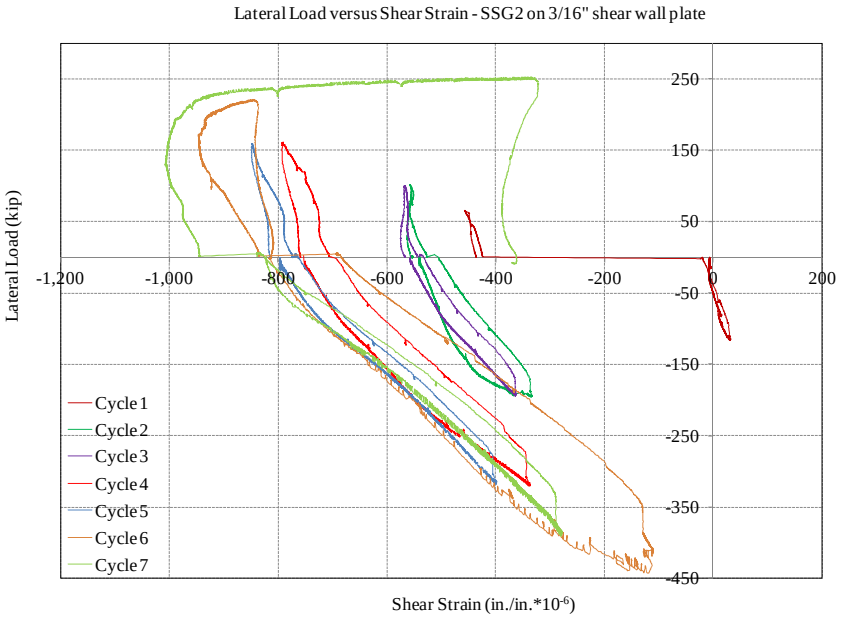

Figure D.107 Lateral load versus shear strain on shear wall plate – SSG2

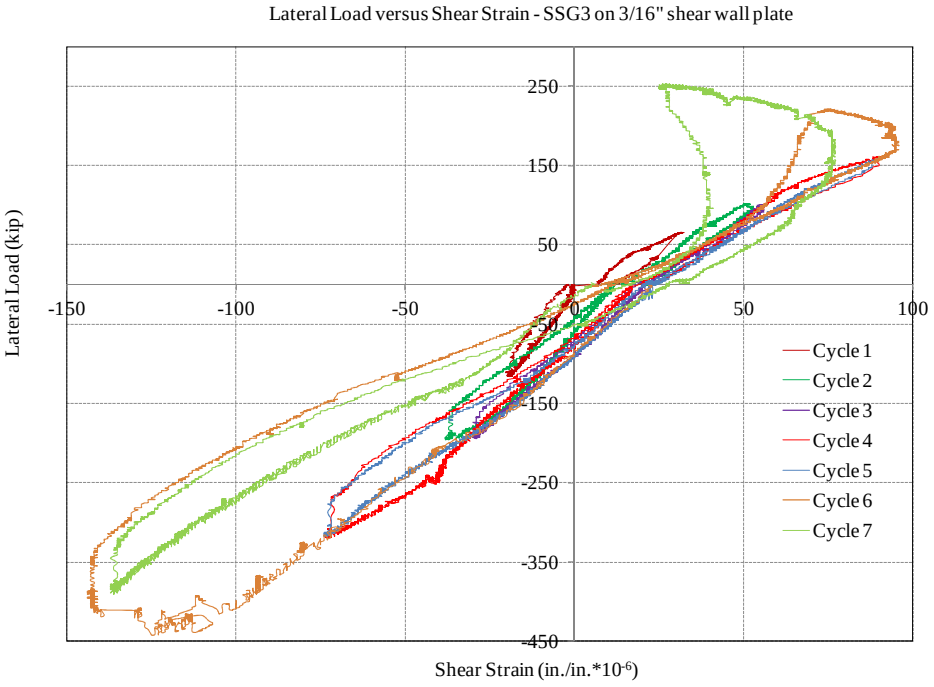

Figure D.108 Lateral load versus shear strain on shear wall plate – SSG3

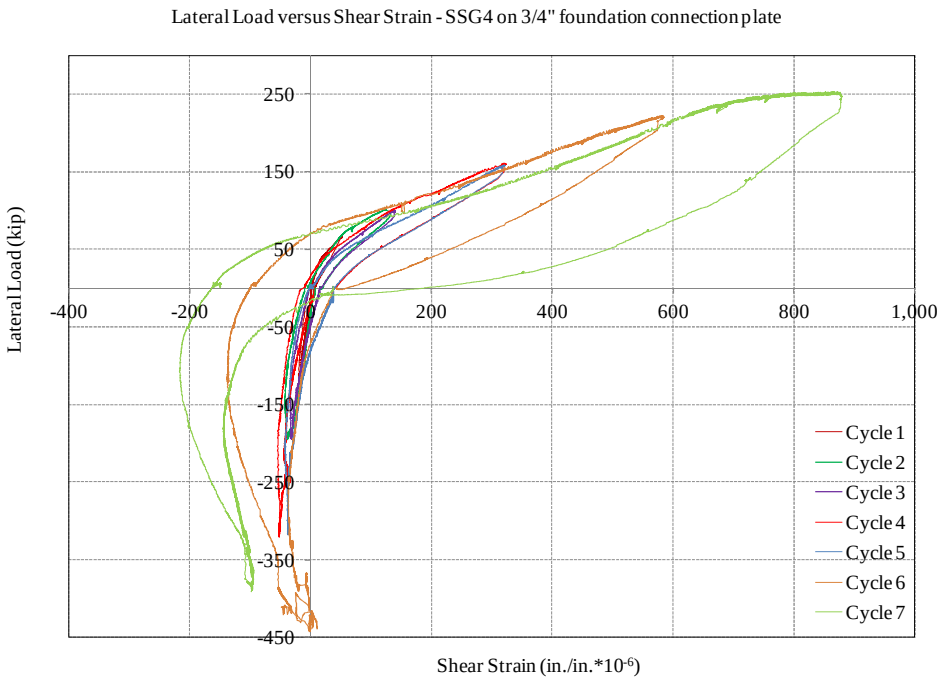

Figure D.109 Lateral load versus shear strain on shear wall plate – SSG4

D.10: Shear and flexural deformations along the web of the specimen in first and second stories

Lateral load versus shear and flexural displacements for the first and second stories are presented in Figs. D.110 through D.113. The instrumentation and calculation methods to determine the shear and flexural displacements are described by Massone and Wallace (2004). See Section 6.5.9 for details on instrumentation to measure shear and flexural displacements along the web of the specimen. Refer to Fig. 6.45 for a schematic diagram of the gauges used to measure the shear and flexural displacements along the web. The shear and flexural displacements were calculated using Equations 4, 5, and 6 from Massone and Wallace (2004).

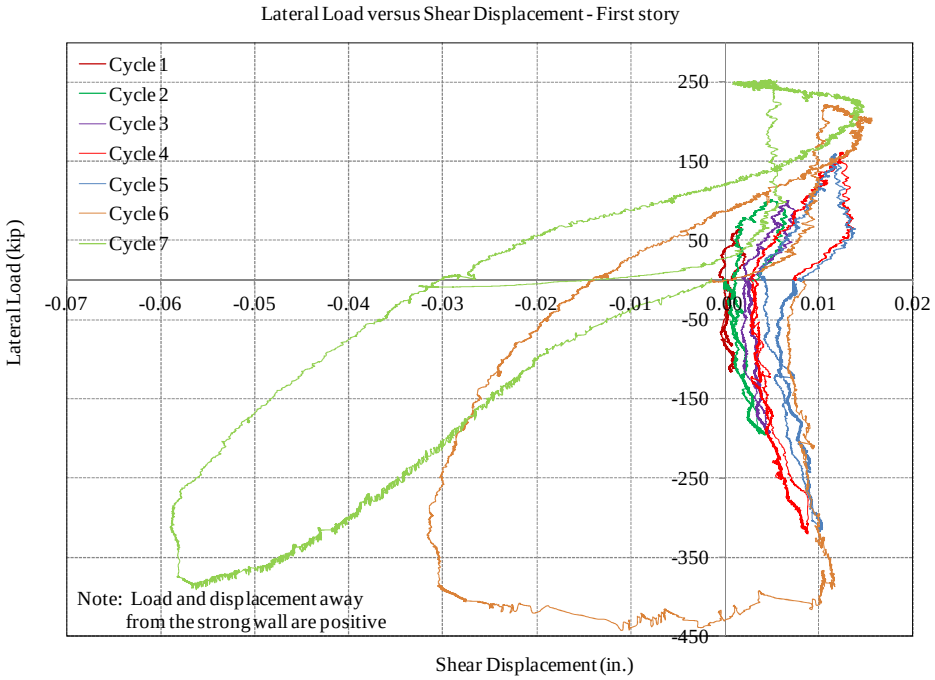

Figure D.110 Lateral load versus shear displacement along the web – First story

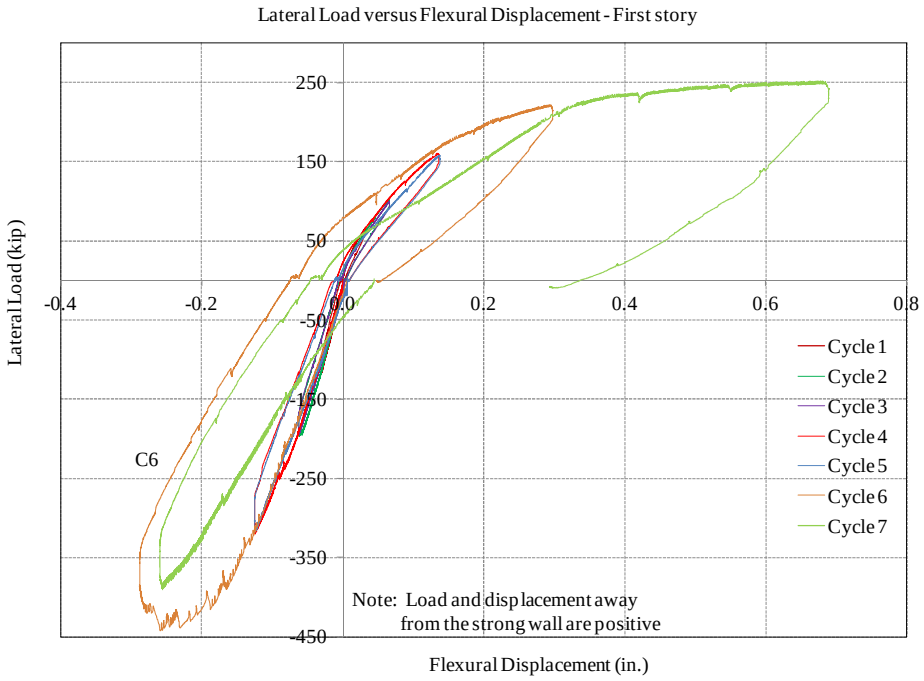

Figure D.111 Lateral load versus flexural displacement along the web – First story

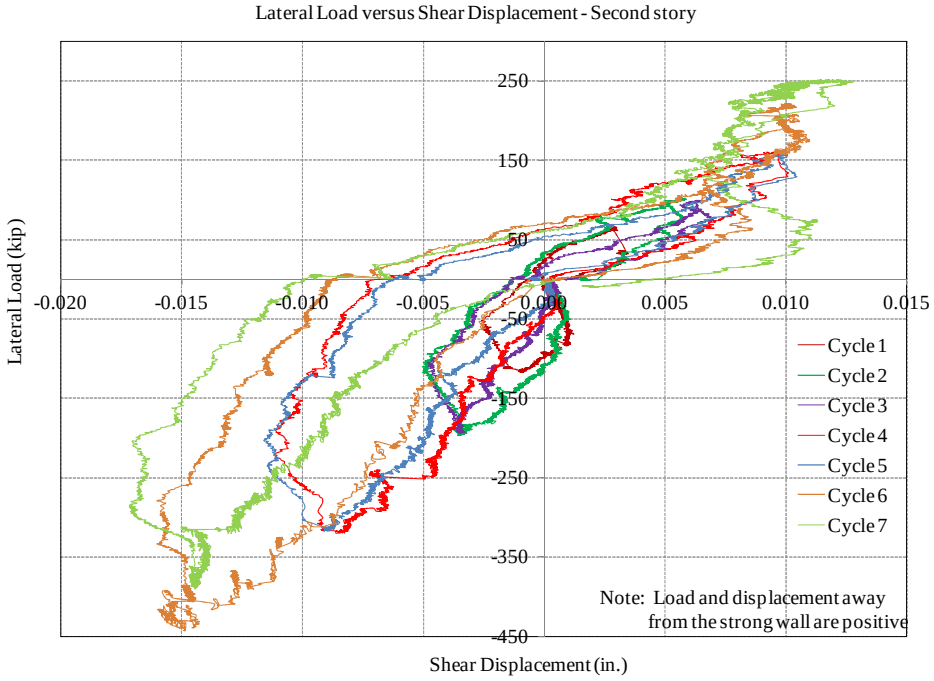

Figure D.112 Lateral load versus shear displacement along the web – Second story

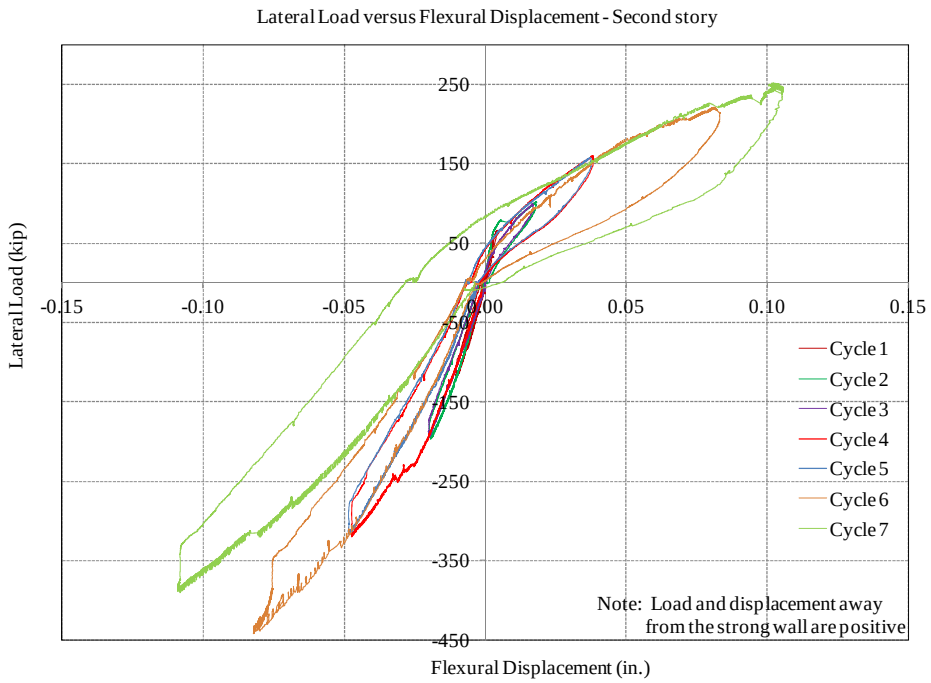

Figure D.113 Lateral load versus flexural displacement along the web – Second story